Dynamique spatio-temporelle des efflorescences de Pseudo-nitzschia australis en mer d'Iroise : une étude pluridisciplinaire combinant l'expression des gènes, l'environnement et l'hydrodynamique

Léa Prigent

COLLEGE SCIENCES DOCTORAL DE LA MER BRETAGNE ET DU LITTORAL

Université de Bretagne Occidentale

THESE DE DOCTORAT DE

L'UNIVERSITE
DE BRETAGNE OCCIDENTALE

ECOLE DOCTORALE N° 598
Sciences de la Mer et du Littoral
Spécialité : *Ecologie Marine*

Par
Léa PRIGENT

Spatio-temporal dynamics of *Pseudo-nitzschia australis* bloom in the Iroise Sea: A multi-disciplinary study combining gene expression, environment and hydrodynamics

Thèse présentée et soutenue à l'IUEM, Plouzané, le 5 décembre 2023
Unité de recherche : IFREMER – ODE – DYNECO - Pelagos

Rapporteurs avant soutenance :

Mariella FERRANTE Senior researcher, Stazione Zoologica Anton Dohrn, Naples, Italie
Cécile LEPERE Professeure d'Université, Université Clermont Auvergne

Composition du Jury :

Président :	Rodolphe LEMEE	Professeur d'Université, CNRS, Sorbonne Université
Rapporteurs :	Mariella FERRANTE	Senior researcher, Stazione Zoologica Anton Dohrn, Naples, Italie
	Cécile LEPERE	Professeure d'Université, Université Clermont Auvergne
Examinateurs :	Rodolphe LEMEE	Professeur d'Université, CNRS, Sorbonne Université
	Philippe PONDAVEN	Maitre de conférences, Université de Bretagne Occidentale
Dir. de thèse :	Mickael LE GAC	Cadre de recherche, Ifremer Centre Bretagne
Invité(s)		
Co-dir. de thèse :	Martin PLUS	Cadre de recherche, Ifremer Centre Bretagne
	Mariella FERRANTE	Senior researcher, Stazione Zoologica Anton Dohrn, Naples, Italie
	Guillaume CHARRIA	Cadre de recherche, Ifremer Centre Bretagne

Remerciements

Au terme de cette aventure académique, je tiens à remercier toutes les personnes qui ont contribué de près ou de loin à la réalisation de cette thèse. Le chemin a été long et rempli de défis, mais il restera à jamais la plus belle expérience que j'ai eue jusqu'à maintenant.

Il est tout naturel que mes premiers remerciements se tournent vers mon directeur de thèse, Mickael. Mes mots ne seront jamais assez forts pour exprimer toute la gratitude que j'ai à ton égard. Je te remercie de m'avoir appris tant de choses, avec ce calme et cette patience infinis qui te définisse. Je me souviendrai toujours de ta lutte acharnée « corrélation n'est pas causalité » ou « sois explicite », merci de m'avoir toujours autant poussée à aller au bout de mes idées. J'ai eu beaucoup de chance d'avoir appris à tes côtés.

Je dois également énormément de remerciements à Martin, mon deuxième encadrant. Merci de m'avoir initiée à l'hydrodynamique avec autant de patience, merci d'avoir été aussi posé face à la personne stressée que je suis ! Tu ne le sais peut-être pas encore, mais merci aussi de m'avoir appris autant de mots et d'expressions que j'ai découvert au fur et à mesure de tes corrections !

J'ai eu beaucoup de chance de vous avoir eu tous les deux comme encadrants.

Merci aux membres de mon comité de thèse, Franck Dumas, Mathilde Schapira, et Lucie Bittner pour votre gentillesse, et pour les échanges scientifiques que nous avons eus.

Merci également aux membres du jury, Cécile Lepère, Mariella Ferrante, Rodolphe Lemée, Guillaume Charria, Philippe Pondaven, qui ont si gentiment accepté de relire ma thèse et/ou de venir y assister à l'autre bout du pays. Thank you Mariella for the various discussions we've had, and for agreeing to review my manuscript.

De grands remerciements vont aussi à Valérie Dérolez et Béatrice Bec pour m'avoir envoyé cette offre de thèse, pour m'avoir fait découvrir le monde merveilleux du phytoplancton et pour votre super encadrement lors de mon stage de M2.

J’ai pu arriver au bout de mes travaux de thèse grâce à un travail d’équipe avec de nombreux collaborateurs, Florian, Marie, Emilie, Julien, Aouregan, Audrey, Anne, Fabienne, merci pour votre disponibilité et votre aide si précieuse au cours de ces 3 années. J’ai vraiment pris plaisir à travailler avec vous !
Julien, j’ai eu beaucoup de chance d’avoir pu bénéficier de ton expérience. Merci d’avoir pris le temps de m’apprendre tant de chose sur les manips de laboratoire ou encore sur le terrain.
Chantal, merci de m’avoir donné de ton temps qui était si précieux pour m’assister lors de l’identification des petites *Pseudo-nitzschia* au microscope, merci de m’avoir initiée et d’avoir pris le temps de m’indiquer le nom des différentes espèces phytoplanctoniques qui se dévoilaient à nous sous le microscope.
Merci Nicolas Chomérat pour toutes les informations sur l’identification des *Pseudo-nitzschia,* et le partage de superbes photos !
Merci également à Sébastien Petton et Solène Le Gac d’avoir répondu à nombreuses de mes questions par rapport à CROCO, et à Matthieu Caillaud pour la configuration du modèle CROCO-Iroise !

Mes pensées vont également à toutes les personnes de DYNECO, un grand merci à Marc, Hugo, Raffaele, Cécile, Erwan, Sophie, Mathilde, Rachel, Marine, Gabin, Aurélien, Benjamin, Flavia, Anne, Françoise et Claire.

Mais également :

Ma jojo, je souhaite t’exprimer toute ma reconnaissance. Tu es une belle personne, et mon vœu le plus cher serait que tu t’en persuades ! Tes attentions délicates, régulières me sont allées droit au cœur. 1000 mercis d’avoir été là !
Ma petite Véro, merci pour tous tes petits conseils « bienfait des plantes » et les différentes discussions sur les animaux, sur la vie ! Merci pour ton aide sur les différentes démarches administratives.
Marie-Mad, j’ai vraiment apprécié les différentes discussions qu’on a eues, elles vont me manquer, et grâce à toi je connais un peu l’histoire de l’Ifremer (mais chut) !
Aurore, j’ai appris à vraiment te connaître sur la fin, tu es vraiment une super personne ! Je te souhaite pleins de bonnes choses.

Michèle, merci pour ta gentillesse et pour tous tes conseils ! J'espère que plus jamais, personne ne t'oubliera pour manger ! Merci aussi à ta super binôme Aline ! Les pauses café du midi vont me manquer !
Aline G. au son de ma voix tu m'as reconnue, quelle surprise de te découvrir à mon arrivée à l'Ifremer de Brest, et toi lors de ton premier jour ! Tu es une personne en or, je te souhaite plein de réussite dans tes projets qu'ils soient personnels ou professionnels. Merci pour ton écoute, tes différents conseils. J'espère de tout mon cœur avoir l'occasion de te revoir !
J'en arrive à toi, ma Touria, j'ai découvert une personne extrêmement généreuse, merci pour ton écoute, tes petites attentions si nombreuses. Je reste persuadée que si le monde était rempli de gens comme toi, Touria, il n'y aurait que des gens heureux. Alors un énorme MERCI pour tout ce que tu as fait pour moi.
Pour terminer, je tiens à remercier la dernière recrue, Erwan avec qui j'ai eu la chance de partager le bureau ces derniers mois ! Merci pour ta gentillesse, ta bonne humeur à toute épreuve. J'ai hâte qu'on aille boire des coups tous ensemble ! Tu seras tranquille pour tes pâtés de campagne maintenant !

Ces 3 dernières années de thèse m'ont permis de rencontrer un grand nombre de personnes,

Valérie Stiger, avec qui j'ai eu la chance de travailler pour donner des cours, ça a été un véritable plaisir de te connaître, tu as su me faire partager ta passion de l'enseignement et pour ça merci beaucoup !
Je ne peux évidemment ne pas citer les personnes passées, présentes et nouvellement arrivées dans l'open space, merci pour votre bonne humeur ! Laure (pour ton écoute, ta gentillesse, et toutes tes petites attentions), Irene (pour ta présence généreuse et ton écoute bénite sur ces derniers mois), Thomas (pour nos petites discussions philosophiques sur la vie et la thèse), Mathisse (pour ta bonne humeur constante). Et également Marion, Alex, Bastien, Lucas, Maéva et Chloé et enfin Clément. Clément, mon binôme d'année de thèse ! Je remercie aussi énormément ta petite femme génialissime, Gaelle. Merci aussi à Mathieu !

Je tiens aussi à remercier les deux super doctorantes de Dhyzed, Caroline et Adèle, ça a été un énorme plaisir de vous rencontrer. Dans la team doctorant, je remercie aussi Alisson, je te souhaite pleins de bonnes choses pour ta thèse !

Je remercie aussi un ancien de l'open space, Kévin, qui malgré son départ à mon arrivée a su me prodiguer de nombreux conseils sur ces 3 ans ! J'ai hâte de vous revoir avec Angelica !

Mais je retiens surtout de l'open space ma rencontre avec deux super personnes qui sont actuellement mes amies, Lyndsay et Lou.
Lyndsay, merci pour ton accueil à mon arrivée sur Brest, merci pour ta présence, ton écoute, tes conseils, qu'est-ce que j'aurais fait sans toi ? Je remercie également ton binôme de vie, Lucas. Je suis fière de vous avoir connu et de vous avoir à mes côtés. J'ai hâte de vous accompagner dans les différentes étapes de la vie !
MA Lou ! Tu as été un peu comme ma « grande sœur de thèse », je te remercie du fond du cœur pour tout ce que tu m'as apportée sur ces 3 dernières années : ton écoute, ton aide, tous les petits à-côtés, comme nos petites soirées chez Luigi, et les promenades qui se terminent entourées de gens à…(je m'arrête là…). Un grand merci à Val aussi pour les petites soirées passées tous ensemble. J'ai hâte de revenir vous voir dans votre petit cocon parisien !
Enfin, j'arrive à toi mon Pierre, merci tout simplement d'être apparu dans ma vie. Tu as eu un rôle tellement important pour moi sur cette dernière année, tu as toujours été là pour m'écouter, m'aider sur mes scripts R, mais surtout tu m'as apportée tellement de rire. Je crois que je n'ai jamais autant rigolé que cette année. Il me tarde de te revoir ! (J'espère que ça ne va pas chnouffer à Nice !)
Merci aussi aux deux petites stagiaires de cette dernière année, Julie et Raphaelle, vous êtes formidables les filles ! J'ai hâte de vous revoir !

Je remercie également mes différents amis, de Brest et d'ailleurs,

Marie, merci de m'avoir fait découvrir ta terre natale à mon arrivée sur Brest, merci pour tes encouragements et pour ta présence, nos échanges quasi quotidiens et ta bonne humeur. Tu es une personne en or, et j'ai hâte de partager de nouveau, de bons moments avec toi.
Je remercie également mes meilleurs amis, les triplés, qui m'ont depuis toujours, toujours soutenu malgré la distance ! Je vous aime tellement fort !
Je remercie également les copains de Brest, Sullivan et Théo, pour nos différentes soirées et après-midi escalade, je suis contente de vous avoir rencontré.
Merci à Anne et à Tof, 1000 mercis, d'avoir contribué à notre bien être sur Brest. J'ai hâte qu'on se refasse pleins de petits repas autour du feu !

Thank you Maike, From Sweden, France and Portugal, I'm coming soon to see you in Germany!
Ma Emeline, partie si loin, à l'autre bout du monde, merci aussi pour tous ces bons moments sur La Rochelle, puis sur Brest !
Un grand merci aussi à Kenza, Marine, Elodie, Angelina, Fanny et ma Maumau !

Et enfin, à David Cox et Steven pour les relectures !

Et bien évidemment, je ne peux oublier ma super famille.
Avec avant tout mes parents adorés, merci pour votre amour inconditionnel, merci de m'avoir toujours poussée dans mes retranchements et de m'avoir donné la possibilité de faire les études que je voulais, c'est grâce à vous tout ça. Je vous aime tellement fort. J'ai également une pensée pour toi, ma Gaelle.
Merci papi, mamie, tatie, J-M, Julien, nanou, Steven & family, pour votre présence et vos encouragements constants.
Merci à ma belle-famille pour votre soutien et pour tous les moments partagés sur les terres corréziennes et bretonnes !

J'en arrive à toi mon Pierre-Léo, merci d'avoir traversé la France pour venir jusqu'à Brest. Merci pour tout l'amour que tu me donnes depuis toutes ces années. Si ces dernières années ont été intenses, elles nous montrent qu'ensemble nous pouvons tout affronter. Je suis fière de partager ma vie avec toi, et j'ai hâte de découvrir le futur à tes côtés.

Je termine par remercier mon chat, Phyto, car il m'a peut-être réveillée à 6 heures tous les matins pendant ma thèse, week-end compris, mais c'est juste parce qu'il voulait que je réussisse.

Table des matières

Introduction 14
1.1 Phytoplankton in the global ocean 15
1.1.1 The ecological role of phytoplankton: from primary production to the marine food chain 15
1.1.2 A wide range of sizes and shapes 18
1.1.3 The diversified group of diatoms 19
1.1.3.1 A unique morphology 20
1.1.3.2 The central role of sexual reproduction in the life cycle 23
1.2 Phytoplankton blooms 26
1.2.1 A complex event 26
1.2.1.1 Concept and theory 27
1.2.1.2 What is a bloom? 30
1.2.1.3 Conceptual definitions 30
1.2.1.3.1 Threshold- and anomaly based bloom 31
1.2.1.3.2 Advective blooms 31
1.2.1.3.3 Ecological definitions of blooms 32
1.2.2 Understanding the study area through spatiotemporal analysis of blooms 33
1.2.2.1 Multiple environmental variables impact the spatio-temporal bloom development 33
1.2.2.1.1 Factors that can limit a bloom 34
1.2.2.1.2 Factors favoring one species over another 35
1.2.2.2 *In situ* Bloom monitoring methods 38
1.2.3 Harmful algae blooms (HABs) 40
1.3 The diatom genus *Pseudo-nitzschia* 43
1.3.1 Generalities 43
1.3.2 Taxonomy 44
1.3.3 A cosmopolitan genus 48
1.3.3.1 A complicated identification, and the progress of “omics” methods. 50
1.3.3.2 Highly contrasting development conditions 54
1.3.4 *Pseudo-nitzschia* in France 58
1.3.4.1 Regular coastal surveillance, the REPHY 58
1.3.4.2 West-Brittany, an area regularly affected by *Pseudo-nitzschia* toxic blooms 62

1.4 The MASCOET project 68
1.5 Thesis objectives 69

Early spring small scale spatio-temporal shift in coastal diatom communities 77
2.1 Introduction 82
2.2 Materials and Methods 84
2.2.1 Study area 84
2.2.2 Environmental analysis 85
2.2.3 Biological analysis 85
2.2.3.1 Cell Counts 85
2.2.3.2 RNA extraction, library preparation and sequencing 86
2.2.3.3 Sequences preparations and bioinformatic pipeline 86
2.2.3.4 RbcL marker choice for diatom identifications 87
2.2.4 Statistical analysis 88
2.3 Results 89
2.3.1 Spatial and inter-annual environmental differences 89
2.3.2 Similar succession of diatom communities shifted in time between stations 91
2.3.3 Community changes related to temporal environmental changes 95
2.4 Discussion 96

Caractérisation interannuelle de la connectivité hydrodynamique entre la baie de Douarnenez et la rade de Brest 106
3.1 Introduction 112
3.2 Matériels et Méthodes 115
3.2.1 Description générale de la zone d'étude 115
3.2.2 Le modèle CROCO 118
3.2.3 Le modèle CROCO Iroise 120
3.2.3.1 Emprise, bathymétrie et discrétisation horizontale et verticale 120
3.2.3.2 Forçages, conditions aux limites et conditions initiales du modèle 121
3.2.3.3 Validation du modèle 122
3.2.4 Caractérisation de la connectivité hydrodynamique, méthodes et analyses des simulations 124
3.2.4.1 Transport Eulérien 125
3.2.4.1.1 Première approche, méthode des quadrillages 125
3.2.4.1.2 Deuxième approche, méthode qualitative 131
3.2.4.2 Transport Lagrangien 132
3.3 Résultats 134

3.3.1 Validations du modèle 134
3.3.1.1 Validation des marées 134
3.3.1.2 Validation des courants 135
3.3.1.3 Validation de la salinité et de la température 137
3.3.2 Caractérisation interannuelle des vents et des marées en mars dans la zone d'étude 139
3.3.2.1 Des vents majoritairement d'Ouest 140
3.3.2.2 Caractérisation des marées 141
3.3.3 Connectivités moyennes sur les 4 années simulées (Pmax et Tmax) 143
3.3.4 Des conditions hydrodynamiques plus calmes en baie de Douarnenez 145
3.3.5 Une connectivité interannuelle Sud-Nord marquée entre la baie de Douarnenez et la rade de Brest 146
3.4 Discussion 153

Spatio-temporal dynamics of *Pseudo-nitzschia australis* during a bloom: from gene expression to hydrodynamic 161
4.1 Introduction 167
4.2 Materials and Methods 170
4.2.1 Sampling areas and strategy 170
4.2.2 Environmental data 171
4.2.2.1 Abiotic parameters 171
4.2.2.2 Biotic parameters 172
4.2.2.2.1 Cellular abundances 172
4.2.2.2.2 Biomass 172
4.2.2.2.3 Toxins (particulate and dissolved) 173
4.2.2.2.4 Gene expression data 174
4.2.2.2.4.1 RNA extraction, library preparation and sequencing 174
4.2.2.2.4.2 Sequence assembly and gene annotation 174
4.2.2.2.4.3 Relative abundances of *P. australis* 175
4.2.2.2.4.4 Analysis of *P. australis* expressed genes 175
4.2.3 Hydrodynamic connectivities 175
4.2.3.1 The local hydrodynamic model: CROCO-Iroise 175
4.2.3.2 Hydrodynamic transport time analysis (Eulerian and Lagrangian transports) 177
4.2.3.2.1 Eulerian transport 177
4.2.3.2.2 Lagrangian transport 178
4.2.4 Statistical analysis 179
4.3 Results 179

4.3.1 Spatio-temporal dynamic of *P. australis* and the relationship with environment ……179
4.3.2 Does the spatio-temporal dynamics of expressed transcripts show a shift?..... 186
4.3.3 Does gene expression differ depending on the local environment?..... 188
4.4 Discussion 189

Sexual reproduction, a major event determining the dynamics of gene expression during a *P. australis* bloom? 197
5.1 Introduction 202
5.2 Materials and Methods 204
5.2.1 Field sampling and metatranscriptomic samples..... 204
5.2.2 Environmental data 204
5.2.3 RNA extraction, library preparation and sequencing..... 204
5.2.4 Bioinformatic analysis..... 205
5.2.4.1 Community analysis..... 205
5.2.4.2 Gene expressions and functions analysis 206
5.3 Results 208
5.3.1 A blooming period 208
5.3.2 Environmental conditions 211
5.3.3 Gene expression dynamics change over the bloom period 212
5.3.4 Expression of genes related to sexual reproduction during bloom 218
5.3.5 Identification of toxins biosynthesis genes 220
5.4 Discussion 220
5.4.1 Gene expression dynamics was marked over time..... 220
5.4.2 Sexual reproduction, a major event during a *P. australis* bloom? 224

Discussion..... 230
6.1 Summary of the results..... 231
6.2 The importance of combining analysis methods..... 233
6.3 *P. australis* blooms in Western Finistère: an origin, the Bay of Douarnenez..... 237
6.4 Is there sexual reproduction without bloom? 242

Bibliography..... 251

Supplementary material 295

Chapter 1

Introduction

1.1 Phytoplankton in the global ocean

1.1.1 The ecological role of phytoplankton: from primary production to the marine food chain

Although the oceans cover 70% of the Earth's surface, our knowledge of biodiversity patterns in marine phytoplankton is very limited compared to plants in the terrestrial world (Irigoien et al., 2004).

The term "plankton" originated in Homer's Odyssey, where it was used to describe the animals that "wandered" (from the ancient Greek planktós) on the surface of the sea. Phytoplankton refers to all plant micro-organisms (from the ancient Greek phyton) living in suspension in the euphotic zone of oceans and aquatic environments and drifting with the currents, whether or not they are motile.

Phytoplankton are eukaryotic and prokaryotic photoautotrophic micro-organisms, i.e. capable of photosynthesis and producing organic matter and oxygen from water, carbon dioxide and light energy. Phytoplankton are capable of capturing light energy through their pigments (structural or acquired through symbiosis or kleptoplastid processes) and transforming this energy into chemical energy needed to synthesise their own organic matter, thereby performing photosynthesis. This bioenergetic process requires the input of light energy and water to reduce inorganic carbon (CO_2) and form the organic matter they need for their metabolism, as well as inorganic nutrients to manufacture the elements they need for growth. Moreover, photosynthesis also causes phytoplankton to act as a sink for inorganic carbon, since it is capable of sequestering this carbon.

As a result, phytoplankton account for around 45% of the Earth's net primary production (Falkowski, 1994; Falkowski et al., 1998; Gregg et al., 2003) and more than 75% of the primary production of the oceans (Falkowski et al., 2004) but only 1% of the Earth's biomass (Falkowski et al., 2003; Gregg et al., 2003).

In addition to producing a considerable quantity of oxygen required for the respiration process of other organisms, phytoplankton are also involved in numerous biogeochemical cycles: the

carbon, oxygen, nitrogen, phosphorus, silicon and calcium cycles (Falkowski, 1994; Falkowski et al., 1998; Gregg et al., 2003). These roles allow phytoplankton to occupy an important place in ecosystems as the basis of most marine food webs. Indeed, over 99% of organisms are linked directly or indirectly to phytoplankton as a source of food. It enables organic matter to be exported to higher levels via predation. This predation pressure affects the growth, cellular processes and composition of phytoplankton communities (Lampert et al., 1986; Rassoulzadegan et al., 1988). This interaction is referred to as 'top-down' control. However, food webs are not linear and are the result of complex interactions between organisms (food webs that also include parasitism).

Phytoplankton are also involved in the microbial loop (fig. 1). The term was coined in 1983 by Azam et al.. Since then, it has become an essential part of the vocabulary of biological oceanography. The article summarized and linked a series of discoveries made over the previous decade by several marine biologists. First, it was shown that the classical view of the structure of marine plankton communities, as presented by Steele (1976) for example, was incomplete and oversimplified. Although the existence of minuscule phototrophs, bacteria and heterotrophic protists in the marine water column had long been recognised, most biological oceanographers thought that what really mattered in the water column's carbon cycle was just the production of large phytoplankton (in particular diatoms and dinoflagellates), which served as food for zooplankton (mainly copepods) which in turn served as food for small fish (Fenchel, 2008).

Later, with the development of new tools for observing microorganisms, such as the epifluorescence microscope or the scanning electron microscope (Hobbie et al., 1977) it was recognised that bacteria play a substantial role comparable to primary producers in terms of the cycling of elements in the water column (Kirchman et al., 1982). This simplistic basic model has gradually been modified, and the microbial food web has become a fundamental element in our understanding of how marine food webs function.

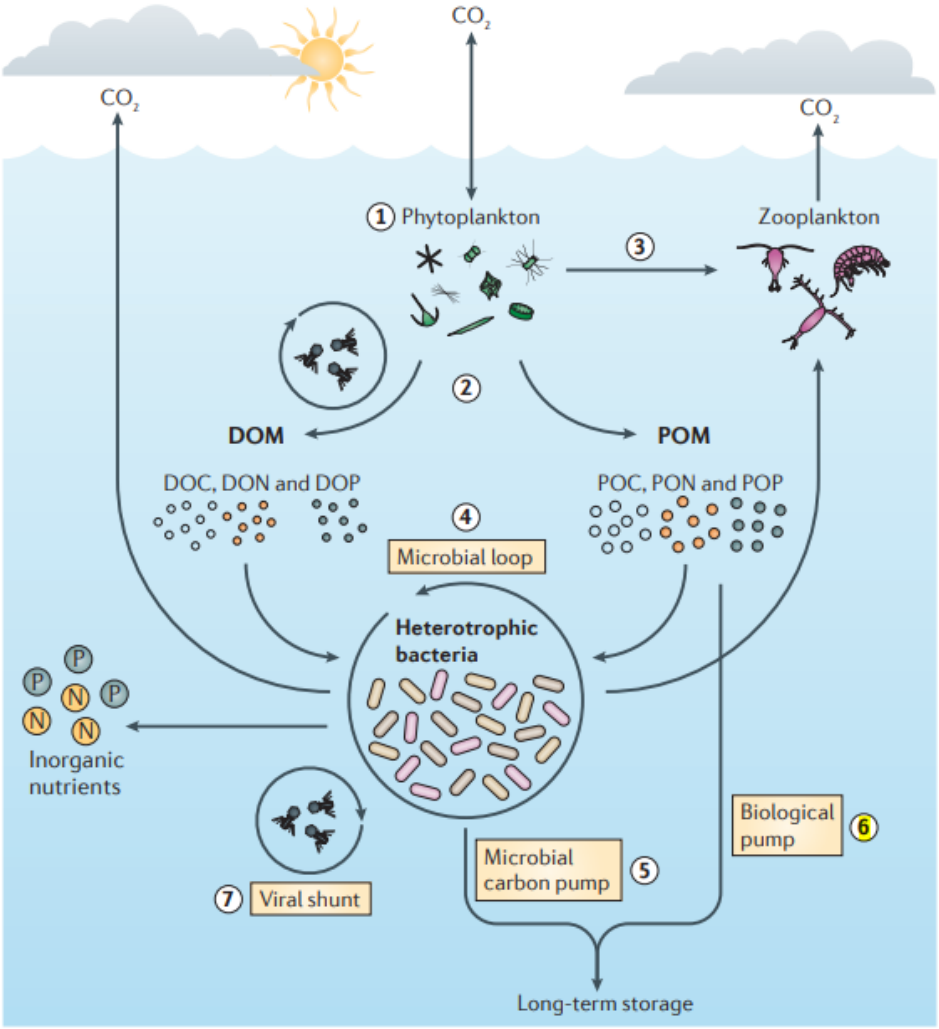

Fig. 1: Representation of the microbial food web taken from Buchan et al., *2014. (1) Photosynthesis; (2) release of dissolved organic matter (DOM) and particulate organic matter (POM); (3) consumption of phytoplankton by zooplankton; (4) mineralisation and recycling of organic matter in the microbial loop; (5) microbial carbon pump; (6) biological pump: export of particulate organic matter from the surface to the deep layers and (7) viral contamination, which allows the release of dissolved and particulate matter during cell lysis of phytoplankton and bacteria.*

As figure 1 illustrates, starting from the role of phytoplankton described above, it produces dissolved organic matter (including: DOM = dissolved organic carbon (DOC) + dissolved organic nitrogen (DON) + dissolved organic phosphate (DOP)) and particulate organic matter (POM = particulate organic carbon (POC) + particulate organic nitrogen (PON) + particulate organic phosphate (POP)) which is made available via excretion and also via cell lysis, for example.

The organic matter produced in this way can be used to produce bacterial biomass, which is recovered by the microbial food web and transported to higher trophic levels ("microbial loop" for the recovery of detrital organic matter). The result of these reactions is organic carbon available to the food web and, at the same time, inorganic carbon, which is once again available

to phytoplankton and can find its way back into the atmosphere. The degradation of DOM and POM by heterotrophic prokaryotes will also lead to the remineralisation of nutrients in inorganic forms, which can be used again by phytoplankton in regenerated primary production. This regenerated production should be contrasted with new production, which corresponds to the use of nutrient salts produced by the remineralisation of nutrients in the deep layers and brought to the surface. This new production also corresponds to the supply of nutrients of continental origin. The nutrients feeding the new and regenerated production (including that from continental inputs, whether anthropogenic or not) exert a bottom-up control, since they regulate the metabolic parameters of the phytoplankton.

1.1.2 A wide range of sizes and shapes

Phytoplankton is an extremely diverse set of microorganisms spanning more than 7 orders of magnitude in cell volume (Beardall et al., 2009) and an enormous range of cell morphologies, bio(geo)chemical functions, elemental requirements and trophic strategies (Dutkiewicz et al., 2020). Depending on the research questions and the degree of specificity required, different approaches can be used to classify and study phytoplankton.

The simplest classification of phytoplankton is to split them into size classes since it does not require any expertise in the classification or identification of phytoplankton. The division is as follow: picophytoplankton (0.2 - 2 µm), nanophytoplankton (2 - 20 µm), microphytoplankton (20 - 200 µm) and mesophytoplankton (2 - 20 mm).

Among these groups, phytoplankton encompasses a great diversity of organisms, it being estimated that there are more than 70,000 marine and freshwater species (Guiry, 2012). These species are grouped into different taxonomic groups.
Over the last few decades, the tree of life has been radically redesigned several times on the basis of data derived from improved microscopic techniques and molecular phylogenies (Simon et al., 2009). Even more recently, the evidence in support of the tree has shifted from a synthesis of molecular phylogenetics and biological characters to a purely molecular phylogenetics (reviewed in Burki et al., 2020).
Existing marine phytoplankton species are found in two domains of life: the Bacteria and Eucarya. The eukaryotic side primarily consists of larger organisms like diatoms and dinoflagellates, as well as numerous smaller microorganisms such as haptophytes,

pelagophyceans, prasinophyceans, cryptophyceans, euglenoids, and chlorarachniophyceans. On the bacterial side, the dominant species are the tiny picocyanobacteria Prochlorococcus and Synechococcus, as well as the nitrogen fixers Trichodesmium, Crocosphaera, and Richelia.
Among these groups, diatoms, dinoflagellates and to a lesser extend haptophytes and green algae are the most diversified groups with respectively, approximately, 40, 40, 10 and 6% of the described phytoplanktonic eukaryote species (Simon et al., 2009).

Beside the high taxonomic diversity, these different groups display different pigment assemblages, which is characteristic of a highly functional diversity. Most of these organisms are present as individual free-floating cells, although some tend to form chains (e.g., certain diatoms), colonies (e.g., Phaeocystis and Trichodesmium), or establish symbiotic relationships with other species (e.g., Richelia). Moreover, the traditional perception of these organisms as simple autotrophs has been increasingly challenged, as many of them are now known to be mixotrophs. This means they possess the capability of phagotrophy, consuming bacteria and small protists, or osmotrophy, taking up dissolved organic substances (Karlusich et al., 2020 and references therein).

Another way to classify organisms, which is fairly recent, is the development of functional ecology as a discipline in itself within the general ecology of organisms in attempting to provide new answers to explain and describe the diversity observed within phytoplankton communities. Based on a systems and integrative approach, it combines the physiological traits of organisms with their function within their ecosystem to study community dynamics and the role of each organism (Litchman and Klausmeier, 2008).
As an example of functional ecology, we can cite the size of phytoplankton cells, which influences all ecological functions and therefore conditions other ecological traits. Smaller cells will increase the surface/volume ratio and therefore favour the assimilation and use of nutrients (Chisholm, 1992), but will be more easily ingested by predators (Straile, 1997).

1.1.3 The diversified group of diatoms

Diatom (Bacillariophyceae) is the most diverse group of eukaryotic phytoplankton. They can be planktonic, benthic, epiphytic, epizoic, endozoic, endophytic and also live in air (Hasle and Syvertsen, 1997). Approximately 40% of all marine phytoplankton described species are diatoms and they are of crucial importance from an ecological and biogeochemical point of

view, especially in nutrient-rich systems (Falkowski et al., 2004). On a global scale it can be estimated that diatoms contribute at least 20% of annual primary productivity, equivalent to the tropical rain forests (Field et al., 1998).

The first illustrations of diatoms (Bacillariophyta) are found in an article from 1703 in Transactions of the Royal Society showing unmistakable drawings of the diatom Tabellaria (Dolan, 2019). It was only 80 years later that we find the first formally identified diatom, the colonial *Bacillaria paxillifera*, discovered and described in 1783 by Danish naturalist Otto Friedrich Müller. Like many others after him, he wrongly thought that it was an animal due to its ability to move (Mann, 2002). It was only in the 19th century that they were included in the plant kingdom after being confirmed as photosynthetic organisms (Simon et al., 2009).

Diatoms are believed to have appeared around 200 million years ago as a result of a secondary endosymbiotic event between a red eukaryotic alga and a heterotrophic flagellate (Medlin et al., 2000). Diatom cells therefore have characteristics that make them very different from the classic cellular structures of higher plants and animals.

1.1.3.1 A unique morphology

Most diatoms are identified by the species-specific morphology of their amorphous silica cell wall, which vary from each other at the nanometer scale (Lopes et al., 2005). Diatom cells are encased within a special cell wall called the frustule, which is well preserved in the fossil record. They usually exist as single cells with a size between 5 µm and 5 mm depending on the species: they often form chains and colonies.

A first distinction among diatoms traditionally starts from the symmetry of their frustule: based on the morphology of their siliceous frustule, diatoms can be divided into two major groups, subdivided into 2 subgroups:

- Centric diatoms have valve striae (rows of pores) arranged basically with central symmetry. In this case, the symmetry can be unipolar (**radial centrics**) or multipolar (**multipolar centrics**)
- Pennate diatoms have valve striae arranged basically linearly. Within the latter, the frustule of **raphid pennates** has a slit called a raphe. **Araphid pennates** lack such slits.

Different phylogenetic studies have shown that “radial centrics" represent the deepest branch, whilst “bi- and multipolar centrics" appeared later (Simon et al., 2009). Figure 2 shows an example of cells from each of the groups

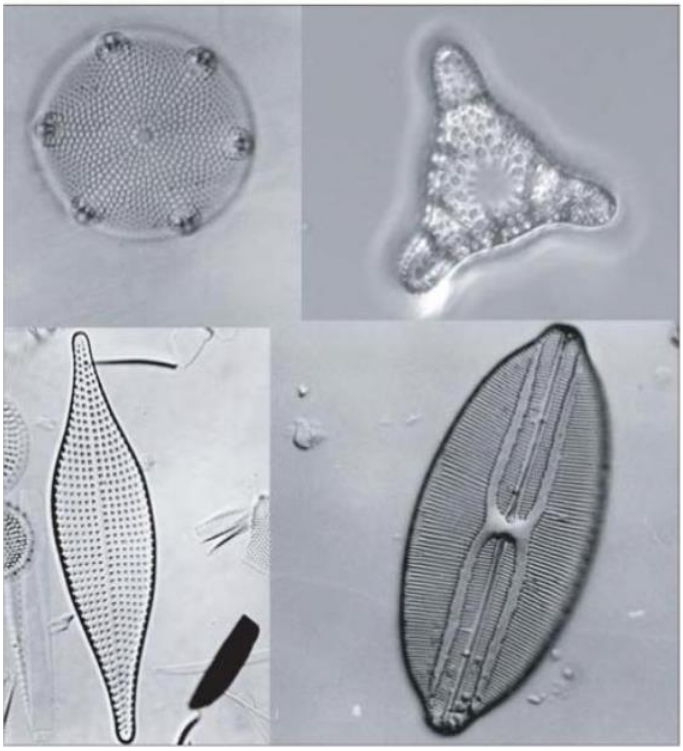

Fig. 2: Diatoms representative of the different groups, top left: radial centric (class Coscinodiscophyceae); top right: bipolar multipolar centric (Mediophyceae), lower left: araphid pennate (Bacillariophyceae) and lower right: raphid pennate (Bacillariophyceae); Credit L.K Medlin, 2009.

For a long time, classification was based on the morphological differences described above. In the era of molecular biology, the comparative analysis of rRNA sequences provided insights into the contemporary phylogenetic relationships among diatoms at higher taxonomic levels (Medlin et al., 1996). Subsequently, this led to the establishment of three diatom classes: specifically, clade 1 comprising Coscinodiscophyceae (radial centric diatoms), clade 2 encompassing Mediophyceae (bi- or multipolar centric diatoms, including radial Thalassiosirales), and clade 3, comprising Bacillariophyceae (pennate diatoms) (Medlin and Kaczmarska, 2004).

More recently, Medlin, in 2016 reviews the various known classifications of diatoms (division Bacillariophyta) and updates them taking into account the latest molecular and genetic

advances. Diatoms are classified in the Heterokontophyta lineage and the Bacillarophyta division, then following classification into 2 sub-divisions, and 3 classes:

- Subdivision Coscinodiscophytina
    - Class Coscinodiscophyceae (= radial centrics)
- Subdivision Bacillariophytina
    - Class Mediophyceae (= polar centrics)
    - Class Bacillariophyceae (= pennates)
        - Subclass Urneidophycidae (= araphid pennates)
        - Subclass Fragilariophycidae (= araphid pennates)
        - Subclass Bacillariophycidae (= raphid pennates)

To date it has been accepted that we know less than 10% of the identified diversity in the marine microbial world and the diatoms are no exception (Medlin, 2018).

From the greek diatomos, meaning cut in two, diatoms are composed of two asymmetrical valves. One large valve, the epivalve, and a smaller one, the hypovalve, are interlocked by a girdle composed of fine structures called pleural bands (figure 3). This structure forms the frustule that protects the cell (De Tommasi et al., 2017).

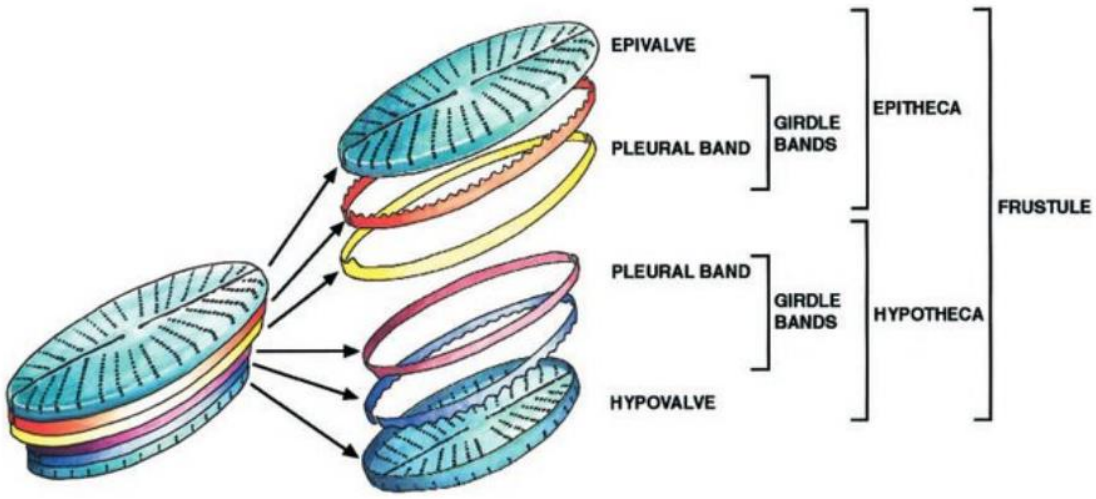

Fig. 3: Schematic overview of the siliceous components of diatom cell walls. Drawing by Ian Nettleton (Zurzolo and Bowler, 2001).

The frustule acts as a physical barrier and offers an ecological advantage against predation by limiting the action of grazers and the access of parasites (Hamm et al., 2003). The cells will also be more resistant to pressure. In fact, biogenic silica is more resistant than exoskeletons

made of calcium (coccolithophorids) or cellulose (dinoflagellates) (Kooistra et al., 2007). The frustule can also play a protective role against abiotic factors; for example, silica absorbs UV-B rays. In addition, cells can adapt their buoyancy via variations in frustule density and the presence of vacuoles in the cell. This mechanism allows the cells to position themselves optimally in the water column according to their needs. Raven and Waite (2004) suggest that this morphological feature also enables a cell to sink more quickly when it is parasitised, thereby slowing the spread of disease within the population.

1.1.3.2 The central role of sexual reproduction in the life cycle

Typically, the diatom life cycle comprises two principal phases: a prolonged vegetative phase lasting months to years, during which the cells divide mitotically (diploid stages), and a comparatively short phase that includes sexual reproduction (haploid stages) (figure 4).
In diatoms, the sexual phase plays a crucial role in the life cycle due to the constraint imposed by the rigid silica frustule. As diatoms undergo an extended period of mitotic divisions, their cell size gradually decreases as vegetative growth progresses. During these divisions, the two daughter cells retain one maternal theca (slightly unequal) and a new smaller hypotheca is synthesized (figure 4). Consequently, the two daughter cells differ in size, leading to a decrease in cell size across the population as cell divisions continue. Eventually, this miniaturization process can lead to cell death when cells reach a critical size that becomes incompatible with survival. At a certain point, when the cells fall below a species-specific size threshold for sexualization (sexualisation size threshold (SST)), the formation of gametes occurs through meiosis, followed by gamete conjugation. The zygote resulting from this process is not surrounded by a rigid siliceous frustule, thereby allowing it to expand and form the auxospore, within which a cell of the maximum species-specific size develops.
Whilst the fundamental pattern of sexual behavior in diatoms is generally preserved, there are significant distinctions between centric and pennate diatoms, as illustrated in figure 4. These differences can be explained by distinct lifestyles that have shaped traits related to sexual reproduction.

Centric diatoms are predominantly planktonic and homothallic, following meiosis, they produce large macrogametes (egg cells) and small uniflagellated microgametes (sperm cells). Within a strain, some cells produce egg-cells and others sperm cells, the latter, the male gamete, are flagellated and can swim through the water column to find the female gamete.

In contrast, pennate diatoms primarily include benthic species, with raphid pennates gliding on surfaces and guided by sex pheromones to find their partners (Gillard et al., 2013).

They are predominantly heterothallic, where gamete formation occurs when two strains of opposite mating types (MT+ and MT-) come into close contact. Gametangial cells pair side by side, and meiosis takes place. The conjugation of haploid gametes results in the formation of a zygote that expands into an auxospore. Within the auxospore, the large initial cell is synthesized (Chepurnov et al., 2004; Montresor et al., 2016).

Our knowledge of the sexual behavior of araphid diatoms remains limited (Montresor et al., 2016).

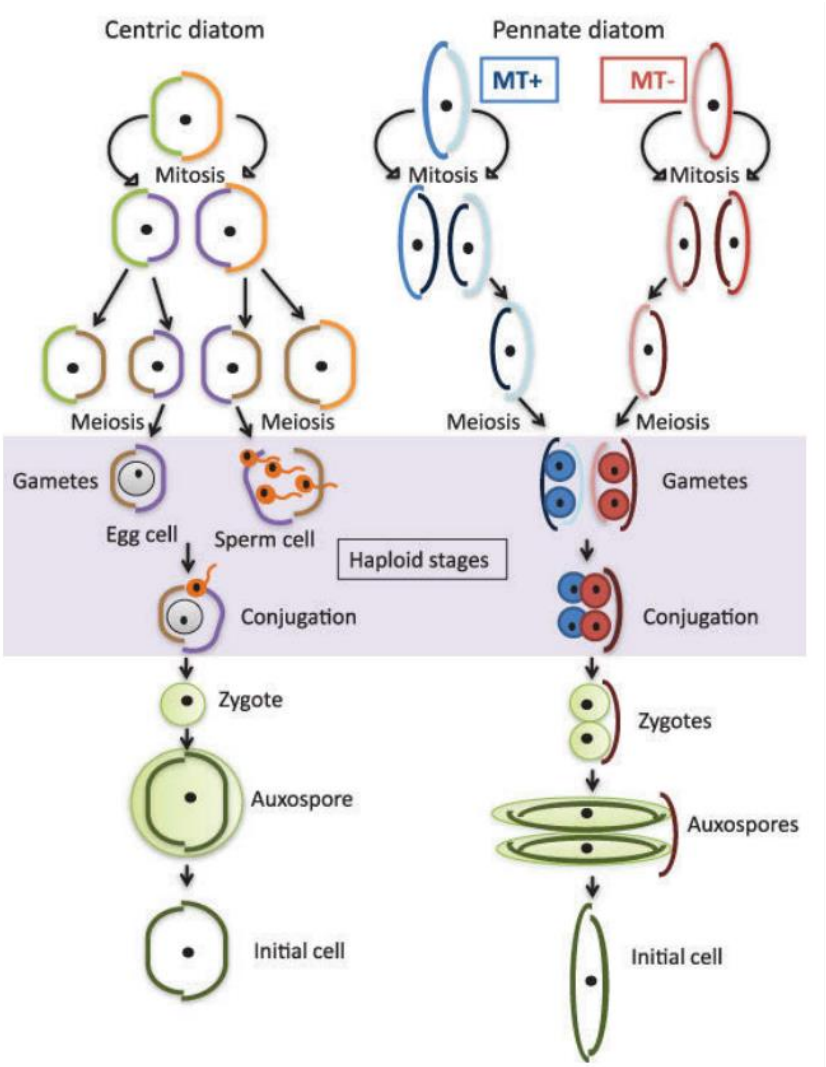

Fig. 4: Schematic drawing of the life cycle of a centric, and a pennate diatom (taken from Montresor et al., 2016).

Numerous studies are currently investigating sexual reproduction through *in vitro* and molecular approaches to gain a deeper understanding of this complex process in diatoms (Basu et al., 2017; Bilcke et al., 2021; Ferrante et al., 2019; Marotta et al., 2022; Russo et al., 2021, 2018).

Among this research, many aim to understand the initiation of sexual reproduction in pennate diatoms, characterised by the interaction of vegetative cells below the SST from compatible mating types (MT - and MT+).

Recent studies have shown that some pennate diatoms release sex pheromones to recognise and locate suitable partners (Gillard et al., 2013; Moeys et al., 2016). To date, sex pheromones in diatoms have only been described in one benthic species, *Seminavis robusta*. In this species, a pheromone called SIP+ (sex inducing pheromone +) is produced by MT+ cells to stimulate MT- cells (Moeys et al., 2016), which in turn produce a second pheromone, the small amino acid diproline, which strongly attracts MT+ cells to promote pairing (Fiorini et al., 2020; Gillard et al., 2013).

Currently, two genetic models are mainly used to understand in vitro sexual reproduction: *Seminavis robusta* (Chepurnov et al., 2008) and *Pseudo-nitzschia multistriata* (Basu et al., 2017) due to the complete sequencing of their genome. For the latter species, the genome was sequenced in 2015, enabling an initial investigation into the signaling pathways used in the early stages of sexual reproduction (Basu et al., 2017). More recently, Annunziata et al., in 2022 used transcriptomics to study changes in gene expression during an *in vitro* sexual reproduction experiment (Annunziata et al., 2022). This study showed a strong change in numerous metabolic functions (mainly photosynthesis, fatty acid biosynthesis, nutrient transport and assimilation) during sexual reproduction. However, no pheromone has yet been described for this species (Ferrante et al., 2023). The genes regulated during sexual reproduction can be used as an indicator of pheromone perception, which has enabled the sex pheromones of *P. multistriata* to be identified (Ferrante et al., 2023; Marotta et al., 2022).

A transcriptomic approach was also used to explore the differences between the two MTs and led to the discovery of the first MT determining gene in diatoms. The MRP3 gene is expressed in a monoallelic manner only in MT+ strains and regulates the expression of four MR (Mating type Related) genes, two specifics for MT+ (MRP1 and MRP2) and two for MT- (MRM1 and MRM2), whose functions are unknown. Notably, a transgenic MT- expressing exogenous MRP3 exhibited sex reversal and a typical MT+ MR gene expression profile (Russo et al., 2018). In the *P. multistriata* life cycle, opposing MTs only produce gametes when they are shorter than 55 μm (D'Alelio et al., 2009). The molecular mechanism linking cell size to the

initiation of sexual reproduction remains to be identified (Ferrante et al., 2023) and references therein).

All of this highlights the largely unexplored complexity of partner identification *in natura* and recognition in diatoms, a key stage in sexual reproduction.

Very few studies have reported observations of diatom sexual events in the natural environment. Sexual stages of *Pseudo-nitzschia* species in their natural environment have been observed and reported twice (Holtermann et al., 2010; Sarno et al., 2010). In Europe, sexual stages of two species of *Pseudo-nitzschia* were detected at the Long Term Ecological Research Station MareChiara in the Bay of Naples (Mediterranean Sea), where they accounted for 9.2 and 14.3% of the total number of cells of *P. cf. delicatissima* and *P. cf. calliantha*, respectively (Sarno et al., 2010). Another massive sex event has been reported along the Washington coast (USA) involving *P. australis* and *P. pungens*. Auxospores were detected for a long time period (about 3 weeks) and accounted for 59% of the *P. australis* population at the end of the bloom (Holtermann et al., 2010).
A few observations of sexual reproduction stages have also been observed in the natural environment for other diatom species. This is the case of the oceanic diatom *Fragilariopsis kerguelensis*: auxospore formation by the pennate diatom *Fragilariopsis kerguelensis* has been observed during an iron-induced bloom in the Southern Ocean (Assmy et al., 2006). Observations of vegetative cells of the harmful diatom *Eucampia zodiacus* have also been reported in the Seto Inland Sea, in Japan (Nishikawa et al., 2013).

This evidence of sex in the natural environment has been observed morphologically (Holtermann et al., 2010; Sarno et al., 2010), but to date, little is known about sexual reproduction *in situ*.

1.2 Phytoplankton blooms

1.2.1 A complex event

Depending on the region of the world, the annual cycles of phytoplankton blooms differ considerably. Large-scale patterns of diatom distributions from ocean-colour remote sensing (Alvain et al., 2008; Bracher et al., 2009) along with field observations (Buitenhuis et al., 2013; Leblanc et al., 2012) reveal that they are an important component of phytoplankton biomass at

high latitudes during spring (in April–June in the Northern Hemisphere and October–December in the Southern Ocean) and in equatorial and coastal upwelling regions. They are present at lower levels in mid-ocean subtropical gyres (Tréguer et al., 2018). In areas where blooms are recurrent and predictable, these events have governed the evolution of the life cycles and migratory behaviour of organisms ranging from zooplankton to whales and birds (e.g. Cushing, 1990, 1969; Longhurst, 2007). In all cases, phytoplankton blooms are the consequence of imbalances in the ecosystem between the rates of phytoplankton division and loss, that are the results of both biotic and abiotic factors (Behrenfeld and Boss, 2018). Chlorophyll a is commonly used as an index of phytoplankton biomass.

1.2.1.1 Concept and theory

In temperate and subpolar regions, the production cycle starts with phytoplankton spring blooms. Inter-annual changes in the timing of these blooms lead to a match or mismatch between phytoplankton division and zooplankton grazing. This ultimately determines the recruitment success of higher trophic levels like fish (Cushing, 1990). This remarkable phenomenon has been the subject of scientific investigation since the 19th century (Banse, 1992). We can note that winter blooms are also known to occur in marine ecosystems but they are less common that spring blooms (Trombetta et al., 2019).
The transition from the cold, clear waters of winter, characterized by low light levels and frequent storms, to the plankton-rich waters of spring and early summer is the driving force behind the North Atlantic bloom. This transformation naturally raises the question of what enhances upper ocean growth conditions during spring to stimulate phytoplankton growth.

Analogous to the spring growth of terrestrial vegetation in temperate ecosystems, where increased cell division leads to biomass accumulation, the blooms in temperate waters appear to be linked to improved growth conditions for phytoplankton.
To date, concerning the spring bloom in deeper areas, three theories have been proposed concerning the complex phenomenon of spring bloom. The first is the “critical depth hypothesis” (Sverdrup, 1953), the second, the “critical turbulence hypothesis” (Huisman et al., 1999), and finally, “the disturbance-recovery hypothesis” (Banse, 1992; Behrenfeld, 2010; Behrenfeld et al., 2013). All three use the concept of the critical depth in one form or another, either to argue in its favour, to complement it, or to argue against it (Kovač et al., 2021).

The concept of a "critical depth," introduced by Gran and Braarud in 1935, encapsulates the relationship between growth conditions and phytoplankton biomass. It was later formalized by Sverdrup (1953) into what is now known as the "Critical Depth Hypothesis." This hypothesis serves as a foundation for understanding the mechanisms behind the North Atlantic bloom and its annual resurgence, generating enduring interest among scientists. However, although studied for 70 years (Sverdrup, 1953), the optimal conditions that trigger the initiation of phytoplankton growing period in ocean waters in early spring are not well understood (Sathyendranath et al., 2015).

The first theory on the factors involved in the initiation of blooms was proposed by Sverdrup in 1953 during observations of blooms in the offshore areas of the North Atlantic (Sverdrup, 1953). In this theory, known as the "Critical depth hypothesis", he stated that "*For the spring phytoplankton bloom to begin, the production of organic matter by photosynthesis must exceed the destruction by respiration in the surface layer"*. With this sentence, he defined phytoplankton growth as an imbalance resulting from two competing factors: photosynthesis and respiration. However, as the photosynthesis capacity of autotrophs is correlated with the penetration of light into the water column, it decreases with depth. On the other hand, Sverdrup assumed that the mortality rate is constant throughout the water column, leading to the existence of a "critical depth", above which photosynthetic growth exceeds losses (positive net growth) and therefore allows the initiation of blooms. Thus, at the end of winter, when the lower limit of the surface mixed layer goes above this "critical depth", the total production integrated in this layer is greater than the mortality, initiating a phytoplankton bloom.

Huisman et al. (1999) agree with Sverdrup, proposing that in addition to the classical critical depth theory (Sverdrup, 1953), which operates in well-mixed environments, there is another mechanism based on turbulent mixing. It states that if turbulent mixing is below a critical turbulence, phytoplankton growth rates exceed vertical mixing rates and a bloom develops whatever the depth. This is the "Critical Turbulence Depth hypothesis".

Banse (1994), and later Behrenfeld (2010) and Behrenfeld et al. (2013) question Sverdrup's theory by hypothesising that the phytoplankton bloom is due to a disturbance that temporarily breaks the close relationship between phytoplankton and grazers. Behrenfeld in 2010 suggested abandoning Sverdrup's critical depth concept, largely because he thought that Sverdrup misunderstood phytoplankton losses. In his scenario the "dilution-Recoupling Hypothesis", he focuses on the balance between phytoplankton growth and grazing, and the seasonally varying physical processes influencing this balance (= disturbance). In the North Atlantic, it would be

the lower limit of the mixing layer during the winter that would be the disturbance factor. In winter, when the lower limit of the mixing layer is deeper, the prey and their predators are diluted in the water column. This leads to lower grazing pressure on phytoplankton, resulting in a slow phytoplankton growth rate. However, the growth rate still surpasses the mortality rate, leading to a modest increase in biomass accumulation. In contrast, as spring arrives, the lower limit of the surface mixed layer rises, concentrating planktonic organisms and nutrients within the euphotic layer. This concentration leads to heightened photosynthetic activity, fostering significant phytoplankton growth, known as blooms. Nevertheless, this increase in phytoplankton population also attracts a larger number of grazers. Consequently, there is a lag period during which phytoplankton mortality due to grazing becomes more pronounced, and predation pressure begins to exceed the rate of phytoplankton growth, ultimately bringing the bloom to an end.

However, Behrenfeld et al. (2013) point out that in other systems, the disturbance factors that disrupt predator-prey interactions may be different and play an equivalent role in the onset of blooms. For example, in upwellings, nutrients are the disturbance factor (Wilkerson et al., 2006). The upwelling of nutrient-rich water in the euphotic zone, due to winds in coastal upwelling zones for example, provides phytoplankton with the nutrient resources it needs for its growth, thus exceeding the losses due to grazing.

Other examples include the forcing of the monsoon in the Arabian Sea (Marra and Barber, 2005) and the deposition of iron in nutrient-rich, chlorophyll-poor waters (Hamme et al., 2010). In each case, a disturbance 'opens a window' for phytoplankton division to temporarily outpace losses, and in all cases, subsequent ecosystem feedbacks tighten predator-prey coupling again to reclose this window over the course of the bloom.

However, no consensus has emerged from these different concepts especially because most of these concepts have been defined at specific temporal and spatial scales (Caracciolo et al., 2021; Chiswell et al., 2015). Phytoplankton blooms are ecologically complex events, with characteristics differing between regions and from year to year. Mechanisms driving this variability will continue to be debated.

1.2.1.2 What is a bloom?

It is interesting to note that the previous paragraph on the theories of the development of blooms does not give a precise and quantitative answer as to what a bloom is. In fact, the fundamental question that the bloom hypotheses attempt to explain are the conditions necessary for the accumulation of phytoplankton biomass. To answer this question, it is obviously necessary to assess temporal variations in biomass or cell abundance, but a large number of publications on blooms do not report rates of variation.
In view of all that has been said above, this lack of clear bloom definition can compromise the validity of the conclusions of a given study and contributes significantly to the current confusion and debate in the bloom literature (Behrenfeld and Boss, 2018).

In many cases, blooms have been described as periods of rapid (or even "explosive", Platt et al., 1991) growth in phytoplankton biomass. However, this definition is unsatisfactory because, although some blooms happen quickly, others develop over long periods and have rates of biomass accumulation equivalent to only one or two doublings per month (Behrenfeld, 2010). More generally, blooms are understood as a condition of elevated phytoplankton concentration, although there is no established quantitative threshold defining "elevated." The concentration of the chlorophyll is commonly used as an index of phytoplankton abundance, and has the benefit of being detectable from space (Behrenfeld and Boss, 2014; McClain, 2009).

1.2.1.3 Conceptual definitions

A bloom can be characterized as such without having a very large quantity of biomass, and the fact that there is no clear and universal definition of what a bloom is can lead to contradictions in the current scientific literature. In his review, Kutser (2009) warned in the introduction that the term ''bloom'' is ''relative'' because it is used to describe phytoplankton events with contrastingly different biomass concentrations.
A synthesis of a set of conceptual definitions of blooms based on the literature was proposed by Isles and Pomati, 2021. The main results are presented below:

1.2.1.3.1 Threshold- and anomaly based bloom

Definitions based on thresholds of phytoplankton biomass or based on anomalies are common in the literature on “harmful algal blooms” (HABs, more information about this concept below). We consider this definition to be useful for sanitary monitoring but less useful from an ecological point of view.

This term includes toxic species that express toxicity to higher trophic levels, largely fish, shellfish, marine mammals, or humans, and include also high-biomass events which, although often including non-toxic phytoplankton species, nevertheless seriously alter ecosystems through hypoxia/anoxia, altered food web efficiency, stimulation of pathogenic bacteria or other ecological consequences (Wells et al., 2015). In current monitoring networks, specific thresholds have been set so that if concentrations or levels of toxins exceed these thresholds, measures are taken to protect the population. The definition of harmful blooms clearly reveals that it is not appropriate to define blooms in terms of abundance levels, whether biomass or numerical cell abundance, as no two species have the same impact at the same concentration, e.g. Dinophysis is highly toxic, even at low concentrations (Reguera et al., 2012). What's more, as pointed out in the article published by Smayda in 1997, according to current language this would be a "harmful bloom", but from a traditional biological oceanographic and ecosystem point of view, it would be neither a bloom nor a harmful bloom! At yet another level, ingestion of only 6-11 cells of toxic *Alexandrium tamarense* was lethal to first-feeding sea bream (*Pagrus major*) larvae, and only one cell of a more toxic strain was lethal to capelin (*Mallotus villolus*) and herring (*Clupea harengus harengus*) larvae (Smayda, 1997 and references therein).

As pointed out in previous work (Isles and Pomati, 2021), these events are defined as unpredictable and outside the baseline of the system (e.g. seasonal blooms) (Miller et al., 2013), making these events more complicated to understand. However, depending on the environment, HABs may be rare events or common, depending on the ecosystem.

1.2.1.3.2 Advective blooms

Isles and Pomati (2021) define “advective blooms” as those in which the variability in a time-series of algal biomass is dominated by spatial transport of existing biomass rather than biological growth and loss processes. Advection can act both vertically and horizontally and accumulate cells at the surface or in more "confined" areas or at the coast under the effect of

currents, resulting in a high local concentration of cells. Three-dimensional hydrodynamic models driven by meteorological forecasts are best suited for understanding lateral advective blooms (Davidson et al., 2016), although models using convolutional neural networks and satellite images have also shown promising results and are likely to become more widely used (Barzegar et al., 2020).

1.2.1.3.3 Ecological definitions of blooms

Several "ecological" definitions of blooms have been proposed that focus on processes governing phytoplankton growth and loss rates, as well as phytoplankton community structure. This type of definition embraces principally the spring bloom and grazing-resistant summer blooms. During the spring bloom, there is a rapid proliferation of readily consumable species, supported by an important abundance of nutrients. This results in a temporary buildup of phytoplankton until grazers respond to the ample food supply by increasing their populations (Sommer et al., 1986). In contrast, during a summer bloom, certain phytoplankton species can reach high cell densities despite having relatively low intrinsic growth rates. This is achieved through defence mechanisms that limit grazing pressure, such as the formation of large mucilaginous or filamentous colonies, which act as physical barriers against grazing (Reynolds, 2007).

We can also note that for nontoxic species, biomass is the criterion most often used to establish bloom status (Smayda, 1997). Furthermore, when we consider a bloom, the first thought that comes to mind is that of spring. The proof is in the different concepts and theories of bloom initiation presented in the previous section (2.1.1).
More generally, conceptual, experimental and modeling approaches to bloom are based primarily on a diatom template (which dominate spring blooms). This reflects the historical focus of marine phytoplankton ecologists on the annual, high biomass spring bloom dominated by diatoms, whereas HAB, for example, are mainly dinoflagellate events (Smayda, 1997). In the same way, blooms during other seasons following episodic events such as heavy rainfall are often ignored, or blooms from other phylogenetic groups are considered transient and ephemeral. As suggested in the review by Smayda in 1997, a dogma has emerged that the spring bloom is the only event that determines marine trophic dynamics. From reading numerous papers on blooms, it is clear that this focus is based on technical limitations, particularly related to identification. Bloom abundance and fluctuations are usually expressed in terms of

community biomass, with chlorophyll quantity generally being the index of abundance representing the total community (and reflecting the productivity). But it is not the only reason why spring blooms are considered mainly with its associated biomass. They are ecological hotspots, and the life cycles and migration patterns of many grazers and carnivores are evolutionarily tuned to the timing and location of these major events (Longhurst, 2007). Changes in bloom phenology (temporal and seasonal variations) may have catastrophic implications for higher trophic level (Behrenfeld and Boss, 2014 and references therein). It is only recently that it is been widely recognized by biologists, thanks to organism-oriented ecologists, that the trophic consequences of blooms vary according to the species present (Smayda, 1997) (e.g. different nutritional values, different growth rates, production of toxins…).

1.2.2 Understanding the study area through spatiotemporal analysis of blooms

1.2.2.1 Multiple environmental variables impact the spatio-temporal bloom development

Bloom's events are characterized by the development and accumulation of one or many species, resulting from a combination of physical, chemical, and biological mechanisms. They can be initiated from cells present at low concentrations, sometimes persisting for months before a bloom develops (the hidden flora concept) (Anderson et al., 2012). In other cases, cells are delivered into a specific region via advection after developing elsewhere (e.g. Raine et al., 2010). In this case it is difficult to attribute a cause to this development via the local environment in which the cells are found, which makes studying them not an easy task.
However, once a population is established, its range and biomass are affected by physical controls such as the transport and accumulation of biomass in response to water flows (e.g. Franks and Anderson, 1992), by the swimming behavior of organisms (Kamykowski, 1974), and by the maintenance of suitable environmental conditions. These factors all interact to determine the timing, location, and ultimate biomass achieved by the bloom (Anderson et al., 2012).

Differents parameters influencing the initiation or maintenance of phytoplankton blooms are described below:

1.2.2.1.1 Factors that can limit a bloom

- Light

First of all, as photo-autotrophic organisms, phytoplankton perform photosynthesis, in which light is an essential element. They need light energy and nutrient nutrients, which are essential for their development. But this light is heterogeneous in space and time. In the water column, this light diminishes with depth, and can also be influenced by suspended matter (detritus or living matter, and dissolved compounds) which can either absorb the light or deflect it (Yentsch, 1962). The latter can create spatial heterogeneities. The spectrum of light used for photosynthesis is between 400 nm and 700 nm and is defined as the PAR (i.e. Photosynthetic Active Radiation) that will be absorbed by the photosynthetic pigments. Thus, it is in the euphotic zone, which extends between the surface and depth where light intensity corresponds to 1% of incident light, that phytoplankton carry out photosynthesis (Reynolds, 2006). As well as fluctuating in the water column, light also varies temporally, defining circadian cycles. In high-latitude areas, the variability of the photoperiod over the year influences the seasonal phytoplankton cycle (Reynolds, 2006).

- Nutrients

Phytoplankton require macro- and micro-nutrients to develop and perform metabolic processes. These include: carbon (in the form of bicarbonate), hydrogen, oxygen, phosphorus (phosphate), potassium, iodide, nitrogen (in the form of nitrate, nitrite and ammonium), silica (in the form of silicates, only in diatoms), manganese, calcium, iron, copper, zinc and molybdenum. Physical processes such as turbulence are therefore important in allowing the mixing of the water column and the import of nutrients into the euphotic zone. This implies that these nutrients are highly heterogeneous in space, with estuaries and coasts, for example, richer in nutrients than offshore waters. And like light, there is also a temporal dynamic. This is linked to the seasons, with periods of higher rainfall (and therefore higher flows in the rivers carrying nutrients), and also to the stratification of the water in calmer periods, preventing the circulation of nutrients.

- Temperature

One of the main factors affecting phytoplankton primary productivity is temperature (Lewandowska and Sommer, 2010; Thyssen et al., 2011). Only a few organisms show positive net photosynthetic activity below the freezing point (Boyd et al., 2013; Staehr and Sand-Jensen,

2006). Increasing temperatures increase productivity up to a certain optimum beyond which there is a decrease or cessation of active carbon sequestration or death of organisms, i.e. species are adapted to a thermal window for photosynthetic productivity (Hader and Gao, 2015; Huertas et al., 2011).

- Biotic interactions

In addition to the bottom-up relationships mentioned above, top-down regulations play an important role in phytoplankton development. Among these, predation and parasitism strongly regulate phytoplankton biomass (Cloern and Dufford, 2005; Reynolds, 2006).

- Hydrodynamic processes

The marine environment is heterogeneous due to spatial differences in temperature, salinity, turbidity, etc. linked to distance from the coast, rivers, towns, etc., each of these factors being subject to continuous variations (Reynolds, 2006). As a result, the spatial distribution of phytoplankton is heterogeneous. The hydrodynamic processes associated with the different zones have a considerable influence on the distribution of phytoplankton cells. They can influence their distribution by bringing nutrient-rich water into contact with the cells in the euphotic zone, by creating and disturbing zones of high density of individuals and by transporting the cells away from their growth zones (Peters and Marrasé, 2000).

The distribution of phytoplankton species is the result of all these 'external' factors, but it is important to note that the significant physiological and morphological diversity that exists in phytoplankton is the result of numerous life strategies and adaptations to the environment. The shape and size of the cells, buoyancy (via gas vacuoles or the accumulation of lipids), chain formation and motility (via flagella) of certain species also influence the dynamics of these organisms.

1.2.2.1.2 Factors favoring one species over another

Species composition in bloom is largely determined by mechanisms such as resource competition, selective grazing, and selection on the life cycle properties of individual species (Riegman et al., 1996). In this paragraph, various reasons for one species prevailing over another are outlined.

First, the role of phytoplankton traits, a characterization of functional traits (growth rate, cell size, and composition of photosynthetic pigments…) can help in predicting what group of species is likely to dominate the bloom (Margalef, 1978). The latter point was discussed by Lewandowska et al., in 2015, who suggest that the onset of spring phytoplankton blooms depends on both allogenic factors (water column mixing, temperature, zooplankton grazing, etc.) and autogenic factors (species physiology and characteristics, life cycle, etc.). Both allogenic and autogenic factors affect the balance between reproduction and mortality, with allogenic factors additionally responsible for resource supply. In this study, they hypothesize that blooming will only occur if there are species with a combination of characteristics adapted to the environmental conditions at a given time and place. Various examples of this type are found in the literature, and are explained by the species' own physiology, its dominance over another. A metatranscriptomic study investigated a natural assemblage that changed from diatom dominance (*Skeletonema*) to dinoflagellate bloom (*Prorocentrum donghaiense*). The results reveal distinct metabolic pathways between diatoms and dinoflagellates, potentially defining distinct ecological niches for these two lineages. *P. donghaiense* possesses a more diversified light energy and phosphate acquisition strategy, as well as antimicrobial defence, which could lead them to out-compete diatoms and form blooms (Zhang et al., 2019). One study tested the competition between three bloom-forming marine phytoplankton (the diatom *Skeletonema costatum* and the dinoflagellates *Prorocentrum minimum* and *Alexandrium tamarense*) under nutrient-limited conditions. Results indicated that the diatom was a poor competitor to both dinoflagellates under phosphate-limited conditions; however, it grew well under nitrate-limited conditions when dinoflagellate growth was close to detection limits (Hu et al., 2011). Similarly, between two dinoflagellate species, under PO4-depleted conditions, *Heteroscapsa triquetra* stopped growing after two days, both in monospecific cultures and in mixed batch cultures, while *Alexandrium minutum* grew progressively from day two to the end of the experiment (Labry et al., 2008). In these experiments, *A. minutum* was found to be a "storage specialist" for phosphorus (P), accumulating phosphate (PO4) during pulses for later use, ensuring survival during scarcity, and then using stored P for cell growth. Conversely, *H. triquetra* exhibited a "velocity-adapted" strategy, quickly utilizing available PO4 to boost its cell division rate (Labry et al., 2008).

Finally, a study of diatom species in the Arctic Ocean has revealed a gradient in the respective light intensity of species for maximum growth, suggesting a plasticity in light response that aligns with the successive dominance of species (Croteau et al., 2022).

But the current inquiry is, among the multitude of existing species, there are inevitably those that share identical physiological characteristics for their development. How does this dynamic operate? Although the answers to this question remain somewhat unclear at present, it steers us towards two strategies that constitute the second and third potential reasons for the domination of one species over another.

Second, allelopathy, a process by which certain compounds are produced and released by phytoplankton to inhibit their competitors, plays an important role in species competition (Smayda, 1997). Diatoms are known to secrete various allelopathic compounds, including polyunsaturated fatty acids (PUFAs), polyunsaturated aldehydes (PUAs), as well as polyphenolic and halogenated compounds (Ianora et al., 2011; Wichard et al., 2005). Among these, different types of PUAs have been associated with various functions, such as inter- or intra-species signaling and negative impact on reproduction in marine organisms (Cózar et al., 2018). Although PUAs are thought to target mainly zooplankton, they also influence the dynamics and structure of the phytoplankton community by inhibiting the growth of other phytoplankton species (Gallina et al., 2016; Ianora et al., 2011; Ianora and Miralto, 2010; Ribalet et al., 2007; Wang et al., 2021).
Similarly, the production of transparent exopolymeric substances (TEPs) can have a coagulant effect that can reduce the predation effect on phytoplankton, they also protect against viral attacks and concentrate nutrient salts (Mari and Rassoulzadegan, 2004). In a study exploring biofouling, *Pseudo-nitzschia sp*.'s ability to produce transparent exopolymer particles (TEPs) was associated with increased picophytoplankton densities (especially of *Prochlorococcus*), but justified by a decrease in phosphate and nitrogen concentrations (Leterme et al., 2016).

Third, chain-forming diatoms, although the evolutionary logic behind chain formation in phytoplankton is poorly understood and has historically focused on resource accessibility. Earlier work mainly considered chain formation as an adaptation to optimize descent rate in order to improve nutrient uptake by maintaining high concentration gradients under turbulent conditions (Smayda, 1970). Chains are formed when daughter cells remain attached to each other after cell division, creating highly elongated structures. But studies have shown that predators, such as copepods, prefer to feed on chains. For example, experiments have shown a similar response in the chain-forming diatom *Skeletonema sp.* and the dinoflagellate *Alexandrium sp.* in the presence of mesozooplankton. In the presence of predators, species show reduced chain formation and, consequently, reduced grazing mortality (Bergkvist et al., 2012;

Bjærke et al., 2015; Selander et al., 2011). However, suppressing chain length in diatoms is not a suitable mechanism for avoiding grazing, as it has been observed that zooplankton prefer to feed on solitary cells and short chains (Bergkvist et al., 2012; Bjærke et al., 2015). Despite a functional role that remains largely unknown, it is clear that chain formation must be an advantage for the developing species.

1.2.2.2 *In situ* Bloom monitoring methods

The monitoring of phytoplankton blooms can be accomplished through three distinct methods: *in situ* observations, automated observation stations equipped with underwater sensors, and satellite remote sensing.

While *in situ* observations offer the advantage of delivering more precise data regarding phytoplankton blooms (O'Reilly et al., 1998), this approach comes with inherent challenges. It is characterized by its time-intensive and labor-demanding nature due to the considerable time and effort required for water sampling and subsequent laboratory analyses.

Many methods can be used for the laboratory analysis of phytoplankton. This methods including light microscopy (abundances of the community), electron microscope for higher resolution images (allows better species identification, useful for differentiating cryptic or pseudo-cryptic species), pigment analysis by high-performance liquid chromatography (HPLC, quantifies the composition and concentration of phytoplankton specific pigments), genetic analysis (metabarcoding, metatranscriptomic, relative abundance of the community), spectrophotometry (phytoplankton biomass, detection of light absorbance by chlorophyll), fluorometry (phytoplankton biomass, detection of chlorophyll fluorescence), and flow cytometry (absolute count of different phytoplankton size ranges) (these methods are reviewed in Erickson et al., 2012).

Additionally, *in situ* observations hinge upon manual water sampling conducted at predetermined sites and regular intervals (such as biweekly or monthly) or during shorter research cruises. Consequently, the insights into phytoplankton dynamics are limited. Phytoplankton blooms can be brief (2 weeks/1 month), and higher frequency monitoring needs to be done. Moreover, relying on a sparse set of measurements from *in situ* observations to represent the broader spatial and temporal distribution of phytoplankton blooms poses a potential hurdle in comprehending the full extent of a bloom. In addition, for all the reasons

cited in the previous paragraph, it is necessary to know the sampling zone in order to be sure that the spatial scale of monitoring was conducted in the representative conditions in which the organisms developed.

During the last two decades, tremendous improvements in sensor technology, as well as in data processing, have allowed the construction of autonomous systems that are capable of monitoring key physical, chemical and biological parameters of aquatic environments, and thus, of supporting long-term time series (Blain et al., 2004). The automatic observation station with underwater sensors, a technology commonly equipped with a range of instruments (such as those measuring chlorophyll, temperature, salinity, turbidity, and pH), has the capacity to continuously monitor changes in phytoplankton blooms and various associated parameters in real-time (Bowling et al., 2016; Van Beusekom et al., 2009). However, its effectiveness for phytoplankton bloom monitoring is hampered by three primary limitations. First, its monitoring precision is highly vulnerable to environmental factors; especially in the sea, because of the rough conditions prevailing at sea during storms or strong tidal currents. In addition, biofouling of the sensors in such a highly productive environment is a major problem and optical and chemical sensors are particularly vulnerable (Blain et al., 2004). Second, the underwater observation stations gather data on phytoplankton blooms at specific locations, lacking the capability to provide insights into the broader geographic distribution of such blooms (Wang et al., 2022). Third, taxonomic resolution remains at very broad levels, with information that can be at best over phytoplanktonic size ranges. Detailed information on the specific composition of these blooms therefore remains difficult to obtain.

With its ability to perform large-scale, long-duration, and periodic monitoring at a lower cost, satellite remote sensing has become a powerful approach for ocean water observation, as it allows detailed observations of important biogeochemical parameters related to water quality dynamic processes to be obtained (Bonansea et al., 2015; Sagan et al., 2020). The unique spectral absorption characteristics of phytoplankton pigments enable the use of satellite remote sensing to detect phytoplankton dynamics (Devred et al., 2011). Over the past three decades, satellite remote sensing has been widely used to reveal the spatial and temporal distributions of several metrics of phytoplankton dynamics, e.g., water surface chlorophyll a concentrations (Chla), bloom areas, and phenology in inland and oceanic waters (Gons, 2002; Kahru et al., 2011; Kutser, 2004; Matthews et al., 2012; O'Reilly et al., 1998; Palmer et al., 2015; Sagan et al., 2020; Shi et al., 2019; Tebbs et al., 2013). In particular, Chla is most widely used to quantify

phytoplankton bloom, as this photosynthetic pigment exists in all algal species (Le et al., 2009; Neil et al., 2019). However, satellite remote sensing has some limitations to routinely monitor phytoplankton blooms for the following reasons. The limited availability of high-quality satellite images due to cloud cover and satellite temporal resolutions may be insufficient to capture the rapid evolution of phytoplankton blooms. Low spatial and spectral resolutions (which do not allow precise taxonomic detection) limit the use of satellite remote sensing data for monitoring phytoplankton. Finally, many phytoplankton blooms occurring deep in the water column or with extremely low Chla (<0.1 mg m3) remain unreported because they are not always observed in satellite images but yet are known to occur (e.g. Blondeau-Patissier et al., 2014; Dore et al., 2008; Villareal et al., 2011).

All these different methods have their advantages and disadvantages. And depending on the questions you have and the degree of precision you require, some of these methods may be completely satisfactory.

1.2.3 Harmful algae blooms (HABs)

As mentioned above, the phytoplankton is a critical food for filter feeding bivalve shellfish as well as the larvae of commercially important crustaceans and finfish. They are at the base of the food chain. In most instances, the proliferation of these algae, where the cell count can reach millions per litre, proves to be advantageous for both aquaculture and wild fisheries operations. Nonetheless, there are circumstances where algal blooms can lead to adverse effects, resulting in substantial economic losses for aquaculture, fisheries, and tourism, while also causing significant environmental and human health impacts. When deleterious effects occur during blooms, the phenomenon is known as "harmful algal blooms" (HABs). The HAB designation is a societal concept rather than a scientific definition; Blooms are considered to fit the HAB criterion if they cause injury to human health or socioeconomic interests, or to components of aquatic ecosystems (Anderson et al., 2012).

When considering this event, it is important to make a distinction between the different types of damage resulting from the blooms. One type of harm may be related to oxygen depletion, smothering or abrasion of fish gills associated with a high phytoplankton biomass. And there can be harmful effects without very high biomass due to the production of phycotoxins (Hallegraeff, 2003).

a brief history

The earliest documented mention of a harmful algal bloom is believed to originate from around 1000 B.C. in the Bible. The passage describes a scene where "all the waters that were in the river were turned to blood. And the fish that was in the river died; and the river stank, and the Egyptians could not drink of the water of the river" (Exodus 7: 20–1). In this particular instance, an algal bloom composed of non-toxic species became so densely concentrated that it led to oxygen-depleted conditions, resulting in the widespread mortality of both fish and invertebrates. Oxygen depletion can stem from heightened algal respiration, particularly at night or in low light conditions during the day, but more commonly occurs due to bacterial respiration during the decay of the bloom. Surprisingly, even primarily non-toxic bloom-forming algae can sometimes trigger significant disruptions in ecosystems, leading to unsightly occurrences of dead fish, slime and foam that deter tourism and recreational activities.
One of the earliest documented cases of human poisoning resulting from the consumption of shellfish contaminated with dinoflagellate toxins dates back to 1793, when Captain George Vancouver and his crew landed in an area now known as Poison Cove in British Columbia. Vancouver noted that local Indian tribes considered it taboo to consume shellfish when the seawater displayed bioluminescence due to dinoflagellate blooms (Dale and Yentsch, 1978; Hallegraeff, 2003).

Phytoplankton can damage human health in a number of ways. The most prevalent is through exposure to biotoxins. Various toxins exist with differing modes of action for human health: direct ingestion/contact, aerosolized transport, or concentrating/vectoring by a marine organism that is then eaten (typically shellfish).
The main route of transfer, which is the most closely monitored in Europe, involves the ingestion of toxins contained in filter-feeding bivalves collected during periods of risk, particularly mussels, cockles, scallops and oysters. These organisms will concentrate the toxins in their tissues during toxic blooms and will gradually depurate themselves depending on the species after the bloom. Cyanobacteria, diatoms, and dinoflagellates are the chief contributors to phytoplankton toxins that are harmful to humans and other aquatic organisms (Pradhan et al., 2022).
Phycotoxins are classified according to the symptoms they cause and the chemical nature of the toxic compounds (James et al., 2010). They are presented in table 1.

Table 1: Summary of the different syndromes induced by phycotoxins, their mode of action and the names of the most common species inducing them (Grattan et al., 2016; Hess et al., 2015; Loeffler et al., 2019).

Syndromes	Toxins	Mode of action	Toxic phytoplankton species
Amnesic Shellfish Poisoning (ASP)	domoic acid	Binding to glutamate receptors in neural cells causing constant influyx of Ca2-	*Pseudo-nitzschia spp.*
Azaspiracid Shellfish Poisoning (AZP)	azaspiracid	Cytotoxic, affect cytoskeleton arrangements, and inhibit potassium channels (hERG) and voltage-gated sodium channels	*Azadinium spinosum*
Ciguatera Fish Poisoning (CFP)	Ciguatoxins Palytoxines Imine cyclique	persistent activation of voltage-gated sodium channels, increasing neuronal excitability and neurotransmitter release, impairing synaptic vesicle recycling, and causing cellular swelling	*Gambierdiscus spp.* *Ostreopsis spp.*
Diarrhetic Shellfish Poisoning (DSP)	okadaic acid dinophysistoxins	Inhibition of activity of protein phosphatase 1 and 2	*Dinophysis spp.* *Prorocentrum spp.*
Neurotoxic Shellfish Poisoning (NSP)	Brevetoxin Yssotoxine	Binding to voltage-sensitive sodium channels causing membrane depolarization	*Karenia brevis* *Protoceratium spp.*
Paralytic Shellfish Poisoning (PSP)	Saxitoxin	Inhibition of voltage-gated sodium channels in neural cells	*Alexandrium spp.* *Gymnodinium spp* *Pyrodinium spp.*

A monitoring effort or a global increase in HABs?

In view of the increasing knowledge concerning phytoplankton and the growing number of studies on the subject, the number of HAB events reported in the literature seems to have increased on a global scale. And the initial synthesis to provide trends in their impacts were by Anderson (1989) and Hallegraeff (1993). They argued that there had been a global increase in the frequency, magnitude and geographic extent of HAB. Multiple reasons were suggested to account for this phenomenon. These reasons were: natural dispersal of species by currents and storms, dispersal through human activities such as ballast water discharge and shellfish translocations, improved detection of the species and their toxins, the improving scientist communications, the increasing of aquaculture in coastal waters, and stimulation of HABs as a result of cultural eutrophication or perhaps even climate change.

A study by Hallegraeff et al., 2021 showed that this was not the case between 1985 and 2018, by studying the Harmful Algae Event Database and Ocean Biodiversity Information System. They suggest that increased monitoring efforts associated with increased aquaculture production are responsible for the perceived increase in harmful algal events and that there is no empirical support for general statements about increasing global trends.

1.3 The diatom genus *Pseudo-nitzschia*

1.3.1 Generalities

The genus *Pseudo-nitzschia* belongs to the class Bacillariophyceae (or diatoms). It is represented by elongated cells, linked together at the ends to form chains (Fig. 5).

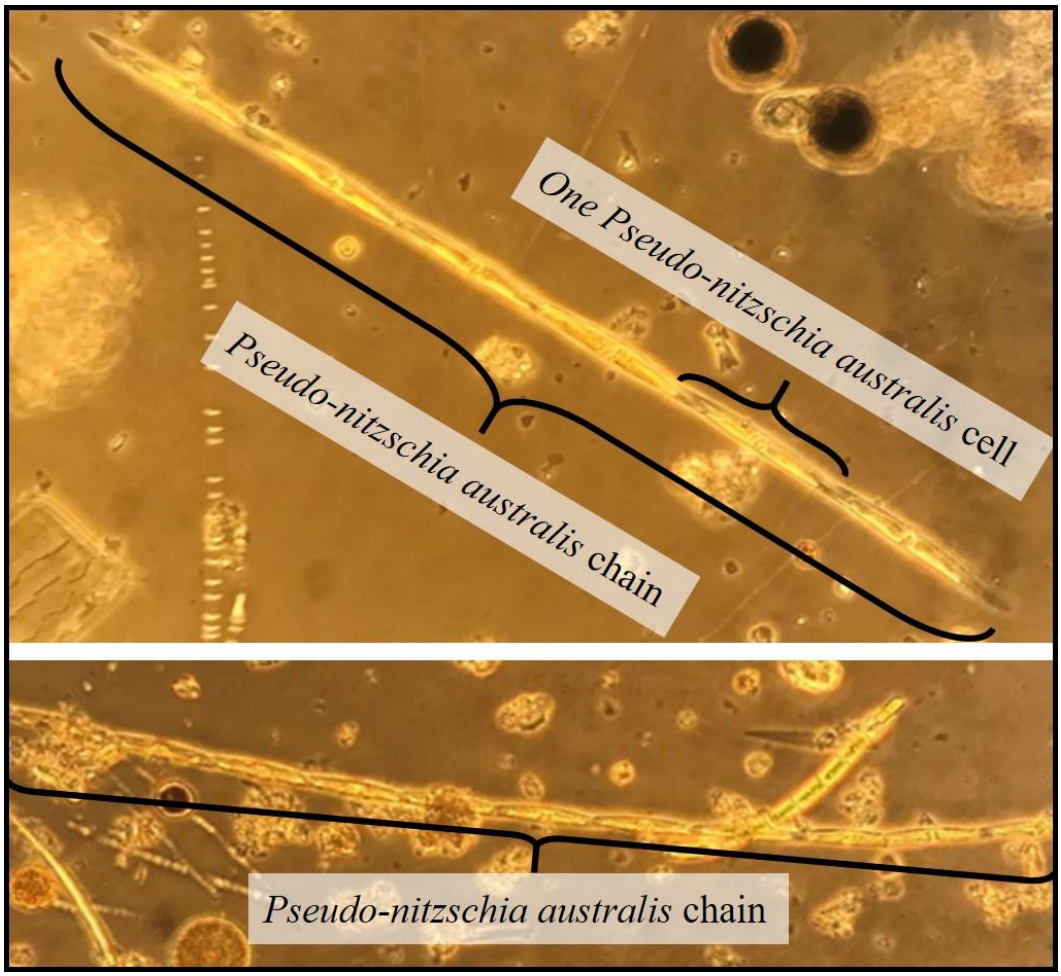

Fig. 5: Pseudo-nitzschia australis cells observed under light microscopy (x40). The cells come from in situ samples collected in March 2021 in Douarnenez Bay (West Brittany, France).

In 1987, global attention was drawn to the fact that certain diatoms possess toxicity. It was during this time that the pennate diatom *Pseudo-nitzschia multiseries* was identified as the source of the neurotoxic amino acid domoic acid (DA), a discovery attributed to Bates et al. in 1998. This neurotoxin was responsible for the deaths of at least three elderly individuals and the illness of over 100 others in eastern Canada, at the Prince Edward Island (DA concentrations ranging between 1 and 128 mg/100g of mussel tissue). The symptoms observed were abdominal cramps, vomiting, and neurologic responses characterized by disorientation and memory loss

that could persist indefinitely. Due to the latter, the term Amnesic Shellfish Poisoning (ASP) was given to this clinical syndrome (Bates et al., 1998).

This event marked the first instance of a diatom being recognized as a producer of a neurotoxin. *Pseudo-nitzschia* is not the only genus produced DA; previously, in the 1950s, DA was known to be produced by the seaweed *Chondria armata* (Meda et al., 1986), used to treat intestinal parasites in Japanese children (as detailed in Lelong et al., 2012). And another pennate diatom genus, *Nitzschia*, has also been found to house two new DA-producing species: *N. navis-varingica* (Lundholm and Jvind Moestrup, 2000) and *N. bizertensis* (Smida et al., 2014).

However, the diatom *Pseudo-nitzschia* is responsible for the single ASP poisoning syndrome reported, and is the most prevalent DA producing organisms (Pinto et al., 2023; Visciano et al., 2016). DA has been detected in numerous bivalves and some other species that uptake it either through filtration of phytoplankton or as a result of grazing on benthic algae. Beyond bivalves, occasional accumulation of DA has been observed in other organisms like crabs, octopuses, fish and even marine mammals (Lefebvre et al., 2002). Since DA mostly stays in the stomach and intestines of these animals, their edible parts usually don't have much or any of the toxin that could harm humans (Pinto et al., 2023 and references therein).

Pseudo-nitzschia is a relatively young genus (Mann et al., 2021), currently, this genus includes 58 described species with 27 species of them described as toxic and produced DA (Guiry and Guiry, 2021; Lundholm, 2021; https://en.wikipedia.org/wiki/Pseudo-nitzschia). In 2018 when the literature review on *Pseudo-nitzschia* was published by Bates et al., there were 52 species of *Pseudo-nitzschia* identified, including 26 toxic species. Notably, this review also revealed an increase of 12 species compared to earlier reviews in 2012 (Lelong et al., 2012; Trainer et al., 2012).

1.3.2 Taxonomy

The diatom *Pseudo-nitzschia* H. Peragallo was first identified as *Nitzschia* (Peragallo and Peragallo, 1900), and separated from the section of Nitzschia Hassall after the comparison of morphological characteristics between both genera (Hasle, 1994, 1993). Before 1994, classification of *Pseudo-nitzschia* species was based on the transapical axis.

Later, taxonomy studies of *Pseudo-nitzschia* species were further refined with the improvement of electron microscopes. By using the scanning electron microscope (SEM) and transmission

electron microscope (TEM), the fine details of frustule ultrastructure can be more precisely observed.
Thanks to it, morphological characteristics (i.e. valve shape, structure of apex, cell overlapping, absent or present of central interspace, number of fibulae and striae, number of poroids and poroid hymen, and valvopula) were used in species delineation (Lundholm et al., 2012, 2006, 2003, 2002; Quijano-Scheggia et al., 2009).

At the time, cryptic (i.e., distinguishable only by molecular methods) and pseudo-cryptic (i.e., also distinguishable by fine ultrastructural characters via electron microscopy) species were discovered especially in the *P. pseudodelicatissim*a complex sensu lato (one row of complex poroids) (Lundholm et al., 2003), and in the *P. delicatissima* complex sensu lato (two rows of simple poroids) (Lundholm et al., 2006). This made species identifications based on morphological characters problematic (Lim et al., 2018).

Indeed, in 2003, *P. pseudodelicatissima* complex was first discovered due to the unclear delineation of the *P. pseudodelicatissima* and *P. cuspidata*: based on the morphology, the only morphological difference was on valve shape (Lundholm et al., 2003). In 2009, *P. arenysensis* was described as a cryptic species from *P. delicatissima*, but both were sexually incompatible (Quijano-Scheggia et al., 2009).

Finally, molecular tools improved and helped to alleviate these drawbacks, but selecting the appropriate genetic markers was crucial (Lim et al., 2018).
Since the early 2000s, significant progress has been made in understanding *Pseudo-nitzschia* species through molecular techniques. Sequencing of the large subunit of ribosomal DNA (LSU rDNA, Lundholm et al., 2002), and investigation into the highly polymorphic ITS1-5.8S-ITS2 region (Internal Transcribed Spacer, a non-coding region of rDNA) (Lundholm et al., 2003) facilitated the development of phylogenetic trees that categorized these species. Moreover, to enhance the accuracy of the *Pseudo-nitzschia* phylogeny, researchers directed their efforts towards analyzing the structure of the ITS2 region. This region (Lim et al., 2018, 2013; Teng et al., 2014), has proven to be more reliable for constructing phylogenetic trees (Lim et al., 2013).

With the target of the genome to assess the phylogeny of *Pseudo-nitzschia* shown with the internal transcribed spacers (ITS) (region ITS2), difference among *P. arenysensis* and *P. delicatissima* were identified (Quijano-Scheggia et al., 2009).

After that, a number of species complexes have been identified in *Pseudo-nitzschia*, with the help of molecular tools. And today, this genus harbors even more diversity than presently described, as morphological variation that does not agree with any present species description continues to be detected (Lim et al., 2018; Trainer et al., 2012 and reference therein).
In 2018, in order to reconcile the phylogenetic and morphological classifications, Lim et al. developed the phylogenetic tree of *Pseudo-nitzschia* species based on sequencing of the ITS2 region. In this phylogeny, morphological criteria for the ultrastructure of the frustule were also taken into account (fig. 6).

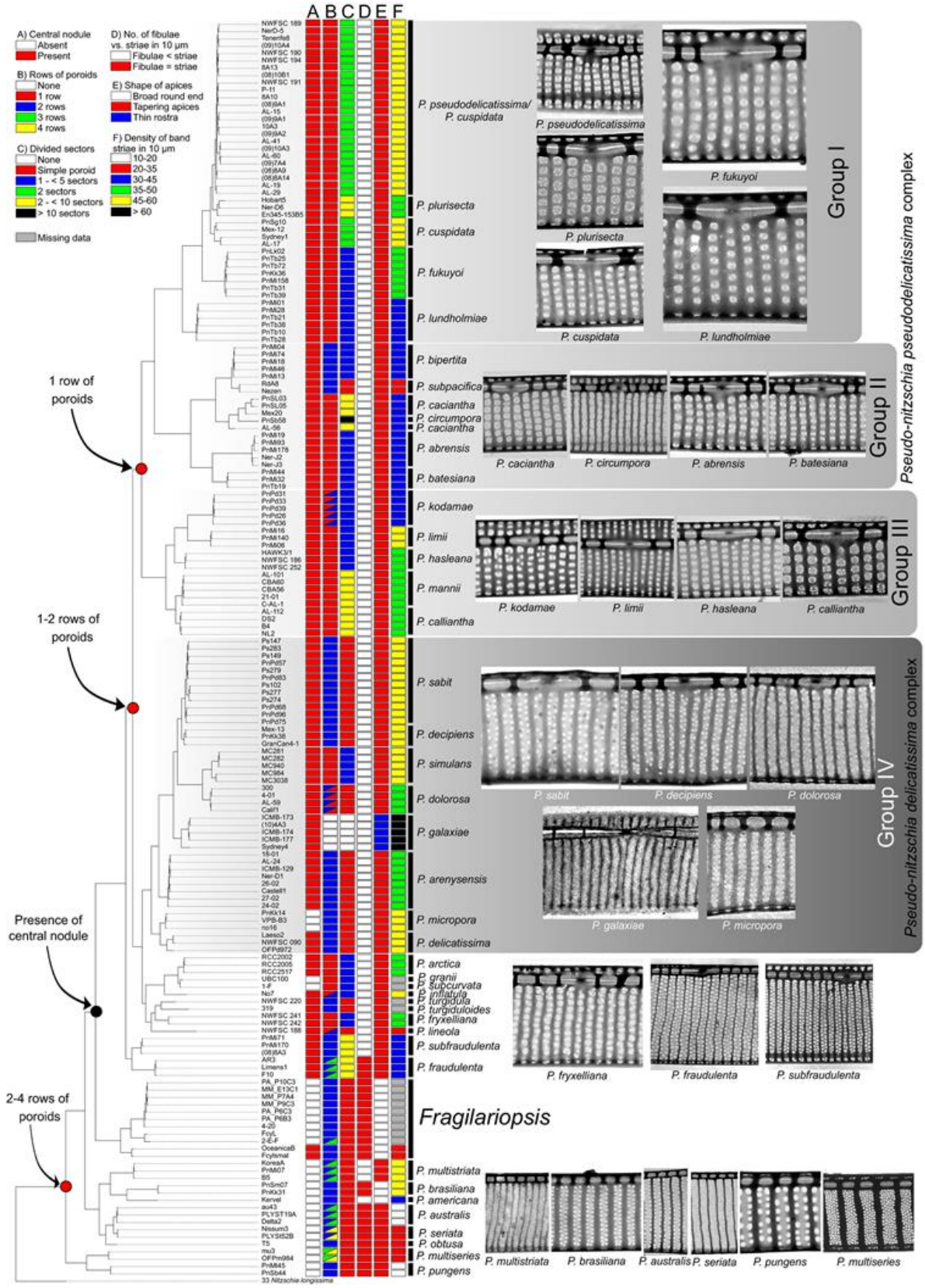

Fig. 6: ITS2 Bayesian tree of Pseudo-nitzschia, with the inclusion of morphological characters (A) presence/absence of central nodule, (B) number of rows of poroids, (C) divided sectors of poroids, (D) number of fibulae and striae in 10 µm, (E) shape of apices, and (F) density of band striae in 10 µm. TEM micrographs of Pseudo-nitzschia spp. showing the central part of valve; note the poroid structure, rows of poroids, and central nodule. Taken from Lim et al., 2018.

1.3.3 A cosmopolitan genus

In alignment with earlier microscopic observations indicating the widespread nature of the *Pseudo-nitzschia* genus (Hasle, 2002), a comprehensive metabarcoding investigation (targeting the V9-18S rRNA region) identified this genus as comprising 4.4% of diatom ribotype sequences. Notably, it contained the highest count of operational taxonomic units (OTUs) among pennate diatoms on a global scale (Malviya et al., 2016).

The different reports of *Pseudo-nitzschia* observations are reported on figure 7 (Bates et al., 2019; Lelong et al., 2012; Trainer et al., 2012) showing its presence in all oceans of the world, including the Arctic (Percopo et al., 2016) and the Antarctic (Almandoz et al., 2008).

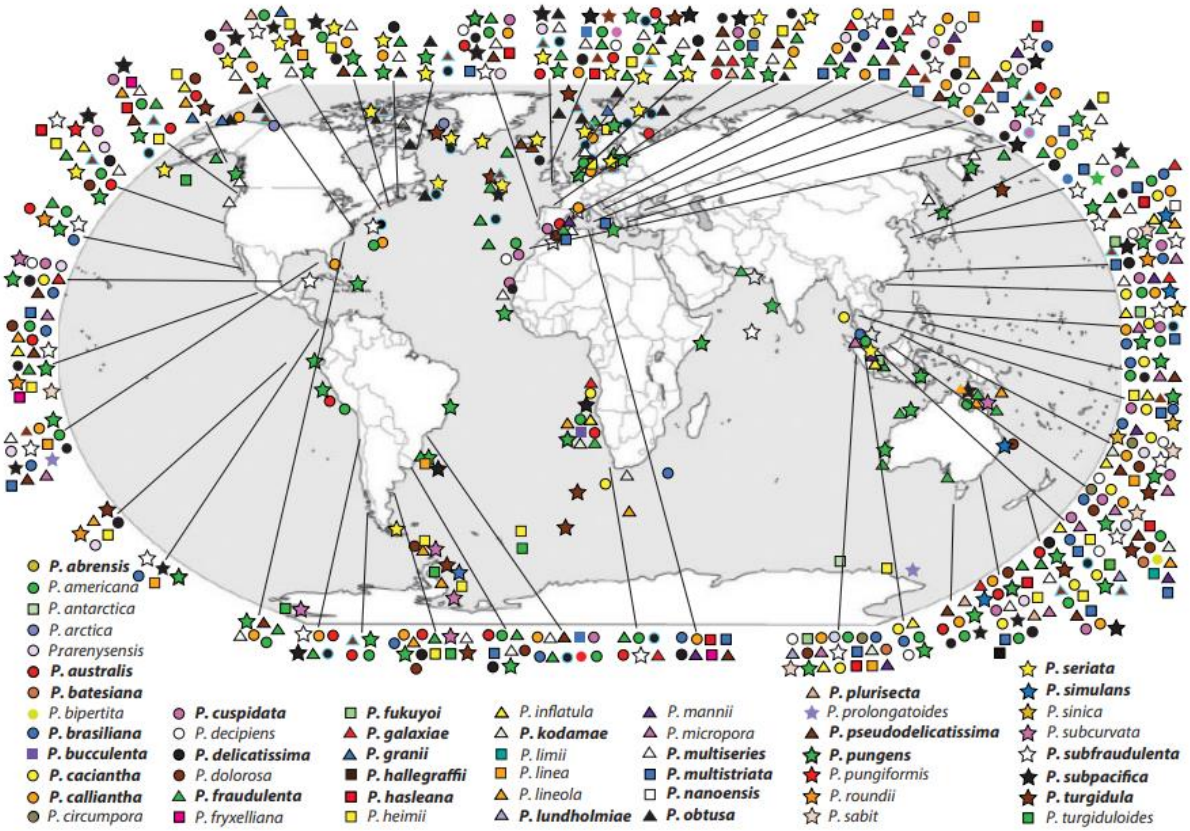

Fig. 7: World distribution of all described Pseudo-nitzschia spp., updated from Lelong et al., 2012 and Trainer et al., 2012. Toxigenic species are in bold note that only certain strains of these species are toxigenic at some locations (Bates et al., 2019).

Fig. 8: Global distribution of the ASP event recorded up to 2023. The figure was taken from the website US National Office for Harmful Algal Blooms, Woods Hole Oceanographic Institution.

There have been many worldwide reports of DA contamination of seafood and mortalities to marine animals and birds (see fig. 8) (Beltrán et al., 1997). In 1998, a notable incident that generated worldwide publicity was when 70 sea lions were washed up onto beaches in California. It was evident that they were suffering from neurological problems and 47 animals died. Subsequent analysis identified DA in fecal samples from these animals and in anchovies collected nearby (Scholin et al., 2000).

In a separate event back in 1991, an outbreak of DA poisoning was reported in Monterey Bay, California, USA. During this episode, pelicans and cormorants were behaving strangely like vomiting, exhibiting unusual head movements, scratching, with many deaths (Walz et al., 1994). A similar event happened in the summer of 1961, near Santa Cruz in California. Flocks of shearwaters began acting erratically, flying into houses and cars, pecking people, breaking windows and vomiting. This latter incident likely inspired the creation of Alfred Hitchcock's

film "The Birds" in 1963. Over the subsequent years, several similar incidents occurred along the same coastline which have been attributed to DA produced by blooms of *Pseudo-nitzschia spp.* (Trainer et al., 2008). After these events, monitoring programs were initiated in Europe, and DA was found in shellfish from Galicia, Spain (Míguez and Fernlindez, 1996), Ireland (James et al., 2000), Portugal (Vale and Sampayo, 2001), Scotland (Hess et al., 2001) and France (Amzil et al., 2001). In Ireland, only the king scallop (Pecten maximus) exhibited high levels of toxin. After that DA has also been found in many organisms around the world (see Gibble et al., 2021; James et al., 2010; Kvrgić et al., 2022; Wang et al., 2023).

1.3.3.1 A complicated identification, and the progress of "omics" methods.

While traditional observation techniques based on light microscopy, relying on cell structure and frustule morphology, remain vital for studying *Pseudo-nitzschia* species, evaluating their diversity and categorizing them into complexes, the complexity of this task is amplified by the limited number of distinguishing characteristics within *Pseudo-nitzschia*. The presence of significant intraspecific variation in morphometry (Cerino et al., 2005; Lundholm et al., 2002) and the potential for morphological data to overlap between different species contribute to the intricacy of this work.

Because of the complexity, classification of complexes has been routinely able to differentiate under light microscope the complex seriata (width > 3µm) and the complex delicatissima (width < 3 µm) groups (Hasle, 1965; Hasle and Syvertsen, 1997). This classification is still used today in routine monitoring programmes.

Table 2: Examples of species associated with the two Pseudo-nitzschia complexes: P. delicatissima and P. seriata.

Complexes	Valve width	Some examples of species
Pseudo-nitzchia delicatissima	< 3 µm	*P. delicatissima; P. calliantha; P. pseudodelicatissima; P. subcurvata; P. americana*
Pseudo-nitzschia seriata	> 3 µm	*P. australis; P. seriata; P. subpacifica; P. fraudulenta; P. multiseries; P. pungens*

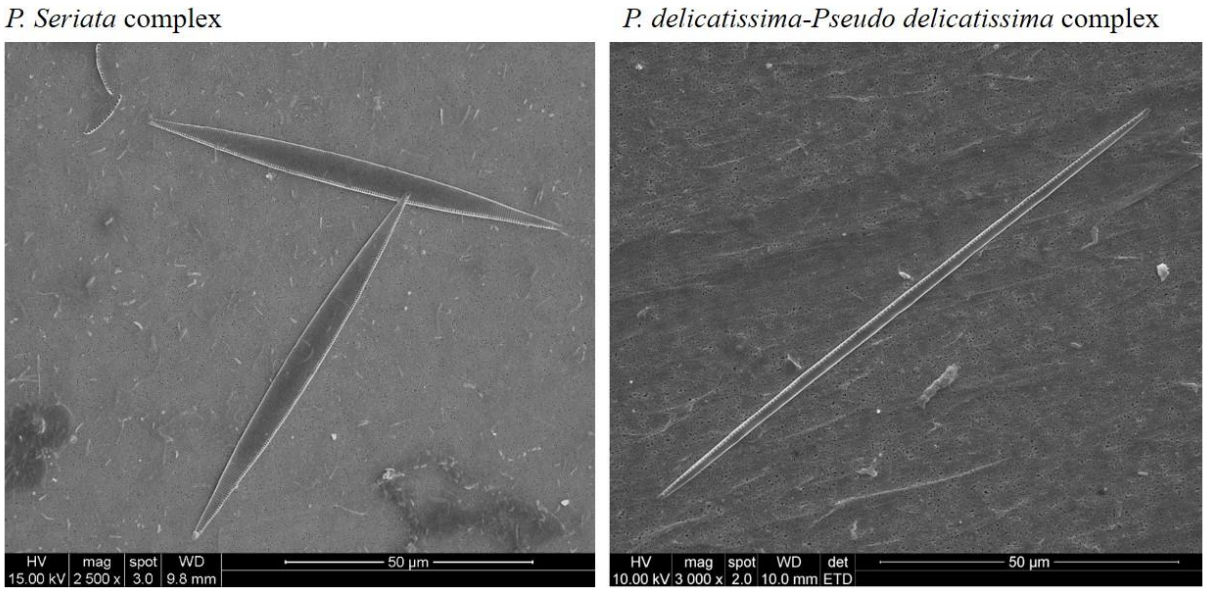

Fig. 9: Electron microscopy photos of two Pseudo-nitzschia species, the one on the left belongs to the P. seriata complex (the P. fraudulenta species) and the one on the right to the P. delicatissima-pseudo delicatissima complex. © E. Nézan / N. Chomérat

In-depth examination of morphology is sometimes impossible without light microscopy, as in the case of *P. multiseries* and *P. pungens*, which are very similar (fig. 10). Their identification requires the use of electronic microscopy to count the number of rows of poroids in the striae: 2 for *P. pungens* and 3-4 for *P. multiseries* (an illustration of the differences on the cell surfaces is shown in fig. 11).

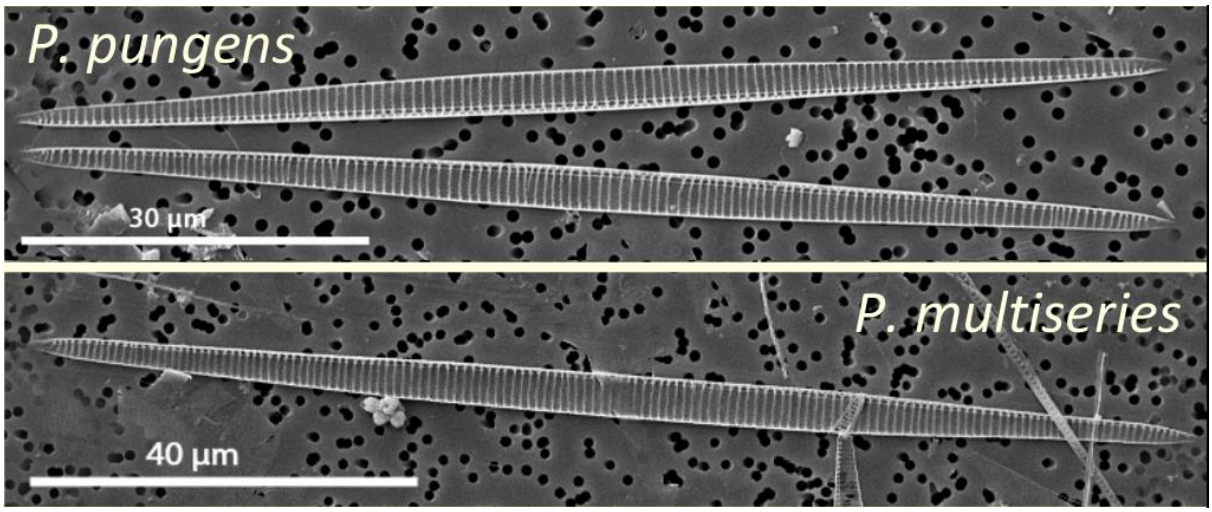

Fig. 10: Electron microscopy photos showing the resemblance between P. pungens and P. multiseries cells. © E. Nézan / N. Chomérat

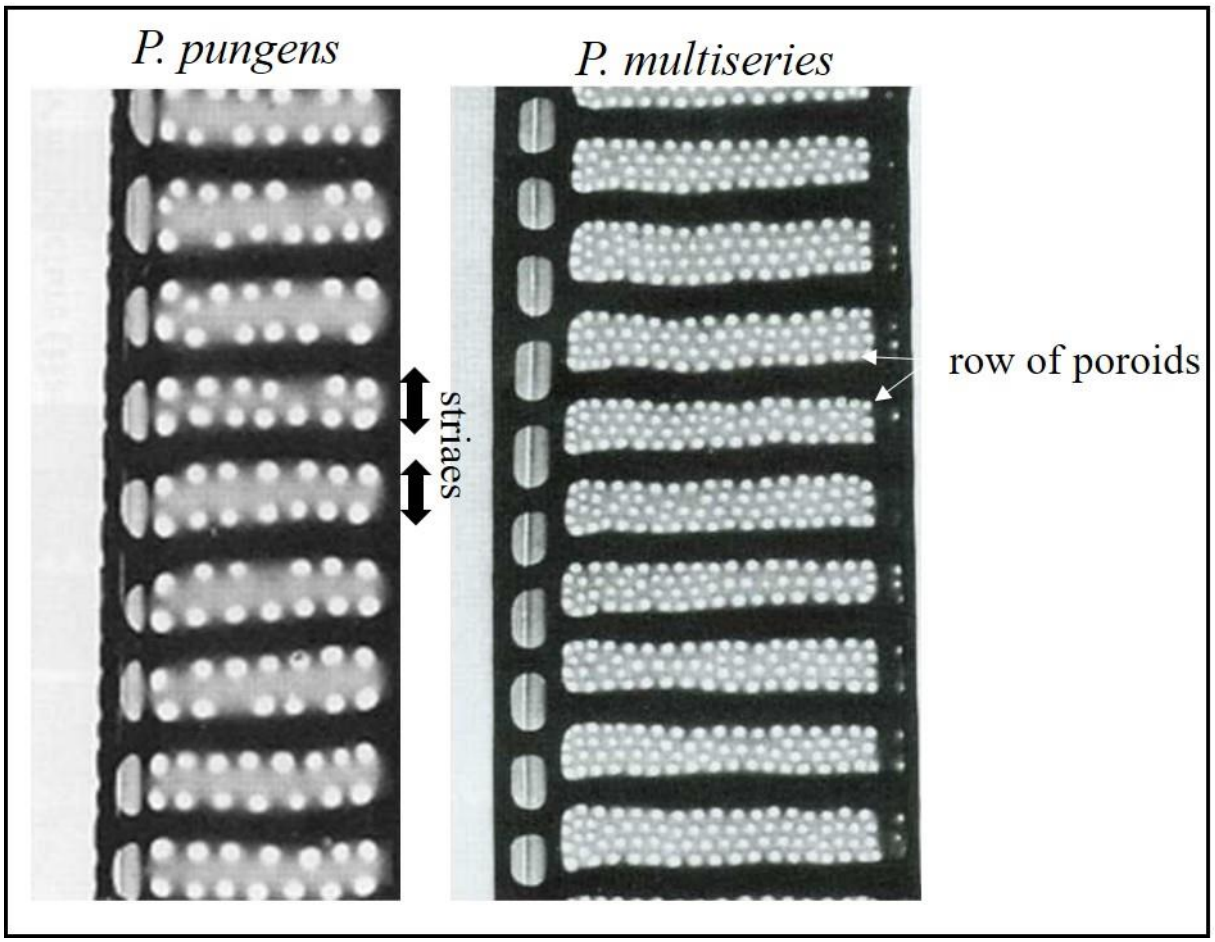

Fig. 11: electron microscopy photos of the cell surfaces of P. pungens and P. multiseries. © E. Nézan / N. Chomérat

However, for other species, even the use of this advanced technique may not reveal the full complexity (Amato et al., 2007; Stern et al., 2018). There are many cases of cryptic and pseudocryptic species within distinct clades and, consequently, genetic tools are being used to address this challenge (Amato et al., 2007; Lelong et al., 2012; Lundholm et al., 2006). This is particularly the case for the *P. delicatissima* complex, which cannot be recognized by electron microscopy, as the details (number of poroid rows, arrangement of sectors in the poroids) are necessary for species identification. The identification is very complicated and requires transmission electron microscopy; scanning electron microscopy is also very inadequate.

More generally, many species in this genus require molecular biology to be sure of their identification. Numerous markers can be used: nuclear-encoded ribosomal RNA genes (SSU, LSU rDNAs and ITS) (e.g. Lim et al., 2018); the mitochondrial encoded cytochrome c oxidase subunit 1 (cox1) gene (Lundholm et al., 2012; Tan et al., 2015); the chloroplast encoded RuBisCO large subunit (rbcL) gene (Amato et al., 2007; D'Alelio and Ruggiero, 2015; Lundholm et al., 2012); and the RuBisCO small subunit (rbcS) gene (Delaney et al., 2011).

Pseudo-nitzschia species can also be identified *in situ* by applying High Throughput Sequencing on phylogenetic markers. These methods are principally metabarcoding, but metatranscriptomic can also be used to characterize the community composition and the *Pseudo-nitzschia* species (see chapter 1) (e.g. Malviya et al., 2016). The challenge is to select a suitable marker for barcode identification. If the marker is too variable, the diversity is overestimated (Bates et al., 2019).

Apart from the advancements made in identifying *Pseudo-nitzschia*, the existence of 'omic' resources including genomics, transcriptomics, and proteomics, along with genomic tools accessible for a growing array of phytoplankton species, provides the opportunity to explore inquiries pertaining to the molecular processes governing their physiology, life cycle characteristics, responsiveness to environmental cues, and engagements with other elements of the planktonic ecosystem (for instance, Bates et al., 2019; Moeys et al., 2016).

Moreover, conventional genomics is often based upon the sequencing and annotation of whole genomes with subsequent bioinformatic focus on the structure and function of key groups of genes (Anderson et al., 2012). Until now, genomic resources have been established for two *Pseudo-nitzschia* species that produce domoic acid (DA). The first is *P. multiseries*, which can be accessed through the Joint Genome Institute (JGI) website (http://genome.jgi.doe.gov/Psemu1/Psemu1.home.html). Alongside this, mitochondrial (Yuan et al., 2016) and plastidial (Cao et al., 2016) genomes are also available. The second species, *P. multistriata*, possesses a comprehensively annotated nuclear genome and extensive transcriptomic datasets (Basu et al., 2017). Partial genomic sequencing data are available for *P. australis* (Stone, 2017).

The genome size of *P. multiseries* is approximately 219 Mbp, while *P. multistriata* has a genome size of about 59 Mbp (Basu et al., 2017). *P. australis*, on the other hand, has an even larger genome size estimated to be around 900 Mbp based on draft assembly. It is important to note that this estimate includes bacterial reads, substantial repeated elements, and heterozygous regions (Stone, 2017), and further investigation is needed to confirm it.

In order to investigate *Pseudo-nitzschia* either *in situ* and *in vitro* on various aspects, transcriptomic resources for several *Pseudo-nitzschia* species have been produced within the Marine Microbial Eukaryote Transcriptome Sequencing Project (Keeling et al., 2014) (e.g. Patil et al., 2015), and will enable comparative approaches to assess functional differences (e.g. Di Dato et al., 2015), and understand the genes expressed by the species in various conditions (Bates et al., 2019; Lema et al., 2017).

1.3.3.2 Highly contrasting development conditions

To understand the factors behind HABs, it is necessary to correlate species growth with environmental factors. However, given the diversity of *Pseudo-nitzschia* species and the habitats in which they occur, there is no unifying principle that explains blooms in all habitats (Trainer et al., 2012).

In the literature about the development of *Pseudo-nitzschia* species *in situ*, there is inter-annual and seasonal variability in their abundance, sometimes species-specific and typical of certain geographical regions. The growth and distribution of *Pseudo-nitzschia*, as all microalgae, is subject to various physico-chemical factors such as salinity (Thessen et al., 2005), temperature (Caroppo et al., 2005; Lundholm et al., 1997; Quiroga, 2006), pH (Lundholm et al., 2004), photoperiod (Fehling et al., 2006), nutrient concentrations such as nitrates, phosphates and silicates (Bates et al., 1993; Spatharis et al., 2007), stratification of the water column, wind, currents, etc., as well as biological factors such as predators, parasites and competing species (Lelong et al., 2012).
The influence of these factors on DA production has also been explored suggesting that, in the case of nutrients, when these are limiting, DA is produced as part of a cell stress response (Pan et al., 1998; Trainer et al., 2012). This is not the case for nutrients containing nitrogen, as nitrogen is required for DA synthesis (Bates et al., 1998, 1991). Furthermore, DA production has also been correlated with increasing temperature (Lewis et al., 1993), decreasing temperature (Lundholm et al., 1994), irradiance (Fehling et al., 2005), and pH (Lundholm et al., 2004).

However, due to the limitations and difficulties in identifying species of this genus, there is a lack in the interpretation of *Pseudo-nitzschia* bloom dynamics at the species level (Quijano-Scheggia et al., 2008).
Indeed, there is conflicting evidence regarding the environmental conditions that facilitate the blooming of various species complexes. Certain individual species might exhibit distinct preferences for environmental factors compared to their representative complexes, and this discrepancy could be the underlying reason for inconsistencies found in the published literature. As an illustration, Thorel et al. (2017) establish a connection between the presence of *P. delicatissima* and low Si:N ratios. Within the same study region, a contrary association is noted for the *P. delicatissima* complex concerning nitrate, as demonstrated by Downes-Tettmar et al.

(2013). In addition, conflicting results have emerged from different studies regarding the environmental conditions linked to the same *Pseudo-nitzschia* species. To illustrate it, *P. delicatissima* and *P. pungens* were observed in salinities ranging from 20.8 to 38 in the western Mediterranean (Quijano-Scheggia et al., 2008), while a survey of the Bay of Seine (Thorel et al., 2017) found a trend that was the opposite: *P. pungens* was found in 32–33.5 salinity waters, while *P. delicatissima* was found in 31.6–32.8 salinity waters.

Moreover, numerous species within the genus have been observed to inhabit the same geographical region, sometimes even coexisting simultaneously. However, in most cases, the distinctions in species niches are significant enough to result in recognizable phenological patterns throughout the year. Temperature primarily, and to a certain extent nutrient concentration, appear to be the driving forces behind the phenological separation among *Pseudo-nitzschia* species (Percopo et al., 2022). Additionally, certain blooms are dominated by a single species, whereas others encompass a mix of multiple species. *Pseudo-nitzschia* blooms can vary in duration, with some being brief (lasting days to weeks), while others extend spatially over substantial areas and endure for months (Bates et al., 2018).
For all these reasons, the study and specific attribution of parameters allowing the development of *Pseudo-nitzschia* is complicated.

In this paragraph, I will summarize some environmental conditions found in *in situ* studies around the world that have been correlated with the development of *Pseudo-nitzschia* bloom.

In tropical and sub-tropical waters, the genus *Pseudo-nitzschia* is found year-round. A long term monitoring (from 2005 to 2018), showed that this genus accounted for about 15 % of total diatom abundance and peaked in spring and autumn, with occasional outbreaks during summer and large inter-annual fluctuations (Turk Dermastia et al., 2020). This study showed that the *P. delicatissima* complex, composed of at least four species (*P. delicatissim*a, *P. calliantha*, *P. mannii* and *P. galaxiae*), preferentially occurs in summer and spring conditions, while the *seriata* complex (composed of *P. multistriata*, *P. pungens*, *P. fraudulenta* and *P. subfraudulenta*) peaks in autumn (Turk Dermastia et al., 2020). In another study carried out in Tunisia, the presence of species from the *P. delicatissima* complex were less abundant when nitrate and silicate concentrations were high. Blooms of *P. multistriata*, on the other hand, were linked to reduced salinity and nitrate levels, whereas blooms of *P. brasiliana* coincided with

higher salinity, as well as increased nitrate and silicate concentrations, coupled with diminished nitrite and phosphate levels (Sahraoui et al., 2012).

Examining the development of *Pseudo-nitzschia* in Argentina waters, dense populations of *P. pungens* and *P. australis* were identified under conditions of low nutrient concentrations, associated with elevated temperatures and salinity. Conversely, the remaining species (*P. heimii*, *P. lineola*, *P. turgidula*, and *P. turgiduloides*) exhibited preference for lower temperatures and salinities, and high nutrient concentrations (Almandoz et al., 2008, 2007). In the northern Gulf of Mexico, *Pseudo-nitzschia* abundance peaked in spring, corresponding to the average maximum in river flow, with another small peak in fall during wind events that mixed the stratified water column (Dortch et al., 1997). On the coasts of California (USA) and the Baja California peninsula (Mexico), the development of *P. australis* seemed to be favoured over other *Pseudo-nitzschia* species by the increased in nutrient concentrations, particularly silicates (Bowers et al., 2018; García-Mendoza et al., 2009).

In northern hemisphere temperate waters, *Pseudo-nitzschia* species are mostly found during the spring and summer period, when the light intensity, photoperiod and temperature increases (Delegrange et al., 2018; Fehling et al., 2006; Husson et al., 2016). A second bloom of lesser intensity can also be observed in autumn.

A study in the Western English Channel in 2009 revealed fluctuations in *Pseudo-nitzschia* species and DA levels throughout the year. Two peaks of abundances were observed: in June/July and August. In August, this dominance was influenced by various factors including temperature, duration of daylight, rainfall, phosphate, and salinity, whereas *P. pungens/multiseries*-group were significantly influenced by macronutrients. The *P. seriata*-group was significantly influenced by temperature and nitrate. DA was detected over a five-week period from May to July with a maximum in June (0.4 ng DA L−1). When DA was present, the surface waters were limited by silicate and nitrate. DA was significantly correlated with the presence of the *P. seriata*-group and the *P. pungens/multiseries*-group (Downes-Tettmar et al., 2013). A study compared the development and these two complexes (Houliez et al., 2023). This study was carried out in the eastern English Channel and southern North Sea with the aim to investigate the drivers of the *Pseudo-nitzschia* bloom from 1992 to 2020. They identified *P. seriata* and *P. delicatissima* complexes all year round, but they bloomed at different periods because they occupied different realized ecological niches. The *P. delicatissima* complex typically bloomed in spring whereas the *P. seriata* complex bloomed more frequently in June. Both complexes are favored by low-silicate environments and

relatively low turbulence but responded differently to water temperature, light, ammonium, phosphate and nitrite + nitrate conditions (Houliez et al., 2023).

Many studies identified a link between *Pseudo-nitzschia* and nutrients, and some studies also observed that *Pseudo-nitzschia* were linked to hydrodynamic features. A study on the Washington coast identified that the Juan de Fuca Eddy acts as an incubation site for *Pseudo-nitzschia* blooms (Trainer et al., 2002). In the Santa Barbara Channel, convergent eddies were found to aggregate preexisting, low density blooms until their densities increased from $5*10^5$ to more than 2×10^6 (Anderson et al., 2006). Bloom development and transport has also been connected to wind direction and upwelling conditions in Washington (MacFadyen et al., 2005), California (Schnetzer et al., 2013), Portugal (Palma et al., 2010), and Ireland (Cusack et al., 2015).

Concerning the southern hemisphere, a study in the south-west of Australia identified high cell concentrations of *P. delicatissima* gp. linked with an increase in soluble reactive phosphorus and a decrease in total nitrogen (Ajani et al., 2020). Another study identified higher cell abundances of *Pseudo-nitzschia* spp. during the late fall, winter, and early spring, when temperatures in the lagoon are cooler and salinity higher in the western part of India (Southern Indian River Lagoon) (Schreiber et al., 2023).

Finally, studies concerning *Pseudo-nitzschia* on subpolar and polar regions are more scarce. A study in Alaska waters during summer (August) and fall (October-November) identified that *Pseudo-nitzschia* species exhibit distinct patterns across variations in latitude, longitude, temperature, and salinity conditions. For instance, the presence of *P. pungens* was closely linked to temperature, as the species is conspicuously absent from areas characterized by cold, saline water masses and ice formations. On the other hand, species like *P. artica* and *P. granii* demonstrate an affinity for less saline waters, while *P. obtusa* tends to thrive in environments characterized by higher salinity levels, colder temperatures, and increased nutrient concentrations (Hubbard et al., 2023).

To conclude this part, results related to the development of *Pseudo-nitzschia* species from all the world's seas and geographical regions collectively underscore the diverse range of environmental conditions associated with their development. These outcomes further emphasize the importance of conducting species-specific studies within localized contexts to gain a comprehensive understanding of their growth patterns and behavior.

1.3.4 *Pseudo-nitzschia* in France

1.3.4.1 Regular coastal surveillance, the REPHY

In France, the establishment of REPHY (Observation and Surveillance Network for Phytoplankton and Hydrology in coastal waters; REPHY, 2022) and REPHYTOX (Monitoring Network for Phycotoxins in marine organisms; REPHYTOX, 2022) can be traced back to 1984. This initiative was prompted following major developments of the toxic dinoflagellate *Dinophysis* on the coasts of Brittany and Normandy, which led to numerous shellfish poisoning cases in 1983 and 1984 (Lassus et al., 1988).

The REPHY and REPHYTOX are closely associated, since the monitoring of toxic phytoplankton by REPHY is used for triggering toxin analysis by REPHYTOX and for a better understanding of shellfish contamination.

The objective of REPHYTOX is to identify and track three classes of toxins that can accumulate in bivalve molluscs. These toxins are subject to European regulations and fall into the following categories: lipophilic toxins (including DST), PST, and AST. These toxins correspondingly give rise to distinct human syndromes: DSP (Diarrhetic Shellfish Poisoning), PSP (Paralytic Shellfish Poisoning), and ASP (Amnesic Shellfish Poisoning) (see table 1). And the REPHY is divided into three components: Observation, Surveillance and Health (Belin and Soudant, 2018).

The Observation component is geared towards addressing several research inquiries, such as: (i) investigating how phytoplankton communities respond to alterations in the environment (for example, Hernández-Fariñas et al., 2014); (ii) contributing to the delineation of ecological niches for phytoplankton (Hernández Fariñas et al., 2015); (iii) identifying changes in phenology (Guallar et al., 2017); and (iv) participating in the characterization of traits and functional groupings (David et al., 2012).

Parallel to the Observation aspect, the Surveillance component primarily aims to assess coastal water quality using indicators, especially those that align with the criteria outlined in the European directives WFD (Water Framework Directive) and MSFD (Marine Strategy Framework Directive).

In tandem with the aforementioned components, the Health component contributes to the initiation of shellfish sampling, as conducted within the framework of the REPHYTOX network. This addition supplements the findings already obtained regarding toxic species through the other two components. The REPHYTOX monitoring initiative pertains to shellfish harvested for professional purposes within their natural environments, encompassing production areas, natural populations, and professional fishing zones. Beyond its role in furnishing essential information to the relevant authorities managing public health risks, this monitoring system also generates scientifically valuable data (Belin et al., 2021).

The monitoring programs REPHY and REPHYTOX cover the entire metropolitan French coastline (fig. 12)

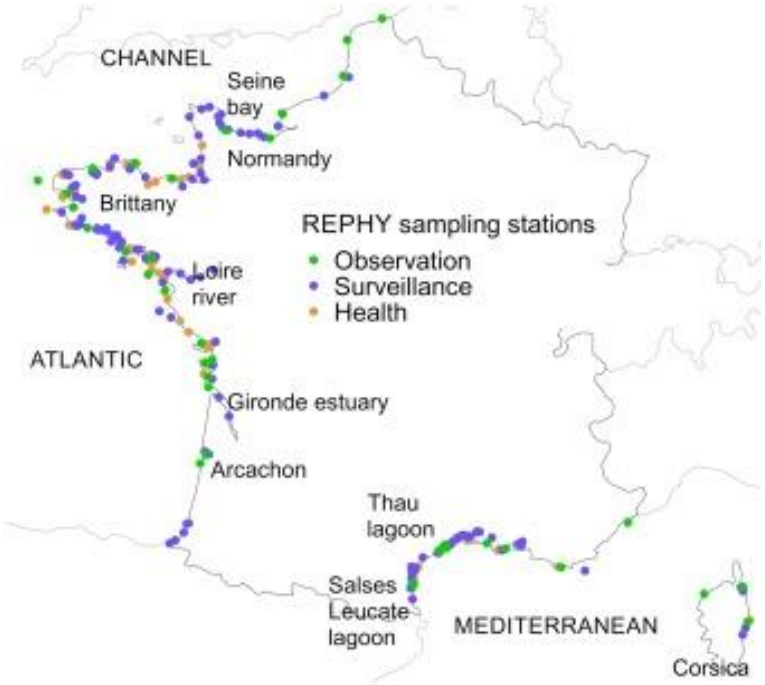

Fig. 12: Sampling stations of the REPHY network, classified by their components: Observation (36), Surveillance (116) and strictly Health (71). Taken from Belin et al., 2021.

- ***Pseudo-nitzschia* monitoring by REPHY**

REPHY sampling takes place every 15 days throughout the year, and samples are observed using optical microscopy. In line with historical data, alert thresholds have been established.

Due to the intricacies tied to identifying species within this genus via light microscopy (referred to as cryptic species), the identifications within the REPHY data are mainly linked to groups of so-called "complex" species.

To illustrate, the complexes encompassing *Pseudo-nitzschia* species were extracted from REPHY data in Finistère area (West-Brittany, France):

- *Pseudo-nitzschia*, *americana* complex (*P. americana* + *P. brasiliana*)
- *Pseudo-nitzschia*, *delicatissima* complex, fines group (*P. caliantha* + *P. delicatissima* + *P. pseudodelicatissima* + *P. subscurvata*)
- *Pseudo-nitzschia*, *seriata* complex, slender group (*P. multiseries* + *P. pungen*s)
- *Pseudo-nitzschia*, *seriata* complex, broad group (*P. australis* + *P. fraudulenta* + *P. seriata* + *P. subpacifica*)
- *Pseudo-nitzschia*, asymmetric broad group (*P. australis* + *P. fraudulenta* + *P. seriata* + *P. subpacifica*)
- *Pseudo-nitzschia*, broad symmetrical group (*P. fraudulenta*)
- *Pseudo-nitzschia*, sigmoid group (*P. multistriata*)

These different groups demonstrate the diversity and difficulty of identifying species of the genus by optical microscopy, even for experienced experimenters such as those at REPHY.

Given the presence of multi-species groups, quantifying the percentage contribution of toxic species in these blooms in comparison to non-toxic species is complicated. However, specific groups do contain a higher proportion of toxic species, and the alert thresholds established in the REPHY system to initiate Amnesic Shellfish Poisoning (ASP) analysis account for this.

REPHY and REPHYTOX data have shown that shellfish only become toxic after the development of at least 100,000 cells of the *P. seriata* complex per litre, and 300,000 for the *P. delicatissima* complex.

Once species have been detected above these thresholds, weekly monitoring of phytoplankton as well toxins in shellfish is initiated. A fishing ban is imposed if shellfish levels exceed 20 mg/kg of flesh.

In certain situations, toxic phytoplankton monitoring is not entirely reliable for ensuring toxin absence in shellfish (due to the 15-day sampling frequency). For example, lipophilic toxins were occasionally detected in shellfish prior to the detection of Dinophysis (REPHY, 2022). To address this, toxin screening is systematically conducted in "risk zones" and during "risk

periods" as defined by historical results from the past three years. Additionally, offshore and deep-sea shellfish deposits underwent bi-weekly monitoring for all three toxin categories, commencing one month before the shellfish harvesting period and continuing throughout.

- **REPHY studies along the French coastline of *Pseudo-nitzschia* and its toxin**

An analysis conducted on REPHY data spanning the period from 1999 to 2018 (Belin et al., 2021) unveiled that the genus *Pseudo-nitzschia* consistently ranked among the top five frequently encountered taxonomic units along the French coastline, regardless of the region. Proliferations of over 1 million cells/L were observed from March to November in the Channel and Atlantic, and all year round in the western Mediterranean, with up to 60 million cells/L. Several *Pseudo-nitzschia* species exist in France, including *P. delicatissima*, *P. fraudulenta*, *P. multiseries*, *P. multistriata*, and *P. pungens*, with some of them being toxic (Lassus et al., 2015). However, among them, *P. australis* and *P. Pseudodelicatissima* have been pinpointed as responsible for Amnesic Shellfish Poisoning (ASP) events (Amzil et al., 2001; Nezan et al., 2006). Two maps: figures 13 and 14 represented respectively the occurrences of the taxonomic unit *Pseudo-nitzschia* and the number of years with at least one ASP event over the French coast within a 20 years period (1999-2018, Belin et al., 2021).

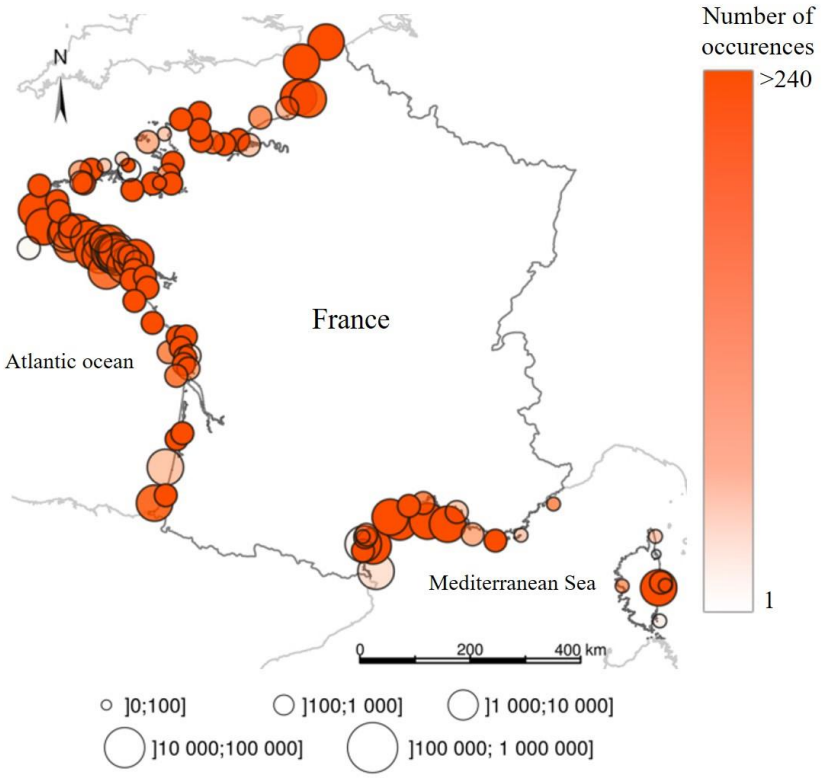

Fig. 13: Maps showing the occurrence of the taxonomic unit Pseudo-nitzschia over 20 years (1999-2018) along the french coast. The size of the circles is proportional to the P90 of the cell concentration. Transparency of colors varies according to the occurrence of Pseudo-nitzschia. Taken and modified from Belin et al., 2021.

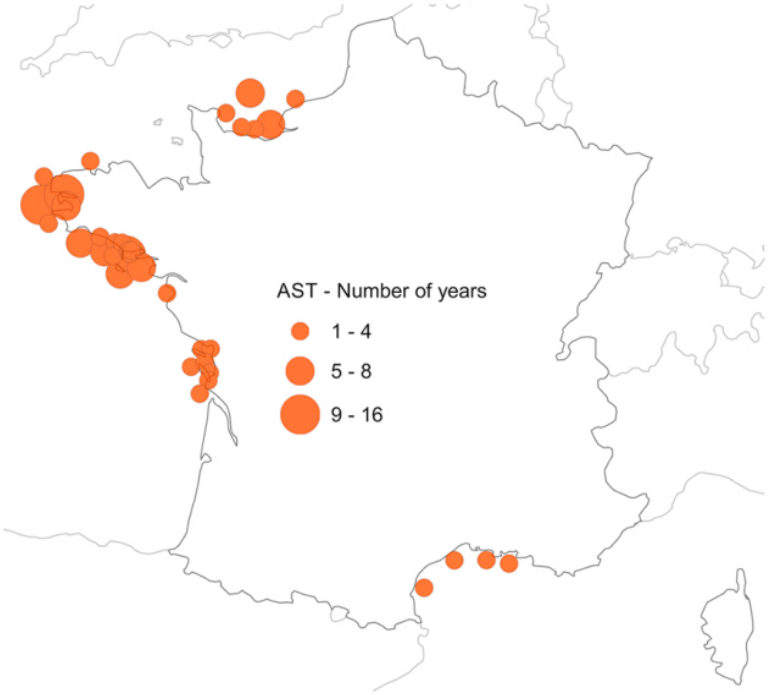

Fig. 14: Maps showing the number of years associated with at least one AST (Amnesic Shellfish Toxins >20 mg/kg) event over 20 years (1999-2018) along the French coast. The size of the circle is proportional to the number of years. Taken and modified from Belin et al., 2021.

Figure 13 shows a widespread presence of *Pseudo-nitzschia* along the entire French coast between 1998 and 2018. Surprisingly, despite its widespread presence, toxicity seems to be more localized (figure 14). Toxicity events seem to be less frequent on the Mediterranean coast, and on the southern half of the Atlantic coast and northern France. However, the Bay of Seine and Brittany seem to be regularly affected by toxicity events.

1.3.4.2 West-Brittany, an area regularly affected by *Pseudo-nitzschia* toxic blooms

- **A strong impact on fisheries**

The French coast has been regularly affected by the harmful effects of toxins for more than 30 years, the main problem being related to the contamination of bivalve molluscs, leading to bans on the fishing and sale of these shellfish during periods of variable duration (Belin et al., 2021). In Brittany, king scallop fisheries of *Pecten maximus* are regularly impacted by ASP events, leading to numerous closures and consequently significant economic losses. The exploitation of this species is particularly problematic since during blooms of toxigenic *Pseudo-nitzschia* species, scallops can accumulate amounts up to ~3,000 mg DA kg^{-1} in the digestive gland (Blanco et al., 2006), and retain them long term, even for years, due to its extremely low depuration rates, from 0.025 to 0.007 d^{-1} in contrast to various other bivalves (Blanco et al.,

2006, 2002; García-Corona et al., 2022). For example, according to CDPMEM 29 data (https://www.comitedespeches-finistere.fr/), ASP events have led to a 40% reduction in the fleet between 2010 and 2020. The threshold for non-consumption stands at 20 mg of domoic acid per kilogram of flesh. However, a derogation is possible up to 25 mg/kg of flesh if an accredited decortication chain is set up. In this case, only the muscle and gonad portions are retained (EFSA Panel on Contaminants in the Food Chain, Alexander et al., 2009). The toxin is concentrated in the tissues of the shell, notably in the digestive gland (hepatopancreas), but the muscle is only slightly affected by the toxin (Douglas et al., 1997), which makes it possible to set up a shell peeling or enucleation chain.

Generally, the REPHY monitoring along the French coast observed the higher concentrations of *Pseudo-nitzschia* species in April-June (Husson et al., 2016). Conversely, scallops (*Pecten maximus*) could be contaminated all year round in the Channel (Amzil et al., 2009) or in the Atlantic, with the fishing periods extending from October to March. And the highest concentrations of AST were identified in Brittany (West-France). Indeed, in April 2014, the concentration of AST in the Bay of Brest was 861 mg/kg for *Pecten maximus*. At the same date, a concentration of 221 mg/kg was found in *Mytilus sp*. and 110 mg/kg in *Crassostrea gigas* tissues in the Bay of Brest. In April 2017, a concentration of 133 mg/kg was identified in *Donax trunculus* in western Brittany; in April 2010, in southern Brittany, a concentration of 123 mg/kg was observed for *Ruditapes philippinarum*. For the other shellfish, domoic acid was found with a maxima less than 100 mg/kg in Brittany (Belin et al., 2021).

In these various cases, *P. australis* appears to be the main culprit of the contaminations (Amzil et al., 2001; Nezan et al., 2006). This toxic species is indeed responsible for recurrent blooms in western Brittany causing ASP events.

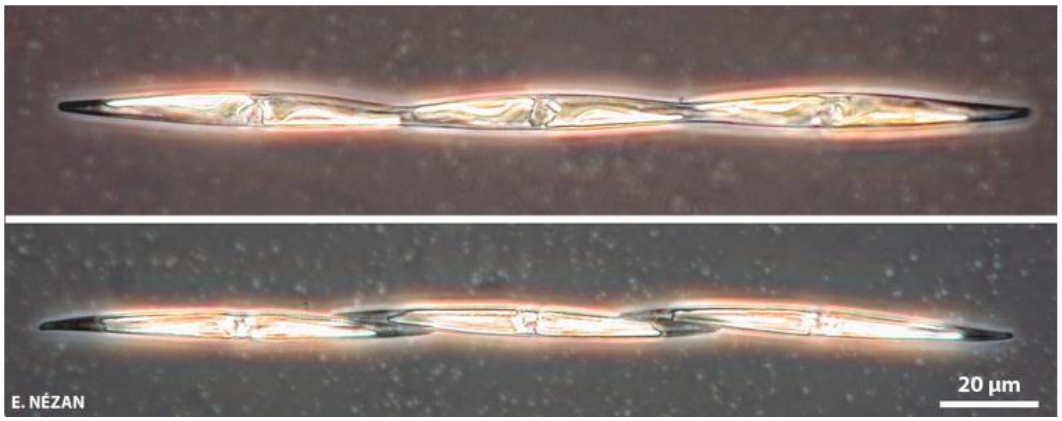

Fig. 15: Electronic microscopy photos of P. australis species forming chains (3 cells). © E. Nézan / N. Chomérat

The various observations of this species by the REPHY have been collected in the area and are presented in figure 11 (red points). The locations of the various monitoring stations in west-Brittany are shown in figure 16.

It should first be noted that the genus *Pseudo-nitzschia* was identified by the REPHY since the start of data banking in 1987. The observations of the REPHY data (figure 11) showed that complexes associated with *P. australis* have only been identified since 2006, while ASP rates have been found since 2000.

The toxic species *P. australis* is also associated to 2 REPHY identification complexes in West-Finistère:

- *Pseudo-nitzschia*, asymmetrical large group (*P. australis* + *P. seriata* + P. *subpacifica*)
- *Pseudo-nitzschia*, seriata complex, large group (*P. australis* + *P. fraudulenta* + *P. seriata* + *P. subpacifica*)

The REPHY results grouping these 2 complexes plus *P. australis* when identified, and the ASP levels in bivalves between 1987 and 2023 in West-Brittany are shown in figure 17.

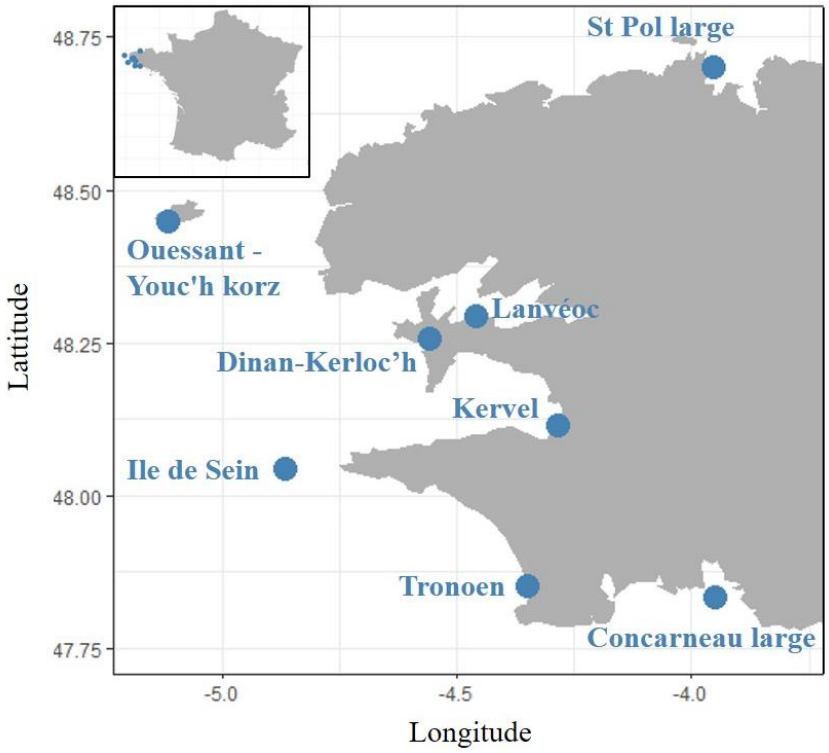

Fig. 16: Localisation of the REPHY monitoring stations in West Brittany (Finistère, France).

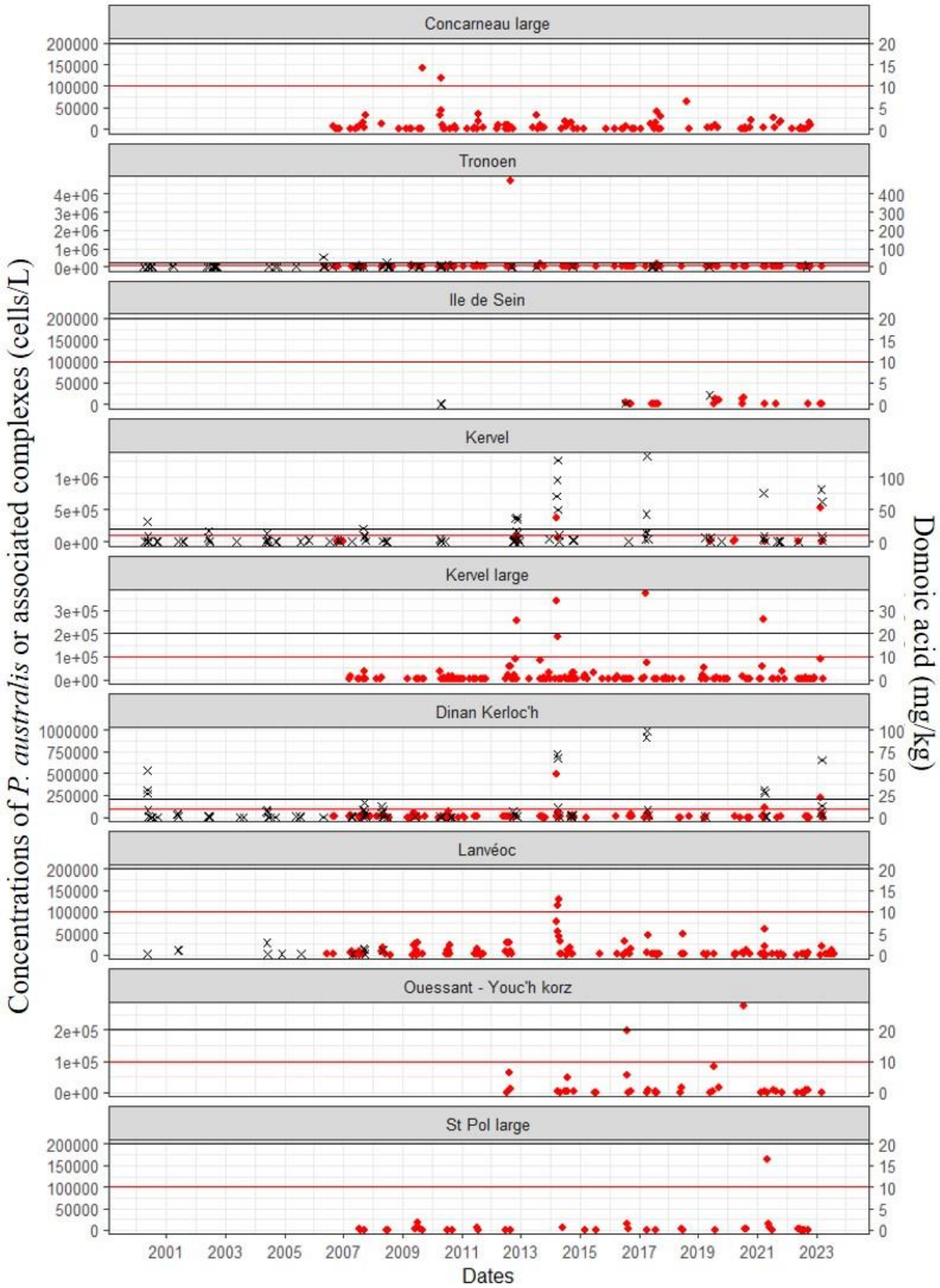

Fig. 17: Evolution of P. australis or its associated complexes' cell concentrations (cells/L) between 2000 and 2023 (red circles) and ASP levels (mg/kg of shellfish tissue) (black crosses). The associated critical thresholds are represented by a horizontal line, red for cell concentrations (100,000 cells/L) and black for ASP levels (20 mg/kg).

Although *P. australis* was only identified as a species through light microscopy relatively late (2004), the initial occurrences of ASP events (>20 mg/kg), as documented by REPHY, occurred in the year 2000. The first of these events took place in May at Dinan-Kerloc'h, where ASP concentrations reached as high as 53.04 mg/kg in bivalve flesh. At this time, ASP concentrations peaked at 31.88 mg/kg at Kervel on May 15th. Concentrations did not exceed 0.15 mg/kg in the Bay of Brest (Lanvéoc).

Subsequently, an ASP event was observed in 2006 at Tronoen, with measured concentrations of 52.50 mg/kg in bivalve flesh. Following these events, ASP became a common occurrence in West Finistère.

In 2009, in western Brittany, REPHY detected the first confirmed *P. australis* blooms exceeding the 100,000 cell/L threshold. Specifically, in Concarneau (south-Finistère), a count of 140,800 cells/L was recorded on September 7th. Six months later, on April 20th in 2010, another observation noted 118,000 cells/L. However, the first substantial bloom, which belonged to the seriata complex large group, was observed at Tronoen in 2012, on September 3rd.

In the Bay of Douarnenez, at Kervel, the first documented *P. australis* bloom was confirmed on November 12th in 2012, with an abundance of 256,600 cells/L. On the same year, ASP was identified on October 30th at Kervel, with a concentration of 36.40 mg/kg of flesh, and it remained above the threshold until November 19th, with a concentration of 34.10 mg/kg of flesh.

In 2014, there was a significant proliferation of *P. australis*, marked by its initial detection on March 17th at Kervel-Large, where cell counts reached 344,000 cells/l. Subsequently, on March 24th, *P. australis* was identified at Dinan-Kerloc'h, with a count of 494,600 cells/l. Shortly thereafter, on April 14th, in the Bay of Brest at the REPHY Lanvéoc station, *P. australis* concentrations were measured at 128,000 cells/L. This event triggered a substantial closure of the fishery due to ASP occurrences, as concentrations in the flesh surged to 126.4 mg/kg on March 31st at Kervel. In Dinan-Kerloc'h, the highest recorded level of ASP was 72.10 mg/kg of flesh on March 24th.

Just as fisheries were recovering from the extended closures in 2014, another significant event unfolded in 2017. During this year, *P. australis* concentrations reached 373,000 cells/L at Kervel large. Furthermore, the highest ASP levels in bivalves were recorded on April 8th, with 133 mg/kg at Kervel and 98.50 mg/kg at Dinan-Kerloc'h. At this time, the maximum number of cells found in the Bay of Brest was 44,800 cells/L on April 18th.

Moving ahead to 2021, *P. australis* was detected on March 22nd at Kervel large, with a cell count of 263,300 cell/L accompanied by ASP levels reaching 75.73 mg/kg on March 21st. Subsequently, on March 30th, *P. australis* was identified at Dinan-Kerloc'h, registering 114,000 cells/L, while ASP levels were measured at 30.80 and 27.57 mg/kg of flesh on March 29th and April 6th, respectively. This presence of *P. australis* extended further north on Finistère on May 5th, where cell counts reached 163,000 cells/L.

In 2023, a significant milestone was reached as the largest *P. australis* bloom ever recorded since the initiation of REPHY monitoring was identified. Specifically, on February 27th, 526,700 cells/L was observed at Kervel-Large, followed by another substantial observation of 215,000 cells/L at Dinan-Kerloc'h on February 28th. During this period, ASP concentrations reached 81.37 mg/kg at Kervel on February 28th (and 61.48 mg/kg on March 6th), and 65.45 mg/kg in bivalves at Dinan-Kerloc'h on March 5th.

A brief history of king scallops in Brittany (focus on the Bay of Brest):

This species is relatively recent in the history of French fisheries. The first documentary mention of this species dates back to 1915 (Fifas, 2004). Before the 19th century, this species was relatively scarce. The emergence of stocks of interest is thought to be due to climate change, which has led to a warming of the climate since the end of the Little Ice Age (a phase of cooling in the climate lasting between five and six centuries, between the beginning of the 14th century and the end of the 19th century) and the start of the industrial era (Fifas, 2004).

The Bay of Brest was the first place to be exploited, especially in the years following the Second World War. This fishery had major economic benefits for the Brest region (Pauchet, 2017). The abundance of the stock and the motorisation of the fishing fleet in the 1950s meant that shellfishing was a profitable and structuring activity in the Bay of Brest (Fifas, 2004; Pauchet, 2017). It should also be noted that Brittany also had another very large king scallop resource at that time, which is now the largest in the region located in the Bay of Saint-Brieuc. Fishing in this area exceeded production in the bay of Brest following a cold spell in the winter of 1962/1963, which decimated stocks (Fifas, 2004). However, overfishing in the Bay of Saint-Brieuc decimated stocks following the development of fishing techniques. Following this event, in 1973, the first shellfish fishing licence was created to prevent the arrival of outside fishing boats and thus protect the stock. But this was not enough, and a significant drop in production began to be seen in the 1980s. Faced with a general decline in Brittany, fishermen, managers and scientists decided to reseed the Bay of Brest with juvenile shellfish to support the fishing

industry. This led to the creation of the Tinduff hatchery, which is still in operation today. But the predators of shellfish: starfish and competitors for the environment: slipper limpets (*Crepidula fornicata*) appeared. The general decline in stocks, particularly in the Bay of Brest (early 1960s), had an upheaval effect on the profession. This was reflected in a significant drop in the number of boats involved in this fishery (271 boats in 1953 compared with 33 today, in 2023).

All in all, the decline in the scallop population, combined with the ASP events, are further weakening the shellfish fleets, which are seeing their revenues dwindle. In fact, fishing for shucking or closing causes a significant economic loss. A shell sold for shucking is also less expensive than a fresh shell (information from the Finistère fisheries committee).

1.4 The MASCOET project

In the context of scallop toxicity explained in the previous section, the MASCOET project (Maintien du stock de coquillages en lien avec la problématique des efflorescences toxiques) was created (https://mascoet.ifremer.fr/). This project is funded mainly by FFP (France Filière Pêche) but also by Brest Métropole, and will cover a period of 5 years, starting in 2019. The project is coordinated by the DYNECO unit and LEMAR, in partnership with several fisheries committees (CDPMEM29, CDPMEM22, CRPMEM Bretagne, CDPMEM17, CRPMEM Normandie, CDPMEM56 and COREPEM) and with the support of the Tinduff hatchery.

The aim of the project is to improve our understanding of the ecological mechanisms that have led to the closure of scallop fisheries since 2000 due to ASP toxicities. These toxicities linked to toxic blooms have mainly affected the Bay of Brest, the Bay of Seine and Southern Brittany in France. Within the MASCOET project, the Bay of Brest will be the pilot site, but the knowledge acquired will extend beyond this single site.

The project is divided into four components:

1. Understanding the determinism of the appearance of toxic blooms;
2. Understanding why the decontamination of scallops is very slow compared with that of other pectinids, notably the black scallop;
3. Improve knowledge of the ecology and population dynamics of the scallop in order to:
4. Improve the management of fishing activity, which may shift to this resource during toxic episodes.

As part of this project, my thesis took part in the first component. The aim was to gain insight into the toxic blooms of *P. australis* occurring in Western-Brittany (Finistère, France).

The PhD thesis (2020-2023) was co-financed by France Filière Pêche (50%) and La région Bretagne (50%).

1.5 Thesis objectives

This thesis takes place in the context of the toxic blooms of *P. australis*, which have been impacting the Bay of Douarnenez and the Bay of Brest in Brittany since the year 2000 (fig. 17). The study encompassed the geographical region spanning the Bay of Douarnenez, the Iroise sea, and the Bay of Brest (West-Finistère, Brittany, France, Fig 16).
Throughout this PhD project, we explored the spatiotemporal development of *P. australis* in West-Finistère using a variety of analytical approaches, combining gene expression, environment and hydrodynamic modeling. These various approaches have allowed us to gain a comprehensive perspective on the blooms, all centered on a central question:

In this area, previous observations, particularly those conducted by the REPHY have revealed a shifting pattern in the spatial and temporal occurrence of blooms, with successive

developments of blooms from the southern part of the study area and progressing towards the Bay of Brest (figures 18, 19). To illustrate, during the largest *P. australis* blooms observed over the last decade by the REPHY, the figure 18 shows that *P. australis* blooms were first identified in the Bay of Douarnenez (Kervel large) and then in the Bay of Brest (Lanvéoc). In addition, cells were mainly found in high quantities in the Bay of Douarnenez, except for 2014 and 2017 (is this due to the sampling frequencies?).

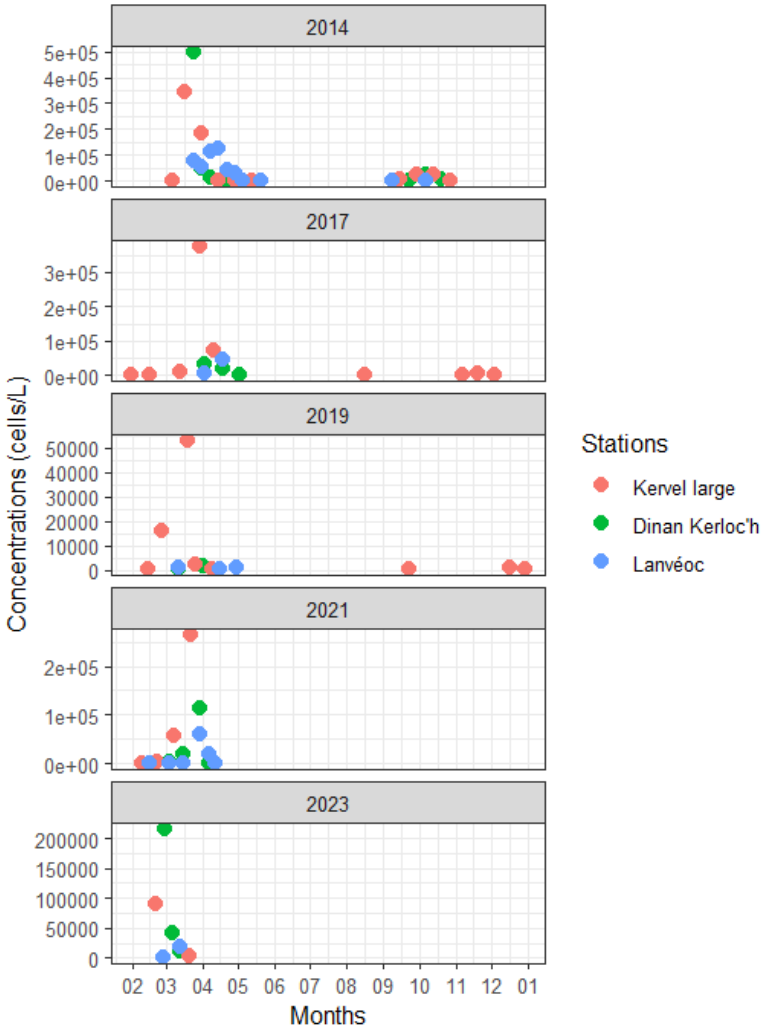

Fig. 18: Cell abundances associated with the species P. australis observed during large blooms (>100,000 cells/L) in 2014, 2017, 2019, 2021 and 2023 between the Bay of Douarnenez and the Bay of Brest.

More specifically, this phenomenon prompts the following question:

What is the spatio-temporal dynamic of *P. australis* blooms in West-Finistère?

To answer this question, the PhD thesis seeks to corroborate or refute the following hypotheses:

1. The bloom originates in one location and subsequently spreads across space and time.
2. Multiple distinct blooms develop independently.

In addition to addressing these hypotheses, the present thesis also aimed to answer the following question:

What are the drivers behind the development of *P. australis* in West-Finistère?

In order to understand the factors intrinsic to the development of *P. australis*, the thesis also seeks to verify the following hypotheses:

1. The development of *P. australis* is directly linked to environmental conditions.
2. The development of *P. australis* is linked to environmental conditions and also to the phenology (life cycle) of the species.

To answer these different questions, the study approach focused on *in situ* analysis of *P. australis* blooms and related environmental variables collected (table 2) at four monitoring stations located from the Bay of Douarnenez (Telgruc), through the Iroise Sea (Dinan-Kerloc'h) to the Bay of Brest (Sainte-Anne and Lanvéoc) (figure 19).

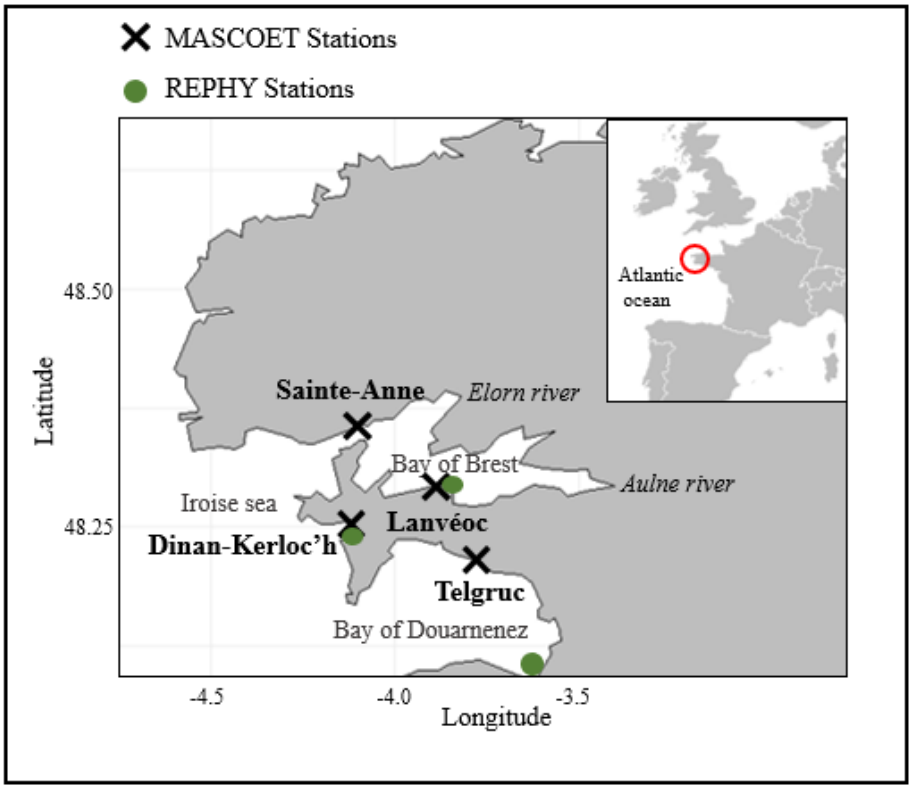

Fig. 19: Monitoring stations (crosses) and surrounding REPHY stations (green dots).

Fig. 20: Picture of thesis sampling locations.

During two *P. australis* blooms, in 2019 and 2021, initially detected by the REPHY in the Bay of Douarnenez, bi-weekly samplings were conducted at four stations located from the south (Bay of Douarnenez) to the north (Bay of Brest) of the study area. In 2019, sampling was carried out between March 1st and 29th; in 2021, this was between February 22nd and April 16th.

In 2017, an opportunistic daily monitoring between April 4th and 24th during a *P. australis* bloom was carried out in the Bay of Brest (Sainte-Anne Stations).

The details of these different monitoring (data collected ect.) are outlined in the table 2 provided below.

Table 2: Data acquired during 2017, 2019 and 2021 monitoring of P. australis blooms, and data collected (stars) from various environmental monitoring in the study area (Marel-Iroise buoy (Rimmelin-Maury et al., 2023), Somlit (http://somlit.epoc.u-bordeaux1.fr), Coriolis observations (http://www.coriolis.eu.org) and models (AROME model (Seity et al., 2011), CROCO-IROISE model (www.croco-ocean.org).

	2017	2019	2021
Stations	Sainte-Anne	Telgruc / Dinan-Kerloc'h / Sainte-Anne / Lanvéoc	Telgruc / Dinan-Kerloc'h / Sainte-Anne / Lanvéoc
Monitoring period	From April 4th to April 24th	From March 1st to March 29th	From February 22nd to April 16th
Sampling frequency	Daily	Bi-weekly	Bi-weekly
Number of monitoring days	14	9	16
Biotic variables	-RNA samples	-RNA samples, -Pico, Nano and -Microphytoplankton abundances (cell/mL) -Cell concentration of dominant species (cell/L; obtained by light microscopy)	-RNA samples -Fractionated chlorophyll a -*Pseudo-nitzschia spp.* count (cell/L; light microscopy); -pico, nano and micro abundances (cell/mL) and biomass (µg/L) -particulate (pg/cell) and disolved (pg/mL) toxins
Abiotic variables	*Somlit data (weekly): Silicate, Phosphate, Nitrate (µmol/L) *Météo-France AROME numerical model (1 hour frequency): PAR (µE/m2/s) *Marel-Iroise data (20 mins frequency): Temperature (°C); Salinity (PSU); Turbidity	Temperature (°C); salinity (PSU) ; nutrients (Silicate, Phosphate, Nitrate; µmol/L) *Coriolis database observations (high frequency): wave height (m) *Météo-France AROME numerical model (1 hour frequency): PAR (µE/m2/s)	Temperature (°C); salinity (PSU) ; nutrients (silicate, phosphate, nitrate; µmol/L); suspended matter (mg/L) *Coriolis database observations (high frequency): wave height (m) *Météo-France AROME numerical model (1 hour frequency): PAR (µE/m2/s) *CROCO-Iroise model (every 30mins): currents speed (m/s)

In order to address the various issues raised in the thesis, the present manuscript is structured into four main chapters, each of them addressing a particular aspect of the general problematic.

In the **chapter 2**, we studied the succession of coastal phytoplankton communities on a small spatio-temporal scale (from the Bay of Douarnenez to the Bay of Brest). These successions were correlated to environmental parameters, for the two years of monitoring carried out in 2019 and 2021. An essential step in the study of microorganism's ecology is to determine community composition. In this chapter, we set up an analysis pipeline using

metatranscriptomic samples to: 1) determine the eukaryotic community composition and 2) determine the diatom community composition at the species/genus levels.
This study was the subject of an article (currently under review by Estuarine, Coastal and Shelf Science): Early spring small scale spatio-temporal shift in coastal diatom communities (Léa Prigent, Julien Quéré, Marie Latimier, Florian Caradec, Emilie Rabiller, Martin Plus, Mickaël Le Gac).

The French phytoplankton monitoring network (REPHY, 2022) has regularly observed blooms in early spring. These blooms exhibit a shifting pattern from south to north, extending from the Bay of Douarnenez to the Bay of Brest, although this observation lacks confirmation. This observation aligns with findings presented in chapter 2.
In **chapter 3**, our objective was to understand the movement of blooms in West-Finistère. To achieve this, we used a 3D hydrodynamic model: CROCO (Coastal and Regional Ocean Community model) configured in our study area. Four hydrodynamic simulations over the month of March (the period when *P. australis* blooms are most frequently observed in the area) were carried out for four years with varying degrees of blooms (2014, 2017, 2019 and 2021). Two transport methods were used to model hydrodynamic connectivity and tracer transport along the Finistère coast. First, the connectivity between zones was studied using an Eulerian approach to monitor the concentrations of passive tracers (a proxy for phytoplankton biomass), their dilution and their transport, between different west Finisterian zones over time. Second, a Lagrangian approach was used to track the trajectory of individual particles (similar to groups of phytoplankton cells) over time. The modelling approaches focused exclusively on the physical processes likely to influence bloom dispersion.

Chapter 4 looks specifically at a *P. australis* bloom monitored in 2021. Blooms are classically studied by focusing on the absolute or relative abundance of species (chapter 2). In chapter 4, we studied the spatio-temporal evolution of the physiological state of *P. australis* as it responds to the impact of the environment as a whole. In order to gain an overview of the processes governing phytoplankton blooms, hydrodynamic connectivity was also analyzed. Taken together, gene expression analysis and hydrodynamics provided insights into the spatio-temporal dynamics of *P. australis* blooms in West-Finistère. This chapter is currently being prepared for publication.

Finally, in **chapter 5**, the physiological state of *P. australis* was analyzed over the entire period of a bloom. This study focused on the analysis of metatranscriptomic samples collected in the Bay of Brest during a *P. australis* bloom in 2017. Genes expressed by this species were analyzed to determine how gene expression changed during the bloom, and what were the functions associated with genes displaying a dynamic expression. In order to understand the physiological changes that occur during a bloom, the functions of these genes were analyzed in terms of functional categories (Gene Ontology analysis), and with a focus on genes specifically involved in the diatom life cycle (sexual reproduction) and domoic acid biosynthesis. An article is under preparation for ISME journal.

Chapter 2

Early spring small scale spatio-temporal shift in coastal diatom communities

Léa Prigent[a], Julien Quéré[a], Marie Latimier[a], Florian Caradec[a], Emilie Rabiller[a], Martin Plus[a], Mickaël Le Gac[a]

[a]Ifremer, DYNECO, F-29280 Plouzané, France.

Context

The objective of the thesis is to understand the drivers of the development of the toxic *P. australis* blooms in West-Brittany.

In the present chapter, the main objective was to **understand the spatio-temporal dynamic of diatoms community (to which the genus *Pseudo-nitzschia* belongs) at the lowest taxonomic level (species or genus) in relation to the biotic and abiotic environment.** For that, two monitorings were carried out during *P. australis* development periods, in early spring 2019 and 2021.

However, one of the main difficulties in studying micro-organism populations in ecology lies in their accurate detection. Monitoring phytoplankton communities has long been achieved on the basis of microscopic observations. Although traditional optical microscopy remains the standard means of characterising community composition, it has its limitations when it comes to certain species that cannot be easily visualised or distinguished solely by their morphological characteristics (Hallegraeff et al., 2004). These species, which show little or no morphological differences, are known as cryptic or pseudocryptic species. Several pseudocryptic species have been described in *Pseudo-nitzschia spp.*, for example: *P. arenysensis*, *P. caciantha*, *P. calliantha*, *P. decipiens*, *P. dolorosa*, *P. mannii*, *P. arctica*, and three varieties of *P. pungens* (Amato et al., 2007; Amato and Montresor, 2008; Casteleyn et al., 2008; Churro et al., 2009; Lundholm et al., 2006, 2003; Orsini et al., 2004; Percopo et al., 2016; Quijano-Scheggia et al., 2009). Although toxicity events are mainly due to a few species, understanding toxicity events can only be done by analysing *Pseudo-nitzschia* blooms at the specific level.

In this context, in this chapter, the first step was to identify the spatio-temporal composition of the community at the lowest taxonomic level. To achieve this objective, metatranscriptomic samples were used to determine the composition of the active diatom community. Using this method, *Pseudo-nitzschia* species were identified to the species level.

Thanks to a conclusive pipeline for community identification, this chapter has been able to highlight:

- Early spring small scale spatio-temporal study displayed a time-shift in diatom successions in a coastal temperate dynamic area.

- Temporal changes in diatom succession were mainly correlated with seasonal evolution of environmental parameters (PAR and temperature) and also phosphate.

This chapter was submitted on Estuarine, Coastal and Shelf Sciences.

Graphical abstract

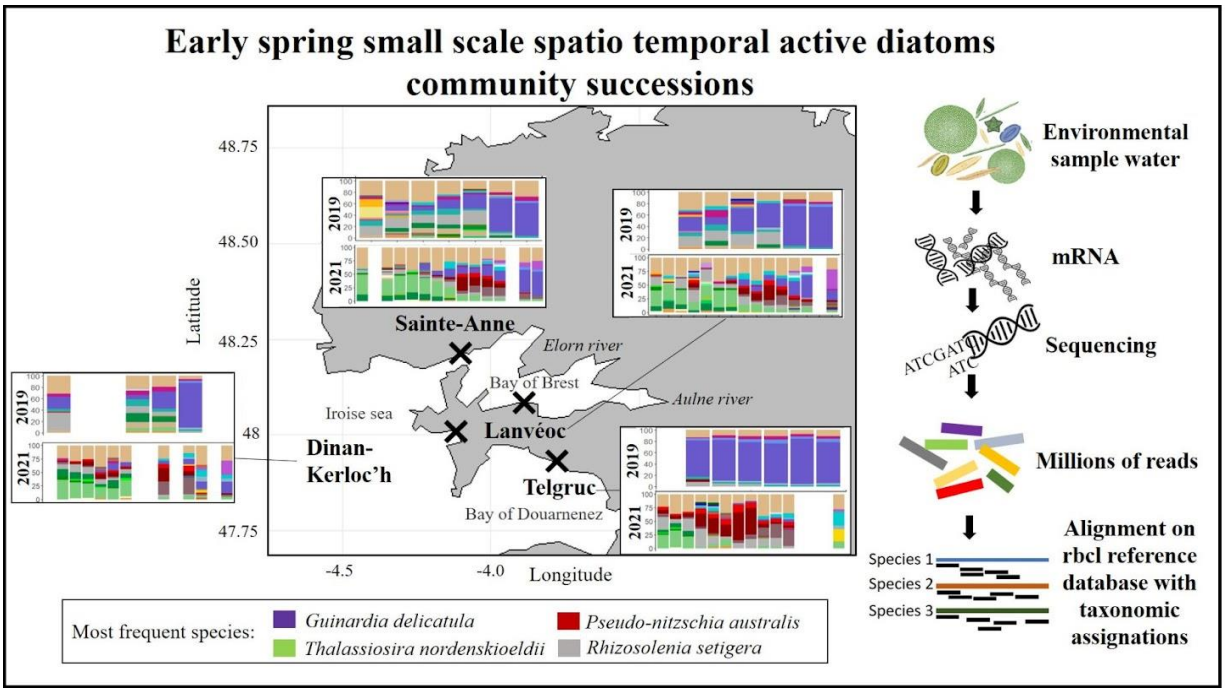

Résumé :

L'étude des changements spatio-temporels à petite échelle dans les communautés de phytoplancton est importante pour comprendre le fonctionnement d'un écosystème, en particulier lorsqu'il est sujet à des proliférations d'algues nuisibles. La succession à court terme des communautés phytoplanctoniques et en particulier de diatomées a été étudiée sur deux ans au début du printemps (mars-avril) dans quatre stations côtières d'Europe occidentale en relation avec des paramètres biotiques et abiotiques. La composition globale de la communauté a été caractérisée au niveau des classes, et les diatomées ont été identifiées au niveau des espèces ou des genres à l'aide d'échantillons métatranscriptomiques. Dans les quatre stations, les communautés de diatomées étaient similaires mais présentaient un décalage dans le temps, les changements dans la succession des communautés se produisant d'abord dans la station la plus méridionale. Les changements temporels dans les successions de diatomées ont été principalement attribués à l'évolution saisonnière des paramètres environnementaux caractéristiques de l'hémisphère Nord : la température et le rayonnement photosynthétiquement actif (PAR), ainsi que le phosphate. La principale différence entre les deux années a été la présence en 2021 des espèces toxiques *Pseudo-nitzschia australis* et *Pseudo-nitzschia fraudulenta*, moins toxiques, qui se développent régulièrement dans la zone au début du printemps. Leur présence était associée à une salinité plus faible et à une faible concentration

de phosphate. Cette étude suggère que la compréhension de la dynamique spatio-temporelle des communautés de phytoplancton à petite échelle peut aider à anticiper les successions d'espèces. Une telle anticipation peut être particulièrement utile dans les zones soumises à des proliférations d'algues nuisibles.

Abstract:

Studying small scale spatio-temporal changes in phytoplankton communities is important to understand the functioning of an ecosystem, particularly when it is subject to harmful algal blooms. The short-term succession within phytoplankton and especially diatom communities was investigated over 2 years at the beginning of spring (March-April) at four nearby coastal stations of western Europe and in relation to biotic and abiotic parameters. Overall community composition was characterized at the class level and the diatoms were identified at the species or genus levels using metatranscriptomic samples. At the four stations, diatom communities were similar but showed a time-shift with changes in succession occuring first at the southernmost station. Temporal changes in diatom successions were mainly attributed to the seasonal evolution of environmental parameters characteristic of the northern hemisphere: temperature and photosynthetically active radiation and also phosphate. The main difference between the two years was the presence in 2021 of the toxic species *Pseudo-nitzschia australis* and the less toxic *Pseudo-nitzschia fraudulenta*, which regularly bloom in the area in early spring. Their presence was associated with lower salinity and low phosphate concentration. This study suggests that understanding spatio-temporal dynamics of phytoplankton communities at small scale may help anticipate species successions. Such anticipation may be especially useful in areas subjected to harmful algal blooms.

2.1 Introduction

Phytoplankton is a key component of aquatic ecosystems, it plays an essential role in maintaining the structure and functioning of marine coastal systems. Marine phytoplankton sustain pelagic food webs (Fenchel, 1988) and directly affect biogeochemical cycles and climate (Holligan, 1992). Many studies investigated their dynamics at large temporal and spatial scales, either focusing on seasonal or interannual variations in phytoplankton communities (Barrera-Alba et al., 2019; Dong et al., 2021; Eriksen et al., 2018) or on long term changes in response to eutrophication, climate changes or additional human disturbances (Chen et al., 2010; Kim et al., 2020).

These studies characterized responses of phytoplankton to environmental and/or biological changes (Rantajarvi, 1998; Schiewer, 1998). The driving factors tend to vary according to geographical areas (Leonilde et al., 2017) as well as habitat type (river, estuary, lagoon, bay, sea...) (Sarker et al., 2021). For example, in tropical ecosystems nutrients and zooplankton grazing were identified as the most important predictors for phytoplankton community in the Bay of Bengal (Sarker et al., 2021), whereas in temperate ecosystems, light, temperature and more generally seasonality tend to be the main drivers (Edwards et al., 2016; Paches et al., 2019; Wiltshire et al., 2015). Large time-scale studies mainly focused on large taxonomic groups of phytoplankton (Liu et al., 2022; Paches et al., 2019) and/or functional groups (Kim et al., 2020). However, fluctuation in species assemblage over short spatial or temporal scales may also be of primary ecological interest to understand microbial dynamics (Martin-Platero et al., 2018; O'Boyle and Silke, 2010). For instance, in relation to different tolerance to environmental conditions, distinct species have been identified as characteristic of different stages of the seasonal growth period (Heino and Soininen, 2006; Hernández Fariñas et al., 2015; O'Boyle and Silke, 2010). However, as the generation time of some protists may be less than a day, large scale studies can miss fundamental ecological processes (bloom, community responses to localized weather events or to species-species interactions) and successions that are more noticeable on shorter time scales (i.e days) (Berdjeb et al., 2018). Moreover, Harmful Algal Blooms (HAB) often result from a local development of species over short-time scales (commonly 1–3 weeks) (Masó and Garcés, 2006).

The monitoring of phytoplankton communities has long been carried on the basis of microscopic observations. Although traditional light microscopy is still the standard mean of characterizing community composition, it has limitations when dealing with certain species that cannot be easily visualized or that cannot be discriminated based on morphological

characteristics alone (Hallegraeff et al., 2004). These species that have no or very small morphological differences are referred to as cryptic or pseudocryptic species. Furthermore, microscopic identification is time-consuming and highly dependent on the level of expertise of the analyst. Molecular genetic techniques, such as DNA metabarcoding enable high throughput profiling of microbial communities and is less dependent on taxonomic expertise (Rees et al., 2014; Trebitz et al., 2017). However, such environmental DNA (eDNA)-based methods may display a high rate of false positives (detection of species absent from the sampled environment) (Cristescu, 2019; Yates et al., 2021). Moreover, in metabarcoding studies, the choice of the genetic marker is a trade-off between the ability to exhaustively characterize community compositions with moderate taxonomic resolution and to precisely identify the species. In the present study, as an alternative, metatranscriptomic samples were used to determine the community composition. Such an approach was chosen because RNA has a lower persistence rate in the environment and a rapid turnover, which could decrease the rate of false positives and enable to specifically focus on the active community associated with the sampling location, which is important for estimating biosecurity risks, and for gaining insight into community succession on short time scales (Cristescu, 2019; Fuhrman et al., 2015). Moreover, metatranscriptomic involves the sequencing of all expressed genes, without targeting a specific locus. Such non-targeted sequencing offers the possibility to align reads against several reference databases. This enables overall community composition characterization at moderate taxonomic resolution using conserved markers such as the small subunit ribosomal ribonucleic acid (SSU rRNA; Guillou et al., 2012; Pruesse et al., 2007) and to obtain species level resolution for phylum of interest, using faster evolving genes such as rbcl (Rimet et al., 2019), ITS or COI (Guo et al., 2015; Moniz and Kaczmarska, 2009).

In this study, an *in situ* metatranscriptomic approach was carried out to study the total eukaryotic communities, with a strong focus on diatoms at a small spatio-temporal scale in a dynamic and productive system situated in Western Europe. The objective of the present study was to expand our knowledge of the small-scale spatial and temporal variability of protistan community composition at the beginning of spring.

During this period, we hypothesize that four coastal areas with different degrees of exposure to the open-ocean have different environmental conditions that may favor distinct diatom community dynamics. In order to test this hypothesis, during two years, the composition of early spring coastal communities in relation to environmental conditions was followed twice a week for about a month at four coastal stations. The variation in diatom community composition was compared between monitoring stations because (1) diatoms are the dominant class at the

beginning of spring on the North-Eastern Atlantic coast and (2) this period is prone to the emergence of the toxic diatom *Pseudo-nitzschia australis* (Nezan et al., 2010, observations from the French phytoplankton and phycotoxin monitoring network: REPHY).

Community composition was then related to environmental variables in order to discuss the variability of diatom communities at small spatial and temporal scales and the use of metatranscriptomic samples for further studies.

2.2 Materials and Methods

2.2.1 Study area

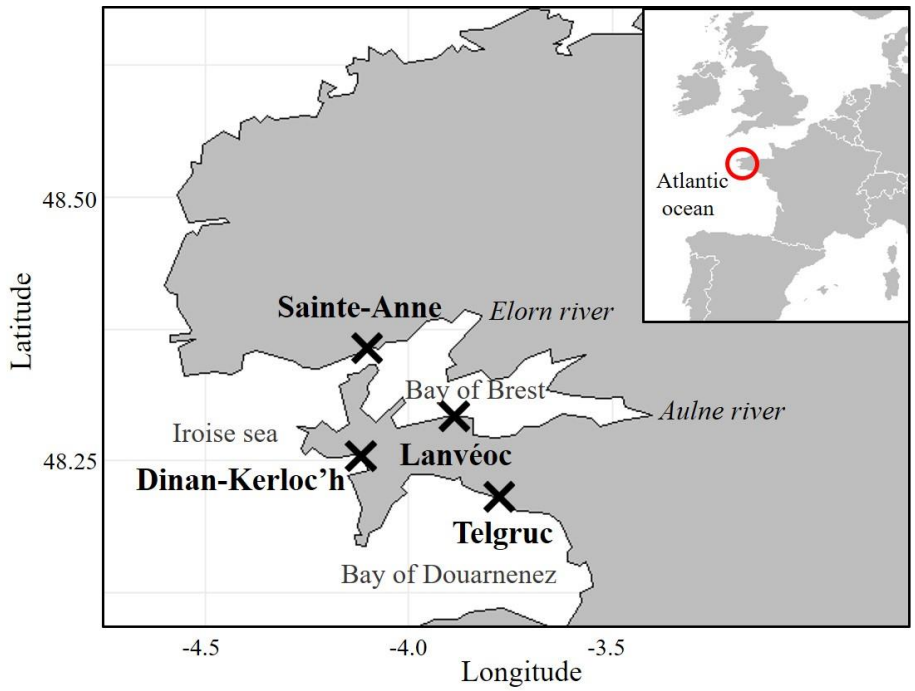

Fig 1: Sampling areas located in the Bay of Brest (Sainte-Anne, Lanvéoc), the Bay of Douarnenez (Telgruc) and the Iroise sea (Dinan-Kerloc'h), France, Western Europe

Following initial detection of the toxic *P. australis* species by the French phytoplankton monitoring network (REPHY), water samples were collected bi-weekly from shore in the Bay of Brest and Iroise sea in March 2019 (from March 1st to March 29th) and between February and April 2021 (from February 26th to April 16th) at four monitoring stations (Fig. 1, from south to north: Telgruc, Dinan-Kerloc'h, Lanvéoc and Sainte-Anne).

Two monitoring stations are located in the Bay of Brest (Lanvéoc: *48.292921, -4.458473*, Sainte-Anne: *48.360160, -4.553163*). The Bay of Brest is a semi-enclosed embayment of 180 km^2 connected to shelf waters by a narrow strait (2 km wide, 40m deep) (Quéguiner and Tréguer, 1984). The two main freshwater inputs in the area (Aulne and Elorn

rivers) flow into the Bay of Brest (average annual flow 21 and 5 m^3 s^{-1}, respectively), where an intense tidal mixing prevails (maximum tidal amplitude 8 m, tide periodicity: 12 h) that allows fast mixing exchanges with the Atlantic Ocean (Le Pape et al., 1996). In this shallow macrotidal area, tidal currents and wind ensure a good vertical mixing of the waters (Beucher et al., 2004). This is also the case for the other two monitoring stations (Dinan-Kerloc'h: 48.257071, -4.560974 and Telgruc: 48.209933, -4.373308). Unlike the Bay of Brest, these two stations only receive very small riverine inputs with mean flows below 2 $m^3.s^{-1}$ (Guillam et al., 2020; Merceron et al., 2007).

2.2.2 Environmental analysis

During the sampling period, salinity and sea surface temperature (°C) were measured *in situ* using Cond 3110 portable thermo-salinometer (WTW, a xylem brand, Germany). Water samples were filtered and prepared immediately after collection on the shore, for later analysis in the laboratory.

Nitrate, nitrite, phosphate and silicate concentrations (µmol/L) were measured by segmented flow analysis, following Aminot and Kérouel, 2007.

The tidal amplitude (m) is recorded in Brest city harbour (048° 23’ 00.0” N, 004° 30’ 00.0” W) by the French Naval Hydrographic and Oceanographic Service (https://maree.shom.fr/). The average photosynthetically active radiation (PAR, µE/m2/s) is provided at each station by Météo-France AROME numerical model (Seity et al., 2011) for which the mean between 10 am and 4 pm at the sea surface has been calculated. Daily average wave height (m) is taken from the Coriolis database observations (http://www.coriolis.eu.org).

2.2.3 Biological analysis

2.2.3.1 Cell Counts

Pico (0-3 µm) -nano (3-20 µm) and -microphytoplankton (> 20 µm) abundances were measured by flow cytometry using a CytoSense (Cytobuoy b.v., Netherlands), (laser 488 nm). Water samples (4 mL) were pre-filtered (200 µm) and fixed with glutaraldehyde and pluronic at a final concentration of 10%. Samples were stored at -80°C prior to analyses. Densities of each phytoplankton group were obtained in 2 runs with different speeds to increase the number of events to characterize the signal amplitudes and shapes. Size calibration was based on reference beads.

2.2.3.2 RNA extraction, library preparation and sequencing

For total RNA extraction, directly after the sampling, 4-5L subsurface water samples were filtered on 10 µm polycarbonate filters using a peristaltic pump. Filters were frozen in liquid nitrogen in RNA later (Fisher Scientific, Illkirch, France) and stored at −80 °C until RNA extraction. Total RNA was extracted by sonicating the filters on ice (Vibra-cell 75115, Bioblock Scientific, Illkirch, France) for 30 seconds at 35% intensity in LBP buffer (Macherey-Nagel, Duren, Germany). Extraction was performed using the NucleoSpin® RNA Plus kit (Macherey-Nagel) following the manufacturer's protocol. Library preparation was performed using the Illumina mRNA TruSeq stranded kit starting from 0.5 µg of total RNA. Paired-end sequencing was performed using 2 × 150 bp cycles on Illumina Hiseq3000 (2019 samples) and Novaseq6000 (2021 samples) at the GeT-PlaGe France Genomics sequencing platform (Toulouse, France). Generated fastQ files have been deposited to the European Nucleotide Archive (ERR9850438-460, 557-562, 566-569, 572-574, 577-584, 589-592, 600-607, 610-613, 619-621, 624-633).

2.2.3.3 Sequences preparations and bioinformatic pipeline

Prior to read mapping, raw reads were initially characterized with FASTQC (http://www.bioinformatics.bbsrc.ac.uk/projects/fastqc/) in order to assess read quality and quantity. TRIMMOMATIC (Version0.36) (Bolger et al., 2014) was then used to trim ambiguous, low quality reads and sequencing adapters with parameters: ILLUMINACLIP:adapter.fasta:2:30:10:8 LEADING:30 TRAILING:30 MAXINFO:40:0.5 MINLEN:80. Forward trimmed reads were aligned on two reference databases using blastn (-max_target_seqs 10 -evalue 1e-10) (Fig 2.A, B). The first one, the Protist Ribosomal Reference database (PR2, Guillou et al., 2012), is a manually curated database for 18S rRNA sequences, which enables complete characterization of the eukaryotic community, but at low taxonomic resolution, especially for diatoms. The second one, Diat_barcode (Rimet et al., 2019), is a manually curated database for diatom based on *rbcL*, a chloroplast marker. It was used to obtain a better taxonomic resolution for diatoms, at the species or genus levels. Homology between environmental reads and sequences from the two databases were determined based on e-values. The e-value represents the number of homologous sequences that one would expect to obtain at random. It is calculated as a function of the raw score (bit-score, alignment score), the alignment length (base pair alignment length of the environmental read on the query sequence) and also the database size (González-Pech et al., 2019).

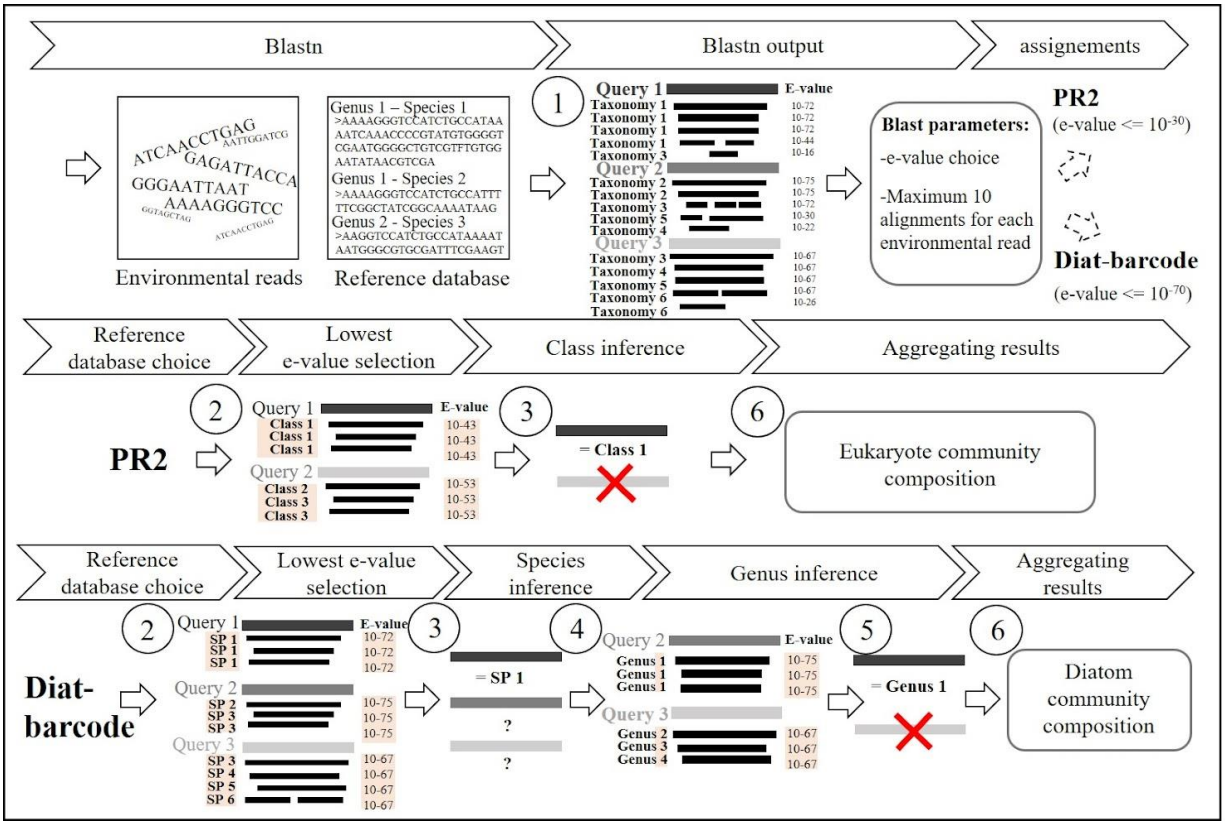

Fig. 2: Blast output analysis pipeline

Blast outputs were analyzed using R software (version 3.2.3; R Core Team 2014). Following preliminary investigation to identify appropriate thresholds (provided in supplementary materials A), reads displaying minimum e-values >= 10^{-30} against Diat_barcode and >= 10^{-70} against PR2 were filtered out. For each of the remaining reads, the database sequences displaying the lowest e-value (up to ten) were considered. For PR2, if all the database sequences displaying the lowest e-value belonged to a given class, reads were assigned to this class. For diat_barcode, if all the database sequences displaying the lowest e-value belonged to a given species or genus, reads were assigned to this species or genus respectively. Otherwise, reads were not considered. Relative community composition was obtained by dividing the number of reads assigned to a given taxonomic level (class, genus or species) by the total number of taxonomically assigned reads in each sample. In the study the relative abundances are expressed in percentage. For the different analyses, only class, genus, or species with a relative abundance >2% were considered.

2.2.3.4 RbcL marker choice for diatom identifications

In the present study, diatom community composition species assignment was based on the number of *rbcL* reads obtained for the various species in each sample. However, this number

of reads may not only be affected by the species' relative abundance in the community. It could also be affected by constitutive gene expression differences between species (for instance if *rbcL* is systematically more expressed by species A than by species B, which would lead to a systematic over- or under-estimation of some species depending on their rbcL expression level. Such bias could be similar to the one due to 18S rRNA gene copy number variation across protist species widely documented in metabarcoding studies (Martin et al., 2022). It could also be affected by differential expression between species across environmental conditions (for instance if *rbcL* is more expressed by species A in sample X and by species B in sample Y). This second type of potential bias could be much more problematic than the previous one, as it could entirely blur the species relative abundance signal. However, *rbcL* encodes for the Rubisco, a key and very abundant enzyme involved in photosynthesis and *rbcL* gene expression has previously been documented as correlated with overall cellular activity total RNA content and carbon fixation in natural diatom communities (John et al., 2007) and was more expressed at the onset of blooms in mesocosms (Wyman et al., 2000). Moreover, we re-analysed a previously generated gene the expression dataset (Lema et al., 2019) to determine how *rbcL* gene expression changes for seven *Pseudo-nitzschia* strains belonging to three different species in three experimental conditions. Results indicated a systematic *rbcL* over-expression for one species (*P. pungens*) compared to another one (*P. australis*) that could lead to an overestimation of *P. pungens* relative abundance compared to *P. australis* (about three times). However, gene expression appeared constant across strains and media (see supplementary materials F). Altogether, this suggests that relative abundance estimates based on *rbcL* gene expression may be a good proxy of the biologically active community composition, although some of the species may be systematically over-represented. This aspect is further discussed, in the discussion section, in light of the community composition results.

2.2.4 Statistical analysis

All statistical analyses and graphics were performed with R software v. 3.2.3 (R Core Team, 2014).

A principal Component Analysis (PCA, factoextra R package, Kassambara and Mundt, 2017) was used to assess temporal and/or spatial relationships between the samples based on the environmental variables along a reduced number of axes. The analysis involved all environmental parameters, including physico-chemical parameters (temperature and salinity, PAR, tidal amplitude, wave heights and nutrients concentrations) and biological parameters

(Pico-, nano and micro-phytoplankton abundances). Prior to these analyses, all variables were centered and scaled in order to make them dimensionally homogeneous. To investigate the spatial and temporal evolution of the diatom communities, a Principal Coordinate Analysis (PCOA; vegan package, Oksanen et al., 2007) using the Bray Curtis distance was used. The correlation between biological, physico-chemical parameters and relative community composition was tested using a Distance-based Redundancy analysis using the Bray-Curtis distance (dbRDA; vegan package). An analysis of variance (ANOVA) was then used to verify the significance of the overall analysis and each axis. The non-parametric Kruskal-Wallis test was performed to determine whether there were any temporal or spatial differences in environmental parameters between samples.

2.3 Results

2.3.1 Spatial and inter-annual environmental differences

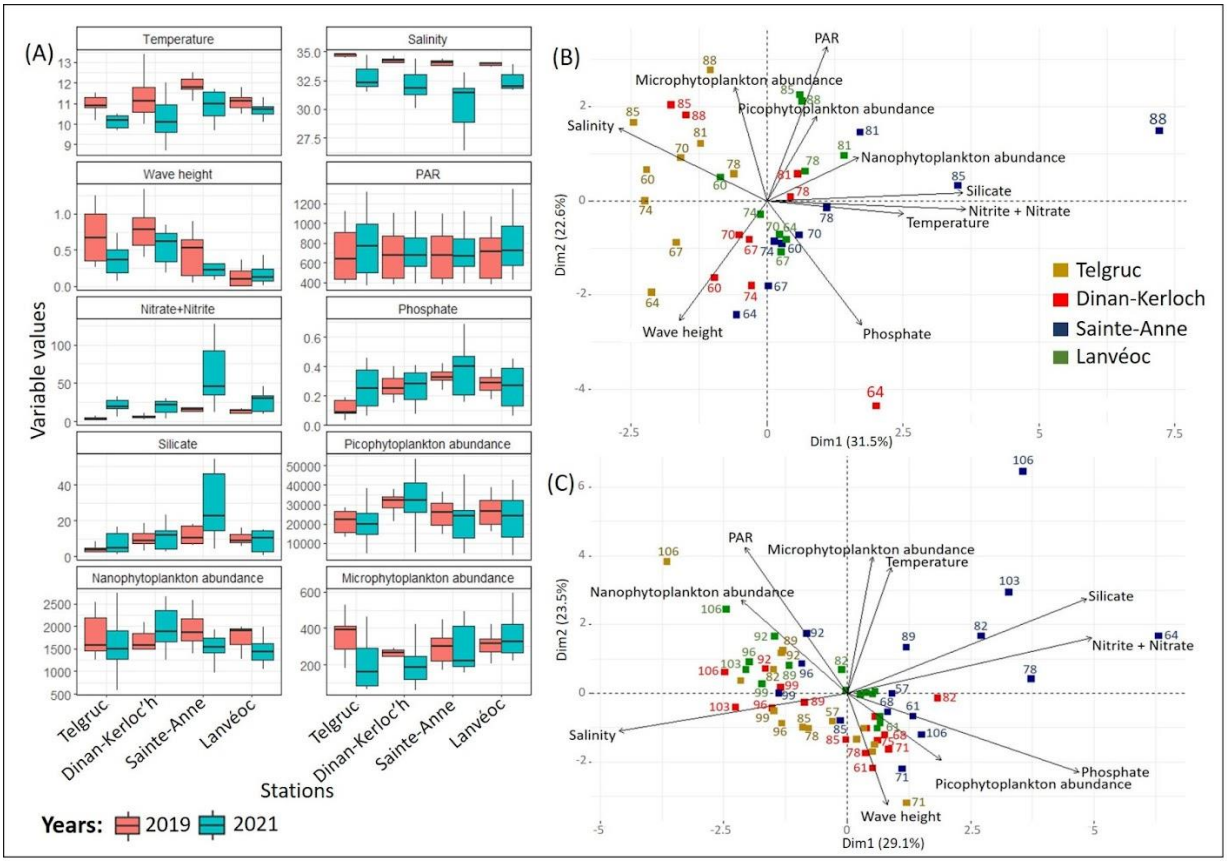

Fig. 3: (A) Interannual variability of biotic and abiotic parameters (outliers were removed of the graphics); (B) 2019 and (C) 2021 Principal Component Analysis (PCA) showing correlations between biotic and abiotic variables collected at the different monitoring stations (Dinan-Kerloc'h, Lanvéoc, Sainte-Anne and Telgruc). all the parameter's values are indicated in supplementary materials B. Numbers indicate sampling dates (julian days).

First of all, concerning interannual variability (Fig.3A), 2021 differed from 2019 by significantly lower salinity (Kruskal-Wallis, $p=2.03e^{-10}$), temperature ($p=3.81e^{-5}$) and significantly higher nitrate+nitrite concentration ($p=4.92e^{-9}$). Regarding the spatial variation for both years, the temperature was higher in Sainte-Anne ($p=0.005$) as well as the nutrients (Nitrate+Nitrite: $p = 2.85e^{-5}$; Phosphate: $p=0.006$; Silicates: $p=3.9e^{-5}$). Whereas salinity was significantly higher in Telgruc compared to the other stations ($p=0.005$). In general, results indicated lower temperature and higher wave heights in the southernmost station (Telgruc) and the open-ocean station (Dinan-Kerloc'h) compared to the Bay of Brest (Sainte-Anne and Lanvéoc) over the two years of sampling.

In addition, the intra-annual variability was analyzed using PCA. For both years, the first axis separated the samples spatially and the second axis separated them temporally.

The 2019 PCA (fig.3B) indicated that the first axis explained 31.5% of the variance and separated the samples with higher salinity from samples characterized by higher temperature and nitrate+nitrite (N) and silicate (Si) concentrations. The 2nd axis (22.6% of the variance) separated the samples with higher PAR from samples with low PAR and high phosphate (PO4) concentrations. Spatially, the first axis opposed the samples from Sainte-Anne which have higher concentrations of Si (13.4 ± 8.8 µmol/L; mean±standard deviation) and N (19.9 ± 11 µmol/L) and low salinity (33.7 ± 0.92) compared to the Telgruc station (Si: 4.9 ± 3.3 µmol/L; N: 3.8 ± 2.1 µmol/L; salinity: 34.7±0.1). Sainte-Anne waters also differed from Dinan-Kerloc'h and Lanvéoc but to a lesser extent. Concerning the temporal variation, the 2nd axis indicated logically an increase in PAR values during the monitoring period, coupled with calmer water (low wave heights) (Fig.3B).

In 2021, the PCA indicated that the first axis explains 29.1% of the variance and separated the high salinity samples from samples with higher temperature and nutrient (N, Si and P) concentrations. While, as in 2019, the 2nd axis (23.5% of the variance) separated temporally the samples with high PAR, temperature and microphytoplankton abundances from samples characterized by high wave heights. As in 2019 again, the 1st axis identified Sainte-Anne samples which have highly variable Si (38±40.9 µmol/L) and N (73.4±68.5 µmol/L) concentrations. The three other stations are characterized by higher salinity and less nutrient concentrations. Temporally, the 2nd axis identified samples which at the beginning of the monitoring period have higher wave heights, picophytoplankton abundances and PO4 concentrations and at the end of the monitoring period, samples with higher PAR and nanophytoplankton abundances (fig.3C).

2.3.2 Similar succession of diatom communities shifted in time between stations

In 2019, a total of 15 classes of eukaryotes with relative abundances over 2% were identified. The class Bacillariophyta, also known as diatoms, was the most abundant and ranged between 25.23% (Lanvéoc, 2019-03-22) and 91.38% (Telgruc, 2019-03-26) of the total abundance. *Spirotrichea* was the second most common class found in the Bay of Brest and at Kerloc'h; whereas the *Prymnesiophyceae* were mostly found at the Telgruc station. Urochordata was also commonly found in the samples (supplementary materials D for class relative abundances).

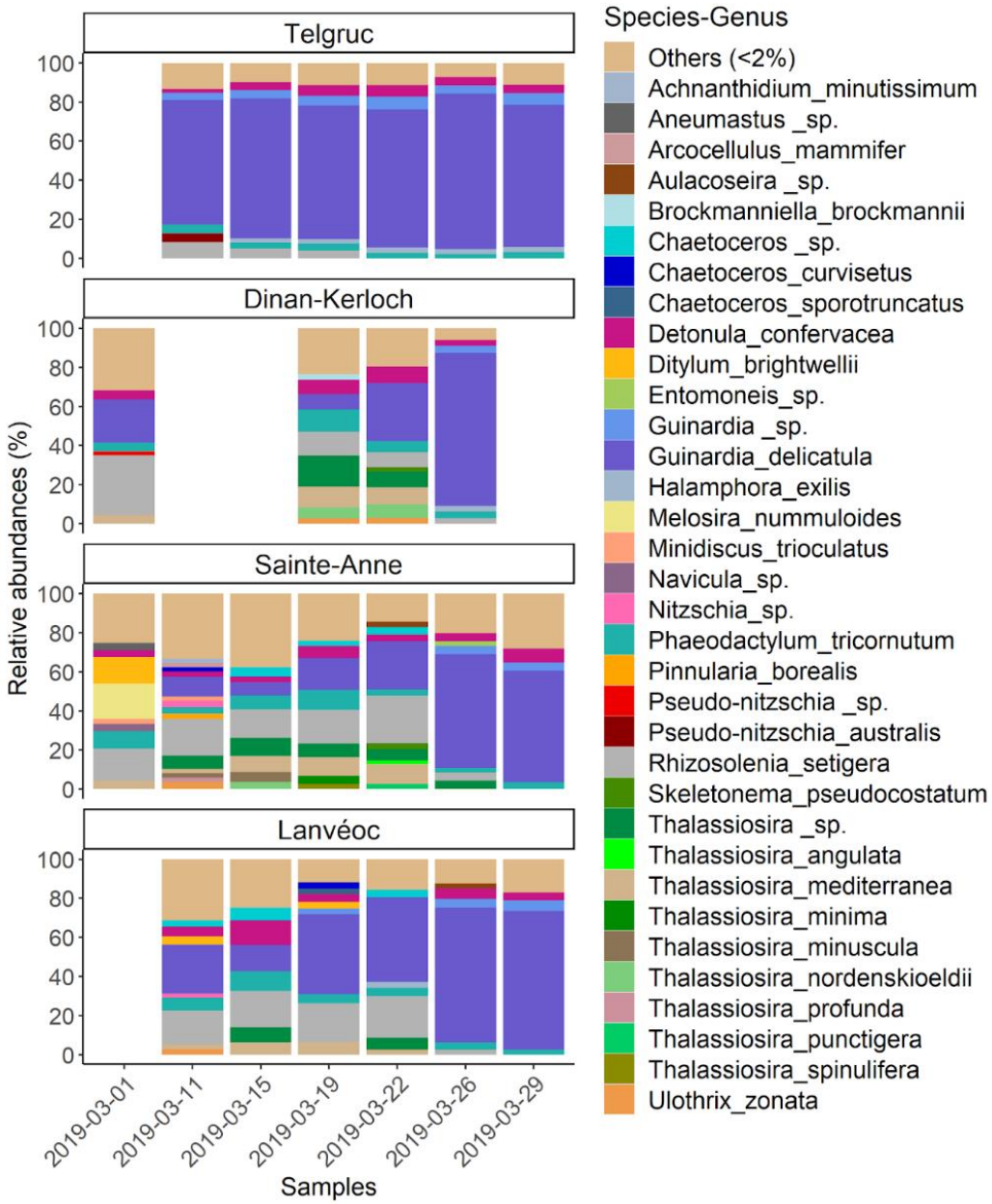

Fig. 4: Relative abundances of the diatom community composition during the 2019 monitoring (the category others regroup genus/species lower than 2% of total abundance). Blank areas correspond to missing data.

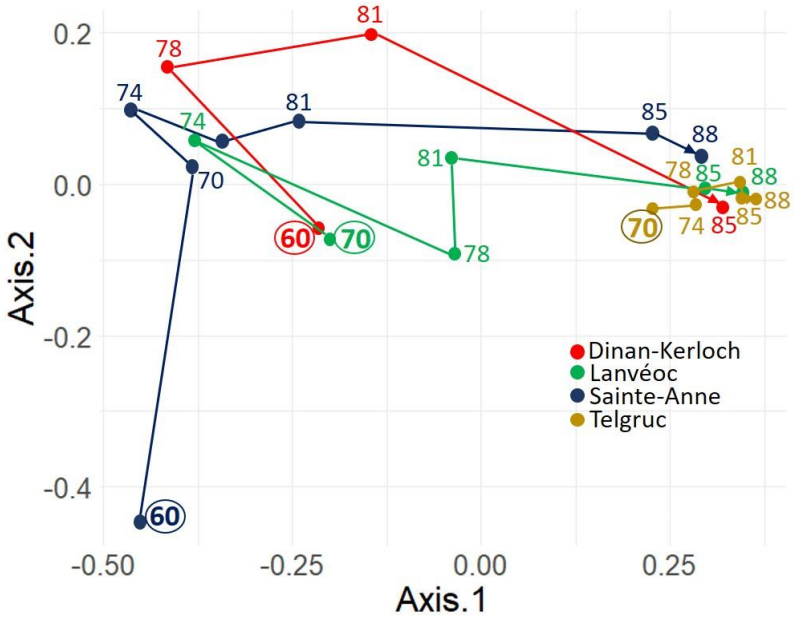

Fig. 5: PCOA based on Bray-Curtis distances showing the temporal trajectories of diatom communities for the 2019 monitoring. The red, green, blue and yellow trajectories represent the temporal trajectory of the Dinan-Kerloc'h, Lanvéoc, Saint-Anne and Telgruc communities, respectively. The numbers indicate the sampling dates (julian days) and the first samples are shown in bold-circled (the lines don't show continuous sequences all the time due to lack of some samples).

In 2019, a total of 34 species or genus of diatoms were found in all the samples. At the beginning of the time-serie the Sainte-Anne diatom composition was very different from the other stations, with some species only displaying relatively high abundance at this station, such as *Melosira nummuloides* and *Ditylum brightwellii* on march 1st. After this date, the same diatom species were found in high relative abundance at Lanvéoc and Dinan-Kerloc'h stations, but no species dominated the community before march 26th, although there was an increase of the diatom *Rhizosolenia setigera*, the genus *Thalassiosira* sp. and *Detonula confervacea* mainly (fig. 4). At the end of the survey, these stations all converged toward a community gradually dominated by the species *Guinardia delicatula.* This was clearly shown by the converging trajectories due to an increase in the relative abundance of *G. delicatula* from march 26th onward (day 81, fig. 5). Contrary to Sainte-Anne, Lanvéoc and Dinan-Kerloc'h, a stable dominance of *G. delicatula* was observed at Telgruc throughout the monitoring period (fig. 4), which is shown in the PCOA by a short trajectory (fig. 5, yellow trajectory). Results showed that during March 2019, the diatom community at Dinan-Kerloc'h, Sainte-Anne and Lanvéoc all evolved towards a composition similar to the one observed in Telgruc (fig. 4 and 5).

According to metatranscriptomic samples, *P. australis* represented 4.5% of the diatoms in Telgruc on March 11th and the genus *Pseudo-nitzschia* sp. 2% in Dinan-Kerloc'h on March 1st.

Light microscopic counts of the genus *Pseudo-nitzschia* were respectively 66,000 cells/L and 500 cells/L in these samples (supplementary materials E). It should be noted that according to microscopic samples, the highest *Pseudo-nitzschia* abundance was 88,760 cells/l on march 15th at Telgruc, while in this same sample the *Pseudo-nitzschia* relative abundance was lower than 2% according to the metatranscriptomic samples (fig. 4).

In 2021, a total of 25 classes of eukaryotes were identified and as in 2019, diatoms were the most abundant class and ranged between 27.74% (Lanvéoc, 2021-03-02) and 85.86% (Telgruc, 2021-03-19) of the total reads. Euglenozoa, Urochordata and Prymnesiophyceae were commonly found in the samples but in lower relative abundance (supplementary materials D.2 for all community information).

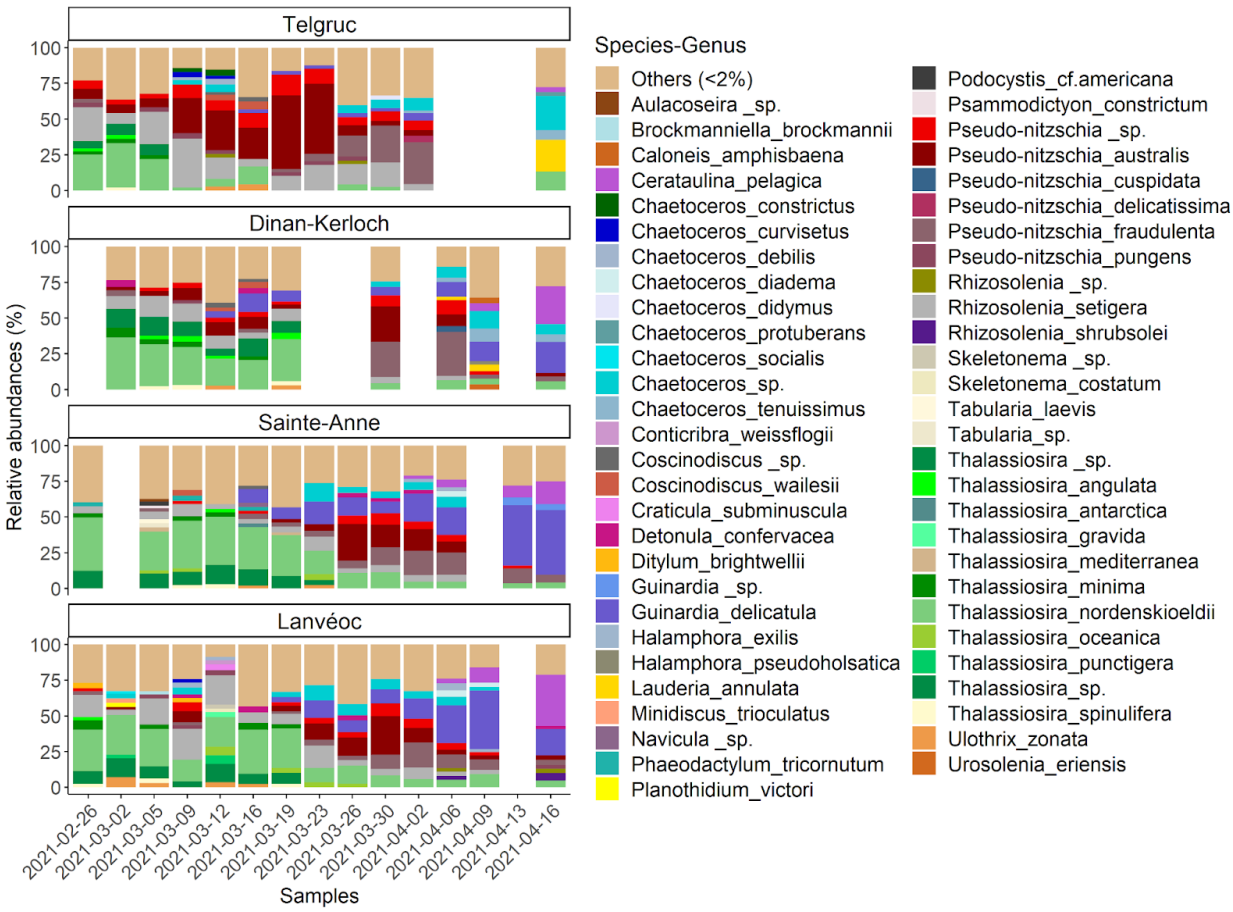

Fig. 6: Relative abundances of the diatom community composition of the 2021 monitoring (the category others regroup genus/species lower than 2%). Blank areas correspond to missing data.

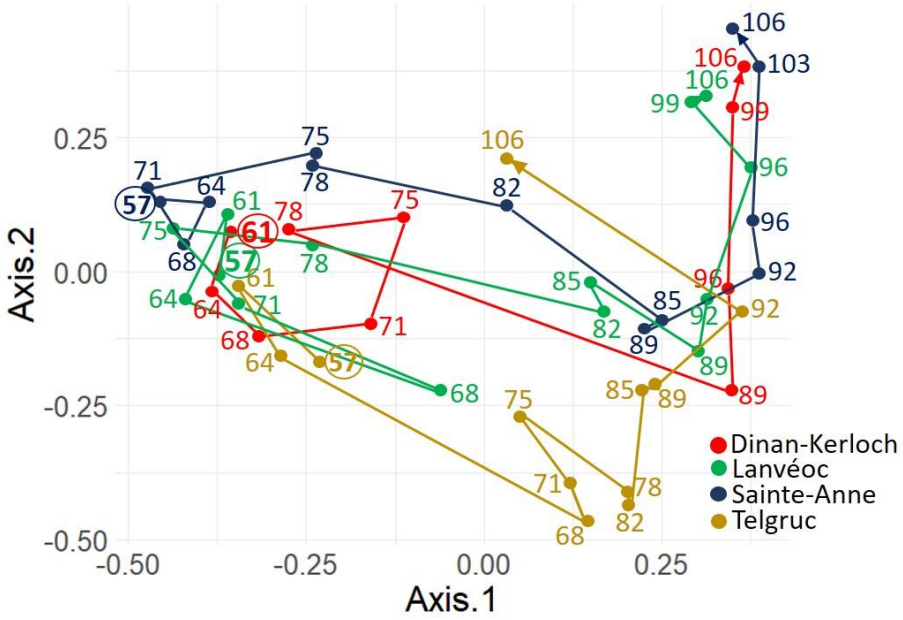

Fig. 7: PCOA based on Bray-Curtis distances showing the temporal trajectories of the diatom communities of the 2021 monitoring. The red trajectory represents the temporal trajectory of the communities present in the Dinan-Kerloc'h samples, the green one those of Lanvéoc, the blue one those of Sainte-Anne and finally the yellow one those of Telgruc. The numbers indicate sampling dates (julian days) and the first samples are shown in bold-circled (the lines do not show continuous sequences all the time due to lack of some samples).

The longer monitoring in 2021 (26th of February to 16th of April) showed a clear succession of communities over a 1.6-month period (fig.5) where a total of 75 diatom species or genus represented more than 2% of diatom relative abundance in at least one sample. In 2021, the samples from the four stations showed at the beginning of the survey a dominance of the genus *Thalassiosira* with the species *T. nordenskioeldii* and *T. minima* mainly. Then the diatom community shifted, with a strong decrease in *Thalassiosira* relative abundance and an increase in *Pseudo-nitzschia australis* abundances. As illustrated on fig. 6 this shift first occurred in Telgruc around March 9th and around two weeks later (March 23rd) in the three other stations. This dynamic is also illustrated on fig. 7 with similar community composition in all four stations at the beginning of the survey (clustering of the samples to the left of the first axis) and successions occurring first in Telgruc (68-78 julian days, corresponding to march 9th to 19th) and then in the three other stations (Dinan-Kerloc'h, Lanvéoc and Sainte-Anne), indicating a change in the relative abundance of the community in advance in Telgruc. In concordance, microscopic quantifications indicated *Pseudo-nitzschia* abundances higher than 100,000 cells/l on march 9th and a maximum of about 500,000 cells/l on march 23rd in Telgruc, while maximum densities were reached on march 30th in Lanvéoc (~60,000 cells/l) and on April 2nd in Dinan-Kerloc'h (~200,000 cells/l) and Sainte-Anne (60,000 cells/l). At the end of the monitoring

period we observed an increased dominance of *G. delicatula*, (except for Telgruc) as occurred in 2019. At the very end, an increase of the diatom species *C. pelagica* was observed (fig.6).

In a nutshell, the two years of monitoring showed similar changes in community composition relative abundance, but with a time-shift in diatom successions with Telgruc, the southernmost station, showing advanced changes compared to the other stations.

2.3.3 Community changes related to temporal environmental changes

For both monitoring years, correlations between diatom communities and the associated environmental factors at the 4 stations were shown by the dbRDA plot (fig. 8).

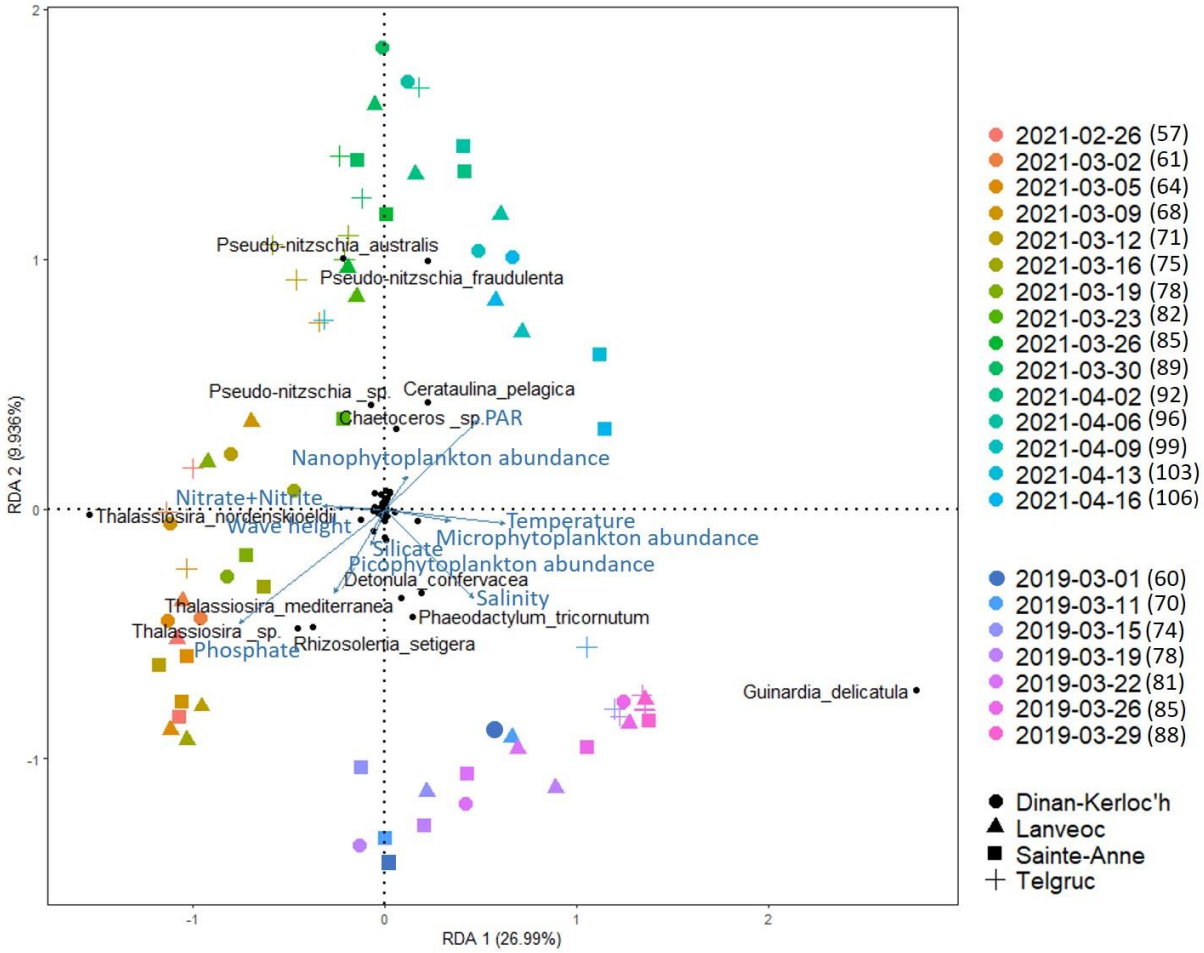

Fig. 8: Distance-based redundancy analysis (db-RDA) based on Bray Curtis similarity of the diatom community structure (relative abundance >2%) and its association with environmental variables of the 2019 and 2021 monitoring. Sampling dates (colors) and sampling stations (shapes) are indicated.

First of all, the first two axes of the dbRDA explained 36.93% of the variation in diatom structure. It revealed interannual differences in phytoplankton assemblages and mainly identified two clusters of samples (right-left of the graph) corresponding to 2021 and 2019

samplings respectively. Years were mainly separated based on two diatoms: *G. delicatula* which dominated the 2019 samples (fig.4), and the genus *Pseudo-nitzschia* (*P. australis*, *P. fraudulenta* and *Pseudo-nitzschia* sp.) present in 2021 but absent in the 2019 samples. Salinity and temperature were the main environmental variables correlated with the dominance of *G. delicatula* in 2019. In 2021, the presence of *P. australis*, *P. fraudulenta* and to a lesser extent *Pseudo-nitzschia sp.* were negatively correlated to salinity and PO4. Nevertheless, other species participated in clustering both years. In 2019, firstly, we can notice the presence of *Phaeodactylum tricornutum* and *D. confervacea* both positively correlated to salinity. And in 2021, *C. pelagica* and *Chaetoceros* sp. are identified as negatively correlated with phosphate, picophytoplankton abundance, but positively correlated with Si, nanophytoplankton abundance and PAR.

The greatest variation in the diatom community composition was found temporally. The first axis clearly separated communities dominated by *T. nordenskioeldii* at the beginning of 2021 at all sampling sites and by *G. delicatula* toward the end of both years. The only noticeable exception was Telgruc. At this site, *G. delicatula* dominated the entire 2019 survey but was virtually not detected in 2021.

Within each year and site, a temporal species succession was identified in relation to environmental parameters (except in 2019 for Telgruc), PO4 and PAR were the major factors which explained the composition of the community, with higher PO4 concentrations and lower PAR occurring at the beginning of the surveys.

2.4 Discussion

This study investigated the phytoplankton community succession on a small spatial and temporal scale during early springs (February to April) during two years (2019 and 2021), in relation with abiotic and biotic parameters (phytoplankton size abundances and accompanying species). Metatranscriptomic samples were used to describe the whole phytoplankton community composition at four study sites located in western Europe, an area subject to harmful algae blooms. The communities showed the same evolution in their successions in relation to the seasonal evolution of temperature, PAR and phosphate. But this succession presents a time-shift, the southern station showing changes earlier, followed by the other 3 stations. Another difference in terms of species dominance is that in 2021, the toxic species *P. australis* and *P. fraudulenta* dominated the community from mid-March to the first days of April, specially at the Southernmost station (Telgruc).

- **Metatranscriptomic samples identify the eukaryotic community in coastal waters**

In this study, metatranscriptomic samples were used to characterize the phytoplankton community composition. Thanks to this, a characterisation at different levels was possible: at large group and diatom specific level since different reference banks (respectively PR2 and diat_barcode databank) were used. Overall community composition was identified using PR2 reference database based on 18S rDNA (Guillou et al., 2012; https://pr2-data base.org/), a marker classically used in metabarcoding studies. This allowed to characterize the whole eukaryotic community, but at moderate taxonomic resolution (higher than genus) for certain phylum. This is especially the case for diatoms, the dominant phylum in this study which are known to be dominant in the Bay of Brest and Iroise sea throughout the year (Del Amo et al., 1997; Quéguiner and Tréguer, 1984; Ramond et al., 2021). To overcome this issue, diatoms were identified at low taxonomic level (species or genus) using the same environmental sequence datasets, but aligned on a different reference bank: Diat.barcode based on rbcl, a chloroplast marker suitable for species-level identification of diatoms (Rimet et al., 2019; https://www6.inra.fr/carrtel-collection_eng/Barcoding-database). Such an approach enabled the identification of species frequently found on the East Atlantic coast in early spring. During the 2 years some diatoms were found recurrent as is the case of *G. delicatula*, *R. setigera* and the genus *Thalassiosira sp.* (mainly *T. nordenskioeldii* and *T. minima*). This homogeneity in the most dominant species during the two years corroborated a study carried out in the west English Channel which showed such stability in the planktonic community composition over 8 years of study (Caracciolo et al., 2022). During both years, the pelagic genus *Thalassiosira* sp. was dominant in the samples at the beginning of the monitoring correlated with lower temperature and PAR. Within this genus, *T. nordenskioeldii* was the species regularly identified in the samples. This species is a typical cold-water species, described from Arctic waters (Gómez, 2008), and is a potential biological indicator of the cold, well-mixed water conditions of west Europe coast. Our observations tend to confirm this since this species was found early in the surveys during both years, in the rather cold waters of early March (around 9-10°C in 2021). It was also identified in the 1960s and also between 2000 and 2010 in the south west English Channel (Guilloux et al., 2013; Jacques, 1963; Paulmier, 1969). In addition to this genus, *Pseudo-nitzschia* sp. (identified mainly in the middle of the 2021 monitoring and in very low relative abundance at one station in 2019) and *Chaetoceros* sp. were cosmopolitan genera also present in the samples. These genera are identified as recurrent bloomers typical of marine systems (Assmy et al., 2008). The species *G. delicatula* was also identified in samples from

both years. In 2019, this pelagic chain species was the most dominant species. Indeed, it dominated the diatom community during the whole period in the southern station and at the end of the survey in the other stations. In 2021, it was less abundant but nevertheless identified as a major component of the community in the Bay of Brest during the second half of the survey. Its presence seems to be recurrent over this period. This was not surprising as it is known on the North-Eastern Atlantic coast to be a recurrent species in early spring phytoplankton blooms, such as in the Seine estuary (Jouenne et al., 2007), the northeastern English Channel (Gómez and Souissi, 2007), the German Bight (Schlüter et al., 2012), and the west coast of the Irish Sea (Gowen, 1999). Closer to our study area, in the south west English Channel, *G. delicatula* has been found in numerous community studies. It is one of the most dominant species in planktonic communities in the Atlantic, English Channel (Arsenieff et al., 2020; Caracciolo et al., 2022; Grall, 1972; Guilloux et al., 2013; Jacques, 1963; Martin-Jézéquel et al., 1992; Sournia and Birrien, 1995) and North Sea (Wiltshire et al., 2010) and appears to do particularly well in temperate tidal mixing habitats (Gómez and Souissi, 2007; Hernández-Fariñas et al., 2014; Peacock et al., 2014; Schlüter et al., 2012; Wiltshire et al., 2010).

All these results were consistent with other studies where species identifications were made either by light microscopy or metabarcoding. Precise taxonomic level identification is important in community ecology studies, especially when dealing with HABs, since not all species of the same genus are toxic as is the case for *Pseudo-nitzschia* sp.. The identification method proposed in the present study allowed us to identify species within the genus *Pseudo-nitzschia* and *Thalassiosira,* difficult to identify by light microscopy. Within the genus *Pseudo-nitzschia sp.* 56 species were previously described of which 26 are confirmed toxigenic (Bates et al., 2018; Lundholm, 2022). However, some method limitations should be noted. In 2019, microscopic observations indicated the presence of *Pseudo-nitzschia* species in the sampled communities, but these species were almost not detected using the metatranscriptomic samples (4.5% on March 11st and then less than 2%). In 2021, the presence of *Pseudo-nitzschia* species was detected using both approaches. Such results may be explained by different reasons. First, this may be due to the presence of *Pseudo-nitzschia* species in 2019 that didn't dominate the community in relative abundance. Whereas in 2021, its presence was more important in relative abundance. Another hypothesis may be a difference in rbcl expression between species. In the present study, diatom community composition was based on the number of *rbcL* reads obtained for the various species in each sample. As stated in the method section such estimation of community composition might be biased by either constitutive gene expression differences

between species or, more problematically by differential gene expression between species across environmental conditions. In addition to the arguments developed in the method section, we would like to emphasize that the extremely clear spatio-temporal species succession patterns reported in the present study strongly suggest an absence of major differential gene expression bias. We acknowledge a potential systematic bias leading to the over- or under-representation of some species (as other methods such as metabarcoding), but such a bias does not interfere with spatio-temporal succession patterns which are the main focus of the present study. In addition, it is also important to note that each method has its own biases. Indeed, optical microscopy, with its much smaller volumes of water used compared to molecular methods, as well results largely influenced by the taxonomist's expertise, and counts that are more difficult when there are many chains of diatoms, can over- or underestimate species richness in environmental samples (Vuorio et al., 2020).

- **West coast of Brittany interannual variability of *Pseudo-nitzschia* bloom**

In 2021, the study provided detailed records of the *Pseudo-nitzschia* within the community, at the species level and described its relationship with both the surrounding environmental conditions and biotic factors such as the accompanying phytoplankton community. The study period (March-April) is prone to the emergence of the toxic diatom *Pseudo-nitzschia australis in* Brittany coast (2014, 2017, 2019 and 2021 for the latest years; Nezan et al., 2010; REPHY, 2022) a harmful diatom known to produce the neurotoxin domoic acid (Garrison et al., 1992).

Over the past decades, numerous monitoring programmes for toxic phytoplankton have been set up on coasts around the world in response to the increasing impact of HAB events. These monitoring programmes are very important and provide periodic information on phytoplankton species and environmental variables of invaluable ecological importance (Edwards et al., 2010). In the present study, a rapid succession of phytoplankton communities and therefore toxic species in early spring was identified. In 2021, the genus *Pseudo-nitzschia* and the species *P. australis* dominated the community at each station over a relatively short time period, ranging from 6 to 11 days. Which can fall through the cracks of some monitoring programmes displaying monitoring frequency of 15 days (REPHY, Pannard et al., 2008), and consequently limits the use of the data to understand the ecology of a species.
Moreover, monitoring data from many countries are mostly related to species groups called “complex”, for example the delicatissima/pseudodelicatissima and the seriata complex for the *Pseudo-nitzschia* genus based on cell size (Belin et al., 2021; Downes-Tettmar et al., 2013;

Turk Dermastia et al., 2020). It is therefore not possible to quantify the percentage of the contribution of toxic species in blooms compared to that of non-toxic species. However, some groups contain more toxic species, and the alert thresholds defined in REPHY in France to trigger toxin analysis in shellfish take this into account (Belin et al., 2021). Despite this, the data from this monitoring programme are sufficient for HAB monitoring but are limited for work on ecological niches or high frequency bloom monitoring.

We advocate the importance of sampling over short periods of time to understand toxic blooms over their entire development period.

In our survey, for all stations, *P. australis* was found to be dominant over different time periods, and always accompanied by other species, in particular two less toxic *Pseudo-nitzschia* species: *P. fraudulenta* and in lower relative abundance the species *P. pungens*. Other diatoms such as *R. setigera, T. nordenskioeldii* and *Chaetoceros* sp. were also found in the same samples as *P. australis*. Some studies also showed non mono-specific *Pseudo-nitzschia* species composition during blooms (Quijano-Scheggia et al., 2008; Smith et al., 2018).

In our study, the genus *Pseudo-nitzschia* and the toxic species *P. australis* were identified in 2021 at all stations, and only in the sample from one station in 2019. The difference between the two monitoring years was that in 2021, salinity and nutrients were lower, especially nitrate. Concerning environmental parameters and the *Pseudo-nitzschia* genus presence, the twice a week survey frequency identified salinity as the most correlated environmental variable with difference in community composition between the two sampling years. Salinity was significantly lower in 2021 compared to 2019 and was correlated with the presence of *P. australis*. In 2021, results displayed *P. australis* correlated with lower salinity and phosphate.

Many studies showed different *Pseudo-nitzschia* sp. responses to environmental variables. Several authors identified temperature and nutrients as main environmental parameters determining dominance amongst *Pseudo-nitzschia* species (Bowers et al., 2018; Klein et al., 2010; Trainer et al., 2012). Some studies found that *Pseudo-nitzschia* blooms are associated with high nutrient concentrations, cold waters and high salinity in East and West America (Trainer et al., 2002, 2000). Others identified *P. australis* associated with high temperature and silicate-rich waters in the Bay of Seine (France, Klein et al., 2010). Whereas Almandoz et al. (2007) showed that *P. australis* reached high densities especially with high salinity and low NO_3^- and PO4 concentrations in South America. Husson et al. (2016), for their part, identified irradiance and temperature as playing a major role on *Pseudo-nitzschia* blooms initiation in spring along the French Atlantic and English Channel coasts. Finally, Thorel et al. (2014) stated the large temperature growth range of *P. australis* depending on the region.

Given our results, a direct link between high relative abundances of *P. australis* and lower salinity in 2021 compared to 2019 appeared unlikely. First because although significant, the magnitude of salinity variation between but also within each year was rather moderate (from 27 to 35). Second because at salinities of 30 and 35, a laboratory study showed that the growth rate of two strains of *P. australis* did not seem to change (Ayache et al., 2020). However, salinity is a conservative tracer indicative of riverine inputs. As a result, nutrient fluxes must have been higher in 2021 than in 2019, and the similar nutrient concentration between these two years probably reflected a faster nutrient consumption by the community.

For all these reasons, we suggest further studies in the area during *P. australis* blooms. Moreover, considering contrasting literature results on the environment associated with the development of the species, we advocate the importance to study locally i.e in the ecosystem of interest, to understand the development of the genus *Pseudo-nitzschia* at this location. Indeed, some studies suggested that the high intraspecific variability among *Pseudo-nitzschia* species may be related to the origin of the strains (ecotypes) (Lelong et al., 2012; Thorel et al., 2014).

- **Diatom community successions from south to north over the time**

Over the two years, the diatom community succession at the beginning of spring was similar, and results indicated a shift that occurs first in the southernmost area. To our knowledge, this study is the first to compare diatom communities in different close areas in a small-time scale that showed a spatial shift in community succession. Different authors in the study area have highlighted the constant mixing of the waters of the bays with the adjacent Iroise sea explained by the strong impact of the tidal cycle (Delmas and Treguer, 1983; Le Pape et al., 1996; Quéguiner and Tréguer, 1984), which suggests that phytoplankton community homogeneity is expected across the area. But this was not reflected in our results. Indeed, at the same day of sampling the four stations had different communities, suggesting that on the same sampling day, the water masses and consequently phytoplankton communities differed between the Bay of Brest and the adjacent areas. Moreover, results showed that stations differed in environmental parameters (temperature, salinity and nutrients). But this was not associated with any difference in diatom communities between stations over the monitoring period. For both years, temporal variations on PO4, temperature and PAR were the main variables correlated with community changes. Phosphate decreased on average, but did not drop to low values over

the survey. And not surprisingly, temperature and PAR were variables which increased in relation to the typical seasonal pattern of the northern hemisphere.

Another study also identified in the English Channel, nutrient stock and light availability as main environmental drivers that influenced phytoplankton community structure on a short-time scale (Houliez et al., 2015; Pannard et al., 2008). However, in the present study 37% of the diatom variability was correlated with the parameters studied, which suggests that other variables must be considered such as micronutrients; competition; grazing or parasite pressure (Litchman and Klausmeier, 2008). Despite this, a good part of the variation was explained by typical spring time parameters. And results suggest that in addition to the known seasonal variability of community change (Caracciolo et al., 2022), environmental temporality on a small time scale also drives community change.

Although small-scale spatial and high time-frequency studies are rare, two previous studies also identified that protist successions were more influenced by temporal than spatial factors at small spatio-temporal scales. A study conducted on the Southern California coast for 12 consecutive days in May 2011 showed that changes in protist community composition at small spatial scales were smaller than changes at small temporal scales (Lie et al., 2013). Another study in a Washington State fjord with sampling at 2- or 5-day intervals in July 2005 reported significant changes in protist community composition over time but not between stations (Menden-Deuer, 2008). Protists can respond rapidly to biotic and abiotic factors as their high maximal growth rates allow them the potential to increase rapidly in abundance (Lie et al., 2013; Rose and Caron, 2007). Lie et al. (2013) detected rapid shifts during 3 successive days in protistan communities which suggest very rapid growth of some species. In these studies, community changes were not correlated with measured variables.

Finally, the present results indicated that the southernmost station (Telgruc) showed early changes in the succession of diatom communities compared to the 3 stations studied (Dinan-Kerloc'h; Sainte-Anne and Lanvéoc) which had fairly homogeneous succession changes in their community. Only the species *Guinardia delicatula* in 2021 was not found to be dominant in the samples from Telgruc (which also had missing samples), whereas it was in the samples from the other three stations. The environmental parameters between the stations were different, however the same species were found in the communities of all stations. None of the measured parameters highlighted an advance in environmental parameter changes at the southernmost station. The successions of communities reacting only to temporal changes without correlation

with environmental parameters allowed us to make two non-mutually exclusive hypotheses. The first was that environmental parameters allowed the development of each community locally and variables not considered in the study were in advance at Telgruc. The second hypothesis was that the stations were hydrodynamically connected, and the species initially developed at Telgruc, the southernmost station, before being transported by the currents. In order to test these hypotheses, further studies are needed to determine whether the different study areas are hydrodynamically connected which would also guide future studies to understand the development of toxic species in the area. In addition, although the focus of the present study was on the relative abundance of species within the communities, it should be noted that the metatranscriptomic datasets may also be used to determine gene expression of the various species within the community. Such analyses would not only allow to determine whether relative abundance of the species change in community but also whether physiological changes occur within each species in relation with space, time and environmental parameters.

The study area is an important fishing area, mainly recognised for the Bay of Brest by the scallop fishery (Husson et al., 2016) and by the grooved shell fishery for the Bay of Douarnenez (Thébaud et al., 2005), but frequently impacted by toxic algal blooms. And we suggest that the Bay of Douarnenez (the southernmost bay) could be a monitoring point to anticipate early spring blooms, particularly of *P. australis* in the Bay of Brest (the northernmost bay). A precise understanding of the spatio-temporal dynamics of phytoplanktonic communities at small scales may enable the development of monitoring strategies that could help anticipate HAB. As suggested by the present study such strategies could for instance focus on sampling points displaying early shifts in community composition compared to nearby areas of primary socio-economical or ecological interests.

Conclusion

Understanding phytoplankton dynamics requires high frequency spatial sampling to resolve the small scale and spatial distribution especially in high productive periods such as spring. During two years, phytoplankton community succession in nearby areas situated on the west coast of France are spatially homogeneous with a temporal evolution associated with temperature, PAR and phosphate. The only major difference is the presence of toxic species *P. australis* and *P. fraudulenta* in the less salty waters of 2021. The successional dynamics show a south-north shift, which suggests that anticipation of HABs is possible from the southernmost bay to anticipate the arrival of toxic species in the northernmost bay. Further studies are needed to

determine whether the different study areas are hydrodynamically connected which would also guide future studies to understand the transport of toxic species in the area. The results of the present study provide new insight into phytoplankton dynamics during early spring in a temperate dynamic area.

Chapitre 3

Caractérisation interannuelle de la connectivité hydrodynamique entre la baie de Douarnenez et la rade de Brest

Léa Prigent[a], Mickaël Le Gac[a], Martin Plus[a]

[a]Ifremer, DYNECO, F-29280 Plouzané, France.

Context

With the taxonomic assignment findings from the analysis of the two spatio-temporal monitoring of *P. australis* bloom detailed in chapter 2, we were able to establish the presence of a fairly homogeneous diatom community during early spring in West-Brittany. This community displayed a south-to-north succession pattern between the Bay of Douarnenez and the Bay of Brest. Although the environmental analysis was insufficient to explain this shift, we did identify a significant correlation in the succession of diatom communities concerning the changing temperature, PAR, and phosphate levels over time.

In support of other observations, although this could not be formally demonstrated (given the observations available), the hypothesis of a South-North shift has already been advanced by the REPHY, with the observation of *P. australis* blooms in the Bay of Brest always preceded by blooms in the Bay of Douarnenez.

Naturally, the question arises of a possible anticipation of *P. australis* before its development in the Bay of Brest.

To answer this question, a realistic 3D hydrodynamic model: CROCO (Coastal and Regional Ocean Community model) was configured for the Finistère area. The main objective was to understand the potential movement of *P. australis* blooms in the West-Finistère area (Brittany) through the study of hydrodynamic connectivity.

For that, hydrodynamic connectivity existing in March was analyzed and compared during four different years (2014, 2017, 2019 and 2021) during periods of *P. australis* bloom.

This chapter seeks to answer the following questions:

What hydrodynamic connectivity exists in West-Brittany? Are the hydrodynamics the same during the 4 years of blooms? Could a south-north hydrodynamic pattern explain the observed south to north bloom patterns?

To investigate the hydrodynamic connectivity, two modelling methods commonly used to simulate the transport of tracers in an area were used: the Eulerian method and the Lagrangian

method. Eulerian models simulate the dispersion/advection of tracers in concentration at fixed locations, while Lagrangian models follow the trajectory of moving particles in space and time (Curchitser et al., 2013).

Four hydrodynamic simulations over the month of March were performed for four years with more or less significant blooms (2014, 2017, 2019 and 2021). These different simulations have been compared and discussed in this chapter.

This chapter mainly highlight :

- Over the four years of simulation, a marked hydrodynamic connectivity between the Bay of Douarnenez and the Bay of Brest.

- Higher retention of water masses in the Bay of Douarnenez

Résumé graphique :

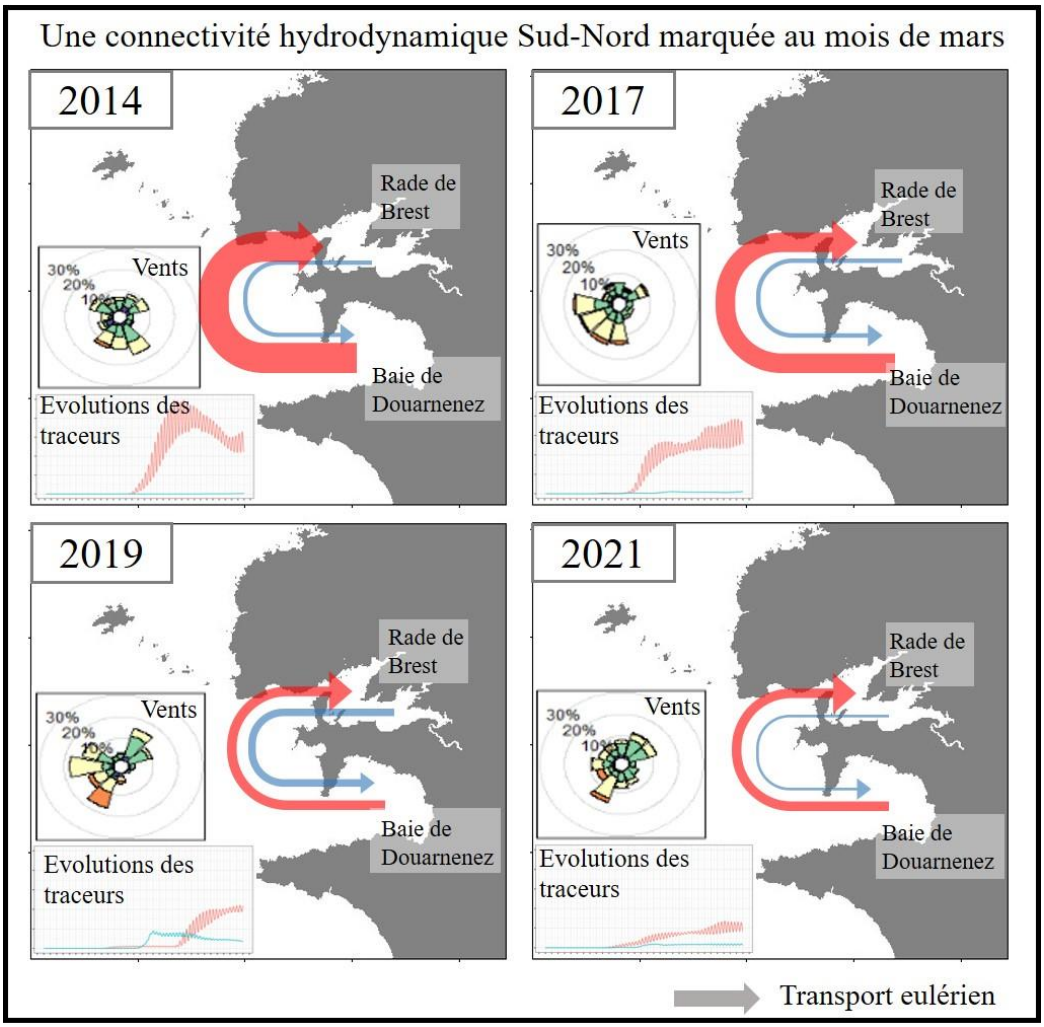

Résumé :

Le phytoplancton joue un rôle majeur dans les écosystèmes aquatiques et dans le cycle du carbone à l'échelle mondiale. Il est influencé par un ensemble de facteurs biotiques et abiotiques, et lorsque la productivité est élevée, le phytoplancton connaît une croissance exponentielle et forme des efflorescences. Ces efflorescences sont majoritairement bénéfiques pour la vie aquatique et soutiennent la chaîne trophique mais peuvent dans certains cas être le résultat du développement d'espèces toxiques et avoir des effets négatifs sur les écosystèmes aquatiques (par exemple, appauvrissement en oxygène, changement de la couleur de l'eau, obstruction des branchies de poissons, ou toxicité) et impacter négativement la santé humaine. Dans les écosystèmes aquatiques tempérés, les efflorescences printanières sont les plus importantes, principalement liées à la présence de nutriments accumulés durant l'hiver et à l'augmentation saisonnière de la température et de la luminosité. La région Ouest-Finistère est

régulièrement touchée par les efflorescences de la diatomée toxique *Pseudo-nitzschia australis* au début du printemps résultant en la fermeture de pêcheries due à des contaminations de bivalves. En France, la surveillance du phytoplancton est assurée par le réseau REPHY (Réseau d'Observation et de Surveillance du Phytoplancton et des Phycotoxines). Les observations de ce dernier ont permis d'identifier une tendance à un développement dans un premier temps en Baie de Douarnenez (BDZ), puis quelques temps après plus au Nord, en Rade de Brest (RDB). Nous avons, dans le cadre de cette thèse, également observé ce phénomène lors d'une efflorescence de *P. australis* au début du printemps 2021 (chapitre 2). Suite à ces différentes observations, l'objectif de ce chapitre est d'identifier la connectivité hydrodynamique existante en Ouest-Finistère, et plus particulièrement en périodes connues d'efflorescences de *P. australis*. Pour cela, un modèle hydrodynamique réaliste 3D : CROCO (Coastal and Regional Ocean Community model) a été configuré pour notre zone d'étude. Quatre simulations correspondant aux mois de mars 2014, 2017, 2019 et 2021 ont été réalisées et analysées. Le mois de mars a été choisi car il correspond à la période la plus propice aux efflorescences de *P. australis*. Grâce à des simulations de traceurs passifs eulériens et de particules Lagrangiennes, nous avons mis en évidence une connectivité hydrodynamique marquée entre la BDZ et la RDB en relation principalement avec les directions du vent et les coefficients de marée. En effet, les vents d'Est ou très variables en direction ont eu tendance à disperser les traceurs initialisés en BDZ, vers le large, alors que les vents venant du Sud et d'Ouest ont eu tendance à entraîner ces traceurs vers la RDB. Les transports de traceurs entre ces deux zones étaient d'une quinzaine de jours en moyenne sur toutes les simulations, avec un maximum de masse de traceurs entre 22 et 31 jours selon les années.

Abstract:

Phytoplankton plays a major role in aquatic ecosystems and in the global carbon cycle. It is influenced by a range of biotic and abiotic factors, and when productivity is high, phytoplankton grow exponentially and form blooms. Most of these blooms are beneficial for the aquatic life and support the trophic chain, but in some cases, they can be the result of the development of toxic species and can have negative effects on the aquatic ecosystems (for example, oxygen depletion, change in water colour, obstruction of fish gills, or toxicity) and negatively impact human health. In temperate aquatic ecosystems, spring blooms are the most significant, mainly due to the presence of nutrients accumulated over the winter and the seasonal increase in temperature and light levels. The West-Finistère (Brittany) region is regularly affected by

blooms of the toxic diatom *Pseudo-nitzschia australis* in early spring, resulting in the closure of fisheries due to contamination of bivalves. In France, the REPHY network (Réseau d'Observation et de Surveillance du Phytoplancton et des Phycotoxines) is in charge of monitoring the phytoplankton. Observations from this network have identified a trend towards the development of phytoplankton, initially in the south of Finistère (in the Bay of Douarnenez, BDZ), then some time later further north (in the Rade de Brest, RDB). As part of this thesis, we also observed this phenomenon during a *P. australis* bloom in early spring 2021 (chapter 2). Following these observations, the aim of this chapter is to identify the hydrodynamic connectivity existing in West Finistère, and more specifically during known periods of *P. australis* blooms. To achieve this, a realistic 3D hydrodynamic model: CROCO (Coastal and Regional Ocean Community model) was configured for the study area. Four simulations corresponding to the months of March 2014, 2017, 2019 and 2021 were carried out and analysed. March was chosen because it is the most suitable period for *P. australis* blooms. Using simulations of passive Eulerian tracers and Lagrangian particles, we demonstrated a marked hydrodynamic connectivity between the BDZ and the RDB, mainly in relation to wind directions and tidal coefficients. Easterly winds or winds of very variable direction have tended to disperse tracers initialised in the BDZ towards the open sea, whereas southerly and westerly winds have tended to carry these tracers towards the RDB. The transport of tracers between these two zones took around fifteen days on average over all the simulations, with a maximum mass of tracers between 22 and 31 days depending on the year.

3.1 Introduction

Les efflorescences de phytoplancton sont des éléments clés de la dynamique des écosystèmes côtiers. Elles sont importantes car elles modifient la composition élémentaire des eaux, constituent une source de nourriture pour les niveaux trophiques supérieurs, mais peuvent affecter la couleur de l'eau et ses aspects sanitaires pour les consommateurs.

Les variations spatiales et temporelles de l'abondance et de la composition du phytoplancton sont régies par des interactions complexes entre les processus physiologiques et physiques. Les efflorescences sont le résultat d'une croissance accrue et d'une accumulation de biomasse résultant de la balance entre production/mortalité locale et dilution hydrodynamique (Lucas et al., 1999). Les taux de croissance sont contrôlés par différentes variables environnementales propres à la physiologie de chaque espèce, comme par exemple les concentrations en nutriments, la température de l'eau, et la luminosité. Et l'accumulation de biomasse peut-être considérablement réduite voir stoppée par la pression de broutage, qui est elle-même dépendante du transport. Ainsi, Les processus hydrodynamiques comme par exemple, les courants induits par les marées et le vent ainsi que le mélange turbulent vertical régulent le taux de transport du phytoplancton entre les différents régimes de lumière/pâturage et jouent un rôle important dans l'explication de la variabilité à court terme des efflorescences (Barbosa and Chícharo, 2011; Rowe et al., 2016; Zhou et al., 2023).

Dans l'étude des mouvements spatiaux des efflorescences, les modèles hydrodynamiques de circulation océanique sont des outils puissants, surtout si l'on considère la difficulté d'obtenir des données de terrain relatives à ceux-ci. Des observations venant de suivis côtiers peuvent donner des indications sur l'emplacement où les efflorescences ont tendance à se développer mais ne fournissent pas d'information sur leur taille. Une méthode pour obtenir ces informations peut être l'observation satellitaire de la chlorophylle de surface. Celle-ci peut couvrir de vastes zones à une résolution qui peut être relativement fine (quelques dizaines/centaines de mètres). Cependant, ces observations concernent uniquement les eaux de surfaces, et selon les périodes et les zones d'intérêt, la couverture nuageuse et/ou la turbidité peuvent constituer des limites importantes de cette méthode (Fernandes-Salvador et al., 2021; Spyrakos et al., 2011). De ce fait, les modèles numériques sont des outils pertinents dans la compréhension d'écosystèmes complexes et l'estimation de la connectivité entre zones. Le terme de connectivité peut être pensé différemment selon la discipline d'intérêt. Ce concept peut se référer uniquement au transport physique de particules passives (approche Lagrangienne), à l'advection/dispersion de traceurs passifs (approche Eulérienne) ou peut inclure différentes interactions biologiques avec

l'environnement au cours du cycle de vie pélagique d'un individu (Ghezzo et al., 2015). Dans l'environnement côtier, le concept de connectivité a été principalement appliqué aux études sur la dispersion des larves en utilisant des simulations lagrangiennes de suivi de particules (Ghezzo et al., 2015; Ménesguen et al., 2018; Thomas et al., 2016) et aux études sur la compréhension des trajectoires de dispersion de contaminants organiques pour notamment déterminer la probabilité de contamination, et les voies d'accès entre les sources de pollution et les écosystèmes aquatiques extrêmement précieux (Lindo-Atichati et al., 2019). Pourtant, assez peu d'études se sont intéressées à la connectivité hydrodynamique pour mieux comprendre le déplacement spatial de certaines efflorescences pouvant avoir des effets néfastes sur les pêcheries, les écosystèmes côtiers, la santé publique et les économies côtières. Ces efflorescences sont connues sous le nom d'efflorescences algales nuisibles (HAB, Anderson et al., 2015). La connaissance de leur dynamique apparaît comme un élément essentiel. Pour les HAB où le transport physique peut constituer un contrôle dominant de la distribution des efflorescences, l'approche lagrangienne s'est avérée efficace dans l'étude spatiale des efflorescences. Elle consiste à suivre des particules passives ou des individus ayant un comportement dans l'espace et le temps. D'ailleurs, la grande majorité des études traitant de ce sujet utilise cette méthode (McGillicuddy, 2010). Par exemple, Giddings et al. (2014) ont utilisé des modèles de suivi des particules pour étudier deux voies de transport vers les zones connues où se forment des HAB dans le Nord-Ouest du Pacifique Américain. Li et al., (2014) ont libéré des particules de manière quasi continue sur 7 sites précédemment suspectés d'être des régions sources potentielles d'*Alexandrium fundyense* et ont suivi leur déplacement dans le golfe du Maine. Pinto et al. (2016) ont suivi des particules passives dans un modèle de circulation 3D de la côte ibérique et ont montré la possibilité d'une présence locale de HAB basée sur le transport de cellules toxiques à partir de sources ponctuelles éloignées. Hickey et al., (2013) ont utilisé une approche similaire en lâchant des particules dans un modèle contraint des courants côtiers de l'Oregon et du Washington pour évaluer les influences de l'emplacement de la source, du forçage du vent, et de la présence et des mouvements des panaches d'eau douce sur l'occurrence des efflorescences de *Pseudo-nitzschia* dans la région. Lai and Yin (2014) ont réalisé des expériences approfondies à l'aide de leur modèle physique 3D, afin de vérifier si les zones de convergence physique pouvaient expliquer les HAB localement denses. Ils ont utilisé des particules à flottabilité neutre et à migration verticale dans leur modèle d'une baie du Nord-Est de Hong-Kong, en testant les effets de la stratification et du vent sur l'accumulation des particules dérivantes. Enfin, la modélisation a également démontré que certaines HAB peuvent

être transportées sur de grandes distances avant d'avoir un impact sur les sites d'aquaculture (Fernandes-Salvador et al., 2021).

Les études de transport eulériens sont plus rares et moins traditionnelles dans les études s'intéressant aux efflorescences. Ces approches sont principalement utilisées depuis les années 1970 pour simuler l'eutrophisation, la qualité de l'eau et les processus biogéochimiques (par exemple, Chapra, 2008; Hellweger et al., 2016; Vinçon-Leite and Casenave, 2019). Elles consistent à suivre le panache de dilution, qui d'après nous se rapprocherait plus du comportement des efflorescences, que le suivi particulaire apporté par les simulations lagrangiennes. Les modèles eulériens présentent trois avantages principaux. Tout d'abord, leur forme est relativement simple et, par conséquent, les exigences en matière de connaissances et de données sont moindres (Hellweger et al., 2016). Deuxièmement, ces modèles fournissent une description pratique des équations régissant la masse et la quantité de mouvement qui sont fondamentales pour décrire le mélange et le transport dans les systèmes aquatiques (Soontiens et al., 2019). Troisièmement, les simulations eulériennes sont directement couplées à des modèles hydrodynamiques ; en effet, les modèles hydrodynamiques sont basés sur des formulations eulériennes, qui simulent déjà la salinité et la température qui sont des traceurs eulériens (Ranjbar et al., 2021; Soontiens et al., 2019). Enfin, les simulations eulériennes peuvent être plus facilement comparées avec les observations satellites (Wynne et al., 2011).

Dans la présente étude, nous nous sommes intéressés à comprendre le mouvement des efflorescences dans la zone Ouest-Finistère (Bretagne), régulièrement touchée par les efflorescences de la diatomée toxique *Pseudo-nitzschia australis*. Ces efflorescences sont régulièrement repérées par le réseau français de surveillance du phytoplancton (REPHY, 2022) au début du printemps. Sans que cela n'ait pu être démontré formellement (compte tenu des observations disponibles), l'hypothèse d'un décalage Sud-Nord a cependant été émise, les efflorescences de la rade de Brest (RDB) étant toujours précédées par des efflorescences en baie de Douarnenez (BDZ). Par contre, dans le chapitre 2, nous avons pu mettre en évidence ce décalage sur la même période.

Partant de ces observations, nous nous sommes intéressés aux connectivités hydrodynamiques existantes en période connues d'efflorescences de *P. australi*s dans l'Ouest-Finistère. Pour ce faire, un modèle hydrodynamique réaliste 3D : CROCO (Coastal and Regional Ocean Community model) a été configuré pour la zone Finistère. Des simulations hydrodynamiques sur le mois de mars ont été faites sur quatre années ayant connues des efflorescences plus ou moins importantes (2014, 2017, 2019 et 2021). Afin de modéliser la connectivité hydrodynamique et le transport de traceurs le long de la côte finistérienne, deux méthodes de

transports ont été utilisées. Dans un premier temps, la connectivité entre les zones a été étudiée grâce à une approche Eulérienne qui a permis de suivre les concentrations de traceurs passifs (proxy de la biomasse phytoplanctonique), leur dilution et leur transport, entre différentes zones ouest-Finistérienne au cours du temps. Et dans un second temps, une approche Lagrangienne a permis de suivre la trajectoire de particules individuelles (s'apparentant à des groupes de cellules phytoplanctoniques) au cours du temps.

Les approches de modélisation utilisées dans la présente étude se concentrent exclusivement sur les processus physiques susceptibles d'influencer la dispersion d'efflorescence. Les efflorescences provoquées par différentes espèces de *Pseudo-nitzschia*, dont *P. australis*, ne sont pas entièrement comprises en raison de résultats contrastés concernant leurs conditions de développement dans la littérature (Bates et al., 1998; Bates and Trainer, 2006). Cela suggère la nécessité de mener des recherches exhaustives sur le développement de cette espèce à l'échelle locale. La décision de ne pas tenir compte de ce comportement découle du besoin d'approfondir notre compréhension de l'écologie de l'espèce à simuler. Par conséquent, tout comme les études menées par Stumpf et al., 2009; Velo-Suárez et al., 2010; Wynne et al., 2011, les processus biogéochimiques et l'écologie propre des espèces phytoplanctoniques n'ont pas été pris en compte.

3.2 Matériels et Méthodes

3.2.1 Description générale de la zone d'étude

Le Finistère est situé à l'extrémité Ouest de la Bretagne. Il est bordé au Nord par la Manche, à l'Ouest la mer d'Iroise et au Sud par l'océan Atlantique (fig.1).

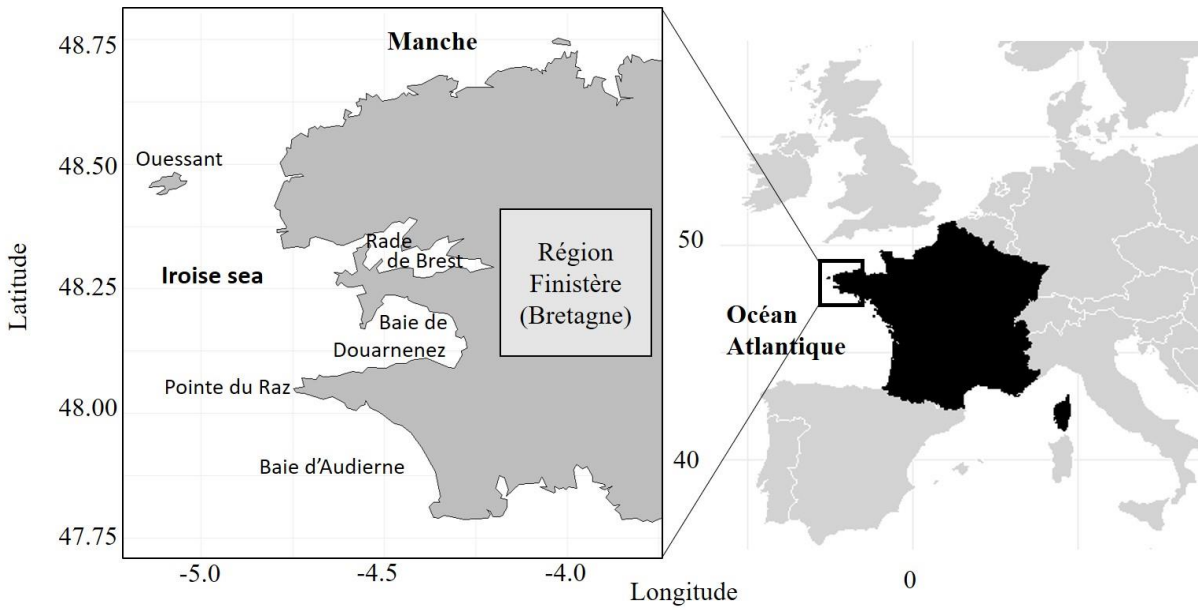

Fig. 1 : Carte de la zone d'étude, le Finistère (Bretagne).

Dans le cadre de notre étude, nous nous intéresserons particulièrement à la partie occidentale de ce département. L'Ouest-Finistère est caractérisé par un littoral relativement fractal, dans lequel de nombreux environnements côtiers sont interconnectés et présentent des caractéristiques hydrologiques (ouverture à l'océan, arrivée plus ou moins importante d'eau douce...) différentes résultant en un système globalement hétérogène. Dans la présente étude, nous nous sommes principalement intéressés à deux zones où des efflorescences régulières de *Pseudo-nitzschia australis* sont identifiées au début du printemps : la baie de Douarnenez (BDZ) et la rade de Brest (RDB) connectées par la mer d'Iroise.

La RDB est un système macrotidal semi-fermé peu profond qui s'étend sur 180 km², avec moins de 15% de sa surface totale dont la profondeur est supérieure à 15 mètres et 50% inférieur à 5 mètres (fig. 3 ; Petton et al., 2020). Cette rade est caractérisée par une marée semi-diurne et un marnage compris entre 1,2 et 7,3 mètres. Le goulet, 1,8 km de large et 6 km de long, est la zone de communication avec la mer d'Iroise (Le Pape and Menesguen, 1997). Il présente les profondeurs les plus importantes (jusqu'à 50 mètres) et les courants y sont les plus forts (jusqu'à 3 m/s en vives eaux). D'une manière générale la RDB est un écosystème énergétique caractérisé par un mélange complexe attribué à la marée, reproductible à chaque cycle et tout au long de l'année. Cet important flux de va-et-vient présent à chaque marée empêche toute stratification durable (Le Pape and Menesguen, 1997), et provoque un mélange vertical intense en hiver et au début de printemps (Cadier et al., 2017). Sur les périodes plus calmes, estivales, les eaux de l'embouchure de l'estuaire de l'Aulne peuvent présenter une stratification haline temporaire.

L'hydrologie de la rade de Brest est dominée par des écoulements d'eau douce provenant principalement de 2 fleuves. L'Aulne fournit 63% des apports annuels d'eau douce (bassin versant de 1875 km^2) et 15% proviennent de l'Elorn (bassin versant de 385 km^2). Des rivières plus petites, La Douffine et la Mignonne fournissent respectivement 8% et 5% des apports d'eau douce (Auffret, 1983). En plus de la marée, les vents peuvent générer du mélange (Petton et al., 2020). Par exemple, des vents forts de sud-ouest (plus de 15 $m.s^{-1}$) peuvent générer des vagues de vent avec des hauteurs significatives de plus de 80 cm dans la partie nord de la baie et dans l'anse de Daoulas (Guillou, 2007; Petton et al., 2020). Dans la zone d'étude, les vents du Sud-Ouest et du Nord-Est sont les principales directions des vents saisonniers (Petton et al., 2020).
En sortie de la rade, la mer d'Iroise est l'un des principaux écosystèmes de front de marée au monde (fig.1), cette mer épicontinentale présente un cycle saisonnier marqué par l'interaction entre le forçage atmosphérique et les courants de marée sur le fond marin peu profond (moyenne de 110 mètres) au-dessus du plateau continental (Le Fèvre and Grall, 1970; Mariette et al., 1982). Du printemps à l'automne, et particulièrement marqué en été, le front de marée d'Ouessant est le principal élément de la structure hydrologique de la mer d'Iroise. Il est situé à quelques kilomètres au large d'Ouessant et rejoint la côte à proximité de la pointe du Raz. Ce front est généré par la présence de forts courants de marée interférant avec l'établissement de la thermocline saisonnière. Le front constitue alors la zone de rencontre entre les eaux stratifiées du large et les eaux côtières mélangées. Le gradient de densité s'équilibre par un courant qui se superpose aux courants de marée et aux courants induits par le vent (Cadier et al., 2017; Le Fevre et al., 1983; Mariette and Le Cann, 1985).
En ce qui concerne la marée, l'onde est semi-diurne (dont le marnage varie de 3 mètres à 7 mètres) et les courants résiduels de marée moyens se propage vers le Nord à l'extrémité Ouest de la Bretagne (Muller et al., 2010). L'interaction avec le littoral et la bathymétrie provoque des courants de l'ordre de 1,55 m/s le long de la côte Nord, autour des îles de Sein et d'Ouessant. S'ils peuvent atteindre jusqu'à 4,11 m/s aux marées de vives eaux dans certains chenaux (Le Duff et al., 1999), ils sont localement assez faibles dans les baies, entre les îles et le long de la côte Sud (0,51 m/s). La circulation, dont l'intensité locale varie d'une région à l'autre, est également contrainte par les courants et les vagues générés par les contraintes du vent de surface.
Enfin, nous nous intéressons à la BDZ, une zone semi-fermée de 350 km^2 peu profonde avec un maximum de 40 mètres. C'est une baie ouverte sur la mer d'Iroise, particulièrement soumise aux houles dominantes d'Ouest (Quiniou, 1986). La configuration de la côte, la bathymétrie et le régime de marée dans la baie conduisent à des courants relativement faibles qui varient entre

0,1 et 1 m/s (Le Fèvre and Grall, 1970). Cette zone est relativement bien brassée par les courants de marées et les vents une bonne partie de l'année, mais présente régulièrement des stratifications thermiques durant les périodes estivales (de juin à septembre) dans sa zone centrale (Guillam et al., 2020; Le Corre et al., 1992).

3.2.2 Le modèle CROCO

Les simulations hydrodynamiques ont été réalisées à l'aide du modèle communautaire CROCO (Coastal and Regional Ocean Community model, https://www.croco-ocean.org/) basé sur le modèle ROMS-AGRIF (Debreu et al., 2012; Shchepetkin and McWilliams, 2005). Dans la version par défaut que nous avons utilisé, ce modèle tridimensionnel à surface libre résout les équations primitives simplifiées de Navier-Stokes, sous les hypothèses d'hydrostaticité, de Boussinesq et d'incompressibilité, ainsi que l'équation non-linéaire d'advection-diffusion de traceurs tels que la température, la salinité ou de tout autre éventuel traceur conservatif ou non. Nous avons choisi ce modèle pour sa capacité à résoudre les très fines échelles pour des zones peu profondes, importantes dans la zone côtière, ainsi que leurs intéractions avec les processus à plus grande échelle.
Une description détaillée des caractéristiques du modèles CROCO est disponible sur la page https://croco-ocean.gitlabpages.inria.fr/croco_doc/ mais, de manière très succinte et simplifiée, les discrétisations spatiales et temporelles de ce modèle peuvent être décrites comme suit :

- La grille spatiale horizontale est une grille Arakawa de type C décentrée où l'élévation de la surface libre, la densité et les traceurs sont calculés au centre de chaque maille, alors que les composantes u et v des courants horizontaux sont calculées respectivement à gauche (sur l'axe est-ouest) et en bas (sur l'axe nord-sud) de chaque maille (fig. 2)

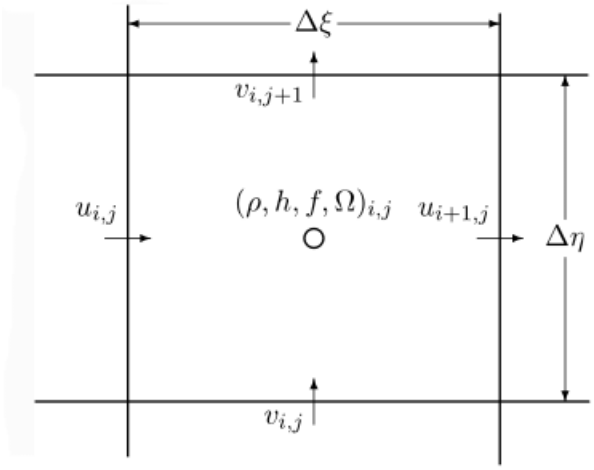

Fig. 2 : Schéma de la grille Arakawa C et position des différentes composantes du modèle (tiré de Couvelard, 2007. Structure et dynamique des jets barotropes créés pas les îles du Pacifique Sud-Ouest).

- La discrétisation spatiale verticale est de type sigma généralisé, qui impose un même nombre de mailles sur tout le domaine, épousant la topographie (fig. 3).

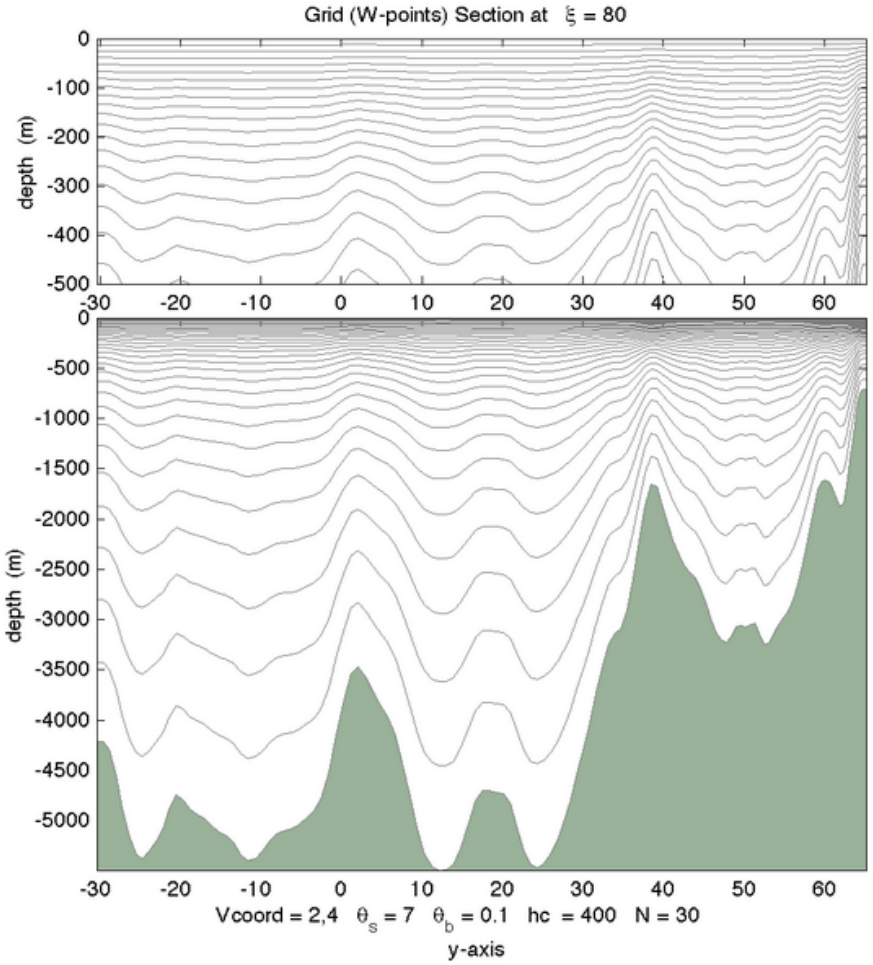

Fig. 3 : Exemple de discrétisation verticale en coordonnées sigma (tiré de la documentation ROMS, https://www.myroms.org/wiki/Vertical_S-coordinate)

Une paramétrisation permet le raffinement de l'épaisseur des mailles près du fond et près de la surface suivant la profondeur.

- Le découpage temporel est hérité de ROMS : un pas de temps pour la dynamique 3D (mode interne, lent) et un autre pour la dynamique 2D (mode externe, rapide). Ces pas de temps sont calculés de façon à respecter le critère CFL (abréviation de Courant, Friedrichs, Lewy), et empêcher ainsi qu'un mouvement ne puisse se propager au-delà d'une maille au cours d'un seul pas de temps.

3.2.3 Le modèle CROCO Iroise

3.2.3.1 Emprise, bathymétrie et discrétisation horizontale et verticale

Le modèle CROCO Iroise dont l'emprise est présentée ci-dessous (fig. 4), s'étend entre 47.9025 N au milieu de la baie d'Audierne à 48.61624 °N au niveau de la commune de Plouguerneau (Finistère, Bretagne) ; et entre -4.087421 °E et -5.292648 °E, à l'ouest de l'île d'Ouessant.

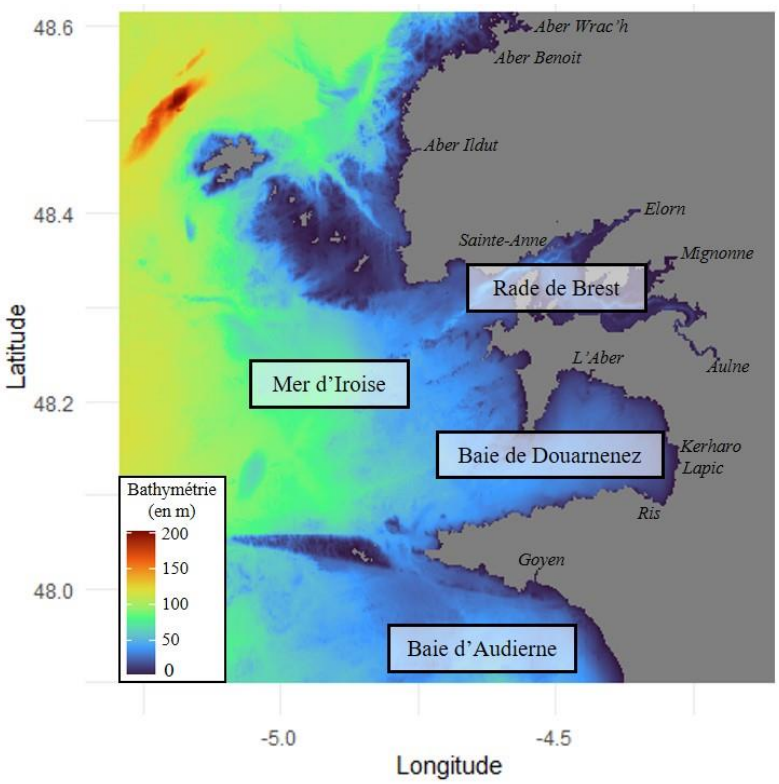

Fig. 4 : Emprise du modèle CROCO Iroise. Les différentes zones d'intérêts, les rivières et la bathymétrie sont indiquées.

Sur l'horizontale, le modèle s'étend sur une grille de 404 x 441 mailles carrées d'une résolution de 200 mètres. L'emprise totale du modèle est donc de 81.2 km Ouest-Est et 88,6 km Sud-Nord. Sur la verticale, 30 niveaux sont pris en compte selon le système de coordonnées sigma simple.

La paramétrisation de ce dernier est faite de façon à ce que contrairement aux coordonnées sigma généralisés décrites précédemment, il n'y ait pas de raffinement en surface et au fond suivant la profondeur. Cela est principalement expliqué par une emprise du modèle principalement côtière dont les profondeurs sont relativement faibles (inférieures à 200 mètres). Le niveau sigma 30 représente la surface et le niveau sigma 1 le fond.
La bathymétrie du modèle (visible dans la figure 4) a été construite à partir des données MNT bathymétrique de la façade Atlantique (Projet Homonim) d'une résolution de 0,001° (~ 111 mètres) (SHOM, 2015).

3.2.3.2 Forçages, conditions aux limites et conditions initiales du modèle

Les différents forçages du modèle sont de type réaliste de façon à simuler l'hydrodynamique de la manière la plus proche de la réalité possible :

(1) Les débits journaliers des 7 fleuves côtiers les plus importants de notre emprise (Aulne, Elorn, Mignonne, Aber Ildut, Aber Benoît et Aber Wrac'h ; fig. 4) proviennent de la banque HYDRO (hydroPortail ; https://www.hydro.eaufrance.fr). Pour les plus petits fleuves (Sainte-Anne, l'Aber, le Kerharo, Lapic, Ris ; fig. 4) absents de la banque HYDRO, des climatologies de débits mensuels ou annuels ont été créées sur la base de données de la littérature quand elles étaient disponibles ou à partir des surfaces de bassin-versant.

(2) Les forçages atmosphériques sont issus du modèle AROME (Météo France, Seity et al., 2011), et concernent : la température (t2m), l'humidité (rh), la nébulosité (fcc), les précipitations (rain), le vent local à 10 mètres (U(10m) et V(10m)), la pression au niveau de la mer (P(mer)), le flux thermique descendant au sol (swhf) et le rayonnement de surface (swhf et lwhf).

(3) Aux trois frontières ouvertes du modèle (Nord, Sud et Ouest), les conditions aux limites suivantes sont appliquées. Les variations de hauteur d'eau dues à la marée sont calculées sur la base de l'Atlas Previmer avec 37 ondes de marées. Pour les traceurs température et salinité les sorties d'un modèle de plus grande emprise sont utilisées après interpolation sur notre grille CROCO-IROISE (MARS3D, configuration MANGAE2500).
Les conditions initiales pour les différentes variables sont issues des sorties MARS3D-MANGAE2500 interpolées sur la grille. Afin de s'éloigner de ces conditions initiales et de

rejoindre un signal cohérent sur ces paramètres, un *spin-up* de 1 mois a été réalisé systématiquement avant toute simulation.

3.2.3.3 Validation du modèle

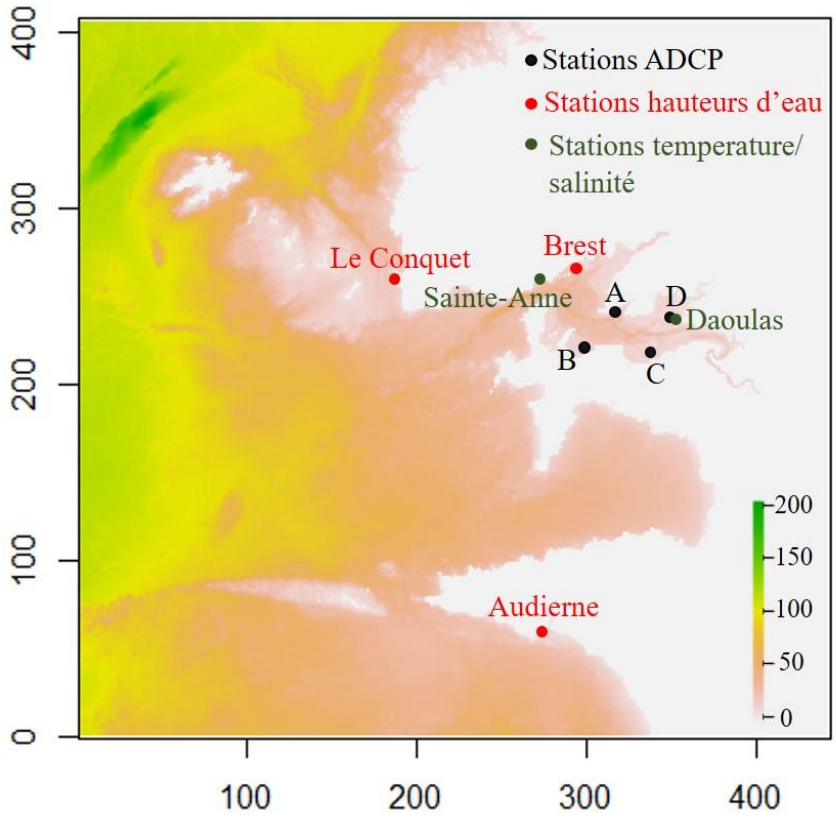

Fig. 5 : Stations de suivis in situ utilisées pour les comparaisons aux données simulées. Les couleurs représentent la source des données : Marégraphes du Shom-Refmar pour les rouges (REFMAR. http://dx.doi.org/10.17183/REFMAR), Stations d'océanographie côtière opérationnelles pour les verts (Coriolis Côtier, https://data.coriolis-cotier.org/cotier), mesures ponctuelles pour les noires (Petton et al., 2016).

Afin de s'assurer de la fiabilité du modèle hydrodynamique, et d'avoir une idée de sa capacité à reproduire les conditions hydrodynamiques réelles, les données simulées ont été comparées à des données mesurées *in situ*. La validation a porté sur les variables suivantes : la hauteur d'eau (la marée), les vitesses et directions des courants baroclines, la température et la salinité.
Selon les périodes de disponibilité des différentes variables, pouvant provenir de suivis spécifiques, les périodes de validation peuvent différer.

Les variations de hauteur d'eau (marée) proviennent de 3 stations marégraphiques (REFMAR, http://dx.doi.org/10.17183/REFMAR) : Brest (48.38290024; -4.49503994), Le Conquet (48.359098; -4.78075) et Audierne port (48.02155; -4.537583 (stations en rouge, fig. 5). Le

paramètre zh_ref des métadonnées indique la hauteur d'eau et a été comparé à la valeur zeta venant du modèle CROCO entre le 1er et le 15 mars 2021.

Les données de courants proviennent de profileurs acoustiques ADCP placés dans l'Anse de l'Auberlac'h (station A ; 48.32719, -4.429694), et l'Anse du Fret (station B ; 48.29158, -4.484111) pendant un mois, puis déplacés vers le Lomergat (station C, 48.28769, -4.369667) et l'Anse du Roz (station D ; 48.32069, -4.339944) pendant un autre mois (stations en noire, fig. 5). Ces données sont des moyennes des courants (vitesse et direction) sur 10 minutes et ont été fournies par Petton et al., 2016. Les mesures de courants zonaux (Ouest-Est, composante Uz) et de courants méridionaux (sud-nord, composante Vz) ont été comparées avec le modèle CROCO Iroise sur les périodes du 5 au 10 octobre pour les stations A et B et entre le 25 et 30 novembre pour les stations C et D.

Enfin, les données de salinité et de température proviennent de deux stations de suivis haute fréquence (stations en vert, fig. 5). La première, la bouée COAST-HF MAREL-Iroise (48.357, -4.582) est située à l'entrée de la RDB et enregistre des données toutes les 20 minutes à 2 mètres de profondeur depuis l'année 2000 (Rimmelin-Maury et al., 2023). La deuxième station est appelée Pointe du Château (48.335; -4.319, station Daoulas sur la fig. 5) et est située sur une ferme ostréicole dans la zone intertidale gérée par le réseau d'observatoires de l'Ifremer ECOSCOPA. Les données de température et de salinité sont disponibles à une fréquence de 15 minutes depuis 2008 (Petton et al., 2022). Dû à la position des différentes stations de prélèvement, les données de surface (niveau sigma = 29) du modèle ont été comparées à la bouée Marel-Iroise, et les données de fond (niveau sigma=10) ont été comparées avec la station de de la Pointe du Château. Cette validation a été réalisée sur l'année 2021 entre le 1er janvier et 31 juin.

Afin de comparer les données simulées et observées, différents indicateurs ont été calculés :

- L'Erreur Moyenne absolue (mean absolute error, MAE), définie comme la moyenne de la différence absolue entre les valeurs modélisées et les valeurs mesurées *in situ*.

MAE = $$\mathrm{MAE} = \frac{\sum_{i=1}^{n} |y_i - x_i|}{n}$$

Où y sont les valeurs de données mesurées, x les valeurs de données simulées et n le nombre d'observations.

-L'Erreur maximale absolue (Maxerr), définie comme étant la plus grande différence absolue entre les valeurs modélisées et les valeurs mesurées *in situ*.

- L'erreur minimale absolue (Minerr), définie à l'inverse du Maxerr comme la différence la plus faible absolue entre valeurs modélisées et les valeurs mesurées *in situ*.

- La déviation de la racine de la moyenne des carrés (RMSD, Root-Mean-Square Deviation), représente la moyenne quadratique des différences entre les valeurs obtenues par le modèle et les valeurs mesurées *in situ.*

RMSD = $\sqrt{\frac{\sum_{i=1}^{n}(X_i - Y_i)^2}{n}}$

Où x sont les données observées, y les données simulées et n le nombre d'observations

- Les résultats du test de régression linéaires. Le coefficient de corrélation r^2, la p-value et le degré de liberté sont indiqués.

3.2.4 Caractérisation de la connectivité hydrodynamique, méthodes et analyses des simulations

Des simulations de transport de traceurs eulériens et lagrangiens ont été réalisées pour déterminer la connectivité hydrodynamique Ouest-Finistère ayant eu lieu durant les mois de mars (du 1er au 31) 2014, 2017, 2019 et 2021.

La connectivité hydrodynamique a été caractérisée respectivement :
- par le suivi des masses de traceurs issus d'une zone d'initialisation, arrivant dans une zone d'arrivée (pourcentage maximal de la masse initiale émise (Pmax), temps d'arrivée (Tmax)) pour les simulations Eulériennes.
- par le suivi des trajectoires et du nombre de particules issues d'une zone d'initialisation et arrivant dans une zone d'arrivée, pour les simulations Lagrangiennes.

L'advection/dispersion des traceurs Eulériens se fait online, au même pas de temps que le calcul des équations primitives hydrodynamiques. Un pas de temps de sortie a été configuré toutes les 30 minutes du 1er mars au 31 mars minuit.

Le calcul du transport des particules Lagrangienne se fait offline, en utilisant les sorties des simulations précédentes (toutes les 30 minutes). Le transport Lagrangien a été caractérisé sur 15 jours, avec un lâché au 1er mars.

La manière dont sont calculés les indicateurs de connectivité que nous avons retenus est décrite ci-après.

3.2.4.1 Transport Eulérien

Dans ce chapitre, deux approches ont été utilisées : une première visant à caractériser globalement la connectivité existante sur une partie de l'emprise du modèle et la deuxième visant à se focaliser sur les deux zones impactées par les efflorescences toxiques : la BDZ et la RDB.

3.2.4.1.1 Première approche, méthode des quadrillages

- Description

Sur une partie de l'emprise du modèle, 21 zones d'une surface de 50 x 50 mailles de grille ont été sélectionnées (fig. 6). De manière à répondre du mieux possible à notre problématique, les zones qui nous intéressent se limitent aux zones proches de la côte et englobent la BDZ et la RDB. Chacune de ces zones représente à la fois une zone de départ d'un traceur eulérien conservatif et une zone d'observation de l'arrivée des traceurs issus des 20 autres zones.

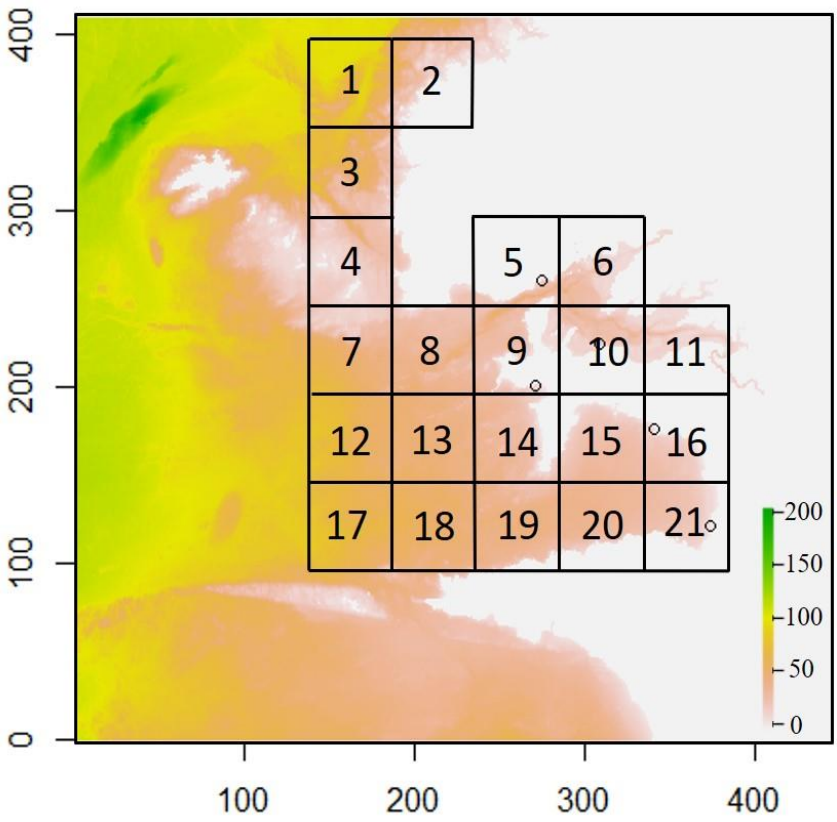

Fig. 6 : Quadrillage de l'emprise du modèle CROCO-Iroise en 21 zones.

La taille des zones de départ et d'arrivée des traceurs a été décidée sur la base de compromis entre les facteurs suivants : les échelles spatiales sur lesquelles se développent les efflorescences, la topographie/morphologie complexe du trait de côte Finistérien, et le temps de calcul lié aux nombres de traceurs à transporter.

Même en acceptant un coût de calcul plus élevé, une délimitation de zones plus petites ne nous semblait pas idéale du fait d'un manque d'informations précises sur la surface des efflorescences phytoplanctonique, mais également dû au fait qu'il faut trouver un juste milieu entre le nombre de traceurs émis et le temps de simulation ayant une influence sur le coût de calcul.

Sans espérer pouvoir caractériser la variabilité totale interannuelle pour laquelle il faudrait simuler beaucoup de périodes et d'années. Dans la présente étude, le choix a été fait de caractériser la connectivité sur différentes périodes favorables au développement de l'espèce toxique *P. australis*.

Ainsi, 21 traceurs différents ont été lâchés au même moment le premier mars et suivis pendant une période d'un mois. Quatre simulations réalistes ont été réalisées pour les mois de mars 2014, 2017, 2019 et 2021. Le mois de mars a été choisi car il s'agit d'une période reconnue (REPHY, 2022) dans la région pour les efflorescences de *P. australis*, et les années ont été

choisies suite à des efflorescences identifiées plus ou moins importantes. En 2014 et 2017, d'importantes efflorescences de *P. australis* ont été notées, associées à des évènements ASP ; en 2021, bien que moins importantes, *P. australis* s'est développé dans la région avec également des évènements ASP ; enfin, en 2019, l'efflorescence de *P. australis* a été moins prononcée (voir introduction).

- Indicateurs de connectivité

Le découpage du trait de côte et les forts gradients bathymétriques imposent des volumes de zones différents, donc des quantités initiales de traceurs différents. De façon à supprimer ce biais, la masse initiale de traceur dans chaque zone a été calculée, et les quantités observées dans les différentes zones d'arrivée sont rapportées à cette masse initiale. Les résultats seront donc présentés ci-après en pourcentage de la masse initiale.

Dans un premier temps, les caractéristiques de la structure verticale des masses d'eau en mars ont été regardées (fig. 7 et 8). Des différences de densité de l'eau de mer engendre des mouvements, par des différences de température et de salinité des masses d'eau (circulation thermo-haline). Les profils en profondeur de la salinité et de la température réalisés par le REPHY (REPHY, 2022) ont montré une absence de stratification sur les mois de mars 2014, 2017, 2019 et 2021 au Sud de la BDZ (à la station de Kervel), et au Sud de la RDB (à la station de Lanvéoc).
Les profils de température et salinité sont représentés dans la figure 7, et ceux de la masse volumique potentielle ($\rho = 1000 - 0{,}12 * T + 0{,}35 * S$ (en $kg.m^{-3}$) où ρ est la masse volumique, T la température, et S la salinité) dans la figure 8.

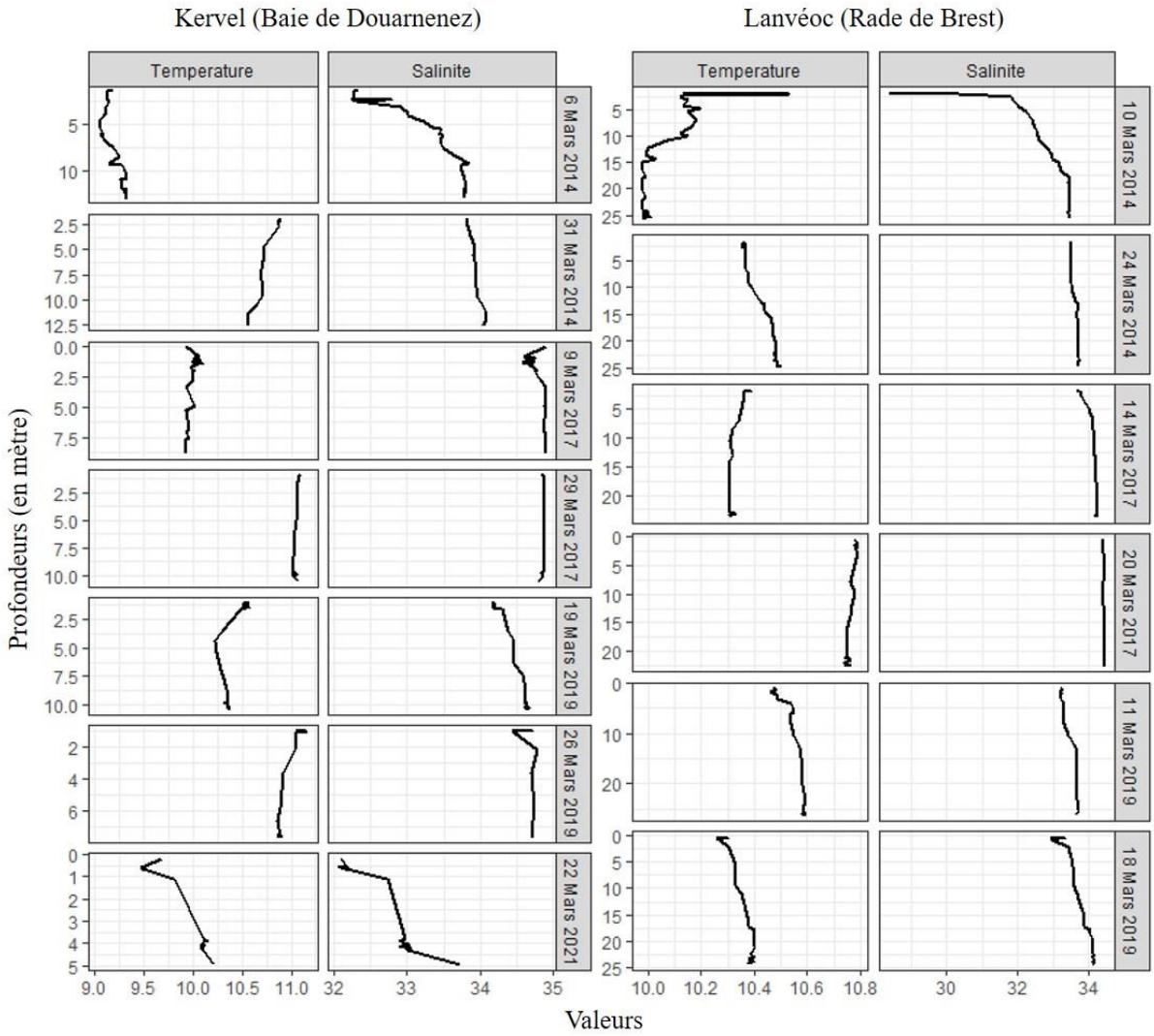

Fig. 7 : Profils verticaux de température (°C) et de salinité (PSU) réalisés par le REPHY en BDZ (station Kervel) et en RDB (station Lanvéoc).

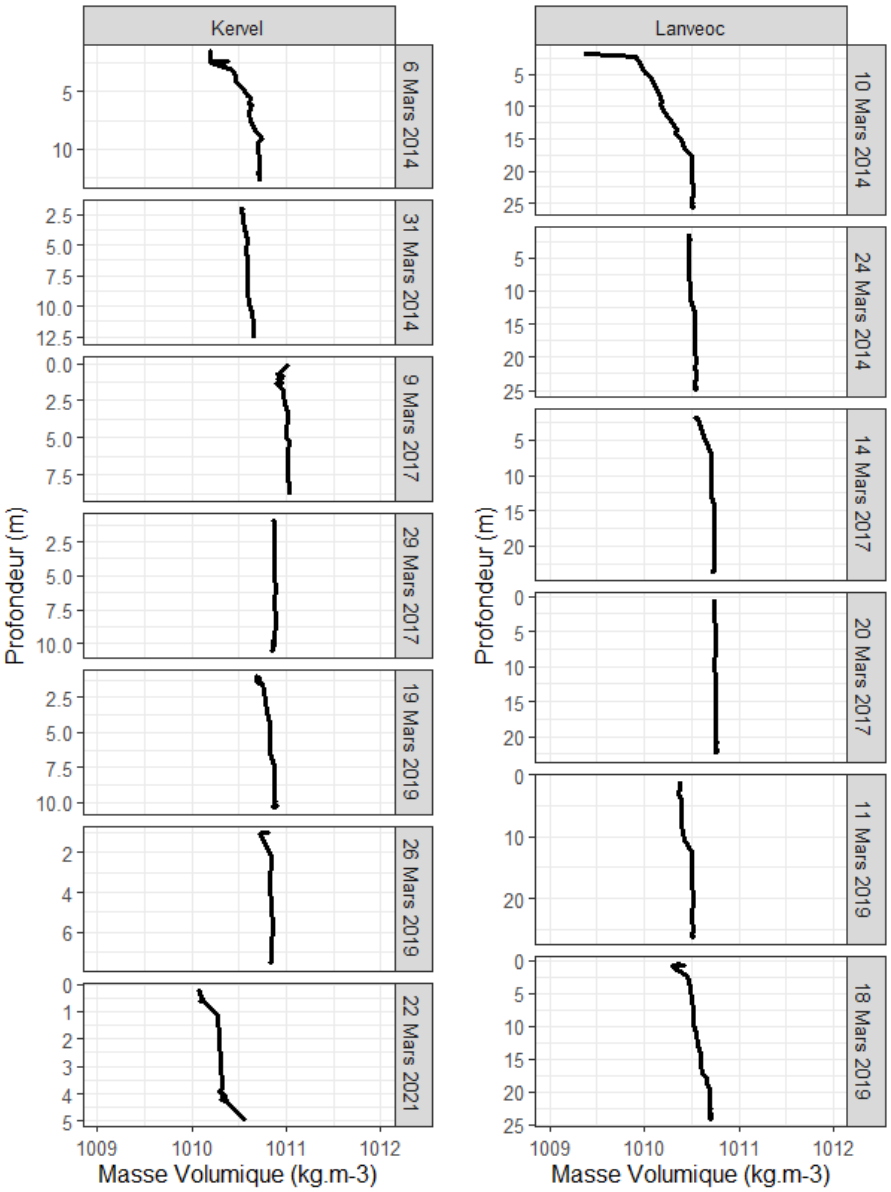

Fig. 8 : Profil vertical de l'évolution de la masse volumique (kg.m^{-3}) en BDZ (station Kervel) et en RDB (station Lanvéoc).

L'observation des figures 7 et 8 nous confirme l'absence de stratification sur les mois de mars que ce soit dans la BDZ ou la RDB, une concentration de 100% de traceur a donc été initialisée sur toute la colonne d'eau (les 30 couches sigma) aux 21 zones.

Ensuite, pour permettre une comparaison des quantités de traceurs qui parviennent à une station donnée, nous avons calculé le pourcentage de la masse initiale pour chaque traceur de la façon suivante :

1. La masse totale de chaque traceur dans chaque zone à chaque pas de temps a été calculée.

2. La masse totale de traceur arrivée dans une zone a été divisée par la masse initiale partie d'une autre zone.

Ainsi, pour chacun des traceurs, l'évolution du pourcentage de masse initiale a été identifiée et analysée sur toute la durée des simulations.

Les connectivités hydrodynamiques entre chacune des 21 zones ont été caractérisées grâce à deux indicateurs **:** le pourcentage maximal de masse initiale de traceur (Pmax) et le temps associé à ce maximum (Tmax) (fig. 9).

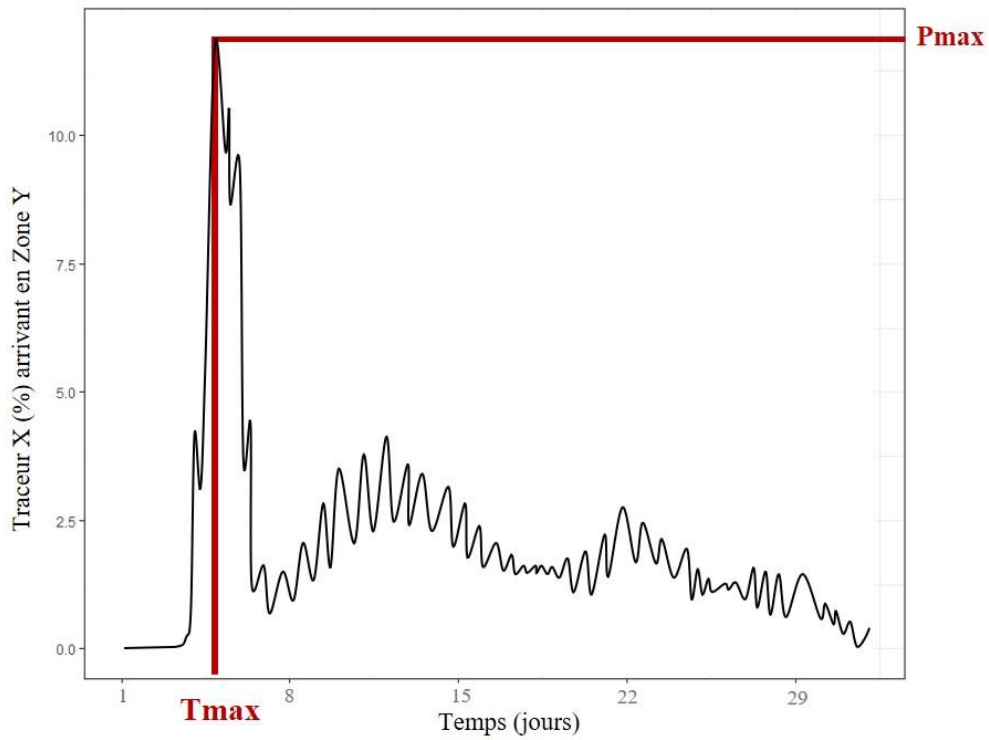

Fig. 9 : Indicateurs de connectivité (en rouge), la ligne noire représente l'évolution du pourcentage de masse initiale du traceur partant d'une zone X et qui arrive dans une autre zone Y.

Face à la problématique des efflorescences motivant la présente étude, les aspects masse de traceur et temps de transport nous semblent d'égal intérêt. Nous avons donc fait le choix de caractériser la connectivité eulérienne hydrodynamique entre deux zones à la fois par la quantité maximale et par le temps mis par un traceur pour atteindre la zone d'arrivée. Ces choix ont été motivés par le fait que nous considérons qu'un maximum de cellules doivent être déplacées pour qu'elles puissent se développer dans une zone. En effet, nous avons plus haut dans le chapitre évoqué des différences de courants entre la baie de Douarnenez et la rade de Brest, plus fort en rade de Brest. Ainsi, afin que des cellules se développent dans une zone où potentiellement les taux de croissance sont nuls ou négatifs, il est important que l'importation

de biomasse soit plus rapide par rapport à l'exportation ou aux pertes locales pour que cette dernière s'accumule (Lucas and Deleersnijder, 2020).

Les différents indicateurs de connectivités ont été représentés sous la forme de matrices 21 x 21, avec l'axe des abscisses représentant les zones de départ et l'axe des ordonnées les zones d'arrivée.

Il convient également de noter que le volume mouillé de chaque zone est différent. Nous avons donc fait le choix comme décrit auparavant de diviser la masse de traceur dans une zone d'arrivée par la masse initiale émise dans la zone de départ. Ceci implique d'adopter une lecture horizontale des matrices de connectivité Pmax, zone d'arrivée par zone d'arrivée. Par contre, la matrice de connectivité Tmax peut être lue dans les deux sens.

- Départ haute-mer *versus* basse-mer

Des départs de traceurs à marée basse et à marée haute ont été testés afin de vérifier si des différences importantes sont identifiées en termes de résultats sur les indicateurs. Les différences entre les valeurs des indicateurs ont été calculées et vérifiées entre les deux départs. Les différences de Pmax ont impacté seulement les zones proches. Les départs aux différentes marées ont entraîné des sorties plus ou moins rapides des traceurs dans les zones toutefois, les différences nous semblaient négligeables. Les plus grandes différences étaient principalement sur les lâchers de traceurs en dehors des baies. Par exemple, la différence de Pmax entre 2 marées du traceur 7 allant à la zone 12 était de 41.4% en 2021, cette valeur était plus importante à marée haute, mais les Tmax étaient similaires (de 0,2 jour). Par contre, aucune différence de Pmax n'a été identifiée entre le traceur partant de la BDZ (zone 16) et arrivant en RDB (zone 10), seul un écart de 0.2 jour à été identifié sur le Tmax, un peu plus rapide en haute mer.

Ainsi, par souci de simplification, nous présenterons ci-après les résultats concernant les départs de traceurs réalisés au moment de la marée haute.

3.2.4.1.2 Deuxième approche, méthode qualitative

Dans cette deuxième approche principalement qualitative, les directions du panache du traceur de surface ont été observés sur 8 jours au départ de la BDZ pour toutes les années simulées.

Afin de comprendre les relations avec les conditions environnementales, les directions et les surfaces des panaches ont été mis en relation avec le vent et les intensités de marée.

Seul le traceur de surface a été observé car les panaches sont similaires sur toute la colonne d'eau (fig. 10).

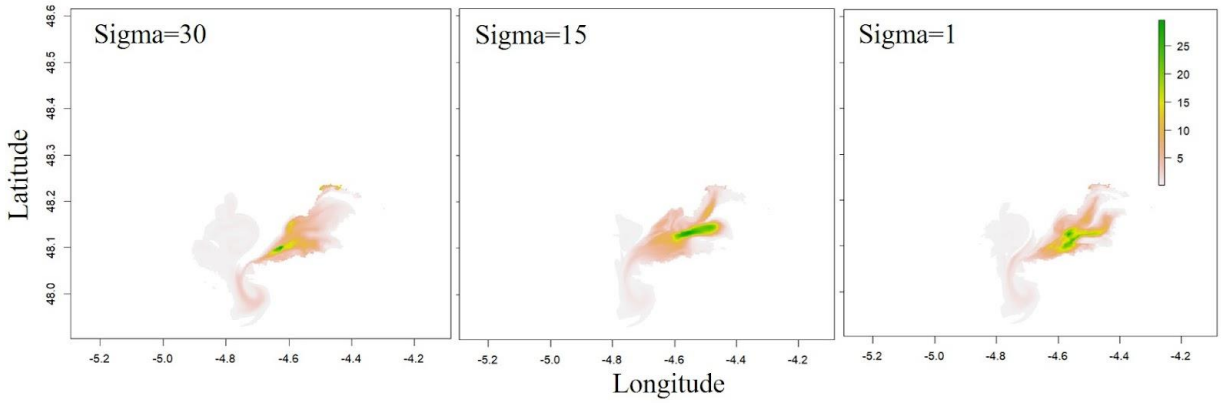

Fig. 10 : Panache du traceur eulérien au bout de 5 jours au départ de la zone 16 (Nord-Est de la BDZ, fig. 6) à différents niveaux de profondeur dans la colonne d'eau. Pour rappel, le sigma de 30 représente la surface, et le sigma de 1 représente le fond de la colonne d'eau. Les couleurs représentent le pourcentage du traceur initial.

3.2.4.2 Transport Lagrangien

En plus du transport Eulérien, qui apporte de l'information sur les connectivités entre les zones par l'utilisation d'indicateurs, le transport Lagrangien nous a permis d'observer les trajectoires de particules individuelles lâchées initialement en un point de suivi situé au Nord-Est de la BDZ, à la station Telgruc.

Le choix de faire partir les simulations à cette station a été motivé par différentes raisons. Cette station a fait l'objet de deux suivis lors de cette thèse, suite à une première identification d*e P. australis* dans une station REPHY située au Sud-Est de la BDZ (Kervel, (REPHY, 2022). Lors de ces suivis en mars 2019 et entre février et avril et mars 2021, des décalages Sud-Nord dans l'identification des diatomées et *P. australis* ont été observés avec une première détection à Telgruc avant d'être observés plus au Nord (chapitres 2 et 4). De plus, des abondances relatives de *P. australis* et des abondances absolues beaucoup plus importantes ont été identifiées à cette station (chapitre 4).

Les champs de courants calculés pour les 4 années de simulations par le modèle hydrodynamique CROCO ont été utilisés et le transport de particules Lagrangienne a été réalisé

offline, grâce au logiciel ICHTHYOP, développé par l'IRD et décrit dans Lett et al., 2008 (https://www.ichthyop.org/).

Pour cet exercice, le modèle ICHTHYOP a été exécuté en faisant partir 1000 particules dans un cylindre de centre 48.209933, -4.373308, au niveau d'une station de suivi d'intérêt, Telgruc. Le cylindre possède un rayon de 500 mètres sur une profondeur de 10 mètres (à partir de la surface). Les particules ont été initialisées comme n'ayant aucun comportement. La dispersion horizontale (par défaut de 10^9 m^2/s^3 sur le logiciel) a été par défaut activée (par défaut de données sur la turbulence, non représenté dans le modèle hydrodynamique CROCO de base), de façon à ce que deux particules partant d'un endroit proche ne suivent pas exactement le même chemin au fil de simulation. De même, la dispersion verticale a été activée.

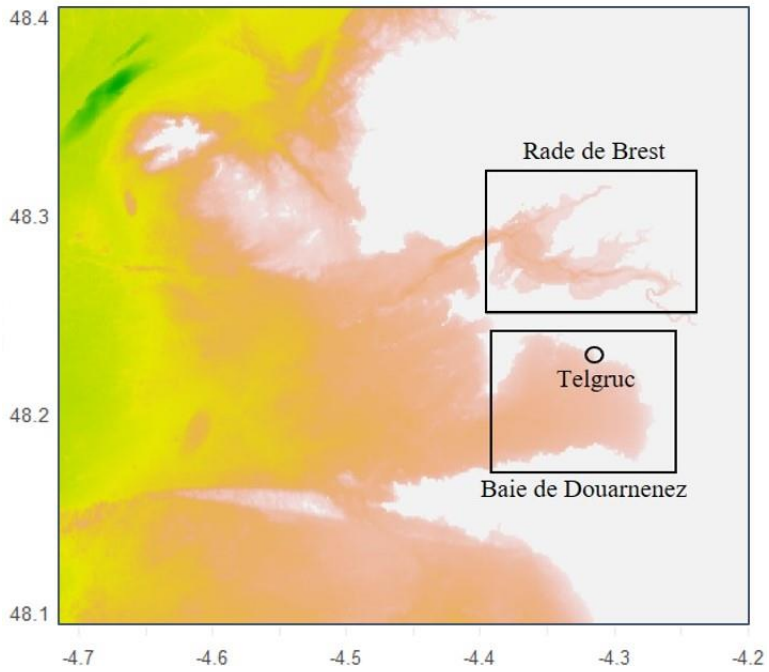

Fig. 11 : Carte représentant la zone de départ au niveau de la station Telgruc (cercle) en BDZ et les zones d'arrivée des particules lagrangiennes suite aux simulations (rectangles), au niveau de la BDZ pour caractériser l'autoconnectivité et au niveau de la RDB.

La connectivité entre la zone de départ à Telgruc et la Rade de Brest a été caractérisée par le nombre de particules cumulées rejoignant la RDB depuis la station Telgruc sur une période de simulation de 15 jours. De plus, les simulations lagrangiennes permettent d'observer les trajectoires privilégiées par les particules ainsi que le nombre de particules qui restent piégées dans la BDZ (autoconnectivité).

3.3 Résultats

3.3.1 Validations du modèle

3.3.1.1 Validation des marées

La figure 12 présente les résultats des comparaisons réalisées entre les mesures et les hauteurs d'eau simulées aux 3 stations marégraphiques.

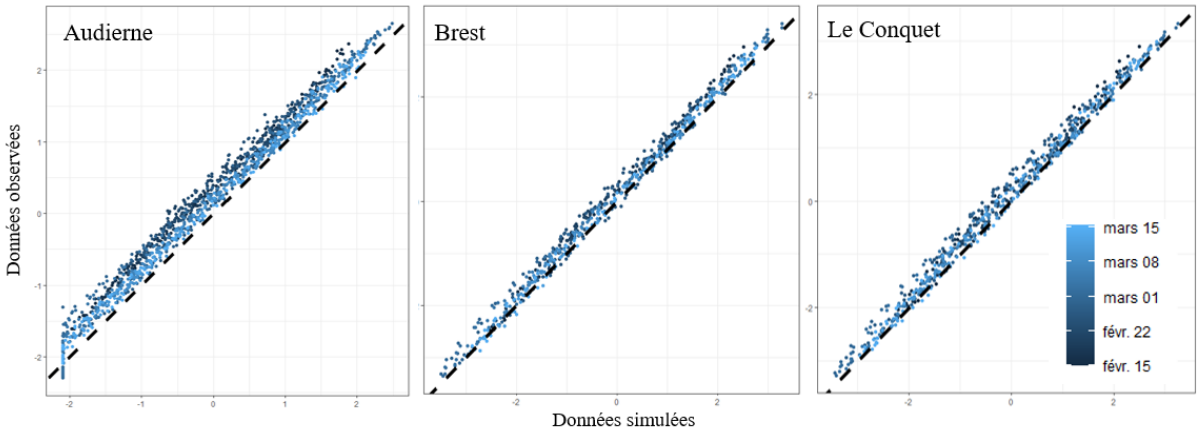

Fig. 12 : Comparaisons des hauteurs d'eau (en mètres) entre les données simulées par le modèle CROCO et les données observées par les marégraphes du SHOM. Les comparaisons ont été réalisées entre le 1er et le 15 mars 2021.

Tableau 1 : Indicateurs de la qualité du modèle à reproduire les variations de hauteurs d'eau aux ports d'Audierne, de Brest et du Conquet.

	MAE	Maxerr	Minerr	RMSD	r^2	Df	*p-value*
Audierne Port	0.26	0.80	0	0.30	0.99	1335	< 0.001
Brest	0.17	0.50	0	0.21	0.99	683	< 0.001
Le Conquet	0.18	0.57	0	0.23	0.99	683	< 0.001

La figure 12 indique une bonne capacité du modèle à reproduire la phase et l'amplitude de marée aux 3 stations avec un RMSD maximum de 0,30 cm à Audierne. Cette station présente également les différences les plus importantes comparées aux deux autres avec des erreurs moyennes de 0.26 cm, et un maximum de différence relativement faible à 0.80 cm (tableau 1). En général, ce qui ressort dans les comparaisons pour les différentes stations est un biais systématique qui montre une légère sous-estimation des hauteurs d'eau du modèle. De plus, les simulations apparaissent plus proches des données observées lors des vives eaux plutôt qu'en mortes eaux. Il est possible qu'une légère erreur sur les niveaux moyens soit à l'origine de ce

biais, mais nous n'avons pas eu le temps de vérifier cela. Les erreurs restent néanmoins très satisfaisantes.

3.3.1.2 Validation des courants

La figure 13 présente les résultats des comparaisons réalisées entre les courants mesurés et simulés en 4 stations en rade de Brest.

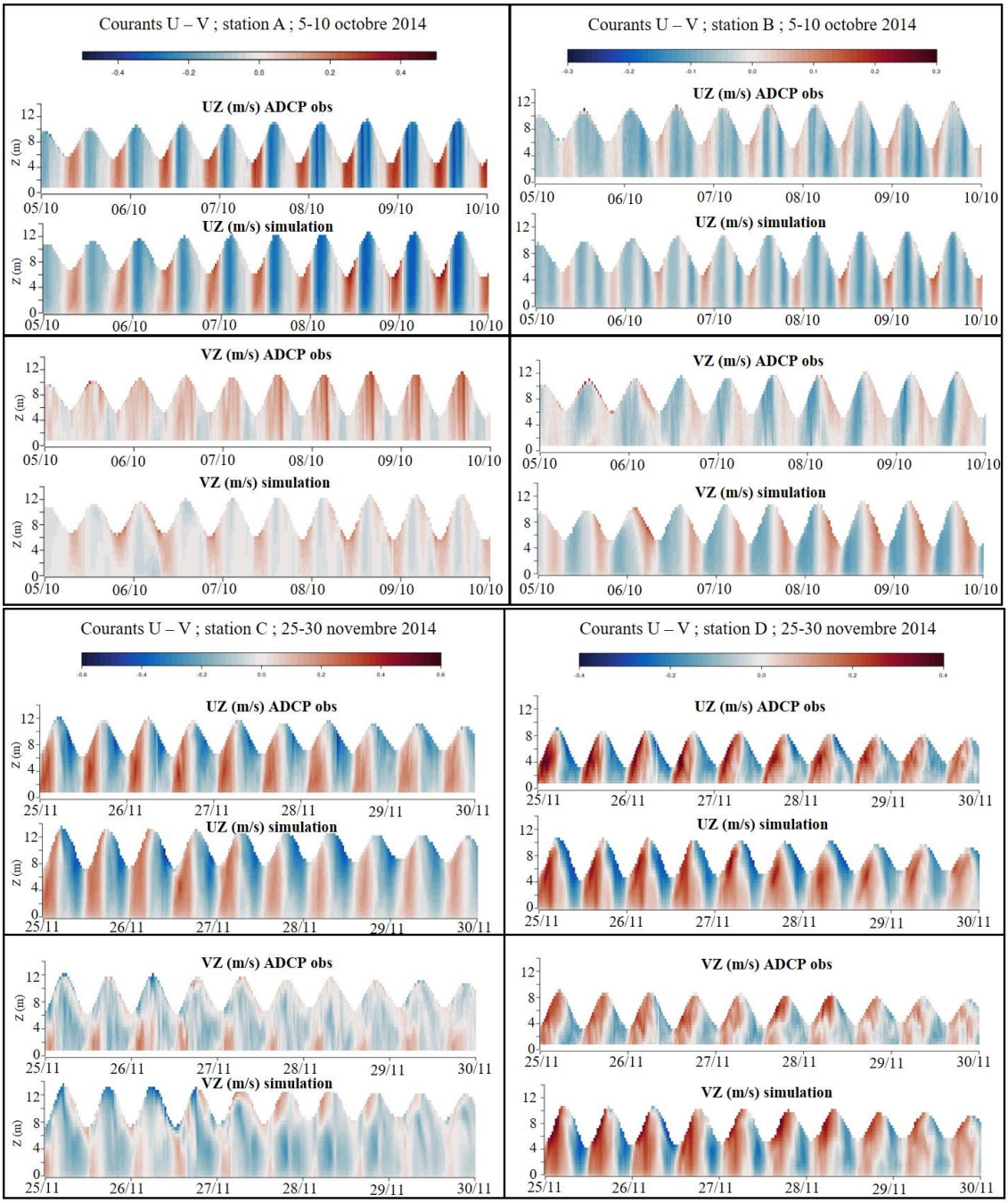

Fig. 13 : Séries temporelles des composantes U et V des courants baroclines simulées et mesurées aux stations A, B, C et D. Deux périodes de 5 jours ont été comparées (5-10 octobre 2014 pour les stations A et B, et 25-30 novembre 2014 pour les stations C et D).

La figure 13 montre que, pour toutes les stations, les courants U et V simulés présentent des dynamiques similaires à celles qui ont été observées *in situ* par ADCP. Les maximums et les minimums des courants simulés sont en phase avec les minimums et maximums des courants observés. Seuls les courants V, notamment à la station A mais également à la station C semblent sous-estimés par rapport aux données mesurées, une surestimation est à noter pour la station B.

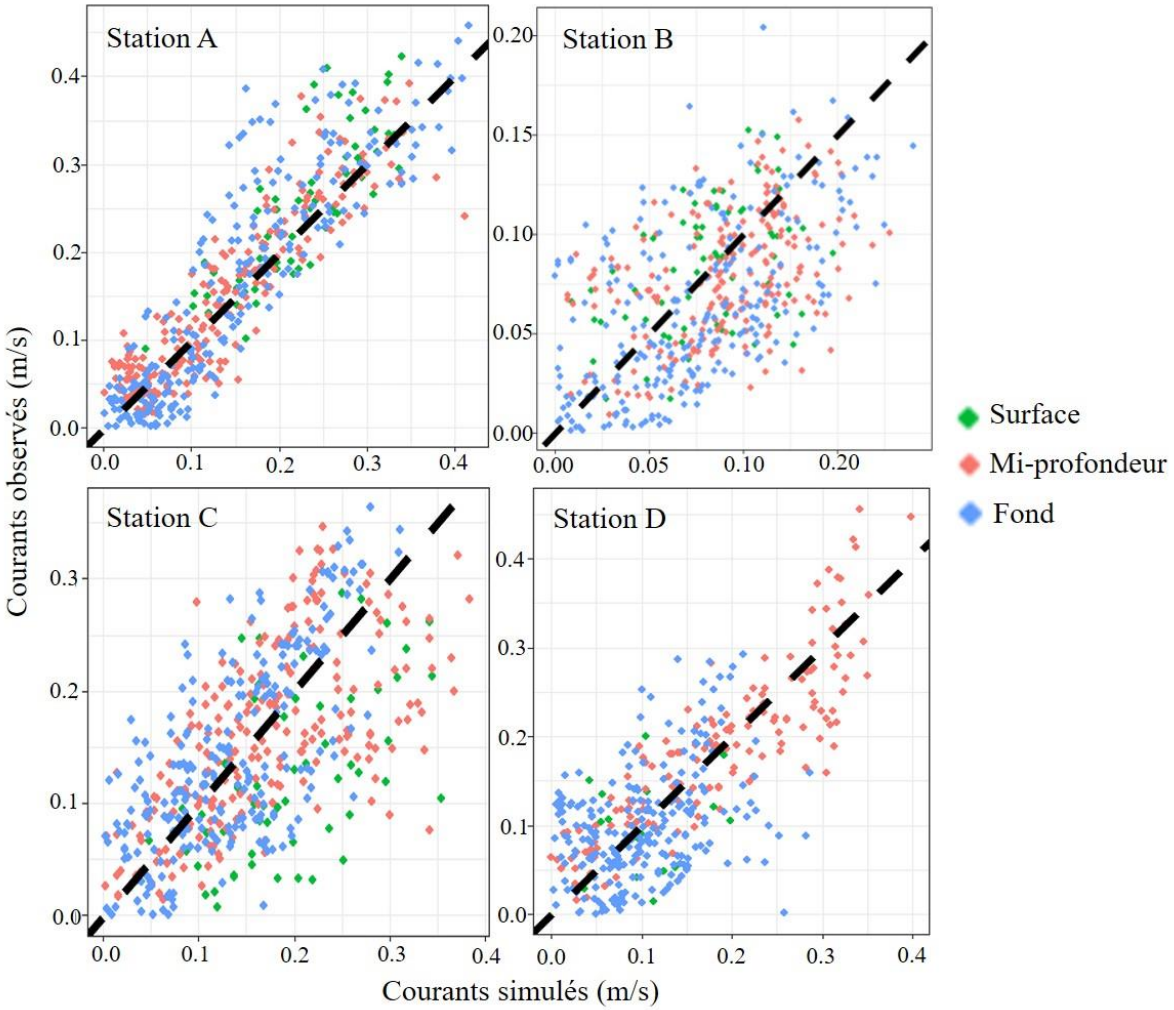

Fig. 14 : Comparaisons des vitesses de courants (en m/s) à 3 niveaux de profondeur (1.3 mètres du fond, à mi- profondeur et en surface) entre les données de courants simulées et les données observées au niveau des stations A, B entre le 5 et 10 octobre 2014 et les stations C et D entre le 25 et 30 novembre 2014.

Tableau 2 : Indicateurs de la qualité du modèle, comparaisons entre les données simulées et observées de courants aux stations A, B, C et D.

	MAE	Maxerr	Minerr	RMSD	r^2	Df	*p-value*
Station A	0.04	0.22	0	0.05	0.81	516	< 0.001
Station B	0.03	0.1	0	0.04	0.28	520	< 0.001
Station C	0.06	0.27	0	0.07	0.39	521	< 0.001
Station D	0.04	0.26	0	0.06	0.56	414	< 0.001

Afin de regarder plus en détail les comparaisons *in situ*/modèle, les vitesses de courants ont été extraites entre le 5 et 10 octobre 2014 au niveau des stations A et B et entre le 25 et 30 novembre aux stations C et D. Les valeurs ont été comparées. La fig. 14 indique une bonne capacité générale du modèle à représenter les données observées, avec un RMSD moyen de 0,06 m/s et une erreur moyenne de 0.04 m/s aux 4 stations (tableau 2).

3.3.1.3 Validation de la salinité et de la température

La salinité et la température ont été comparées à deux stations, Daoulas et Sainte-Anne (fig. 14), entre le 1er janvier et le 30 juin 2021.

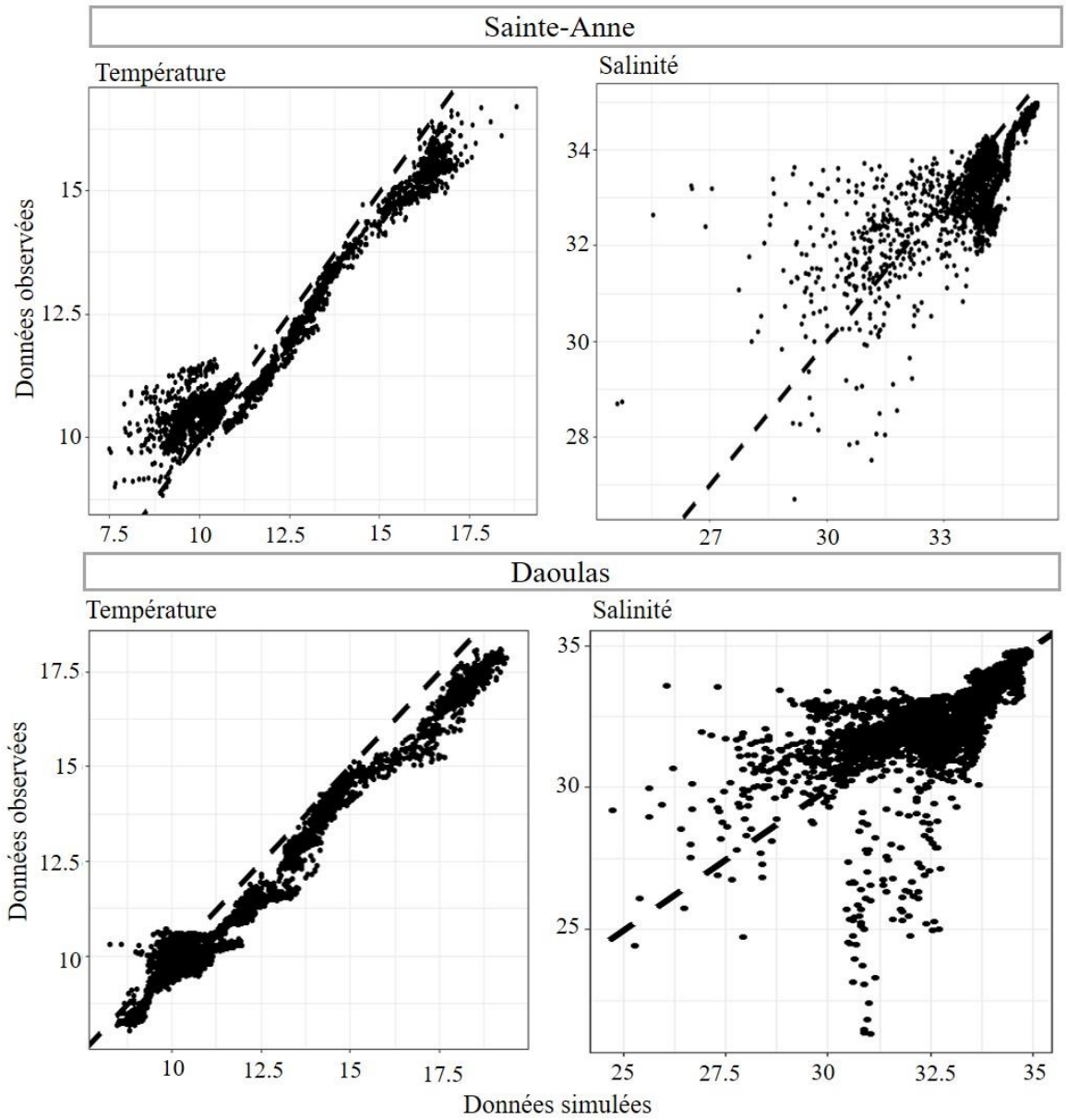

Fig. 15 : Relations entre la salinité (PSU) et la température (en °C) simulées et mesurées à deux stations : Sainte-Anne (en haut) et Daoulas (en bas) entre le 1er janvier et le 30 juin 2021.

Tableau 3 : Indicateurs de la qualité du modèle, comparaisons entre les données simulées et observées à 2 stations : Sainte-Anne et Daoulas pour la salinité et la température.

	MAE	Maxerr	Minerr	RMSD	r^2	Df	*p-value*
Salinité – Sainte-Anne	0.76	7.1	0	0.96	0.60	4201	< 0.001
Température – Sainte-Anne	0.56	2.81	0	0.67	0.95	4201	< 0.001
Salinité - Daoulas	0.73	9.71	0	1.22	0.51	4310	< 0.001
Température - Daoulas	0.66	2.4	0	0.77	0.98	4310	< 0.001

D'une manière générale, les comparaisons sur ces deux paramètres sont satisfaisantes (avec des r^2 compris entre 0.51 et 0.98, tableau 3) qui indiquent que la variabilité temporelle est relativement bien captée par le modèle.
Toutefois, il est à noter que le modèle CROCO a tendance à surestimer les valeurs de salinité au niveau de la station de Sainte-Anne (fig. 15). Cette observation pourrait s'expliquer par une arrivée d'eau locale non prise en compte dans le modèle. Et toujours à Sainte-Anne, les températures faibles sont sous-estimées. Cette observation peut être attribuée à des conditions limites du modèle inexactes, ou peut résulter d'une limitation dans le bilan radiatif du modèle (énergie reçue, devenir de l'énergie arrivant sur les fonds…)
Quant à la station Daoulas, globalement la dynamique saisonnière de la salinité est moins bien captée (r^2=0.51) qu'à la station Sainte-Anne (r^2= 0.60). Des différences de salinité peuvent être assez importantes entre ce qui a été mesuré et simulé, avec un maximum d'erreur à 9.71 PSU et un RMSD de 1.22 PSU, toutefois, l'erreur moyenne est relativement satisfaisante avec une valeur de 0.73 PSU (tableau 3). Contrairement à la salinité, la température simulée suit assez bien la dynamique de ce qui a été mesurée, avec un r^2 de 0.98.

D'une manière générale, les différentes validations effectuées dans le présent chapitre ont été faites afin de s'assurer de la capacité du modèle à reproduire les grandes caractéristiques hydrodynamiques dans la zone considérée. La validation effectuée dans l'étude n'est faite que 6 mois et ne permet pas vraiment de conclure sur la capacité du modèle à reproduire les variations saisonnières. Une validation poussée du modèle CROCO nécessiterait beaucoup plus de comparaisons sur des périodes plus importantes.
Toutefois, les validations de la température et de la salinité se sont avérées satisfaisantes dans l'étude pour aborder de manière confiante le déplacement des traceurs dans l'étude de la connectivité.

3.3.2 Caractérisation interannuelle des vents et des marées en mars dans la zone d'étude

3.3.2.1 Des vents majoritairement d'Ouest

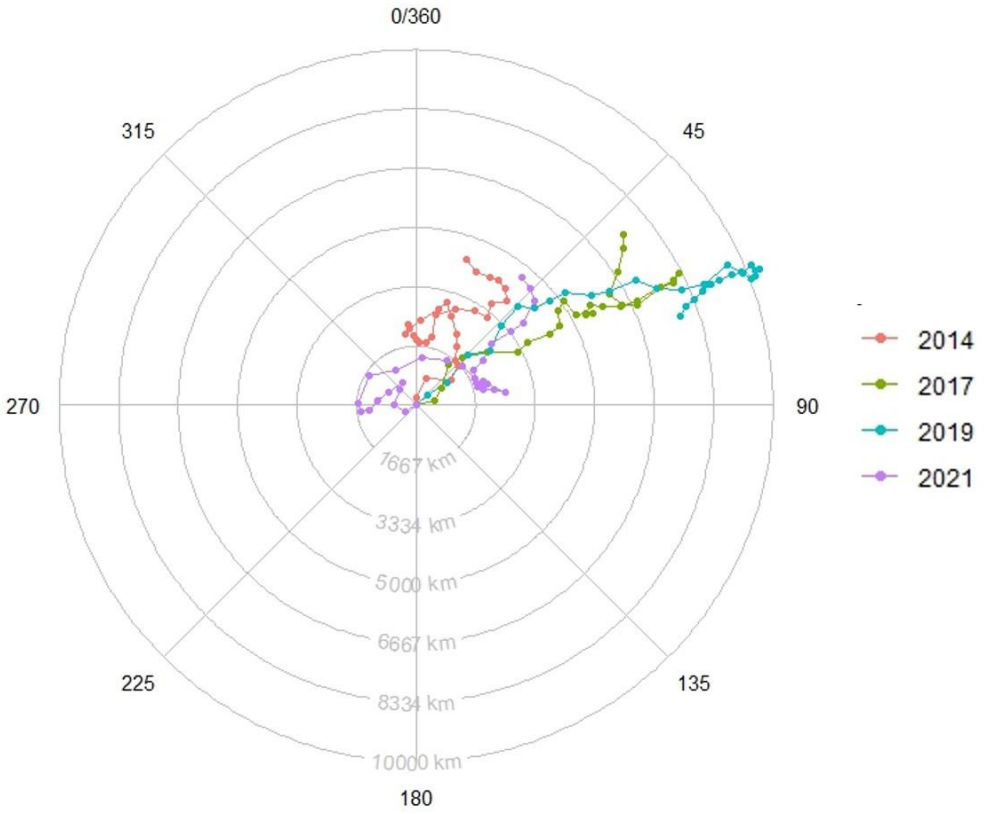

Fig. 16 : Hodographe représentant quotidiennement sur les mois de mars 2014 (en rouge), 2017 (en vert), 2019 (en bleu) et en 2021 (en violet) l'évolution de la direction (direction des traits depuis l'origine) et de la force (espace entre 2 points) du vent. Dans la figure la lecture se fait en fonction de la direction du vent ; par exemple un vent plus ou moins fort du sud (180°) poussera les points plus ou moins vite vers le nord (0°, en haut de la figure).

Les directions et forces du vent sont représentées dans la figure 16. Les quatre années présentaient des régimes de vent majoritairement du Sud-Ouest, mais quelques différences sont tout de même à noter.

Tout d'abord, en 2014, sur les 7 premiers jours du mois de mars les vents provenaient principalement du Sud, avec néanmoins un vent d'Ouest qui présentait une vitesse maximale de 8.2 m/s. Après cette première semaine, les vents étaient assez changeants avant d'être de l'Ouest entre le 19ième et le 24ième jour du mois. À la fin du mois, les vents étaient principalement du Sud-Est.

Deuxièmement, en 2017, les vents étaient principalement du Sud-Ouest, puis du Sud à la fin du mois. Les vents étaient assez forts sur la 1ère semaine avec un pic à 9.8 m/s le 6 mars.

Ensuite, en 2019, tout comme 2017, les vents étaient principalement du Sud-Ouest, avec un changement sur la dernière semaine du mois de mars où ils étaient principalement du Nord-Est. En général, cette année-là, la première semaine a connu des vents assez forts avec une moyenne

maximale de 11.2 m/s le 3 mars, les vents étaient plus faibles à partir du 18 mars où ils étaient principalement inférieurs à 4 m/s jusqu'à la fin du mois.

Pour terminer, les vents en 2021 présentaient des directions assez changeantes au fil du mois de mars, avec une vitesse maximale des vents entre le 10 et le 14 mars (supérieure à 8 m/s). Les 3 premiers jours de mars présentaient des vents d'Est, puis entre le 3ième et le 5ième jour ils étaient du Sud avant d'être du Nord-Est jusqu'au 9ième jour du mois. Les vents ont ensuite été du Sud-Ouest avec des petits changements de directions entre le jour 15 à 23 avec des vents progressivement du Nord, puis d'Ouest et enfin du Sud. La dernière semaine du mois de mars 2021 a principalement connu des vents du Sud-Ouest.

3.3.2.2 Caractérisation des marées

Tableau 4 : Coefficient de marées entre le 1er mars et le 31 mars pour les quatre années de simulation : 2014, 2017, 2019 et 2021 récupérées sur le site marée-info. Les couleurs rougeâtres représentent les périodes de vives eaux et les couleurs bleuâtre, les périodes de mortes eaux.

	2014		2017		2019		2021	
01	108	112	103	101	37	40	106	106
02	114	115	99	95	45	50	105	102
03	114	112	90	84	55	60	98	93
04	108	102	77	70	65	70	87	79
05	96	89	63	57	74	78	71	63
06	80	72	51	48	81	83	55	49
07	64	56	48		86	87	44	
08	48	41	51	56	88	88	42	43
09	35	32	62	69	88	86	48	54
10	32		75	81	85	82	60	67
11	34	38	86	90	79	74	72	78
12	43	50	93	96	70	65	83	86
13	55	61	97	97	59	54	89	91
14	67	72	97	95	49	44	92	92
15	77	81	93	89	42	41	92	90
16	85	88	85	81	44		88	85
17	91	93	76	70	50	58	82	77
18	94	94	64	58	66	76	72	67
19	93	92	52	45	85	93	61	55
20	90	87	40	34	100	107	49	43
21	83	78	31	29	111	114	37	32
22	73	67	30		115	115	28	26
23	61	55	34	40	113	109	28	
24	51	48	47	54	104	97	33	40
25	47		62	69	90	82	48	56
26	50	55	77	84	73	64	65	74
27	62	70	91	96	55	47	82	90
28	78	85	101	105	40	35	97	103
29	93	99	108	109	32		107	111
30	104	107	109	108	31	34	112	112
31	109	109	104	100	39	44	111	107

Les coefficients ont été récupérés entre le 1er et 31 mars pour les différentes années simulées (tableau 4). Dans un premier temps, il est important de souligner qu'à cette période de l'année, nous sommes en période d'équinoxe, ce qui se traduit par des marées de grandes amplitudes, avec des coefficients très élevés qui dépassent généralement les 110.

Lorsqu'on regarde les coefficients des 3 années sur le mois de mars, les coefficients de 2017 étaient légèrement inférieurs aux autres années. Globalement, les années 2014, 2017 et 2021 étaient assez similaires sur leur cycle de marée, avec un début de mois en déchet c'est-à-dire dont les coefficients de marée diminuent et dont les premiers jours présentaient de forts coefficients de marée (>90).

Au contraire, 2019 a connu des marées en revif au début du mois, c'est-à-dire des coefficients de marée faibles qui augmentent. En 2019, les grands coefficients de marée ont été présents entre le 19 et le 25 mars.

3.3.3 Connectivités moyennes sur les 4 années simulées (Pmax et Tmax)

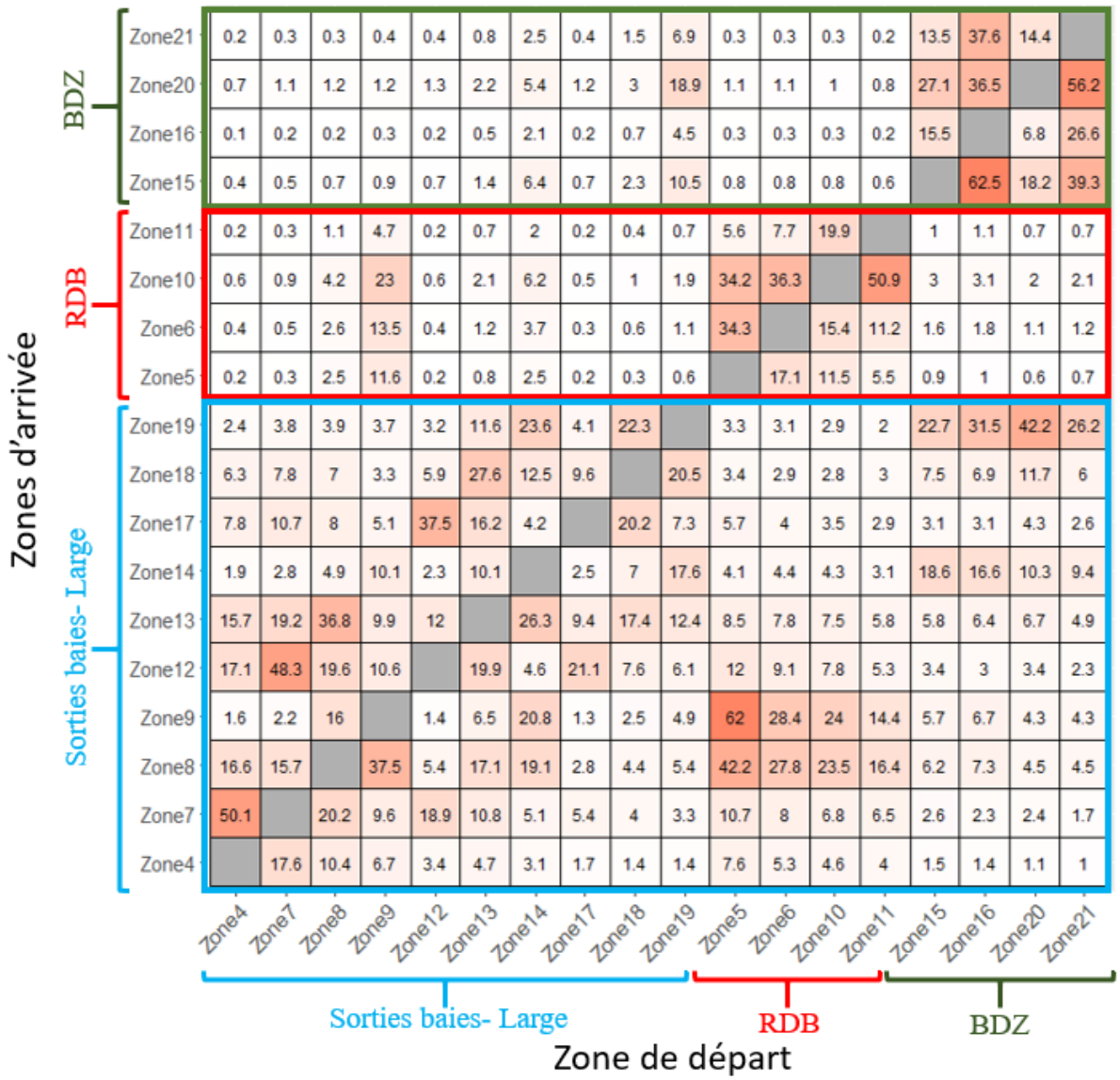

Fig. 17 : Matrices de connectivité Pmax ; La matrice est à lire à l'horizontale en considérant dans les différentes zones, l'arrivée des traceurs venant des 19 autres stations. Par exemple, la zone 7 a reçu en moyenne sur les 4 années un Pmax de 50.1 % du traceur parti de la zone 4.

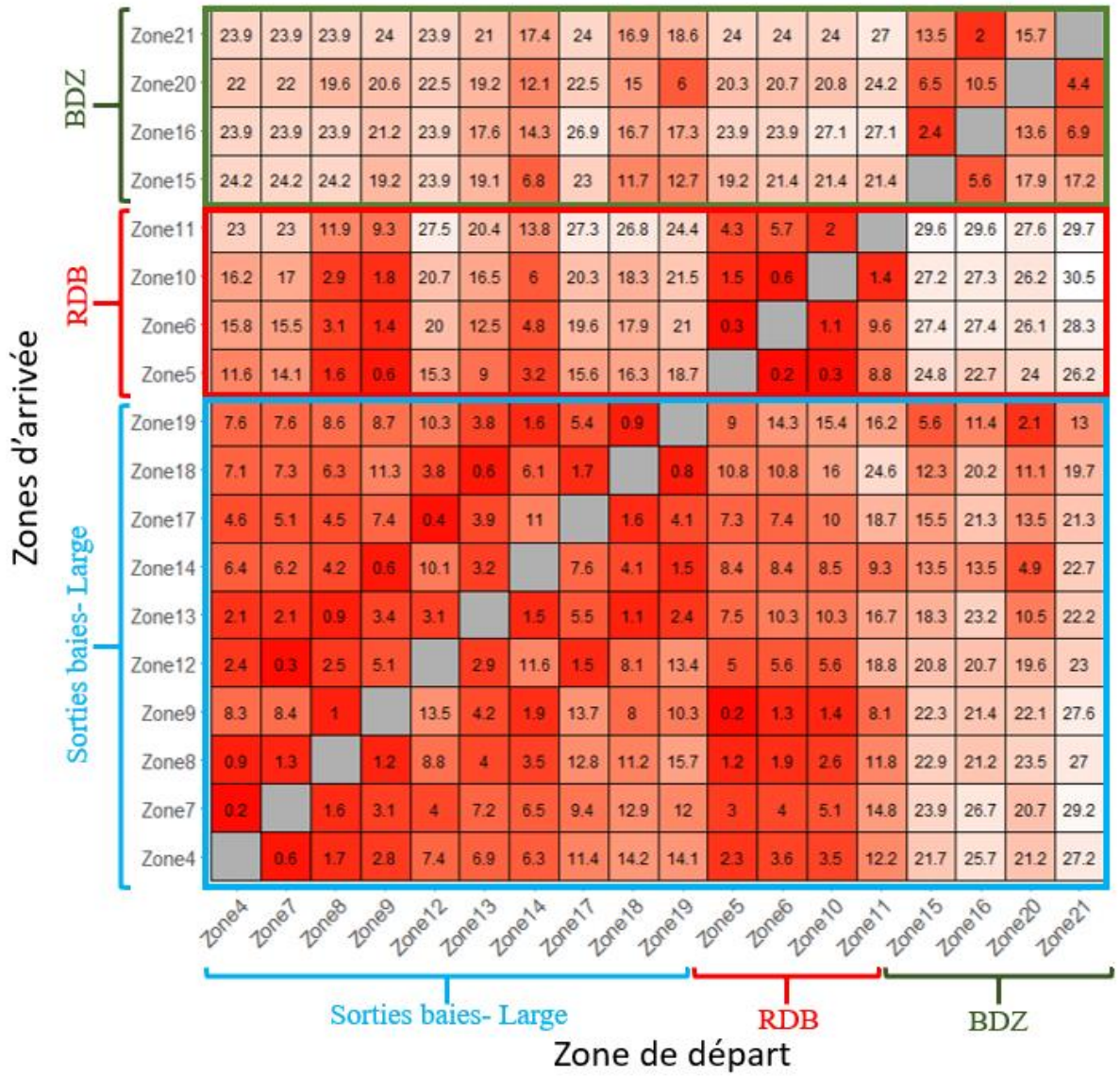

Fig. 18 : Matrices de connectivité Tmax ; La matrice est à lire à l'horizontale en considérant dans les différentes zones, l'arrivée des traceurs venant des 19 autres stations. Par exemple, la zone 7 a reçu en moyenne sur les 4 années un Tmax du traceur parti de la zone 4 en 0.2 jour.

Les figures 17 et 18 représentent respectivement les matrices de connectivité des valeurs moyennes de Pmax et les temps associés (Tmax). En raison de leur proximité avec les limites du modèle, les zones 1, 2 et 3 ne sont pas incluses dans les matrices.

L'analyse des matrices fait logiquement apparaître une forte connectivité (forts Pmax, et faibles Tmax) entre les zones proches les unes des autres.

Globalement, les valeurs de Pmax les plus élevées étaient dans les zones respectivement de la BDZ et de la RDB. Par exemple, pour toutes les années, en moyenne, la plus grande valeur du Pmax a été trouvée à l'arrivée du traceur parti de la station 16 à la station 15 (62.5%), en BDZ.

La deuxième valeur la plus élevée du Pmax a été observée à l'arrivée du traceur 5 dans la zone 9 (62%) en sortie de la RDB. Toutefois, nous pouvons noter que les Tmax associés aux Pmax des zones de la RDB (zones 5-6-10-11) présentent des valeurs plus faibles (< 5 jours) que ceux de la BDZ (> 5 jours sauf pour le traceur 16 arrivant dans la zone 21 ; zones 15-16-20-21). Ce qui suggère des retenues des traceurs plus importantes dans cette dernière. D'ailleurs, en BDZ, une valeur relativement importante de Pmax (39,3%) en zone 15 a été retrouvée avec une valeur importante de Tmax (17,2 jours) en provenance de la zone 21.

Entre la RDB et la BDZ, les valeurs de Pmax et Tmax moyennées montrent peu de connectivité. Au départ de la BDZ, les Pmax sont inférieurs à 2% et les Tmax supérieurs à 24 jours. Au départ de la RDB, les valeurs sont encore plus faibles, avec des valeurs moyennes de Pmax globalement inférieures à 1% et des Tmax associés supérieurs à 19 jours.

Enfin, pour terminer, les résultats des Pmax et Tmax plus au large montrent des valeurs de connectivité plus élevées dans le sens Nord-Sud que Sud-Nord. Pour illustrer, entre la zone 12 et la zone 7, dans le sens Sud-Nord (traceur de la zone 7 à la zone 12) le Pmax moyen était de 18,9% (Tmax = 4 jours), alors que dans le sens Nord-Sud (traceur de la zone 12 à la zone 7), le Pmax moyen était de 48,3% (Tmax = 0,3 jours). Plus au nord de l'emprise du modèle, plus à la côte, ce schéma est identique. Par exemple entre la zone 7 et 4, le traceur au départ de la zone 7 avait en moyenne un Tmax à 17,6% (Tmax = 0,6) alors qu'au départ de la zone 4, le Pmax moyen était de 50,1% (Tmax = 0,2).

3.3.4 Des conditions hydrodynamiques plus calmes en baie de Douarnenez

Dans un souci de simplification, nous avons choisi de ne pas inclure les matrices de connectivité Pmax et Cmax pour chaque année dans la partie principale du chapitre. Elles sont consultables dans la partie matérielle supplémentaire.
Toutefois, l'analyse des matrices de connectivité indiquent des différences interannuelles dans le temps de passage des traceurs Eulériens entre zones au sein des deux baies de l'étude. Prenons deux zones côte à côte orientées Est-Ouest dans chacune des baies. Par exemple en 2014 (mais cela est également le cas quelque soit l'année simulée), en RDB, le pourcentage maximal de traceur partant de la zone 11 et arrivant à la zone 10 était de 63,5% en 0,2 jour. Ceci suggère une arrivée très rapide du traceur. Au contraire, en BDZ, le pourcentage maximal de traceur

partant de la zone 16 et arrivant à la zone 15 était de 70,7% et est arrivé en 9,5 jours, évoquant cette fois-ci, une rétention plus importante qu'en RDB.

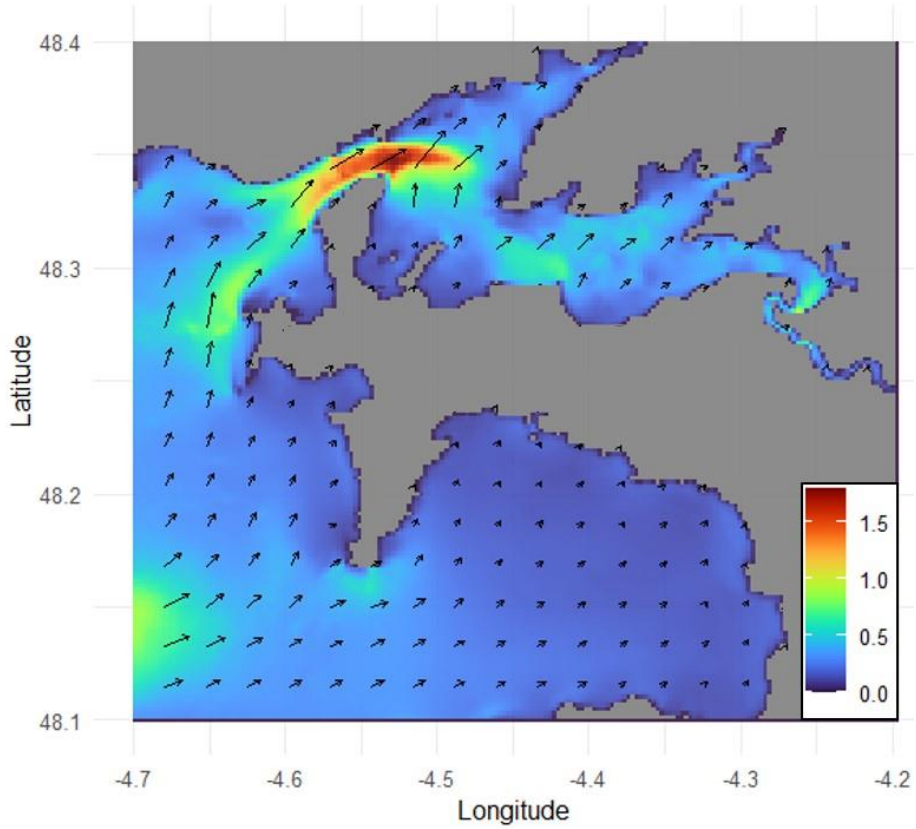

Fig. 19 : Percentile 90 des vitesses de courant (m/s) en mars 2014 (du 1er au 31) observées au niveau de la RDB et la BDZ.

Une explication à ces différences peut être donnée par les courants. La figure 19 illustre le percentile 90 des vitesses de courants sur l'emprise du modèle CROCO Iroise en 2014 (mais les schémas des vitesses de courants sont les mêmes pour toutes les années). Les courants étaient beaucoup plus faibles en BDZ avec un percentile 90 maximum de 0,35 m/s à l'entrée de la baie et une moyenne de 0.17 m/s sur toute la baie. Alors qu'en RDB le percentile 90 maximal était de 1,79 m/s situé au niveau du goulet de la rade, et la moyenne des percentiles 90 était sur toute la rade de 0,35 m/s, deux fois plus important qu'en BDZ (fig. 19).

3.3.5 Une connectivité interannuelle Sud-Nord marquée entre la baie de Douarnenez et la rade de Brest

Afin de vérifier l'hypothèse de développement de micro-algues dans un premier temps au niveau de la BDZ puis quelques temps après en RDB, nous avons spécifiquement étudié la connectivité hydrodynamique entre la BDZ et la RDB.

En se basant sur des suivis réalisés au préalable, le Nord-Est de la BDZ (zone 16) et le Sud de la RDB (zone 10) ont été choisis respectivement comme zone de départ et d'arrivée dans l'étude du transport Eulérien entre les deux baies.

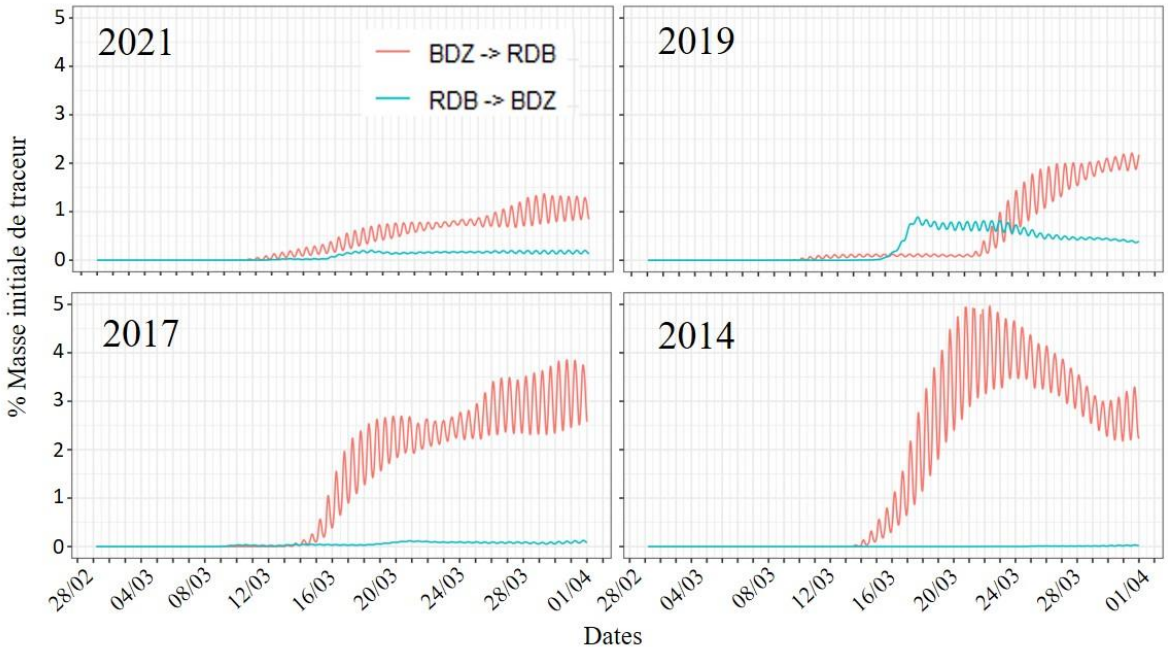

Fig. 20 : Évolution du pourcentage de masse initiale entre la BDZ (zone 16, fig.6) et la RDB (zone 10, fig.6). Les dynamiques sud-nord (BDZ vers RDB) et Nord-Sud (RDB vers BDZ) sont présentées respectivement de couleur rouge et bleue.

La figure 20 montre l'évolution de la masse initiale de deux traceurs respectivement lâchés au Nord-Est de la BDZ (zone 16), et au Sud de la RDB (zone 10) (fig. 6).

D'une manière générale, les connectivités calculées par le modèle ont montré que la dynamique Sud-Nord (BDZ vers RDB) était beaucoup plus importante que la dynamique Nord-Sud (RDB vers BDZ). Cette dynamique était fortement marquée notamment pour les années 2014 et 2017 et plus faible, même si elle était présente en 2019 et en 2021.

Selon les années, les simulations ont montré différentes dynamiques de connectivités entre les deux zones (10 et 16). Le Pmax de 2014 a été le plus important (5.2%), suivi de 2017 (3.9%), puis 2021 (1.4%) et enfin 2019 (0.9%).

En 2014, le début du mois de mars a été caractérisé par de très forts coefficients et des vents plutôt faibles et orientés au sud. La connectivité BDZ vers RDB est importante. Le traceur est

arrivé en RDB à environ 15 jours, assez rapidement, les quantités ont augmenté pour atteindre un Tmax en 21.7 jours avec un Pmax de 5.2%.

En 2017, les coefficients de marée ont été aussi très forts au début du mois mais les vents ont été plus soutenus et de Sud-Ouest. Le traceur est arrivé aux environs de 14 jours, dans les mêmes gammes de temps que 2014. Mais la connectivité a été légèrement plus faible avec un Tmax de 28.8 jours et un Pmax associé de 3.9%.

En 2019, les coefficients de marée étaient faibles au début du mois de mars et en revifs (ils augmentent). Les vents étaient plutôt soutenus du Sud-Ouest et s'orientant à l'Ouest à la mi-mars. La dynamique des traceurs partant de la BDZ et de la RDB divergeait des autres années. En particulier, une dynamique de traceur dans le sens Nord-Sud a été identifiée, de la RDB vers la BDZ, avec un Pmax beaucoup plus important que les autres années (0.9% avec un Tmax de 17 jours). Également, ce qui différencie 2019 également des autres années a été une connectivité entre la BDZ et la RDB plus faible avec un Tmax de 30.5 jours et un Pmax de 2.2%. Le traceur était néanmoins arrivé assez tôt aux alentours de 10 jours (>0.1%).

Pour terminer, en 2021, les coefficients de marée étaient forts au début du mois de mars, et les vents étaient orientés à l'Est, puis ont tourné à l'Ouest vers le 10 mars. Ces conditions ont pu expliquer une arrivée plus rapide mais plus diluée des traceurs en RDB. Puisque, tout comme 2019, 2021 a présenté un Pmax entre la BDZ et la RDB assez faible de 1.37% avec un Tmax de 28.1 jours. De même, l'arrivée de traceur a été beaucoup plus rapide que ce Pmax (>0.1% aux alentours de 12 jours), mais en faible quantité.

Afin d'observer l'impact des vents et des coefficients de marée sur les premiers jours de lâchers de traceurs, la figure 21 compare l'évolution à la surface, des traceurs au bout de 1 jour, 3 jours et 8 jours.

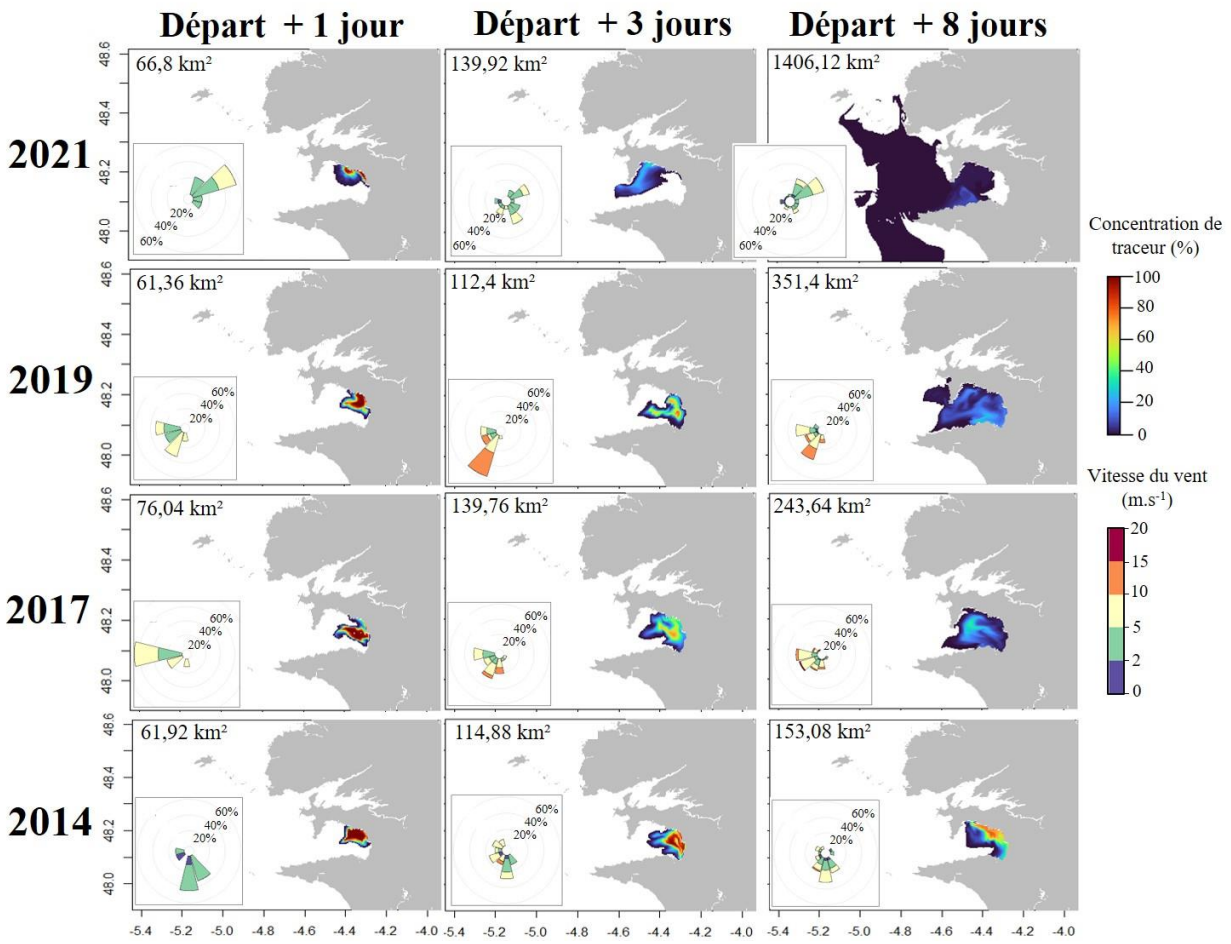

Fig. 21 : Évolution du traceur eulérien (en km²) situé à la surface de la colonne d'eau au départ de la BDZ (zone 16) au bout de 1, 3 et 8 jours. L'orientation, la fréquence (longueur), et la vitesse (les couleurs) des vents sont indiqués par des roses des vents pour chaque période.

Au cours des 8 premiers jours de simulation, la dispersion du panache des traceurs au départ de la BDZ (de la zone 16, fig. 21) varie selon les années. Ces différences semblent être en accord avec l'évolution des pourcentages de masse de traceurs observés entre la BDZ et la RDB dans la figure 20.

En effet, en 2021 rapidement au bout de 3 jours le traceur a commencé à sortir de la BDZ, puis s'est rapidement dispersé dans la mer d'Iroise (surface de 1406 km²) avec des pourcentages de masses initiales par conséquent faibles dus à une dilution rapide avec les eaux du large, cela appuie les résultats de la fig. 22 qui montrent des pourcentages ne dépassant pas 1.4% de la masse initiale lors de la simulation. Cette année-là, la sortie rapide de la BDZ a été observée couplée à des vents du Nord-Est et de fortes marées (fig. 16 et tableau 4).

En 2019, le panache du traceur se retrouve au bout de 8 jours sorti de la RDB. Le traceur se retrouve de façon relativement homogène dans la BDZ. Les vents sont principalement du Sud-Ouest, et il semblerait que malgré cette orientation des vents, qui pouvait laisser penser à une rétention du traceur dans la BDZ, que les fortes marées à partir du 5 mars ont favorisé une sortie du panache de traceur en dehors de la baie (fig. 21). L'année 2019 est la seule des 4 années à avoir présenté de faibles coefficients au début du mois de mars, le traceur a été lâché lors d'une période de revif qui peut avoir favorisé une sortie du panache hors de la BDZ.

En 2017, le traceur a une surface un peu plus faible qu'en 2019 (243 km²) avec un panache qui semblait plutôt orienté et condensé au niveau Nord de la BDZ ainsi qu'à sa sortie. Les fortes marées des 4 premiers jours de mars n'ont pas montré une relation avec la sortie du panache sur cette période. Les vents majoritairement d'Ouest ont dû permettre une rétention du panache dans la baie. Au bout de 8 jours, le panache présentait une surface plus faible qu'en 2019 de 243 km², sans doute dû aux faibles marées qui ont eu lieu à partir du 5 mars.

Enfin, en 2014, la surface du panache au cours du temps est restée relativement faible comparée aux autres années avec un maximum de 153 km² au bout de 8 jours, neuf fois plus faible qu'en 2021. Le traceur présentait des pourcentages de masses initiales supérieures à 60% au niveau de la côte Nord-Est de la BDZ. Les vents principalement du sud peuvent être une explication à ce schéma de dynamique (fig.16). Si les marées avaient les mêmes dynamiques d'évolution qu'en 2017, les vents du Sud de 2014, même faibles, ont entraîné un auto-confinement plus important du traceur dans la BDZ (fig. 21).

Pour terminer, dans un but d'étudier les trajectoires empruntées par les traceurs, des simulations de transport de particules Lagrangiennes ont été réalisées sur les 15 premiers jours de mars, visibles sur la figure 22. Au niveau de la station Telgruc (cf chapitre 2) située au Nord-Est de la BDZ, 1000 particules ont été lâchées, le nombre de particules restées en BDZ (auto-confinement) et passées en RDB ont été comptabilisées.

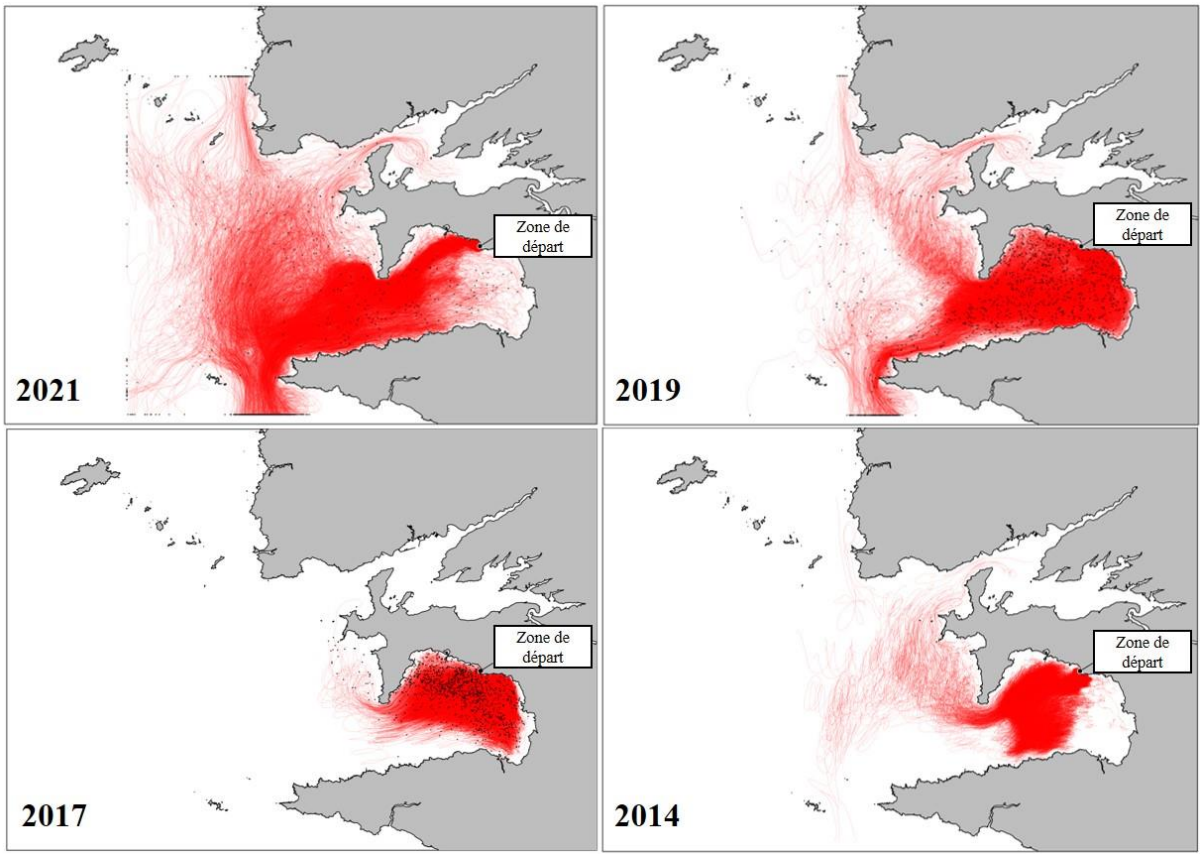

Fig. 22 : Carte des trajectoires de 1000 particules Lagrangiennes au départ de Telgruc au Nord-Est de la BDZ du 1er au 15 mars pour les années 2014, 2017, 2019 et 2021.

Tableau 5 : Résultats des simulations Lagrangiennes. Le nombre de particules restées dans la BDZ (auto confinement) et le nombre de particules passées en RDB sont indiqués entre le 1er et le 15 mars pour les années 2014, 2017, 2019 et 2021.

	Période	Autoconfinement en Baie de Douarnenez	Passage en Rade de Brest
2021	1-15	70	8
2019	1-15	569	11
2017	1-15	969	0
2014	1-15	850	5

Les résultats de simulations Lagrangiennes (fig. 22) sont en accord avec les dynamiques des traceurs Eulériens de surface observés dans la figure 21.

En effet, en 2021, comme pour la simulation Eulérienne qui montrait une sortie rapide du traceur de surface de la BDZ dès 3 jours (fig. 21). Les simulations Lagrangiennes ont montré qu'au bout de 15 jours, sur les 1000 particules lâchées au nord de la BDZ, il ne restait que 70

particules, dont 8 en RDB (tableau 5). Les trajectoires des particules ont été identifiées dispersées sur une grande partie de l'emprise du modèle et présentaient des trajectoires assez contrastées entre elles. Un grand nombre des particules initialement lâchées se sont dirigées assez rapidement au large des côtes, et ne présentaient pas de trajectoire réellement côtière en BDZ, suggérant un mouvement important des masses d'eau sur les 15 premiers jours de mars. A noter également qu'une grande majorité des particules ont présenté une trajectoire orientée vers le Sud de l'emprise du modèle, peut être favorisée par les vents du Nord-Est.

En 2019, tout comme ce qui a été déjà démontré sur les différentes analyses de connectivités Eulériennes (fig. 20 et 21), la connectivité cette année-là était assez intermédiaire.
Les simulations lagrangiennes ont montré qu'une grande majorité des particules sont restées en BDZ au bout de 15 jours (569) avec un nombre assez comparable entre le nombre de cellules arrivées en RDB cette année et le nombre arrivé en 2021 (11) (tableau 5). Même si elles n'ont pas été majoritaires, les cellules sorties de la BDZ ont néanmoins eu des trajectoires orientées vers le Sud comme la simulation de 2021, malgré des vents du Sud-Ouest (fig.15).

En 2017 et en 2014, l'auto confinement qui a été identifié lors des 8 premiers jours en Eulérien (fig. 21) se confirmait assez bien avec le transport de particules Lagrangiennes. On a comptabilisé respectivement 969 et 850 particules restées en BDZ lors des 15 premiers jours de simulation.

En 2017, le transport des particules en BDZ était principalement côtier, orienté plutôt à l'Est et au Nord, les vents d'Ouest assez forts identifiés sur la figure 16 semblaient être la principale explication à cette trajectoire.
En 2014, les particules étaient principalement situées au centre de la BDZ, avec très peu particules qui se sont dirigées au niveau côtier Ouest de la BDZ. Cela pouvait être expliqué par des vents principalement du Sud qui n'ont pas entraîné les masses d'eau sur le côté Est de la BDZ. Les particules sorties de la BDZ au contraire de 2019 et 2021 ont présenté une trajectoire orientée vers le Nord (fig. 22).

Pour résumer, l'analyse de 4 années de simulations sur 1 mois ont montré que les coefficients de marée et les directions de vents semblent expliquer les différents interannuelles de connectivité entre la BDZ et la RDB.

L'analyse des différents résultats semblent indiquer que les conditions les plus favorables à la connectivité BDZ vers la RDB sont les vents du Sud (2014). En moindre mesure les vents du Sud-Ouest (2017). Ces deux conditions associées à de forts coefficients de marée, en déchet, au moment du lâché ont montré les connectivités les plus importantes vers la RDB.

Les conditions qui ont été les plus défavorables à la connectivité ont été les vents d'Est associés à de forts coefficients de marée qui ont dilué rapidement le panache de traceur (2021). A noter également que les coefficients de marées en revif (qui augmentent) ont favorisé une sortie et dilution du panache de la BDZ (2019).

3.4 Discussion

La présente étude a cherché à comprendre la connectivité hydrodynamique existant au début du printemps entre différentes masses d'eau de l'Ouest Finistère. Une attention particulière a été portée à la connectivité entre la baie de Douarnenez et la rade de Brest, deux zones touchées de manière décalée dans le temps par les efflorescences toxiques de la diatomée *Pseudo-nitzschia australis*. Nous avons utilisé afin de répondre aux objectifs de l'étude, le modèle hydrodynamique 3D CROCO Iroise. Des traceurs Eulériens et Lagrangiens ont été lâchés au début du mois de mars et suivis durant un mois. Sur les différentes années modélisées (2014, 2017, 2019 et 2021), une connectivité Sud-Nord au départ de la BDZ vers la RDB a été identifiée, et des différences interannuelles dans ces connectivités ont pu être mises en avant. L'intensité de ces connectivités printanières en Ouest-Finistère semble particulièrement liée aux vents et aux marées.

La mer d'Iroise est une zone reconnue comme complexe en termes d'hydrodynamique en raison de ses irrégularités topographiques, de la présence de forts courants de marée et de sa situation géographique particulière, située dans un système atmosphérique de basse pression. Elle est soumise à des marées semi-diurnes, et présente de forts courants de marée, notamment au printemps (lors des marées d'équinoxe de mars) pouvant aller localement jusqu'à 8 nœuds, le vent joue également un rôle important sur les courants (Muller et al., 2009). Ce dernier point appuie les résultats trouvés dans la présente étude dans laquelle le transport des traceurs semble fortement lié aux vents. Si on s'intéresse plus à l'hydrodynamique des baies qui sont d'un intérêt majeur dans notre étude et interconnectées à la mer d'Iroise, il est bien connu que la RDB

présente un faible temps de renouvellement des eaux dû aux fortes marées comme l'ont montré Le Pape et Menesguen (1997). Ces auteurs ajoutent que ces forts taux de renouvellement, à l'origine d'échanges rapides entre la rade de Brest et la mer d'Iroise, limitent les fortes biomasses planctoniques en favorisant l'export rapide des efflorescences. Cela a été observé dans la présente étude, par le temps relativement faible de rétention des traceurs en RDB, qui indique une connectivité significative entre ces zones. Ces deux zones peuvent ainsi, en cas d'efflorescences phytoplanctoniques être toutes deux impactées. L'hydrodynamique en BDZ est caractérisée par de faibles courants et un confinement important des eaux (Ayata et al., 2010; Dubois et Colombo, 2014), ce qui est également confirmé par nos résultats.

De manière générale, les résultats obtenus révèlent une tendance au transport du Sud vers le Nord entre la BDZ et la RDB. Il est important de noter que bien que cette connectivité semble être influencée par les différentes intensités et directions des vents, elle découle logiquement aussi de l'onde de marée présente sur le plateau continental Nord-Européen. Cette onde de marée est bien documentée et sa résiduelle transporte les masses d'eau du Sud-Ouest vers le Nord-Est (Mariette et al., 1982; Muller et al., 2009).

A noter que les traceurs eulériens et lagrangiens choisis dans la présente étude étaient inertes et passifs et ne reflètent donc que l'effet du forçage purement physique exercé par les flux d'eau. Dans le contexte de simulation d'efflorescences, ils n'ont pas la capacité d'informer sur des mécanismes biologiques (par exemple, la croissance ou la migration verticale) qui répondent à des facteurs tels que la lumière et les nutriments qui, à leur tour, peuvent moduler les distributions de la population. Étant donné que ni la lumière ni les nutriments ne sont connus comme limitants dans la zone à cette période (Morin et al., 1991), nous nous attendons à ce que ces mécanismes biologiques ne modulent que légèrement nos résultats et n'entraînent pas de distorsions majeures. Une simulation couplant l'hydrodynamique et la biologie nous permettrait de confirmer cette hypothèse.

En accord avec les résultats de ce chapitre, différentes études ont mis en avant le rôle clé des facteurs physiques tels que le vent et/ou les courants, qui provoquent l'accumulation et la dispersion des cellules phytoplanctoniques (Koike et al., 2001; Koukaras, 2004; Soudant et al., 1997). Soudant et al. (1997) ont expliqué la dynamique de population d'un dinoflagellé en Normandie (France) à l'aide d'une régression linéaire dynamique. Ces auteurs ont conclu que la disparition des cellules dans la zone étudiée était principalement due aux vents et aux marées qui induisent la dispersion par dilution et par le mouvement des masses d'eau.

Dans une autre étude, l'application d'un modèle 3D à la dynamique de la population d'une espèce de HAB (*Dinophysis acuminata*) a montré que des simulations de transport lagrangien sont capables de reproduire les schémas de dispersion de cette espèce observés *in situ* (Velo-Suárez et al., 2010). Les résultats ont indiqué que les processus physiques seuls pouvaient expliquer la dispersion des cellules dans la zone. Les comparaisons entre les données de l'étude (concentrations cellulaires) et les résultats du modèle (pourcentage de rétention des particules Lagrangiennes) se sont montrées concluantes, malgré les simplifications utilisées dans le modèle (c'est-à-dire le mouvement passif des particules) (Velo-Suárez et al., 2010).
Malgré tout, il est important de rester prudent sur les résultats de la présente étude, puisqu'il s'agit des résultats de 4 années de simulation, sur un mois précis. Les différentes simulations ont montré que les vents et les marées, respectivement, selon leur orientation et leur force favorisent la connectivité entre les zones. Prenons l'exemple de deux années 2021 et 2014 qui ont présenté des connectivités entre la BDZ et la RDB respectivement relativement faibles et fortes. Les vents avec des directions variables ou d'Est ont eu tendance à disperser et donc diluer les traceurs eulériens sur les 15 premiers jours de simulation dans la zone d'étude en 2021. Ce qui a été confirmé par les trajectoires des traceurs Lagrangiens, qui ont montré une trajectoire très étendue et dispersée dans l'emprise du modèle au départ de la BDZ. Au contraire, en 2014, au départ de la BDZ, les vents du sud ont favorisé le passage du traceur Eulérien en plus grande quantité vers la RDB. Les traceurs lagrangiens, ont montré des trajectoires moins dispersées et orientées vers le Nord quand ils étaient sortis de la BDZ ce qui indique un rôle central du vent dans ces trajectoires. Face aux résultats des simulations interannuelles, il semblerait que la connectivité soit favorisée par des vents du Sud, et du Sud-Ouest, mais un lien plus complexe avec les marées est également à noter. En effet, en 2017 (vents d'Ouest) et 2014 (vents du Sud), la connectivité entre BDZ et RDB était forte. Lors de la simulation de 2019, les vents avaient des directions relativement identiques à 2017 avec pourtant une connectivité entre les deux baies beaucoup plus faibles. La différence venant des coefficients de marée, qui, en revif début 2019 a probablement dilué beaucoup plus le traceur au début du mois.

Malgré ces différences, toutes les années simulées ont connu des développements de *P. australis*, même si les abondances de l'espèce toxique ont été différentes selon ces années (REPHY, 2022). Le REPHY a identifié des concentrations cellulaires atteignant 494 600 cell/L de P. australis en mars 2014, 373 000 cell/L en 2017 ; 263 300 cell/L en 2021 ; et un maximum de 80 660 cell/L au mois de mars 2019 (REPHY, 2022). Même si des simulations et des données

plus précises sur les différentes efflorescences seraient nécessaires pour confirmer cela, il semblerait que pour les années 2014 et 2017 où les concentrations cellulaires ont été identifié en plus grand nombre soient également les années où les traceurs en BDZ ont été “confinés” plus longtemps.

Plus généralement, même si des différences d’intensité d’efflorescences ont été détecté, il aurait été intéressant de simuler une année neutre, c'est-à-dire sans efflorescence identifiée, et de modéliser un nombre plus important d'années pour pouvoir apporter de manière la plus précise qu’il soit des conclusions sur l’hydrodynamique dans la zone.

De plus, dans la présente étude, toutes les simulations ont été lancées à la même date. le 1er mars, dans un but de pouvoir comparer les différentes années sur une même période, or, les efflorescences n’ont pas précisément démarré à cette date. Il est ainsi important de garder en tête que les simulations réalisées dans la présente étude peuvent ne pas représenter la période “précise” d’efflorescences de *P. australis*, mais apporte une première vision élargie de la connectivité hydrodynamique présente dans la zone, et permet de se rendre compte des différences interannuelles pouvant se présenter. Pour information, une simulation en lien avec des données *in situ* collectées lors d’un suivi spatio-temporel de bloom de *P. australis* en 2021 a été réalisée, les résultats sont présentés dans le chapitre 4 de la thèse.

Malgré tout, grâce aux suivis réalisés dans le présent travail de thèse (chapitre 2), lors d’efflorescences de *P. australis* en 2021 (et dans une moindre mesure en 2019 du fait de concentrations observées beaucoup plus faibles), les observations *in situ* peuvent être mises en relation avec les résultats des simulations. Les résultats des présentes simulations montrent que l’hydrodynamique peut potentiellement expliquer les décalages spatio-temporels Sud-Nord observés dans le chapitre 2.

Concernant, les choix dans les approches d’analyse de la connectivité en Ouest-Finistère, le choix s’est porté en premier lieu sur l’utilisation de l’approche Eulérienne. Nous avons considéré que l’advection/dispersion d’un traceur était plus représentatif d’une efflorescence, d’un patch de biomasse phytoplanctonique, que la dispersion de particules individuelles. Toutefois, les résultats de la simulation Lagrangienne sur 15 jours a montré les mêmes schémas de dispersion que les traceurs eulériens observés jusqu’au 8ème jour dans la présente étude. Ainsi, comme Nicolle et al. (2013) qui a étudié la dérive des larves dans la Manche, nous n’avons pas trouvé de différences significatives entre la modélisation Lagrangienne et Eulérienne. Récemment, Zhou et al., (2023) ont réalisé une évaluation complète des modèles de transport Lagrangiens et Eulériens pour la prévision des efflorescences algales nuisibles de

cyanobactéries dans le lac Érié. L'étude a comparé trois types de modèles 3D : 1) un modèle Lagrangien de particules, 2) un modèle Eulérien de traceurs, et 3) un modèle de particules porteuses de propriétés qui utilisent une approche hybride eulérienne-lagrangienne. Les résultats ont indiqué que les trois modèles de transport présentaient des niveaux de compétence similaires, le modèle Eulérien surpassant les autres dans l'évaluation globale. Dans l'étude, ils ont démontré que l'Eulérien peut mieux représenter les champs continus de concentration que le Lagrangien, et dans l'évaluation il a été le plus performant des trois méthodes pour prédire un évènement de HAB observé (Zhou et al., 2023).

Par conséquent, dans cette étude nous avons principalement quantifié le transport par des simulations Eulériennes, et observé ce transport par des simulations Lagrangiennes.

Cependant, à notre connaissance, assez peu d'études se sont intéressées à la connectivité entre zones par l'utilisation de traceurs eulériens (Lagarde et al., 2019; Ménesguen et al., 2018; Zhou et al., 2023). Une étude sur les schémas spatiaux de recrutement des huîtres a utilisé ce type de traceur pour travailler sur la connectivité entre zones de recrutement dans la lagune de Thau (Sète, France) (Lagarde et al., 2019). Ces auteurs ont défini comme indicateur la connectivité hydrodynamique entre un volume d'émission de traceur fini d'une zone conchylicole (VE) et un volume de destination fini (VD) comme la quantité d'un traceur conservatif passif libéré de VE et entrant dans VD sur une période de temps donnée (ΔT) (Lagarde et al., 2019).

Dans la présente étude le choix a été fait de travailler sur le pourcentage maximal de masse initiale (Pmax) et sur le temps associé (Tmax) afin de permettre la comparaison sur une même zone d'arrivée des traceurs arrivant des différentes zones. Ce choix nous a permis d'illustrer une relation quantitative (Pmax) mais également temporelle (Tmax) entre des zones sources et des zones puits. Le choix du Pmax est principalement basé sur le postulat qu'un minimum de cellules d'une espèce doit être transportées pour qu'elles puissent ensuite se développer et dominer la communauté. Les efflorescences étant des phénomènes relativement courts (quelques semaines), il nous a paru important d'incorporer la composante temporelle associée. Comme nous, une étude s'est intéressée à la connexion potentielle de HAB entre sites en Philippines par l'utilisation de traceurs. Ils ont défini la connectivité entre deux zones par la concentration moyenne maximale de traceur en surface qui n'a pas augmenté ou diminué de plus de 30 %, 3 heures avant et 3 heures après son arrivée dans une zone (Punongbayan et al., 2022).

De plus, si on s'intéresse à la possibilité d'utiliser d'autres indicateurs, dans le cas de notre étude, l'établissement d'un seuil pour établir la connectivité entre zones n'aurait pas été une solution. En effet, les connectivités entre zones étant très variables, certaines sont très fortement

connectées (Pmax important), d'autres plus faiblement (Pmax plus faible). Mais malgré tout, même si elle est faible, la connectivité est existante. L'établissement d'un seuil pour définir la connectivité entre les zones aurait pu limiter l'information. Pour illustrer ce propos, la connectivité entre la BDZ et la RDB varie énormément selon les années simulées, avec des valeurs variant entre 0,9% (en 2019) à 5,2% (en 2014). Pourtant, même si la connectivité est faible en 2019, les deux baies restent malgré tout connectées.

Dans la présente étude, le choix de quadriller la zone de notre étude et la présence d'un littoral découpé et d'un fort gradient bathymétrique en Ouest-Finistère imposent quelques limites à l'interprétation des résultats des matrices de connectivité qui ne peuvent être lues que dans un sens (dans notre cas, horizontalement). Les différences en volumes mouillés entre les zones quadrillées ont rendu impossible les comparaisons entre les arrivés de traceurs d'une zone à une autre. Puisqu'il est logique que la masse maximale d'un traceur pouvant arriver dans une zone dépend aussi du volume de cette zone. Pour résoudre ceci, il aurait fallu diviser le pourcentage de masse initiale arrivant dans chaque zone par le volume moyen des zones, on obtiendrait ainsi une concentration de traceur par volume d'eau. Cependant, contrairement à la méthode que nous avons choisie (pourcentage de masse initiale), les comparaisons pour une zone d'arrivée des quantités de traceurs venant de toutes les autres zones n'auraient pas pu être comparées (lecture horizontale de la matrice de connectivité). En connaissant les limites associées à ces deux méthodes, nous avons fait le choix dans l'étude de nous intéresser au pourcentage de masse initiale émit d'une zone en direction des autres zones. Il est également à noter que quelque soit la méthode, le Tmax reste constant, seule la valeur du Pmax varie. Par conséquent, le Tmax peut être interprété dans les deux sens dans les matrices de connectivité.
Enfin, une autre limite est liée à l'analyse des connectivités entre zones proches des limites de l'emprise du modèle (principalement pour les zones du Nord). En effet le devenir de la masse des traceurs quittant le domaine par les limites océaniques du modèle (et revenant éventuellement à l'intérieur du domaine par le jeu des marées), n'est pas connu précisément. Nous ne pouvons donc accorder le même intérêt aux zones proches des limites du modèle (zones 1 et 2 par exemple). Cependant, dans le cadre de notre étude les zones d'intérêt sont la RDB et la BDZ situées loin des limites océaniques ouvertes.

Pour conclure, comme souligné pour d'autres écosystèmes par Berdalet et al., 2014; Chen et al., 2003; Raine et al., 2010, notre étude montre que le forçage physique à lui seul ne suffit sans doute pas à expliquer la dynamique des efflorescences dans l'Ouest Finistère, mais il est

fondamental dans la compréhension de leur développement. La formation d'efflorescences résulte du bilan entre la vitesse d'augmentation du nombre de cellule à un moment donné (croissance biologique, baisse de la mortalité) et la dilution de ces cellules due au mouvement des masses d'eau (hydrodynamique) (Escalera et al., 2010; Roelke and Buyukates, 2001). Dans notre cas, cette accumulation peut tout à fait avoir lieu en BDZ, où les courants sont beaucoup plus faibles qu'ailleurs et où les résultats ont montré un certain confinement des traceurs selon les conditions environnementales. D'ailleurs, ce dernier point a déjà été remarqué dans une étude sur les connectivités de populations larvaires dans le Nord-Est européen (Ayata et al., 2010). Dans cette étude, la BDZ a montré les plus forts taux de rétention de particules Lagrangiennes : 61.83 ± 16.49 %, lors de simulations de 4 mois sur les mois de mars, mai et juillet 2003 (Ayata et al., 2010).

De même, la question de savoir si les augmentations soudaines du nombre de cellules entraînant des efflorescences en Ouest-Finistère résultent d'une croissance locale ou d'un transport qui amène des populations d'ailleurs, n'est pas encore tranchée. Il serait intéressant de modéliser des départs de traceurs sur une zone géographique encore plus vaste, ayant dans son emprise le Sud-Finistère (baie d'Audierne). Cela permettrait de confirmer que les hypothèses concernant le développement initial des efflorescences dans la zone de Baie de Douarnenez (BDZ) ne soient pas le résultat du transport d'efflorescences provenant d'une zone située plus au sud. Mais pour aller encore plus loin, il serait intéressant d'inclure à notre approche la dynamique biologique, pour évaluer non seulement les chemins empruntés par les cellules, mais aussi la probabilité de croissance et de mortalité le long de ces voies, et le rôle de la migration verticale et des paramètres environnementaux (température, ensoleillement, nutriments…) sur la dynamique des espèces (Gillibrand et al., 2016; Zhou et al., 2023).

Tous ces résultats contribuent à l'amélioration des connaissances de l'hydrodynamique au niveau du littoral Ouest Finistère. De plus, ces premières connaissances acquises pourront être utiles pour cibler au mieux les zones à privilégier pour le suivi côtier d'efflorescences toxiques et également avoir une connaissance temporelle sur leur déplacement.

Chapter 4

Spatio-temporal dynamics of *Pseudo-nitzschia australis* during a bloom: from gene expression to hydrodynamic

Léa Prigent[a], Julien Quéré[a], Marie Latimier[a], Florian Caradec[a], Fabienne Hervé[b], Lauriane Baudy[b], Zouher Amzil[b], Emilie Rabiller[a], Martin Plus[a], Mickaël Le Gac[a]

[a]Ifremer, DYNECO, F-29280 Plouzané, France.

[b]Ifremer, PHYTOX Unit, METALG Laboratory, F-44300 Nantes, France.

Context

The first two chapters provided us with a better understanding of the study area (community composition, community succession, and hydrodynamics) in March.

The chapter 2 revealed a homogeneous diatom community throughout West Finistère, with a staggered succession between south and north. In Chapter 3, we demonstrated a marked south-north hydrodynamic connectivity between the Bay of Douarnenez and the Bay of Brest during simulations over the month of March (*P. australis* development period) over 4 years. This hydrodynamics was shown to be linked to wind direction and tides. In addition, the modelling identified a higher retention of water masses in the Bay of Douarnenez.

However, the environmental conditions (physical, biotic and abiotic) leading the species *P. australis* to develop in early spring in the study area are still unclear.

Hydrodynamic modelling provides valuable information about the potential movements of blooms in a given area, while analysis of the genes expressed allows us to determine whether significant physiological changes result from modifications in the environmental conditions under which cells develop from one area to another.

With this in mind, in the present chapter 4, we combined analyses of *in situ* environmental parameters, hydrodynamic connectivity (simulation over the specific bloom monitoring period) and metatranscriptomics to gain a better understanding of the spatio-temporal dynamics of *P. australis* blooms. and answer the following question:
How is *P. australis* developing in western Brittany? Can its spatio-temporal dynamics be explained by the local environment? Hydrodynamics?

To answer it, correlations between different environmental variables were first observed. Secondly, the hydrodynamic times were compared with the appearance times of *P. australis* at the various monitoring stations. Finally, the physiological state of this species was compared at the different stations over time using metatranscriptomics.

By combining the various results obtained, the aim of chapter 4 was to provide answers to the hypotheses of the thesis:
→ Do *P. australis* blooms develop in one area and then move over time as a result of hydrodynamics?
→ Or do local environmental conditions favour the development of *P. australis*?

This chapter mainly highlight :

- The possibility that the Bay of Douarnenez serves as the initial growth area for *P. australis*, mainly due to its higher water retention rate, with subsequent northward development driven by hydrodynamics.

Graphical abstract :

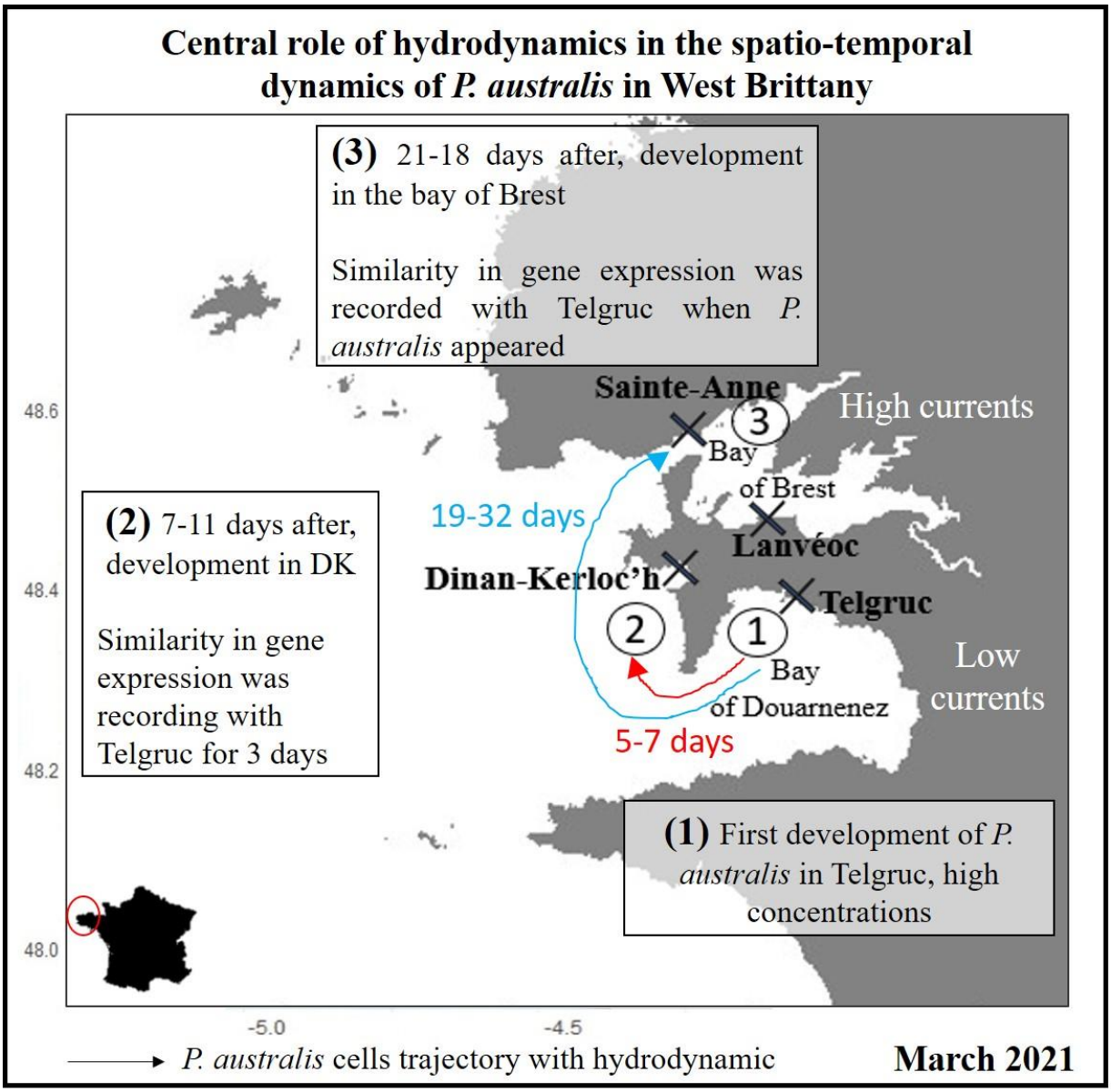

Résumé :

Au cours des dernières décennies, la diatomée pennée *Pseudo-nitzschia*, un genre cosmopolite, a été associée à de nombreux événements toxiques dans le monde entier. En France, la majorité des événements toxiques ont été liés à l'espèce *P. australis*. Elle est apparue pour la première fois dans l'Ouest de la Bretagne (Europe occidentale) en 2006. Depuis, elle fait des apparitions récurrentes sur les côtes bretonnes, causant des pertes économiques par la fermeture de pêcheries. Cependant, aucune étude spécifique n'a été menée localement pour comprendre son développement. En combinant des analyses *in situ*, de connectivité hydrodynamique et d'expression des gènes, cette étude vise à comprendre la dynamique spatio-temporelle d'un

bloom de *P. australis* dans l'Ouest de la Bretagne. Des échantillonnages ont été réalisés au début du printemps (mars-avril) 2021 dans quatre stations côtières proches, toutes les deux semaines. L'espèce *P. australis* a été trouvée en forte abondance relative à la station la plus méridionale, Telgruc, puis a été identifiée plus au Nord à Dinan-Kerloc'h et enfin dans la rade de Brest (aux stations de Sainte-Anne et Lanvéoc). En utilisant un modèle hydrodynamique 3D (CROCO-Iroise), nous avons pu corréler les temps de connectivité hydrodynamique et les temps d'apparition de *P. australis* entre les stations. Grâce à cela, nous avons trouvé une bonne corrélation entre les temps de connectivité hydrodynamique et l'apparition de *P. australis* entre Telgruc et les autres stations plus au Nord. L'état physiologique des cellules aux différentes stations a montré une similarité de quelques jours avec la station Telgruc, en baie de Douarnenez avant de diverger. La corrélation entre l'expression des gènes et l'environnement n'a pas permis d'expliquer ces similitudes d'expression des gènes entre les stations. Ceci implique que l'hydrodynamique exerce probablement une influence significative sur le mouvement spatio-temporel de l'efflorescence de *P. australis* en Bretagne occidentale. Nous émettons l'hypothèse que la baie de Douarnenez sert de zone de croissance initiale pour *P. australis*, principalement en raison de son taux de rétention d'eau plus élevé, avec un développement ultérieur vers le nord entraîné par l'hydrodynamisme.

Abstract:

Over the last decades, the pennate diatom *Pseudo-nitzschia*, a cosmopolitan genus, has been linked to many toxic events worldwide. In France, the majority of toxicity events have been linked to the *P. australi*s species. It first appeared in western Brittany (western Europe) in 2006. Since then, it has made recurring appearances on Brittany's coasts, causing economic losses through fishery closures. However, no specific studies have been carried out locally to understand its development. Combining *in situ* analyses, hydrodynamic connectivity and gene expression, this study aimed to understand the spatio-temporal dynamics of a bloom of *P. australis* in western Brittany. Samplings were carried out at the beginning of spring (March-April) 2021 at four nearby coastal stations biweekly. *P. australis* was found in high relative abundance at the southernmost station, Telgruc, and was then identified further north at Dinan-Kerloc'h and finally in the Bay of Brest (at the Sainte-Anne and Lanvéoc stations). Using a 3D hydrodynamic model (CROCO-Iroise), we were able to correlate hydrodynamic connectivity and shifts in *P. australis* occurrence between stations. Thanks to this, we found a good

correlation between hydrodynamic connectivity times and the appearance of *P. australis* between Telgruc and the other stations further north. In order to understand it, the physiological state of the cells between stations were observed. The latter showed a correlation of a few days in gene expression between the stations and Telgruc before diverging. However, the correlation between gene expression and the environment did not explain these gene expression similarities among the stations. This implies that hydrodynamics likely exerts a significant influence on the spatio-temporal movement of the *P. australis* bloom in West-Brittany. And we hypothesize that the Bay of Douarnenez serves as the initial growth area for *P. australis*, mainly due to its higher water retention rate, with subsequent northward development driven by hydrodynamics.

4.1 Introduction

Coastal environments are highly productive ecosystems and provide important socio-economic resources and services. However, due to their proximity to land, ocean and atmosphere, coastal waters present complex seasonal patterns, with high variability both between and within ecosystems (Cloern and Jassby, 2008). In temperate waters, much of the seasonal variability is imposed directly or indirectly by the annual cycle of solar radiation (Cloern and Jassby, 2010; Sverdrup, 1953). One of the main characteristics of the latter is the spring phytoplankton bloom following the increase in light and temperature and the presence of nutrients accumulated during the winter period. In addition to seasonal phytoplankton blooms, which are somewhat predictable, unusually high biomass levels of certain phytoplankton species can also occur as a localized phenomenon in space and time, in response to particular environmental and ecological conditions (Paerl, 1988). This phenomenon is known as harmful algal blooms (HAB). Some of these HAB can have deleterious consequences for other organisms in the aquatic ecosystem or for human health and the economy (Llebot et al., 2011; Smayda, 1997; Solé et al., 2006). Field studies on HABs provide important information on the factors that potentially favour the formation, propagation and disappearance of blooms. Most research investigating the dynamic of blooms focuses on the bottom-up control of environmental variables (mainly the impact of temperature, light and nutrients) (Reynolds, 2006). Although this approach is effective in understanding the relationships between phytoplankton and their environment, it does not appear to be sufficient to provide an in-depth understanding of the processes structuring phytoplankton communities (Verity and Smetacek, 1996). It often ignores numerous mechanisms such as hydrodynamics in the developpement, migration and persistence of blooms (Houliez et al., 2021). Ocean currents and tides have been shown to play a key role in the bloom dynamics, since they can influence cell dispersion, influencing bloom propagation and intensity (Anglès et al., 2008; Aoki et al., 2012). For example, Basterretxea et al. (2005) have demonstrated through numerical simulations that wind-induced currents can accumulate phytoplankton cells in areas close to the coast, favouring the appearance and persistence of blooms. However, hydrodynamics alone can ignore important physiological aspects linked to bloom-forming species, and the various environmental parameters surrounding a bloom and maintaining its persistence (growth rate, nutrients) or, on the contrary, its termination (grazing, virus, nutrients, stress). Even if the HAB modelisation can be linked to behavior (growth, vertical migration, etc.) (e.g. McGillicuddy, 2010; Vanhoutte-Brunier et al., 2008), given the complexity of this event, it is impossible to be exhaustive.

Blooms are classically studied by focusing on species absolute or relative abundances. In order to gain a thorough comprehension of the intricate occurrence of phytoplankton blooms, it is advisable to investigate the physiological condition of the blooming species throughout these events thanks to metatranscriptomic. This can provide an answer to the impact of the environment as a whole on the physiological state of cells as blooms progress through time and space (Anderson, 2009; Ge et al., 2013; Hoffmann and Willi, 2008; Kolody et al., 2022; Metegnier et al., 2020).

Taken together, the study of the hydrodynamics, environment and gene expression could provide essential information to better understand the spatio-temporal development of blooms. Such an approach could link the physical and biological processes that govern phytoplankton blooms. For instance, it could highlight the physiological conditions triggering blooms and the cellular mechanisms by which cells adapt to the local environment during bloom displacement. More specifically, in a spatio-temporal study, it could highlight whether the bloom is localized or the result of a displacement by comparing the genes expressed between areas. To illustrate, if gene expression initially matches between zones and then diverges with a time lag, this may mean that cells have been transported from one zone to another and are adapting to local conditions in the zone to which they have been moved.

Among HABs, blooms associated with the genus *Pseudo-nitzschia* are particularly critical since some species produce domoic acid, a neurotoxin responsible for amnesic shellfish poisoning syndrome (ASP) in humans through the consumption of filter-feeding molluscs, and mortality in mammals and seabirds through the transfer and bioaccumulation of the toxin in the food web (Husson et al., 2016; Lelong et al., 2012; Trainer et al., 2012).

Pseudo-nitzschia blooms and the resulting toxicity are a worldwide problem. In France, western Brittany (Figure 1) is regularly affected, mainly in early spring, by the species *Pseudo-nitzschia australis*, the most toxic of the genus (REPHY, 2022). Despite these frequent occurrences, and the economic importance of the area due to its many fisheries, very few studies have looked into the causes of its development in western Brittany. The only information available concerns its first suspected detection in 1995 in the Bay of Brest and its first major bloom detected in March 2010 in the Bay of Douarnenez (Nezan et al., 2010). Since then *Pseudo-nitzschia spp* blooms, (REPHY, 2022) have been regularly identified in western Brittany. Two studies have analysed the REPHY monitoring data at the genus taxonomic level, and the first study has shown the recurrent and general occurrence of *Pseudo-nitzschia* blooms throughout the French coast between 1987 and 2018 (Belin et al., 2021). And a second study showed that: (i) the extent and characteristics of the blooms, as well as the frequency of associated toxicity events, vary

considerably from one area to another; (ii) ASP contaminations are always preceded by major blooms; (iii) irradiation and temperature play a major role in triggering blooms in spring; (iv) ASP events tend to be more frequent in bays strongly influenced by nutrient inputs (Husson et al., 2016).

In the present study, using a multidisciplinary approach combining the study of *in situ* environmental parameters, hydrodynamic connectivity and gene expression dynamics, we were interested in understanding the spatio-temporal dynamics of a bloom of the toxic species *P. australis* in West-Brittany.

We worked on a spatio-temporal bloom of *P. australis* in order to: 1) understand the local environment in which it develops; 2) understand the hydrodynamic connectivity in the study area; 3) study the spatio-temporal evolution of the cells' physiological state. All these approaches were analyzed with the aim of providing a general overview of the conditions and the way in which *P. australis* develops in Western Brittany. More specifically, we asked the following questions: 1. Can the spatio-temporal dynamic of *P. australis* be explained by biotic/abiotic parameters and hydrodynamics? 2. Does gene expression also display a spatio-temporal shift?

In this chapter, based on the coupled results of environment, hydrodynamic connectivity and gene expression, we made 3 hypotheses:

(1) blooms develop according to an "internal clock". This development is independent of environmental conditions and hydrodynamics. In our results, we expect the same gene expression dynamics at each station over time (independent of hydrodynamic connectivity and environmental conditions). Cell densities may differ between sites due to dilution.
(2) Blooms develop in an area, and cells are transported. We expect division rates to decrease with distance from this zone. Densities at sink zones depend on hydrodynamic connectivity and dilution. Gene expression in sink zones is more or less similar to that in the source zone.
(3) Bloom development is governed by environmental conditions. In the results, gene expression is expected to be similar when environmental conditions are the same, regardless of connectivity. Observed cell concentrations are dependent on environmental conditions and dilution.

4.2 Materials and Methods

4.2.1 Sampling areas and strategy

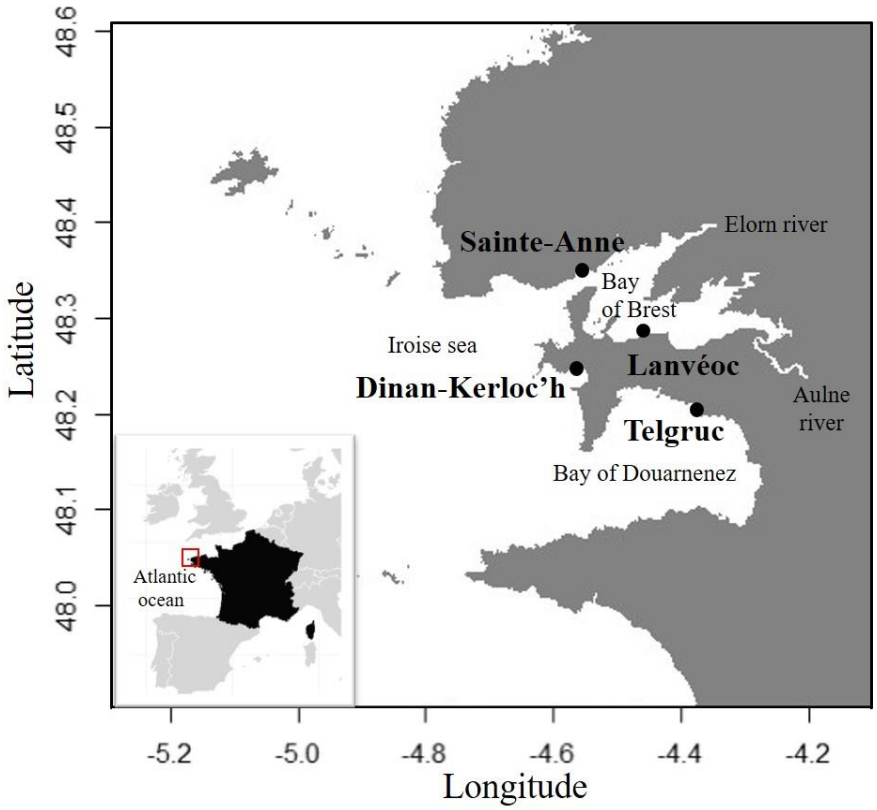

Fig. 1: Map of stations sampled in West-Brittany (West of France). From north to south, the stations were sampled from the Bay of Douarnenez (Telgruc), then in the Iroise Sea (Dinan-Kerloc'h) and finally in the Bay of Brest (Sainte-Anne and Lanvéoc).

The study took place in the westernmost part of France, in western Brittany. Following initial detection of the toxic *P. australis* species by the French phytoplankton monitoring network (REPHY) in south-east Finistère (Bay of Douarnenez), water samples were taken twice a week from shore. The monitoring was carried out in 2021 between February 26th and April 16th at four monitoring stations (fig. 1, from south to north: Telgruc: 48.209933, -4.373308; Dinan-Kerloc'h: 48.257071, -4.560974; Lanvéoc: *48.292921, -4.458473* and Sainte-Anne: *48.360160, -4.553163*).

The Telgruc point was the most southerly point sampled. It is located in the Bay of Douarnenez, a semi-enclosed shallow bay (350 km², maximum depth 40 metres). This bay is open to the Iroise Sea, which means that it is particularly exposed to the prevailing westerly swells (Quiniou, 1986), although it has relatively low currents (Le Fèvre and Grall, 1970, chapter 3). North of the Bay of Douarnenez, Dinan-Kerloc'h is a station more open to the Iroise Sea.

Finally, two stations: Sainte-Anne and Lanvéoc were sampled in the Bay of Brest, a semi enclosed, shallow coastal ecosystem (180 km²) connected with the Iroise sea by a narrow strait (2 km wide, 40m deep) (Quéguiner and Tréguer, 1984). In the bay, two main rivers (Aulne and Elorn) are responsible for 80% of the total freshwater inputs and an intense tidal mixing (almost 8m during spring tides and a periodicity of 12h) assure important exchanges with the Atlantic Ocean (Le Pape et al., 1996). The mean annual flow rates taken from the literature for the Aulne and Elorn rivers are of the order of 24 and 6 m^3 s^{-1}, respectively (Daniel, 1995). Flow rates over time are irregular, with winter flood periods (October to March) followed by low summer water levels (Quéguiner, 1982). In comparison, the Bay of Douarnenez received low riverine inputs with mean flows below 2 $m^3.s^{-1}$ (Guillam et al., 2020; Merceron et al., 2007).
For all the stations, the tidal current and the wind allow vertical mixing during the monitoring period.

4.2.2 Environmental data

During the sampling, several biotic and abiotic environmental parameters were collected.

4.2.2.1 Abiotic parameters

Salinity and sea surface temperature (°C) were measured *in situ* using Cond 3110 portable thermo-salinometer (WTW, a xylem brand, Germany). Water samples were filtered and prepared immediately after sampling, for later nutrient analysis in the laboratory. Nitrate, nitrite, phosphate and silicate concentrations (µmol/L) were then measured by segmented flow analysis, following Aminot and Kérouel (2007).
Suspended matter concentration was measured. Clean Whatman GF/F 45 fiberglass filters combusted at 500°C for one hour in order to remove organic traces and to solidify them were weighed (=weight 1). One litre of water was filtered (= volume) through the pre-treated filters. The filters were then dried at 60°C for 24 hours and weighed (=weight 2). By subtracting the weight 1 from weight 2, the suspended matter concentration (mg/L) was obtained (Aminot and Kérouel, 2004).
Currents were obtained using the CROCO-Iroise 3D hydrodynamic model (described in chapter 2). The average speed current over the whole water column was calculated and averaged over the 12 hours preceding the sampling time, representative of a tidal cycle.
Finally, the photosynthetically active radiation (PAR, µE/m2/s) average between sunrise and sampling was calculated at each station using the outputs of the numerical model AROME of

Météo-France (Seity et al., 2011). This choice was made in order to obtain an average proxy of the light energy received by the cells before sampling.

4.2.2.2 Biotic parameters

4.2.2.2.1 Cellular abundances

First, pico (0-3 µm) -nano (3-20 µm) and -microphytoplankton (> 20 µm) abundances were measured by flow cytometry using a CytoSense (Cytobuoy b.v., Netherlands) (laser 488 nm). Water samples (4 mL) were pre-filtered (200 µm) and fixed with glutaraldehyde and pluronic at a final concentration of 10%. Samples were stored at -80°C prior to analyses. Densities of each phytoplankton group were obtained in 2 runs with different speeds to increase the number of events. Size calibration was based on reference beads.

Second, *Pseudo-nitzschia* cells at the genus level were counted. After the sampling, 500 mL of sea water was preserved using acid Lugol's solution (2 $mL.L^{-1}$). The Utermöhl (1931) method was used to identify and count the cells. The Utermöhl method consists in transfering 10 mL, after homogenisation, into a sedimentation chamber for at least 8 hours before identifying and counting *Pseudo-nitzschia spp.* cells under a light microscope. Cell densities of *Pseudo-nitzschia spp.* per litres were then obtained.

4.2.2.2.2 Biomass

Chlorophyll-a concentrations were calculated using Aminot and Kérouel (2004). For total chlorophyll *a* concentration, 150 mL of water was filtered through a 25 mm glass fiber filter (GF/F; Whatman). For the size-fractionated chlorophyll *a* concentration, 150 mL of water was filtered through polycarbonate filters with pore sizes of 20 and 3 µm. After filtration, the filters were wrapped with aluminium foil to prevent photolysis and stored in a freezer until further analysis. Chlorophyll *a* was extracted with 90% acetone for 18–20 hours in the dark at 4 ◦C, and the concentration was measured using a fluorometer (*LS 50B Perkin Elmer*). Biomass (µg/L) of pico-, nano- and microphytoplankton were then calculated.

4.2.2.2.3 Toxins (particulate and dissolved)

After sampling, a volume of 1 litre of sea surface water was filtered through a 47 mm glass fibre (GF/F, Whatman) to determine the intracellular toxins. The filtrates were then used for determining dissolved toxins. Samples of filters and filtrates were stored at -20°C until analysis. To extract intracellular/particulate toxins, 250 mg glass beads (150-250 µm) and 2.5 mL MeOH/H_2O mixture (50/50: v/v) were added to the filters and stored at -80°C for 1 hour. Then, a mixer mill (MM400; Retsch) was used for mechanical grinding for 20 minutes at 30 Hz. Then, the samples were centrifuged (10 min, 4,300g, 4°C), and the supernatants were filtered through a 0.2-µm nylon filter (Nanosep MF; Pall). The filtered samples were then stored at -20°C until further analysis.

To determine extracellular toxins, solid-phase extraction (Bond Elut C18 200mg cartridges; Agilent) was employed to eliminate salts and concentrate the toxins. The SPE column was conditioned with 10 mL of methanol followed by 10 mL of Milli-Q water. The sample (100 mL of seawater) was acidified at 0.2% with aqueous formic acid before passing through the SPE column. The cartridge was rinsed with 10 mL of 0.2% aqueous formic acid and dried for 1 min. Toxins adsorbed on the cartridge were eluted using 2 mL of methanol/water (50/50: v/v) into a glass vial. The eluate was stored at -20°C until analysis.

Toxins analyses were performed using Ultra Fast Liquid Chromatography (UFLC) (Shimadzu) coupled to an ABSciex 4000 QTrap (triple quadrupole mass spectrometer). LC-MS/MS parameters are described in Caruana et al (2019). A certified domoic acid standard (CNRC, Halifax, Canada) was used for external calibration range (0.3-500 ng mL^{-1}) in order to quantify domoic acid. The limit of detection (LOD) and limit of quantification (LOQ) were respectively 0.1 and 0.25 ng mL^{-1}, corresponding to 1 and 2.5 pg DA on the column. Values were analysed with Analyst 1.7.2, ABSciex software and the content of intra-and extracellular toxins were expressed in pg mL^{-1}.

After, the quantities of toxins per cell were calculated (pg $cell^{-1}$), for that, the number of *Pseudo-nitzschia spp.* counted by light microscopy was divided by the percentage of *P. australis* across all the *Pseudo-nitzschia* identified by metatranscriptomic samples (chapter 2, rbcl marker aligned with the diat_barcode reference bank).

4.2.2.2.4 Gene expression data

4.2.2.2.4.1 RNA extraction, library preparation and sequencing

For total RNA extraction, directly after the sampling, 4-5 litres of water were filtered on 10 µm polycarbonate filters using a peristaltic pump. Filters were frozen in liquid nitrogen in RNA later (Fisher Scientific, Illkirch, France) and stored at −80 °C until RNA extraction. Total RNA was extracted by sonicating the filters on ice (Vibra-cell 75115, Bioblock Scientific, Illkirch, France) for 30 seconds at 35% intensity in LBP buffer (Macherey-Nagel, Duren, Germany). Extraction was performed using the NucleoSpin® RNA Plus kit (Macherey-Nagel) following the manufacturer's protocol. Library preparation was performed using the Illumina mRNA TruSeq stranded kit starting from 0.5 µg of total RNA. Paired-end sequencing was performed using 2 × 150 bp cycles on Illumina Novaseq6000 (2021 samples) at the GeT-PlaGe France Genomics sequencing platform (Toulouse, France). Generated fastQ files have been deposited to the European Nucleotide Archive (ERR9850557-562, 566-569, 572-574, 577-584, 589-592, 597, 600-607, 610-613, 619-621, 624-633).

After this step, samples from April 6th and April 9th in Telgruc; March 23rd, March 26th and April 2nd in Dinan-Kerloc'h; and April 9th in Sainte-Anne could not be sequenced due to low RNA concentrations. These samples were considered as missing data in the present study.

4.2.2.2.4.2 Sequence assembly and gene annotation

Prior to read mapping, raw reads were initially characterised with FASTQC (http://www.bioinformatics.bbsrc.ac.uk/projects/fastqc/) in order to assess read quality and quantity. TRIMMOMATIC (Version0.36) (Bolger et al., 2014) was then used to trim ambiguous, low quality reads and sequencing adapters with parameters: ILLUMINACLIP:adapter.fasta:2:30:10:8 LEADING:30 TRAILING:30 MAXINFO:40:0.5 MINLEN:80. After, using the BWA-MEM aligner (Lie et al., 2013), trimmed reads were aligned to a metareference corresponding to the combination of 315 species specific reference transcriptomes, representing 213 unique genera (Metegnier et al., 2020). It mostly corresponded to the resources developed during the Marine Microbial Eukaryotic Transcriptome Sequencing Project (MMETSP, Keeling et al., 2014) with the addition of reference transcriptomes obtained for three Pseudo-nitzschia species (*Pseudo-nitzschia australis, Pseudo-nitzschia fraudulenta* and *Pseudo-nitzschia pungens*) based on local strains (Lema et al., 2019). Samtools was used to discard reads displaying low quality alignments (MapQ<10), to remove read pairs that did

not align to the same transcript and to generate the raw read count expression matrix (Li et al., 2009).

4.2.2.2.4.3 Relative abundances of *P. australis*

Relative abundance of *P. australis* was obtained by dividing the number of reads assigned to it by the total number of taxonomically assigned reads in each sample. In the study the relative abundances are expressed in percentage. For the different analyses, *P. australis* was considered as present in the sampled community when its relative abundance was higher than 2%. The date when *P. australis* relative abundance first reach 2% was also retained. Due to our bi-weekly monitoring, we consider that the appearance of *P. australis* occurs between the last day of its absence and the moment of its detection. The indicator of its appearance thus obtained are day slices. This choice was made partly because there was no way of knowing when the species appeared between two samplings.

4.2.2.2.4.4 Analysis of *P. australis* expressed genes

Raw read counts corresponding to *P. australis* contigs were extracted. Transcripts covered by more than 10 reads on average across samples were first extracted, then those with a relative abundance higher than 2% belonging to *P. australis* were kept for further analysis. Following these filtering steps, a total of 24 samples and 14 924 transcripts were kept.

After preliminary analysis, one sample (Dinan-Kerloc'h on April 9th) was removed due to the absence of reads in various transcripts, and was found to be an outlier. After that, in order to minimise differences between samples, the dataset was normalised using Deseq2 Variance Stabilizing Transformation (Love et al., 2014).

4.2.3 Hydrodynamic connectivities

4.2.3.1 The local hydrodynamic model: CROCO-Iroise

We set up a three-dimensional hydrodynamic Coastal and Regional Ocean Community model (CROCO) (www.croco-ocean.org) over the West-Finistère (geographic extends between 47.9025 N and 48.61624 N; and between -4.087421 E and -5.292648 E). For our application, CROCO-IROISE solves the primitive and free surface equations under the hydrostatic and Boussinesq assumptions (Shchepetkin and McWilliams, 2005) over a regular grid with a horizontal resolution of 200 m and 30 sigma layers over the vertical (see chapter 2).

The bathymetry (fig.2) was constructed from MNT bathymetric data of the Atlantic coast (Homonim Project) with a resolution of 0.001° (~111 metres) (SHOM, 2015).

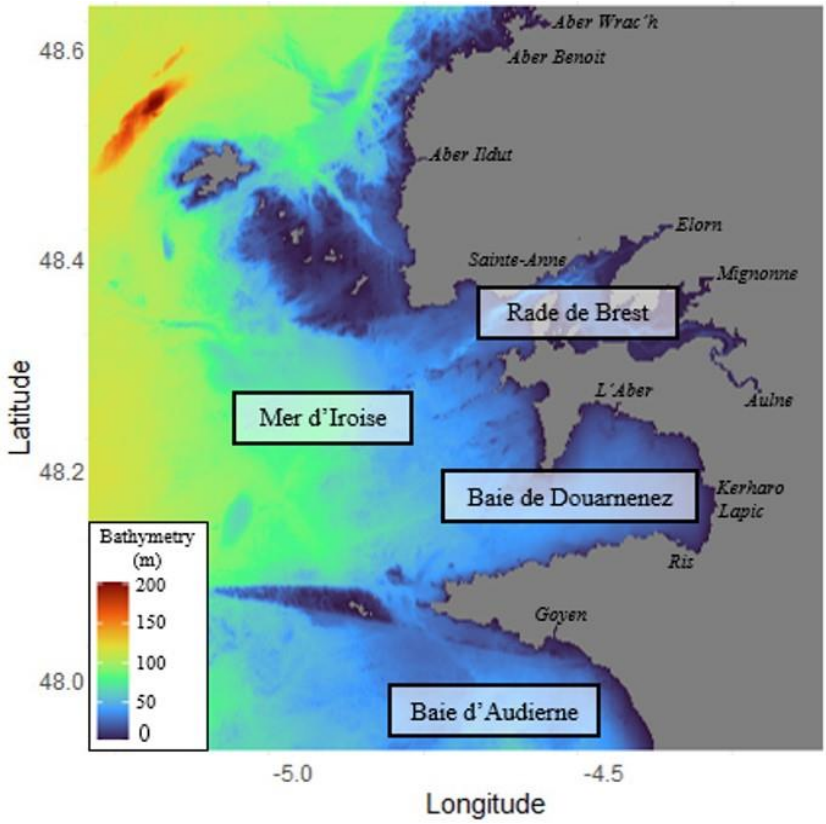

Fig. 2: CROCO-Iroise model footprint; the different areas of interest, and rivers are indicated.

The model is forced by various realistic forcings in order to simulate representative hydrodynamics. The forcings concern the daily flows of the various rivers shown in fig. 2, most of them were taken from the HYDRO database (http://www.hydro.eaufrance.fr/). For the smaller rivers, not present in the HYDRO database, monthly or annual flow climatologies were created on the basis of grey literature data when available or using watershed surfaces. The atmospheric forcings were derived from the AROME model (Météo France, Seity et al., 2011), and concerns: temperature, humidity, cloud cover, precipitation, local wind direction at 10 metres, sea level pressure, downward heat flux to the ground and surface radiation. In addition, the model is forced along the open boundaries by the sea-surface elevation obtained from the Previmer Atlas, and salinity and temperature were obtained from a wider model over the whole Iroise Sea that encompasses the targeted area (MARS3D, configuration MANGAE2500, with a 2.5 km resolution, interpolated on our grid).

In order to move on from the initial conditions mentioned above, and to get a coherent hydrodynamical signal: a 1-month spin-up was carried out.

The model has demonstrated its ability to reproduce the main characteristics of ocean flows (tidal amplitude and phase, 3D currents, salinity and temperature) with a good level of realism as shown in the chapter 3.

4.2.3.2 Hydrodynamic transport time analysis (Eulerian and Lagrangian transports)

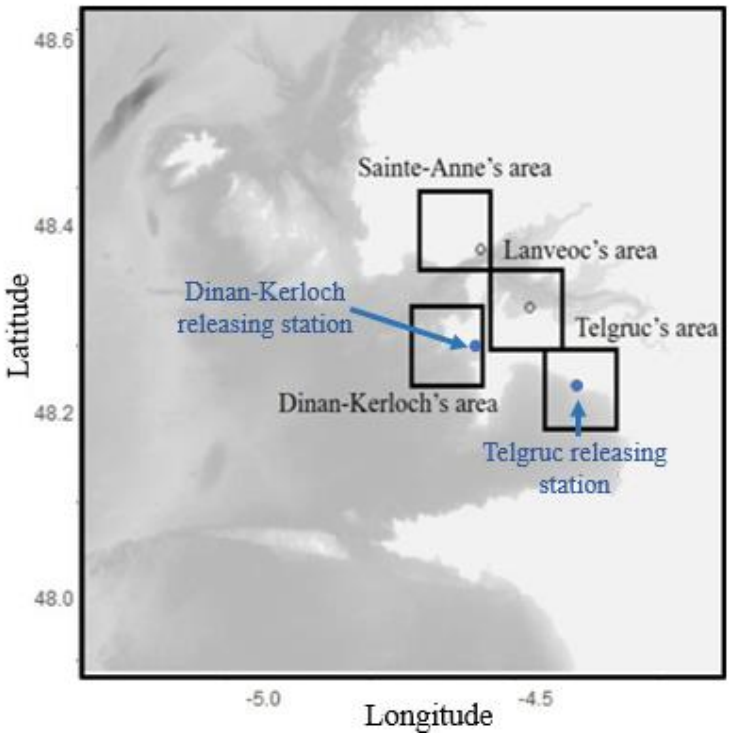

Fig. 4: Location of Eulerian tracer release and arrival zones drawn in black. Departure zones of the Lagrangian particles are represented by the blue dots. The dots represented the sampling stations.

4.2.3.2.1 Eulerian transport

The hydrodynamic connectivity between station' areas was characterised by the results of Eulerian's tracer transport carried out over the sampling period (from 2021-02-26 to 2021-04-16).

As described in chapter 3, four 50x50 grid-mesh zones were selected as tracer departure and arrival zones. Differing from the chapter 3, the zones were remodelled to encompass the monitoring zones (fig. 4) and the simulations were initialised when *P. australis* appeared in order to simulate a representative bloom and facilitate comparison with the metatranscriptomic data: two simulations were run. In the first one, tracers were released from Telgruc's area on

February 26th, and in the second one tracers were released from Dinan Kerloc'h's area on March 9th.

An initial concentration of 100% tracer was released over the entire water column (the 30 sigma layers) at the 2 zones. Then, to enable comparison of the quantities of tracer arriving at a given station, the initial mass percentage for each tracer was calculated as described in chapter 3.

Connectivity from Telgruc was analysed towards Dinan-Kerloc'h, Sainte-Anne and Lanvéoc; and connectivity from Dinan-Kerloc'h was analysed towards Sainte-Anne and Lanvéoc (fig. 4). Connectivity was characterized by two indicators, one representing the time of arrival of a tracer in a zone with an initial mass >0.1% (Tmin) and the time associated with the maximum mass (Tmax) of this tracer.

The selection of the tracer arrival threshold: >0.1% was based on (i) the highest observed percentage of tracer mass (maximum of 0.15% between Telgruc and Lanvéoc), and marked shifts in the percentage of tracer mass arrival that occurred beyond this threshold.

4.2.3.2.2 Lagrangian transport

In addition to Eulerian transport, which provides information on connectivity between zones through the use of temporal indicators, Lagrangian transport has enabled us to observe the trajectories of individual particles.

The transport trajectory between stations was observed using particle transports released on February 26th at Telgruc and March 9th at Dinan-Kerloc'h for a period of 7 days.

The Lagrangian particle transport was carried out using ICHTHYOP software, developed by IRD and described in Lett et al., 2008 (https://www.ichthyop.org/). CROCO Iroise model provided the 3D current fields every 30 minutes.

For both simulations 100,000 fictive particles were released at the surface within a cylinder (radius of 1000 m, 10 m deep), at the two following locations: 48.209933 N, -4.373308 E and 48.257071 N, -4.560974 E for Telgruc and Dinan-Kerloc'h respectively (see fig. 4).
The particles have been initialised as having no behaviour, no buoyancy and do not run aground. A forward Euler numerical scheme is used to discretize the transport equations. Computational

time step *dt* was set to 40 seconds in order not to break the CFL criterion (*U*dt*)/*dX* <= 0.7, where *U* is the speed current in m/s and *dX* is the grid cell length in m. Default horizontal dispersion parameter according to the formulation of Peliz et al. (2007) was kept unchanged (10^{-9} m^2/s^3).

4.2.4 Statistical analysis

All statistical analyses and graphics were performed with R software v. 3.2.3 (R Core Team, 2014).

First, a principal Component Analysis (PCA, factoextra R package, Kassambara and Mundt, 2017) was used to assess temporal and/or spatial relationships between the samples based on the environmental variables along a reduced number of axes. The analysis involved physico-chemical parameters (temperature and salinity, PAR, suspended matters, current speeds, and nutrients concentrations) and biological parameters (pico-, nano and micro-phytoplankton abundances and biomass). Prior to these analyses, all variables were centered and scaled in order to make them dimensionally homogeneous.

Second, to determine the spatio-temporal evolution of gene expression, a PCA was performed on all the expressed genes.

Finally, the correlation between biological, physico-chemical parameters and gene expressions was tested using a canonical correlation analysis (CCA analysis, vegan package, Oksanen et al., 2007).

4.3 Results

4.3.1 Spatio-temporal dynamic of *P. australis* and the relationship with environment

During 2.5 months (between February 26th and April 16th) an *in situ* survey during a *P. australis* bloom was performed in four different sampling points. Based on metatranscriptomic samples, spatio-temporal *P. australis* composition was identified. Environmental reads corresponding to *P. australis* contigs were extracted and the relative abundances of *P. australis* transcripts were calculated (figure 5).

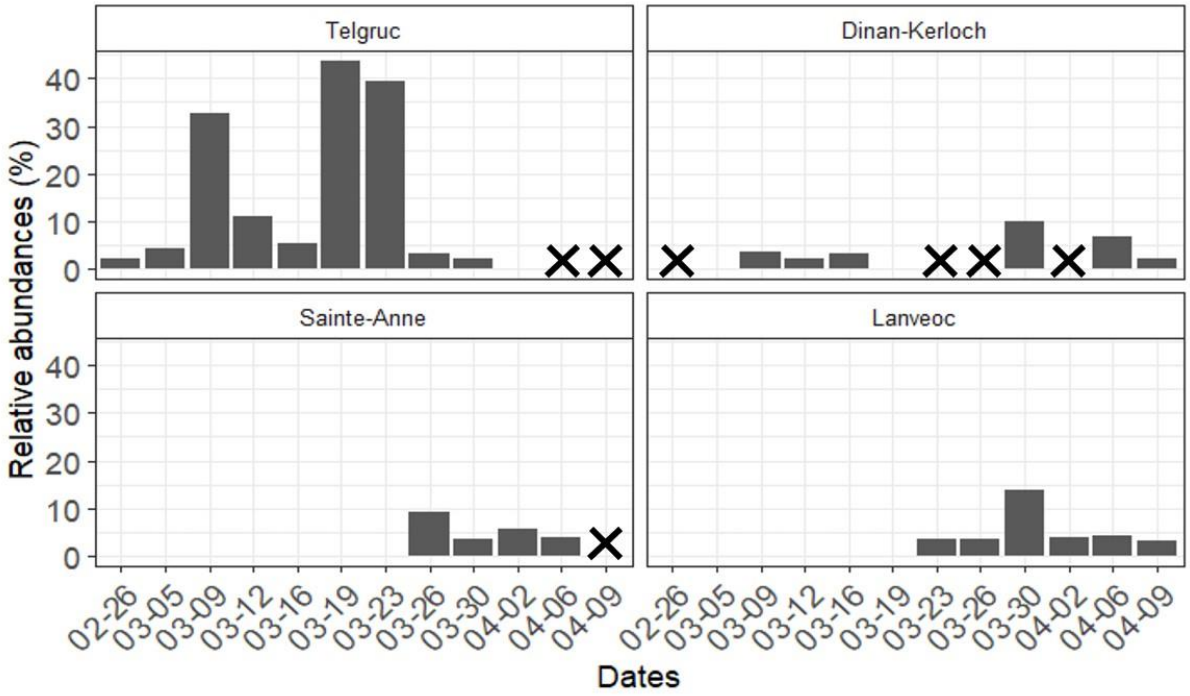

Fig. 5: Relative abundances of transcripts expressed by P. australis between February 26th and April 16th. Crosses correspond to missing data and the white areas correspond to samples where P. australis had not been detected (relative abundance < 2%).

At Telgruc, relative abundances of *P. australis* were above 2% from the beginning of sampling on February 26th until March 30th. A first strong relative abundance of 32.5% was observed on March 9th A maximum of 43.5% was reached on March 19th before decreasing strongly until the species was not detected on March 30th.

At Dinan-Kerloc'h, the maximum values were identified on March 30th (10.1%) and April 6th (6.9%), although its presence has been identified since March 9th, there are some missing samples.

Sainte-Anne and Lanvéoc showed fairly similar results temporally with maximum relative abundance on March 26th (9.2%) at Sainte-Anne and March 30th (13.6%) for Lanvéoc (fig. 5).

Globally, a spatio-temporal shift was identified with first a development in Telgruc (from February 26th), then in Dinan-Kerloc'h (from March 9th) and finally in the Bay of Brest (from March 23d first at Lanvéoc and then at Sainte-Anne).

In order to understand the development and the south-north shift, biotic and abiotic environmental variability was analysed using a PCA (fig. 6).

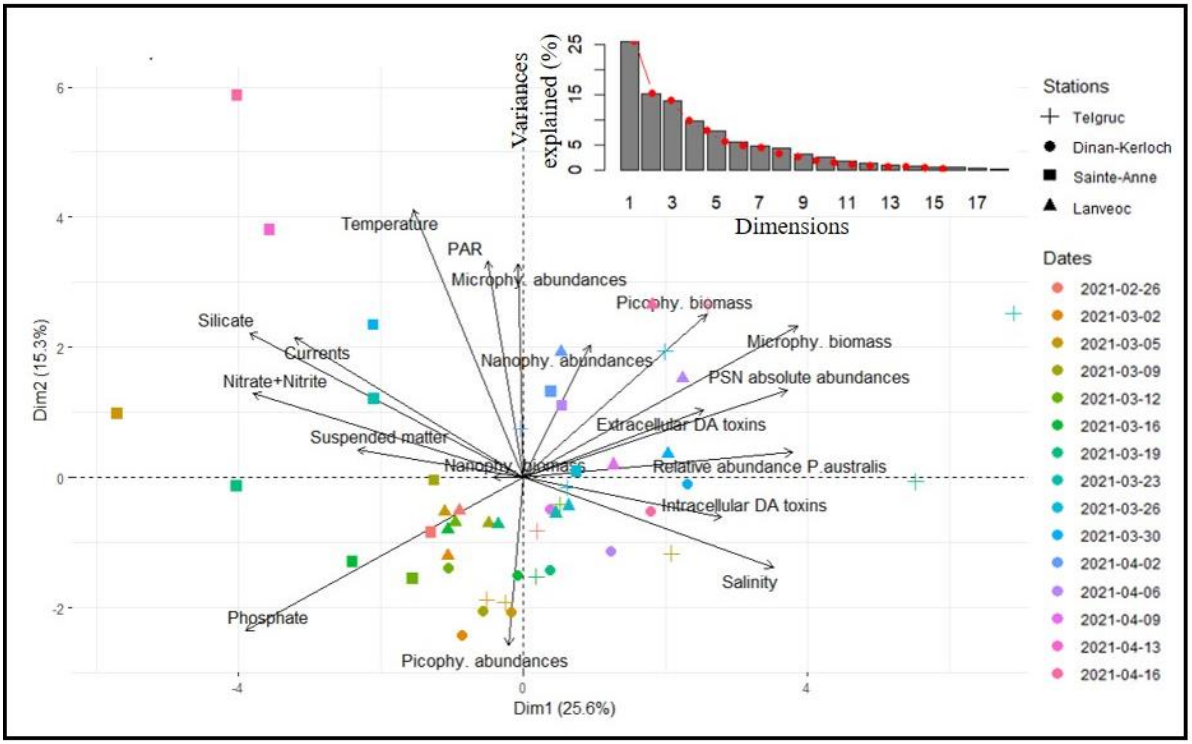

Fig. 6: First two components of PCA showing relationships between biotic and abiotic environments and samples. Sampling dates (colors) and sampling stations (shapes) are indicated. The black arrows represent the biotic and abiotic variables.

The first two PCA axes explain 40.9% of the variance, of which 25.6% is explained by the 1st axis (fig. 6).

It is important to notice that the absolute counts of *Pseudo-nitzschia* were correlated to the relative abundance of *P. australis* and both of them correlated to the microphytoplankton biomass. This certainly supported the bloom of this species. Extra- and intracellular toxins were observed in higher quantities when the presence of *P. australis* was higher. *P. australis* was mainly found in high abundance in Telgruc in the middle of the sampling period, and in Lanvéoc towards the end. Overall, phosphate concentration tended to be lower during the second half of the survey, when *P. australis* was more abundant.

With regard to spatial variability, environmental conditions in Sainte-Anne often contrasted with the other stations, and especially with those recorded in Telgruc. Saint-Anne was characterised by a freshwater-impacted environment, reflected by higher nutrient concentrations (silicates and nitrates + nitrites), warmer waters, more suspended matter, higher current velocities and lower salinity.

Finally, concerning the temporal variability, picophytoplankton abundances and phosphate concentration were higher at the beginning of the monitoring. Temperature, PAR and microphytoplankton abundances tended to increase toward the end of the sampling period (Figure 6, Supplementary figure 1). Altogether, these results do not support a spatio-temporal

shift in terms of environmental parameters, suggesting that the spatio-temporal time shift in the apparition of *P. australis* cannot be explained by the measured environmental parameters.

3.2 Does the time associated with hydrodynamic transport coincide with the spatio-temporal shift of *P. australis*?

Hydrodynamic connectivity was investigated as an alternative to better understand the functioning of the area and find a potential explanation for the temporal shift between stations.

Simulations were used to investigate if hydrodynamic connectivities could elucidate the spatio-temporal shift observed in the appearance of *P. australis*. Following the initial detection of *P. australis* during the survey, tracers were released on February 26th from Telgruc and on March 9th from Dinan-Kerloc'h. The analysis focused on examining the connectivity between these stations and those located further to the north. The figure 7 showed the evolution of tracer arrival in the different zones over time as well as the relative abundances of *P. australis*.

From the start of monitoring (February 26th), there was a higher hydrodynamic connectivity from Telgruc to Dinan-Kerloc'h compared with the other stations. Even if the tracer masses remained low (maximum of 2.5%), the associated time was rather low, and tracers arrived in 7 days (March 5th).
In comparison, only 0.15% of Telgruc's tracer mass reached Sainte-Anne and Lanvéoc after 32 days.

During the subsequent simulation involving the tracer released at Dinan-Kerloc'h on March 9th, the mass of maximum tracer released was 14% at Sainte-Anne (after 3 days) and 15% at Lanvéoc (after 5 days).

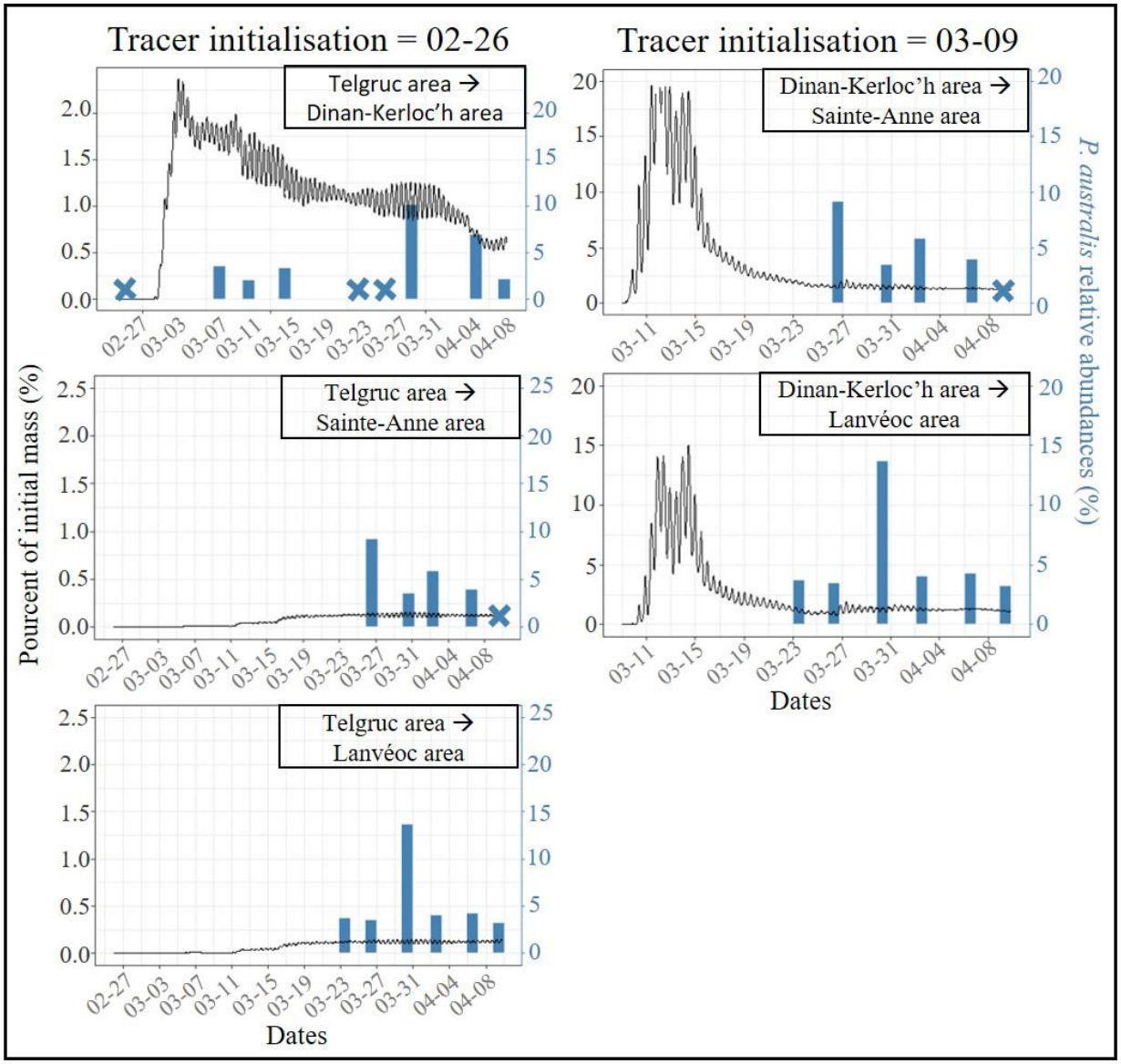

Fig. 7: Evolution of the percentage of mass of tracer leaving a zone and arriving in the other zones (black line). The left-hand column shows the arrival of tracers initialised in Telgruc on February 26th, heading for Dinan-Kerloc'h, Sainte-Anne and Lanvéoc. The right-hand column shows the arrival of tracers initialised in Dinan-Kerloc'h on March 9th, heading for Sainte-Anne and Lanvéoc. The blue bars represent the relative abundance of P. australis in the arriving area and crosses correspond to missing data (fig. 5). The scales between the two starting zones are different.

Hydrodynamic connectivity and *P. australis* emergence were compared in table 1.

Table 1: Time lags observed (P. australis relative abundances, first row) and simulated (Tmin - Tmax of tracers, second row).

	Telgruc's initialisation (02-26)			**Dinan-Kerloc'h's initialisation (03-09)**	
	Dinan-Kerloc'h	**Sainte-Anne**	**Lanvéoc**	**Sainte-Anne**	**Lanvéoc**
Identification of *P.australis* relative abundances (days)	7-11	25-28	21-25	14-17	10-14
	Box 1	**Box 2**	**Box 3**	**Boxes 2**	**Box 3**
Eulerian connectivity (days)	5-7	19-32	19-32	0.3-3	1-5

First, the time scales associated with hydrodynamic connectivity and the identification of *P. australis* between Telgruc and Dinan-Kerloc'h were in agreement (table 1). From Telgruc, a maximum mass of tracer reached Dinan-Kerloc'h with a Tmin and 5 days and a Tmax of 7 days, a time gap of 7 to 11 days was found between the detection of *P. australis* at Telgruc and its subsequent appearance at Dinan-Kerloc'h. This result may support a possible role of hydrodynamics in the identification of *P. australis* at Dinan-Kerloc'h.

Second, regarding the arrival of tracers to the Bay of Brest, comparisons between the hydrodynamics connectivity and the appearance of *P. australis* were consistent from Telgruc and inconsistent from Dinan-Kerloc'h.

Indeed, starting from Telgruc, the simulation results indicated that tracers reached the Bay of Brest between 19 (Tmin) and 32 (Tmax) days and the identification of the species was identified after 25-28 days to Sainte-Anne and 21-25 days to Lanvéoc.

But significant differences were observed between the identification times of *P. australis* and the tracer transport time from Dinan-Kerloc'h to the Bay of Brest. After being initialised from Dinan-Kerloch on March 9th, the simulation results indicated that the tracer reached the Bay of Brest quickly with a Tmin of 0.3 days and a Tmax of 5 days, and *P. australis* was identified after 14-17 days at Sainte-Anne and 10-14 days at Lanvéoc.

From a hydrodynamic perspective, the time gap between the emergence of *P. australis* in Dinan-Kerloc'h and the Bay of Brest does not align with the idea of particles originating from Dinan-Kerloc'h being transported.

Lagrangian particle trajectories were observed for 7 days from Telgruc and Dinan-Kerloc'h in order to see their directions between the stations (fig.8).

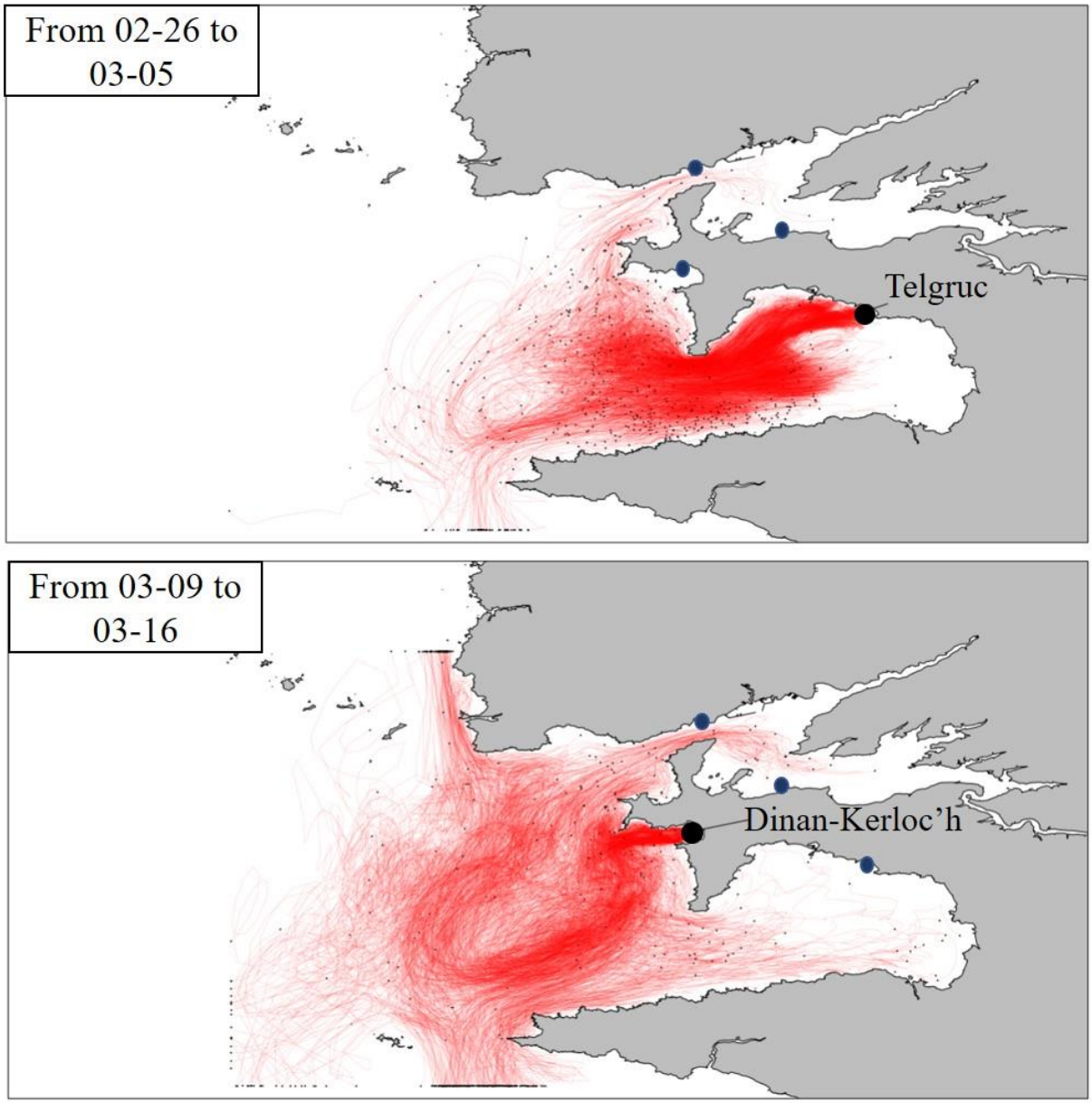

Fig. 8: Map of the trajectories of 100,000 Lagrangian particles from Telgruc from February 26th to March 05th (top map) and from Dinan-Kerloc'h from March 09th to March 16th (bottom map). Other monitoring stations are indicated by blue dots. The red lines represent the trajectories of the particles emitted, and the black dots represent the arrival position of these particles after 7 days of simulation.

Particle trajectories from Telgruc showed predominantly coastal trajectories, mainly towards the Dinan-Kerloc'h area, but a large majority headed south towards the Bay of Douarnenez, or outside the model's footprint (to the south). It is also interesting to note that a very small number of them end up in the Bay of Douarnenez after 7 days and those that were there were more likely to be located in the southern part of the bay. The trajectories also revealed that particles were not required to transit through Dinan-Kerloc'h as they made their way to the Bay of Brest. A fraction of particles was carried offshore from Dinan-Kerloc'h and proceeded towards the Bay of Brest.

By contrast, on departure from Dinan-Kerloc'h on March 9th, particles tended to disperse within the simulation zone. Many of them exit the model footprint to the south and south-west, and even to the north. A small number of particles are moving towards the Bay of Douarnenez, and a few particless are moving directly from Dinan-Kerloc'h to the Bay of Brest, but it would appear that the majority of them, before reaching the Bay of Brest, head south and pass offshore (fig. 8).

4.3.2 Does the spatio-temporal dynamics of expressed transcripts show a shift?

Next, we investigated whether the physiological state of *P. australis* cells changed during the bloom and whether these changes followed a spatio-temporal pattern

Our approach is based on the global gene expression as a proxy of physiological state. This approach enables us to capture the temporal and spatial variability between cells, without specifically characterizing this physiological state.

To determine gene expression dynamics of *P. australis* according to sampling dates and stations, a PCA was performed to visualise the variability between samples for 14 924 expressed genes. The two first PCA components explained 22.2% of the dataset variability and showed that the higher variability on gene expression was not spatial but temporal (fig. 9).
When two samples are close in the PCA, this indicates that at least part of the gene expression is similar.

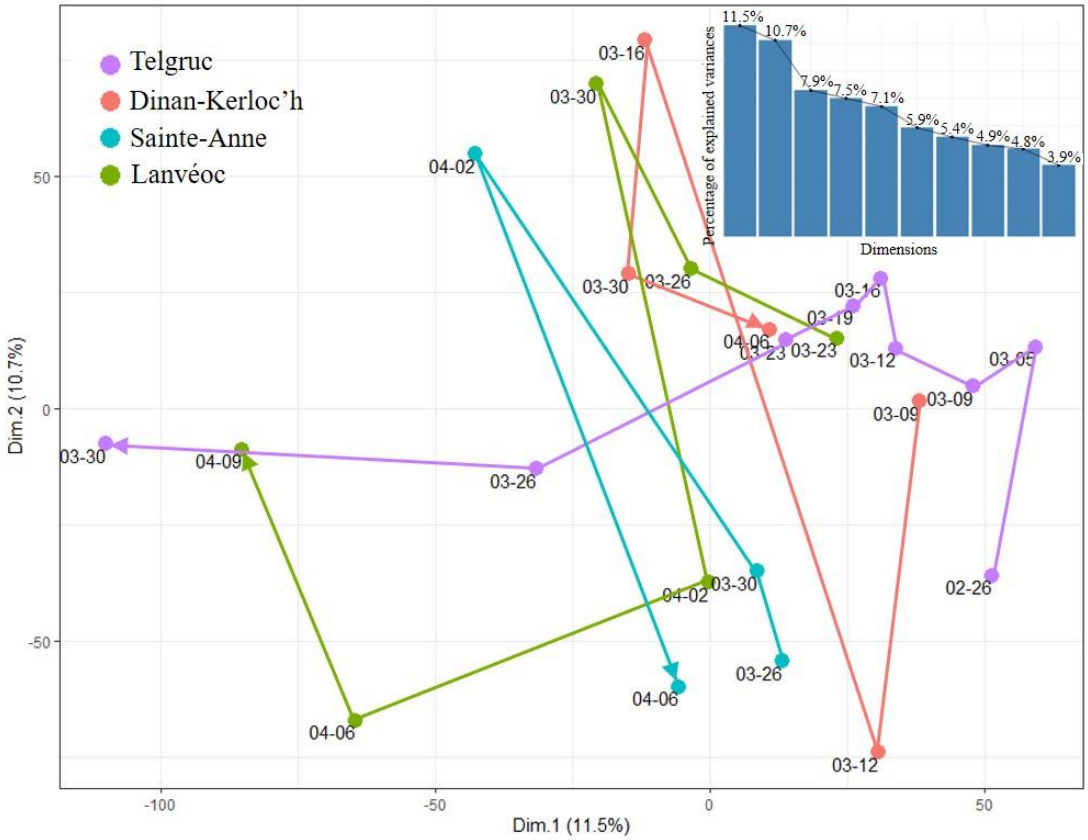

Fig. 9: PCA on all genes expressed by P. australis. The dots indicate the dates, and the colours indicate the different stations. The lines link the samples of each station from the beginning to the end of the sampling.

The first axis (accounting for 11.5% of the variability) illustrates the temporal changes of *P. australis* gene expression. Along this axis, temporal change of *P. australis* gene expression was mainly marked for Telgruc. Lanvéoc displayed the second most notable temporal changes in gene expression. On the contrary, gene expression changes for Dinan-Kerloc'h and Sainte-Anne were more restrained along this first axis and displayed higher changes along the second one.

On March 9th, when *P. australis* was first detected at Dinan-Kerloc'h, gene expression was similar in Dinan-Kerloc'h and Telgruc. On March 12th, expression remained similar according to the first axis but diverged along the second axis. After this date, gene expression in Dinan-Kerloc'h and Telgruc tend to diverge. On April 6th, end of *P. australis* presence in Dinan-Kerloc'h, gene expression in Dinan-Kerloc'h was similar to that shown in Telgruc on March 23^{d}

On March 23^{d}, *P. australis* was detected at Lanvéoc. At this date the expression was similar to the one observed in Telgruc on March 19th and March 23^{d}. Then gene expression at these two stations tend to diverge till the end of the bloom.

P. australis was then detected at Sainte-Anne (March 26th), and gene expression was similar to Telgruc on March 23d and March 19th and Lanveoc on March 23d only according to the first axis. According to this same axis, on March 30th, expression was similar in Lanveoc, Saint-Anne and Dinan-Kerloc'h.

Finally, at the end of the bloom, gene expression was similar at Telgruc (March 30th) and Lanvéoc (April 9th), but not at the other two stations.

Although these results represent only part of the variability in *P. australis* gene expression, they highlighted a strong relationship between stations on some of the expressed genes, in particular between Telgruc and the other stations.

4.3.3 Does gene expression differ depending on the local environment?

Finally, we tested whether the cell physiological states were correlated with environmental variables.

In figure 10, we investigated the relationship between gene expression and the environment using a canonical correspondence analysis (CCA).

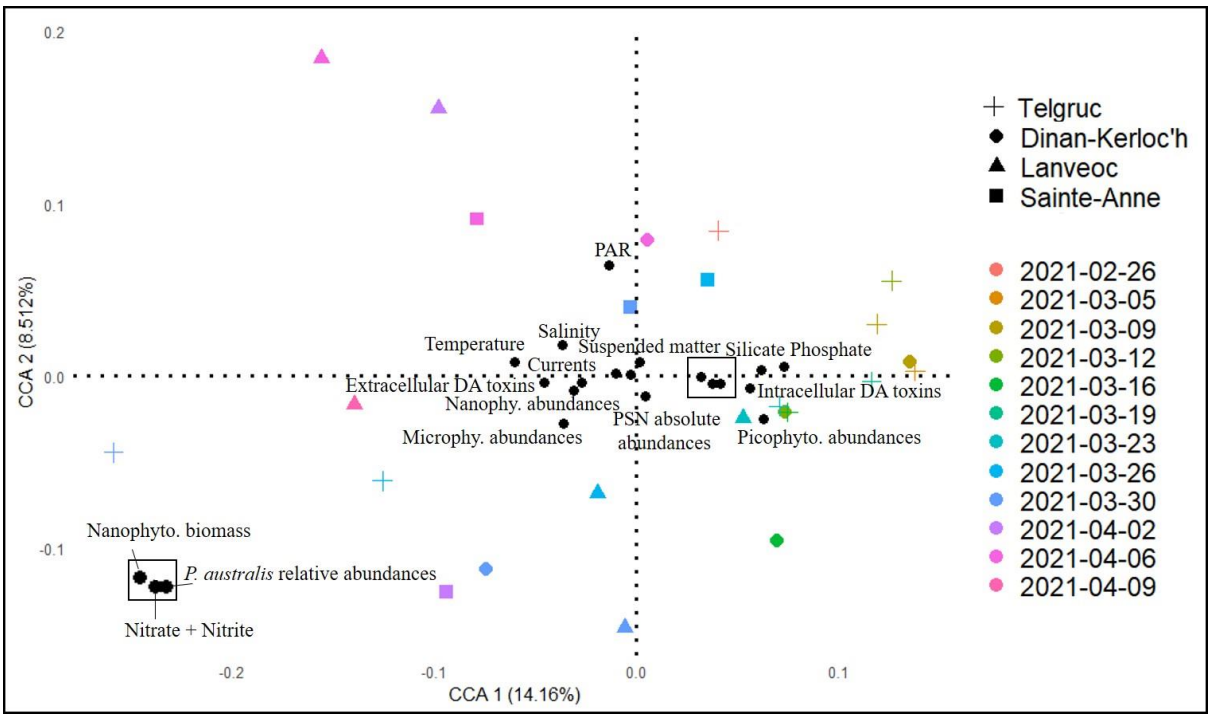

Fig. 10: Canonical Correlation Analysis (CCA) of the genes expressed by P. australis in each sample (shapes and colors) and its association with environmental variables. Sampling dates (colors) and sampling stations (shapes) are indicated. Black dots are quantitative explanatory environmental variables with their position indicating their direction of increase. For clarity, the black rectangle represents a zoom on some environmental variables.

The first axis (accounting for 14.2% of the variance) explained the temporal evolution in gene expression. Gene expression at the beginning of the bloom was on the right side while at the end it was on the left.
On this first axis, at the beginning of the bloom, gene expression was correlated with phosphate and to lesser extent silicate, picophytoplankton abundances and intracellular toxins. At the end of the bloom, gene expression was correlated with higher temperature and extracellular toxins.
On the second axis (accounting for 8.5% of the variance), especially for Dinan-Kerloc'h, Sainte-Anne and Lanvéoc, the end of the bloom was correlated with higher PAR.

More generally, it seems that gene expression is correlated with the seasonal evolution already observed in figure 6.

4.4 Discussion

In this study, metatranscriptomic samples were used to characterize the emergence of the toxic diatom *P. australis* in four stations of West Brittany in March 2021. Its first appearance at the different stations followed a south-north gradient, with a time lag.
Indeed, the species was first identified in the south of the study area (Bay of Douarnenez, Telgruc) the 26th of February before being observed between 7 and 11 days after at the next station (Dinan-Kerloc'h), and again 10 and 17 days after further north at the stations of the Bay of Brest (Sainte-Anne and Lanvéoc).

As said before, cells of *P. australis* were first identified at Telgruc on February 26th. Starting from March 5th until March 23rd, *P. australis* cells were actively growing at the Telgruc sampling point. This is supported by the increase in absolute *Pseudo-nitzschia* cell densities (supplementary materials, fig 1) and very strong relative abundance of the *P. australis* species within the genus (the latter being especially visible in the figure 6 of chapter 2). Even when tidal coefficients and subsequent dilution were increasing (between March 10 to 16), absolute *Pseudo-nitzschia* cell densities tend to be stable. As a result, the gene expression pattern in Telgruc from March 5th to 23rd should reflect the fact that the cells were actively growing. The shift in gene expression after March 23rd, might reflect a transition from actively growing to non-growing cells. To validate these hypotheses, our metatranscriptomic dataset could be used to study the expression of specific gene functions.

The actively growing cells in Telgruc were probably transported by currents toward Dinan Kerloc'h and started to be detected at this station around March 9th. This is in phase with the simulated hydrodynamic connectivity time between these two stations. When they reached this station, cells were in the same physiological state as the actively growing cells from Telgruc. An alternative explanation would be that gene expression in Telgruc and Dinan Kerloc'h around March 9th were similar because the environmental conditions were similar at the two stations. The environment variables were relatively similar at this time, however, on the 16th it was also the case but gene expression started to diverge. This would tend to favor the hydrodynamic connectivity hypothesis rather than the environmental one to explain the gene expression similarities observed on March 9th.

At Dinan Kerloc'h absolute *Pseudo-nitzschia* cell densities (and thus *P. australis* densities) remained low during the entire period of monitoring, suggesting that either cells were not actively growing (or at least displayed a low growth rate) or growth rate was unable to cope with local dilution rate at this station. In any case, we observed a divergence in gene expression between Telgruc and Dinan-Kerloc'h after March 9th. From this date, it is conceivable that a growing cell population arriving (consistently) from Telgruc by the currents is mixed with another cell population that was moved earlier from Telgruc (or another place) but is no longer dividing. Around March 30th, absolute *Pseudo-nitzschia* cell abundances increase at this station. We have three possible hypotheses for this, first, this may result from an active local growth of *P. australis* (to be tested by looking at gene expression of specific genes), second, the hydrodynamic transport of the dense bloom from the Bay of Douarnenez (unlikely because gene expression is quite different in Telgruc and Dinan-Kerloc'h on March 30th) and third, the active development of *P. fraudulenta* (its relative abundance strongly increased in Dinan-Kerloc'h around this date, cf figure 6 of chapter 1).

The time lag between *P. australis* appearance in the Telgruc area and the Bay of Brest is compatible with hydrodynamic connectivity time. We may thus wonder if the healthy dividing cells from the Bay of Douarnenez could have travelled to the Bay of Brest and be directly responsible for the increase in cell densities observed in this area. If it is the case, the cells would have travelled from the Bay of Douarnenez to the Bay of Brest without transiting by the Dinan-Kerloc'h area. Interestingly, the Lagrangian simulations seem to support this since some particles show trajectories that avoid Dinan-Kerloc'h area but still reach the Bay of Brest. Eulerian simulations showed very short transport time between Dinan-Kerloc'h and the Bay of Brest through the apparition of *P. australis* in Sainte-Anne or Lanveoc is later (fig. 4). This

could be explained either by a retention of cells in the Bay of Dinan (the Dinan-Kerloc'h area for releasing the tracer being not representative for the sole Dinan-Kerloc'h station) or that the first slight apparition of *P. australis* in Dinan-Kerloc'h (7^{th} to 15^{th} of March) remained unperceived in the Bay of Brest while the second apparition on March the 27^{th} was strong enough to be transferred and perceived in our metatranscriptomic results.

When they first appeared in the Bay of Brest, *P. australis* cells gene expression displayed some similarity with the Telgruc *P. australis* cells sampled at the same date. Two alternative hypotheses may explain this pattern. First, it could mean that gene expression changed independently depending on local environmental conditions and that conditions were similar in the Bay of Brest and Telgruc. However, at the time of *P. australis* appearance in the Bay of Brest, environmental conditions were not more similar in the Bay of Brest and Telgruc than at other sampling dates. Second, it could mean that gene expression changed synchronously in the actively dividing cells across the entire study area during up to 30 days (table 1). It could either be due to environmental conditions changing in a synchronous fashion across the entire study area or to an internal clock governing changes in gene expression more or less independently of environmental conditions. It should be noted that in the present study, the major changes in environmental conditions reflect the transition from winter to spring and these changes display a similar trend across the entire study area (increase in temperature, PAR, and decrease in nutrients due to consumption). We may also wonder, at what point our intertidal sampled sites might overestimate the spatial differences in environmental conditions across the entire area. More specifically temperature, salinity, and nutrient concentrations may vary rather quickly at intertidal sites but these changes can be short term, limited in space and may not reflect the environmental conditions encountered by most of the cells across the entire study area. In further studies, we could envisage monitoring the salinity and temperature conditions encountered by the particles during Lagrangian simulations. With the present data, it seems difficult to tear apart the environmental vs internal clock explanation.

After the initial cell arrivals in the Bay of Brest, gene expression diverged from Telgruc as well as between Sainte-Anne and Lanvéoc. As already developed for Dinan Kerloc'h, this may reflect active cells arriving continuously by transport, and mixing with other cells arrived earlier, and/or in a distinct physiological state (which have stopped dividing?).

One major question remains. At what point did *P. australis* cells actively divide in the Bay of Brest? Concentrations of *Pseudo-nitzschia* counts were much higher in the Bay of Douarnenez

compared to the Bay of Brest, with a maximum of 498,000 cell/L at Telgruc, while in the Bay of Brest the maximum counts were 59,700 cell/L at Sainte-Anne and 63,500 cell/L at Lanvéoc (see supplementary materials and relative abundances fig. 6, chapter 2). This is further reinforced by the findings of REPHY's observations (REPHY, 2022, see introduction) of *P. australis* over the last decade, consistently revealing higher quantities in the Bay of Douarnenez compared to the Bay of Brest. It is well known that there's a difference in the speed of currents between the Bay of Douarnenez, which are much lower (Le Fèvre and Grall, 1970) than those prevailing in the Bay of Brest (Le Pape et al., 1996; Le Pape and Menesguen, 1997). This is confirmed by additional calculations we did, taking advantage of our Eulerian simulation of tracer dilution in 2021 (see Supplementary materials 3). Indeed, the calculated e-flushing times (the time needed for dilution to drop the tracer quantity to 37% of initial quantity in a particular area) were much longer in the Bay of Douarnenez and Lanvéoc area (2 and 3 days, respectively), than in Dinan-Kerloc'h (0.6 days), and in Sainte-Anne (0.1 days). This makes the Bay of Douarnenez a more retentive zone as previously stated by Merceron et al. (2007). Various studies have shown that a long residence time of water in an ecosystem favors phytoplankton development and retention (Artigas et al., 2014; Drouzy et al., 2019; Lucas and Deleersnijder, 2020; Ruiz-Villarreal et al., 2016; Velo-Suárez et al., 2010), while regions with a short residence time limit the development of high phytoplankton biomass, despite local conditions favorable to the development of a bloom (Lucas and Deleersnijder, 2020). One study on the east coast of the United States (Cape Cod) showed that one important factor controlling the *Alexandrium fundyense* bloom was the water retention (Ralston et al., 2015). The differences in dilution rate may therefore explain the differences in *P. australis* concentrations observed between the Bay of Douarnenez and the Bay of Brest. More specifically, this may indicate that the balance between growth rate and dilution rate is a major factor explaining the differences in cell abundances between the two bays. Reaching high cell densities in the Bay of Brest would need higher growth rates than in the the Bay of Douarnenez. Moving from purely hydrodynamic toward biological models including cell growth rate could help addressing this problem. Even a simple 0D model with two test cases may help.

With this last point, we may even wonder whether the observed spatio-temporal time shift might not simply be the result of the growth rate vs dilution difference between the two bays. However, such a simple explanation seems unlikely given that the time lag is visible for different species (chapter 2) and also exists towards the end of the blooming period, which

cannot be explained by differences in dilution rates. In addition, flushing times are relatively long at Lanvéoc.

Finally, taken together, the results seem to suggest a hydrodynamic transport of cells from Telgruc. This would suggest that the Bay of Douarnenez is a source area of the *P. australis* blooms in West-Brittany. Although the content of this chapter is based on a single spatio-temporal monitoring study of *P. australis*, it is worth pointing out that REPHY's observations of *P. australis* blooms have always begun in the Bay of Douarnenez, and then extended to the bay of Brest. Different studies have highlighted the transport of HAB, from a source area where blooms are induced to a sink area (e.g. Giddings et al., 2014; MacFadyen et al., 2005). MacFadyen et al. (2005), by studying the trajectories of ARGOS-tracked drifters and particles in a model, demonstrated that a seasonal cold eddy located off the mouth of the Strait of Juan de Fuca was involved as an initiation site for toxic HABs (in particular *Pseudo-nitzschia spp.*) affecting the Washington coast. Giddings et al. (2014), further investigated the development of *Pseudo-nitzschia* on the Washington coast using a realistic simulation model. They highlighted that transport pathways are seasonal, with transport to the Washington coast from a northern source (the Juan de Fuca eddy) during the summer/fall upwelling season and from a southern source (Heceta Bank) during winter/early spring due to predominant wind-driven currents.

Another crucial aspect to consider when examining *P. australis* blooms is their toxicity. If cells can be transported, is it possible that toxins can too? In the present study, the measured particulate and dissolved toxins reveal a peak of intracellular toxicity at Telgruc when *P. australis* cells divided on March 19th, with 203,800 cells of *Pseudo-nitzschia* per litre (the maximum absolute concentration was on the 23rd with 498,000 cells/L). Seven days later, a major peak in extracellular toxins was observed in Dinan-Kerloc'h (March 26th). This observation raises the question of whether this extracellular peak, which is not observed at the other stations, could be the result of the large bloom peak of Telgruc. In addition, the hydrodynamic time intervals correspond (7 days between the two peaks). REPHY data (REPHY, 2022) measured domoic acid concentrations above the sanitary threshold (20 mg/kg bivalve flesh) three times higher in the Bay of Douarnenez (Kervel) than in Dinan-Kerloc'h. These observations showed that in 2021, Kervel station as well Dinan-Kerloc’h has been heavily impacted by *P. australis*.

In the Bay of Brest, toxins did not exceed sanitary thresholds (REPHY, 2022). This is confirmed by the present study, with lower toxin concentrations in the Bay of Brest. Nonetheless, for both

Sainte-Anne and Lanvéoc stations, it seems that particulate toxin peaks precede dissolved toxin peaks. The particulate peaks seem to arrive at the same time as our identification of *P. australis* in the Bay of Brest. Moreover, the hydrodynamic times coincide with transport from the Bay of Douarnenez. Is this the result of cell transport in active division?

Environmental stress has not been identified in the literature as a precondition for toxin release in *P. australis*. In our current study, there does not appear to be any nutrient limitation in the Bay of Douarnenez or the Bay of Brest at the time of the intracellular toxin peak observed at the different stations. Unlike other *Pseudo-nitzschia* species (see Lelong et al., 2012), experiments on *P. australis* cells collected in the English Channel produced domoic acid under equilibrated growth, without nutrient limitation (Thorel et al., 2014). Furthermore, in their study, Thorel et al. (2014) also found higher concentrations of domoic acid in the cells during the exponential growth phase. These observations are in line with other studies carried out on *P. australis* strains, which have shown that cells produce domoic acid during the exponential growth phase (Lelong et al., 2012; Martin-Jézéquel et al., 2015; Schnetzer et al., 2017). Moreover, in the chapter 5 of this thesis, gene expression over the entire period of a *P. australis* bloom revealed higher expression of genes related to the toxin biosynthesis during the first (exponential growth) and third (decrease) period of the bloom.

Thus, as mentioned earlier in this discussion, the toxin study showed that it could be that the cells arriving in the Bay of Brest were in an exponential growth phase. If so, this could explain the similarities in gene expression between the Bay of Douarnenez and the Bay of Brest.

To conclude this chapter, the coupled results from the environment, hydrodynamics and gene expression indicated that the cells were transported from the Bay of Douarnenez to the Bay of Brest. Cells arriving at the various stations showed a similar physiological state at Telgruc (in the Bay of Douarnenez), before diverging. Further investigation is needed to gain a deeper understanding of this final aspect.

It should be noted that in the present study, we were addressing the complexity of *P. australis* development by simulating its movement through behaviourless particles. It is possible to add the organism of interest's biology and behavioral characteristics (such as growth rate, grazing rate, etc.) (Xiong et al., 2023). But this point requires a high knowledge of the organisms, and a lack of parameters can alter the simulation. In addition, we are aware that in the present study the pattern of gene expression was used as a global description of the physiological state of the cells. This approach remains somewhat broad and preliminary, and additional research is

required, especially regarding the exploration of functions associated with similarities in gene expression between stations.

Nevertheless, the coupling between the hydrodynamic modeling and the spatio-temporal physiological state study of *P. australis* cells provides relevant information and appears as two complementary analyses in the understanding of bloom dynamics. Indeed, taken separately, these two methods showed a strong correlation between the Bay of Douarnenez and the other stations. The coupled study of the two methods therefore lends weight to the conclusions of this chapter. It is also important to note that the study of the environment is also a support to the transport, since the different stations showed different environments at the moment of *P. australis* emergence. We therefore suggest conducting further comprehensive investigations into the local environmental conditions conducive to the development of *P. australis* in the Bay of Douarnenez during early spring

Chapter 5

Sexual reproduction, a major event determining the dynamics of gene expression during a *P. australis* bloom?

Léa Prigent[a], *Julien Quéré*[a], *Martin Plus*[a], *Mickaël Le Gac*[a]

[a]*Ifremer, DYNECO, F-29280 Plouzané, France.*

Context

In chapter 3 we identified a south-north hydrodynamic connectivity at the time of *P. australis* development. In chapter 4, we identified consistent results between this hydrodynamics and the transport of Eulerian tracers from the Bay of Douarnenez.
However, we have not established a clear link between *P. australis* development and the biotic and/or abiotic environment.

To understand the development of a bloom, particularly of toxic species, it seems crucial to identify it from start to finish, and discern the environmental parameters that lead the causative species to dominate the community. Nevertheless, as previously discussed in earlier chapters, pinpointing the pertinent environmental variables can be a complex task. Indeed, the exhaustiveness of environmental conditions is very complicated to obtain. However, by studying the genes expressed during a bloom, transcriptomics can provide many answers about the mechanisms that lead one species to develop rather than another.

For this reason, in this chapter, metatranscriptomic samples collected during the entire period of a *P. australis* blooms (3 weeks) in April 2017 in the Bay of Brest were analyzed.
Metatranscriptomics studies the genome-wide transcription and transcriptional regulation of all organisms in a given environment or at a specific time, by extracting RNA from all organisms directly from environmental samples (Lin, 2021).

By studying all the genes expressed specifically by *P. australis* during its bloom, the chapter 5 introduces the first study focused on understanding *in situ* blooms through gene expression. This study can shed light on mechanisms governing blooms that cannot be detected by traditional studies of the environment-species development linkage. And could provide relevant answers to the question of what causes a bloom?

Thanks to a study of the genes specifically expressed by *P. australis* during its bloom, we posed two mains questions:

How does gene expression change during a bloom? What are the functions of the genes showing a change in their expression dynamics?

In order to understand the physiological transitions occurring during a bloom, gene functions were analyzed in terms of broad functional categories as well as focusing on genes specifically involved in the diatom life cycle (especially the sexual reproduction) and domoic acid biosynthesis.

This chapter will be valorized and submitted to the ISME journal.

Graphical Abstract :

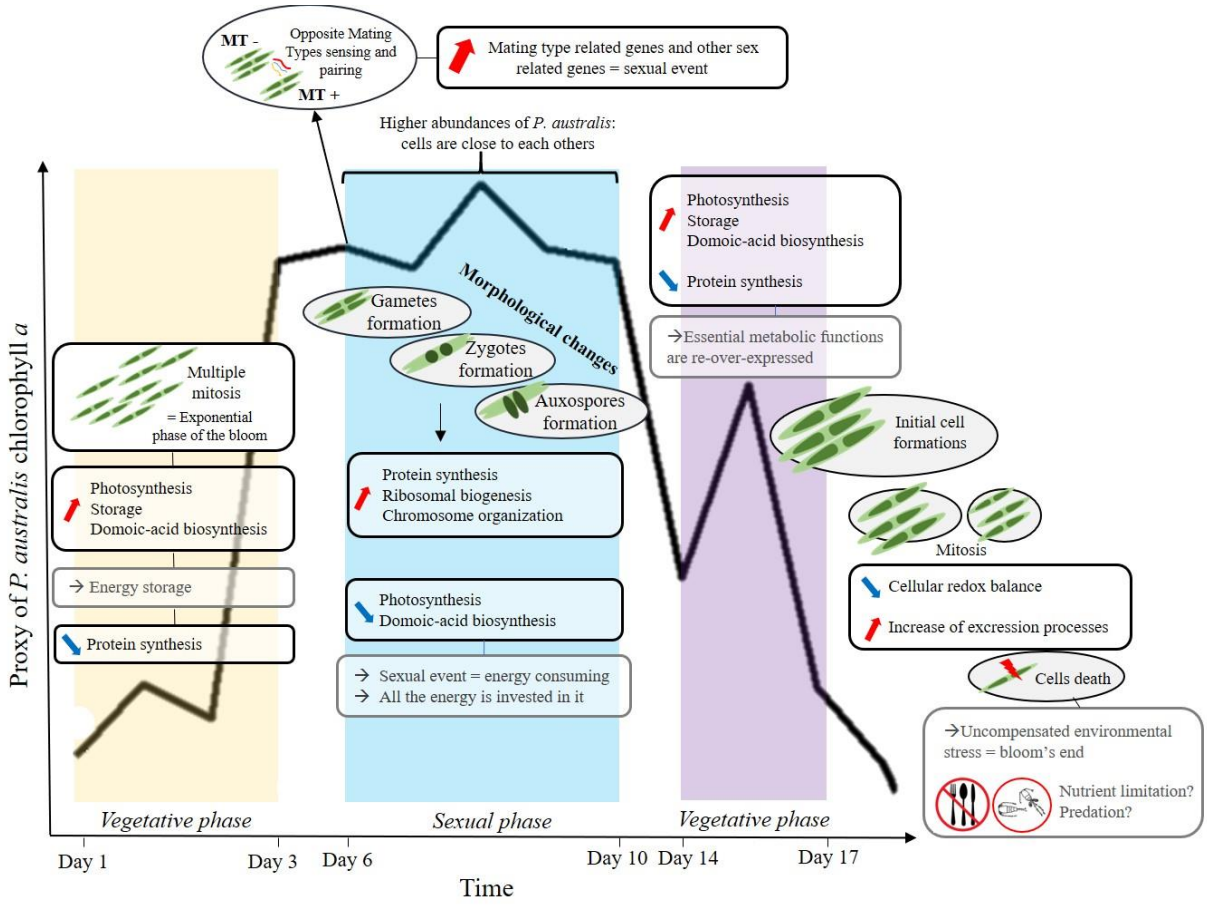

Résumé :

Les efflorescences phytoplanctoniques sont un phénomène important et répandu dans tous les écosystèmes aquatiques, soutenant les réseaux alimentaires et les services écosystémiques essentiels. Les études écologiques ont fourni des informations précieuses sur le lien entre les variables environnementales et les successions d'espèces *in situ*. Cependant, la physiologie *in situ* des espèces lors des efflorescences reste mal caractérisée. L'utilisation de la métatranscriptomique peut désormais y remédier. Pendant un mois, en avril 2017, un échantillonnage d'échantillons métatranscriptomique a été réalisé lors de l'efflorescence de l'espèce toxique *Pseudo-nitzschia australis* dans la rade de Brest (Bretagne, France). Ces échantillons ont été analysés pour étudier pour la première fois la dynamique d'expression des gènes pendant toute la durée d'une efflorescence *in situ*. En utilisant une approche globale, plusieurs grandes catégories fonctionnelles de gènes ont montré une forte dynamique temporelle dans leur expression. Au début de l'efflorescence, les gènes impliqués dans la photosynthèse, la production d'énergie, le stockage ainsi que dans la biosynthèse des toxines

étaient fortement exprimés et, dans une moindre mesure, à la fin de l'efflorescence. Au milieu de l'efflorescence, un changement abrupt dans l'expression des gènes a été identifié au moment où l'abondance relative de *P. australis* était la plus élevée. A ce moment-là, nous avons pu mettre en évidence une expression marquée de gènes liés à la reproduction sexuée. Par la suite, de nombreux changements dans la dynamique d'expression des gènes ont été observés, les gènes impliqués dans la biogenèse des ribosomes, la synthèse des protéines et la division cellulaire ont été surexprimés pendant quelques jours. Dans l'ensemble, cette étude met en évidence des fonctions clés présentant une expression dynamique *in situ* et illustre comment des fonctions étudiées en *in vitro* peuvent aider à comprendre les efflorescences *in situ*.

Abstract

Phytoplankton blooms are an important, widespread phenomenon in all aquatic ecosystems, supporting food webs and essential ecosystem services. Ecological studies have provided valuable insights about the link between environmental variables and species successions *in situ.* However, the *in situ* physiology of blooming species remains poorly characterized. This may now be addressed by using metatranscriptomic. During one month, in April 2017, a metatranscriptomic sampling was carried out during the bloom of the toxin producing species *Pseudo-nitzschia australis* in the Bay of Brest (Brittany, France). These samples were analyzed to investigate for the first time gene expression dynamics during the entire period of a bloom *in situ*. Using a global approach, several functional gene categories displayed a strong temporal pattern of differential gene expression. At the beginning of the bloom, genes involved in photosynthesis, energy production, storage as well as in toxin's biosynthesis were highly expressed and to a lesser extend at the end of the bloom. In the middle of the bloom, an abrupt change in gene expression was identified at the time of highest *P. australis*'s relative abundances with a marked expression of genes related to sexual reproduction. Following this, genes involved in ribosome biogenesis, protein synthesis and cell division were overexpressed for a few days. Altogether, this study highlights key functions displaying dynamic expression *in situ* and illustrates how functions mainly studied *in vitro* may help understand *in situ* blooms.

5.1 Introduction

Phytoplankton plays a major role in aquatic ecosystems. It has a remarkable morphological and functional diversity and contributes to about half of the Earth's primary productivity (Field et al., 1998). Among this group, diatoms represent one of the most diverse and dominant protists (Armbrust, 2009; Kooistra et al., 2007). When environmental conditions are favorable, diatoms can temporarily proliferate in high densities (up to millions of cells per liter) and form a natural phenomenon called bloom. To form a bloom, species must display high growth rate and low mortality (Ji et al., 2018).

Improving our understanding of algal blooms requires the ability to detect entire bloom events (from start to the end), to identify the parameters that lead the causative species to dominate the community and/or to understand the physiology of the causative species. Up to now, the processes of initiation, maintenance and termination of blooms are poorly understood. During the last decades a number of research studies have been carried out to identify the ecological and physiological factors that trigger the initiation and influence the magnitude of these events. Abiotic factors influencing species occurrence and dynamics include hydrodynamic processes, environmental conditions (temperature, salinity), and nutrient availability (Zhou et al., 2018), whereas biotic factors include grazing, pathogenicity, parasitism, and the microbial community composition (Carnicer et al., 2015; Zhou et al., 2018). However, each ecosystem and study area have its own environmental characteristics and the impact of these factors may differ between ecosystems, and bloom expansions are still unclear. Few studies have investigated these blooms *in situ* at the physiological level. By simultaneously quantifying the expression of thousands of genes, metatranscriptomic enables to characterize the cellular strategies of various organisms (Metegnier et al., 2020). These transcriptomic analyses of the natural community (metatranscriptomic) remain scarce but are beginning to shed light on mechanisms that could govern the dominance of a species during blooms.

Some studies have investigated the expression of genes of microorganisms *in situ*. A study during a bloom of the dinoflagellate *Alexandrium minutum* identified a low expression of photosynthesis and central metabolism genes during a bloom (Metegnier et al., 2020). Other studies investigating bloom formation have highlighted the over-expression of genes in response to high nutrient demands. For example, compared to a laboratory culture, the dinoflagellate *A. fundyense* over-expressed genes related to nitrogen fixation, CO2 concentration and saxitoxin production during a natural bloom (Zhuang et al., 2015). Another study observed that dinoflagellates increased the expression of genes involved in N, P and Fe

acquisition (Gong et al., 2018). The raphidophyte *Heterosigma akashiwo* displayed a strong upregulation of phosphate and dissolved organic phosphorus (DOP) uptake genes during a bloom, compared to the pre-bloom period, suggesting that rapid phosphorus uptake and efficient DOP utilization may be a driving force for bloom initiation in this species (Ji et al., 2018). However, no metatranscriptomics study has been carried out during the entire duration of a diatom bloom.

The dynamics of communities are strongly dependent on the life cycle of the individual species (Basu et al., 2017). Diatoms have unique life cycles during which multiple mitoses lead to cell size reduction until a sexualization size threshold (SST) is reached. Below this threshold, sexual reproduction occurs, restoring the original cell size. Sexual reproduction is an obligate phase in diatom life cycles, important not only for recombination, but also to escape the miniaturization process (Basu et al., 2017; Montresor et al., 2016). Pennate diatoms have a heterothallic mating system and sex occurs between strains of opposite mating type (MT+ and MT-). This is the case of the genus *Pseudo-nitzschia* (Annunziata et al., 2022; Russo et al., 2018).

The harmful algal genus *Pseudo-nitzschia* is a diatom of increasing global occurrence and concern (Bates et al., 2018; Trainer et al., 2012). Species of this genus are cosmopolitan, persisting in all seas and oceans at a wide range of temperature conditions (Hasle, 2002), and their distributions span estuaries, coastal and open ocean (Bates et al., 2018). Some *Pseudo-nitzschia* species produce domoic acid (DA), a neurotoxin responsible for Amnesic Shellfish Poisoning. A total of 58 *Pseudo-nitzschia* species have been identified worldwide, and at least half are confirmed DA producers (Bates et al., 2018). These species are often extremely difficult to distinguish morphologically from one another, and several species, producing DA or not, often co-occur during multi-species blooms. This is a considerable hurdle to understand the physiological dynamics of a specific species in relation to environmental conditions *in situ*. In the present study, a metatranscriptomic sampling was carried out during the entire time course of a bloom of one of the most toxic *Pseudo-nitzschia* species, *P. australis*. These samples were analyzed to investigate how gene expression changed and what are the functions of the genes displaying dynamic expression. In order to understand the physiological transitions occurring during a bloom, these gene functions were analyzed in terms of broad functional categories as well as focusing on genes specifically involved in diatom life cycle and domoic acid biosynthesis.

5.2 Materials and Methods

5.2.1 Field sampling and metatranscriptomic samples

During one month in April 2017, 26 samples were obtained daily (except Saturdays and Sundays) during a *Pseudo-nitzschia australis* bloom. Duplicate water samples were collected from shore at a single site (48.360160; - 4.553163) in the Bay of Brest (Brittany, North-West of France) as close as possible to high tide. Water samples (between 6 and 15.1 liters) were filtered onto polycarbonate filter (10 µm, 47 mm) using a peristaltic pump before being frozen in liquid nitrogen after stabilization using RNA later (Fisher Scientific, Illkirch, France). Then, samples were transferred to our laboratory and stored at −80 °C before extraction.

5.2.2 Environmental data

Nutrients concentrations (nitrate, phosphate and silicate, in µmol/L) were provided by the French marine monitoring network: SOMLIT (http://somlit.epoc.u-bordeaux1.fr, Service d'Observation en Milieu LITtoral). Sampling is carried out at sub-surface and in constant tidal conditions at high tide, weekly and at − 2 m at the Brest station (48,2129, -4,3305)
The buoy MAREL Iroise provided temperature (°C), conductivity, turbidity (NTU) and chlorophyll fluorescence which is a proxy of the phytoplankton biomass (Fluorescein Fluorescence Units (FFU)) measured every 20 min at a depth of 2m, at a location situated at 50 m from the SOMLIT-Brest station (Rimmelin-Maury et al., 2023). Finally, the photosynthetically active radiations at the sea surface is provided by Météo-France AROME numerical model (1.3 km resolution, Seity et al., 2011).

5.2.3 RNA extraction, library preparation and sequencing

Total RNA was extracted by sonicating filters on ice (Vibra-cell 75115, Bioblock Scientific, Illkirch, France) for 30 seconds at 35% intensity in LBP buffer (Macherey-Nagel, Duren, Germany). Extraction was performed using NucleoSpin® RNA Plus kit (Macherey-Nagel) following the manufacturer's protocol. Library preparation was performed using the Illumina mRNA TruSeq stranded kit starting from 0.5 µg of total RNA. A total of 26 samples were paired-end sequenced using 2 × 150 bp cycles on Illumina Novaseq6000 at the GeT-PlaGe France Genomics sequencing platform (Toulouse, France). To avoid batch effects, samples

were randomized for RNA extraction, library preparation and sequencing. Generated fastQ files have been deposited to ENA with accession numbers ERR9850563-65, 570-571, 575-576, 585-588, 593-596, 598-599, 608-609, 614-618, 622-623.

5.2.4 Bioinformatic analysis

Prior to read mapping, raw reads quality were assessed using FastQC (http://www.bioinformatics.bbsrc.ac.uk/projects/fastqc/), and Trimmomatic63 (V. 0.33, Bolger et al., 2014) was used to trim ambiguous, low quality reads and sequencing adapters with parameters ILLUMINACLIP: Adapt.fasta: 2 :30 :10 :8 LEADING: 3 TRAILING: 3 MAXINFO:135:0.8 MINLEN: 80.

5.2.4.1 Community analysis

Similarity between the forward trimmed reads and two reference databases were identified using blastn (-max_target_seqs 10 -evalue $1e^{-10}$). Trimmed reads were aligned to two different databanks following the protocol used in Prigent et al. (submitted). For a complete characterization of the eukaryotic community: the manually curated protist Ribosomal Reference database (PR2, Guillou et al., 2012) based on 18S rRNA sequences was used. For a more precise taxonomic characterization of the diatoms, the sequences were aligned to the reference bank Diat_barcode (Rimet et al., 2019), based on the chloroplast marker rbcL. Homology between environmental reads and sequences from the two databases were determined based on e-values (chapter 2).

Blast outputs were analyzed using R (version 3.2.3; R Core Team, 2014). Following the methods introduced in chapter 2, reads displaying minimum e-values <= 10^{-30} against Diat_barcode and <= 10^{-70} against PR2 were filtered out. For each of the remaining reads, the database sequences displaying the lowest e-value (up to ten) were considered. For PR2, if all the database sequences displaying the lowest e-value belonged to a given class, reads were assigned to this class. For diat_barcode, if all the database sequences displaying the lowest e-value belonged to a given species or genus, reads were assigned to this species or genus respectively. Otherwise, reads were not considered. The relative abundances of the communities were obtained for each sample by dividing the sum of the reads associated with each species, genera or class, by the total number of aligned reads.

5.2.4.2 Gene expressions and functions analysis

- Reference transcriptomes and alignment

Using the BWA-MEM aligner (Li, 2013), trimmed reads were aligned to a metareference corresponding to the combination of 315 species specific reference transcriptomes, representing 213 unique genera (Metegnier et al., 2020). It mostly corresponded to the resources developed during the Marine Microbial Eukaryotic Transcriptome Sequencing Project (MMETSP, Keeling et al., 2014) with the addition of reference transcriptomes obtained for three *Pseudo-nitzschia* species (*Pseudo-nitzschia australis*, *Pseudo-nitzschia fraudulenta* and *Pseudo-nitzschia pungens*) based on local strains (Lema et al., 2019).

Samtools was used to discard reads displaying low quality alignments (MapQ<10), to remove read pairs that did not align to the same transcript and to generate the raw read count expression matrix (Li et al., 2009). Raw read counts corresponding to *P. australis* contigs were then extracted.

- Overall gene expression dynamics

After preliminary analyses, the April 24th samples were excluded due to low relative abundances of *P. australis*, and transcripts covered by less than 5 reads on average across samples were discarded from the analyses. In order to minimize differences between samples, the dataset was normalized using Deseq2 rlog transformation (Love et al., 2014).
Differential expression (DE) analyses were performed using the DESeq2 package (Love et al., 2014). A PCA based on the 25,140 transcripts identified three sample groups ("early" for the beginning of the bloom: 04/04; 04/05, 04/06 and 04/07; "middle" for the middle of the bloom: 04/10, 04/11, 04/12, 04/13 and 04/14; and "late" for end of the bloom: 04/18, 04/19, 04/20 and 04/21; see results).

After checking the homogeneity of the replicates (fig. 4), reads from replicates were pooled by summing the expression matrices.
Pairwise DE was tested between sample groups using Wald tests (implemented in DESeq2) considering a negative binomial generalized linear model with a false discovery rate (FDR) threshold set at qvalue = 0.05. Considering the identified transcripts as significant, expression profiles across samples were clustered according to negative binomial models as implemented in MBCluster.Seq, using expectation-maximization algorithm for estimating model parameters

and cluster membership (Si et al., 2014). Different cluster sizes were visually inspected and clusters with similar profiles were merged, finally 6 clusters were selected (fig.5).
Gene expression is reported as the log 2-fold change (log2FC) of the expression of a given transcript over the median expression considering all samples. It is calculated as: log2(2Xi/2X) where Xi is the rlog transformation (regularized log transformation, as implemented in DESeq2) of the number of reads mapping to a given transcript for each samples i and $\bar{X}$ is the rlog transformation of the number of reads mapping to a given transcript for all samples.

In parallel, WGCNA R package (Langfelder and Horvath, 2008) was used to see if there are expression patterns that are not captured by the differences between sample groups. For that, 24,117 contigs displaying an average normalized read count (2^{rlog}) > 2 per sample were grouped into modules of co-expressed transcripts across the 24 samples (Supplementary material 5). A soft-thresholding power of 8 and bicor correlation were used as parameters. Module identification was performed using dynamic tree cut with minimum cluster size of 1,000 transcripts, and modules displaying a Pearson correlation >0.95 were merged. Clustering results using WGCNA and deseq2/MBClusters showed similar results. Hereafter, only results from MBClusters cluster's analyses were reported.

Reference transcriptome annotation was previously performed (Lema et al., 2019). It was based on sequence similarity with the manually curated Uniprot database as inferred using blastx and considering e-value $<10^{-3}$. Based on this result reference contigs were classified in various Gene Ontology (GO) categories (http://geneontology.org/). Overrepresentation of GO categories in the identified clusters were tested for functional gene categories represented by at least five transcripts, using Fisher Exact tests followed by a false discovery rate (FDR) correction for multiple testing with a significance threshold set at q-value = 0.05. Fisher Exact tests odds ratios (ORs) were reported. Only GO categories containing more than five differential expressed transcripts in a given cluster were considered. However, the hierarchical Gene Ontology classification system leads to redundancies (i.e. a similar set of genes can be found in different GO categories). To take account of this redundancy, GO categories displaying an overlap coefficient: GOi GOjmin(GOi,GOj) > 0.8 (where GOj is the size of the GO category j) were clustered (Lema et al., 2019).

- Candidate gene identifications

On April 4th, a strong over-expression of DE genes was identified and the associated functions were investigated. For this purpose, sequence similarity between these genes and proteins of identified function in the NR and uniprot-swissprot databases was searched using blastx with an e-value $<10^{-3}$. The homologous proteins with the lowest e-value were selected.

In addition, genes involved in *P. australis* toxin production and sexual reproduction were searched. Homologs of the *dabA*, *dabB*, *dabC* and *dabD* genes involved in domoic acid production in *Pseudo-nitzschia multiseries* (Brunson et al., 2018) were identified using tblastn. Similarly, homologs of 384 genes (supplementary material table 2) identified as involved in sexual reproduction in *Pseudo-nitzschia multistriata* (Annunziata et al., 2022; Basu et al., 2017; Patil et al., 2015; Russo et al., 2018 and personal communication of G. Bilcke) were used as queries against *P. australis* transcriptome using tblastn (e-value $<10^{-3}$) and keeping the contig displaying the lowest e-value.

5.3 Results

5.3.1 A blooming period

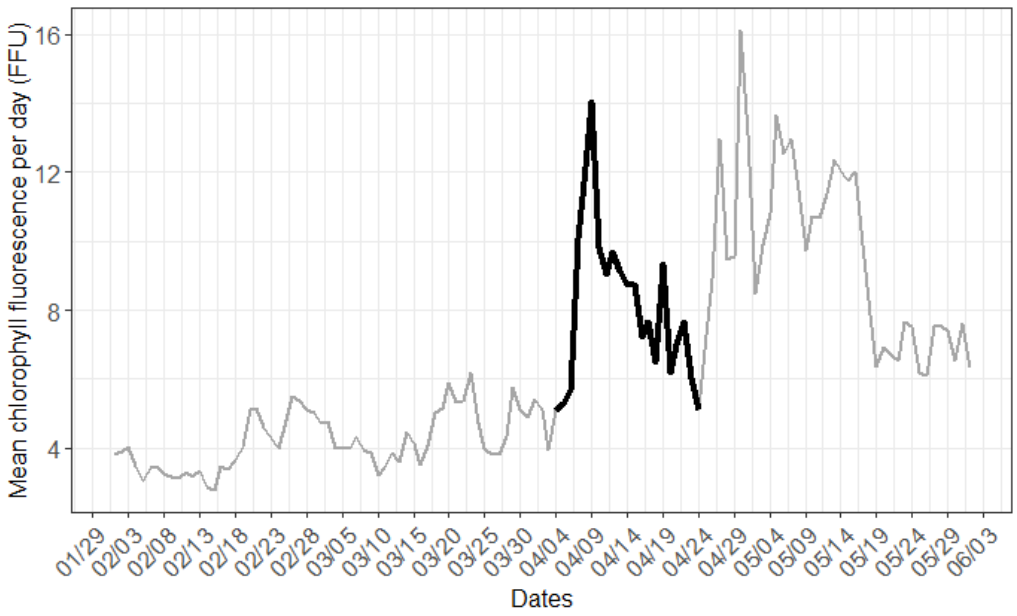

Fig. 1: Temporal evolution of the mean chlorophyll fluorescence per day between 2017-02-01 and 2017-05-30. The survey period is shown in black.

The temporal evolution of the chlorophyll biomass was shown daily between February 1st and May 30th. The results clearly indicated that the study period coincided with the first major spring

bloom of 2017. This bloom had a chlorophyll peak on April 9th with a value of 14.04 FFU which then decreased until it reached 5.1 FFU on April 24th.

The composition of the eukaryotic community was identified using metatranscriptomic samples between April 4th and April 24th. A total of 15 phylums of eukaryotes with relative abundances over 2% were identified. The phylum *Bacillariophyta*, also known as diatoms, was the most abundant and ranged between 38% (April 20th) and 81% (April 6th) of the total abundance. Urochordata was a phylum also present throughout the monitoring with a maximum relative abundance of 29 and 26% on April 12nd. Dinophyceae, Prymnesiophyceae and Spirotrichea were also present in all samples but in a relative abundance not exceeding 14%. Finally, the presence of Arthropoda, mainly corresponding to copepods, was identified at the end of the monitoring period with a maximum relative abundance of 20% on April 19th (supplementary material fig. 3 and 4).

The dominant diatoms were then identified at the species and/or genus levels (fig.2).

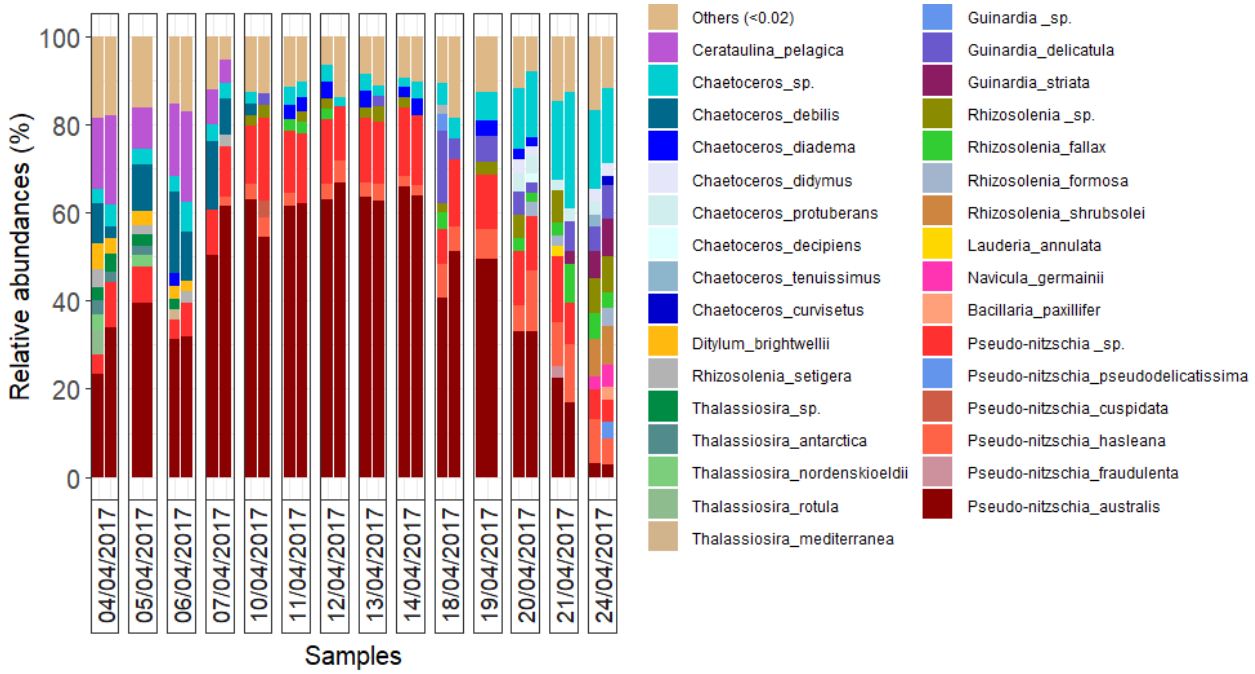

Fig. 2: Relative abundances of the diatom community composition during the 2017 monitoring (the category others regroup genus/species lower than 2%).

Among the diatoms, *P. australis* was the dominant species in the community. The results clearly indicated the evolution of the bloom with lower relative abundances at the beginning and at the end of the monitoring. Its relative abundance was maximum between April 10th and 14th (values between 54% on April 10th and 67% on April 12th).

Other *Pseudo-nitzschia* species were also detected. More specifically, *P. hasleana* was present throughout the monitoring period with a maximum relative abundance of 13% on April 20th and April 21st when the abundances of *P. australis* were decreasing. The other species, *P. fraudulenta, P. pseudodelicatissima, P. cuspidata* displayed less than 3% relative abundance. Reads for which species assignment was not possible were grouped under *Pseudo-nitzschia* sp. and represented relative abundances between 4.1% on April 4th and 15.9% on April 11th.

Other diatom species were identified, such as *Cerataulina pelagica* and *Chaetoceros debilis* which were abundant before the bloom peak, i.e. before April 10th. From April 18th, the relative abundance of *P. australis* decreased, and the species *P. hasleana*, the genus Chaetoceros and to a lesser extent the diatom *Guinardia delicatula* increased in relative abundance. On April 24th, *P. australis* no longer dominated the diatom community (fig.2).

5.3.2 Environmental conditions

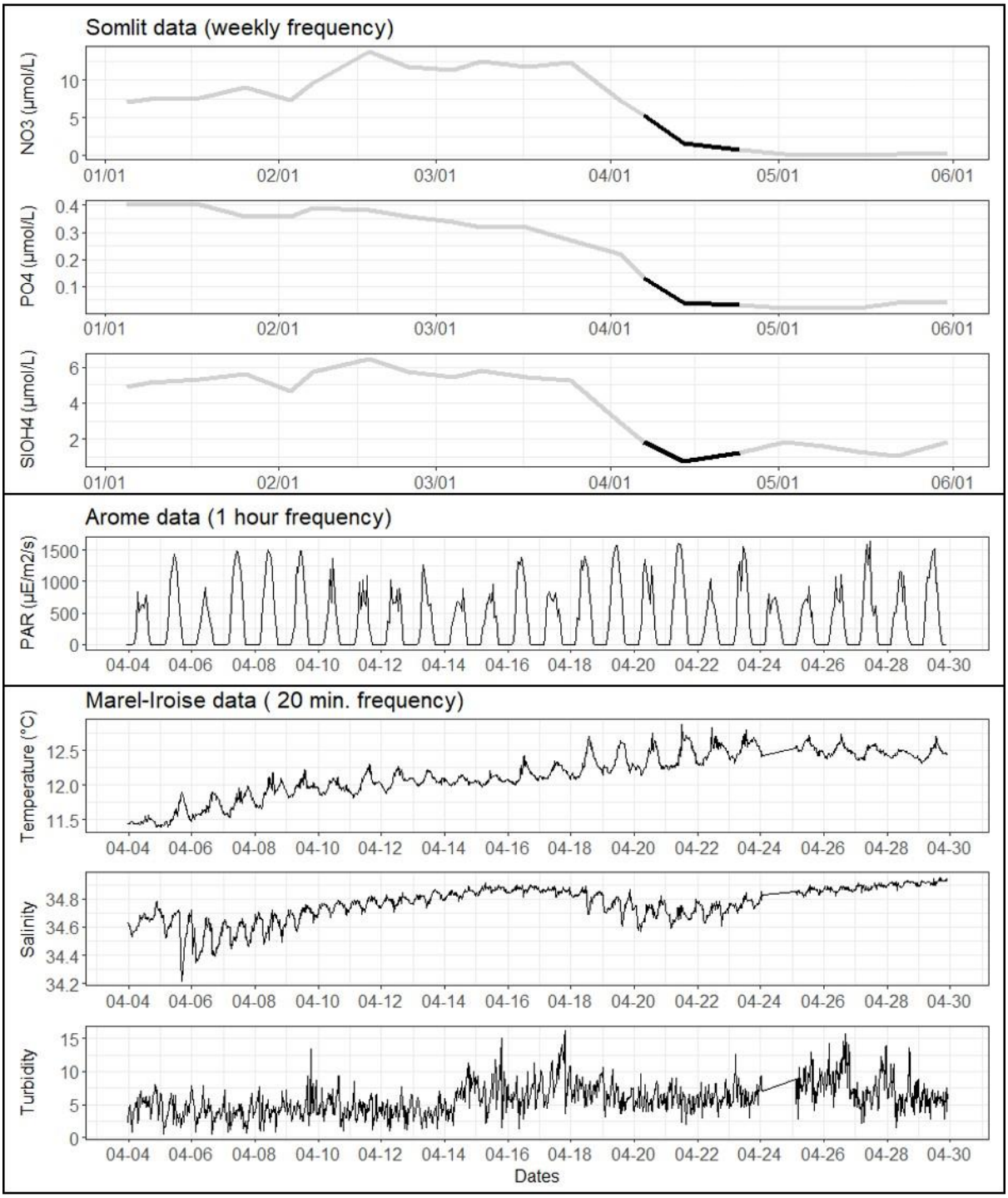

Fig. 3: Temporal evolution of abiotic parameters during the sampling period for nutrients: Nitrate (NO3), Phosphate (PO4) and Silicate (SiOH4) (Somlit data), Photosynthetically Active Radiation (PAR, Arome data) and temperature, salinity and turbidity (NTU) (Marel-Iroise buoy). The black line on the first three graphs represent the sampling period, due to the lower sampling frequency on Somlit data (1 time per week), a longer period is shown to get an insight into the evolution of the nutrients.

The weekly nutrient data showed a decrease in concentration during the monitoring period (black line) that began upstream. Nitrates and silicates showed fairly similar dynamics in the

evolution of their concentrations with maximum values reached on February 17th with 13.7 µmol/L and 6.48 µmol/L respectively. Phosphate concentrations declined more slowly from January 1st, but became more marked from April 3rd onwards (from 12 µmol/L on March 25th to 7.18 µmol/L). During the monitoring period, between April 3rd and April 24th, concentrations decreased from 7.2 µmol/L to 0.7 µmol/L for nitrates; from 0.2 µmol/L to 0.03 µmol/L for phosphates and from 2.84 µmol/L to 1.23 µmol/L for silicates. The PAR was variable without a clear trend over the period of the survey. Peaks on PAR were identified between April 7th and 9th and between April 18th and 21st with maximum values above 1000 µE/m2/S.

Maximum daily values below 800 µE/m2/S for several consecutive days were recorded between April 10th and 15th. Temperature, salinity and turbidity varied according to the tidal cycle, which displays high amplitude in the study area. The variations in salinity seemed to be well related to these cycles (supplementary material table 1), with lower salinity values during low tidal coefficients (tidal amplitude < 4 meters), and higher values during higher tidal coefficients (tidal amplitude > 4 meters) due to the large influx of marine water into the area. In general, some trends regarding temperature and turbidity can be noted. An increase, typical of northern hemisphere spring, was identified, with values ranging from an average of 11.5°C at the beginning of the survey period on April 4th to 12.5°C at the end of the survey on April 24th.

Over the monitoring period, lower turbidity was recorded between April 5th and 13th with daily average values below 5 NTU, before increasing from April 14th (fig. 3). These results suggested little freshwater inflow, or a quiet period over the survey period.

5.3.3 Gene expression dynamics change over the bloom period

To determine gene expression dynamics of *P. australis*, a principal component analysis (PCA) was performed to visualize the variability between samples containing 25,140 expressed genes. The two first PCA components explained 66% of the dataset variability (Fig.4). Three groups of samples displaying similar gene expression were identified and corresponded to samples from April 4th to 7th (early), the April 10th to 14th (middle) and April 18th to 21st (late).

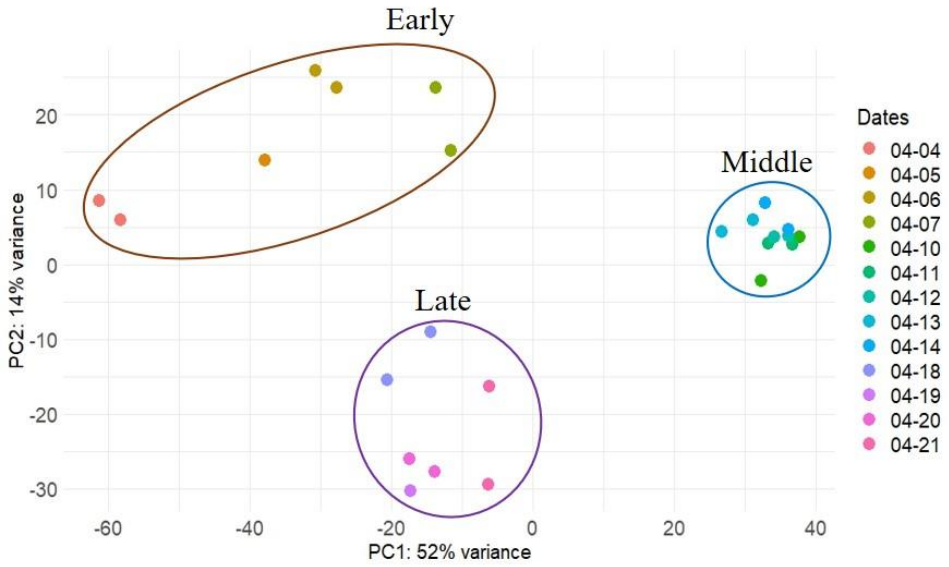

Fig. 4: Principal component analysis of normalized gene expression profiles for each sample.

A total of 8,252 genes were identified as differentially expressed between the three groups of samples. These genes were grouped into 6 clusters based on gene expression changes across samples (fig. 5). The clusters contained between 75 (cluster 6) and 2591 (cluster 2) genes. Overall, these gene clusters displayed pronounced gene expression differences between the early, middle and late groups of samples, with major shifts in gene expression occurring on April 10th and 18th.

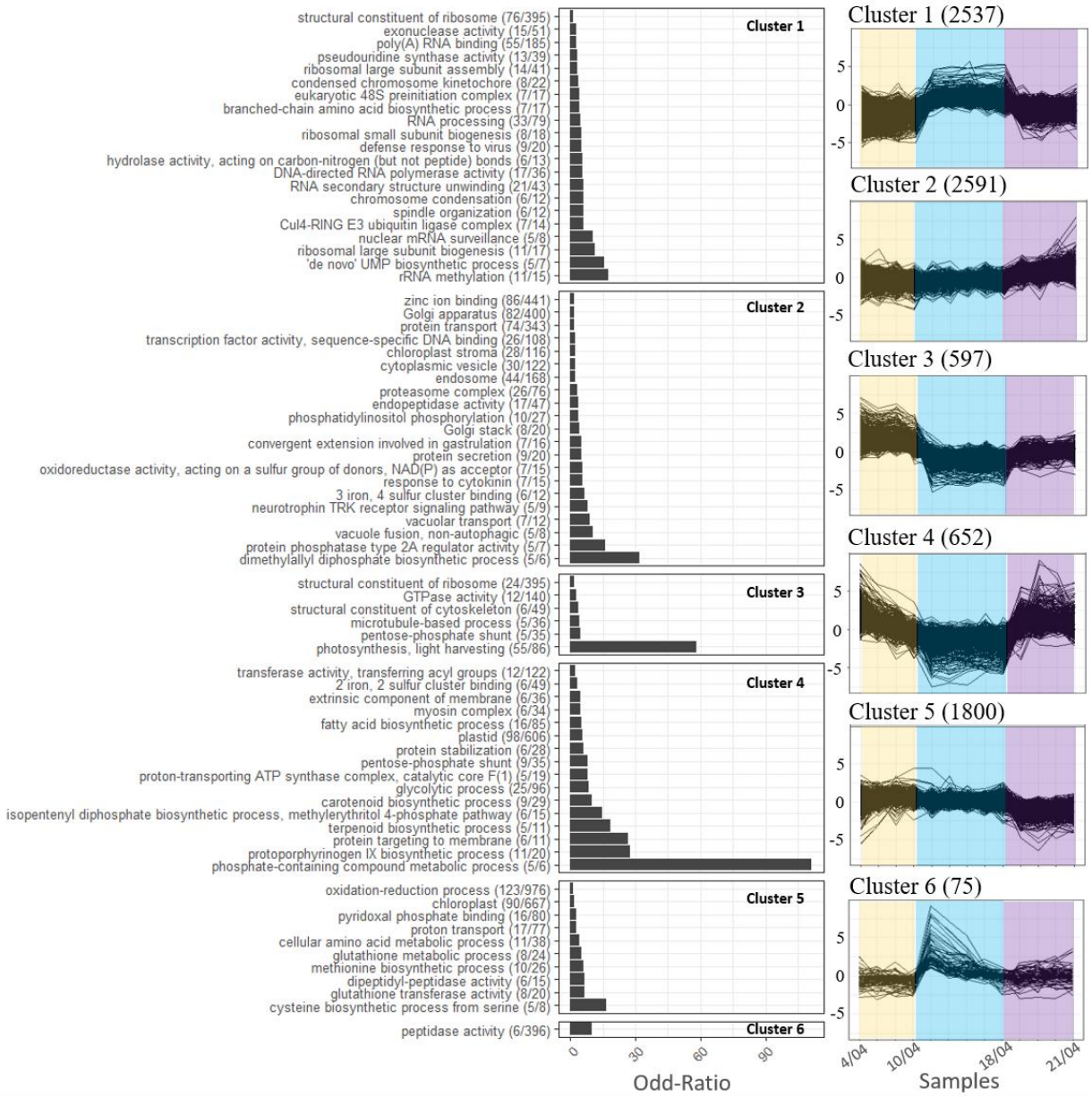

Fig 5: Right side: clusters of DE genes displaying similar gene expression dynamics (expressed as log2FC) across samples. The number of transcripts belonging to each cluster is indicated in parenthesis. Left side: overrepresented Biological Process in each cluster (GO terms). Go terms (y axis) were presented based on their odd-ratio (x axis). For each GO term, the number of transcripts identified over the total number of transcripts contained in it and presented in P. australis transcriptome, is indicated in parenthesis.

The over-representation of gene functions was analyzed in the 6 clusters. At the beginning of the bloom (from April 3rd to April 10th), cells appeared to be engaging in high levels of photosynthesis, as indicated by the over-representation of "Photosynthesis, light-harvesting" in cluster 3. In addition, although decreasing during this first phase, there was also over-representation of processes related to energy production and storage (cluster 4: “glycolytic process”, “pentose phosphate shunt”, “fatty acid biosynthesis” and “proton-transporting ATP

synthase complex"), as well as involving the biosynthesis of a variety of interconnected compounds (terpenoids, fatty acids, carotenoids, protoporphyrinogen IX and isopentenyl diphosphate).

In the second phase (from April 10th to 14th), two main groups of functions were overrepresented (cluster 1). The first one was related to ribosomal biogenesis and protein synthesis: "DNA-directed RNA polymerase activity", "'de novo' UMP biosynthetic process", "ribosomal large subunit assembly", "structural constituent of ribosome", "ribosomal large subunit biogenesis", "RNA secondary structure unwinding", "pseudouridine synthase activity", "RNA processing, exonuclease activity", and "poly(A) RNA binding". This could indicate that the cells were experiencing high rates of protein synthesis and required additional ribosomes to meet this demand. The second one was related to the organization of chromosomes: "chromosome condensation", "condensed chromosome kinetochore" and "spindle organization". A GO function "defense response to virus" was overrepresented as well during this stage.

In a last phase (from April 14th to 21st), cells appeared to display a slight increase in their photosynthesis (cluster 3) and a more pronounced increase in processes related to energy production and storage, as well as involving the biosynthesis of a variety of interconnected compounds (cluster 4). We also note the very strong overrepresentation of "phosphate-containing compound metabolic process" (odd-ratio of 111) which may indicate tight regulation of phosphate utilization during this last phase. This last phase is also characterized by an under-representation of various functions related to the cellular redox balance (cluster). More specifically, this is the case of the functions: such as "oxidation-reduction process", "glutathione transferase activity" and "glutathione metabolic process". More indirectly, the category "methionine biosynthetic process" may also be related to the redox balance as methionine, is a precursor for the synthesis of S-adenosylmethionine, which is involved in a variety of cellular methylation reactions, some of which are involved in redox regulation. Finally, related to "cysteine biosynthetic process from serine", cysteine is also important for redox regulation as it contains a thiol group that can be oxidized and reduced in response to changes in the cellular redox state. Cysteine is also a precursor for the synthesis of glutathione, which is an important antioxidant molecule that helps to maintain the cellular redox balance. Overall these results suggest a decreased level of the cellular redox balance toward the end of the bloom.

Throughout the bloom (from April 5th to 21st), there was a moderate but rather constant increase in several processes related to excretion processes: "cytoplasmic vesicle", "vacuolar transport", "Golgi apparatus", "Golgi stack", “vacuole fusion, non-autophagic", "endosome" and more specifically related to proteins: "endopeptidase activity", "protein secretion", "protein transport", "proteasome complex". Associated with this, we noted the extremely strong overrepresentation of "dimethylallyl diphosphate biosynthetic process". Dimethylallyl diphosphate (DMAPP) is an important precursor for the synthesis of isoprenoids. In diatoms, DMAPP is synthesized through the methylerythritol phosphate (MEP) pathway, which provides precursors for the synthesis of pigments such as chlorophyll, carotenoids, as well as phytohormones and secondary metabolites. Among isoprenoids are terpenoids, carotenoids, protoporphyrinogen IX and isopentenyl diphosphate, compounds with biosynthesis genes overrepresented during the last phase of the bloom (cluster 4). It is also important to note that DMAPP is a domoic acid precursor.

Finally, between the early and middle phases, genes belonging to cluster 6 display a transitory but extremely high over-expression (among the highest observed in the present study). In this cluster, the only over-represented GO category is “peptidase activity” which may indicate a metabolic shift.

In order to understand the major changes that occurred on April 10th, the annotation of individual genes belonging to cluster 6 were analyzed.

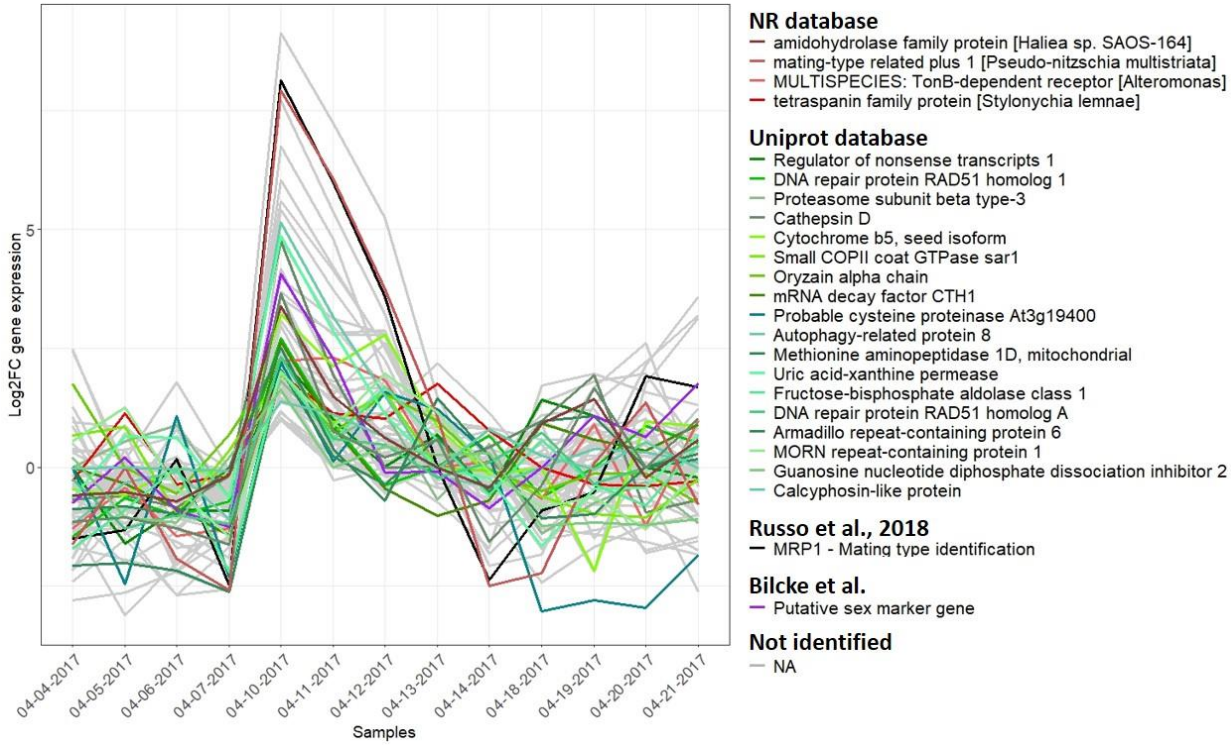

Fig. 6: Function of the genes belonging to cluster 6. Homology searches were carried out on the UNIPROT and NR database and by searching for candidate genes identified in the literature.

In total, 75 genes belonged to cluster 6. No homology was identified for 50 of these genes, although some of them displayed high over-expression levels on April 10th, such as for instance comp21766_c0_seq1 (log2FC of 9.1), comp49603_c0_seq1 (log2FC of 6.7), comp52530_c0_seq1 (log2FC of 6) and comp53321_c0_seq1(log2FC of 5.4).

The two annotated genes displaying the highest over-expression levels on April 10th (log2FC of 8.1 and 7.9 for comp38021_c0_seq2 and comp53010_c0_seq1) were homologous to the "mating type related plus 1" gene identified in *P. multistriata*. Several other genes that may be related to sexual reproduction, also belonged to cluster 6. It was the case of a gene identified as sex marker (comp44166_c0_seq1; Bilcke XXX, log2FC of 4.1), two Rad51 homologous (log2FC of 2.7 and 2.3) identified as an important gene family whose members are employed in homologous recombination during both mitotic and meiotic DNA repair (Patil et al., 2015), as well two genes homologous to cathepsin D (Log2FC of 4.8 and 3.7) identified as molecular proxy of sexualisation in MT- (Marotta et al., 2022).

Other genes that were highly over-expressed and annotated on April 10th included functions related to autophagy: "Autophagy-related protein 8" (log2FC 5.2), "uric acid-xanthine permease" (log2FC 4.9), associated with "amidohydrolase family protein" function (log2FC 3.4) as well "Cytochrome b5, seed isoform" (log2FC 3.2). The other annotated genes identified with a lower overexpression (< log2FC of 3) were involved in multiple functions: glucose

metabolism, membrane and cell wall proteins, mRNA transport and monitoring, transport regulation...

5.3.4 Expression of genes related to sexual reproduction during bloom

Altogether, the pattern of expression presented above suggested a potential sexual reproduction event. To further investigate this, a focus was made on genes whose expression changed *in vitro* during a sexual reproduction. We reviewed the literature focusing on transcriptomic analyses performed during sexual reproduction experiments in diatoms and identified a total of 348 genes (Supplementary material table 2; (Annunziata et al., 2022; Basu et al., 2017; Patil et al., 2015; Russo et al., 2018 and genes shared by Bilcke G. (*in prep*). Among these genes, 298 found homology to the reference transcriptome of *P. australis*. These genes were over-represented in the clusters presented above (p-value $1.9e^{-07}$, Odd-ratio 1.77, two-sided Fisher Exact test), with 161 genes belonging to the clusters (fig.5).

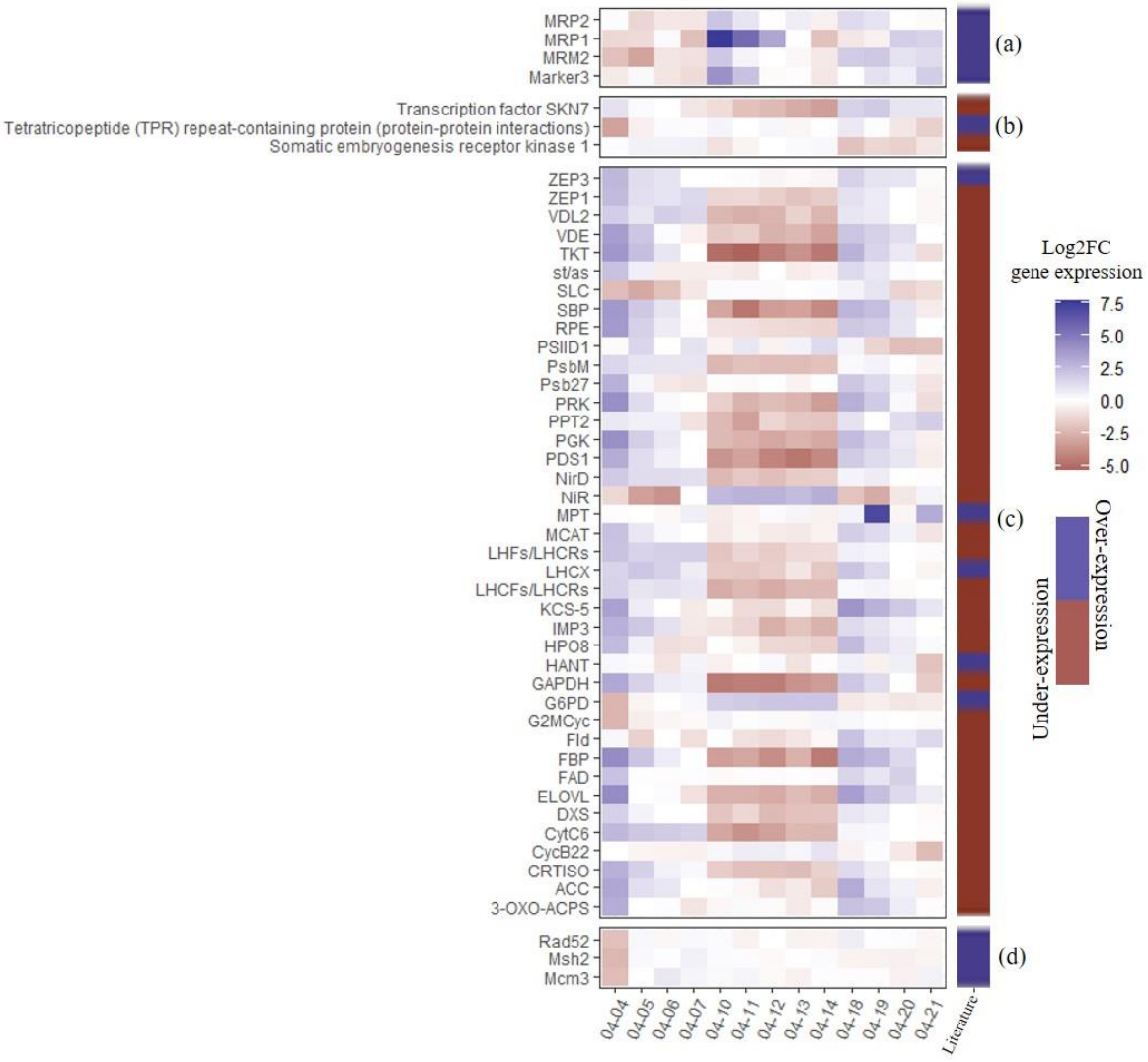

Fig. 7: Comparison of the expression level (under- in brown and over-expressed in blue) of genes identified as differentially expressed or involved in sexual reproduction in the literature with their homologs identified in the P. australis reference transcriptome. For readability, only homologous genes displaying absolute log2FC > 2 are represented in the figure. The different letters represent gene expression analysis's timings after sexual reproduction in the literature: (a) Directly (Russo et al., 2018 and Bilcke. G personal communication); (b) 6h after opposite MT contact (Basu et al., 2017) (c) From 1 hour to 5 days (Annunziata et al., 2022) and (d) Sexual reproduction period (Patil et al., 2015). All homologous genes identified are found in the supplementary material (table 2) in comparison with the literature.

First of all, mating type (MT) related genes, that were over-expressed at the time of sexual reproduction during *in-vitro* studies (Russo et al., 2018), tend to be over-expressed on April 10th (fig.7a). This was the case of MRP1 (log2FC=7.6, as already seen above), but also, to a lesser extent, of MRP2 (log2FC=2.1) and MRM2 (log2FC=2). In addition, another gene identified as a sex marker (Bilcke G., personal communication) showed an over-expression with a logFC of 4. Of the remaining mating type related genes, no MRM1 homolog was identified in *P. australis* reference transcriptome and MRP3 displayed a rather stable expression level throughout the bloom.

Second, numerous genes identified as down regulated from a few hours to a few days after opposite MT contact during *in vitro* studies (Annunziata et al., 2022; Basu et al., 2017) were under-expressed between April 10^{th} and 18^{th} (Fig. 7b and c).

From 1 hour to 5 days (Annunziata et al., 2022), there was an over-representation of the under-expressed genes in the clusters 3-4 (p-value < $2.2\ e^{-16}$, Odd-ratio 16.48, two-sided Fisher Exact test) as well as over-expressed genes in cluster 1 (p-value < $2.2\ e^{-16}$, Odd-ratio 2.82, two-sided Fisher Exact test).

The only two notable exceptions were the glucose-6-phosphate dehydrogenase (G6PD) also under-expressed *in vitro* and nitrite reductase (NiR) that were up-regulated between April 10th and 18th (Fig. 7c) and under-expressed *in vitro*.

Third, the genes identified as involved in diatom meiosis *in vitro* (Patil et al., 2015) displayed a rather stable expression throughout the bloom (Fig. 7d). The only exceptions were a handful of genes displaying slightly lower expression (log2FC < -2) on April 4^{th} (Fig. 7d).

5.3.5 Identification of toxins biosynthesis genes

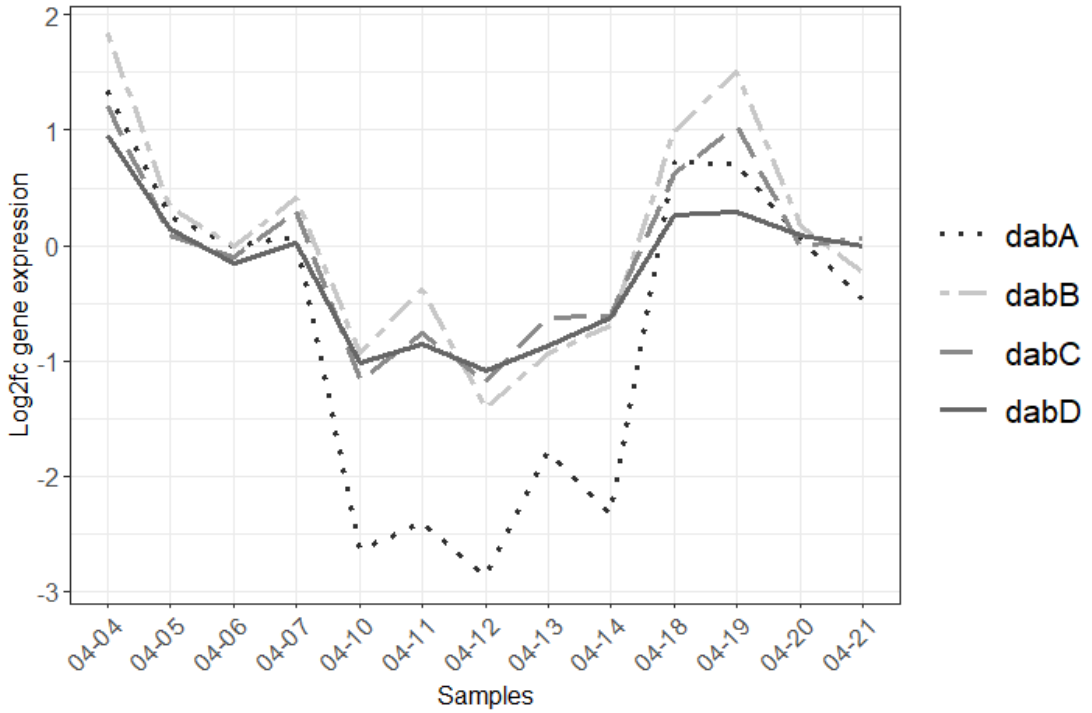

Fig. 8: DA biosynthesis gene expression dynamics in P. australis.

The four genes (*dab ABCD*) identified as involved in the biosynthesis of DA in *P. multiseries* (Brunson et al., 2018) were identified in *P. australis* transcriptome. The four genes displayed similar expression dynamics with over-expression decreasing during the early phase, under-expression during the middle phase before being over-expressed during the late phase (fig. 8). The under-expression during the middle phase was especially strong for *dabA* (a minimum log2FC of -2.9). Among these genes, two (*dabA* and *dabB*) showed a significant difference in expression during the survey and belonged to cluster 4 (see supplementary material fig 7).

5.4 Discussion

5.4.1 Gene expression dynamics was marked over time

The gene expression dynamics of *P. australis* showed strong temporal changes during a three-week bloom. These changes mostly occurred between three main periods of relatively stable expression. The results are discussed: 1. to determine whether changes in gene expression may be related to environmental parameters, 2. to relate the functions of the genes displaying dynamic expression to bloom progression and 3. to illustrate that a punctual sexual reproduction event may be one of the main drivers of bloom progression.

Biotic and abiotic environment in relation with gene expression dynamic changes?

Different studies showed that in natural ecosystems, microorganisms have different metabolic processes in response to different environmental conditions (Gong et al., 2018; see Kolody et al., 2022).

First, concerning the biotic environment, it is interesting to notice the dominance of diatoms throughout the *P. australis* bloom monitoring. A co-occurrence of different accompanying species throughout the bloom was identified with progressive changes throughout the bloom. At the beginning, the species *Cerataulina pelagica*, *Ditylum brightwellii*, and the genera *Thalassiosira* and *Chaetoceros* were mainly present. From the middle, *P. australis* and the genus *Pseudo-nitzschia* largely dominated the diatom community (> 50%) before decreasing in relative abundance, accompanied by an increase of the species *Guinardia delicatula*, and species of the genus *Chaetoceros* and *Rhizosolenia*. These different changes in the community seemed to take place over 3 periods as did the dynamics of gene expression. We note that the dominance of *P. australis* in the middle of the bloom did not seem to reduce the number of accompanying species compared to the early and late bloom's samples. This contrasts with one documented consequence of a HAB event can be the alteration of the accompanying phytoplankton community. For instance, during a *H. akashiwo* bloom, a significant shift in the phytoplankton community was revealed by 18S rDNA sequencing and microscopic observations, suggesting a negative influence of *H. akashiwo* high abundances on the community diversity (Ji et al., 2018).

At the end of the bloom period, copepod relative abundance, especially the species *Acartia clausii*, increased. It is known that grazers like copepods contribute to bloom termination (Turner, 2014). It was also shown *in vitro* that DA production was induced by the presence of copepods in *P. seriata*, suggesting that domoic acid production may be related to grazing defense (Tammilehto et al., 2015). In the present study, expression of genes related to DA biosynthesis increased at the end of the *P. australis* bloom. However, expression of DA biosynthesis genes was also high at the beginning of the bloom with very few or no copepods at all. The over-expression of DA genes at the beginning of the bloom might also suggest a possible advantage given by DA for community dominance. But literature's results remain contrasted, and the role of DA in terms of competitive advantage is not fully elucidated (Zabaglo et al., 2016). Although the literature has not shown a direct link, we believe that DA is an advantage during a bloom for two reasons: firstly, to dominate the community, and secondly, to defend against grazers. Moreover, except for DA genes, no competition-related

gene functions as stress-related appeared to explain gene expression changes by species successions.

Second, phytoplankton gene expressions have been shown to be strongly affected by abiotic parameters. For example, in an upper estuary, where nutrients are replete, a community highly expressed photosynthesis, carbon fixation and other growth-related genes. In the lower estuary, where nutrients can be temporarily limiting, phytoplankton increased gene expression related to nutrient acquisition processes to scavenge the scarce nutrients from the environment in order to meet the nutrient needs (Gong et al., 2018). In the present study, changes in environmental parameters such as turbidity, temperature, salinity, PAR and nutrients were not consistent with gene expression changes. During the time course of the bloom, a continuous decrease in nutrient concentrations was measured, but genes related to nutrient uptake or assimilation did not display significant expression changes. This contrasted with several studies identifying nutrient related gene expression as a major signal in early bloom (Gong et al., 2018; Ji et al., 2018; Zhuang et al., 2015). Moreover, *in situ* measurement of temperature did not coincide with marked changes in gene expression. Salinity and turbidity were mainly linked to the tidal cycle and could not explain the strong changes in gene expression. PAR values fluctuated during the time course of the bloom, with higher PAR values recorded during the early and late phase and lower values during the middle phase. This may be directly linked to the expression of genes related to photosynthesis that tend to display higher expression during the early and late phases and lower expression during the middle phase. We also note that several studies have shown under-expression of photosynthesis related genes after sexual reproduction *in vitro* (Annunziata et al., 2022; Basu et al., 2017; Montresor et al., 2016). As a result, low expression of photosynthesis related genes might also be a direct consequence of the sexual reproduction event that occurred during the bloom (see below).

Moreover, daily rhythms of photosynthesis are common in photosynthetic organisms, and chloroplast genes are usually most highly expressed in the middle of the day (Reynolds et al., 1993). For instance, a study on the dinoflagellate *H. akashiwo* identified that genes involved in photosynthesis and carbon fixation displayed high expression in the middle of the day when light intensity was highest (Ji et al., 2018).

In the present monitoring, samples were collected close to high tide and therefore at different times of the day. However, the time of sampling was not correlated with the expression levels of genes related to photosynthesis.

Important metabolic functions are down-regulated in the middle of the bloom

Six gene clusters displaying dynamic gene expression across the three bloom periods were identified.

At the beginning of the bloom (early period), genes involved in photosynthesis displayed high expression levels. Genes related to this biological process have previously been identified as displaying dynamic expression *in situ* in diatoms (Alexander et al., 2015; Gong et al., 2018; Metegnier et al., 2020). In the present study, photosynthesis decreased sharply when the relative abundance of *P. australis* appeared to be the greatest. This is also the case for transcripts involved in storage and sugar metabolism. These functions related to energy production and phytoplankton growth appeared to have an important role in the early stages of the bloom, until the relative abundance of *P. australis* peaked to the highest levels. DA biosynthesis was also over-expressed at this time, DA synthesis requires energy and a certain level of light suggesting a strong link with photosynthesis (Brunson et al., 2018), this was confirmed in the present study with similar dynamics expressions of these functions.

After this early period, a marked transition in gene expression took place and the expression of the former genes strongly decreased. During the middle period, different functions showed an over-expression, such as ribosomal biogenesis and protein synthesis. The over-expression of these functions seemed to contradict the under-expression of photosynthesis genes, since photosynthesis is generally the primary energy source, whereas protein synthesis is the primary energy sink (McCain et al., 2022). This suggested that during the middle bloom period the accumulated energy was used up.

At the end of the bloom, decreased expression of genes involved in cellular redox balance and more specifically related to glutathione were also identified. Environmental stress can lead to perturbations in oxygenic metabolism and induce oxidative stress by overproduction of reactive oxygen species (ROS) which can alter the redox balance in a cell and be toxic at high levels (Volpert et al., 2018). Cells have developed different antioxidant mechanisms, including glutathione, to overcome this toxicity. As a result, changes identified in the expression of genes related to redox potential at the end of the bloom may suggest a disequilibrium in the redox potential, known to increase deteriorative processes and cell senescence (Bidle, 2016; Kranner et al., 2006) that could explain the termination of the bloom.

Finally, we may note throughout the bloom a moderate but rather constant increase in several processes related to excretion processes. Extracellular vesicles are produced by many organisms, carrying a wide repertoire of molecules, e.g. proteins, lipids, different types of RNA.

Currently, the understanding of their functions is still very limited, and different studies highlight their importance in a myriad of functions particularly involved in cell-cell signaling, especially during stress conditions and host-pathogen interactions (Aguilera et al., 2022; Schatz et al., 2021). Interestingly, a study on vesicles excreted by *Prochlorococcus* suggested a role of these vesicles in mitigating ROS toxicity (Biller et al., 2022). According to the present study, this might also be related to cell redox balance and bloom termination

5.4.2 Sexual reproduction, a major event during a *P. australis* bloom?

The knowledge of diatom life cycles mostly comes from laboratory studies. In these experiments numerous genes differentially expressed during sexual reproduction experiments were identified (Annunziata et al., 2022; Basu et al., 2017; Ferrante et al., 2019; Patil et al., 2015; Russo et al., 2018).

In the present study, a strong gene expression signal compatible with a transient and synchronized sexual reproduction event *in situ* was identified.

First, a transient gene expression pattern was identified between the early and middle bloom phases. The expression of several genes tended to indicate that sexual reproduction was actually occuring in a synchronized fashion at the time of sampling. This was the case of the mating type related gene: MRP1. This gene is MT+ specific and strongly upregulated during the early phase of sex (Russo et al., 2018). A study identified this gene as a key regulator of the MT− sexualization mechanism (Marotta et al., 2022). In the present study, two homologs of this gene were identified and they were both among the most highly overexpressed genes between the early and middle phases. To a lesser extent, other mating type related genes (MRP2 and MRM2) were over-expressed at this date. This was also the case of other putative sex marker genes. Among them, one marker was found strongly expressed during sexual reproduction in several diatoms (Bilcke G., personal communication). In addition, two cathepsin D homologs displayed high expression levels. Different studies have identified high expression of this gene during sexual reproduction (Basu et al., 2017; Marotta et al., 2022). Moreover, in *Saccharomyces cerevisiae*, Cathepsin D is a peptidase that degrades pheromones to generate a gradient useful for detecting the closest mating partner (Barkai et al., 1998).

Second, following this transient expression pattern, *in situ* gene expression dynamics is extremely similar to the one observed a few days after sexual reproduction during experiments. More specifically, *in vitro*, *P. multistriata* showed a down-regulation of many genes involved

in major metabolic processes such as photosynthesis, nutrient transport and assimilation, fatty acid biosynthesis and carbon assimilation after sexual reproduction (Annunziata et al., 2022). These genes were over-represented in different clusters with a high odd-ratio (16.48) compared to the over-expressed genes also over-represented but with a smaller odd-ratio (2.82). A large proportion of the genes displaying low expression in Annunziata et al. (2022) also displayed low expression levels during the middle phase of the bloom. Most of the genes seemed to be under- more than over-expressed after the sex event. More specifically, during this phase, the most down-regulated process was photosynthesis as well as related processes such as carotenoid biosynthesis. This down-regulation is described as a method to decrease the input of photochemical energy in a way to protect cell health during the sexual phase (Annunziata et al., 2022).

In addition, genes involved in fatty acid biosynthesis were down-regulated in the same period. When their growth is stopped caused by multiple reasons (nutrient starvation, pharmacology) it is known that microalgae accumulate lipids in specific compartments called lipid droplets (LD) (Annunziata et al., 2022). LDs can store reserves of energy, membrane components, carbon skeletons, carotenoids and proteins (Leyland et al., 2020). This was hypothesized to be linked with the sex event, and permitted to store energy: consequence of cell division arrest highlighted in different studies (Annunziata et al., 2022; Basu et al., 2017; Scalco et al., 2014), or a strategy used by the cells to transfer storage molecules to the F1 generation (Annunziata et al., 2022). Together, these two important metabolic processes seemed to indicate that, at the early and end bloom's period, cells produced and stored energy that would be used for sex. Mate finding and sexual reproduction are known to be energetically costly (Lewis, 1987). Interestingly, even if it was difficult to make a functional link, it is worth noting the over-expression of the "glucose-6 phosphate dehydrogenase" gene which is related to the carbon assimilation process. This enzyme involved in the pentose phosphate pathway was also over-expressed *in vitro* (Annunziata et al., 2022).

In addition to photosynthesis and fatty-acid biosynthesis, genes involved in DA biosynthesis were also under-expressed for few days from the moment sexual reproduction started. A study of Bates et al. in 1998 documented that short, old cells after many generations of vegetative division produced less DA than new, large cells formed after sexual reproduction. Because blooms are the result of mitosis resulting in short cells, a large number could produce DA in the early period; before sex event (middle period). At the end of the bloom, the population mainly composed of new cells increased DA gene expressions. However, no direct role has been demonstrated for this toxin in sexual reproduction (Bates et al., 1998), but this result could

explain under-expression of the DA biosynthesis gene expression during the bloom when a sex event took place.

Moreover, different studies showed that cells involved in sexual reproduction blocked cell divisions (mitosis) for few days, halting population growth (Annunziata et al., 2022; Basu et al., 2017; Scalco et al., 2014). In this study, as we saw above, genes involved in protein synthesis and ribosomal biogenesis were over-expressed in the middle of the bloom, in addition with the over-expression of chromosome organization genes functions. The amount of ribosomal protein and protein encoding transcripts has previously been shown to be positively correlated with metabolic rates and growth (Gifford et al., 2013; Gong et al., 2018; Wei et al., 2001). This over-expression runs inverse to the growth arrests identified in the literature according growth rate analyses, at the time of sexual events. A study on the diatom *S. marinoi* supported our results since no evidence of marked growth arrest was identified and no major signals related to cell cycle control were detected. However, blooms are the result of numbers of cell division (Smayda, 1997) and in the study, the increased cell divisions during the middle period does not seem consistent with what would be expected, i.e at the beginning of the bloom. Indeed, at this time the greatest abundance of cells seems to be already present (chlorophyll a values) compared to the early and end period and the relative abundance of *P. australis* had already been reached.

Pseudo-nitzschia life cycle is characterized by a size-reduction-restitution life in which cells of opposite mating type (+ and -) produce gametes when they reach a certain threshold of cell size and population concentration, at which a sexual event can take place. Meiosis is characteristic of this stage, and the genes of this function identified in the study and known to play a role in DNA duplication, chromosome maintenance and stability and DNA repair were found to be relatively stable during the monitoring with the exception of a Rad51 A-1 homolog at the beginning of the middle monitoring phase. One explanation already raised in the article of Ferrante et al. in 2019, could be that their expression levels were already sufficient to allow for the meiotic machinery to function during the progression of sexual reproduction. Genes involved in meiosis were detected in the transcriptome of the sexualized diatom *S. marinoi* during the switch from vegetative lifestyle to sexual reproduction (Ferrante et al., 2019). It should be noted that the sexual phase in diatoms is also characterized by strong morphological changes after pairing with different stages (gametes, zygotes, auxospores) before returning to the initial state. And we wonder if genes involved in protein synthesis, ribosomal biogenesis were not the result of these major morphological changes that would require high protein requirements, for example the formation of the siliceous shells typical of diatoms after the

auxospore state. Moreover, genes related to the organization of chromosomes were over-expressed at this time and are necessary for meiosis to function properly (Murray and Szostak, 1985). The time associated with the sexual phase in literature seemed to be in line with the present study (Basu et al., 2017). Indeed, after a short time sensing between the different mating types (that we assumed to be the peak of the cluster 6; fig 6); the sexual phase, with numerous morphological changes took place with over-expression of genes involved in protein synthesis. At the same time, different metabolic functions were under-expressed as photosynthesis, fatty acid biosynthesis as well domoic acid biosynthesis. These profound changes took place during the sexual phase, which according to the literature seemed to take place for several days (Annunziata et al., 2022; Basu et al., 2017; Scalco et al., 2014).

Added to the laboratory studies information about sexual reproduction, some rare morphological observations of natural populations were reported anyway. The paucity of reports is due to different reasons: (1) low sampling frequencies and the limitations of visual identifications of sexual stages, inherent limitations of sampling and counting procedure; (2) Sexual reproduction in diatoms in the field is thought to occur on average every three years, whilst the mating cells and auxospores are formed over 2–4 days (Davidovich and Bates, 1998). These varying time scales means that studying this process in its natural environment is very difficult (Kim et al., 2023).

However, this is not impossible, as regular monitoring could enable this phenomenon to be observed *in situ*, as diatom species don't bloom all the same year, and synchronization between cells has been observed *in situ* during sex event. This was particularly observed in the present study by strong over- and under-expression of genes during the time course of a *P. australis* bloom. Sexual stages in natural environment of *Pseudo-nitzschia* species have been observed and reported twice (Holtermann et al., 2010; Sarno et al., 2010). In Europe, sexual stages of two species of *Pseudo-nitzschia* were detected at the Long Term Ecological Research Station MareChiara in the Bay of Naples (Mediterranean Sea), where they accounted for 9.2 and 14.3% of the total number of cells of *P. cf. delicatissima* and *P. cf. calliantha*, respectively (Sarno et al., 2010). Another massive sex event has been reported along the Washington coast (USA) involving *P. australis* and *P. pungens*. Auxospores were detected for a long time period (about 3 weeks) and accounted for 59% of the *P. australis* population at the end of the bloom (Holtermann et al., 2010).

In addition to the synchronous aspect, the observation of sex *in situ* has shown that several factors must be in place to allow it. Firstly, the cells must reach a sexualisation size threshold

(SST) (Basu et al., 2017). Secondly, a threshold cell concentration is required in order to allow vegetative cell's encounter and subsequent gametogenesis. This requirement can be met at the end of the exponential growth phase of the bloom (D'Alelio et al., 2009; Scalco et al., 2014). Because the major changes were present from a sample which appeared to be consistent with a dominance of *P. australis*, we assumed that the latter argument coupled with all the others presented in this section was in favour of the detection of sexual reproduction in the samples studied with the perception of chemical cues deriving from mating partner at the beginning of the middle period followed by many changes in the population genes expression described above. We believe that this event determined the entire gene expression dynamic during a bloom.

Conclusion

This study is the first to identify gene expression dynamics during the all-time course of *a P. australis* bloom in the natural environment. Analysis of these genes revealed a strong dynamic during the bloom characterized by 3 distinct periods. Based on numerous signals found on *in vitro* sexual reproduction experiments, we believe that sexual reproduction is the key event in the blooming of *P. australi*s, that impacts all gene expression dynamics. Different points are in agreement with this: 1) the strong over-expression of MRP1 gene (mating type related plus gene); 2) over-expression of genes related to sexual reproduction (mating type related genes, Rad51 A-1, Cathepsin D, putative sexual markers ect); 3) prolonged changes in genes related to metabolic functions during several days (photosynthesis, carbon assimilation, cell growth, fatty acid biosynthesis, AD biosynthesis); and 4) common changes in gene expression with genes identified as marker of sexual reproduction in the literature. All these different observations suggested that *P. australis* cells have been sexually reproducing for a few days. And we hypothesize that as soon as the cells receive the chemical signals related to sexual reproduction, they reduce different metabolism processes in order to promote this event. Our data provide a baseline for future gene expression dynamic studies of natural bloom.

Chapter 6

Discussion

The general aim of the thesis was to understand the spatio-temporal development dynamics of toxic blooms of *Pseudo-nitzschia australis* in Western Brittany (France). To achieve this, our original approach was to combine different analytical methods. By simultaneously exploring gene expression, the environment (both biotic and abiotic), and hydrodynamics, we were able to gain a comprehensive understanding at different scales of *P. australis* blooms in Western Brittany.

6.1 Summary of the results

Phytoplankton is by definition a group of 'wandering' organisms, subject to the influence of marine environment driving their movements and their development. Consequently, understanding a given area can involve characterising the phytoplankton composition at different sites within that area. Does this composition vary between the different stations in the zone? If so, what are the causes?

The aim of the chapter 2 was to characterise the spatio-temporal dynamic of the diatom community (to which the genus *Pseudo-nitzschia* belongs) by identifying its composition at the lowest taxonomic level (species/genus) in relation to the biotic and abiotic environment. During two periods in late winter/early spring, four contrasting sites differing in terms of their openness to the ocean and the amount of freshwater received were analysed along the on western coast of Brittany (chapter 2). In this chapter, using high-frequency monitoring, we have highlighted a relatively homogeneous diatom community, over 2 years of monitoring, in spring 2019 and 2021. More specifically, using metatranscriptomic samples, we identified species frequently found on the East Atlantic coast in early spring, as is the case of *Guinardia delicatula*, *Rhizosolenia setigera* and the genus *Thalassiosira sp.* (mainly *T. nordenskioeldii* and *T. minima*). Within this homogeneity, one of the major points to note is the shift in the succession of communities in a South-North direction between the stations monitored. The station located furthest south showed earlier changes in its succession than the stations further north. We also identified that changes in the succession of diatoms (the dominant phylum) were mainly correlated with seasonal changes in PAR and temperature, and a decrease in phosphate.

However, there was no local explanation for this shift. However, there was no local explanation for this shift, no time lag in environmental changes was identified. Also, some stations differed in environment, e.g. the Bay of Brest is more impacted by freshwater.

The second approach in this thesis was to characterise the hydrodynamics in the study area (chapter 3). Is it an explanation for the development pattern observed in chapter 2? The idea was to characterise and compare the existing hydrodynamic connectivity in the West-Brittany area in the month of March over different years during which *P. australis* blooms were observed. Eulerian simulations over the study area showed a marked connectivity between the Bay of Douarnenez and the Bay of Brest, whatever the year. However, our connectivity indicators (Pmax, the maximum tracer concentration arriving in an area; and Tmax, the time corresponding to Pmax in that area) were highly variable, illustrating a variable connectivity intensity between the Bay of Douarnenez and the Bay of Brest, amongst the year. For instance, the average Pmax from the Bay of Douarnenez to the Bay of Brest was around 5 times greater in 2014 than in 2019. When the winds were from the south or south-west, with increasing tide amplitude, connectivity was stronger than when the winds were from the east, or when the tides had coefficients that increased. This suggested that the variability of the results obtained from the simulations is partly due to the wind direction and the tide.

In chapter 4, the study of hydrodynamic connectivity was coupled with the results of the 2021 monitoring, where a major *P. australis* bloom was observed (488,000 cell/L of *Pseudo-nitzschia spp.* counted on March 23rd, with a dominance of *P. australis*). Based on these results, we found a good concordance between hydrodynamic connectivity times and the appearance of *P. australis. P. australis* was first observed in Telgruc. It then appeared in Dinan-Kerloc'h between 7 and 11 days later, which coincided with the estimated time of the hydrodynamic transport (5-7 days). Then, *P. australis* cells emerged in the Bay of Brest between 21-28 days which also coincided with the time of the estimated hydrodynamic transport from Telgruc (19-32 days). However, from Dinan-Kerloc'h to the Bay of Brest, there was a discrepancy between hydrodynamic and appearance time of *P. australis*. These results suggest a development in the Bay of Douarnenez, which would thus be a 'hot spot' for the development of *P. australis* in the area. We assume that transport from this area leads to the development of *P. australis* cells into the Bay of Brest. Various reasons highlighted by the results of the chapter 4 support this hypothesis: (1) a South-North hydrodynamic transport which indicates that *P. australis* cells from the Bay of Douarnenez may travel to the Bay of Brest; (2) Weaker dilution of water masses in the Bay of Douarnenez than in the other study areas which favors phytoplankton development and retention; (3) Physiological state similar to the appearance of the cells at the various stations

with Telgruc, in the Bay of Douarnenez which suggests a strong link between the Bay of Douarnenez and the different stations; (4) This last point, independently of local environmental conditions, since at the time of the gene expression similarities, the environment was not similar between stations.

In Chapter 5, in order to better comprehend the physiological state of the *P. australis* cells during a bloom, we specifically studied the genes expressed by this species throughout the period of its development in the Bay of Brest. We studied the genes expressed during a high-frequency bloom monitoring period. Analysis of these genes revealed a strong dynamic during the bloom, characterised by 3 distinct periods. Among the genes expressed, numerous signals related to sexual events *in vitro* were also identified during the bloom: (1) the strong over-expression of MRP1 gene (mating type related plus gene); (2) over-expression of genes related to sexual reproduction (mating type related genes, Rad51 A-1, Cathepsin D, putative sexual markers ect); (3) prolonged changes in genes related to metabolic functions during several days (photosynthesis, carbon assimilation, cell growth, fatty acid biosynthesis, AD biosynthesis); and (4) common changes in gene expression with genes identified as marker of sexual reproduction in the literature. Thanks to these different signals, we have demonstrated that sexual reproduction is a central event which impacts global expression dynamics during a bloom.

6.2 The importance of combining analysis methods

First of all, the point I wish to discuss relates to the choice of analytical methods when studying a bloom. It is essential to point out that all studies, whatever their nature, are often restricted and sometimes conditioned by technical and budgetary constraints.

Coastal systems are among the most dynamic natural systems on Earth, making their study particularly challenging. In coastal regions, environmental conditions can change rapidly due to factors such as wind speed and direction, precipitations, river discharge, waves and tides. Since the growth of phytoplankton is closely dependent on these variations, understanding their dynamics can become a complex task. A holistic approach that integrates a set of monitoring or analysis (i.e. satellite imagery, numerical models, *in situ* observations, molecular biology) may provide different information about coastal ecosystems at different spatial and temporal scales. Of course, none of these tools are perfect, being that each is characterized by intrinsic

errors and therefore specific uncertainties, which is also an important subject of investigation (Martellucci et al., 2021).

In the case of this thesis, the combination of different approaches (fig. 1) enabled us to gain an understanding of *P. australis* blooms in West Finistère.

In fact, is we consider a bloom in an area, notably of HABs, in our case *P. australis*, which can have a negative impact on the surrounding ecosystems (death of organisms due to toxins) and human activities (fishery closures). When we seek to comprehend the occurrence of a phytoplankton bloom, several fundamental questions arise.

Firstly, we inquire about the specific location (Where?) and timing of this species' growth (When?). What factors contribute to its development? Is it influenced by local environmental conditions, biotic or abiotic factors, or hydrodynamic elements that facilitate its proliferation? (How?) Are there any coexisting species that play a role in this process? (With who?) Lastly, why does it thrive during this particular period? (Why?) Is it linked to its life cycle or an environment uniquely suited to its ecological niche, providing a competitive advantage? (fig.1)

Throughout this thesis, we employed a range of analytical techniques to address these inquiries (fig. 1): *in situ* environmental analysis, metatranscriptomics, and hydrodynamic modeling. Each of these approaches yielded insights into distinct aspects of the questions at hand. The synergy resulting from the combination of these methods allowed us to attain more comprehensive and holistic answers.

This raises a point: **Understanding a bloom requires the use of various analysis methods.**

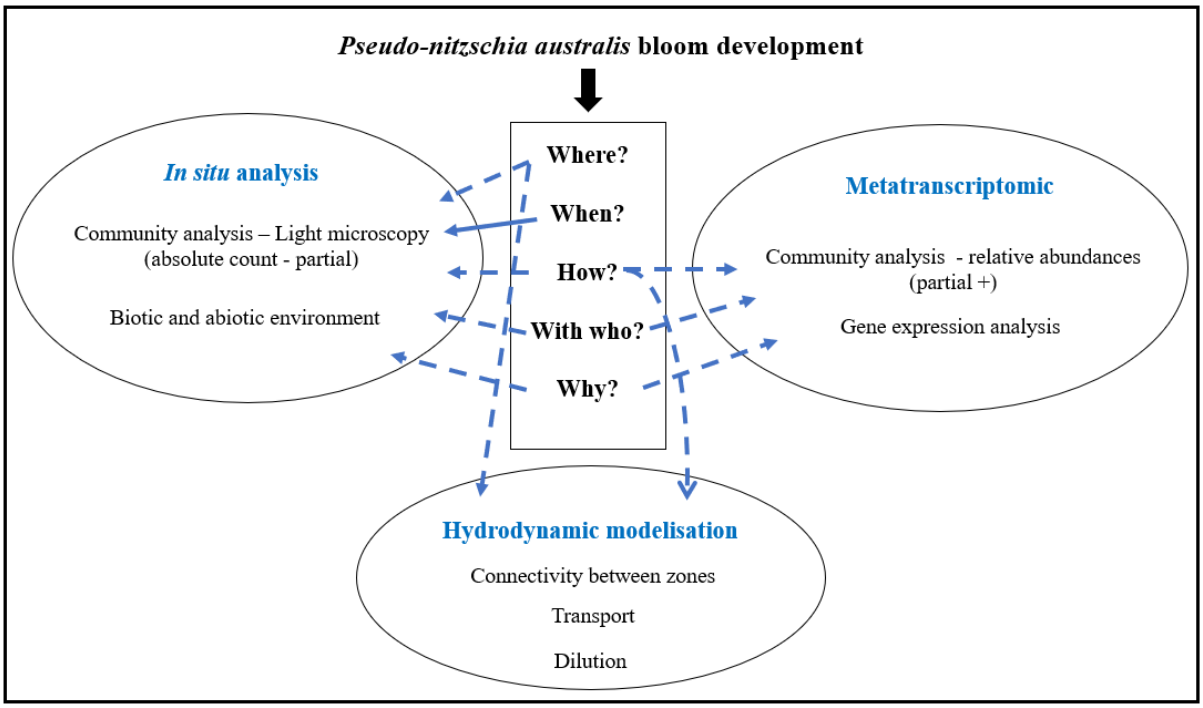

Fig. 1: Conceptual diagram showing the different methods used in the thesis and the questions associated with their use. Full arrows indicate a complete answer to the question, and broken arrows indicate a partial answer.

Considering the methods used in this manuscript "one by one", how far can we go in understanding the bloom? (fig.1).

In the spatio-temporal analysis of a bloom, identifying the composition of the community is a key first step. This enables us to identify the dominant species and its evolution: does it dominate the community on its own? Are there accompanying species?
In a spatial study, if similar communities are identified between study stations, this would indicate a strong link between the areas studied, while different communities would show a cleavage between areas and a different environmental impact.

In this thesis, the first objective was to pinpoint and thoroughly characterize this community at the most precise taxonomic level attainable (e.g species and if not possible: genus). This detailed identification is of great importance for identifying the *P. australis* responsible for the problem, which is difficult to identify within the pseudo-nitzschia genus using light microscopy alone.
The application of metatranscriptomics allowed us to discern the community down to the finest taxonomic level, and to identify *Pseudo-nitzschia* species at the specific level (chapter 2). Nevertheless, while we did acquire data regarding the relative abundances associated with

various species, it is important to note that a species may appear in high relative abundance in metatranscriptomic samples but exhibit low absolute abundance. In order to assess the absolute abundance of a species, it becomes crucial to couple those results with light microscopy counts at higher taxonomic level.
However, light microscopy results are limited not only by the expertise of the observer, but also by the quantity of water analyzed (how representative was it of the environment?) and the various technical biases (are the lugolated cells actually present in the sample analyzed and not stuck to the flask wall?). Various methods can also be used to obtain information on the phytoplankton community. In this thesis, we also used flow cytometry to count cell abundance in phytoplankton size ranges (pico-nano-micro phytoplankton).

Similarly, understanding the process of bloom development cannot be solely achieved through isolated investigations. This is because blooms emerge as a complex interplay of factors encompassing the biotic, abiotic, physical and physiological environment (Anderson et al., 2012). As illustrated in the figure 1, each of the methods used provided insights into only a portion of the potential factors contributing to the bloom development.

Due to the dynamic nature of coastal environments, acquiring data about the specific environmental conditions conducive to species development can be a challenging endeavor. Additionally, it is essential to ascertain whether the sample collection site aligns with the area where the species is likely to thrive. These inquiries can be addressed through hydrodynamic modeling with simulations involving tracers within the region. Eulerian transport proves valuable when investigating the dispersion and dilution of tracers emanating from a zone that may reflect phytoplankton biomass during a bloom. On the other hand, Lagrangian transport tracks particle movements in both space and time, offering insights into potential trajectories. Furthermore, metatranscriptomics, by examining expressed genes, provides a glimpse into the physiological condition of cells at the time of sampling. It can reveal whether the cells were under stress, engaged in intensive cell division, or exhibited overexpression of genes related to nutrient uptake or toxins biosynthesis for example. Collectively, these methods complement each other and contribute to a comprehensive understanding of bloom development.

To conclude this part, it is important to notice that in view of the increasing number of Harmful Algae Bloom (HAB) events, it seems necessary to combine different analysis methods. To

illustrate, the hydrodynamic simulation periods were set on the basis of the development of *P. australis* which was identified using metatranscriptomics.
The different methods used in this thesis provide us a more comprehensive view of the bloom initiation factors, as well as their initial location in Western-Brittany.

6.3 *P. australis* blooms in Western Finistère: an origin, the Bay of Douarnenez

Throughout the thesis, thanks to the coupled analysis of different methods, the results reflected the Bay of Douarnenez as the zone of initiation of *P. australis* blooms. There are many arguments to support this:

- The REPHY identification of *P. australis* blooms, first in the Bay of Douarnenez and then in the Bay of Brest (see introduction).

- Spatio-temporal analysis at 4 stations located on the south-north gradient between the Bay of Douarnenez and the Bay of Brest revealed an early development in the south and a later emergence in the north (chapter 2).

- Hydrodynamic simulations carried out in the study area revealed northward conservative tracer transport and lower dilution of water masses in the Bay of Douarnenez (chapter 3).

- A multi-approach analysis showed consistency between the appearance times of *P. australis* and the simulated hydrodynamic connectivity times between the departure of the tracer at Telgruc and its identification at other stations. We also found a correspondence between the physiological state of the cells at the time of their appearance at the various stations, and the cells of Telgruc (chapter 4).

Blooms of *P. australis* have been a recurring event in the region, with the most recent occurrence in 2023, and they have been happening approximately every 2-3 years for the past decade. For these reasons, we consider the Bay of Douarnenez to be a hot spot for the development of *P. australis* in West- Brittany.

During this thesis, we were particularly interested in the northeastern part of the Bay of Douarnenez, due to the monitoring of the Telgruc station. However, during *P. australis* bloom monitoring in 2021, REPHY data (REPHY, 2022) also observed high and increasing abundances of the toxic species at the Kervel monitoring station located in the south-east of the Bay of Douarnenez. The recorded concentrations were 84,000 cell/L on March 7th and 488,100 cell/L on March 21st. These results coincide with the absolute counts of *Pseudo-nitzschia* at Telgruc: 101,400 cell/L on March 9th and 498,000 cell/L on March 23th. This would indicate that bloom development took place at least in the entire eastern part of the Bay of Douarnenez. This was also confirmed by satellite images obtained by the OC5 algorithm (IFREMER) using MODIS data (NASA) (1 km resolution, fig. 2) As a reminder, the highest cell concentrations in Telgruc were between March 19th and 23th.

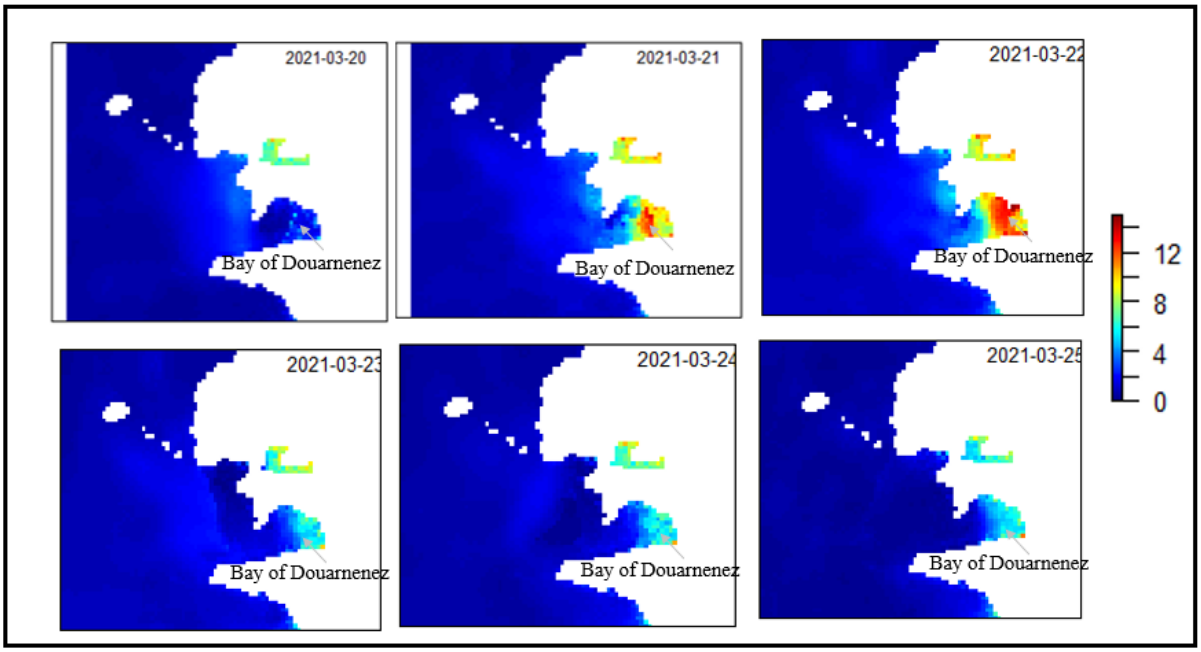

Fig. 2: Chlorophyll a (µmol/L) surface concentrations maps between March 20th and 25th, 2021 in West-Finistère.

The frequency of the term "hot spot" is increasing in the literature related to Harmful Algal Blooms (HABs). This is partially attributable to enhanced sampling efforts and advancements in analytical techniques. Notably, the integration of satellite data (chlorophyll *a*) and numerical models has contributed significantly to our improved understanding of bloom spatial dynamics. In our case, we characterize the hot spot as an area where the initial growth of *P. australis* occurs, and subsequently, due to hydrodynamic conditions, extends its influence to affect other areas.

This phenomenon has been relatively well studied on the United state coast during *P. australis* bloom periods. Regions affected by *Pseudo-nitzschia* extend along the coast of Washington State, with a demonstrated “hot spot” in the Juan de Fuca eddy area, where *Pseudo-nitzschia* blooms occur relatively frequently, associated with high DA concentrations (Trainer et al., 2009, 2002). For cells (thus DA) to reach the coast from the eddy region, toxic cells must first reach a concentration level sufficient to form a bloom. Subsequently, they need to escape the eddy and move southward towards the razor clam beaches, then make their way onto coastal beaches, remaining in the surf zone for a significant period to allow a substantial ingestion of toxic cells by clams. The highest concentrations of toxic cells, along with onshore transport, occur during periods of downwelling winds (storms). On the other hand, the escape from the eddy and the southward movement happen during periods of upwelling winds, as observed by MacFadyen and Hickey in 2010. Another area where toxigenic *Pseudo-nitzschia* blooms initiate, referred to as a "hot spot," is the Heceta Bank off the coast of Oregon, as indicated by Trainer et al. in 2000. In recent years, the impact of DA toxicity on industries such as razor clamming, mussel harvesting, and Dungeness crab fishing appears to be increasing, with extensive and prolonged closures occurring notably from 2003 to 2005, as reported by Tweddle et al., in 2010. Additional hotspot regions in California include Monterey Bay, San Luis Obispo, and Point Conception, as documented by Trainer et al., in 2000.

These various observations indicate that when our focus is on algal blooms, particularly HABs, it is essential to examine these blooms from a spatial perspective. In other words, the region where monitoring occurs might not necessarily coincide with the area where the bloom initially develops. This can introduce biases, particularly in relation to the environmental factors affecting the bloom's development. To illustrate, in our study we took samples from 4 different geographical areas. The environmental characteristics of these areas differed according to their position (more specifically, freshwater inflow, tides, winds, currents). As an illustration, if we consider a location highly influenced by the inflow of freshwater into the Bay of Brest, such as Sainte-Anne, we would observe stronger correlations with factors like nutrients, salinity, or currents compared to the zone we have identified as the initial development area. In this latter zone, salinity levels are higher, and the influence of nutrients and currents is comparatively weaker.

The high spatial and temporal variability of coastal zones makes it difficult to understand the precise trigger of HAB development. A telling example concerns blooms in upwelling regions.

The analysis of *in situ* data have not always produced strong correlations and consistent directional relationships on the occurrence of *Pseudo-nitzschia* in California. For example, it is normal to find strong correlations between *Pseudo-nitzschia* abundances and cooler temperatures and higher salinity, which are direct consequences of upwelling, a primary driver of toxic *Pseudo-nitzschia* blooms (Bates et al., 2018; Lelong et al., 2012; Smith et al., 2018; Trainer et al., 2012, 2010).
In our case, *P. australis* mainly develops in West-Brittany in late winter/early spring period, in a highly dynamic environment, characterized by high tides and strong winds, with significant seasonal changes (increased temperature, increased daylight and irradiance).

But the question remains, to what extent is this development the result of the local environment? The various samples were collected at coastal level, with a strong impact from the coast. This raises the question: to what extent is the coastal environment representative of the developmental environment of *P. australis*? Doesn't the high variability of the environmental parameters collected conceal a signal that would be obvious if we did not sample at the coast?

To make sure of this, it would have been interesting to see the variability of environmental values in the different study areas through coast-to-open-ocean transect sampling. Similarly, it would have shown us the extent of the bloom.

In view of the complexity of blooms, which are influenced by many constantly fluctuating factors, particularly in coastal areas, metatranscriptomics offers the possibility of exploring the responses of cells to the various environmental stresses they are confronted with, using RNA-seq datasets. With this in mind, we are convinced that metatranscriptomics by analyzing all the genes expressed by a specific species represents a solution for capturing the direct impact of the environment on its physiological state. In a variable environment such as the coast, this can provide important information on the role of the different environmental variables on the potential development of cells. In other words, it enables us to gain a more comprehensive understanding of blooms compared to traditional species-environment correlations, as it directly reveals the impact of the environment by the study of the cells at the physiological level. In this study, we were able to highlight the important role of sexual reproduction in the overall dynamics of gene expression during a bloom of *P. australis* in 2017. Furthermore, by studying similarities in the physiological state of the cells during spatio-temporal monitoring in 2019 and 2021, we were able to see that the physiological state at the time of the appearance of

P. australis presented high similarities between the different stations and Telgruc. We would not have been able to obtain this information with the *P. australis* presence/environment link.

- **Some analysis perspectives**

How can we be sure that cells are being transported from the Bay of Douarnenez?

First of all, we can carry out complementary analyses on the spatio-temporal monitoring of 2021. We can analyze the specific functions of expressed genes. When analyzing the spatio-temporal variability that exists during the 2021 bloom, we saw strong similarities at the time of emergence of *P. australis* in Dinan-Kerloch and in the Bay of Brest with Telgruc before diverging. In order to find some explanation about it, we suggest analyzing which genes and associated functions show a change between the initial state of gene expression at cell emergence at the different stations and gene expression after some days.
To address this, we propose two potential approaches that could be tested using the metatranscriptomic dataset of 2021. (1) We could analyze the major categories of functions associated with genes showing similar expression dynamics (identified by WGCNA) in the different study stations using Gene Ontology analysis (http://geneontology.org/). Similarly, a Gene Ontology analysis could be conducted on the genes displaying the highest expression variability on the first axis of the PCA conducted on all the samples of 2021 (fig. 9, chapter 4). (2) We could perform a differential expression analysis by categorizing samples with expression patterns similar to Telgruc together and those with expression patterns distinct from Telgruc together, these groups would be established on the basis of the PCA (fig. 9, chapter 4). After this, a search for functions can be carried out either by GO analysis to obtain broad categories of functions, or on protein sequence libraries such as NR and Uniprot-Swissprot.

Second, to verify this south-north transport, we also propose to carry out sampling cruises between the Bay of Douarnenez and the Bay of Brest at the time of *P. australis* blooms. A precise analysis of the cells could be made by light microscopy, for example, are the cells in the Bay of Douarnenez smaller resulting in numerous divisions compared with the other stations?
An analysis of gene expression could also show whether there are correspondences in expression in space and time between the different samplings (as done in chapter 4).

Lastly, coupling mortality and growth rates to a physical model of cell transport could enable us to check whether hydrodynamic times are consistent with the displacement of *P. australis* in relation to its biology.

How can we improve our knowledge of the ecological niche o*f P. australis*?

In this thesis, we have examined the spatio-temporal dynamics of *P. australis* bloom and identified a south-to-north pattern in its initiation, with the initiation of blooms in the Bay of Douarnenez. However, the specific conditions responsible for this localized growth remain unclear.

We strongly advocate for the implementation of high-frequency monitoring of *P. australis* blooms in the Bay of Douarnenez over an extended period of several years. Long-term data collection efforts could help us identify, through statistical analysis, the favorable conditions that lead to its development, compared with the environmental conditions in years when it doesn't bloom.

The information gathered could significantly contribute to our understanding of its recurrent presence in West-Finistère and potentially facilitate the development of a numerical *P. australis* model development for this region. Indeed, gaining a deeper insight into its ecological behavior could pave the way for the creation of physical-biological models, utilizing data on growth and mortality rates, linked to the environment. Over time, such models could offer fisheries managers and decision-makers real-time predictive tools for monitoring the development and movement of *P. australis*.

The best perspective on *P. australis* blooms understanding remains **long term data acquisition**: the more data we have, the better we'll be able to understand the environmental and/or physical conditions linked to its development in the region.

6.4 Is there sexual reproduction without bloom?

In chapter 5 of this thesis, the expression dynamics of *P. australis* genes were studied throughout the entire course of a bloom in the natural environment. Without any prior consideration, the analysis of *P. australis* expressed genes revealed strong dynamics during the

bloom, characterized by 3 distinct periods. On the basis of numerous signals identified from *in vitro* sexual reproduction experiments and found in our data, we showed that sexual reproduction is the key event in *P. australis* bloom, impacting all gene expression dynamics.
Different points support it: (1) the strong over-expression of MRP1 gene (mating type related plus gene); (2) over-expression of genes related to sexual reproduction (mating type related genes, Rad51 A-1, Cathepsin D, putative sexual markers ect); (3) prolonged changes in genes related to metabolic functions during several days (photosynthesis, carbon assimilation, cell growth, fatty acid biosynthesis, DA biosynthesis); and (4) common changes in gene expression with genes identified as marker of sexual reproduction in the literature.
A progressive reduction in cell size during mitotic cell division is a distinctive feature of diatom species (Montresor et al., 2016). This is due to the presence of a rigid siliceous cell wall (the frustule) composed of two slightly unequal halves. During cell division, daughter cells always synthesize the inner half of the frustule, implying that the average cell size of the population gradually decreases. Sexual reproduction plays a fundamental role in the diatom life cycle. It contributes to increasing genetic diversity through meiotic recombination, and also represents the phase during which large cells are produced to counteract the process of cell size reduction that characterizes these microalgae. It is not only the phase in which genetic recombination occurs when haploid gametes are produced after meiosis, but also the phase in which large cells are regenerated. In many diatoms, large cells are produced following sexual reproduction, during which the zygote (called "auxospore"), which is not surrounded by the rigid frustule, can develop and, during this phase, the initial large cell is synthesized (Ferrante et al., 2019). In this context, it could be envisaged that if sexual reproduction did not occur, the cells would continue to reduce in size, eventually leading to their extinction.

Throughout this thesis, we have been interested in the phenomenon of bloom in *P. australis*, which is the result of massive development when conditions are favorable. Its blooms depend on the rapid asexual reproduction of diatoms by mitosis, which facilitates rapid growth and biomass accumulation, but reduces the average size of the dividing clonal cell. Finally, it appears necessary that during blooms, the cell that reaches a minimum critical size triggers sexual reproduction to restore its maximum size (Sison-Mangus et al., 2022).

Although very few studies have observed sexual reproduction events in the natural environment in diatoms. Auxospore formation has been identified *in situ* in the diatom *Fragilariopsis*

kerguelensis (Assmy et al., 2006). Two studies observed and reported sexual reproduction events in *Pseudo-nitzschia* species (Holtermann et al., 2010; Sarno et al., 2010).
However, given the number of bloom monitoring events, it is not clear why there are so few reports on sexual reproduction in diatoms. As suggested by Montresor et al., in 2016, this may be due to a lack of knowledge of the morphology of sexual stages, which may be rare and therefore easily neglected or underestimated. Indeed, in both events of sexual reproduction observed *in situ* (Holtermann et al., 2010; Sarno et al., 2010), only a certain fraction of the population undergoes sex. In Europe, sexual stages of two species of *Pseudo-nitzschia* were detected at the Long Term Ecological Research Station MareChiara in the Bay of Naples (Mediterranean Sea), where they accounted for 9.2 and 14.3% of the total number of cells of *P. cf. delicatissima* and *P. cf. calliantha*, respectively (Sarno et al., 2010). During another massive sex event reported along the Washington coast (USA) involving *P. australis* and *P. pungens*. Auxospores were detected for a long time period (about 3 weeks) and accounted for 59% of the *P. australis* population at the end of the bloom (Holtermann et al., 2010). Comparable results were reported from laboratory experiments (Scalco et al., 2014).

Another factor to consider is that sexual events are short-term events. This could be due to the fact that the sexual phase occurs under very specific conditions, requiring an appropriate cell concentration, a precise cell size (in the life cycle of *P. multistriata*, opposite MTs produce gametes only when they are shorter than 55 µm (D'Alelio et al., 2009), and possibly other external cues. When pennate diatom strains of opposite mating types are mixed under laboratory conditions, gametogenesis is only recorded for a few hours/days (Scalco et al., 2016, 2014; Vanormelingen et al., 2013). Gamete formation in centric homothallic diatoms also occurs within a short time interval (typically ~2 days) in culture (Koester et al., 2007). In the field, sexual reproduction in diatoms is estimated to occur on average every three years, with mating cells and auxospores forming in 2 to 4 days (Davidovich and Bates, 1998). The recurrence of blooms reported in the article is in line with observations made by REPHY (REPHY, 2022) in Western Brittany. Since 2014, significant *P. australis* blooms (> 100,000 cells/L) have occurred at intervals of approximately every 2 to 3 years, specifically in 2014, 2017, 2019, 2021, and 2023. These variable and tight timescales (both for development and for sampling sexual events) make it very difficult to study this process in its natural environment (Kim et al., 2023).

During the bloom study in 2017, the sexual reproduction event (4 days long) seemed to condition the entire gene expression dynamics of *P. australis*. This leads us to pose the following questions:

Is it possible for sexual reproduction to occur independently of a bloom event? Furthermore, could there be a biological cycle, akin to a biological clock, where, under specific environmental conditions, cells divide extensively (resulting in a bloom) in order to facilitate pairing and initiate sexual reproduction?

One study has already mentioned a synchronicity in *P. australis* bloom development along the West Coast of the United States. This synchronicity was observed from southern California to central California (Du et al., 2016). With regard to the cyclical nature of the blooms, *P. multistriata* blooms in the Gulf of Naples occur with great regularity. Peak abundance occurs every year, between late summer and early autumn, but cohorts of large cells, resulting from sexual events, have only been found to be present one year in two (D'Alelio et al., 2010). Moreover, the authors predicted, following the results of a population growth model, that *P. multistriata* would become locally extinct if sexual reproduction did not occur within 4 years (D'Alelio et al., 2010).

In this thesis, the environmental conditions that caused *P. australis* to develop are still unclear. Since the species was first identified in West Brittany by the REPHY, the species developed rather recurrently over the late winter/early spring period, with large blooms detected by the REPHY in 2014, 2017, 2019, 2021, 2023 (see introduction). This suggests that this period provides the ideal environmental conditions for its development. To illustrate, in the 2021's monitoring, the environmental changes were rather linked to the temporal evolution typical of early spring (increase of PAR and temperature, high nutrients). Previous studies showed that *Pseudo-nitzschia spp.* has been observed on different French coastal areas from spring to early summer when light intensity and photoperiod increase (Belin et al., 2021; Husson et al., 2016; Thorel et al., 2017). More generally, different studies have highlighted that *Pseudo-nitzschia spp.* blooms in coastal ecosystems are especially common in nutrient-rich waters with high nutrient inputs (Lundholm et al., 2010; Parsons and Dortch, 2002). Some studies identified *P. australis* blooms in coastal upwelling systems (e.g. Anderson et al., 2006; Schnetzer et al., 2013; Torres Palenzuela et al., 2019). Generally, high nutrient conditions are known to be well present at the beginning of spring, or autumn, in temperate coastal areas with the increase in river flows.

Furthermore, given the identification of *P. australis* blooms at regular frequencies in the study area, this prompts us to inquire **whether the internal biological clock of *P. australis* may exert an influence on the timing of its sexual reproduction event.**

We also wonder whether *P. australis* could survive despite unfavorable environmental conditions that would prevent it from developing in a given year. More specifically, **could the recent lack of development of *P. australis* in certain regions of the world be the result of unfavorable environmental conditions that prevented this species from growing, reproducing and eventually disappearing locally, even if it had a significant impact for several years?**

Take the most notable example: a major toxicity event was identified in northeastern Canada in the Prince Edward Island, in 1987, when hundreds of people were poisoned and three died after eating shellfish contaminated with *P. multiseries*. At that time, the toxin reached among the highest levels recorded (790 mg DA g^{-1}) in blue mussels (Davidovich and Bates, 1998). After this initial event, there were several years of shellfish harvest closures due to domoic acid contaminations in mussels. These closures affected the eastern part of the island (in 1987, 1988, 1999), as well as the northern part of the island (in 1990, 1991, 1992, 1993 and 1999) caused by the toxic species *P. multiseries* before declining (Bates, 2004). The last harvest closure occurred in 2002, covering most of the southern Gulf of St. Lawrence (north of the island), but this time caused by a massive bloom of toxic *P. seriata* (Bates et al., 2002). Since then, no toxic events have been reported at this location, and *P. multiseries* has not been detected there (Trainer et al., 2012).

Another more local example concerns the Bay of Seine (Normandy) in France. Historically, this region has experienced two major toxicity crises caused by domoic acid produced by diatoms *Pseudo-nitzschia spp*. These events occurred in 2004 (as reported by Nezan et al., 2006) as well as in 2011 and 2012 (according to Ifremer data). These incidents led to the partial closure of the scallop fishery in the Bay of Seine for several months. Since then, no more toxic blooms of this type have been detected in the area.

If sexual reproduction plays a crucial role in the survival of a species in its environment, it could become the central element to be monitored in the natural environment.

Overall, sexual reproduction improves the population's chances of coping with environmental changes (e.g. global warming) (Ruggiero et al., 2018), thus contributing to the persistence of the species in its natural environment.

To conclude this section, I recommend field studies aimed at targeting genes associated with sexual reproduction, which have been identified in the laboratory (Annunziata et al., 2022; Basu et al., 2017; Patil et al., 2015; Russo et al., 2018). It is important to note that the sampling frequency during proliferation periods may not be sufficient to observe the sexual reproduction event. Indeed, as we pointed out earlier, sexual reproduction is a short-term process, and it may be necessary to increase the sampling frequency to detect it.
As an example, in this thesis, during the 2019 and 2021 bi-weekly monitoring, specific efforts were made to detect these markers, but the signal seems to be much less obvious than during the daily monitoring in 2017, due to the lower sampling that doesn't allow us to easily capture changes in the genes that could have been related to this short event. Further studies are needed for these two years.

In addition, I recommend additional long-term studies to examine the possibility of cyclicity within toxic species bloom, and *P. australis* in particular. These studies could help identify: (i) any exceptional events that may have prevented this species from developing, or even disappearing locally; (ii) to improve our overall understanding of its ecology.

- **Do accompanying species play a role in the sexual reproduction of *Pseudo-nitzschia in situ*?**

To conclude this discussion, I would like to address a point raised in the paper by Ferrante et al, 2023 about the "mystery of how planktonic cells of *P. multistriat*a, unable to swim, can find their partners and pair up in the 3D space of the water column".
During the 3 years that *P. australis* has been monitored, the species has always been identified with accompanying species during its blooms. During the 3 surveys, the species most frequently found were *Chaetoceros spp., Guinardia delicatula, Rhizosolenia setigera* and *Cerataulina pelagica* (chapter 2). These species all form chains. We therefore wonder whether the presence of these species does not favour *P. australis* cells pairing and sexual reproduction.

Various studies identified specific blooms of *Pseudo-nitzschia* with other accompanying species (e.g. Clark et al., 2019; Houliez et al., 2023). One study identified *P. pseudodelicatissima* populations within *Chaetoceros socialis* colonies during 3 weeks in the field (fig. 3) (Rines et al., 2002). During their study, the authors observed different cell sizes ranging from 48 to 102 µm (are there species that have reached the size threshold necessary for sexual reproduction?). Only towards the end of the study was *P. pseudodelicatissima* occasionally observed living freely in the water column, independently of *C. socialis*. Concentrations of *P. pseudodelicatissima* then reached ~6 $\times 10^4$ cells l^{-1} (Rines et al., 2002). In this study, since the cells have increased in size, it is very likely that there has been a sexual reproduction event.

Other studies have also demonstrated the colonization of *C. socialis* by various protists (Rines, 1988; Sieracki et al., 1998). For example, long, needle-like '*Nitzschia*' living on *C. socialis* were reported by Margalef et al. (1955) and Taylor (1982).

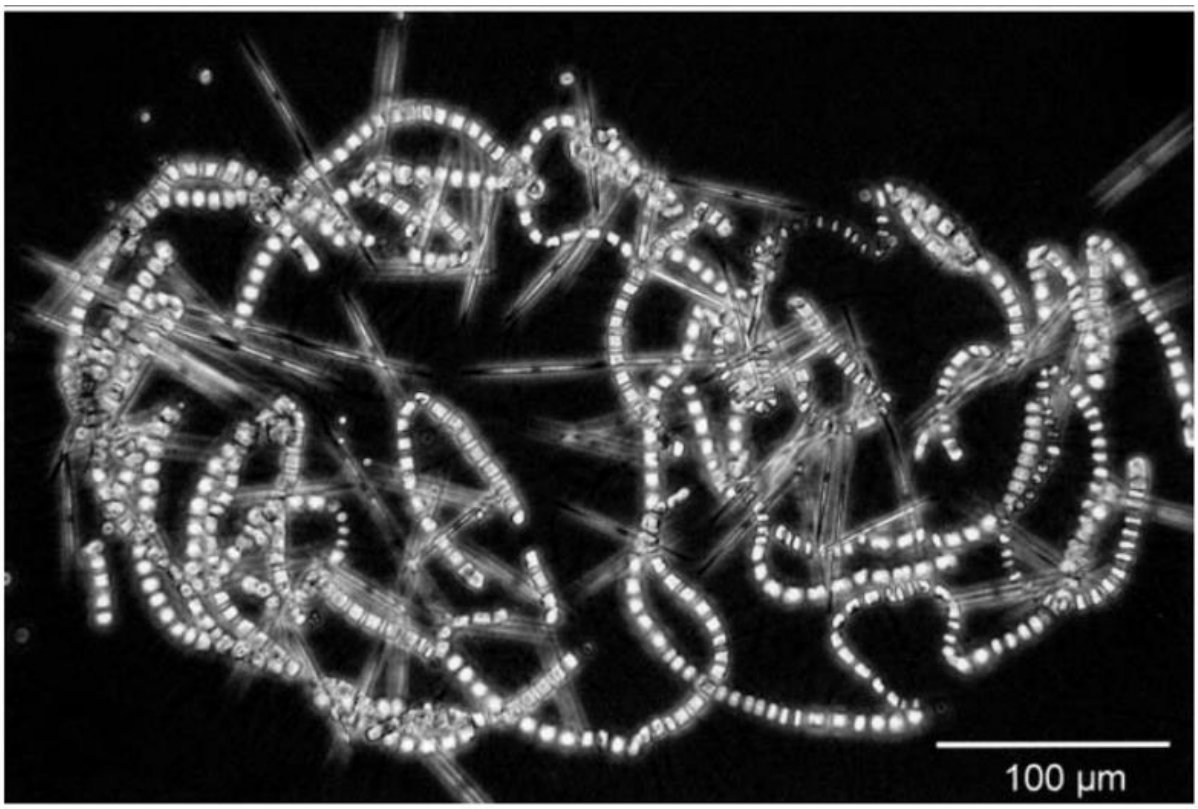

Fig. 3: Light micrographs (phase-contrast) of *P. pseudodelicatissima* cells living within and upon a colony of the diatom *Chaetoceros socialis*, photographed in the field. Picture taken from Rines et al., 2002.

Pseudo-nitzschia spp. are only mobile when they have a substrate on which to slide. Motility is important for sexual reproduction in this genus, as colonies of different mating types must align with each other, or agglutinate (Davidovich and Bates, 1998; Fryxell et al., 1991), and

gametangia need a substrate on which to glide. *C. socialis* provides a substrate in the water column, which can act as a support, an aid, for the completion of the life cycle (Rines et al., 2002). It should also be noted that the hydrodynamics of the environment play a role in encounters between species. I think it is a combination of support from accompanying species and environmental disturbance.

Considering the identification of various diatom species during *P. australis* blooms in the literature and also during the different monitoring made during this thesis, we contemplate whether chain-forming diatoms might play a pivotal role in triggering sexual reproduction in the natural environment. Further research into the role of accompanying species during *P. australis* blooms is encouraged.

Conclusion

Throughout these three years, our approach has been characterised by the use of multidisciplinary approaches, encompassing various scales ranging from the investigation of connectivity between zones through the simulation of tracer transport (Eulerian and Lagrangian), to the study of genes (Metatranscriptomics), including an understanding of the environment. These studies were complementary and contributed to giving us an idea of the spatio-temporal development of *P. australis* blooms in Western Finistère. More generally, we have shed light on mechanisms that were previously poorly understood and rarely observed *in situ*, raising many questions about the biology of blooms. The results clearly the fact that the study of *P. australis* blooms (and perhaps other diatoms) requires both a study of the environment and a study of the life cycle. There is no doubt that we still have a long way to go to achieve a complete understanding of blooms. I strongly believe that this can only be achieved through interdisciplinary approaches and ambitious exploratory research, such as that carried out in this study.

Bibliography

Aguilera, A., Distéfano, A., Jauzein, C., Correa-Aragunde, N., Martinez, D., Martin, M.V., Sueldo, D.J., 2022. Do photosynthetic cells communicate with each other during cell death? From cyanobacteria to vascular plants. J. Exp. Bot. 73, 7219–7242. https://doi.org/10.1093/jxb/erac363

Ajani, P.A., Larsson, M.E., Woodcock, S., Rubio, A., Farrell, H., Brett, S., Murray, S.A., 2020. Fifteen years of Pseudo-nitzschia in an Australian estuary, including the first potentially toxic P. delicatissima bloom in the southern hemisphere. Estuar. Coast. Shelf Sci. 236, 106651. https://doi.org/10.1016/j.ecss.2020.106651

Alexander, H., Jenkins, B.D., Rynearson, T.A., Dyhrman, S.T., 2015. Metatranscriptome analyses indicate resource partitioning between diatoms in the field. Proc. Natl. Acad. Sci. 112, E2182–E2190. https://doi.org/10.1073/pnas.1421993112

Alexander, J., Benford, D., Boobis, A., Ceccatelli, S., Cravedi, J.-P., Di, A., Doerge, D., Dogliotti, E., Edler, L., Farmer, P., Filipi, M., Fürst, P., Guerin, T., Knutsen, H.K., Machala, M., Mutti, A., Schlatter, J., van Leeuwen, R., Verger, P., 2009. SCIENTIFIC OPINION Cadmium in food Scientific Opinion of the Panel on Contaminants in the Food Chain. EFSA J 980, 1:139.

Almandoz, G.O., Ferrario, M.E., Ferreyra, G.A., Schloss, I.R., Esteves, J.L., Paparazzo, F.E., 2007. The genus Pseudo-nitzschia (Bacillariophyceae) in continental shelf waters of Argentina (Southwestern Atlantic Ocean, 38–55°S). Harmful Algae 6, 93–103. https://doi.org/10.1016/j.hal.2006.07.003

Almandoz, G.O., Ferreyra, G.A., Schloss, I.R., Dogliotti, A.I., Rupolo, V., Paparazzo, F.E., Esteves, J.L., Ferrario, M.E., 2008. Distribution and ecology of Pseudo-nitzschia species (Bacillariophyceae) in surface waters of the Weddell Sea (Antarctica). Polar Biol. 31, 429–442. https://doi.org/10.1007/s00300-007-0369-9

Alvain, S., Moulin, C., Dandonneau, Y., Loisel, H., 2008. Seasonal distribution and succession of dominant phytoplankton groups in the global ocean: A satellite view: PHYTOPLANKTON GROUPS - A SATELLITE VIEW. Glob. Biogeochem. Cycles 22, n/a-n/a. https://doi.org/10.1029/2007GB003154

Amato, A., Kooistra, W., Levialdighiron, J., Mann, D., Proschold, T., Montresor, M., 2007. Reproductive Isolation among Sympatric Cryptic Species in Marine Diatoms. Protist 158, 193–207. https://doi.org/10.1016/j.protis.2006.10.001

Amato, A., Montresor, M., 2008. Morphology, phylogeny, and sexual cycle of Pseudo-nitzschia mannii sp. nov. (Bacillariophyceae): a pseudo-cryptic species within the P. pseudodelicatissima complex. Phycologia 47, 487–497. https://doi.org/10.2216/07-92.1

Aminot, A., Kérouel, R., 2007. Dosage automatique des nutriments dans les eaux marines: méthodes en flux continu. Editions Quae.

Aminot, A., Kérouel, R., 2004. Hydrologie des écosystèmes marins: paramètres et analyses. Editions Quae.

Amzil, Z., Fresnel, J., Gal, D.L., Billard, C., 2001. Domoic acid accumulation in French shellfish in relation to toxic species of Pseudo-nitzschia multiseries and P. pseudodelicatissima.

Amzil, Z., Royer, F., Sibat, M., Fiant, L., Gelin, M., Gal, D.L., Françoise, S., 2009. First report on amnesic and diarrhetic toxins detection in French scallops during 2004–05 monitoring surveys. Sixth Int. Conf. Molluscan Shellfish Saf. Blenh. N. Z. 18-23 March.

Anderson, C., Brzezinski, M., Washburn, L., Kudela, R., 2006. Circulation and environmental conditions during a toxigenic *Pseudo-nitzschia australis* bloom in the Santa Barbara Channel, California. Mar. Ecol. Prog. Ser. 327, 119–133. https://doi.org/10.3354/meps327119

Anderson, C.R., Moore, S.K., Tomlinson, M.C., Silke, J., Cusack, C.K., 2015. Living with Harmful Algal Blooms in a Changing World, in: Coastal and Marine Hazards, Risks, and Disasters. Elsevier, pp. 495–561. https://doi.org/10.1016/B978-0-12-396483-0.00017-0

Anderson, D.M., 2009. Approaches to monitoring, control and management of harmful algal blooms (HABs). Coast. Manag. 6.

Anderson, D.M., 1989. Toxic algal blooms and red tides: A global perspective. Red Tides Biol. Environ. Sci. Toxicol. Proc 1st Int Symp Red Tides Elsevier 11–16.

Anderson, D.M., Cembella, A.D., Hallegraeff, G.M., 2012. Progress in Understanding Harmful Algal Blooms: Paradigm Shifts and New Technologies for Research, Monitoring, and Management. Annu. Rev. Mar. Sci. 4, 143–176. https://doi.org/10.1146/annurev-marine-120308-081121

Anglès, S., Jordi, A., Garcés, E., Masó, M., Basterretxea, G., 2008. High-resolution spatio-temporal distribution of a coastal phytoplankton bloom using laser in situ scattering and transmissometry (LISST). Harmful Algae 7, 808–816. https://doi.org/10.1016/j.hal.2008.04.004

Annunziata, R., Mele, B.H., Marotta, P., Volpe, M., Entrambasaguas, L., Mager, S., Stec, K., d'Alcalà, M.R., Sanges, R., Finazzi, G., Iudicone, D., Montresor, M., Ferrante, M.I., 2022. Trade-off between sex and growth in diatoms: Molecular mechanisms and demographic implications. Sci. Adv. 8, eabj9466. https://doi.org/10.1126/sciadv.abj9466

Aoki, K., Onitsuka, G., Shimizu, M., Kuroda, H., Matsuyama, Y., Kimoto, K., Matsuo, H., Kitadai, Y., Sakurada, K., Nishi, H., Tahara, Y., 2012. Factors controlling the spatio-temporal distribution of the 2009 Chattonella antiqua bloom in the Yatsushiro Sea, Japan. Estuar. Coast. Shelf Sci. 114, 148–155. https://doi.org/10.1016/j.ecss.2012.08.028

Armbrust, E.V., 2009. The life of diatoms in the world's oceans. Nature 459, 185–192. https://doi.org/10.1038/nature08057

Arsenieff, L., Le Gall, F., Rigaut-Jalabert, F., Mahé, F., Sarno, D., Gouhier, L., Baudoux, A.-C., Simon, N., 2020. Diversity and dynamics of relevant nanoplanktonic diatoms in the Western English Channel. ISME J. 14, 1966–1981. https://doi.org/10.1038/s41396-020-0659-6

Artigas, M.L., Llebot, C., Ross, O.N., Neszi, N.Z., Rodellas, V., Garcia-Orellana, J., Masqué, P., Piera, J., Estrada, M., Berdalet, E., 2014. Understanding the spatio-temporal variability of phytoplankton biomass distribution in a microtidal Mediterranean estuary. Deep Sea Res. Part II Top. Stud. Oceanogr. 101, 180–192. https://doi.org/10.1016/j.dsr2.2014.01.006

Assmy, P., Henjes, J., Smetacek, V., Montresor, M., 2006. AUXOSPORE FORMATION BY THE SILICA-SINKING, OCEANIC DIATOM FRAGILARIOPSIS KERGUELENSIS (BACILLARIOPHYCEAE). J. Phycol. 42, 1002–1006. https://doi.org/10.1111/j.1529-8817.2006.00260.x

Assmy, P., Hernández-Becerril, D.U., Montresor, M., 2008. MORPHOLOGICAL VARIABILITY AND LIFE CYCLE TRAITS OF THE TYPE SPECIES OF THE DIATOM GENUS *CHAETOCEROS* , *C. DICHAETA*. J. Phycol. 44, 152–163. https://doi.org/10.1111/j.1529-8817.2007.00430.x

Auffret, A., 1983. Dynamique sédimentaire de la marge continentale celtique - Evolution Cénozoïque - Spécificité du Pleistocène supérieur et de l'Holocène. Université de Bordeaux I, Bordeaux.

Ayache, N., Hervé, F., Lundholm, N., Amzil, Z., Caruana, A.M.N., 2020. Acclimation of the Marine Diatom *Pseudo-nitzschia australis* to Different Salinity Conditions: Effects on Growth, Photosynthetic Activity, and Domoic Acid Content. J. Phycol. 56, 97–109. https://doi.org/10.1111/jpy.12929

Ayata, S.-D., Lazure, P., Thiébaut, É., 2010. How does the connectivity between populations mediate range limits of marine invertebrates? A case study of larval dispersal between the Bay of Biscay and the English Channel (North-East Atlantic). Prog. Oceanogr. 87, 18–36. https://doi.org/10.1016/j.pocean.2010.09.022

Azam, F., Fenchel, T., Field, J., Gray, J., Meyer-Reil, L., Thingstad, F., 1983. The Ecological Role of Water-Column Microbes in the Sea. Mar. Ecol. Prog. Ser. 10, 257–263. https://doi.org/10.3354/meps010257

Banse, K., 1994. Grazing and Zooplankton Production as Key Controls of Phytoplankton Production in the Open Ocean. Oceanography 7, 13–20. https://doi.org/10.5670/oceanog.1994.10

Banse, K. (Ed.), 1992. Grazing, Temporal Changes of Phytoplankton Concentrations, and the Microbial Loop in the Open Sea. Prim. Product. Biogeochem. Cycles Sea, Boston, MA: Springer US 409–440. https://doi.org/10.1007/978-1-4899-0762-2

Barbosa, A.B., Chícharo, M.A., 2011. Hydrology and Biota Interactions as Driving Forces for Ecosystem Functioning, in: Treatise on Estuarine and Coastal Science. Elsevier, pp. 7–47. https://doi.org/10.1016/B978-0-12-374711-2.01002-0

Barkai, N., Rose, M.D., Wingreen, N.S., 1998. Protease helps yeast find mating partners. Nature 396, 422–423. https://doi.org/10.1038/24760

Barrera-Alba, J.J., Abreu, P.C., Tenenbaum, D.R., 2019. Seasonal and inter-annual variability in phytoplankton over a 22-year period in a tropical coastal region in the southwestern Atlantic Ocean. Cont. Shelf Res. 176, 51–63. https://doi.org/10.1016/j.csr.2019.02.011

Barzegar, R., Aalami, M.T., Adamowski, J., 2020. Short-term water quality variable prediction using a hybrid CNN–LSTM deep learning model. Stoch. Environ. Res. Risk Assess. 34, 415–433. https://doi.org/10.1007/s00477-020-01776-2

Basterretxea, G., Garcés, E., Jordi, A., Masó, M., Tintoré, J., 2005. Breeze conditions as a favoring mechanism of Alexandrium taylori blooms at a Mediterranean beach. Estuar. Coast. Shelf Sci. 62, 1–12. https://doi.org/10.1016/j.ecss.2004.07.008

Basu, S., Patil, S., Mapleson, D., Russo, M.T., Vitale, L., Fevola, C., Maumus, F., Casotti, R., Mock, T., Caccamo, M., Montresor, M., Sanges, R., Ferrante, M.I., 2017. Finding a partner in the ocean: molecular and evolutionary bases of the response to sexual cues in a planktonic diatom. New Phytol. 215, 140–156. https://doi.org/10.1111/nph.14557

Bates, S.S., 2004. Amnesic shellfish poisoning: domoic acid production by Pseudo-nitzschia diatoms. Aqua Info Aquac. Notes 16.

Bates, S.S., Freitas, A.S.W.D., Milley, J.E., Pocklington, R., Quilliam, M.A., Smith, J.C., Worms, J., 1991. Controls on Domoic Acid Production by the Diatom *Nitzschia pungens* f. *multiseries* in Culture: Nutrients and Irradïance. Can. J. Fish. Aquat. Sci. 48, 1136–1144. https://doi.org/10.1139/f91-137

Bates, S.S., Garrison, D.L., Horner, R.A., 1998. Bloom Dynamics and Physiology of Domoic-Acid- Producing Pseudo-nitzschia Species.

Bates, S.S., Hubbard, K.A., Lundholm, N., Montresor, M., Leaw, C.P., 2018. Pseudo-nitzschia, Nitzschia, and domoic acid: New research since 2011. Harmful Algae 79, 3–43. https://doi.org/10.1016/j.hal.2018.06.001

Bates, S.S., Léger, C., White, J.M., MacNair, N., Ehrman, J.M., Levasseur, M., Couture, J.-Y., Gagnon, R., Bonneau, E., Michaud, S., 2002. Domoic acid production by the diatom Pseudo-nitzschia seriata causes spring closures of shellfish harvesting for the first time in the Gulf of St. Lawrence, eastern Canada, in: Lawrence, Eastern Canada. Xth Int Conf on Harmful Algae, St. Pete Beach, FL (Abstract) p.

Bates, S.S., Lundholm, N., Hubbard, K.A., Montresor, M., Leaw, C.P., 2019. Toxic and Harmful Marine Diatoms, in: Seckbach, J., Gordon, R. (Eds.), Diatoms: Fundamentals and Applications. Wiley, pp. 389–434. https://doi.org/10.1002/9781119370741.ch17

Bates, S.S., Trainer, V.L., 2006. The Ecology of Harmful Diatoms, in: Granéli, E., Turner, J.T. (Eds.), Ecology of Harmful Algae, Ecological Studies. Springer Berlin Heidelberg, pp. 81–93. https://doi.org/10.1007/978-3-540-32210-8_7

Bates, S.S., Worms, J., Smith, J.C., 1993. Effects of Ammonium and Nitrate on Growth and Domoic Acid Production by *Nitzschia pungens* in Batch Culture. Can. J. Fish. Aquat. Sci. 50, 1248–1254. https://doi.org/10.1139/f93-141

Beardall, J., Allen, D., Bragg, J., Finkel, Z.V., Flynn, K.J., Quigg, A., Rees, T.A.V., Richardson, A., Raven, J.A., 2009. Allometry and stoichiometry of unicellular, colonial and multicellular phytoplankton. New Phytol. 181, 295–309. https://doi.org/10.1111/j.1469-8137.2008.02660.x

Behrenfeld, M.J., 2010. Abandoning Sverdrup's Critical Depth Hypothesis on phytoplankton blooms. Ecology 91, 977–989. https://doi.org/10.1890/09-1207.1

Behrenfeld, M.J., Boss, E.S., 2018. Student's tutorial on bloom hypotheses in the context of phytoplankton annual cycles. Glob. Change Biol. 24, 55–77. https://doi.org/10.1111/gcb.13858

Behrenfeld, M.J., Boss, E.S., 2014. Resurrecting the Ecological Underpinnings of Ocean Plankton Blooms. Annu. Rev. Mar. Sci. 6, 167–194. https://doi.org/10.1146/annurev-marine-052913-021325

Behrenfeld, M.J., Doney, S.C., Lima, I., Boss, E.S., Siegel, D.A., 2013. Annual cycles of ecological disturbance and recovery underlying the subarctic Atlantic spring plankton bloom. Glob. Biogeochem. Cycles 27, 526–540. https://doi.org/10.1002/gbc.20050

Belin, C., Soudant, D., 2018. Trente années d'observation des micro-algues et des toxines d'algues sur le littoral. éditions Quae. https://doi.org/10.35690/978-2-7592-2941-3

Belin, C., Soudant, D., Amzil, Z., 2021. Three decades of data on phytoplankton and phycotoxins on the French coast: Lessons from REPHY and REPHYTOX. Harmful Algae 102, 101733. https://doi.org/10.1016/j.hal.2019.101733

Beltrán, A.S., Palafox-Uribe, M., Grajales-Montiel, J., Cruz-Villacorta, A., Ochoa, J.L., 1997. Sea bird mortality at Cabo San Lucas, Mexico: Evidence that toxic diatom blooms are spreading. Toxicon 35, 447–453. https://doi.org/10.1016/S0041-0101(96)00140-7

Berdalet, E., McManus, M.A., Ross, O.N., Burchard, H., Chavez, F.P., Jaffe, J.S., Jenkinson, I.R., Kudela, R., Lips, I., Lips, U., Lucas, A., Rivas, D., Ruiz-de La Torre, M.C., Ryan, J., Sullivan, J.M., Yamazaki, H., 2014. Understanding harmful algae in stratified systems: Review of progress and future directions. Deep Sea Res. Part II Top. Stud. Oceanogr. 101, 4–20. https://doi.org/10.1016/j.dsr2.2013.09.042

Berdjeb, L., Parada, A., Needham, D.M., Fuhrman, J.A., 2018. Short-term dynamics and interactions of marine protist communities during the spring–summer transition. ISME J. 12, 1907–1917. https://doi.org/10.1038/s41396-018-0097-x

Bergkvist, J., Thor, P., Jakobsen, H.H., Wängberg, S.-Å., Selander, E., 2012. Grazer-induced chain length plasticity reduces grazing risk in a marine diatom. Limnol. Oceanogr. 57, 318–324. https://doi.org/10.4319/lo.2012.57.1.0318

Beucher, C., Tréguer, P., Corvaisier, R., Hapette, A., Elskens, M., 2004. Production and dissolution of biosilica, and changing microphytoplankton dominance in the Bay of Brest (France). Mar. Ecol. Prog. Ser. 267, 57–69. https://doi.org/10.3354/meps267057

Bidle, K.D., 2016. Programmed Cell Death in Unicellular Phytoplankton. Curr. Biol. 26, R594–R607. https://doi.org/10.1016/j.cub.2016.05.056

Bilcke, G., Van den Berge, K., De Decker, S., Bonneure, E., Poulsen, N., Bulankova, P., Osuna-Cruz, C.M., Dickenson, J., Sabbe, K., Pohnert, G., Vandepoele, K., Mangelinckx, S., Clement, L., De Veylder, L., Vyverman, W., 2021. Mating type specific transcriptomic response to sex inducing pheromone in the pennate diatom Seminavis robusta. ISME J. 15, 562–576. https://doi.org/10.1038/s41396-020-00797-7

Biller, S.J., Lundeen, R.A., Hmelo, L.R., Becker, K.W., Arellano, A.A., Dooley, K., Heal, K.R., Carlson, L.T., Van Mooy, B.A.S., Ingalls, A.E., Chisholm, S.W., 2022. Prochlorococcus extracellular vesicles: molecular composition and adsorption to diverse microbes. Environ. Microbiol. 24, 420–435. https://doi.org/10.1111/1462-2920.15834

Bjærke, O., Jonsson, P.R., Alam, A., Selander, E., 2015. Is chain length in phytoplankton regulated to evade predation? J. Plankton Res. fbv076. https://doi.org/10.1093/plankt/fbv076

Blain, S., Guillou, J., Tréguer, P., Woerther, P., Delauney, L., Follenfant, E., Gontier, O., Hamon, M., Leildé, B., Masson, A., Tartu, C., Vuillemin, R., 2004. High frequency monitoring of the coastal marine environment using the MAREL buoy. J Env. Monit 6, 569–575. https://doi.org/10.1039/B314073C

Blanco, J., Acosta, C.P., Bermúdez De La Puente, M., Salgado, C., 2002. Depuration and anatomical distribution of the amnesic shellfish poisoning (ASP) toxin domoic acid in the king scallop Pecten maximus. Aquat. Toxicol. 60, 111–121. https://doi.org/10.1016/S0166-445X(01)00274-0

Blanco, J., Acosta, C.P., Mariño, C., Muñiz, S., Martín, H., Moroño, Á., Correa, J., Arévalo, F., Salgado, C., 2006. Depuration of domoic acid from different body compartments of the king scallop *Pecten maximus* grown in raft culture and natural bed. Aquat. Living Resour. 19, 257–265. https://doi.org/10.1051/alr:2006026

Blondeau-Patissier, D., Gower, J.F.R., Dekker, A.G., Phinn, S.R., Brando, V.E., 2014. A review of ocean color remote sensing methods and statistical techniques for the detection, mapping and analysis of phytoplankton blooms in coastal and open oceans. Prog. Oceanogr. 123, 123–144. https://doi.org/10.1016/j.pocean.2013.12.008

Bolger, A.M., Lohse, M., Usadel, B., 2014. Trimmomatic: a flexible trimmer for Illumina sequence data. Bioinformatics 30, 2114–2120. https://doi.org/10.1093/bioinformatics/btu170

Bonansea, M., Rodriguez, M.C., Pinotti, L., Ferrero, S., 2015. Using multi-temporal Landsat imagery and linear mixed models for assessing water quality parameters in Río Tercero reservoir (Argentina). Remote Sens. Environ. 158, 28–41. https://doi.org/10.1016/j.rse.2014.10.032

Bowers, H.A., Ryan, J.P., Hayashi, K., Woods, A.L., Marin, R., Smith, G.J., Hubbard, K.A., Doucette, G.J., Mikulski, C.M., Gellene, A.G., Zhang, Y., Kudela, R.M., Caron, D.A., Birch, J.M., Scholin, C.A., 2018. Diversity and toxicity of Pseudo-nitzschia species in Monterey Bay: Perspectives from targeted and adaptive sampling. Harmful Algae 78, 129–141. https://doi.org/10.1016/j.hal.2018.08.006

Bowling, L., Egan, S., Holliday, J., Honeyman, G., 2016. Did spatial and temporal variations in water quality influence cyanobacterial abundance, community composition and cell size in the Murray River, Australia during a drought-affected low-flow summer? Hydrobiologia 765, 359–377. https://doi.org/10.1007/s10750-015-2430-y

Boyd, P.W., Rynearson, T.A., Armstrong, E.A., Fu, F., Hayashi, K., Hu, Z., Hutchins, D.A., Kudela, R.M., Litchman, E., Mulholland, M.R., Passow, U., Strzepek, R.F., Whittaker, K.A., Yu, E., Thomas, M.K., 2013. Marine Phytoplankton Temperature versus Growth Responses from Polar to Tropical Waters – Outcome of a Scientific Community-Wide Study. PLoS ONE 8, e63091. https://doi.org/10.1371/journal.pone.0063091

Bracher, A., Vountas, M., Dinter, T., Burrows, J.P., Rottgers, R., Peeken, I., 2009. Quantitative observation of cyanobacteria and diatoms from space using PhytoDOAS on SCIAMACHY data.

Brunson, J.K., McKinnie, S.M.K., Chekan, J.R., McCrow, J.P., Miles, Z.D., Bertrand, E.M., Bielinski, V.A., Luhavaya, H., Oborník, M., Smith, G.J., Hutchins, D.A., Allen, A.E., Moore, B.S., 2018. Biosynthesis of the neurotoxin domoic acid in a bloom-forming diatom. Science 361, 1356–1358. https://doi.org/10.1126/science.aau0382

Buchan, A., LeCleir, G.R., Gulvik, C.A., González, J.M., 2014. Master recyclers: features and functions of bacteria associated with phytoplankton blooms. Nat. Rev. Microbiol. 12, 686–698. https://doi.org/10.1038/nrmicro3326

Buitenhuis, E.T., Vogt, M., Moriarty, R., Bednaršek, N., Doney, S.C., Leblanc, K., Le Quéré, C., Luo, Y.-W., O'Brien, C., O'Brien, T., Peloquin, J., Schiebel, R., Swan, C., 2013. MAREDAT: towards a world atlas of MARine Ecosystem DATa. Earth Syst. Sci. Data 5, 227–239. https://doi.org/10.5194/essd-5-227-2013

Burki, F., Roger, A.J., Brown, M.W., Simpson, A.G.B., 2020. The New Tree of Eukaryotes. Trends Ecol. Evol. 35, 43–55. https://doi.org/10.1016/j.tree.2019.08.008

Cadier, M., Gorgues, T., Sourisseau, M., Edwards, C.A., Aumont, O., Marié, L., Memery, L., 2017. Assessing spatial and temporal variability of phytoplankton communities' composition in the Iroise Sea ecosystem (Brittany, France): A 3D modeling approach. Part 1: Biophysical control over plankton functional types succession and distribution. J. Mar. Syst. 165, 47–68. https://doi.org/10.1016/j.jmarsys.2016.09.009

Cao, M., Yuan, X.-L., Bi, G., 2016. Complete sequence and analysis of plastid genomes of *Pseudo-nitzschia multiseries* (Bacillariophyta). Mitochondrial DNA Part A 27, 2897–2898. https://doi.org/10.3109/19401736.2015.1060428

Caracciolo, M., Rigaut-Jalabert, F., Romac, S., Mahé, F., Forsans, S., Gac, J., Arsenieff, L., Manno, M., Chaffron, S., Cariou, T., Hoebeke, M., Bozec, Y., Goberville, E., Le Gall, F., Guilloux, L., Baudoux, A., de Vargas, C., Not, F., Thiébaut, E., Henry, N., Simon, N., 2022. Seasonal dynamics of marine protist communities in tidally mixed coastal waters. Mol. Ecol. 31, 3761–3783. https://doi.org/10.1111/mec.16539

Caracciolo, M., Rigaut-Jalabert, F., Romac, S., Mahé, F., Forsans, S., Gac, J.-P., Arsenieff, L., Manno, M., Chaffron, S., Cariou, T., Hoebeke, M., Bozec, Y., Goberville, E., Gall, F.L., Guilloux, L., Baudoux, A.-C., de Vargas, C., Not, F., Thiébaut, E., Henry, N., Simon, N., 2021. Seasonal temporal dynamics of marine protists communities in tidally mixed coastal waters (preprint). Ecology. https://doi.org/10.1101/2021.09.15.460302

Carnicer, O., Guallar, C., Andree, K.B., Diogène, J., Fernández-Tejedor, M., 2015. Ostreopsis cf. ovata dynamics in the NW Mediterranean Sea in relation to biotic and abiotic factors. Environ. Res. 143, 89–99. https://doi.org/10.1016/j.envres.2015.08.023

Caroppo, C., Congestri, R., Bracchini, L., Albertano, P., 2005. On the presence of Pseudo-nitzschia calliantha Lundholm, Moestrup et Hasle and Pseudo-nitzschia delicatissima (Cleve) Heiden in the Southern Adriatic Sea (Mediterranean Sea, Italy). J. Plankton Res. 27, 763–774. https://doi.org/10.1093/plankt/fbi050

Casteleyn, G., Chepurnov, V.A., Leliaert, F., Mann, D.G., Bates, S.S., Lundholm, N., Rhodes, L., Sabbe, K., Vyverman, W., 2008. Pseudo-nitzschia pungens (Bacillariophyceae): A cosmopolitan diatom species? Harmful Algae 7, 241–257. https://doi.org/10.1016/j.hal.2007.08.004

Cerino, F., Orsini, L., Sarno, D., Dell'Aversano, C., Tartaglione, L., Zingone, A., 2005. The alternation of different morphotypes in the seasonal cycle of the toxic diatom Pseudo-nitzschia galaxiae. Harmful Algae 4, 33–48. https://doi.org/10.1016/j.hal.2003.10.005

Chapra, S.C., 2008. Surface Water-Quality Modeling. Waveland Press.

Chen, B., Xu, Z., Zhou, Q., Chen, C., Gao, Y., Yang, S., Ji, W., 2010. Long-term changes of phytoplankton community in Xiagu waters of Xiamen, China. Acta Oceanol. Sin. 29, 104–114. https://doi.org/10.1007/s13131-010-0081-4

Chen, C., Zhu, J., Beardsley, R.C., Franks, P.J.S., 2003. Physical-biological sources for dense algal blooms near the Changjiang River: DENSE ALGAL BLOOMS OFF THE CHANGJIANG. Geophys. Res. Lett. 30, n/a-n/a. https://doi.org/10.1029/2002GL016391

Chepurnov, V.A., Mann, D.G., Sabbe, K., Vyverman, W., 2004. Experimental Studies on Sexual Reproduction in Diatoms, in: International Review of Cytology. Elsevier, pp. 91–154. https://doi.org/10.1016/S0074-7696(04)37003-8

Chepurnov, V.A., Mann, D.G., Von Dassow, P., Vanormelingen, P., Gillard, J., Inzé, D., Sabbe, K., Vyverman, W., 2008. In search of new tractable diatoms for experimental biology. BioEssays 30, 692–702. https://doi.org/10.1002/bies.20773

Chisholm, S.W., 1992. Phytoplankton Size, in: Falkowski, P.G., Woodhead, A.D., Vivirito, K. (Eds.), Primary Productivity and Biogeochemical Cycles in the Sea, Environmental Science Research. Springer US, Boston, MA, pp. 213–237. https://doi.org/10.1007/978-1-4899-0762-2_12

Chiswell, S.M., Calil, P.H.R., Boyd, P.W., 2015. Spring blooms and annual cycles of phytoplankton: a unified perspective. J. Plankton Res. 37, 500–508. https://doi.org/10.1093/plankt/fbv021

Churro, C.I., Carreira, C.C., Rodrigues, F.J., Craveiro, S.C., Calado, A.J., Casteleyn, G., Lundholm, N., 2009. DIVERSITY AND ABUNDANCE OF POTENTIALLY TOXIC *PSEUDO-NITZSCHIA* PERAGALLO IN AVEIRO COASTAL LAGOON, PORTUGAL AND DESCRIPTION OF A NEW VARIETY, *P. PUNGENS* VAR. *AVEIRENSIS* VAR. NOV. Diatom Res. 24, 35–62. https://doi.org/10.1080/0269249X.2009.9705782

Clark, S., Hubbard, K.A., Anderson, D.M., McGillicuddy, D.J., Ralston, D.K., Townsend, D.W., 2019. Pseudo-nitzschia bloom dynamics in the Gulf of Maine: 2012–2016. Harmful Algae 88, 101656. https://doi.org/10.1016/j.hal.2019.101656

Cloern, J., Dufford, R., 2005. Phytoplankton community ecology: principles applied in San Francisco Bay. Mar. Ecol. Prog. Ser. 285, 11–28. https://doi.org/10.3354/meps285011

Cloern, J.E., Jassby, A.D., 2010. Patterns and Scales of Phytoplankton Variability in Estuarine–Coastal Ecosystems. Estuaries Coasts 33, 230–241. https://doi.org/10.1007/s12237-009-9195-3

Cloern, J.E., Jassby, A.D., 2008. Complex seasonal patterns of primary producers at the land-sea interface. Ecol. Lett. 11, 1294–1303. https://doi.org/10.1111/j.1461-0248.2008.01244.x

Core Team, R., 2014. R: A language and environment for statistical computing. Vienna, Austria. R Found. Stat. Comput.

Couvelard, X., 2007. Structure et dynamique des jets barotropes créés par les îles du Pacifique Sud-Ouest. Université de Toulouse Paul Sabatier, Toulouse.

Cózar, A., Morillo-García, S., Ortega, M.J., Li, Q.P., Bartual, A., 2018. Macroecological patterns of the phytoplankton production of polyunsaturated aldehydes. Sci. Rep. 8, 12282. https://doi.org/10.1038/s41598-018-29787-8

Cristescu, M.E., 2019. Can Environmental RNA Revolutionize Biodiversity Science? Trends Ecol. Evol. 34, 694–697. https://doi.org/10.1016/j.tree.2019.05.003

Croteau, D., Lacour, T., Schiffrine, N., Morin, P., Forget, M., Bruyant, F., Ferland, J., Lafond, A., Campbell, D.A., Tremblay, J., Babin, M., Lavaud, J., 2022. Shifts in growth light

optima among diatom species support their succession during the spring bloom in the Arctic. J. Ecol. 110, 1356–1375. https://doi.org/10.1111/1365-2745.13874

Curchitser, E., Batchelder, H., Haidvogel, D., Fiechter, J., Runge, J., 2013. Advances in Physical, Biological, and Coupled Ocean Models During the US GLOBEC Program. Oceanography 26, 52–67. https://doi.org/10.5670/oceanog.2013.75

Cusack, C., Mouriño, H., Moita, M.T., Silke, J., 2015. Modelling Pseudo-nitzschia events off southwest Ireland. J. Sea Res. 12.

Cushing, D.H., 1990. Plankton Production and Year-class Strength in Fish Populations: an Update of the Match/Mismatch Hypothesis, in: Advances in Marine Biology. Elsevier, pp. 249–293. https://doi.org/10.1016/S0065-2881(08)60202-3

Cushing, D.H., 1969. The Regularity of the Spawning Season of Some Fishes. ICES J. Mar. Sci. 33, 81–92. https://doi.org/10.1093/icesjms/33.1.81

Dale, B., Yentsch, C.M., 1978. Red Tide and Paralytic Shellfish Poisoning. Oceanus.

D'Alelio, D., Amato, A., Luedeking, A., Montresor, M., 2009. Sexual and vegetative phases in the planktonic diatom Pseudo-nitzschia multistriata. Harmful Algae 8, 225–232. https://doi.org/10.1016/j.hal.2008.05.004

D'Alelio, D., d'Alcalà, M.R., Dubroca, L., Diana Sarn, Zingone, A., Montresor, M., 2010. The time for sex: A biennial life cycle in a marine planktonic diatom. Limnol. Oceanogr. 55, 106–114. https://doi.org/10.4319/lo.2010.55.1.0106

D'Alelio, D., Ruggiero, M.V., 2015. Interspecific plastidial recombination in the diatom genus *Pseudo-nitzschia*. J. Phycol. 51, 1024–1028. https://doi.org/10.1111/jpy.12350

David, V., Ryckaert, M., Karpytchev, M., Bacher, C., Arnaudeau, V., Vidal, N., Maurer, D., Niquil, N., 2012. Spatial and long-term changes in the functional and structural phytoplankton communities along the French Atlantic coast. Estuar. Coast. Shelf Sci. 108, 37–51. https://doi.org/10.1016/j.ecss.2012.02.017

Davidovich, N.A., Bates, S.S., 1998. SEXUAL REPRODUCTION IN THE PENNATE DIATOMS PSEUDO-NITZSCHIA MULTISERIES AND P. PSEUDODELICATISSIMA (BACILLARIOPHYCEAE). J. Phycol. 34, 126–137. https://doi.org/10.1046/j.1529-8817.1998.340126.x

Davidson, K., Anderson, D.M., Mateus, M., Reguera, B., Silke, J., Sourisseau, M., Maguire, J., 2016. Forecasting the risk of harmful algal blooms. Harmful Algae 53, 1–7. https://doi.org/10.1016/j.hal.2015.11.005

De Tommasi, E., Gielis, J., Rogato, A., 2017. Diatom Frustule Morphogenesis and Function: a Multidisciplinary Survey. Mar. Genomics 35, 1–18. https://doi.org/10.1016/j.margen.2017.07.001

Debreu, L., Marchesiello, P., Penven, P., Cambon, G., 2012. Two-way nesting in split-explicit ocean models: Algorithms, implementation and validation. Ocean Model. 49–50, 1–21. https://doi.org/10.1016/j.ocemod.2012.03.003

Del Amo, Y., Quéguiner, B., Tréguer, P., Breton, H., Lampert, L., 1997. Impacts of high-nitrate freshwater inputs on macrotidal ecosystems. II. Specific role of the silicic acid pump in the year-round dominance of diatoms in the Bay of Brest (France). Mar. Ecol. Prog. Ser. 161, 225–237. https://doi.org/10.3354/meps161225

Delaney, J.A., Ulrich, R.M., Paul, J.H., 2011. Detection of the toxic marine diatom Pseudo-nitzschia multiseries using the RuBisCO small subunit (rbcS) gene in two real-time RNA amplification formats. Harmful Algae 11, 54–64. https://doi.org/10.1016/j.hal.2011.07.005

Delegrange, A., Lefebvre, A., Gohin, F., Courcot, L., Vincent, D., 2018. Pseudo-nitzschia sp. diversity and seasonality in the southern North Sea, domoic acid levels and associated phytoplankton communities. Estuar. Coast. Shelf Sci. 214, 194–206. https://doi.org/10.1016/j.ecss.2018.09.030

Delmas, R., Treguer, P., 1983. Evolution saisonnière des nutriments dans un écosystème eutrophe d'Europe occidentale (la rade de Brest). Interactions marines et terrestres. Oceanol. Acta 6(4), 345–356.

Devred, E., Sathyendranath, S., Stuart, V., Platt, T., 2011. A three component classification of phytoplankton absorption spectra: Application to ocean-color data. Remote Sens. Environ. 115, 2255–2266. https://doi.org/10.1016/j.rse.2011.04.025

Di Dato, V., Musacchia, F., Petrosino, G., Patil, S., Montresor, M., Sanges, R., Ferrante, M.I., 2015. Transcriptome sequencing of three Pseudo-nitzschia species reveals comparable gene sets and the presence of Nitric Oxide Synthase genes in diatoms. Sci. Rep. 5, 12329. https://doi.org/10.1038/srep12329

Dolan, J.R., 2019. Unmasking "The Eldest Son of The Father of Protozoology": Charles King. Protist 170, 374–384. https://doi.org/10.1016/j.protis.2019.07.002

Dong, Y., Zuo, L., Ma, W., Chen, Z., Cui, L., Lu, S., 2021. Phytoplankton community organization and succession by sea warming: A case study in thermal discharge area of the northern coastal seawater of China. Mar. Pollut. Bull. 169, 112538. https://doi.org/10.1016/j.marpolbul.2021.112538

Dore, J.E., Letelier, R.M., Church, M.J., Lukas, R., Karl, D.M., 2008. Summer phytoplankton blooms in the oligotrophic North Pacific Subtropical Gyre: Historical perspective and recent observations. Prog. Oceanogr. 76, 2–38. https://doi.org/10.1016/j.pocean.2007.10.002

Dortch, Q., Robichaux, R., Pool, S., Milsted, D., Mire, G., Rabalais, N., Soniat, T., Fryxell, G., Turner, R., Parsons, M., 1997. Abundance and vertical flux of Pseudo-nitzschia in the northern Gulf of Mexico. Mar. Ecol. Prog. Ser. 146, 249–264. https://doi.org/10.3354/meps146249

Douglas, D.J., Kenchington, E.R., Bird, C.J., Pocklington, R., Bradford, B., Silvert, W., 1997. Accumulation of domoic acid by the sea scallop (*Placopecten magellanicus*) fed cultured cells of toxic *Pseudo-nitzschia multiseries*. Can. J. Fish. Aquat. Sci. 54, 907–913. https://doi.org/10.1139/f96-333

Downes-Tettmar, N., Rowland, S., Widdicombe, C., Woodward, M., Llewellyn, C., 2013. Seasonal variation in *Pseudo-nitzschia spp.* and domoic acid in the Western English Channel. Cont. Shelf Res. 53, 40–49. https://doi.org/10.1016/j.csr.2012.10.011

Drouzy, M., Douillet, P., Fernandez, J.-M., Pinazo, C., 2019. Hydrodynamic time parameters response to meteorological and physical forcings: toward a stagnation risk assessment device in coastal areas. Ocean Dyn. 69, 967–987. https://doi.org/10.1007/s10236-019-01283-1

Du, X., Peterson, W., Fisher, J., Hunter, M., Peterson, J., 2016. Initiation and development of a toxic and persistent Pseudo-nitzschia bloom off the Oregon coast in spring/summer 2015. PLoS One 11, e0163977.

Dubois, S.F., Colombo, F., 2014. How picky can you be? Temporal variations in trophic niches of co-occurring suspension-feeding species. Food Webs 1, 1–9. https://doi.org/10.1016/j.fooweb.2014.07.001

Dutkiewicz, S., Cermeno, P., Jahn, O., Follows, M.J., Hickman, A.E., Taniguchi, D.A.A., Ward, B.A., 2020. Dimensions of marine phytoplankton diversity. Biogeosciences 17, 609–634. https://doi.org/10.5194/bg-17-609-2020

Edwards, K.F., Thomas, M.K., Klausmeier, C.A., Litchman, E., 2016. Phytoplankton growth and the interaction of light and temperature: A synthesis at the species and community level: Light-Temperature Interactions. Limnol. Oceanogr. 61, 1232–1244. https://doi.org/10.1002/lno.10282

Edwards, M., Beaugrand, G., Hays, G.C., Koslow, J.A., Richardson, A.J., 2010. Multi-decadal oceanic ecological datasets and their application in marine policy and management. Trends Ecol. Evol. 25, 602–610. https://doi.org/10.1016/j.tree.2010.07.007

Erickson, J.S., Hashemi, N., Sullivan, J.M., Weidemann, A.D., Ligler, F.S., 2012. In Situ Phytoplankton Analysis: There's Plenty of Room at the Bottom. Anal. Chem. 84, 839–850. https://doi.org/10.1021/ac201623k

Eriksen, R., Trull, T., Davies, D., Jansen, P., Davidson, A., Westwood, K., van den Enden, R., 2018. Seasonal succession of phytoplankton community structure from autonomous sampling at the Australian Southern Ocean Time Series (SOTS) observatory. Mar. Ecol. Prog. Ser. 589, 13–31. https://doi.org/10.3354/meps12420

Escalera, L., Reguera, B., Moita, T., Pazos, Y., Cerejo, M., Cabanas, J.M., Ruiz-Villarreal, M., 2010. Bloom dynamics of Dinophysis acuta in an upwelling system: In situ growth versus transport. Harmful Algae 9, 312–322. https://doi.org/10.1016/j.hal.2009.12.002

Falkowski, P.G., 1994. The role of phytoplankton photosynthesis in global biogeochemical cycles. Photosynth. Res. 39, 235–258. https://doi.org/10.1007/BF00014586

Falkowski, P.G., Barber, R.T., Smetacek, V., 1998. Biogeochemical Controls and Feedbacks on Ocean Primary Production. Science 281, 200–206. https://doi.org/10.1126/science.281.5374.200

Falkowski, P.G., Katz, M.E., Knoll, A.H., Quigg, A., Raven, J.A., Schofield, O., Taylor, F.J.R., 2004. The Evolution of Modern Eukaryotic Phytoplankton. Science 305, 354–360. https://doi.org/10.1126/science.1095964

Falkowski, P.G., Laws, E.A., Barber, R.T., Murray, J.W., 2003. Phytoplankton and Their Role in Primary, New, and Export Production, in: Fasham, M.J.R. (Ed.), Ocean Biogeochemistry. Springer Berlin Heidelberg, Berlin, Heidelberg, pp. 99–121. https://doi.org/10.1007/978-3-642-55844-3_5

Fehling, J., Davidson, K., Bates, S.S., 2005. Growth dynamics of non-toxic Pseudo-nitzschia delicatissima and toxic P. seriata (Bacillariophyceae) under simulated spring and summer photoperiods. Harmful Algae 4, 763–769. https://doi.org/10.1016/j.hal.2004.11.002

Fehling, J., Davidson, K., Bolch, C., Tett, P., 2006. Seasonality of Pseudo-nitzschia spp. (Bacillariophyceae) in western Scottish waters. Mar. Ecol. Prog. Ser. 323, 91–105. https://doi.org/10.3354/meps323091

Fenchel, T., 2008. The microbial loop – 25 years later. J. Exp. Mar. Biol. Ecol. 366, 99–103. https://doi.org/10.1016/j.jembe.2008.07.013

Fenchel, T., 1988. Marine Plankton Food Chains. Annu. Rev. Ecol. Syst. 19–38.

Fernandes-Salvador, J.A., Davidson, K., Sourisseau, M., Revilla, M., Schmidt, W., Clarke, D., Miller, P.I., Arce, P., Fernández, R., Maman, L., Silva, A., Whyte, C., Mateo, M., Neira, P., Mateus, M., Ruiz-Villarreal, M., Ferrer, L., Silke, J., 2021. Current Status of Forecasting Toxic Harmful Algae for the North-East Atlantic Shellfish Aquaculture Industry. Front. Mar. Sci. 8, 666583. https://doi.org/10.3389/fmars.2021.666583

Ferrante, Entrambasaguas, Johansson, Töpel, Kremp, Montresor, Godhe, 2019. Exploring Molecular Signs of Sex in the Marine Diatom *Skeletonema marinoi*. Genes 10, 494. https://doi.org/10.3390/genes10070494

Ferrante, M.I., Broccoli, A., Montresor, M., 2023. The pennate diatom *Pseudo-nitzschia multistriata* as a model for diatom life cycles, from the laboratory to the sea. J. Phycol. 59, 637–643. https://doi.org/10.1111/jpy.13342

Field, C.B., Behrenfeld, M.J., Randerson, J.T., Falkowski, P., 1998. Primary Production of the Biosphere: Integrating Terrestrial and Oceanic Components. Science 281, 237–240. https://doi.org/10.1126/science.281.5374.237

Fifas, S., 2004. La coquille Saint Jacques en Bretagne. Dir. Ressour. Vivantes Ifremer 15.

Fiorini, F., Borgonuovo, C., Ferrante, M.I., Brönstrup, M., 2020. A Metabolomics Exploration of the Sexual Phase in the Marine Diatom *Pseudo-nitzschia multistriata*. Mar. Drugs 18, 313. https://doi.org/10.3390/md18060313

Franks, P.J.S., Anderson, D.M., 1992. Alongshore transport of a toxic phytoplankton bloom in a buoyancy current: *Alexandrium tamarense* in the Gulf of Maine. Mar. Biol. 112, 153–164. https://doi.org/10.1007/BF00349739

Fryxell, G.A., Garza, S.A., Roelke, D.L., 1991. AUXOSPORE FORMATION IN AN ANTARCTIC CLONE OF *NITZSCHIA SUBCURVATA* HASLE. Diatom Res. 6, 235–245. https://doi.org/10.1080/0269249X.1991.9705169

Fuhrman, J.A., Cram, J.A., Needham, D.M., 2015. Marine microbial community dynamics and their ecological interpretation. Nat. Rev. Microbiol. 13, 133–146. https://doi.org/10.1038/nrmicro3417

Gallina, A.A., Palumbo, A., Casotti, R., 2016. Oxidative pathways in response to polyunsaturated aldehydes in the marine diatom *Skeletonema marinoi* (Bacillariophyceae). J. Phycol. 52, 590–598. https://doi.org/10.1111/jpy.12421

García-Corona, J.L., Hégaret, H., Deléglise, M., Marzari, A., Rodríguez-Jaramillo, C., Foulon, V., Fabioux, C., 2022. First subcellular localization of the amnesic shellfish toxin, domoic acid, in bivalve tissues: Deciphering the physiological mechanisms involved in its long-retention in the king scallop Pecten maximus. Harmful Algae 116, 102251. https://doi.org/10.1016/j.hal.2022.102251

García-Mendoza, E., Rivas, D., Olivos-Ortiz, A., Almazán-Becerril, A., Castañeda-Vega, C., Peña-Manjarrez, J.L., 2009. A toxic Pseudo-nitzschia bloom in Todos Santos Bay, northwestern Baja California, Mexico. Harmful Algae 8, 493–503. https://doi.org/10.1016/j.hal.2008.10.002

Garrison, D.L., Conrad, S.M., Eilers, P.P., Waldron, E.M., 1992. CONFIRMATION OF DOMOIC ACID PRODUCTION BY PSEUDONITZSCHIA AUSTRALIS (BACILLARIOPHYCEAE) CULTURES1. J. Phycol. 28, 604–607. https://doi.org/10.1111/j.0022-3646.1992.00604.x

Ge, Y., Wang, D.-Z., Chiu, J.-F., Cristobal, S., Sheehan, D., Silvestre, F., Peng, X., Li, H., Gong, Z., Lam, S.H., Wentao, H., Iwahashi, H., Liu, J., Mei, N., Shi, L., Bruno, M., Foth, H., Teichman, K., 2013. Environmental OMICS: Current Status and Future Directions. J. Integr. OMICS 3, 75–87. https://doi.org/10.5584/jiomics.v3i2.141

Ghezzo, M., De Pascalis, F., Umgiesser, G., Zemlys, P., Sigovini, M., Marcos, C., Pérez-Ruzafa, A., 2015. Connectivity in Three European Coastal Lagoons. Estuaries Coasts 38, 1764–1781. https://doi.org/10.1007/s12237-014-9908-0

Gibble, C.M., Kudela, R.M., Knowles, S., Bodenstein, B., Lefebvre, K.A., 2021. Domoic acid and saxitoxin in seabirds in the United States between 2007 and 2018. Harmful Algae 103, 101981. https://doi.org/10.1016/j.hal.2021.101981

Giddings, S.N., MacCready, P., Hickey, B.M., Banas, N.S., Davis, K.A., Siedlecki, S.A., Trainer, V.L., Kudela, R.M., Pelland, N.A., Connolly, T.P., 2014. Hindcasts of potential harmful algal bloom transport pathways on the Pacific Northwest coast. J. Geophys. Res. Oceans 119, 2439–2461. https://doi.org/10.1002/2013JC009622

Gifford, S.M., Sharma, S., Booth, M., Moran, M.A., 2013. Expression patterns reveal niche diversification in a marine microbial assemblage. ISME J. 7, 281–298. https://doi.org/10.1038/ismej.2012.96

Gillard, J., Frenkel, J., Devos, V., Sabbe, K., Paul, C., Rempt, M., Inzé, D., Pohnert, G., Vuylsteke, M., Vyverman, W., 2013. Metabolomics Enables the Structure Elucidation of a Diatom Sex Pheromone. Angew. Chem. Int. Ed. 52, 854–857. https://doi.org/10.1002/anie.201208175

Gillibrand, P.A., Siemering, B., Miller, P.I., Davidson, K., 2016. Individual-based modelling of the development and transport of a *Karenia mikimotoi* bloom on the North-west European continental shelf. Harmful Algae 53, 118–134. https://doi.org/10.1016/j.hal.2015.11.011

Gómez, F., 2008. Phytoplankton invasions: Comments on the validity of categorizing the non-indigenous dinoflagellates and diatoms in European Seas. Mar. Pollut. Bull. 56, 620–628. https://doi.org/10.1016/j.marpolbul.2007.12.014

Gómez, F., Souissi, S., 2007. Unusual diatoms linked to climatic events in the northeastern English Channel. J. Sea Res. 58, 283–290. https://doi.org/10.1016/j.seares.2007.08.002

Gong, W., Paerl, H., Marchetti, A., 2018. Eukaryotic phytoplankton community spatiotemporal dynamics as identified through gene expression within a eutrophic estuary. Environ. Microbiol. 20, 1095–1111. https://doi.org/10.1111/1462-2920.14049

Gons, H.J., 2002. A chlorophyll-retrieval algorithm for satellite imagery (Medium Resolution Imaging Spectrometer) of inland and coastal waters. J. Plankton Res. 24, 947–951. https://doi.org/10.1093/plankt/24.9.947

González-Pech, R.A., Stephens, T.G., Chan, C.X., 2019. Commonly misunderstood parameters of NCBI BLAST and important considerations for users. Bioinformatics 35, 2697–2698. https://doi.org/10.1093/bioinformatics/bty1018

Gowen, R., 1999. Are copepods important grazers of the spring phytoplankton bloom in the western Irish Sea? J. Plankton Res. 21, 465–483. https://doi.org/10.1093/plankt/21.3.465

Grall, J.-R., 1972. Developpement printanier de la Diatomde Rhizosolenia delicatula pros de Roscoff. Mar. Biol. 16, 41–48.

Gran, H.H., Braarud, T., 1935. A quantitative study of the phytoplankton in the Bay of Fundy and the Gulf of Maine (including observations on hydrography, chemistry and turbidity). J. Biol. Board Can. 1(5), 279–467.

Grattan, L.M., Holobaugh, S., Morris, J.G., 2016. Harmful algal blooms and public health. Harmful Algae 57, 2–8. https://doi.org/10.1016/j.hal.2016.05.003

Gregg, W.W., Ginoux, P., Schopf, P.S., Casey, N.W., 2003. Phytoplankton and iron: validation of a global three-dimensional ocean biogeochemical model. Deep Sea Res. Part II Top. Stud. Oceanogr. 50, 3143–3169. https://doi.org/10.1016/j.dsr2.2003.07.013

Guallar, C., Bacher, C., Chapelle, A., 2017. Global and local factors driving the phenology of Alexandrium minutum (Halim) blooms and its toxicity. Harmful Algae 67, 44–60. https://doi.org/10.1016/j.hal.2017.05.005

Guillam, M., Bessin, C., Blanchet-Aurigny, A., Cugier, P., Nicolle, A., Thiébaut, É., Comtet, T., 2020. Vertical distribution of brittle star larvae in two contrasting coastal embayments: implications for larval transport. Sci. Rep. 10, 12033. https://doi.org/10.1038/s41598-020-68750-4

Guillou, L., Bachar, D., Audic, S., Bass, D., Berney, C., Bittner, L., Boutte, C., Burgaud, G., de Vargas, C., Decelle, J., del Campo, J., Dolan, J.R., Dunthorn, M., Edvardsen, B., Holzmann, M., Kooistra, W.H.C.F., Lara, E., Le Bescot, N., Logares, R., Mahé, F., Massana, R., Montresor, M., Morard, R., Not, F., Pawlowski, J., Probert, I., Sauvadet, A.-L., Siano, R., Stoeck, T., Vaulot, D., Zimmermann, P., Christen, R., 2012. The Protist Ribosomal Reference database (PR2): a catalog of unicellular eukaryote Small Sub-Unit rRNA sequences with curated taxonomy. Nucleic Acids Res. 41, D597–D604. https://doi.org/10.1093/nar/gks1160

Guillou, N., 2007. Effects of the heterogeneity of bottom sediments and wave-current interaction on subtidal hydrodynamics and sediment transport—applications to the eastern English Channel and off Brittany. Université de Bretagne Occidentale, Brest.

Guilloux, L., Rigaut-Jalabert, F., Jouenne, F., Ristori, S., Viprey, M., Not, F., Vaulot, D., Simon, N., 2013. An annotated checklist of Marine Phytoplankton taxa at the SOMLIT-Astan time series off Roscoff (Western English Channel, France): data collected from 2000 to 2010 10.

Guiry, M.D., 2012. HOW MANY SPECIES OF ALGAE ARE THERE? J. Phycol. 48, 1057–1063. https://doi.org/10.1111/j.1529-8817.2012.01222.x

Guiry, M.D., Guiry, G.M., 2021. AlgaeBase. World-wide electronic publication. Natl. Univ. Irel. Galway. http://www.algaebase.org

Guo, L., Sui, Z., Zhang, S., Ren, Y., Liu, Y., 2015. Comparison of potential diatom 'barcode' genes (the 18S rRNA gene and ITS, COI, rbcL) and their effectiveness in discriminating and determining species taxonomy in the Bacillariophyta. Int. J. Syst. Evol. Microbiol. 65, 1369–1380. https://doi.org/10.1099/ijs.0.000076

Hader, D.-P., Gao, K., 2015. Interactions of anthropogenic stress factors on marine phytoplankton. Front. Environ. Sci. 3. https://doi.org/10.3389/fenvs.2015.00014

Hallegraeff, G.M., 2003. Harmful algal blooms: a global overview 33, 1–22.

Hallegraeff, G.M., 1993. A review of harmful algal blooms and their apparent global increase. Phycologia 32, 79–99. https://doi.org/10.2216/i0031-8884-32-2-79.1

Hallegraeff, G.M., Anderson, D.M., Belin, C., Bottein, M.-Y.D., Bresnan, E., Chinain, M., Enevoldsen, H., Iwataki, M., Karlson, B., McKenzie, C.H., Sunesen, I., Pitcher, G.C., Provoost, P., Richardson, A., Schweibold, L., Tester, P.A., Trainer, V.L., Yñiguez, A.T., Zingone, A., 2021. Perceived global increase in algal blooms is attributable to intensified monitoring and emerging bloom impacts. Commun. Earth Environ. 2, 117. https://doi.org/10.1038/s43247-021-00178-8

Hallegraeff, G.M., Anderson, D.M., Cembella, A.D., Enevoldsen, H.O., 2004. Manual on harmful marine microalgae. Unesco.

Hamm, C.E., Merkel, R., Springer, O., Jurkojc, P., Maier, C., Prechtel, K., Smetacek, V., 2003. Architecture and material properties of diatom shells provide effective mechanical protection. Nature 421, 841–843. https://doi.org/10.1038/nature01416

Hamme, R.C., Webley, P.W., Crawford, W.R., Whitney, F.A., DeGrandpre, M.D., Emerson, S.R., Eriksen, C.C., Giesbrecht, K.E., Gower, J.F.R., Kavanaugh, M.T., Peña, M.A., Sabine, C.L., Batten, S.D., Coogan, L.A., Grundle, D.S., Lockwood, D., 2010. Volcanic ash fuels anomalous plankton bloom in subarctic northeast Pacific: ASH FUELS ANOMALOUS PLANKTON BLOOM. Geophys. Res. Lett. 37, n/a-n/a. https://doi.org/10.1029/2010GL044629

Hasle, G.R., 2002. Are most of the domoic acid-producing species of the diatom genus Pseudo-nitzschia cosmopolites? Harmful Algae 1, 137–146. https://doi.org/10.1016/S1568-9883(02)00014-8

Hasle, G.R., 1994. PSEUDO-NITZSCHIA AS A GENUS DISTINCT FROM NITZSCHIA (BACILLARIOPHYCEAE) 1. J. Phycol. 30(6), 1036–1039. https://doi.org/10.1111/j.0022-3646.1994.01036.x

Hasle, G.R., 1993. Nomenclatural notes on marine planktonic diatoms. The family Bacillariaceae. Beih. Zur Nova Hedwig. 106, 315–321.

Hasle, G.R., 1965. Nitzschia and Fragilariopsis species studied in the light and electron microscopes. II. The group Pseudonitzschia. Skrift. Nor. Vidensk Akad 18:1-45.

Hasle, G.R., Syvertsen, E.E., 1997. Marine Diatoms (5-386). Identifying Mar. Phytoplankton 1–385.

Heino, J., Soininen, J., 2006. Regional occupancy in unicellular eukaryotes: a reflection of niche breadth, habitat availability or size-related dispersal capacity? Freshw. Biol. 51, 672–685. https://doi.org/10.1111/j.1365-2427.2006.01520.x

Hellweger, F.L., Clegg, R.J., Clark, J.R., Plugge, C.M., Kreft, J.-U., 2016. Advancing microbial sciences by individual-based modelling. Nat. Rev. Microbiol. 14, 461–471. https://doi.org/10.1038/nrmicro.2016.62

Hernández Fariñas, T., Bacher, C., Soudant, D., Belin, C., Barillé, L., 2015. Assessing phytoplankton realized niches using a French national phytoplankton monitoring network. Estuar. Coast. Shelf Sci. 159, 15–27. https://doi.org/10.1016/j.ecss.2015.03.010

Hernández-Fariñas, T., Soudant, D., Barillé, L., Belin, C., Lefebvre, A., Bacher, C., 2014. Temporal changes in the phytoplankton community along the French coast of the eastern English Channel and the southern Bight of the North Sea. ICES J. Mar. Sci. 71, 821–833. https://doi.org/10.1093/icesjms/fst192

Hess, P., Gallacher, S., Bates, L.A., Brown, N., Quilliam, M.A., 2001. Determination and Confirmation of the Amnesic Shellfish Poisoning Toxin, Domoic Acid, in Shellfish from Scotland by Liquid Chromatography and Mass Spectrometry. J. AOAC Int. 84, 1657–1667. https://doi.org/10.1093/jaoac/84.5.1657

Hess, P., Twiner, M.J., Kilcoyne, J., Sosa, S., 2015. Azaspiracid Toxins: Toxicological Profile, in: Gopalakrishnakone, P., Haddad, V., Kem, W.R., Tubaro, A., Kim, E. (Eds.), Marine and Freshwater Toxins. Springer Netherlands, Dordrecht, pp. 1–19. https://doi.org/10.1007/978-94-007-6650-1_20-1

Hickey, B.M., Trainer, V.L., Michael Kosro, P., Adams, N.G., Connolly, T.P., Kachel, N.B., Geier, S.L., 2013. A springtime source of toxic Pseudo-nitzschia cells on razor clam beaches in the Pacific Northwest. Harmful Algae 25, 1–14. https://doi.org/10.1016/j.hal.2013.01.006

Hobbie, J.E., Daley, R.J., Jasper, S., 1977. Use of nuclepore filters for counting bacteria by fluorescence microscopy. Appl. Environ. Microbiol. 33, 1225–1228. https://doi.org/10.1128/aem.33.5.1225-1228.1977

Hoffmann, A.A., Willi, Y., 2008. Detecting genetic responses to environmental change. Nat. Rev. Genet. 9, 421–432. https://doi.org/10.1038/nrg2339

Holligan, P.M., 1992. Do Marine Phytoplankton Influence Global Climate?, in: Falkowski, P.G., Woodhead, A.D., Vivirito, K. (Eds.), Primary Productivity and Biogeochemical Cycles in the Sea. Springer US, Boston, MA, pp. 487–501. https://doi.org/10.1007/978-1-4899-0762-2_25

Holtermann, K.E., Bates, S.S., Trainer, V.L., Odell, A., Armbrust, E.V., 2010. Mass Sexual Reproduction in the Toxigenic Diatoms Pseudo-Nitzschia Australis and P. Pungens (bacillariophyceae) on the Washington Coast, Usa1. J. Phycol. 46, 41–52. https://doi.org/10.1111/j.1529-8817.2009.00792.x

Houliez, E., Lefebvre, S., Dessier, A., Huret, M., Marquis, E., Bréret, M., Dupuy, C., 2021. Spatio-temporal drivers of microphytoplankton community in the Bay of Biscay: Do species ecological niches matter? Prog. Oceanogr. 194, 102558. https://doi.org/10.1016/j.pocean.2021.102558

Houliez, E., Lizon, F., Lefebvre, S., Artigas, L.F., Schmitt, F.G., 2015. Phytoplankton photosynthetic activity dynamics in a temperate macrotidal ecosystem (the Strait of

Dover, eastern English Channel): Time scales of variability and environmental control. J. Mar. Syst. 147, 61–75. https://doi.org/10.1016/j.jmarsys.2014.05.001

Houliez, E., Schmitt, F.G., Breton, E., Skouroliakou, D.-I., Christaki, U., 2023. On the conditions promoting Pseudo-nitzschia spp. blooms in the eastern English Channel and southern North Sea. Harmful Algae 125, 102424. https://doi.org/10.1016/j.hal.2023.102424

Hu, H., Zhang, J., Chen, W., 2011. Competition of bloom-forming marine phytoplankton at low nutrient concentrations. J. Environ. Sci. 23, 656–663. https://doi.org/10.1016/S1001-0742(10)60459-7

Hubbard, K.A., Villac, M.C., Chadwick, C., DeSmidt, A.A., Flewelling, L., Granholm, A., Joseph, M., Wood, T., Fachon, E., Brosnahan, M.L., Richlen, M., Pathare, M., Stockwell, D., Lin, P., Bouchard, J.N., Pickart, R., Anderson, D.M., 2023. Spatiotemporal transitions in Pseudo-nitzschia species assemblages and domoic acid along the Alaska coast. PLOS ONE 18, e0282794. https://doi.org/10.1371/journal.pone.0282794

Huertas, I.E., Rouco, M., López-Rodas, V., Costas, E., 2011. Warming will affect phytoplankton differently: evidence through a mechanistic approach. Proc. R. Soc. B Biol. Sci. 278, 3534–3543. https://doi.org/10.1098/rspb.2011.0160

Huisman, J., Van Oostveen, P., Weissing, F.J., 1999. Critical depth and critical turbulence: Two different mechanisms for the development of phytoplankton blooms. Limnol. Oceanogr. 44, 1781–1787. https://doi.org/10.4319/lo.1999.44.7.1781

Husson, B., Hernández-Fariñas, T., Le Gendre, R., Schapira, M., Chapelle, A., 2016. Two decades of Pseudo-nitzschia spp. blooms and king scallop (Pecten maximus) contamination by domoic acid along the French Atlantic and English Channel coasts: Seasonal dynamics, spatial heterogeneity and interannual variability. Harmful Algae 51, 26–39. https://doi.org/10.1016/j.hal.2015.10.017

Ianora, A., Bentley, M.G., Caldwell, G.S., Casotti, R., Cembella, A.D., Engström-Öst, J., Halsband, C., Sonnenschein, E., Legrand, C., Llewellyn, C.A., Paldavičienë, A., Pilkaityte, R., Pohnert, G., Razinkovas, A., Romano, G., Tillmann, U., Vaiciute, D., 2011. The Relevance of Marine Chemical Ecology to Plankton and Ecosystem Function: An Emerging Field. Mar. Drugs 9, 1625–1648. https://doi.org/10.3390/md9091625

Ianora, A., Miralto, A., 2010. Toxigenic effects of diatoms on grazers, phytoplankton and other microbes: a review. Ecotoxicology 19, 493–511. https://doi.org/10.1007/s10646-009-0434-y

Irigoien, X., Huisman, J., Harris, R.P., 2004. Global biodiversity patterns of marine phytoplankton and zooplankton. Nature 429, 863–867. https://doi.org/10.1038/nature02593

Isles, P.D., Pomati, F., 2021. An operational framework for defining and forecasting phytoplankton blooms. Front. Ecol. Environ. 19, 443–450. https://doi.org/10.1002/fee.2376

Jacques, G., 1963. Variations saisonnières des populations phytoplanctoniques de la région de Roscoff (1962-1963). Thèse 3ième cycle. Fac. Sci. Paris, 88 pp.

James, K.J., Carey, B., O'Halloran, J., Van Pelt, F.N.A.M., Škrabáková, Z., 2010. Shellfish toxicity: human health implications of marine algal toxins. Epidemiol. Infect. 138, 927–940. https://doi.org/10.1017/S0950268810000853

James, K.J., Gillman, M., Lehane, M., Gago-Martinez, A., 2000. New fluorimetric method of liquid chromatography for the determination of the neurotoxin domoic acid in seafood and marine phytoplankton. J. Chromatogr. A 871, 1–6. https://doi.org/10.1016/S0021-9673(99)00917-6

Ji, N., Lin, L., Li, L., Yu, L., Zhang, Y., Luo, H., Li, M., Shi, X., Wang, D.-Z., Lin, S., 2018. Metatranscriptome analysis reveals environmental and diel regulation of a *Heterosigma akashiwo* (raphidophyceae) bloom: Metatranscriptome profiling of *Heterosigma akashiwo*. Environ. Microbiol. 20, 1078–1094. https://doi.org/10.1111/1462-2920.14045

John, D.E., Patterson, S.S., Paul, J.H., 2007. Phytoplankton-Group Specific Quantitative Polymerase Chain Reaction Assays for RuBisCO mRNA Transcripts in Seawater. Mar. Biotechnol. 9, 747–759. https://doi.org/10.1007/s10126-007-9027-z

Jouenne, F., Lefebvre, S., Véron, B., Lagadeuc, Y., 2007. Phytoplankton community structure and primary production in small intertidal estuarine-bay ecosystem (eastern English Channel, France). Mar. Biol. 151, 805–825. https://doi.org/10.1007/s00227-006-0440-z

Kahru, M., Brotas, V., Manzano-Sarabia, M., Mitchell, B.G., 2011. Are phytoplankton blooms occurring earlier in the Arctic?: PHYTOPLANKTON BLOOMS IN THE ARCTIC. Glob. Change Biol. 17, 1733–1739. https://doi.org/10.1111/j.1365-2486.2010.02312.x

Kamykowski, 1974. Possible interactions between phytoplankton and semidiurnal internal tides.

Karlusich, J.J.P., Ibarbalz, F.M., Bowler, C., 2020. Exploration of marine phytoplankton: from their historical appreciation to the omics era. J. Plankton Res. fbaa049. https://doi.org/10.1093/plankt/fbaa049

Kassambara, A., Mundt, F., 2017. Package 'factoextra'. Extract and visualize the results of multivariate data analyses 76(2).

Keeling, P.J., Burki, F., Wilcox, H.M., Allam, B., Allen, E.E., Amaral-Zettler, L.A., Armbrust, E.V., Archibald, J.M., Bharti, A.K., Bell, C.J., Beszteri, B., Bidle, K.D., Cameron, C.T., Campbell, L., Caron, D.A., Cattolico, R.A., Collier, J.L., Coyne, K., Davy, S.K., Deschamps, P., Dyhrman, S.T., Edvardsen, B., Gates, R.D., Gobler, C.J., Greenwood, S.J., Guida, S.M., Jacobi, J.L., Jakobsen, K.S., James, E.R., Jenkins, B., John, U.,

Johnson, M.D., Juhl, A.R., Kamp, A., Katz, L.A., Kiene, R., Kudryavtsev, A., Leander, B.S., Lin, S., Lovejoy, C., Lynn, D., Marchetti, A., McManus, G., Nedelcu, A.M., Menden-Deuer, S., Miceli, C., Mock, T., Montresor, M., Moran, M.A., Murray, S., Nadathur, G., Nagai, S., Ngam, P.B., Palenik, B., Pawlowski, J., Petroni, G., Piganeau, G., Posewitz, M.C., Rengefors, K., Romano, G., Rumpho, M.E., Rynearson, T., Schilling, K.B., Schroeder, D.C., Simpson, A.G.B., Slamovits, C.H., Smith, D.R., Smith, G.J., Smith, S.R., Sosik, H.M., Stief, P., Theriot, E., Twary, S.N., Umale, P.E., Vaulot, D., Wawrik, B., Wheeler, G.L., Wilson, W.H., Xu, Y., Zingone, A., Worden, A.Z., 2014. The Marine Microbial Eukaryote Transcriptome Sequencing Project (MMETSP): Illuminating the Functional Diversity of Eukaryotic Life in the Oceans through Transcriptome Sequencing. PLoS Biol. 12, e1001889. https://doi.org/10.1371/journal.pbio.1001889

Kim, H.G., Hong, S., Kim, D.-K., Joo, G.-J., 2020. Drivers shaping episodic and gradual changes in phytoplankton community succession: Taxonomic versus functional groups. Sci. Total Environ. 734, 138940. https://doi.org/10.1016/j.scitotenv.2020.138940

Kim, J.H., Ajani, P.A., Murray, S.A., Kang, S.-M., Kim, S.-H., Lim, H.C., Teng, S.T., Lim, P.T., Park, B.S., 2023. Abiotic and biotic factors controlling sexual reproduction in populations of Pseudo-nitzschia pungens (Bacillariophyceae). Harmful Algae 123, 102392. https://doi.org/10.1016/j.hal.2023.102392

Kirchman, D., Ducklow, H., Mitchell, R., 1982. Estimates of bacterial growth from changes in uptake rates and biomass. Appl. Environ. Microbiol. 44, 1296–1307. https://doi.org/10.1128/aem.44.6.1296-1307.1982

Klein, C., Claquin, P., Bouchart, V., Le Roy, B., Véron, B., 2010. Dynamics of Pseudo-nitzschia spp. and domoic acid production in a macrotidal ecosystem of the Eastern English Channel (Normandy, France). Harmful Algae 9, 218–226. https://doi.org/10.1016/j.hal.2009.10.004

Koester, J.A., Brawley, S.H., Karp-Boss, L., Mann, D.G., 2007. Sexual reproduction in the marine centric diatom ***Ditylum brightwellii*** (Bacillariophyta). Eur. J. Phycol. 42, 351–366. https://doi.org/10.1080/09670260701562100

Koike, K., Otobe, H., Takagi, M., Yoshida, T., Ogata, T., Ishimaru, T., 2001. Recent Occurrences of Dinophysis fortii (Dinophyceae) in the Okkirai Bay, Sanriku, Northern Japan, and Related Environmental Factors. J. Oceanogr. 57, 165–175. https://doi.org/10.1023/A:1011191124025

Kolody, B.C., Harke, M.J., Hook, S.E., Allen, A.E., 2022. Transcriptomic and metatranscriptomic approaches in phytoplankton: insights and advances, in: Advances in Phytoplankton Ecology. Elsevier, pp. 435–485. https://doi.org/10.1016/B978-0-12-822861-6.00022-4

Kooistra, W.H.C.F., Gersonde, R., Medlin, L.K., Mann, D.G., 2007. The Origin and Evolution of the Diatoms: Their Adaptation to a Planktonic Existence, in: Evolution of Primary Producers in the Sea. Elsevier, pp. 207–249. https://doi.org/10.1016/B978-012370518-1/50012-6

Koukaras, K., 2004. Dinophysis blooms in Greek coastal waters (Thermaikos Gulf, NW Aegean Sea). J. Plankton Res. 26, 445–457. https://doi.org/10.1093/plankt/fbh042

Kovač, Ž., Platt, T., Sathyendranath, S., 2021. Sverdrup meets Lambert: analytical solution for Sverdrup's critical depth. ICES J. Mar. Sci. 78, 1398–1408. https://doi.org/10.1093/icesjms/fsab013

Kranner, I., Birtić, S., Anderson, K.M., Pritchard, H.W., 2006. Glutathione half-cell reduction potential: A universal stress marker and modulator of programmed cell death? Free Radic. Biol. Med. 40, 2155–2165. https://doi.org/10.1016/j.freeradbiomed.2006.02.013

Kutser, T., 2009. Passive optical remote sensing of cyanobacteria and other intense phytoplankton blooms in coastal and inland waters. Int. J. Remote Sens. 30, 4401–4425. https://doi.org/10.1080/01431160802562305

Kutser, T., 2004. Quantitative detection of chlorophyll in cyanobacterial blooms by satellite remote sensing. Limnol. Oceanogr. 49, 2179–2189. https://doi.org/10.4319/lo.2004.49.6.2179

Kvrgić, K., Lešić, T., Džafić, N., Pleadin, J., 2022. Occurrence and Seasonal Monitoring of Domoic Acid in Three Shellfish Species from the Northern Adriatic Sea. Toxins 14, 33. https://doi.org/10.3390/toxins14010033

Labry, C., Erard–Le Denn, E., Chapelle, A., Fauchot, J., Youenou, A., Crassous, M.P., Le Grand, J., Lorgeoux, B., 2008. Competition for phosphorus between two dinoflagellates: A toxic Alexandrium minutum and a non-toxic Heterocapsa triquetra. J. Exp. Mar. Biol. Ecol. 358, 124–135. https://doi.org/10.1016/j.jembe.2008.01.025

Lagarde, F., Fiandrino, A., Ubertini, M., Roque d'Orbcastel, E., Mortreux, S., Chiantella, C., Bec, B., Bonnet, D., Roques, C., Bernard, I., Richard, M., Guyondet, T., Pouvreau, S., Lett, C., 2019. Duality of trophic supply and hydrodynamic connectivity drives spatial patterns of Pacific oyster recruitment. Mar. Ecol. Prog. Ser. 632, 81–100. https://doi.org/10.3354/meps13151

Lai, Z., Yin, K., 2014. Physical–biological coupling induced aggregation mechanism for the formation of high biomass red tides in low nutrient waters. Harmful Algae 31, 66–75. https://doi.org/10.1016/j.hal.2013.09.011

Lampert, W., Fleckner, W., Rai, H., Taylor, B.E., 1986. Phytoplankton control by grazing zooplankton: A study on the spring clear-water phase1. Limnol. Oceanogr. 31, 478–490. https://doi.org/10.4319/lo.1986.31.3.0478

Langfelder, P., Horvath, S., 2008. WGCNA: an R package for weighted correlation network analysis. BMC Bioinformatics 9, 559. https://doi.org/10.1186/1471-2105-9-559

Lassus, P., Bardouil, M., Berthomé, J.-P., Maggi, P., Truquet, P., Le Déan, L., 1988. Seasonal occurrence of *Dinophysis* sp. along the French coast between 1983 and 1987. Aquat. Living Resour. 1, 155–164. https://doi.org/10.1051/alr:1988017

Lassus, P., Chomérat, N., Hess, P., Nézan, E., 2015. Toxic and harmful microalgae of the World Ocean. International Society for the Study of Harmful Algae and the United Nations Educational, Scientific and Cultural Organisation.

Le, C., Li, Y., Zha, Y., Sun, D., 2009. Specific absorption coefficient and the phytoplankton package effect in Lake Taihu, China. Hydrobiologia 619, 27–37. https://doi.org/10.1007/s10750-008-9579-6

Le Corre, P., L'Helguen, S., Morin, P., Birrien, J.L., 1992. Conditions de formation d'eaux colorées toxiques sur le plateau continental Manche - Atlantique; Cas de Gyrodinium cf. aureolum. Hydroécologie Appliquée 4, 173–188. https://doi.org/10.1051/hydro:1992214

Le Duff, M., Hily, C., Glemarec, M., 1999. Environnement naturel de l'Iroise. Bilan des connaissances et intérêt patrimonial.

Le Fèvre, J., Grall, J.R., 1970. On the relationships of Noctiluca swarming off the western coast of brittany with hydrological features and plankton characteristics of the environment. J. Exp. Mar. Biol. Ecol. 4, 287–306. https://doi.org/10.1016/0022-0981(70)90040-7

Le Fevre, J., Le Corre, P., Morin, P., Birrien, J.-L., 1983. The pelagic ecosystem in frontal zones and other environments off the west coast of Brittany. Oceanol. Acta, Special issue.

Le Pape, O., Del Amo, Y., Menesguen, A., Aminot, A., Quequiner, B., Treguer, P., 1996. Resistance of a coastal ecosystem to increasing eutrophic conditions: the Bay of Brest (France), a semi-enclosed zone of Western Europe. Cont. Shelf Res. 16, 1885–1907. https://doi.org/10.1016/0278-4343(95)00068-2

Le Pape, O., Menesguen, A., 1997. Hydrodynamic prevention of eutrophication in the Bay of Brest (France), a modelling approach. J. Mar. Syst. 12, 171–186. https://doi.org/10.1016/S0924-7963(96)00096-6

Leblanc, K., Arístegui, J., Armand, L., Assmy, P., Beker, B., Bode, A., Breton, E., Cornet, V., Gibson, J., Gosselin, M.-P., Kopczynska, E., Marshall, H., Peloquin, J., Piontkovski, S., Poulton, A.J., Quéguiner, B., Schiebel, R., Shipe, R., Stefels, J., Van Leeuwe, M.A., Varela, M., Widdicombe, C., Yallop, M., 2012. A global diatom database – abundance, biovolume and biomass in the world ocean. Earth Syst. Sci. Data 4, 149–165. https://doi.org/10.5194/essd-4-149-2012

Lefebvre, K.A., Bargu, S., Kieckhefer, T., Silver, M.W., 2002. From sanddabs to blue whales: the pervasiveness of domoic acid. Toxicon 40, 971–977. https://doi.org/10.1016/S0041-0101(02)00093-4

Lelong, A., Hégaret, H., Soudant, P., Bates, S.S., 2012. Pseudo-nitzschia (Bacillariophyceae) Species, Domoic Acid and Amnesic Shellfish Poisoning: Revisiting Previous Paradigms. Phycologia 51, 168–216. https://doi.org/10.2216/11-37.1

Lema, K.A., Latimier, M., Nézan, É., Fauchot, J., Le Gac, M., 2017. Inter and intra-specific growth and domoic acid production in relation to nutrient ratios and concentrations in Pseudo-nitzschia : phosphate an important factor. Harmful Algae 64, 11–19. https://doi.org/10.1016/j.hal.2017.03.001

Lema, K.A., Metegnier, G., Quéré, J., Latimier, M., Youenou, A., Lambert, C., Fauchot, J., Le Gac, M., 2019. Inter- and Intra-Specific Transcriptional and Phenotypic Responses of *Pseudo-nitzschia* under Different Nutrient Conditions. Genome Biol. Evol. 11, 731–747. https://doi.org/10.1093/gbe/evz030

Leonilde, R., Elena, L., Elena, S., Francesco, C., Alberto, B., 2017. Individual trait variation in phytoplankton communities across multiple spatial scales. J. Plankton Res. 39, 577–588. https://doi.org/10.1093/plankt/fbx001

Leterme, S.C., Le Lan, C., Hemraj, D.A., Ellis, A.V., 2016. The impact of diatoms on the biofouling of seawater reverse osmosis membranes in a model cross-flow system. Desalination 392, 8–13. https://doi.org/10.1016/j.desal.2016.04.019

Lett, C., Verley, P., Mullon, C., Parada, C., Brochier, T., Penven, P., Blanke, B., 2008. A Lagrangian tool for modelling ichthyoplankton dynamics. Environ. Model. Softw. 23, 1210–1214. https://doi.org/10.1016/j.envsoft.2008.02.005

Lewandowska, A., Sommer, U., 2010. Climate change and the spring bloom: a mesocosm study on the influence of light and temperature on phytoplankton and mesozooplankton. Mar. Ecol. Prog. Ser. 405, 101–111. https://doi.org/10.3354/meps08520

Lewandowska, A.M., Striebel, M., Feudel, U., Hillebrand, H., Sommer, U., 2015. The importance of phytoplankton trait variability in spring bloom formation. ICES J. Mar. Sci. 72, 1908–1915. https://doi.org/10.1093/icesjms/fsv059

Lewis, N., Bates, S.S., McLachlan, J.L., Smith, J.C., 1993. Temperature effects on growth, domoic acid productlon, and morphology of the diatom Nitzschia pungens f multiseries. In: Smayda TJ, Shlrnlzu Y (eds) TOXIC phytoplankton bloon~s in the sea. Elsevier Sci. Publ. Amst. 601–606.

Lewis, W.M., 1987. The cost of sex, in: Stearns, S.C. (Ed.), The Evolution of Sex and Its Consequences, Experientia Supplementum. Birkhäuser Basel, Basel, pp. 33–57. https://doi.org/10.1007/978-3-0348-6273-8_2

Leyland, B., Boussiba, S., Khozin-Goldberg, I., 2020. A Review of Diatom Lipid Droplets. Biology 9, 38. https://doi.org/10.3390/biology9020038

Li, H., 2013. Aligning sequence reads, clone sequences and assembly contigs with BWA-MEM.

Li, H., Handsaker, B., Wysoker, A., Fennell, T., Ruan, J., Homer, N., Marth, G., Abecasis, G., Durbin, R., 1000 Genome Project Data Processing Subgroup, 2009. The Sequence Alignment/Map format and SAMtools. Bioinformatics 25, 2078–2079. https://doi.org/10.1093/bioinformatics/btp352

Li, Y., He, R., Manning, J.P., 2014. Coastal connectivity in the Gulf of Maine in spring and summer of 2004–2009. Deep Sea Res. Part II Top. Stud. Oceanogr. 103, 199–209. https://doi.org/10.1016/j.dsr2.2013.01.037

Lie, A., Kim, D., Schnetzer, A., Caron, D., 2013. Small-scale temporal and spatial variations in protistan community composition at the San Pedro Ocean Time-series station off the

coast of southern California. Aquat. Microb. Ecol. 70, 93–110. https://doi.org/10.3354/ame01652

Lim, H.C., Tan, S.N., Teng, S.T., Lundholm, N., Orive, E., David, H., Quijano-Scheggia, S., Leong, S.C.Y., Wolf, M., Bates, S.S., Lim, P.T., Leaw, C.P., 2018. Phylogeny and species delineation in the marine diatom *Pseudo-nitzschia* (Bacillariophyta) using *cox1* , LSU , and ITS 2 rRNA genes: A perspective in character evolution. J. Phycol. 54, 234–248. https://doi.org/10.1111/jpy.12620

Lim, H.C., Teng, S.T., Leaw, C.P., Lim, P.T., 2013. Three novel species in the *Pseudo-nitzschia pseudodelicatissima* complex: *P . batesiana* sp. nov., *P. lundholmiae* sp. nov., and *P. fukuyoi* sp. nov. (Bacillariophyceae) from the Strait of Malacca, Malaysia. J. Phycol. 49, 902–916. https://doi.org/10.1111/jpy.12101

Lin, X., 2021. The Application of Transcriptomics, Metagenomics, and Metatranscriptomics in Algal Research, in: Gao, K., Hutchins, D.A., Beardall, J. (Eds.), Research Methods of Environmental Physiology in Aquatic Sciences. Springer Singapore, Singapore, pp. 285–291. https://doi.org/10.1007/978-981-15-5354-7_34

Lindo-Atichati, D., Montero, P., Rodil, R., Quintana, J.B., Miró, M., 2019. Modeling Dispersal of UV Filters in Estuaries. Environ. Sci. Technol. 53, 1353–1363. https://doi.org/10.1021/acs.est.8b03725

Litchman, E., Klausmeier, C.A., 2008. Trait-Based Community Ecology of Phytoplankton. Annu. Rev. Ecol. Evol. Syst. 39, 615–639. https://doi.org/10.1146/annurev.ecolsys.39.110707.173549

Liu, S., Cui, Z., Zhao, Y., Chen, N., 2022. Composition and spatial-temporal dynamics of phytoplankton community shaped by environmental selection and interactions in the Jiaozhou Bay. Water Res. 218, 118488. https://doi.org/10.1016/j.watres.2022.118488

Llebot, C., Solé, J., Delgado, M., Fernández-Tejedor, M., Camp, J., Estrada, M., 2011. Hydrographical forcing and phytoplankton variability in two semi-enclosed estuarine bays. J. Mar. Syst. 86, 69–86. https://doi.org/10.1016/j.jmarsys.2011.01.004

Loeffler, Handy, Flores Quintana, Deeds, 2019. Fish Hybridization Leads to Uncertainty Regarding Ciguatera Fish Poisoning Risk; Confirmation of Hybridization and Ciguatoxin Accumulation with Implications for Stakeholders. J. Mar. Sci. Eng. 7, 105. https://doi.org/10.3390/jmse7040105

Longhurst, 2007. Ecological Geography of the Sea. Academic. San Diego.

Lopes, M.R.M., Bicudo, C.E. de M., Ferragut, M.C., 2005. Short term spatial and temporal variation of phytoplankton in a shallow tropical oligotrophic reservoir, southeast Brazil. Hydrobiologia 542, 235–247. https://doi.org/10.1007/s10750-004-8332-z

Love, M.I., Huber, W., Anders, S., 2014. Moderated estimation of fold change and dispersion for RNA-seq data with DESeq2 (preprint). Bioinformatics. https://doi.org/10.1101/002832

Lucas, L., Koseff, J., Cloern, J., Monismith, S., Thompson, J., 1999. Processes governing phytoplankton blooms in estuaries. I:The local production-loss balance. Mar. Ecol. Prog. Ser. 187, 1–15. https://doi.org/10.3354/meps187001

Lucas, L.V., Deleersnijder, E., 2020. Timescale Methods for Simplifying, Understanding and Modeling Biophysical and Water Quality Processes in Coastal Aquatic Ecosystems: A Review. Water 12, 2717. https://doi.org/10.3390/w12102717

Lundholm, N., 2022. Bacillariophyceae [WWW Document]. In: IOC-UNESCO Taxonomic Reference List of Harmful Micro Algae. URL. http://www.marinespecies.org/hab (accessed 02.18.2022).

Lundholm, N., 2021. Bacillariophyceae. In: IOC-UNES-CO Taxonomic Reference List of Harmful Micro Algae. Moestrup, Ø., Akselmann-Cardella, R., Churro, C., Fraga, S., Hoppenrath, M. et al., (Eds). http://www.marinespecies.org/hab

Lundholm, N., Bates, S.S., Baugh, K.A., Bill, B.D., Connell, L.B., Léger, C., Trainer, V.L., 2012. CRYPTIC AND PSEUDO-CRYPTIC DIVERSITY IN DIATOMS-WITH DESCRIPTIONS OF PSEUDO-NITZSCHIA HASLEANA SP. NOV. AND P. FRYXELLIANA SP. NOV.1: CRYPTIC DIVERSITY IN PSEUDO-NITZSCHIA. J. Phycol. 48, 436–454. https://doi.org/10.1111/j.1529-8817.2012.01132.x

Lundholm, N., Clarke, A., Ellegaard, M., 2010. A 100-year record of changing Pseudo-nitzschia species in a sill-fjord in Denmark related to nitrogen loading and temperature. Harmful Algae 9, 449–457.

Lundholm, N., Daugbjerg, N., Moestrup, Ø., 2002. Phylogeny of the Bacillariaceae with emphasis on the genus *Pseudo - nitzschia* (Bacillariophyceae) based on partial LSU rDNA. Eur. J. Phycol. 37, 115–134. https://doi.org/10.1017/S096702620100347X

Lundholm, N., Hansen, P., Kotaki, Y., 2004. Effect of pH on growth and domoic acid production by potentially toxic diatoms of the genera Pseudo-nitzschia and Nitzschia. Mar. Ecol. Prog. Ser. 273, 1–15. https://doi.org/10.3354/meps273001

Lundholm, N., Jvind Moestrup, Ø., 2000. Morphology of the Marine Diatom Nitzschia Navis-Varingica, Sp. Nov. (bacillariophyceae), Another Producer of the Neurotoxin Domoic Acid. J. Phycol. 36, 1162–1174. https://doi.org/10.1046/j.1529-8817.2000.99210.x

Lundholm, N., Moestrup, O., Kotaki, Y., Hoef-Emden, K., Scholin, C., Miller, P., 2006. INTER- AND INTRASPECIFIC VARIATION OF THE PSEUDO-NITZSCHIA DELICATISSIMA COMPLEX (BACILLARIOPHYCEAE) ILLUSTRATED BY RRNA PROBES, MORPHOLOGICAL DATA AND PHYLOGENETIC ANALYSES1. J. Phycol. 42, 464–481. https://doi.org/10.1111/j.1529-8817.2006.00211.x

Lundholm, N., Moestrup, Jvind, Hasle, G.R., Hoef-Emden, K., 2003. A STUDY OF THE PSEUDO-NITZSCHIA PSEUDODELICATISSIMA/CUSPIDATA COMPLEX (BACILLARIOPHYCEAE): WHAT IS P. PSEUDODELICATISSIMA? 1. J. Phycol. 39, 797–813. https://doi.org/10.1046/j.1529-8817.2003.02031.x

Lundholm, N., Skov, J., Pocklington, R., Moestrup, Ø., 1997. Studies on the marine planktonic diatom Pseudo-nitzschia. 2. Autecology of P. pseudodelicatissima based on isolates from Danish coastal waters. Phycologia 36, 381–388. https://doi.org/10.2216/i0031-8884-36-5-381.1

Lundholm, N., Skov, J., Pocklington, R., Moestrup, Ø., 1994. Domoic acid, the toxic amino acid responsible for amnesic shellfish poisoning, now in Pseudonitzschia seriata (Bacillariophyceae) in Europe. Phycologia 33, 475–478. https://doi.org/10.2216/i0031-8884-33-6-475.1

MacFadyen, A., Hickey, B.M., 2010. Generation and evolution of a topographically linked, mesoscale eddy under steady and variable wind-forcing. Cont. Shelf Res. 30, 1387–1402.

MacFadyen, A., Hickey, B.M., Foreman, M.G.G., 2005. Transport of surface waters from the Juan de Fuca eddy region to the Washington coast. Cont. Shelf Res. 25, 2008–2021. https://doi.org/10.1016/j.csr.2005.07.005

Malviya, S., Scalco, E., Audic, S., Vincent, F., Veluchamy, A., Poulain, J., Wincker, P., Iudicone, D., De Vargas, C., Bittner, L., Zingone, A., Bowler, C., 2016. Insights into global diatom distribution and diversity in the world's ocean. Proc. Natl. Acad. Sci. 113. https://doi.org/10.1073/pnas.1509523113

Mann, D.G., 2002. Diatoms: organism and image. In DU Buf , H. and Bayer, M. M. (eds.), Automatic Diatom Identification, Series in Machine Perception and Artificial Intelligence, World Scientific Publishing Co.,Singapore 9–40.

Mann, D.G., Trobajo, R., Sato, S., Li, C., Witkowski, A., Rimet, F., Ashworth, M.P., Hollands, R.M., Theriot, E.C., 2021. Ripe for reassessment: A synthesis of available molecular data for the speciose diatom family Bacillariaceae. Mol. Phylogenet. Evol. 158, 106985. https://doi.org/10.1016/j.ympev.2020.106985

Margalef, 1978. Life-forms of phytoplankton as survival alternatives in an unstable environment. Oceanol. Acta 1(4), 493–509.

Margalef, R., Durán, M., Saiz, F., 1955. El fitoplancton de la ría de Vigo de enero de 1953 a marzo de 1954.

Mari, X., Rassoulzadegan, F., 2004. Role of TEP in the microbial food web structure. I. Grazing behavior of a bacterivorous pelagic ciliate. Mar. Ecol. Prog. Ser. 279, 13–22. https://doi.org/10.3354/meps279013

Mariette, V., Le Cann, B., 1985. Simulation of the formation of Ushant thermal front. Cont. Shelf Res. 4, 637–660. https://doi.org/10.1016/0278-4343(85)90034-2

Mariette, V., Rougier, V., Salomon, J.-C., Simon, B., 1982. Courants de marée en mer d'Iroise. Oceanol. Acta, 5(2) 149–159.

Marotta, P., Borgonuovo, C., Santin, A., Russo, M.T., Manfellotto, F., Montresor, M., De Luca, P., Ferrante, M.I., 2022. Mate Perception and Gene Networks Regulating the Early

Phase of Sex in Pseudo-nitzschia multistriata. J. Mar. Sci. Eng. 10, 1941. https://doi.org/10.3390/jmse10121941

Marra, J., Barber, R.T., 2005. Primary productivity in the Arabian Sea: A synthesis of JGOFS data. Prog. Oceanogr. 65, 159–175. https://doi.org/10.1016/j.pocean.2005.03.004

Martellucci, R., Salon, S., Cossarini, G., Piermattei, V., Marcelli, M., 2021. Coastal phytoplankton bloom dynamics in the Tyrrhenian Sea: Advantage of integrating in situ observations, large-scale analysis and forecast systems. J. Mar. Syst. 218, 103528. https://doi.org/10.1016/j.jmarsys.2021.103528

Martin, J.L., Santi, I., Pitta, P., John, U., Gypens, N., 2022. Towards quantitative metabarcoding of eukaryotic plankton: an approach to improve 18S rRNA gene copy number bias. Metabarcoding Metagenomics 6, e85794. https://doi.org/10.3897/mbmg.6.85794

Martin-Jézéquel, V., Calu, G., Candela, L., Amzil, Z., Jauffrais, T., Séchet, V., Weigel, P., 2015. Effects of Organic and Inorganic Nitrogen on the Growth and Production of Domoic Acid by Pseudo-nitzschia multiseries and P. australis (Bacillariophyceae) in Culture. Mar. Drugs 13, 7067–7086. https://doi.org/10.3390/md13127055

Martin-Jézéquel, V., Sournia, A., Birrien, J.-L., 1992. A daily study of the diatom spring bloom at Roscoff (France) in 1985. III. Free amino acids composition studied by HPLC analysis. J. Plankton Res. 14, 409–421. https://doi.org/10.1093/plankt/14.3.409

Martin-Platero, A.M., Cleary, B., Kauffman, K., Preheim, S.P., McGillicuddy, D.J., Alm, E.J., Polz, M.F., 2018. High resolution time series reveals cohesive but short-lived communities in coastal plankton. Nat. Commun. 9, 266. https://doi.org/10.1038/s41467-017-02571-4

Masó, M., Garcés, E., 2006. Harmful microalgae blooms (HAB); problematic and conditions that induce them. Mar. Pollut. Bull. 53, 620–630. https://doi.org/10.1016/j.marpolbul.2006.08.006

Matthews, M.W., Bernard, S., Robertson, L., 2012. An algorithm for detecting trophic status (chlorophyll-a), cyanobacterial-dominance, surface scums and floating vegetation in inland and coastal waters. Remote Sens. Environ. 124, 637–652.

McCain, J.S.P., Allen, A.E., Bertrand, E.M., 2022. Proteomic traits vary across taxa in a coastal Antarctic phytoplankton bloom. ISME J. 16, 569–579. https://doi.org/10.1038/s41396-021-01084-9

McClain, C.R., 2009. A Decade of Satellite Ocean Color Observations. Annu. Rev. Mar. Sci. 1, 19–42. https://doi.org/10.1146/annurev.marine.010908.163650

McGillicuddy, D.J., 2010. Models of harmful algal blooms: Conceptual, empirical, and numerical approaches. J. Mar. Syst. 83, 105–107. https://doi.org/10.1016/j.jmarsys.2010.06.008

Meda, M., Kodama, T., Yoshizumi, H., Takemoto, T., Nomoto, K., Fujita, T., 1986. Structures of isodomoic acids A, B and C, novel insecticidal amino acids from the red alga Chondria armata. Chem. Pharm. Bull. (Tokyo) 34(11), 4892–4895.

Medlin, L., Kooistra, W.H.C.F., Schmid, A.M., 2000. A review of the evolution of the diatoms-a total approach using molecules, morphology and geology. The origin and early evolution of the diatoms: fossil, molecular and biogeographical approaches. A. Witkowski & J. Sieminska [eds.], Polish Academy of Sciences, Krakow, Poland 13–35.

Medlin, L.K., 2018. Mini review: Diatom species as seen through a molecular window. Braz. J. Bot. 41, 457–469. https://doi.org/10.1007/s40415-018-0444-1

Medlin, L.K., 2016. Evolution of the diatoms: major steps in their evolution and a review of the supporting molecular and morphological evidence. Phycologia 55, 79–103. https://doi.org/10.2216/15-105.1

Medlin, L.K., 2009. Diatoms (Bacillariophyta). Timetree Life 1, 127.

Medlin, L.K., Kaczmarska, I., 2004. Evolution of the diatoms: V. Morphological and cytological support for the major clades and a taxonomic revision. Phycologia 43, 245–270. https://doi.org/10.2216/i0031-8884-43-3-245.1

Medlin, L.K., Kooistra, W.H., Gersonde, R., Wellbrock, U., 1996. Evolution of the diatoms (Bacillariophyta). II. Nuclear-encoded small- subunit rRNA sequence comparisons confirm a paraphyletic origin for the centric diatoms. Mol. Biol. Evol. 13, 67–75. https://doi.org/10.1093/oxfordjournals.molbev.a025571

Menden-Deuer, S., 2008. Spatial and temporal characteristics of plankton-rich layers in a shallow, temperate fjord. Mar. Ecol. Prog. Ser. 355, 21–30. https://doi.org/10.3354/meps07265

Ménesguen, A., Hachet, A., Grégoris, T., 2018. Modelling benthic invasion by the colonial gastropod Crepidula fornicata and its competition with the bivalve Pecten maximus. 2. Coupling the 0D model of colony-forming species to a connectivity matrix for a realistic distributed simulation of benthic invasion. Ecol. Model. 375, 30–44. https://doi.org/10.1016/j.ecolmodel.2018.02.015

Merceron, M., Antoine, V., Auby, I., Morand, P., 2007. In situ growth potential of the subtidal part of green tide forming Ulva spp. stocks. Sci. Total Environ. 384, 293–305. https://doi.org/10.1016/j.scitotenv.2007.05.007

Metegnier, G., Paulino, S., Ramond, P., Siano, R., Sourisseau, M., Destombe, C., Le Gac, M., 2020. Species specific gene expression dynamics during harmful algal blooms. Sci. Rep. 10, 6182. https://doi.org/10.1038/s41598-020-63326-8

Míguez, A., Fernlindez, L., 1996. First detection of domoic acid in Galicia(NW of Spain). Harmful Toxic Algal Blooms 143–145.

Miller, T.R., Beversdorf, L., Chaston, S.D., McMahon, K.D., 2013. Spatiotemporal Molecular Analysis of Cyanobacteria Blooms Reveals Microcystis-Aphanizomenon Interactions. PLoS ONE 8, e74933. https://doi.org/10.1371/journal.pone.0074933

Moeys, S., Frenkel, J., Lembke, C., Gillard, J.T.F., Devos, V., Van Den Berge, K., Bouillon, B., Huysman, M.J.J., De Decker, S., Scharf, J., Bones, A., Brembu, T., Winge, P., Sabbe, K., Vuylsteke, M., Clement, L., De Veylder, L., Pohnert, G., Vyverman, W., 2016. A sex-inducing pheromone triggers cell cycle arrest and mate attraction in the diatom Seminavis robusta. Sci. Rep. 6, 19252. https://doi.org/10.1038/srep19252

Moniz, M.B.J., Kaczmarska, I., 2009. Barcoding diatoms: Is there a good marker? Mol. Ecol. Resour. 9, 65–74. https://doi.org/10.1111/j.1755-0998.2009.02633.x

Montresor, M., Vitale, L., D'Alelio, D., Ferrante, M.I., 2016. Sex in marine planktonic diatoms: insights and challenges. Perspect. Phycol. 3, 61–75. https://doi.org/10.1127/pip/2016/0045

Morin, P., Lecorre, P., Marty, Y., Lhelguen, S., 1991. Evolution printanière des éléments nutritifs et du phytoplancton sur le plateau continental armoricain (Europe du Nord-Ouest). Oceanol. Acta 14(3), 263–279.

Muller, H., Blanke, B., Dumas, F., Lekien, F., Mariette, V., 2009. Estimating the Lagrangian residual circulation in the Iroise Sea. J. Mar. Syst. 78, S17–S36. https://doi.org/10.1016/j.jmarsys.2009.01.008

Muller, H., Blanke, B., Dumas, F., Mariette, V., 2010. Identification of typical scenarios for the surface Lagrangian residual circulation in the Iroise Sea. J. Geophys. Res. 115, C07008. https://doi.org/10.1029/2009JC005834

Murray, A.W., Szostak, J.W., 1985. Chromosome Segregation in Mitosis and Meiosis. Annu. Rev. Cell Biol. 1, 289–315. https://doi.org/10.1146/annurev.cb.01.110185.001445

Neil, C., Spyrakos, E., Hunter, P.D., Tyler, A.N., 2019. A global approach for chlorophyll-a retrieval across optically complex inland waters based on optical water types. Remote Sens. Environ. 229, 159–178. https://doi.org/10.1016/j.rse.2019.04.027

Nezan, E., Antoine, E., Fiant, L., Billard, C., 2006. Identification of Pseudo-nitzschia australis and P. multiseries in the Bay of Seine. Was there a relation to presence of domoic acid in king scallops in autumn 2004? Harmful Algae News 31, 1–3.

Nezan, E., Chomerat, N., Billien, G., Boulben, S., Duval, A., Ryckaert, M., 2010. Pseudo-nitzschia australis on French Atlantic coast - an unusual toxic bloom. Harmful Algae News 41, 1–2.

Nicolle, A., Dumas, F., Foveau, A., Foucher, E., Thiébaut, E., 2013. Modelling larval dispersal of the king scallop (Pecten maximus) in the English Channel: examples from the bay of Saint-Brieuc and the bay of Seine. Ocean Dyn. 63, 661–678. https://doi.org/10.1007/s10236-013-0617-1

Nishikawa, T., Hori, Y., Harada, K., Imai, I., 2013. Annual regularity of reduction and restoration of cell size in the harmful diatom Eucampia zodiacus, and its application to the occurrence prediction of nori bleaching. Plankton Benthos Res. 8, 166–170. https://doi.org/10.3800/pbr.8.166

O'Boyle, S., Silke, J., 2010. A review of phytoplankton ecology in estuarine and coastal waters around Ireland. J. Plankton Res. 32, 99–118. https://doi.org/10.1093/plankt/fbp097

Oksanen, J., Kindt, R., Legendre, P., O'Hara, B., Stevens, M.H.H., Oksnanen, M.J., Suggests, M.A.S.S., 2007. The vegan package. Community Ecol. Package 10(631-637).

O'Reilly, J.E., Maritorena, S., Mitchell, B.G., Siegel, D.A., Carder, K.L., Garver, S.A., Kahru, M., McClain, C., 1998. Ocean color chlorophyll algorithms for SeaWiFS. J. Geophys. Res. Oceans 103, 24937–24953. https://doi.org/10.1029/98JC02160

Orsini, L., Procaccini, G., Sarno, D., Montresor, M., 2004. Multiple rDNA ITS-types within the diatom Pseudo-nitzschia delicatissima (Bacillariophyceae) and their relative abundances across a spring bloom in the Gulf of Naples. Mar. Ecol. Prog. Ser. 271, 87–98. https://doi.org/10.3354/meps271087

Paches, M., Aguado, D., Martínez-Guijarro, R., Romero, I., 2019. Long-term study of seasonal changes in phytoplankton community structure in the western Mediterranean (Valencian Community). Environ. Sci. Pollut. Res. 26, 14266–14276. https://doi.org/10.1007/s11356-019-04660-x

Paerl, H.W., 1988. Nuisance phytoplankton blooms in coastal, estuarine, and inland waters1: Nuisance blooms. Limnol. Oceanogr. 33, 823–843. https://doi.org/10.4319/lo.1988.33.4part2.0823

Palma, S., Mouriño, H., Silva, A., Barão, M.I., Moita, M.T., 2010. Can Pseudo-nitzschia blooms be modeled by coastal upwelling in Lisbon Bay? Harmful Algae 9, 294–303. https://doi.org/10.1016/j.hal.2009.11.006

Palmer, S.C.J., Kutser, T., Hunter, P.D., 2015. Remote sensing of inland waters: Challenges, progress and future directions. Remote Sens. Environ. 157, 1–8. https://doi.org/10.1016/j.rse.2014.09.021

Pan, Y., Bates, S.S., Cembella, A.D., 1998. Environmental Stress and Domoic Acid Production by Pseudo-nitzschia: a Physio- logical Perspective. Nat Toxins.

Pannard, A., Claquin, P., Klein, C., Le Roy, B., Véron, B., 2008. Short-term variability of the phytoplankton community in coastal ecosystem in response to physical and chemical conditions' changes. Estuar. Coast. Shelf Sci. 80, 212–224. https://doi.org/10.1016/j.ecss.2008.08.008

Parsons, M.L., Dortch, Q., 2002. Sedimentological evidence of an increase in *Pseudo-nitzschia* (Bacillariophyceae)abundance in response to coastal eutrophication. Limnol. Oceanogr. 47, 551–558. https://doi.org/10.4319/lo.2002.47.2.0551

Patil, S., Moeys, S., Von Dassow, P., Huysman, M.J.J., Mapleson, D., De Veylder, L., Sanges, R., Vyverman, W., Montresor, M., Ferrante, M.I., 2015. Identification of the meiotic toolkit in diatoms and exploration of meiosis-specific SPO11 and RAD51 homologs in the sexual species Pseudo-nitzschia multistriata and Seminavis robusta. BMC Genomics 16, 930. https://doi.org/10.1186/s12864-015-1983-5

Pauchet, C., 2017. ers une nouvelle gestion de la pêcherie de coquille Saint-Jacques en rade de Brest ? [Mémoire de fin d'étude]. Plouzané IUEMUBO.

Paulmier, G., 1969. Le microplancton des rivières de Morlaix et de la Penzé. Rev. Trav. Inst. Pêch. Marit. 33, 311–332.

Peacock, E., Olson, R., Sosik, H., 2014. Parasitic infection of the diatom Guinardia delicatula, a recurrent and ecologically important phenomenon on the New England Shelf. Mar. Ecol. Prog. Ser. 503, 1–10. https://doi.org/10.3354/meps10784

Peliz, A., Marchesiello, P., Dubert, J., Marta-Almeida, M., Roy, C., Queiroga, H., 2007. A study of crab larvae dispersal on the Western Iberian Shelf: Physical processes. J. Mar. Syst. 68, 215–236. https://doi.org/10.1016/j.jmarsys.2006.11.007

Peragallo, H., Peragallo, M., 1900. Diatomées marines des France, Grez-sur-Loing, 492 pp.

Percopo, I., Ruggiero, M.V., Balzano, S., Gourvil, P., Lundholm, N., Siano, R., Tammilehto, A., Vaulot, D., Sarno, D., 2016. Pseudo-nitzschia arctica sp. nov., a new cold-water cryptic Pseudo-nitzschia species within the P. pseudodelicatissima complex. J. Phycol. 52, 184–199. https://doi.org/10.1111/jpy.12395

Percopo, I., Ruggiero, M.V., Sarno, D., Longobardi, L., Rossi, R., Piredda, R., Zingone, A., 2022. Phenological segregation suggests speciation by time in the planktonic diatom *Pseudo-nitzschia allochrona* sp. nov. Ecol. Evol. 12, e9155. https://doi.org/10.1002/ece3.9155

Peters, F., Marrasé, C., 2000. Effects of turbulence on plankton: an overview of experimental evidence and some theoretical considerations. Mar. Ecol. Prog. Ser. 205, 291–306. https://doi.org/10.3354/meps205291

Petton, S., Le Berre, D., Haurie, A., Pouvreau, S., 2016. HOMER Campaign : Mooring time series. SEANOE. https://doi.org/10.17882/43082

Petton, S., Le Roy, V., Bellec, G., Queau, I., Le Souchu, P., Pouvreau, S., 2022. Marine environmental station database of Daoulas bay. https://doi.org/10.17882/42493

Petton, S., Pouvreau, S., Dumas, F., 2020. Intensive use of Lagrangian trajectories to quantify coastal area dispersion. Ocean Dyn. 70, 541–559. https://doi.org/10.1007/s10236-019-01343-6

Pinto, A., Botelho, M.J., Churro, C., Asselman, J., Pereira, P., Pereira, J.L., 2023. A review on aquatic toxins - Do we really know it all regarding the environmental risk posed by phytoplankton neurotoxins? J. Environ. Manage. 345, 118769. https://doi.org/10.1016/j.jenvman.2023.118769

Pinto, L., Mateus, M., Silva, A., 2016. Modeling the transport pathways of harmful algal blooms in the Iberian coast. Harmful Algae 53, 8–16. https://doi.org/10.1016/j.hal.2015.12.001

Platt, T.C., Bird, D.F., Sathyendranath, S., 1991. Critical depth and marine primary production. Proc. R. Soc. Lond. B Biol. Sci. 246, 205–217. https://doi.org/10.1098/rspb.1991.0146

Pradhan, B., Kim, H., Abassi, S., Ki, J.-S., 2022. Toxic Effects and Tumor Promotion Activity of Marine Phytoplankton Toxins: A Review. Toxins 14, 397. https://doi.org/10.3390/toxins14060397

Pruesse, E., Quast, C., Knittel, K., Fuchs, B.M., Ludwig, W., Peplies, J., Glockner, F.O., 2007. SILVA: a comprehensive online resource for quality checked and aligned ribosomal RNA sequence data compatible with ARB. Nucleic Acids Res. 35, 7188–7196. https://doi.org/10.1093/nar/gkm864

Punongbayan, A.T., Wang, Y.D., Villanoy, C.L., Yñiguez, A.T., 2022. Connections and clustering of Paralytic Shellfish Toxin events among coastal embayments in an archipelago partly mediated by advection. Harmful Algae 111, 102147.

Quéguiner, B., Tréguer, P., 1984. Studies on the Phytoplankton in the Bay of Brest (Western Europe). Seasonal Variations in Composition, Biomass and Production in Relation to Hydrological and Chemical Features (1981 — 1982). Bot. Mar. 27. https://doi.org/10.1515/botm.1984.27.10.449

Quijano-Scheggia, S., Garcés, E., Flo, E., Diogène, J., Camp, J., 2008. Bloom dynamics of the genus Pseudo-nitzschia (Bacillariophyceae) in two coastal bays (NW Mediterranean Sea). SCI MAR 14.

Quijano-Scheggia, S.I., Garcés, E., Lundholm, N., Moestrup, Ø., Andree, K., Camp, J., 2009. Morphology, physiology, molecular phylogeny and sexual compatibility of the cryptic *Pseudo-nitzschia delicatissima* complex (Bacillariophyta), including the description of *P. arenysensis* sp. nov. Phycologia 48, 492–509. https://doi.org/10.2216/08-21.1

Quiniou, L., 1986. Les peuplements de poissons démersaux de la pointe de Bretagne: environnement, biologie, structure démographique, relations trophiques. Université de Bretagne Occidentale, Brest.

Quiroga, I., 2006. *PSEUDO-NITZSCHIA* BLOOMS IN THE BAY OF BANYULS-SUR-MER, NORTHWESTERN MEDITERRANEAN SEA. Diatom Res. 21, 91–104. https://doi.org/10.1080/0269249X.2006.9705654

Raine, R., McDermott, G., Silke, J., Lyons, K., Nolan, G., Cusack, C., 2010. A simple short range model for the prediction of harmful algal events in the bays of southwestern Ireland. J. Mar. Syst. 83, 150–157. https://doi.org/10.1016/j.jmarsys.2010.05.001

Ralston, D.K., Brosnahan, M.L., Fox, S.E., Lee, K.D., Anderson, D.M., 2015. Temperature and residence time controls on an estuarine harmful algal bloom: Modeling hydrodynamics and Alexandrium fundyense in Nauset estuary. Estuaries Coasts 38, 2240–2258.

Ramond, P., Siano, R., Schmitt, S., de Vargas, C., Marié, L., Memery, L., Sourisseau, M., 2021. Phytoplankton taxonomic and functional diversity patterns across a coastal tidal front. Sci. Rep. 11, 2682. https://doi.org/10.1038/s41598-021-82071-0

Ranjbar, M.H., Hamilton, D.P., Etemad-Shahidi, A., Helfer, F., 2021. Individual-based modelling of cyanobacteria blooms: Physical and physiological processes. Sci. Total Environ. 792, 148418. https://doi.org/10.1016/j.scitotenv.2021.148418

Rantajarvi, E., 1998. Effect of sampling frequency on detection of natural variability in phytoplankton: unattended high-frequency measurements on board ferries in the Baltic Sea. ICES J. Mar. Sci. 55, 697–704. https://doi.org/10.1006/jmsc.1998.0384

Rassoulzadegan, F., Laval-Peuto, M., Sheldon, R.W., 1988. Partitioning of the food ration of marine ciliates between pico- and nanoplankton. Hydrobiologia 159, 75–88. https://doi.org/10.1007/BF00007369

Raven, J.A., Waite, A.M., 2004. The evolution of silicification in diatoms: inescapable sinking and sinking as escape? New Phytol. 162, 45–61. https://doi.org/10.1111/j.1469-8137.2004.01022.x

Rees, H.C., Maddison, B.C., Middleditch, D.J., Patmore, J.R.M., Gough, K.C., 2014. REVIEW: The detection of aquatic animal species using environmental DNA - a review of eDNA as a survey tool in ecology. J. Appl. Ecol. 51, 1450–1459. https://doi.org/10.1111/1365-2664.12306

Reguera, B., Velo-Suárez, L., Raine, R., Park, M.G., 2012. Harmful Dinophysis species: A review. Harmful Algae 14, 87–106. https://doi.org/10.1016/j.hal.2011.10.016

REPHY - French Observation and Monitoring program for Phytoplankton and Hydrology in coastal waters, 2022. REPHY dataset - French Observation and Monitoring program for Phytoplankton and Hydrology in coastal waters. Metropolitan data. https://doi.org/10.17882/47248

REPHYTOX-French Monitoring Program For Phycotoxins In Marine Organisms, 2022. REPHYTOX dataset. French Monitoring program for Phycotoxins in marine organisms. Data since 1987. https://doi.org/10.17882/47251

Reynolds, C.S., 2007. Variability in the provision and function of mucilage in phytoplankton: facultative responses to the environment. Hydrobiologia 578, 37–45. https://doi.org/10.1007/s10750-006-0431-6

Reynolds, C.S., 2006. The ecology of phytoplankton. Cambridge University Press.

Ribalet, F., Berges, J.A., Ianora, A., Casotti, R., 2007. Growth inhibition of cultured marine phytoplankton by toxic algal-derived polyunsaturated aldehydes. Aquat. Toxicol. 85, 219–227. https://doi.org/10.1016/j.aquatox.2007.09.006

Riegman, R., Boer, M.D., Domis, L.D.S., 1996. Growth of harmful marine algae in multispecies cultures. J. Plankton Res. 18, 1851–1866. https://doi.org/10.1093/plankt/18.10.1851

Rimet, F., Gusev, E., Kahlert, M., Kelly, M.G., Kulikovskiy, M., Maltsev, Y., Mann, D.G., Pfannkuchen, M., Trobajo, R., Vasselon, V., Zimmermann, J., Bouchez, A., 2019. Diat.barcode, an open-access curated barcode library for diatoms. Sci. Rep. 9, 15116. https://doi.org/10.1038/s41598-019-51500-6

Rimmelin-Maury, P., Charria, G., Repecaud, M., Quemener, L., Beaumont, L., Guillot, A., Gautier, L., Prigent, S., Le Becque, T., Bihannic, I., Bonnat, A., Le Roux, J.-F., Grossteffan, E., Devesa, J., Bozec, Y., Gautier De Charnacé, C., 2023. COAST-HF-Marel-Iroise buoy's time series (French Research Infrastructure ILICO) : long-term high-frequency monitoring of the Bay of Brest and Iroise sea hydrology. https://doi.org/10.17882/74004

Rines, J.E., 1988. The Chaetoceros Ehrenberg (Bacillariophyceae) flora of Narragansett Bay, Rhode Island, USA. Bibl. Phycol. 79, 1–196.

Rines, J.E.B., Donaghay, P.L., Dekshenieks, M.M., Sullivan, J.M., Twardowski, M.S., 2002. Thin layers and camouflage: hidden Pseudo-nitzschia spp.(Bacillariophyceae) populations in a fjord in the San Juan Islands, Washington, USA. Mar. Ecol. Prog. Ser. 225, 123–137.

Roelke, D., Buyukates, Y., 2001. The Diversity of Harmful Algal Bloom-Triggering Mechanisms and the Complexity of Bloom Initiation. Hum. Ecol. Risk Assess. Int. J. 7, 1347–1362. https://doi.org/10.1080/20018091095041

Rose, J.M., Caron, D.A., 2007. Does low temperature constrain the growth rates of heterotrophic protists? Evidence and implications for algal blooms in cold waters. Limnol. Oceanogr. 52, 886–895. https://doi.org/10.4319/lo.2007.52.2.0886

Rowe, M.D., Anderson, E.J., Wynne, T.T., Stumpf, R.P., Fanslow, D.L., Kijanka, K., Vanderploeg, H.A., Strickler, J.R., Davis, T.W., 2016. Vertical distribution of buoyant *Microcystis* blooms in a Lagrangian particle tracking model for short-term forecasts in Lake Erie. J. Geophys. Res. Oceans 121, 5296–5314. https://doi.org/10.1002/2016JC011720

Ruggiero, M.V., D'Alelio, D., Ferrante, M.I., Santoro, M., Vitale, L., Procaccini, G., Montresor, M., 2018. Clonal expansion behind a marine diatom bloom. ISME J. 12, 463–472. https://doi.org/10.1038/ismej.2017.181

Ruiz-Villarreal, M., García-García, L.M., Cobas, M., Díaz, P.A., Reguera, B., 2016. Modelling the hydrodynamic conditions associated with Dinophysis blooms in Galicia (NW Spain). Harmful Algae 53, 40–52. https://doi.org/10.1016/j.hal.2015.12.003

Russo, M.T., Ruggiero, M.V., Manfellotto, F., Scriven, V., Campbell, L., Montresor, M., Ferrante, M.I., 2021. New alleles in the mating type determination region of West Atlantic strains of Pseudo-nitzschia multistriata. Harmful Algae 103, 101995. https://doi.org/10.1016/j.hal.2021.101995

Russo, M.T., Vitale, L., Entrambasaguas, L., Anestis, K., Fattorini, N., Romano, F., Minucci, C., De Luca, P., Biffali, E., Vyverman, W., Sanges, R., Montresor, M., Ferrante, M.I.,

2018. MRP3 is a sex determining gene in the diatom Pseudo-nitzschia multistriata. Nat. Commun. 9, 5050. https://doi.org/10.1038/s41467-018-07496-0

Sagan, V., Peterson, K.T., Maimaitijiang, M., Sidike, P., Sloan, J., Greeling, B.A., Maalouf, S., Adams, C., 2020. Monitoring inland water quality using remote sensing: potential and limitations of spectral indices, bio-optical simulations, machine learning, and cloud computing. Earth-Sci. Rev. 205, 103187. https://doi.org/10.1016/j.earscirev.2020.103187

Sahraoui, I., Grami, B., Bates, S.S., Bouchouicha, D., Chikhaoui, M.A., Mabrouk, H.H., Hlaili, A.S., 2012. Response of potentially toxic Pseudo-nitzschia (Bacillariophyceae) populations and domoic acid to environmental conditions in a eutrophied, SW Mediterranean coastal lagoon (Tunisia). Estuar. Coast. Shelf Sci. 102–103, 95–104. https://doi.org/10.1016/j.ecss.2012.03.018

Sarker, S., Sultana, T., Islam, N., Hossain, M.S., Huda, A.S., Zulkarnain, K., Sharifuzzaman, S., 2021. Phytoplankton ecology in different coastal habitats along the northern Bay of Bengal. Mar. Ecol. 42. https://doi.org/10.1111/maec.12679

Sarno, D., Zingone, A., Montresor, M., 2010. A massive and simultaneous sex event of two Pseudo-nitzschia species. Deep Sea Res. Part II Top. Stud. Oceanogr. 57, 248–255. https://doi.org/10.1016/j.dsr2.2009.09.012

Sathyendranath, S., Ji, R., Browman, H.I., 2015. Revisiting Sverdrup's critical depth hypothesis. ICES J. Mar. Sci. 72, 1892–1896. https://doi.org/10.1093/icesjms/fsv110

Scalco, E., Amato, A., Ferrante, M.I., Montresor, M., 2016. The sexual phase of the diatom Pseudo-nitzschia multistriata: cytological and time-lapse cinematography characterization. Protoplasma 253, 1421–1431. https://doi.org/10.1007/s00709-015-0891-5

Scalco, E., Stec, K., Iudicone, D., Ferrante, M.I., Montresor, M., 2014. The dynamics of sexual phase in the marine diatom *Pseudo-nitzschia multistriata* (Bacillariophyceae). J. Phycol. 50, 817–828. https://doi.org/10.1111/jpy.12225

Schatz, D., Schleyer, G., Saltvedt, M.R., Sandaa, R.-A., Feldmesser, E., Vardi, A., 2021. Ecological significance of extracellular vesicles in modulating host-virus interactions during algal blooms. ISME J. 15, 3714–3721. https://doi.org/10.1038/s41396-021-01018-5

Schiewer, U., 1998. Hypertrophy of a Baltic estuary — Changes in structure and function of the planktonic community. SIL Proc. 1922-2010 26, 1503–1507. https://doi.org/10.1080/03680770.1995.11900978

Schlüter, M.H., Kraberg, A., Wiltshire, K.H., 2012. Long-term changes in the seasonality of selected diatoms related to grazers and environmental conditions. J. Sea Res. 67, 91–97. https://doi.org/10.1016/j.seares.2011.11.001

Schnetzer, A., Jones, B.H., Schaffner, R.A., Cetinic, I., Fitzpatrick, E., Miller, P.E., Seubert, E.L., Caron, D.A., 2013. Coastal upwelling linked to toxic Pseudo-nitzschia australis

blooms in Los Angeles coastal waters, 2005–2007. J. Plankton Res. 35, 1080–1092. https://doi.org/10.1093/plankt/fbt051

Schnetzer, A., Lampe, R.H., Benitez-Nelson, C.R., Marchetti, A., Osburn, C.L., Tatters, A.O., 2017. Marine snow formation by the toxin-producing diatom, Pseudo-nitzschia australis. Harmful Algae 61, 23–30. https://doi.org/10.1016/j.hal.2016.11.008

Scholin, C.A., Gulland, F., Doucette, G.J., Benson, S., Busman, M., Chavez, F.P., Cordaro, J., DeLong, R., De Vogelaere, A., Harvey, J., Haulena, M., Lefebvre, K., Lipscomb, T., Loscutoff, S., Lowenstine, L.J., Marin Iii, R., Miller, P.E., McLellan, W.A., Moeller, P.D.R., Powell, C.L., Rowles, T., Silvagni, P., Silver, M., Spraker, T., Trainer, V., Van Dolah, F.M., 2000. Mortality of sea lions along the central California coast linked to a toxic diatom bloom. Nature 403, 80–84. https://doi.org/10.1038/47481

Schreiber, S., Hanisak, M.D., Perricone, C.S., Fonnegra, A.C., Sullivan, J., McFarland, M., 2023. Pseudo-nitzschia species, toxicity, and dynamics in the southern Indian River Lagoon, FL. Harmful Algae 126, 102437. https://doi.org/10.1016/j.hal.2023.102437

Seity, Y., Brousseau, P., Malardel, S., Hello, G., Bénard, P., Bouttier, F., Lac, C., Masson, V., 2011. The AROME-France Convective-Scale Operational Model. Mon. Weather Rev. 139, 976–991. https://doi.org/10.1175/2010MWR3425.1

Selander, E., Jakobsen, H.H., Lombard, F., Kiørboe, T., 2011. Grazer cues induce stealth behavior in marine dinoflagellates. Proc. Natl. Acad. Sci. 108, 4030–4034. https://doi.org/10.1073/pnas.1011870108

Shchepetkin, A.F., McWilliams, J.C., 2005. The regional oceanic modeling system (ROMS): a split-explicit, free-surface, topography-following-coordinate oceanic model. Ocean Model. 9, 347–404. https://doi.org/10.1016/j.ocemod.2004.08.002

Shi, K., Zhang, Yunlin, Zhang, Yibo, Li, N., Qin, B., Zhu, G., Zhou, Y., 2019. Phenology of Phytoplankton Blooms in a Trophic Lake Observed from Long-Term MODIS Data. Environ. Sci. Technol. 53, 2324–2331. https://doi.org/10.1021/acs.est.8b06887

SHOM, 2015. MNT Bathymétrique de façade Atlantique (Projet Homonim). http://dx.doi.org/10.17183/MNT_ATL100m_HOMONIM_WGS84

Si, Y., Liu, P., Li, P., Brutnell, T.P., 2014. Model-based clustering for RNA-seq data. Bioinformatics 30, 197–205. https://doi.org/10.1093/bioinformatics/btt632

Sieracki, M.E., Gifford, D.J., Gallager, S.M., Davis, C.S., 1998. Ecology of a Chaetoceros socialis Lauder patch on Georges Bank: distribution, microbial associations, and grazing losses. Oceanography 11, 30–35.

Simon, N., Cras, A.-L., Foulon, E., Lemée, R., 2009. Diversity and evolution of marine phytoplankton. C. R. Biol. 332, 159–170. https://doi.org/10.1016/j.crvi.2008.09.009

Sison-Mangus, M.P., Kempnich, M.W., Appiano, M., Mehic, S., Yazzie, T., 2022. Specific bacterial microbiome enhances the sexual reproduction and auxospore production of the marine diatom, Odontella. Plos One 17, e0276305.

Smayda, T.J., 1997. What is a bloom? A commentary. Limnol. Oceanogr. 42, 1132–1136. https://doi.org/10.4319/lo.1997.42.5_part_2.1132

Smayda, T.J., 1970. The suspension and sinking of phytoplankton in the sea. Ocean. Mar Biol Ann Rev 8, 353–414.

Smida, D.B., Lundholm, N., Kooistra, W.H.C.F., Sahraoui, I., Ruggiero, M.V., Kotaki, Y., Ellegaard, M., Lambert, C., Mabrouk, H.H., Hlaili, A.S., 2014. Morphology and molecular phylogeny of Nitzschia bizertensis sp. nov.—A new domoic acid-producer. Harmful Algae 32, 49–63. https://doi.org/10.1016/j.hal.2013.12.004

Smith, J., Gellene, A.G., Hubbard, K.A., Bowers, H.A., Kudela, R.M., Hayashi, K., Caron, D.A., 2018. Pseudo-nitzschia species composition varies concurrently with domoic acid concentrations during two different bloom events in the Southern California Bight. J. Plankton Res. 40, 29–45. https://doi.org/10.1093/plankt/fbx069

Solé, J., Garcia-Ladona, E., Estrada, M., 2006. The role of selective predation in harmful algal blooms. J. Mar. Syst. 62, 46–54. https://doi.org/10.1016/j.jmarsys.2006.04.002

Sommer, U., Gliwicz, Z.M., Lampert, W., Duncan, A., 1986. The PEG-model of seasonal succession of planktonic events in fresh waters. Arch. Für Hydrobiol. 433–471.

Soontiens, N., Binding, C., Fortin, V., Mackay, M., Rao, Y.R., 2019. Algal bloom transport in Lake Erie using remote sensing and hydrodynamic modelling: Sensitivity to buoyancy velocity and initial vertical distribution. J. Gt. Lakes Res. 45, 556–572. https://doi.org/10.1016/j.jglr.2018.10.003

Soudant, D., Beliaeff, B., Thomas, G., 1997. Explaining Dinophysis cf. acuminata abundance in Antifer (Normandy, France) using dynamic linear regression. Mar. Ecol. Prog. Ser. 156, 67–74. https://doi.org/10.3354/meps156067

Sournia, A., Birrien, J.-L., 1995. La série océanographique côtière de Roscoff (Manche occidentale) de 1985 à 1992. Cah. Biol. Mar. 36(1), 8.

Spatharis, S., Danielidis, D.B., Tsirtsis, G., 2007. Recurrent Pseudo-nitzschia calliantha (Bacillariophyceae) and Alexandrium insuetum (Dinophyceae) winter blooms induced by agricultural runoff. Harmful Algae 6, 811–822. https://doi.org/10.1016/j.hal.2007.04.006

Spyrakos, E., González Vilas, L., Torres Palenzuela, J.M., Barton, E.D., 2011. Remote sensing chlorophyll a of optically complex waters (rias Baixas, NW Spain): Application of a regionally specific chlorophyll a algorithm for MERIS full resolution data during an upwelling cycle. Remote Sens. Environ. 115, 2471–2485. https://doi.org/10.1016/j.rse.2011.05.008

Staehr, P.A., Sand-Jensen, K., 2006. Seasonal changes in temperature and nutrient control of photosynthesis, respiration and growth of natural phytoplankton communities. Freshw. Biol. 51, 249–262. https://doi.org/10.1111/j.1365-2427.2005.01490.x

Steele, J.H., 1976. The role of predation in ecosystem models. Mar. Biol. 35, 9–11. https://doi.org/10.1007/BF00386670

Stern, R., Moore, S., Trainer, V., Bill, B., Fischer, A., Batten, S., 2018. Spatial and temporal patterns of Pseudo-nitzschia genetic diversity in the North Pacific Ocean from the Continuous Plankton Recorder survey. Mar. Ecol. Prog. Ser. 606, 7–28. https://doi.org/10.3354/meps12711

Stone, E.E., 2017. Obligate microbial communities associated with the toxic diatom Pseudo-nitzschia australis genome? Implications for genome assemblies. Clark University.

Straile, D., 1997. Gross growth efficiencies of protozoan and metazoan zooplankton and their dependence on food concentration, predator-prey weight ratio, and taxonomic group. Limnol. Oceanogr. 42, 1375–1385. https://doi.org/10.4319/lo.1997.42.6.1375

Stumpf, R.P., Tomlinson, M.C., Calkins, J.A., Kirkpatrick, B., Fisher, K., Nierenberg, K., Currier, R., Wynne, T.T., 2009. Skill assessment for an operational algal bloom forecast system. J. Mar. Syst. 76, 151–161. https://doi.org/10.1016/j.jmarsys.2008.05.016

Sverdrup, H.U., 1953. On conditions for the vernal blooming of phytoplankton. J Cons Int Explor Mer 18(3), 287–295.

Tammilehto, A., Nielsen, T.G., Krock, B., Møller, E.F., Lundholm, N., 2015. Induction of domoic acid production in the toxic diatom Pseudo-nitzschia seriata by calanoid copepods. Aquat. Toxicol. 159, 52–61. https://doi.org/10.1016/j.aquatox.2014.11.026

Tan, S.N., Lim, H.C., Teng, S.T., Lim, P.T., Leaw, C.P., 2015. Pseudo-nitzschia species (Bacillariophyceae) identification and delineation using mitochondrial cox1 gene sequences as compared to LSU rDNA. Fish. Sci. 81, 831–838. https://doi.org/10.1007/s12562-015-0902-7

Taylor, F.J.R., 1982. Symbioses in marine microplankton. Ann Inst Ocean. 58, 61–90.

Tebbs, E.J., Remedios, J.J., Harper, D.M., 2013. Remote sensing of chlorophyll-a as a measure of cyanobacterial biomass in Lake Bogoria, a hypertrophic, saline–alkaline, flamingo lake, using Landsat ETM+. Remote Sens. Environ. 135, 92–106. https://doi.org/10.1016/j.rse.2013.03.024

Teng, S.T., Lim, H.C., Lim, P.T., Dao, V.H., Bates, S.S., Leaw, C.P., 2014. Pseudo-nitzschia kodamae sp. nov. (Bacillariophyceae), a toxigenic species from the Strait of Malacca, Malaysia. Harmful Algae 34, 17–28. https://doi.org/10.1016/j.hal.2014.02.005

Thébaud, O., Gérard, V., Spyros, F., 2005. Incidences des episodes d'efflorescences de micro algues toxiques sur les ecosystemes et sur les pecheries de coquillages.

Thessen, A.E., Dortch, Q., Parsons, M.L., Morrison, W., 2005. EFFECT OF SALINITY ON *PSEUDO-NITZSCHIA* SPECIES (BACILLARIOPHYCEAE) GROWTH AND DISTRIBUTION. J. Phycol. 41, 21–29. https://doi.org/10.1111/j.1529-8817.2005.04077.x

Thomas, Y., Dumas, F., Andréfouët, S., 2016. Larval connectivity of pearl oyster through biophysical modelling; evidence of food limitation and broodstock effect. Estuar. Coast. Shelf Sci. 182, 283–293. https://doi.org/10.1016/j.ecss.2016.03.010

Thorel, M., Claquin, P., Schapira, M., Le Gendre, R., Riou, P., Goux, D., Le Roy, B., Raimbault, V., Deton-Cabanillas, A.-F., Bazin, P., Kientz-Bouchart, V., Fauchot, J., 2017. Nutrient ratios influence variability in Pseudo-nitzschia species diversity and particulate domoic acid production in the Bay of Seine (France). Harmful Algae 68, 192–205. https://doi.org/10.1016/j.hal.2017.07.005

Thorel, M., Fauchot, J., Morelle, J., Raimbault, V., Le Roy, B., Miossec, C., Kientz-Bouchart, V., Claquin, P., 2014. Interactive effects of irradiance and temperature on growth and domoic acid production of the toxic diatom Pseudo-nitzschia australis (Bacillariophyceae). Harmful Algae 39, 232–241. https://doi.org/10.1016/j.hal.2014.07.010

Thyssen, M., Ferreyra, G., Moreau, S., Schloss, I., Denis, M., Demers, S., 2011. The combined effect of ultraviolet B radiation and temperature increase on phytoplankton dynamics and cell cycle using pulse shape recording flow cytometry. J. Exp. Mar. Biol. Ecol. 406, 95–107. https://doi.org/10.1016/j.jembe.2011.06.015

Torres Palenzuela, J.M., González Vilas, L., Bellas, F.M., Garet, E., González-Fernández, Á., Spyrakos, E., 2019. Pseudo-nitzschia blooms in a coastal upwelling system: Remote sensing detection, toxicity and environmental variables. Water 11, 1954.

Trainer, V.L., Adams, N.G., Bill, B.D., Stehr, C.M., Wekell, J.C., Moeller, P., Busman, M., Woodruff, D., 2000. Domoic acid production near California coastal upwelling zones, June 1998. Limnol. Oceanogr. 45, 1818–1833. https://doi.org/10.4319/lo.2000.45.8.1818

Trainer, V.L., Bates, S.S., Lundholm, N., Thessen, A.E., Cochlan, W.P., Adams, N.G., Trick, C.G., 2012. Pseudo-nitzschia physiological ecology, phylogeny, toxicity, monitoring and impacts on ecosystem health. Harmful Algae 14, 271–300. https://doi.org/10.1016/j.hal.2011.10.025

Trainer, V.L., Hickey, B.M., Bates, S.S., 2008. Toxic Diatoms. In: Walsh PJ et al., eds. Oceans and Human Health : Risks and Remedies from the Seas. Amsterdam: Elsevier. Elsevier 219–237.

Trainer, V.L., Hickey, B.M., Horner, R.A., 2002. Biological and physical dynamics of domoic acid production off the Washington coast. Limnol. Oceanogr. 47, 1438–1446. https://doi.org/10.4319/lo.2002.47.5.1438

Trainer, V.L., Pitcher, G.C., Reguera, B., Smayda, T.J., 2010. The distribution and impacts of harmful algal bloom species in eastern boundary upwelling systems. Prog. Oceanogr., Special Issue on Harmful Algal Blooms in Upwelling Systems 85, 33–52. https://doi.org/10.1016/j.pocean.2010.02.003

Trainer, V.L., Wells, M.L., Cochlan, W.P., Trick, C.G., Bill, B.D., Baugh, K.A., Beall, B.F., Herndon, J., Lundholmf, N., 2009. An ecological study of a massive bloom of toxigenic

Pseudo-nitzschia cuspidata off the Washington State coast. Limnol. Oceanogr. 54, 1461–1474. https://doi.org/10.4319/lo.2009.54.5.1461

Trebitz, A.S., Hoffman, J.C., Darling, J.A., Pilgrim, E.M., Kelly, J.R., Brown, E.A., Chadderton, W.L., Egan, S.P., Grey, E.K., Hashsham, S.A., Klymus, K.E., Mahon, A.R., Ram, J.L., Schultz, M.T., Stepien, C.A., Schardt, J.C., 2017. Early detection monitoring for aquatic non-indigenous species: Optimizing surveillance, incorporating advanced technologies, and identifying research needs. J. Environ. Manage. 202, 299–310. https://doi.org/10.1016/j.jenvman.2017.07.045

Tréguer, P., Bowler, C., Moriceau, B., Dutkiewicz, S., Gehlen, M., Aumont, O., Bittner, L., Dugdale, R., Finkel, Z., Iudicone, D., Jahn, O., Guidi, L., Lasbleiz, M., Leblanc, K., Levy, M., Pondaven, P., 2018. Influence of diatom diversity on the ocean biological carbon pump. Nat. Geosci. 11, 27–37. https://doi.org/10.1038/s41561-017-0028-x

Trombetta, T., Vidussi, F., Mas, S., Parin, D., Simier, M., Mostajir, B., 2019. Water temperature drives phytoplankton blooms in coastal waters. PLOS ONE 14, e0214933. https://doi.org/10.1371/journal.pone.0214933

Turk Dermastia, T., Cerino, F., Stanković, D., Francé, J., Ramšak, A., Žnidarič Tušek, M., Beran, A., Natali, V., Cabrini, M., Mozetič, P., 2020. Ecological time series and integrative taxonomy unveil seasonality and diversity of the toxic diatom Pseudo-nitzschia H. Peragallo in the northern Adriatic Sea. Harmful Algae 93, 101773. https://doi.org/10.1016/j.hal.2020.101773

Turner, J.T., 2014. Planktonic marine copepods and harmful algae. Harmful Algae 32, 81–93. https://doi.org/10.1016/j.hal.2013.12.001

Tweddle, J.F., Strutton, P.G., Foley, D.G., O'Higgins, L., Wood, A.M., Scott, B., Everroad, R.C., Peterson, W.T., Cannon, D., Hunter, M., Forster, Z., 2010. Relationships among upwelling, phytoplankton blooms, and phycotoxins in coastal Oregon shellfish. Mar. Ecol. Prog. Ser. 405, 131–145. https://doi.org/10.3354/meps08497

Utermöhl, H., 1931. Neue Wege in der quantitativen Erfassung des Plankton.(Mit besonderer Berücksichtigung des Ultraplanktons.): Mit 4 Abbildungen im Text. SIL Proc. 1922-2010 5, 567–596. https://doi.org/10.1080/03680770.1931.11898492

Vale, P., Sampayo, M.A.M., 2001. Domoic acid in Portuguese shellfish and fish. Toxicon 39, 893–904. https://doi.org/10.1016/S0041-0101(00)00229-4

Van Beusekom, J.E.E., Mengedoht, D., Augustin, C.B., Schilling, M., Boersma, M., 2009. Phytoplankton, protozooplankton and nutrient dynamics in the Bornholm Basin (Baltic Sea) in 2002–2003 during the German GLOBEC Project. Int. J. Earth Sci. 98, 251–260. https://doi.org/10.1007/s00531-007-0231-x

Vanhoutte-Brunier, A., Fernand, L., Ménesguen, A., Lyons, S., Gohin, F., Cugier, P., 2008. Modelling the Karenia mikimotoi bloom that occurred in the western English Channel during summer 2003. Ecol. Model. 210, 351–376.

Vanormelingen, P., Vanelslander, B., Sato, S., Gillard, J., Trobajo, R., Sabbe, K., Vyverman, W., 2013. Heterothallic sexual reproduction in the model diatom *Cylindrotheca*. Eur. J. Phycol. 48, 93–105. https://doi.org/10.1080/09670262.2013.772242

Velo-Suárez, L., Reguera, B., González-Gil, S., Lunven, M., Lazure, P., Nézan, E., Gentien, P., 2010. Application of a 3D Lagrangian model to explain the decline of a Dinophysis acuminata bloom in the Bay of Biscay. J. Mar. Syst. 83, 242–252. https://doi.org/10.1016/j.jmarsys.2010.05.011

Verity, P., Smetacek, V., 1996. Organism life cycles, predation, and the structure of marine pelagic ecosystems. Mar. Ecol. Prog. Ser. 130, 277–293. https://doi.org/10.3354/meps130277

Villareal, T.A., Adornato, L., Wilson, C., Schoenbaechler, C.A., 2011. Summer blooms of diatom-diazotroph assemblages and surface chlorophyll in the North Pacific gyre: A disconnect. J. Geophys. Res. 116, C03001. https://doi.org/10.1029/2010JC006268

Vinçon-Leite, B., Casenave, C., 2019. Modelling eutrophication in lake ecosystems: A review. Sci. Total Environ. 651, 2985–3001. https://doi.org/10.1016/j.scitotenv.2018.09.320

Visciano, P., Schirone, M., Berti, M., Milandri, A., Tofalo, R., Suzzi, G., 2016. Marine Biotoxins: Occurrence, Toxicity, Regulatory Limits and Reference Methods. Front. Microbiol. 7, 1051. https://doi.org/10.3389/fmicb.2016.01051

Volpert, A., Graff Van Creveld, S., Rosenwasser, S., Vardi, A., 2018. Diurnal fluctuations in chloroplast GSH redox state regulate susceptibility to oxidative stress and cell fate in a bloom-forming diatom. J. Phycol. 54, 329–341. https://doi.org/10.1111/jpy.12638

Vuorio, K., Mäki, A., Salmi, P., Aalto, S.L., Tiirola, M., 2020. Consistency of Targeted Metatranscriptomics and Morphological Characterization of Phytoplankton Communities. Front. Microbiol. 11, 96. https://doi.org/10.3389/fmicb.2020.00096

Walz, P.M., Garrison, D.L., Graham, W.M., Cattey, M.A., Tjeerdema, R.S., Silver, M.W., 1994. Domoic acid-producing diatom blooms in Monterey Bay, California: 1991-1993. Nat. Toxins 2, 271–279. https://doi.org/10.1002/nt.2620020505

Wang, W., Shi, K., Zhang, Yibo, Li, N., Sun, X., Zhang, D., Zhang, Yunlin, Qin, B., Zhu, G., 2022. A ground-based remote sensing system for high-frequency and real-time monitoring of phytoplankton blooms. J. Hazard. Mater. 439, 129623. https://doi.org/10.1016/j.jhazmat.2022.129623

Wang, Z., Wang, C., Li, W., Wang, M., Xiao, L., 2021. Interspecies competition between Scrippsiella acuminata and three marine diatoms: Growth inhibition and allelopathic effects. Aquat. Toxicol. 237, 105878. https://doi.org/10.1016/j.aquatox.2021.105878

Wang, Z., Wang, F., Wang, C., Xie, C., Tang, T., Chen, J., Ji, S., Zhang, S., Zhang, Y., Jiang, T., 2023. Annual variation in domoic acid in phytoplankton and shellfish samples from Daya Bay of the South China Sea. Harmful Algae 127, 102438. https://doi.org/10.1016/j.hal.2023.102438

Wei, Y., Lee, J.-M., Richmond, C., Blattner, F.R., Rafalski, J.A., LaRossa, R.A., 2001. High-Density Microarray-Mediated Gene Expression Profiling of *Escherichia coli*. J. Bacteriol. 183, 545–556. https://doi.org/10.1128/JB.183.2.545-556.2001

Wells, M.L., Trainer, V.L., Smayda, T.J., Karlson, B.S.O., Trick, C.G., Kudela, R.M., Ishikawa, A., Bernard, S., Wulff, A., Anderson, D.M., Cochlan, W.P., 2015. Harmful algal blooms and climate change: Learning from the past and present to forecast the future. Harmful Algae 49, 68–93. https://doi.org/10.1016/j.hal.2015.07.009

Wichard, T., Poulet, S.A., Halsband-Lenk, C., Albaina, A., Harris, R., Liu, D., Pohnert, G., 2005. Survey of the Chemical Defence Potential of Diatoms: Screening of Fifty Species for α,β,γ,δ-unsaturated aldehydes. J. Chem. Ecol. 31, 949–958. https://doi.org/10.1007/s10886-005-3615-z

Wilkerson, F.P., Dugdale, R.C., Hogue, V.E., Marchi, A., 2006. Phytoplankton blooms and nitrogen productivity in San Francisco Bay. Estuaries Coasts 29, 401–416. https://doi.org/10.1007/BF02784989

Wiltshire, K.H., Boersma, M., Carstens, K., Kraberg, A.C., Peters, S., Scharfe, M., 2015. Control of phytoplankton in a shelf sea: Determination of the main drivers based on the Helgoland Roads Time Series. J. Sea Res. 105, 42–52. https://doi.org/10.1016/j.seares.2015.06.022

Wiltshire, K.H., Kraberg, A., Bartsch, I., Boersma, M., Franke, H.-D., Freund, J., Gebühr, C., Gerdts, G., Stockmann, K., Wichels, A., 2010. Helgoland Roads, North Sea: 45 Years of Change. Estuaries Coasts 33, 295–310. https://doi.org/10.1007/s12237-009-9228-y

Wyman, M., Davies, J.T., Crawford, D.W., Purdie, D.A., 2000. Molecular and Physiological Responses of Two Classes of Marine Chromophytic Phytoplankton (Diatoms and Prymnesiophytes) during the Development of Nutrient-Stimulated Blooms. Appl. Environ. Microbiol. 66, 2349–2357. https://doi.org/10.1128/AEM.66.6.2349-2357.2000

Wynne, T.T., Stumpf, R.P., Tomlinson, M.C., Schwab, D.J., Watabayashi, G.Y., Christensen, J.D., 2011. Estimating cyanobacterial bloom transport by coupling remotely sensed imagery and a hydrodynamic model. Ecol. Appl. 21, 2709–2721. https://doi.org/10.1890/10-1454.1

Xiong, J., Shen, J., Qin, Q., Tomlinson, M.C., Zhang, Y.J., Cai, X., Ye, F., Cui, L., Mulholland, M.R., 2023. Biophysical interactions control the progression of harmful algal blooms in Chesapeake Bay: A novel Lagrangian particle tracking model with mixotrophic growth and vertical migration. Limnol. Oceanogr. Lett. 8, 498–508. https://doi.org/10.1002/lol2.10308

Yates, M.C., Derry, A.M., Cristescu, M.E., 2021. Environmental RNA: A Revolution in Ecological Resolution? Trends Ecol. Evol. 36, 601–609. https://doi.org/10.1016/j.tree.2021.03.001

Yentsch, C.S., 1962. MEASUREMENT OF VISIBLE LIGHT ABSORPTION BY PARTICULATE MATTER IN THE OCEAN1. Limnol. Oceanogr. 7, 207–217. https://doi.org/10.4319/lo.1962.7.2.0207

Yuan, X.-L., Cao, M., Bi, G.-Q., 2016. The complete mitochondrial genome of *Pseudo-nitzschia multiseries* (Baciuariophyta). Mitochondrial DNA Part A 27, 2777–2778. https://doi.org/10.3109/19401736.2015.1053061

Zabaglo, K., Chrapusta, E., Bober, B., Kaminski, A., Adamski, M., Bialczyk, J., 2016. Environmental roles and biological activity of domoic acid: A review. Algal Res. 8.

Zhang, Y., Lin, X., Shi, X., Lin, L., Luo, H., Li, L., Lin, S., 2019. Metatranscriptomic Signatures Associated With Phytoplankton Regime Shift From Diatom Dominance to a Dinoflagellate Bloom. Front. Microbiol. 10, 590. https://doi.org/10.3389/fmicb.2019.00590

Zhou, J., Richlen, M.L., Sehein, T.R., Kulis, D.M., Anderson, D.M., Cai, Z., 2018. Microbial Community Structure and Associations During a Marine Dinoflagellate Bloom. Front. Microbiol. 9, 1201. https://doi.org/10.3389/fmicb.2018.01201

Zhou, X., Rowe, M., Liu, Q., Xue, P., 2023. Comparison of Eulerian and Lagrangian transport models for harmful algal bloom forecasts in Lake Erie. Environ. Model. Softw. 162, 105641. https://doi.org/10.1016/j.envsoft.2023.105641

Zhuang, Y., Zhang, H., Hannick, L., Lin, S., 2015. Metatranscriptome profiling reveals versatile N-nutrient utilization, CO2 limitation, oxidative stress, and active toxin production in an Alexandrium fundyense bloom. Harmful Algae 42, 60–70. https://doi.org/10.1016/j.hal.2014.12.006

Zurzolo, C., Bowler, C., 2001. Exploring Bioinorganic Pattern Formation in Diatoms. A Story of Polarized Trafficking. Plant Physiol. 127, 1339–1345. https://doi.org/10.1104/pp.010709

Supplementary material

2019 monitoring data

Dates	Stations	Sampling time	Temperature (°C)	Salinity (PSU)	Ammonium (umol/L)	Nitrite (umol/L)	Nitrate+Nitrite (umol/L)	Phosphate (umol/L)	Silicate (umol/L)	Nitrate (umol/L)	N:P	Si:N	N:Si	Si:P	Picophyto_abun (cell/mL)	Nanophyto_abun (cell/mL)	Microphyto_abun (cell/mL)	PAR_10am_4pm (uE/m2/s)	Wave height (m)	*P. australis* (cell/L)	*Pseudo-nitzschia* thin (cell/L)	Symetric Pseudo-nitzschia (cell/L)	*Pseudo-nitzschia* tapered (cell/L)	Dominant species	Concentration (cell/L)
01/03/2019	Dinan-Kerloc'h	11:30	11,80	34,00	0,69	0,18	4,61	0,25	5,10	4,43	0,06	0,85	0,87	20,22	21482,00	1504,70	179,62	451.0856	0.7884167	NA	NA	NA	NA	NA	NA
01/03/2019	Lanveoc	14:40	11,10	34,10	0,51	0,18	3,75	0,09	8,92	3,57	0,03	0,93	0,40	98,04	33714,00	1474,60	214,67	450.1749	0.10691667	NA	NA	NA	NA	NA	NA
01/03/2019	Telgruc	13:30	11,10	34,50	0,53	0,18	3,67	0,09	4,96	3,49	0,02	0,87	0,70	57,18	13500,00	1583,50	528,10	497.1045	0.6638334	NA	NA	NA	NA	NA	NA
01/03/2019	Sainte-Anne	16:45	11,80	34,10	0,33	0,19	15,29	0,37	7,52	15,09	0,02	0,93	2,01	20,26	25909,00	1679,90	345,70	449.4433	0.5360834	NA	NA	NA	NA	NA	NA
05/03/2019	Dinan-Kerloc'h	10:10	12,10	29,10	0,66	0,21	10,63	0,40	18,57	10,42	0,04	0,96	0,56	46,44	15517,00	921,50	244,06	380.1186	1.3425001	NA	NA	NA	NA	NA	NA
05/03/2019	Lanveoc	11:20	11,10	33,70	0,86	0,25	14,94	0,38	8,12	14,69	0,03	0,88	1,81	21,29	32211,00	1591,00	315,50	380.0768	0.3145833	NA	NA	NA	NA	NA	NA
05/03/2019	Telgruc	13:10	10,80	34,80	0,44	0,26	7,05	0,29	3,53	6,79	0,04	0,83	1,92	12,14	13623,00	1466,10	297,90	386.7005	1.179583	NA	NA	NA	NA	NA	NA
05/03/2019	Sainte-Anne	15:30	11,80	34,30	0,44	0,21	12,43	0,36	6,14	12,22	0,03	0,90	1,99	16,82	15863,00	1388,20	218,69	378.7763	0.8977500	NA	NA	NA	NA	NA	NA
08/03/2019	Dinan-Kerloc'h	10:20	10,80	34,30	0,43	0,22	7,50	0,34	8,40	7,28	0,05	0,93	0,87	24,64	31820,00	2668,30	288,80	441.9672	0.9455000	NA	NA	NA	NA	NA	NA
08/03/2019	Lanveoc	13:20	10,80	34,10	0,53	0,21	15,09	0,37	10,28	14,87	0,02	0,93	1,45	28,16	16510,00	1905,80	268,89	441.1571	0.1845000	NA	NA	NA	NA	NA	NA
08/03/2019	Telgruc	11:50	10,80	34,60	0,87	0,19	4,67	0,17	2,86	4,48	0,04	0,73	1,57	17,13	22293,00	2194,00	180,13	406.9742	0.747500	NA	NA	NA	NA	NA	NA
08/03/2019	Sainte-Anne	NA	12,00	34,20	0,43	0,21	14,14	0,32	7,42	13,93	0,02	0,92	1,88	23,18	19438,00	1552,40	184,35	440.4988	0.6448334	NA	NA	NA	NA	NA	NA
11/03/2019	Dinan-Kerloc'h	10:30	10,60	34,10	0,43	0,21	7,42	0,32	8,73	7,21	0,04	0,93	0,83	27,20	34144,00	2080,60	244,10	673.3113	1.1055001	NA	NA	NA	NA	NA	NA
11/03/2019	Lanveoc	13:40	11,10	33,80	0,48	0,22	15,81	0,33	7,86	15,59	0,02	0,92	1,98	24,17	16058,00	1281,20	202,96	818.3499	0.2109167	NA	NA	NA	NA	NA	NA
11/03/2019	Telgruc	12:15	11,50	34,80	0,68	0,19	3,26	0,15	3,57	3,07	0,05	0,80	0,86	24,22	26568,00	2012,70	391,80	846.8979	1.003750	NA	NA	NA	NA	NA	NA
11/03/2019	Sainte-Anne	15:45	12,20	34,40	0,53	0,20	11,71	0,42	10,10	11,51	0,04	0,93	1,14	24,18	22850,00	1859,80	333,30	671.2758	0.5933334	NA	NA	NA	NA	NA	NA
15/03/2019	Dinan-Kerloc'h	11:00	11,10	34,20	0,52	0,18	7,91	0,31	13,15	7,72	0,04	0,95	0,59	42,02	28225,00	1524,40	151,32	433.4675	0.9195000	NA	300,00	NA	NA	NA	NA
15/03/2019	Lanveoc	12:30	10,80	34,00	0,30	0,20	14,24	0,30	7,09	14,04	0,02	0,93	1,98	23,30	28171,00	1938,10	342,40	432.8839	0.3632500	900,00	1500,00	NA	NA	Rhisolenia setigera	20000,00
15/03/2019	Telgruc	9:40	10,80	34,70	0,48	0,17	2,24	0,08	4,15	2,07	0,04	0,86	0,50	49,00	22188,00	2541,20	391,80	433.8287	1.2555001	80660,00	5200,00	800,00	2100,00	Guinardia delicatula	214000,00
15/03/2019	Sainte-Anne	14:45	11,40	34,20	0,34	0,18	13,16	0,34	8,09	12,97	0,03	0,94	1,60	23,92	34594,00	2128,30	283,80	432.1490	0.8292500	NA	600,00	NA	NA	NA	NA
19/03/2019	Dinan-Kerloc'h	13:10	11,80	34,10	0,60	0,17	6,25	0,24	15,61	6,08	0,04	0,95	0,39	65,06	32362,00	1797,50	266,05	676.7523	0.6011304348	500,00	800,00	NA	NA	Skeletonema	5200,00
19/03/2019	Lanveoc	15:35	10,50	33,70	0,24	0,20	16,96	0,24	12,36	16,76	0,01	0,97	1,36	51,44	25109,00	1986,90	298,00	714.3678	0.02350000	500,00	1100,00	NA	NA	Skeletonema	2700,00
19/03/2019	Telgruc	14:30	10,90	34,80	0,34	0,20	7,02	0,19	8,09	6,82	0,03	0,94	0,84	42,42	28419,00	2285,50	249,50	634.0585	0.3534167	30500,00	2100,00	1400,00	2100,00	Guinardia delicatula	299500,00
19/03/2019	Sainte-Anne	NA	11,10	33,80	0,33	0,17	18,65	0,31	17,90	18,48	0,02	0,97	1,03	57,90	14607,00	1753,90	383,40	674.9142	0.2819167	NA	500,00	NA	NA	Centrique	7200,00
22/03/2019	Dinan-Kerloc'h	16:15	13,40	34,40	0,71	0,16	4,73	0,21	11,56	4,57	0,05	0,93	0,40	54,30	32377,00	1578,90	267,90	868.5985	0.5626666667	NA	3100,00	NA	NA	Rhisolenia setigera	4500,00
22/03/2019	Lanveoc	17:30	11,60	33,90	0,31	0,19	14,68	0,29	15,85	14,49	0,02	0,97	0,91	55,19	26268,00	1918,30	334,10	865.2598	0.01691667	NA	1000,00	NA	NA	Guinardia delicatula	4500,00
22/03/2019	Telgruc	14:45	12,90	34,50	0,58	0,15	3,11	0,09	2,73	2,96	0,03	0,79	1,08	31,09	15462,00	1309,10	405,30	903.9522	0.3892500	19500,00	6700,00	1000,00	800,00	Guinardia delicatula	164400,00
22/03/2019	Sainte-Anne	8:00	11,70	33,80	0,38	0,17	18,53	0,33	11,98	18,36	0,02	0,96	1,53	36,50	30820,00	2570,10	448,00	866.4079	0.1491667	NA	NA	NA	NA	Guinardia delicatula	3100,00
26/03/2019	Dinan-Kerloc'h	8:45	10,00	34,60	0,68	0,17	4,42	0,20	7,08	4,25	0,05	0,89	0,60	35,99	36802,00	695,20	466,70	979.7007	0.3991667	2200,00	NA	NA	NA	Guinardia delicatula	53400,00
26/03/2019	Lanveoc	11:35	11,30	34,10	0,28	0,18	11,58	0,25	5,81	11,40	0,02	0,93	1,96	23,71	38565,00	2706,00	421,70	854.1706	0.01141667	NA	NA	NA	NA	Guinardia delicatula	8900,00
26/03/2019	Telgruc	10:15	10,20	34,80	0,51	0,16	1,55	0,05	1,98	1,39	0,04	0,75	0,70	38,37	23975,00	1252,10	NA	919.0933	0.2645833	2200,00	16200,00	800,00	900,00	Guinardia delicatula	1161000,00
26/03/2019	Sainte-Anne	13:40	12,50	33,10	0,51	0,17	30,21	0,29	17,12	30,04	0,01	0,96	1,76	58,70	28768,00	2167,20	170,18	977.3514	0.05241667	NA	NA	NA	NA	NA	NA
29/03/2019	Dinan-Kerloc'h	8:45	10,10	34,40	0,88	0,14	2,44	0,15	3,26	2,29	0,07	0,76	0,70	21,60	37732,00	1837,10	280,29	1099.0514	0.5692500	NA	NA	NA	NA	NA	NA
29/03/2019	Lanveoc	12:30	11,80	34,10	0,36	0,18	9,79	0,18	16,18	9,61	0,02	0,97	0,59	92,44	19681,00	1603,50	464,00	1061.8531	0.01766667	NA	NA	NA	NA	NA	NA
29/03/2019	Telgruc	11:15	11,30	34,80	0,91	0,15	1,79	0,03	12,20	1,64	0,02	0,92	0,13	385,90	27382,00	1446,80	424,90	1118.8655	0.3444167	NA	NA	NA	NA	NA	NA
29/03/2019	Sainte-Anne	14:45	13,50	31,50	0,44	0,21	45,09	0,24	33,95	44,88	0,01	0,98	1,32	141,80	36521,00	3084,00	301,23	1096.5597	0.09208334	NA	NA	NA	NA	NA	NA

2021 monitoring data

Dates	Stations	Sampling time	Temperature (°C)	Salinity (PSU)	Ammonium (µmol/L)	Nitrite (µmol/L)	Nitrate+Nitrite (µmol/L)	Phosphate (µmol/L)	Silicate (µmol/L)	Nitrate (µmol/L)	N:P	Si:N	N:Si	Si:P	Picophyto_biomass (µg/L)	Nanophyto_biomass (µg/L)	Microphyto_biomas (µg/L)	Picophyto_abun (cell/mL)	Nanophyto_abun (cell/mL)	Microphyto_abun (cell/mL)	Suspended matter (mg/L)	PAR since sunrise (µE/m2/s)	Wave height (m)	*Pseudo-nitzschia spp.* (cell/L)	Intra toxins (pg/cell)	Extra toxins (pg/mL)	Currents (m/s)
26/02/2021	Dinan-Kerloc'h	14:30	11	30,8	0,70	0,31	26,73	0,37	18,90	26,42	74,72	0,69	1,45	51,50	0,18	0,66	0,33	32940,00	2649,80	128,03	5091,99	744,00	0,73	1600,00	NA	NA	0,02
26/02/2021	Telgruc	12:00	10,4	32	0,67	0,31	19,50	0,33	11,00	19,20	61,31	0,55	1,83	33,44	0,50	0,53	0,96	19728,70	1832,65	99,94	3085,52	574,60	0,57	14900,00	NA	NA	0,03
26/02/2021	Lanveoc	15:53	10,7	31,8	0,59	0,30	33,69	0,38	14,55	33,39	89,96	0,42	2,36	38,18	0,52	0,40	0,25	36253,00	1496,70	273,46	5398,77	743,00	0,06	200,00	NA	NA	0,10
26/02/2021	Sainte-Anne	8:30	9,7	30,7	0,91	0,24	38,59	0,48	18,70	38,35	82,97	0,47	2,11	39,28	0,61	0,24	0,23	24170,00	1689,70	421,72	3700,31	187,30	0,28	0,00	NA	NA	0,15
02/03/2021	Dinan-Kerloc'h	8:14	9,5	31,8	0,78	0,29	23,61	0,41	13,08	23,31	59,91	0,54	1,86	32,14	0,09	0,77	0,33	27706,60	1679,26	119,07	4203,01	95,60	0,63	1300,00	0,31	20,90	0,03
02/03/2021	Telgruc	10:30	10	32,2	0,97	0,37	30,01	0,40	16,41	29,64	78,23	0,53	1,89	41,43	0,40	0,18	0,27	23242,10	1265,12	130,00	3507,34	212,00	0,44	5300,00	1,59	3,00	0,03
02/03/2021	Lanveoc	11:55	10,1	32	0,60	0,29	32,68	0,40	14,78	32,39	82,37	0,44	2,25	36,58	0,52	0,34	0,33	29926,50	1151,93	249,51	4445,49	257,90	0,11	0,00	0,00	11,10	0,13
02/03/2021	Sainte-Anne	8:20	11,1	31,2	0,63	0,28	45,34	0,46	22,57	45,06	99,07	0,49	2,04	48,64	0,47	0,26	0,35	26066,00	1483,10	239,40	3942,98	95,10	0,21	0,00	NA	0,00	0,19
05/03/2021	Dinan-Kerloc'h	9:25	9,7	31	1,34	0,33	30,00	0,35	16,71	29,67	90,85	0,53	1,88	48,44	0,38	0,59	0,38	32444,40	1883,20	163,14	4911,32	151,40	0,62	2200,00	4,41	0,00	0,03
05/03/2021	Telgruc	11:44	9,7	32,3	2,21	0,30	31,56	0,45	15,26	31,26	74,71	0,45	2,21	33,76	0,00	0,90	0,41	26028,50	1452,70	165,49	3931,21	484,60	0,33	6700,00	3,97	0,00	0,03
05/03/2021	Lanveoc	13:12	9,7	31,9	1,95	0,28	45,89	0,45	14,85	45,61	105,61	0,31	3,22	32,77	0,57	0,54	0,52	24127,70	1343,50	378,70	3644,12	619,10	0,21	0,00	0,00	NA	0,09
05/03/2021	Sainte-Anne	15:45	10,2	31,9	1,48	0,23	284,60	0,69	129,80	284,37	414,60	0,45	2,20	188,12	0,05	0,69	0,20	15983,00	1239,50	207,96	2487,68	627,00	0,29	0,00	0,00	18,20	0,16
09/03/2021	Dinan-Kerloc'h	10:40	9,4	30,1	1,34	0,32	25,07	0,28	15,11	24,75	93,98	0,57	1,75	53,77	0,00	2,87	0,00	53616,00	2228,80	325,70	7986,17	438,70	0,62	23800,00	2,63	NA	0,01
09/03/2021	Telgruc	13:00	9,8	32	1,41	0,36	33,18	0,32	12,89	32,82	107,08	0,37	2,68	39,92	0,31	0,37	1,63	38292,30	931,53	77,84	5609,82	665,70	0,42	101400,00	4,61	324,20	0,02
09/03/2021	Lanveoc	14:30	9,8	31,9	0,73	0,28	37,58	0,36	14,99	37,30	105,53	0,39	2,56	41,29	0,63	0,74	0,00	26844,40	1332,99	375,30	4031,80	672,00	0,06	1700,00	3,57	16,40	0,07
09/03/2021	Sainte-Anne	16:35	10,6	31,5	1,91	0,28	41,05	0,40	18,27	40,77	107,68	0,43	2,35	45,79	0,48	0,45	0,21	25249,60	1921,10	405,00	3888,57	550,40	0,83	0,00	0,00	27,20	0,13
12/03/2021	Dinan-Kerloc'h	14:20	10,9	31,5	1,44	0,29	26,51	0,40	14,05	26,22	69,35	0,50	1,99	34,86	0,00	1,10	0,08	28162,00	1376,60	212,95	4225,23	339,80	0,85	6200,00	4,40	9,10	0,05
12/03/2021	Telgruc	12:10	10,3	31,5	2,04	0,36	26,78	0,46	15,82	26,43	63,20	0,55	1,82	34,70	1,91	0,00	1,39	29684,00	1250,60	88,88	4424,92	295,90	1,65	98200,00	5,06	803,60	0,09
12/03/2021	Lanveoc	16:00	10,8	31,7	0,89	0,28	34,03	0,39	14,11	33,75	88,84	0,40	2,47	35,91	0,42	0,47	0,15	21501,00	1191,80	298,38	3247,46	373,90	0,51	200,00	NA	0,00	0,10
12/03/2021	Sainte-Anne	8:30	10,1	31,4	6,29	0,31	38,23	0,45	15,71	37,92	100,05	0,35	2,83	35,29	0,23	0,88	0,38	28673,00	1631,40	164,76	4334,86	82,50	1,01	600,00	1,09	68,20	0,15
16/03/2021	Dinan-Kerloc'h	14:20	10,9	31,5	2,20	0,31	29,71	0,32	11,82	29,41	99,11	0,37	2,70	36,71	0,27	0,55	0,51	40060,40	1682,15	177,06	5969,04	361,00	0,54	7800,00	3,99	0,00	0,03
16/03/2021	Telgruc	12:10	10,3	31,5	3,21	0,36	30,61	0,40	12,58	30,25	83,73	0,37	2,69	31,14	0,20	0,96	0,93	23939,00	1543,90	83,43	3645,55	317,00	0,37	67000,00	6,48	2,00	0,03
16/03/2021	Lanveoc	16:00	10,8	31,7	12,54	0,27	36,62	0,40	13,29	36,35	123,83	0,27	3,70	33,46	0,49	0,61	0,19	25581,10	1240,70	255,51	3837,18	364,50	0,16	2100,00	0,34	20,80	0,10
16/03/2021	Sainte-Anne	8:30	10,1	31,4	18,29	0,31	55,46	0,53	24,31	55,15	139,93	0,33	3,03	46,14	0,18	1,06	0,66	27520,00	1696,70	159,42	4181,11	99,80	0,22	0,00	0,00	35,00	0,16
19/03/2021	Dinan-Kerloc'h	8:15	10,1	31,7	7,52	0,33	29,11	0,36	11,76	28,78	100,90	0,32	3,11	32,40	1,37	0,00	1,23	25409,50	1247,08	92,91	3813,53	113,70	0,73	1600,00	2,59	102,80	0,02
19/03/2021	Telgruc	9:50	9,8	32,4	2,27	0,39	24,62	0,16	5,71	24,24	169,10	0,21	4,71	35,94	0,00	2,82	3,34	18931,20	1545,38	174,41	2931,91	179,80	0,41	203800,00	18,08	6139,10	0,04
19/03/2021	Lanveoc	11:10	10,4	31,8	0,88	0,25	32,12	0,37	13,01	31,88	88,71	0,39	2,54	34,97	0,67	0,70	0,41	36242,00	1976,80	566,40	5465,44	221,70	0,26	3200,00	4,39	97,20	0,08
19/03/2021	Sainte-Anne	8:24	10,8	27,1	3,90	0,25	127,16	0,48	51,73	126,91	273,61	0,39	2,53	108,00	0,00	1,71	0,35	24725,00	1360,20	211,05	3742,54	113,40	0,22	700,00	1,69	45,20	0,15
23/03/2021	Dinan-Kerloc'h	8:20	8,7	25,2	3,02	0,21	21,98	0,30	23,08	21,77	82,21	0,92	1,08	75,92	0,00	3,29	0,77	52315,10	2347,20	423,10	7820,48	310,60	0,37	34700,00	NA	345,10	0,02
23/03/2021	Telgruc	10:00	9,9	32,7	2,02	0,48	19,29	0,09	1,68	18,81	226,70	0,08	12,68	17,88	2,96	0,00	3,72	19964,10	1924,80	464,95	3132,31	468,80	0,27	498000,00	9,19	8,70	0,01
23/03/2021	Lanveoc	11:30	10,6	32	1,54	0,26	30,14	0,27	10,15	29,88	118,23	0,32	3,12	37,85	1,12	0,45	0,43	42738,80	1518,50	462,10	6328,61	466,20	0,08	8300,00	3,80	330,80	0,04
23/03/2021	Sainte-Anne	14:00	11,4	27,4	1,28	0,31	102,33	0,29	40,69	102,02	354,83	0,39	2,55	139,36	0,92	0,50	0,01	45302,80	1511,90	483,60	6708,29	889,50	0,16	1000,00	5,09	85,80	0,09
26/03/2021	Dinan-Kerloc'h	12:40	10,6	32,1	4,30	0,44	20,85	0,21	3,48	20,41	117,50	0,14	7,22	16,28	0,00	1,60	2,14	47973,00	1663,80	306,20	7094,86	369,04	0,79	22900,00	NA	13720,60	0,04
26/03/2021	Telgruc	10:35	10,4	32,3	3,16	0,47	22,13	0,08	2,14	21,66	324,18	0,08	11,84	27,38	0,57	0,73	0,64	14089,60	1333,92	338,08	2209,24	276,50	1,05	47200,00	0,97	NA	0,05
26/03/2021	Lanveoc	9:00	10,6	31,8	0,76	0,26	25,58	0,20	8,39	25,32	132,32	0,32	3,14	42,18	0,60	0,73	0,85	34379,70	1264,00	591,50	5098,74	147,60	0,43	14400,00	7,53	129,40	0,07
26/03/2021	Sainte-Anne	15:20	10,9	32,3	2,18	0,33	25,25	0,21	8,89	24,92	133,80	0,32	3,09	43,37	0,49	0,53	0,96	29778,50	1195,31	351,70	4431,75	416,20	0,79	44900,00	8,40	1349,90	0,14
30/03/2021	Dinan-Kerloc'h	9:25	11,2	32,6	0,98	0,36	13,05	0,17	3,04	12,69	85,05	0,22	4,62	18,42	0,85	0,72	1,07	41712,00	2148,10	259,18	6269,40	237,10	0,78	125300,00	1,67	6783,80	0,04
30/03/2021	Telgruc	11:00	12,3	32	0,50	0,41	18,72	0,11	1,03	18,30	181,28	0,05	18,61	9,74	0,98	0,32	1,40	17116,80	2727,80	348,50	2839,38	541,10	0,74	202300,00	0,03	4599,90	0,03
30/03/2021	Lanveoc	8:00	10,8	32,7	0,81	0,33	17,34	0,18	4,42	17,01	103,15	0,24	4,11	25,12	0,83	0,37	1,80	21835,30	1436,72	348,30	3329,18	98,90	0,13	63500,00	5,98	3142,10	0,14
30/03/2021	Sainte-Anne	14:40	13,5	30,4	1,83	0,39	60,29	0,42	22,41	59,90	148,63	0,36	2,77	53,61	0,81	0,57	1,30	22632,00	1773,40	193,67	3494,92	860,40	0,32	44800,00	2,99	416,40	0,19
02/04/2021	Dinan-Kerloc'h	11:05	12	32,8	0,89	0,32	12,67	0,10	4,17	12,35	136,98	0,31	3,25	42,15	0,39	0,60	1,78	15468,80	1516,77	59,54	2433,39	629,40	0,34	207200,00	NA	7844,00	0,02
02/04/2021	Telgruc	12:40	12,6	32,9	1,12	0,37	15,81	0,21	2,09	15,45	82,20	0,12	8,12	10,13	0,00	1,49	0,22	8700,70	585,13	162,09	1329,40	802,50	0,23	43300,00	0,07	3725,00	0,04
02/04/2021	Lanveoc	14:15	12,7	33,1	0,66	0,29	13,83	0,18	2,28	13,53	81,39	0,16	6,35	12,81	0,18	1,58	1,37	11963,20	1499,60	325,20	1926,44	897,30	0,34	21600,00	3,39	3720,00	0,11
02/04/2021	Sainte-Anne	8:00	11,1	31,7	0,55	0,30	31,00	0,16	12,73	30,70	202,22	0,40	2,48	81,62	0,72	0,67	1,26	12826,90	1529,00	492,00	2063,24	111,70	0,30	59700,00	1,96	2861,30	0,18
06/04/2021	Dinan-Kerloc'h	12:05	9,8	34,2	1,05	0,31	10,55	0,19	3,93	10,24	62,03	0,34	2,95	21,02	0,09	0,43	0,00	NA	NA	NA	4,90	663,50	0,34	8700,00	0,03	3322,60	0,02
06/04/2021	Telgruc	9:45	8,7	34,1	2,15	0,35	12,19	0,36	4,82	11,84	40,39	0,34	2,97	13,58	0,35	0,33	0,57	NA	NA	81,74	3,56	476,40	0,15	300,00	NA	5,40	0,02
06/04/2021	Lanveoc	13:15	10,6	33,1	0,61	0,29	13,84	0,07	2,33	13,55	212,41	0,16	6,20	34,25	1,55	0,00	1,94	7078,90	1725,31	279,90	1264,02	750,20	0,19	44000,00	1,09	2402,20	0,05
06/04/2021	Sainte-Anne	15:20	11,7	32,3	0,89	0,28	29,80	0,17	11,48	29,52	184,86	0,37	2,67	69,13	0,57	0,48	0,63	5139,30	1496,80	182,63	958,51	664,40	0,10	23500,00	1,56	3270,90	0,10
09/04/2021	Dinan-Kerloc'h	13:30	11,3	33,2	0,89	0,27	9,21	0,21	3,98	8,94	49,03	0,39	2,53	19,34	0,08	0,81	0,24	5428,00	NA	194,70	908,50	511,10	0,19	200,00	3,50	24,70	0,02
09/04/2021	Telgruc	11:35	10,5	34,1	1,21	0,29	11,96	0,25	3,20	11,67	52,92	0,24	4,12	12,86	0,14	0,46	0,06	4604,73	1304,46	64,32	846,69	530,10	0,07	0,00	NA	1,90	0,02
09/04/2021	Lanveoc	10:15	10,9	33	0,77	0,28	9,58	0,07	0,65	9,30	143,79	0,06	15,85	9,07	0,18	0,57	1,58	3859,10	1055,55	222,90	705,99	322,40	0,02	8600,00	1,84	1331,40	0,08
09/04/2021	Sainte-Anne	7:50	11	33,2	0,68	0,21	12,71	0,16	4,16	12,49	81,62	0,31	3,22	25,37	0,06	1,15	0,40	4978,60	963,70	157,02	853,21	82,80	0,09	3300,00	NA	1046,40	0,14
13/04/2021	Dinan-Kerloc'h	8:10	9,5	34,4	0,72	0,26	10,92	0,15	2,47	10,66	80,30	0,21	4,72	17,02	0,66	0,06	0,34	9657,30	5042,20	69,75	2103,18	387,90	0,21	200,00	NA	107,80	0,03
13/04/2021	Telgruc	9:35	9,8	34,7	3,69	0,27	19,53	0,17	3,67	19,26	135,79	0,16	6,33	21,44	0,72	0,77	0,00	6334,00	5219,75	248,21	1654,72	550,60	0,11	0,00	NA	13,40	0,03
13/04/2021	Lanveoc	11:20	11	33,9	0,78	0,25	12,79	0,06	2,68	12,54	212,00	0,20	5,06	41,89	1,33	0,00	2,52	7961,40	2763,46	260,00	1539,38	701,50	0,09	1200,00	NA	50,40	0,11
13/04/2021	Sainte-Anne	14:30	14,5	26,4	1,21	0,30	127,28	0,34	54,57	126,98	377,93	0,42	2,35	160,50	0,93	0,85	1,37	11807,00	3497,40	218,19	2210,06	662,30	0,10	3600,00	0,17	2,10	0,16
16/04/2021	Dinan-Kerloc'h	8:10	9,7	33,9	0,57	0,17	3,45	0,07	4,13	3,28	54,34	1,03	0,97	55,76	1,60	0,76	0,59	31767,40	6382,80	207,48	5458,56	416,80	0,34	0,00	0,00	68,40	0,02
16/04/2021	Telgruc	10:00	10,2	34,5	0,42	0,22	6,44	0,06	3,54	6,22	110,60	0,52	1,94	57,07	2,83	0,83	1,28	29945,50	15823,10	643,66	6547,51	580,30	0,15	0,00	0,00	80,00	0,04
16/04/2021	Lanveoc	12:05	11,3	33,9	0,46	0,19	10,40	0,09	1,73	10,22	124,87	0,16	6,28	19,90	1,60	0,58	2,85	14886,30	4019,50	471,50	2705,29	953,90	0,13	3100,00	0,83	0,00	0,09
16/04/2021	Sainte-Anne	15:35	13,9	26,9	1,43	0,24	81,36	0,21	133,95	81,12	398,02	1,62	0,62	643,99	0,64	1,34	0,39	13154,00	3936,50	983,29	2533,93	963,40	0,14	0,00	0,00	0,00	0,16

Chapter 2

Supplementary material

Early spring small scale spatio-temporal shift in coastal diatom communities

Léa Prigent[a], Julien Quéré[a], Marie Latimier[a], Florian Caradec[a], Emilie Rabiller[a], Martin Plus[a], Mickaël Le Gac[a]

[a]Ifremer, DYNECO, F-29280 Plouzané, France.

A. Different e-value thresholds test (10^{-30}; 10^{-50}; 10^{-70})

A.1. Diatoms community

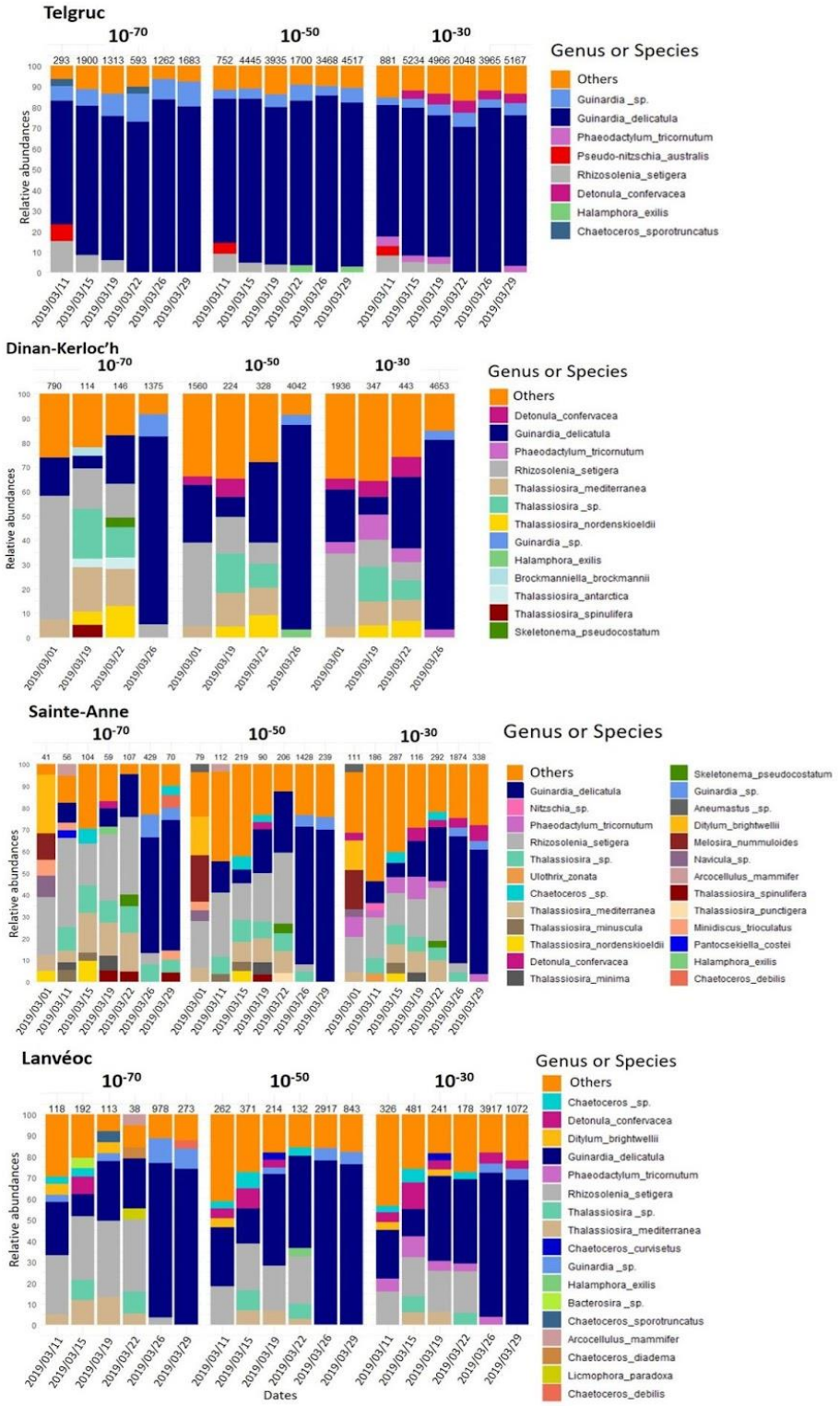

Fig. 1: Comparison of different e-value thresholds of blast outputs for species assignment. The category others regroup class or genus/species lower than 2% of total abundance. The numbers above the barplots are the total number of transcripts for each sample.

A.2. Eukaryote class community

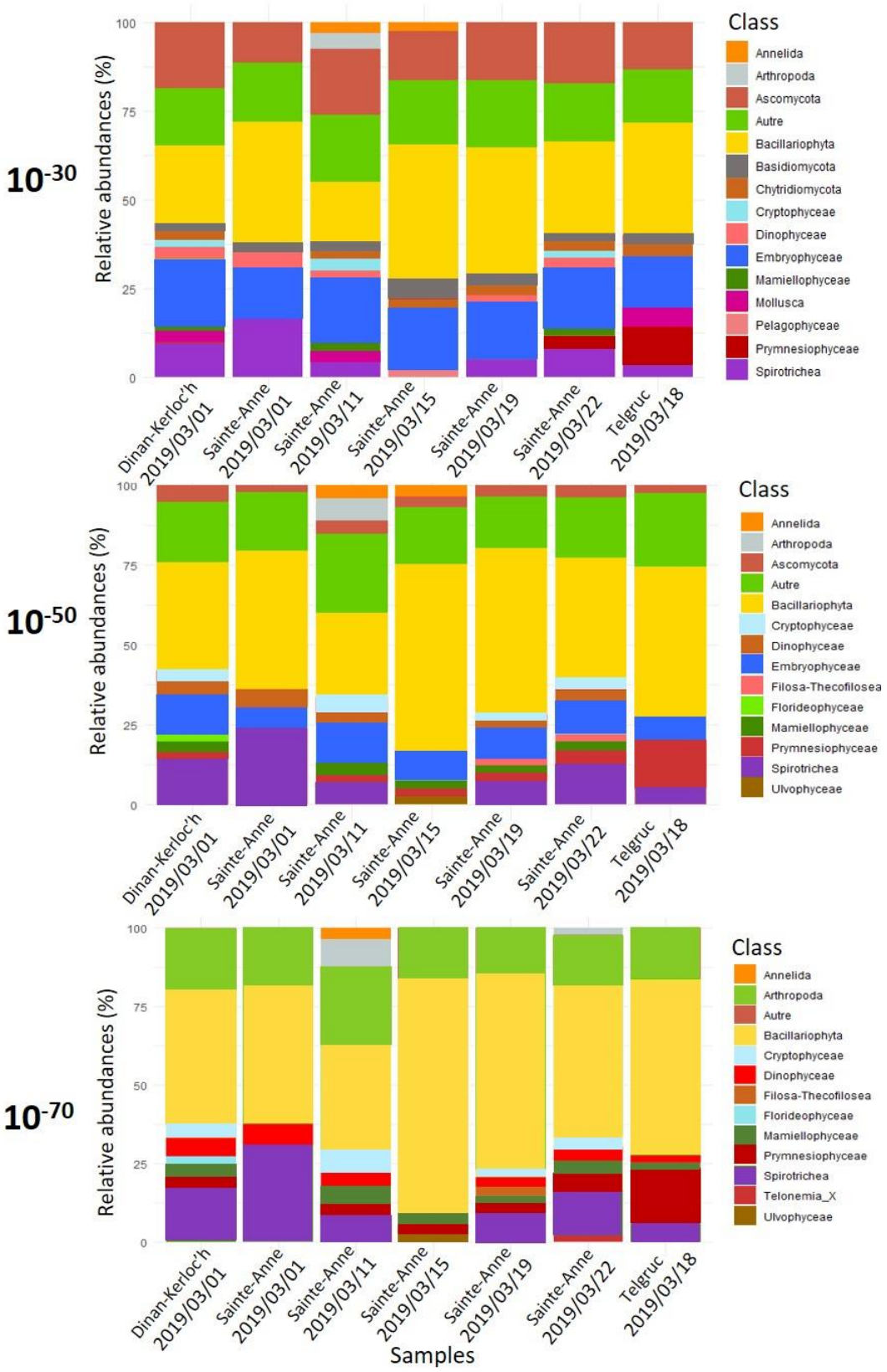

Fig. 2: Comparison of different e-value thresholds of blast outputs for species assignment. The category others regroup class lower than 2% of total abundance. Due to the large output file size, only a few samples were compared.

B. Taxonomic identification, number of corresponding reads

B.1. 2019

Table 1: Number of total environmental reads for each sample, and number of reads used for assignment to genus and species in 2019 samples.

Dates	Stations	Number total reads	Number genus reads	Number diatom reads
2019/03/01	Dinan-Kerloc'h	21376800	Number genus reads	1936
2019/03/01	Lanvéoc	NA	NA	NA
2019/03/01	Telgruc	NA	NA	NA
2019/03/01	Sainte-Anne	10420676	17836	111
2019/03/05	Dinan-Kerloc'h	NA	NA	NA
2019/03/05	Lanvéoc	NA	NA	NA
2019/03/05	Telgruc	NA	NA	NA
2019/03/05	Sainte-Anne	NA	NA	NA
2019/03/08	Dinan-Kerloc'h	NA	NA	NA
2019/03/08	Lanvéoc	NA	NA	NA
2019/03/08	Telgruc	NA	NA	NA
2019/03/08	Sainte-Anne	NA	NA	NA
2019/03/11	Dinan-Kerloc'h	NA	NA	NA
2019/03/11	Lanvéoc	15245583	28420	326
2019/03/11	Telgruc	12643734	28947	886
2019/03/11	Sainte-Anne	11053538	36861	186
2019/03/15	Dinan-Kerloc'h	NA	NA	NA
2019/03/15	Lanvéoc	14584657	42040	481
2019/03/15	Telgruc	12367622	78020	5257
2019/03/15	Sainte-Anne	8539096	19791	287
2019/03/19	Dinan-Kerloc'h	17893311	25200	347
2019/03/19	Lanvéoc	13098667	23277	241
2019/03/19	Telgruc	19086146	55605	5019
2019/03/19	Sainte-Anne	11843341	15259	116
2019/03/22	Dinan-Kerloc'h	14312220	29197	443
2019/03/22	Lanvéoc	11884415	16149	178
2019/03/22	Telgruc	14439424	160325	2067
2019/03/22	Sainte-Anne	13043571	16408	292
2019/03/26	Dinan-Kerloc'h	11399993	136834	4653
2019/03/26	Lanvéoc	11545397	69233	3917
2019/03/26	Telgruc	9409769	240061	3987
2019/03/26	Sainte-Anne	21402032	53917	1874
2019/03/29	Dinan-Kerloc'h	NA	NA	NA
2019/03/29	Lanvéoc	9143197	46062	1072
2019/03/29	Telgruc	13552952	351529	5193
2019/03/29	Sainte-Anne	11861773	26191	338

B.2. 2021

Table 2: Number of total environmental reads for each sample, and number of reads used for assignment to genus and species in 2021 samples.

Dates	Stations	Number total reads	Number genus reads	Number diatom reads
2021/02/26	Dinan-Kerloc'h	31067075	34495	467
2021/02/26	Telgruc	25761923	98008	1097
2021/02/26	Lanvéoc	46038228	223464	1160
2021/02/26	Sainte-Anne	34460848	148128	1465
2021/03/02	Dinan-Kerloc'h	NA	NA	NA
2021/03/02	Telgruc	45204124	574610	4775
2021/03/02	Lanvéoc	53256948	73607	378
2021/03/02	Sainte-Anne	NA	NA	NA
2021/03/05	Dinan-Kerloc'h	44046384	214171	5780
2021/03/05	Telgruc	33265663	89030	1296
2021/03/05	Lanvéoc	38461579	40006	323
2021/03/05	Sainte-Anne	16259233	59805	510
2021/03/09	Dinan-Kerloc'h	59946182	381286	9780
2021/03/09	Telgruc	34176881	75032	1168
2021/03/09	Lanvéoc	31377972	93917	723
2021/03/09	Sainte-Anne	105893092	124456	753
2021/03/12	Dinan-Kerloc'h	30950121	369502	4222
2021/03/12	Telgruc	20418797	33828	587
2021/03/12	Lanvéoc	29635123	25732	116
2021/03/12	Sainte-Anne	37802005	179817	2199
2021/03/16	Dinan-Kerloc'h	43299209	37508	377
2021/03/16	Telgruc	39421780	135929	1438
2021/03/16	Lanvéoc	46422507	96347	589
2021/03/16	Sainte-Anne	25179146	88819	633
2021/03/19	Dinan-Kerloc'h	37480107	60075	780
2021/03/19	Telgruc	47407372	307647	5526
2021/03/19	Lanvéoc	37243840	204075	2392
2021/03/19	Sainte-Anne	42892223	112583	858
2021/03/23	Dinan-Kerloc'h	NA	NA	NA
2021/03/23	Telgruc	34474926	149645	2218
2021/03/23	Lanvéoc	43424475	84276	1404
2021/03/23	Sainte-Anne	37157409	60144	352
2021/03/26	Dinan-Kerloc'h	NA	NA	NA
2021/03/26	Telgruc	24447221	524552	4011
2021/03/26	Lanvéoc	38842577	420746	3813
2021/03/26	Sainte-Anne	36835654	698361	8444
2021/03/30	Dinan-Kerloc'h	27111473	337871	5241
2021/03/30	Telgruc	46464605	176659	1046
2021/03/30	Lanvéoc	35925794	486753	7311
2021/03/30	Sainte-Anne	40642897	205546	1078
2021/04/02	Dinan-Kerloc'h	NA	NA	NA
2021/04/02	Telgruc	36182490	79865	409
2021/04/02	Lanvéoc	28161268	223304	2220
2021/04/02	Sainte-Anne	24103362	106640	1362
2021/04/06	Dinan-Kerloc'h	25095498	58013	884
2021/04/06	Telgruc	NA	NA	NA
2021/04/06	Lanvéoc	33175620	168047	1206
2021/04/06	Sainte-Anne	35410719	278793	2205
2021/04/09	Dinan-Kerloc'h	30709678	74038	410
2021/04/09	Telgruc	NA	NA	NA
2021/04/09	Lanvéoc	40422350	294705	3092
2021/04/09	Sainte-Anne	NA	NA	NA
2021/04/13	Dinan-Kerloc'h	NA	NA	NA
2021/04/13	Telgruc	NA	NA	NA
2021/04/13	Lanvéoc	NA	NA	NA
2021/04/13	Sainte-Anne	36535432	55390	516
2021/04/16	Dinan-Kerloc'h	33459231	611691	6884
2021/04/16	Telgruc	41664174	1584381	5802
2021/04/16	Lanvéoc	34605834	1244546	7405
2021/04/16	Sainte-Anne	38268883	157268	566

C. Environmental data

C.1. 2019

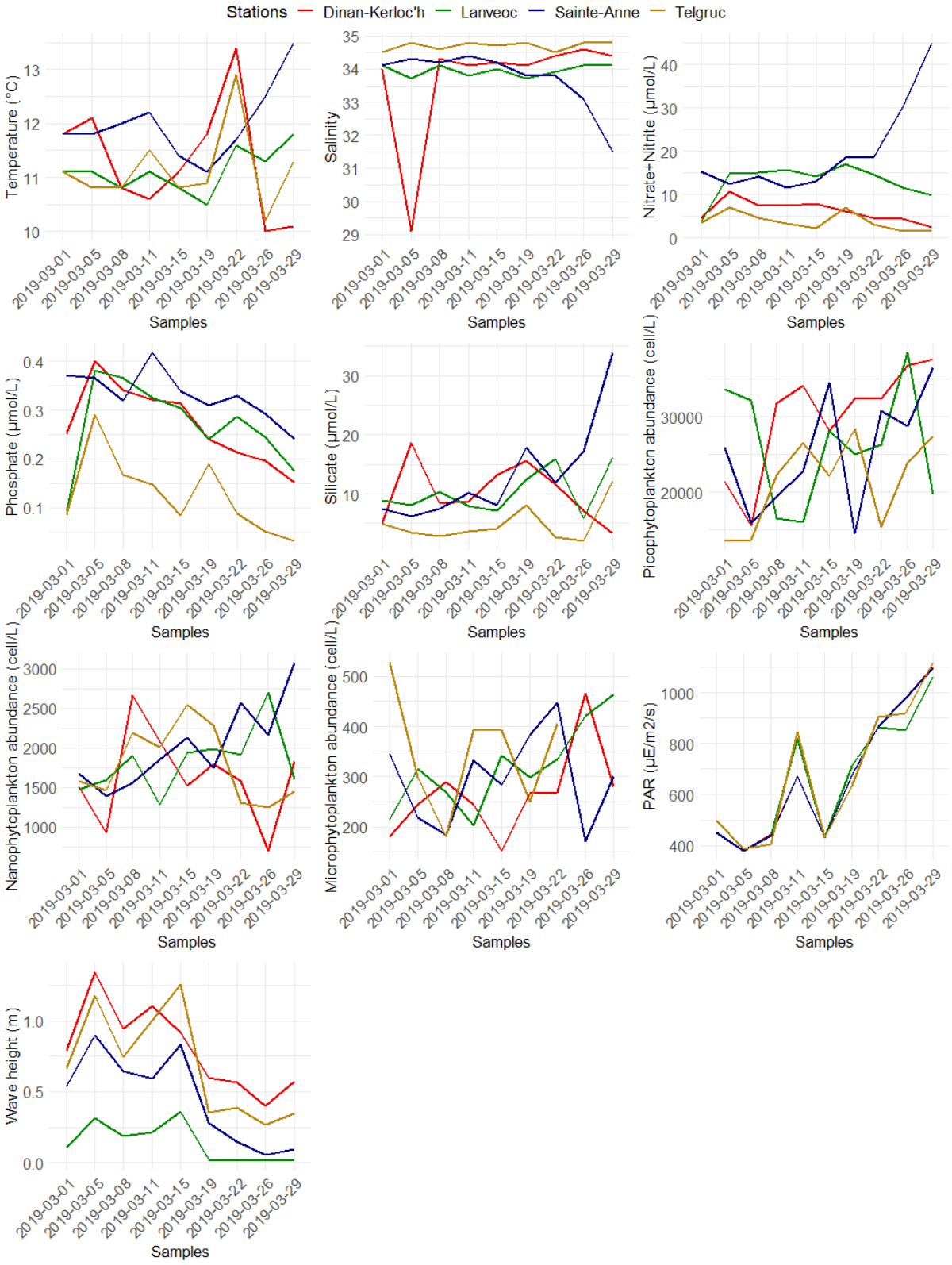

Fig.3: Temporal evolution of environmental parameters during the 2019 monitoring. The different colors correspond to the stations (red: Dinan-Kerloc'h; green: Lanvéoc; blue: Sainte-Anne; yellow: Telgruc)

Table 3: Values of the different parameters used in the 2019 monitoring study according to time and stations.

Sampling stations	03/01	03/05	03/08	03/11	03/15	03/19	03/22	26/03	03/29
Sainte-Anne									
Temperature (°C)	11.8	11.8	12	12.2	11.4	11.1	11.7	12.5	13.5
Salinity	34.1	34.3	34.2	34.4	34.2	33.8	33.8	33.1	31.5
Nitrate + Nitrite (µmol)	15.29	12.43	14.14	11.71	13.16	18.65	18.53	30.21	45.09
Phosphate (µmol)	0.37	0.36	0.32	0.42	0.34	0.31	0.33	0.29	0.24
Silicate (µmol)	7.52	6.14	7.42	10.10	8.09	17.90	11.98	17.12	33.95
Wave height (m)	0.53	0.89	0.64	0.59	0.83	0.28	0.15	0.05	0.09
PAR (µE/m2/s)	449.44	378.77	440.49	671.27	432.14	674.91	866.40	977.35	1096.56
Picophytoplankton abundances (cell/mL)	25909	15863	19438	22850	34594	14607	30820	28768	36521
Nanophytoplankton abundances (cell/mL)	1680	1388	1552	1860	2128	1754	2570	2167	1447
Microphytoplankton abundances (cell/mL)	346	219	184	333	284	383	448	170	301
Lanvéoc									
Temperature (°C)	11.1	11.1	10.8	11.1	10.8	10.5	11.6	11.3	11.8
Salinity	34.1	33.7	34.1	33.8	34	33.7	33.9	34.1	34.1
Nitrate + Nitrite (µmol)	3.75	14.95	15.09	15.81	14.24	16.96	14.68	11.58	9.79
Phosphate (µmol)	0.09	0.38	0.37	0.33	0.30	0.24	0.29	0.25	0.18
Silicate (µmol)	8.92	8.12	10.28	7.86	7.09	12.36	15.85	5.81	16.18
Wave height (m)	0.11	0.31	0.18	0.21	0.36	0.02	0.01	0.01	0.02
PAR (µE/m2/s)	450.17	380.08	441.16	818.35	432.88	714.37	865.26	854.17	1096.55
Picophytoplankton abundances (cell/mL)	33714	32211	16510	16058	28171	25109	26268	38565	19681
Nanophytoplankton abundances (cell/mL)	1475	1591	1906	1281	1938	1987	1918	2706	1603
Microphytoplankton abundances (cell/mL)	215	316	269	203	342	298	334	422	464
Dinan-Kerloc'h									
Temperature (°C)	11.8	12.1	10.8	10.6	11.1	11.8	13.4	10	10.1
Salinity	34	29.1	34.3	34.1	34.2	34.1	34.4	34.6	34.4
Nitrate + Nitrite (µmol)	4.61	10.63	7.50	7.42	7.91	6.25	4.73	4.42	2.44
Phosphate (µmol)	0.25	0.40	0.34	0.32	0.31	0.24	0.21	0.20	0.15
Silicate (µmol)	5.10	18.57	8.40	8.73	13.15	15.61	11.56	7.08	3.26
Wave height (m)	0.78	1.34	0.94	1.11	0.92	0.6	0.56	0.4	0.57
PAR (µE/m2/s)	451.09	380.12	441.97	673.31	433.47	676.75	868.6	979.7	1099.05
Picophytoplankton abundances (cell/mL)	21482	15517	31820	34144	28225	32362	32377	36802	37732
Nanophytoplankton abundances (cell/mL)	1505	922	2668	2081	1524	1798	1579	695	1837
Microphytoplankton abundances (cell/mL)	180	244	289	244	151	266	268	467	280
Telgruc									
Temperature (°C)	11.1	10.8	10.8	11.5	10.8	10.9	12.9	10.2	11.3
Salinity	34.5	34.8	34.6	34.8	34.7	34.8	34.5	34.8	34.8
Nitrate + Nitrite (µmol)	3.67	7.05	4.67	3.26	2.24	7.02	3.11	1.55	1.79
Phosphate (µmol)	0.09	0.29	0.17	0.15	0.08	0.19	0.09	0.05	0.03
Silicate (µmol)	4.96	3.53	2.86	3.57	4.15	8.09	2.73	1.98	12.20
Wave height (m)	0.66	1.18	0.75	1	1.26	0.35	0.39	0.26	0.34
PAR (µE/m2/s)	497.1	386.7	407	846.9	433.83	634.06	903.95	919.09	1118.87
Picophytoplankton abundances (cell/mL)	13500	13623	22293	26568	22188	28419	15462	23975	27382
Nanophytoplankton abundances (cell/mL)	1584	1466	2194	2013	2541	2286	1309	1252	1446
Microphytoplankton abundances (cell/mL)	528	298	180	392	392	250	405	NA	425

C.2. 2021

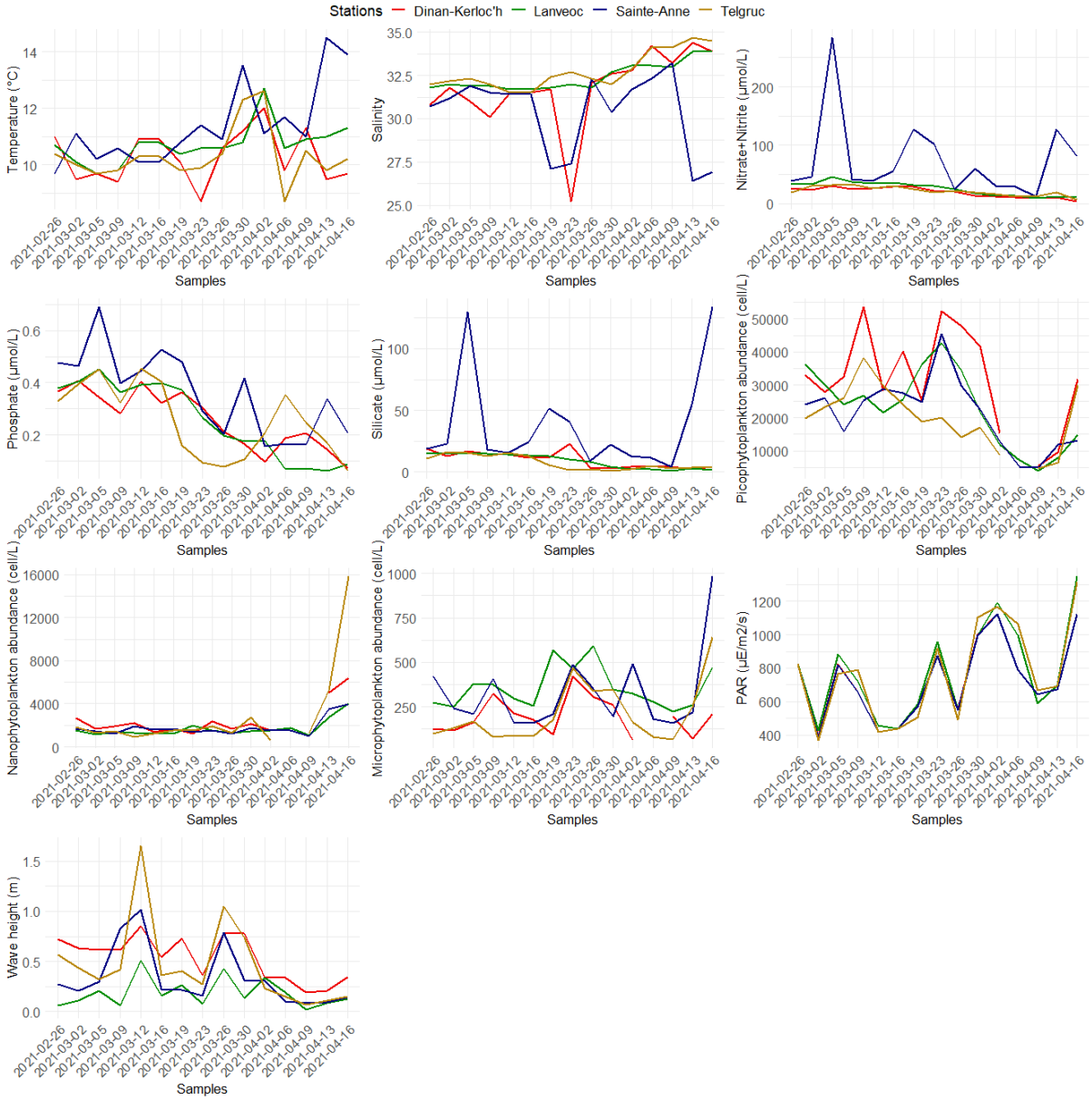

Fig. 4: Temporal evolution of environmental parameters during the 2021 monitoring. The different colors correspond to the stations (red: Dinan-Kerloc'h; green: Lanvéoc; blue: Sainte-Anne; yellow: Telgruc)

Table 4: Values of the different parameters used in the 2019 monitoring study according to time and stations.

Sampling stations	02/26	03/02	03/05	03/09	03/12	03/16	03/19	03/23	03/26	03/30	04/02	04/06	04/09	04/13	04/16
Sainte-Anne															
Temperature (°C)	9.7	11.1	10.2	10.6	10.1	10.1	10.8	11.4	10.9	13.5	11.1	11.7	11	14.5	13.9
Salinity	30.7	31.2	31.9	31.5	31.4	31.4	27.1	27.4	32.3	30.4	31.7	32.3	33.2	26.4	26.9
Nitrate + Nitrite (µmol)	38.59	45.34	284.60	41.05	38.23	55.46	127.16	102.33	25.25	60.29	31	29.80	12.71	127.28	81.36
Phosphate (µmol)	0.48	0.46	0.69	0.40	0.45	0.53	0.48	0.29	0.21	0.42	0.16	0.17	0.16	0.34	0.21
Silicate (µmol)	18.70	22.57	129.80	18.27	15.71	24.31	51.73	40.69	8.89	22.41	12.73	11.48	4.16	54.57	133.95
Wave height (m)	0.28	0.21	0.29	0.83	1.01	0.22	0.22	0.16	0.79	0.32	0.30	0.1	0.1	0.1	0.14
PAR (µE/m2/s)	821.94	386.12	820.14	656.31	416.12	437.48	568.73	870.79	551.74	995.87	1121.16	789.96	642.43	670.16	1122.48
Picophytoplankton abundances (cell/mL)	24170	26066	15983	25249	28673	27520	24725	45302	29779	22632	12826	5139	4979	11807	13154
Nanophytoplankton abundances (cell/mL)	1690	1483	1239	1921	1631	1697	1360	1511	1195	1773	1529	1497	964	3497	3937
Microphytoplankton abundances (cell/mL)	422	239	208	405	165	159	211	484	352	194	492	183	157	218	983
Lanvéoc															
Temperature (°C)	10.7	10.1	9.7	9.8	10.8	10.8	10.4	10.6	10.6	10.8	12.7	10.6	10.9	11	11.3
Salinity	31.8	32	31.9	31.9	31.7	31.7	31.8	32	31.8	32.7	33.1	33.1	33	33.9	33.9
Nitrate + Nitrite (µmol)	33.69	32.68	45.89	37.58	34.03	36.62	32.12	30.14	25.28	17.34	13.83	13.84	9.58	12.79	10.40
Phosphate (µmol)	0.38	0.40	0.45	0.36	0.39	0.40	0.37	0.27	0.20	0.18	0.18	0.07	0.07	0.06	0.09
Silicate (µmol)	14.55	14.78	14.85	14.99	14.11	13.29	13.01	10.15	8.39	4.42	2.28	2.33	0.65	2.68	1.73
Wave height (m)	0.06	0.11	0.21	0.06	0.51	0.16	0.26	0.08	0.43	0.13	0.34	0.19	0.02	0.09	0.12
PAR (µE/m2/s)	823.68	428.14	880.9	723.77	455.97	438.21	586.6	957.87	550.5	993.5	1190.8	997.15	587.9	698.13	1347.92
Picophytoplankton abundances (cell/mL)	36253	29927	24128	26844	21501	25581	36242	42739	34380	21835	11963	7079	3859	7961	14886
Nanophytoplankton abundances (cell/mL)	1497	1152	1344	1333	1192	1241	1977	1519	1264	1437	1500	1725	1056	2763	4020
Microphytoplankton abundances (cell/mL)	273	250	379	375	298	256	566	462	592	348	325	280	223	260	472
Dinan-Kerloc'h															
Temperature (°C)	11	9.5	9.7	9.4	10.9	10.9	10.1	8.7	10.6	11.2	12	9.8	11.3	9.5	9.7
Salinity	30.8	31.8	31	30.1	31.5	31.5	31.7	25.2	32.1	32.6	32.8	34.2	33.2	34.4	33.9
Nitrate + Nitrite (µmol)	26.73	23.61	30	25.07	26.51	29.71	29.11	21.98	20.85	13.05	12.67	10.55	9.21	10.92	3.45
Phosphate (µmol)	0.37	0.41	0.35	0.28	0.40	0.32	0.36	0.30	0.21	0.17	0.10	0.19	0.21	0.15	0.07
Silicate (µmol)	18.90	13.08	16.71	15.11	14.05	11.82	11.76	23.08	3.48	3.04	4.17	3.93	3.98	2.47	4.13
Wave height (m)	0.73	0.63	0.62	0.62	0.85	0.54	0.73	0.37	0.79	0.78	0.34	0.34	0.20	0.21	0.34
PAR (µE/m2/s)	825	387.55	822.86	658.36	417.45	438.79	570.31	872.95	553.16	998.1	1123.56	791.61	643.77	671.48	1124.46
Picophytoplankton abundances (cell/mL)	32940	27707	32444	53616	28162	40060	25410	52315	47973	41712	15469	NA	5428	9657	31767
Nanophytoplankton abundances (cell/mL)	2650	1679	1883	2229	1377	1682	1247	2347	1664	2148	1517	NA	NA	5042	6383
Microphytoplankton abundances (cell/mL)	128	119	163	326	213	177	93	423	306	259	60	NA	195	70	207
Telgruc															
Temperature (°C)	10.4	10	9.7	9.8	10.3	10.3	9.8	9.9	10.4	12.3	12.6	8.7	10.5	9.8	10.2
Salinity	32	32.2	32.3	32	31.5	31.5	32.4	32.7	32.3	32	32.9	34.1	34.1	34.7	34.5
Nitrate + Nitrite (µmol)	19.50	30.01	31.56	33.18	26.78	30.61	24.62	19.29	22.13	18.72	15.81	12.19	11.96	19.53	6.44
Phosphate (µmol)	0.33	0.40	0.45	0.32	0.46	0.40	0.16	0.09	0.08	0.11	0.21	0.36	0.25	0.17	0.06
Silicate (µmol)	11	16.41	15.26	12.89	15.82	12.58	5.71	1.68	2.14	1.03	2.09	4.82	3.20	3.67	3.54
Wave height (m)	0.06	0.11	0.21	0.06	0.51	0.16	0.26	0.08	0.43	0.13	0.34	0.2	0.02	0.09	0.13
PAR (µE/m2/s)	825.89	367.18	765.23	788.39	417.82	439.15	503.88	915.99	491.54	1101.3	1167.79	1065.08	669.12	691.99	1315.36
Picophytoplankton abundances (cell/mL)	19729	23242	26029	38292	29684	23939	18931	19964	14090	17117	8701	NA	4605	6334	29945
Nanophytoplankton abundances (cell/mL)	1833	1265	1453	932	1251	1544	1545	1925	1334	2728	585	NA	1304	5220	15823
Microphytoplankton abundances (cell/mL)	100	130	165	78	89	83	174	465	338	349	162	82	64	248	644

D. Relative abundances class communities

D.1. 2019

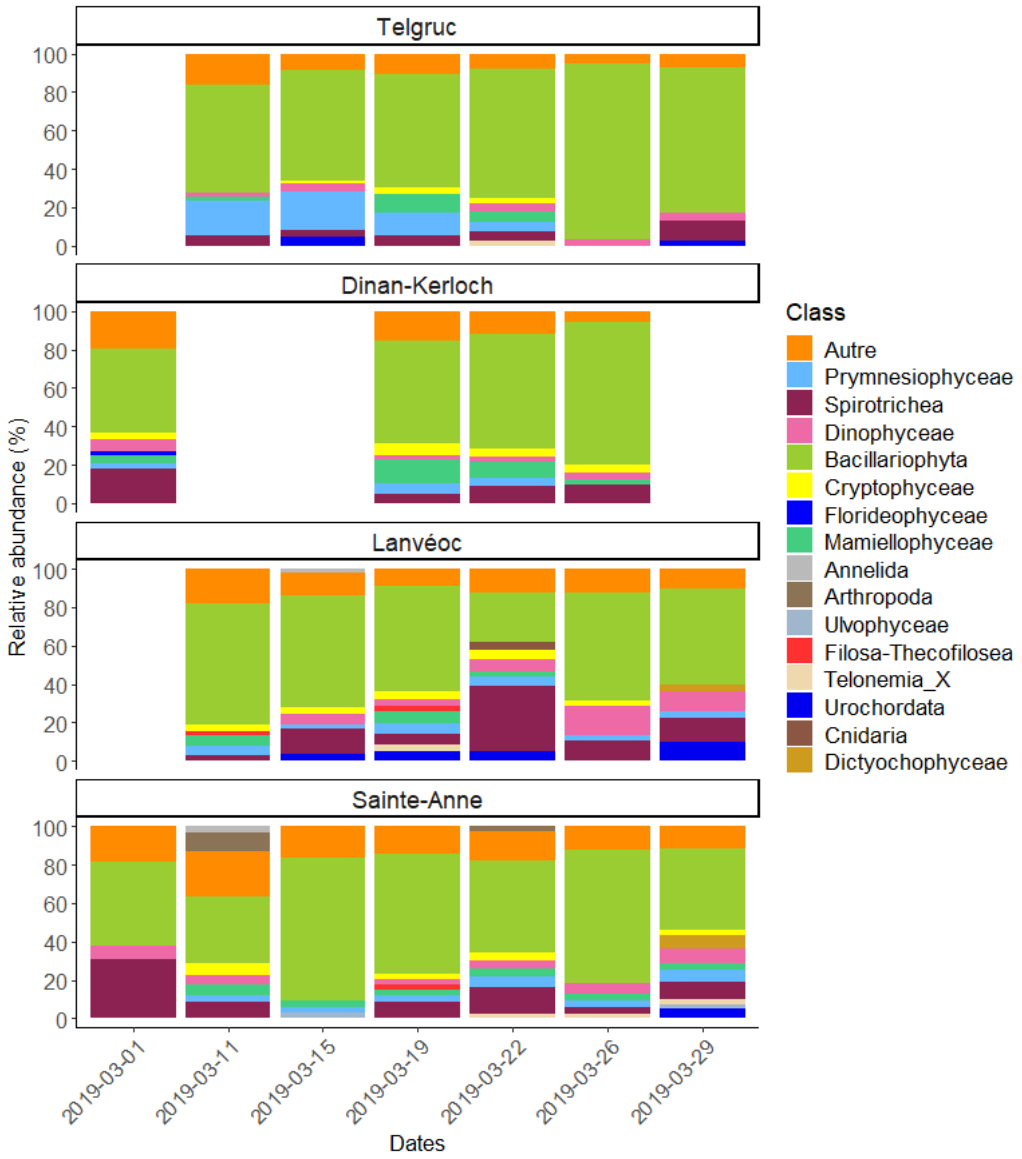

Fig. 5: Relative abundances of the class community composition during the 2019 monitoring (the category others regroup class lower than 2% of total abundance). Blank areas correspond to missing data.

D.2. 2021

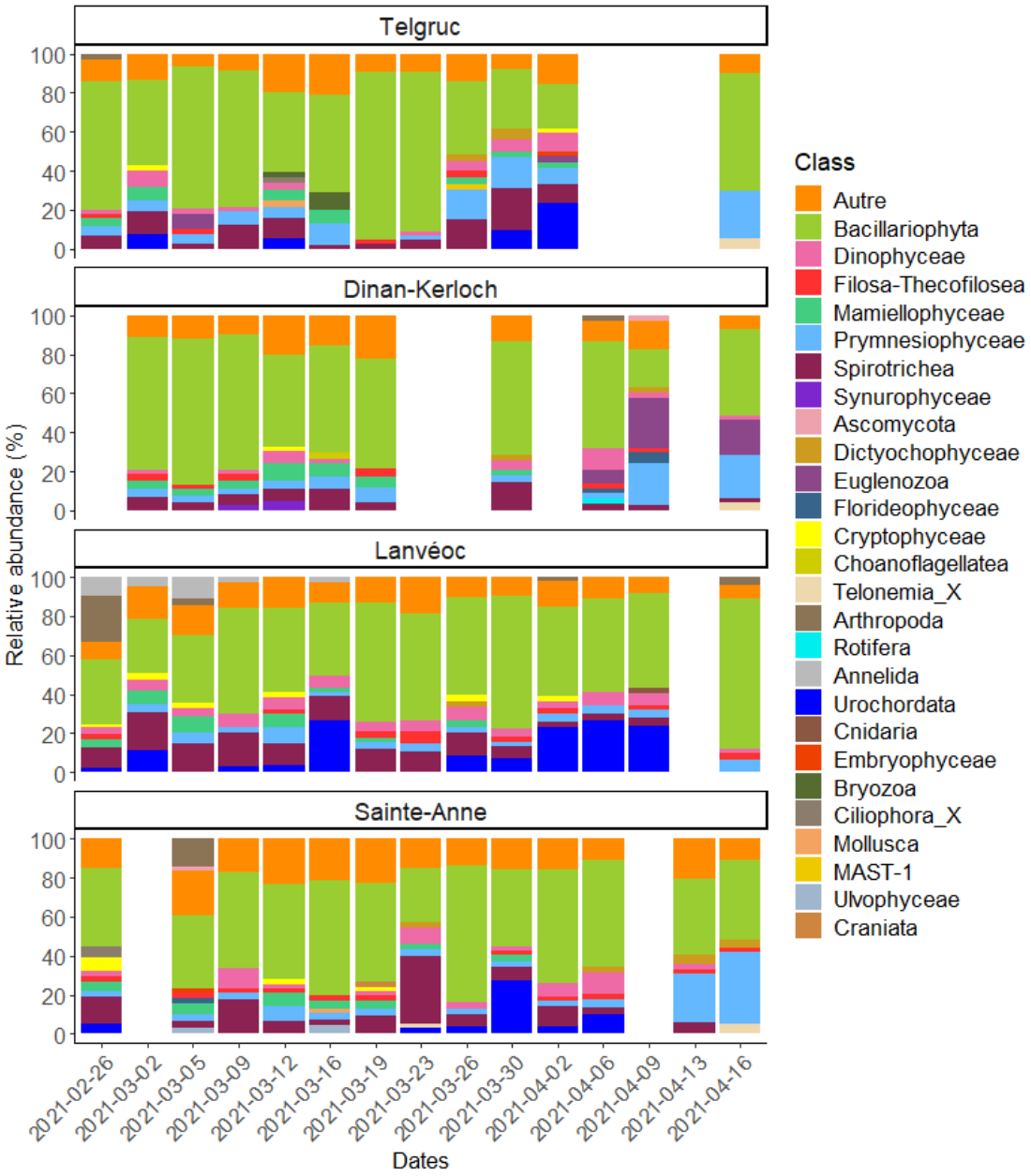

Fig. 6: Relative abundances of the class community composition during the 2021 monitoring (the category others regroup class lower than 2% of total abundance). Blank areas correspond to missing data.

E. *Pseudo-nitzschia sp.* light microscopy counts

Table 5: Light microscopic counts of cells (cell/L) of the genus Pseudo-nitzschia from the 2019 monitoring samples from the 2019/03/01 to 2019/03/29 for the four monitoring stations (Telgruc, Dinan-Kerloc'h, Lanvéoc and Sainte-Anne).

	03/01	03/05	03/08	03/11	03/15	03/19	03/22	26/03	03/29
Telgruc	38100	39300	20700	66000	88760	36100	28000	20100	14400
Dinan-Kerloc'h	500	1100	1400	1100	300	1300	3100	2200	1200
Lanvéoc	200	0	1200	1000	2400	1600	1000	0	500
Sainte-Anne	900	200	300	0	600	400	0	1000	1400

Table 6: Light microscopic counts of cells (cell/L) of the genus Pseudo-nitzschia from the 2021 monitoring samples from the 2021/02/26 to 2021/04/16 for the four monitoring stations (Telgruc, Dinan-Kerloc'h, Lanvéoc and Sainte-Anne).

	26/02	02/03	05/03	09/03	12/03	16/03	19/03	23/03	26/03	30/03	02/04	06/04	09/04	13/04	16/04
Telgruc	14900	5300	6700	101400	98200	67000	203800	498000	47200	202300	43300	300	0	0	0
Dinan-Kerloc'h	1600	1300	2200	23800	6200	7800	1600	34700	22900	125300	207200	8700	200	200	0
Lanvéoc	200	0	0	1700	200	2100	3200	8300	14400	63500	21600	44000	8600	1200	3100
Sainte-Anne	0	0	0	0	600	0	700	1000	44900	44800	59700	23500	3300	3600	0

F. Rbcl gene expression

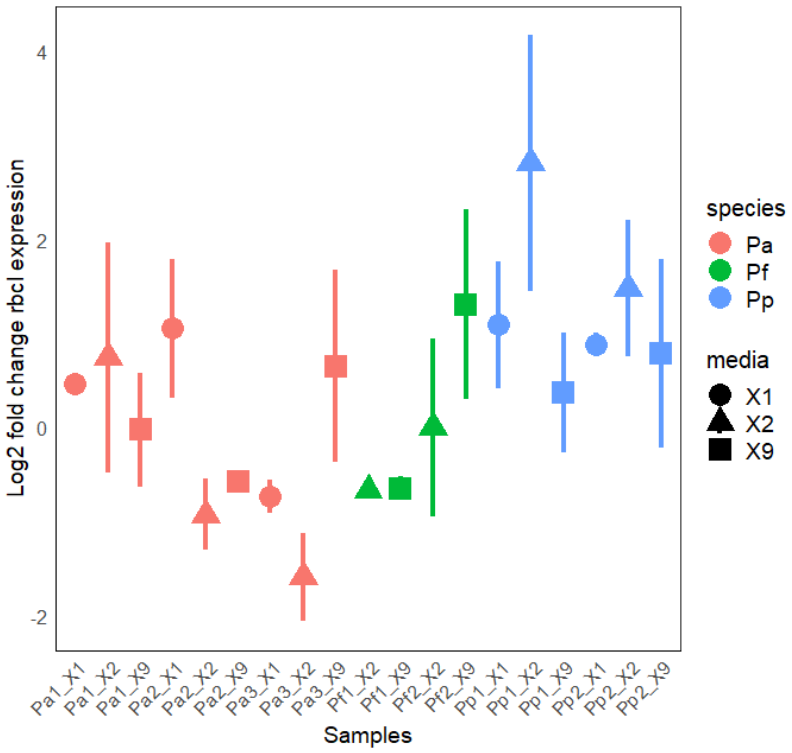

Fig.7: Rbcl gene expression in Pseudo-nitzschia australis (Pa), Pseudo-nitzschia fraudulenta (Pf) and Pseudo-nitzschia pungens (Pp). Shape and colors indicate strains and media, respectively. Media X1 corresponded to low phosphate, media X2 low nitrate and media X9: nutrient replete environment. Different replicates were present for each strain and media, the average expression and standard error is given for each strain in each medium.

More informations about the methods in Lema et al. in 2019.

Chapter 3

Supplementary material

Caractérisation interannuelle de la connectivité hydrodynamique entre la baie de Douarnenez et la rade de Brest

Léa Prigent[a], Mickaël Le Gac[a], Martin Plus[a]

[a]Ifremer, DYNECO, F-29280 Plouzané, France.

Des différences interannuelles de connectivités hydrodynamique

1. Pmax

Matrices de connectivité représentant les Pmax de 19 traceurs dans les 19 zones pour les 4 années simulées. La matrice est à lire à l'horizontale en considérant dans les différentes zones, l'arrivée des traceurs venant des 19 autres stations. Par exemple en 2021, la zone 10 reçoit au maximum 50.1 % du traceur parti de la zone 5.

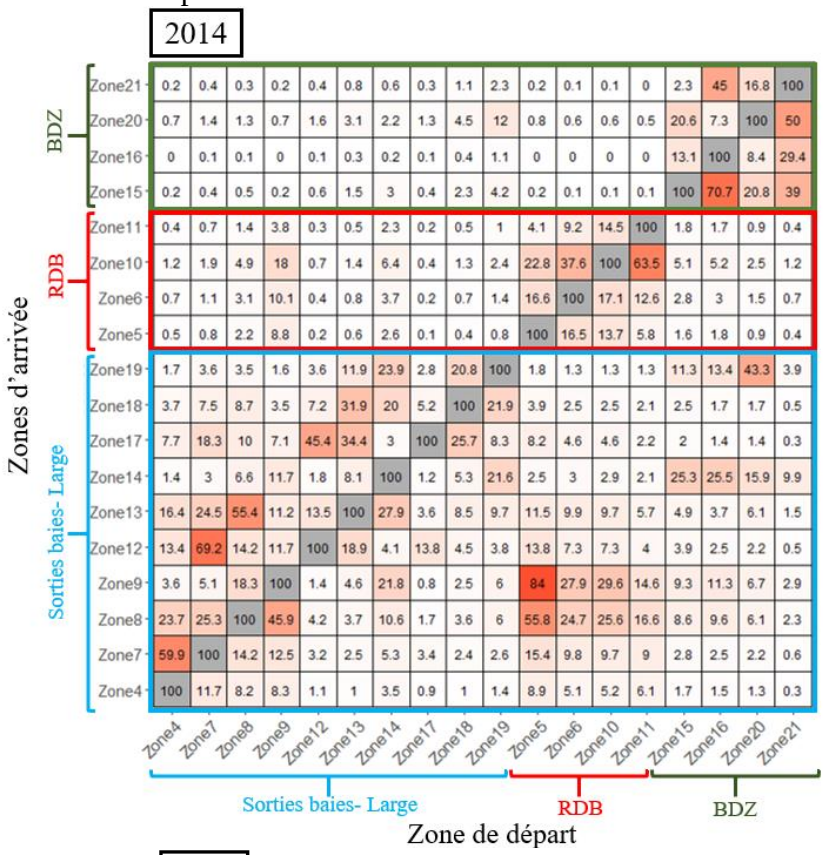

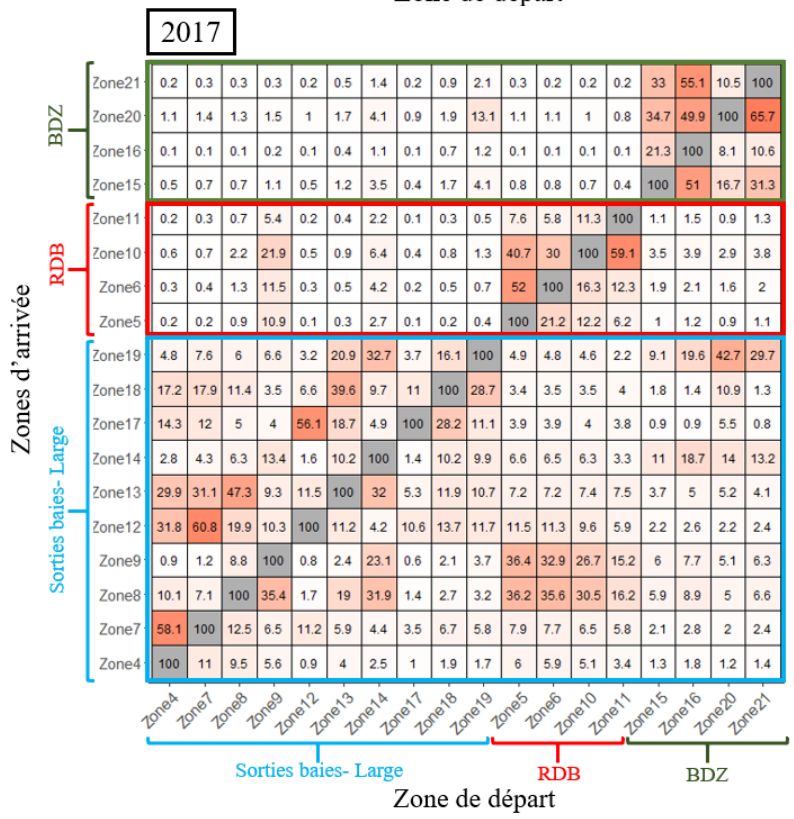

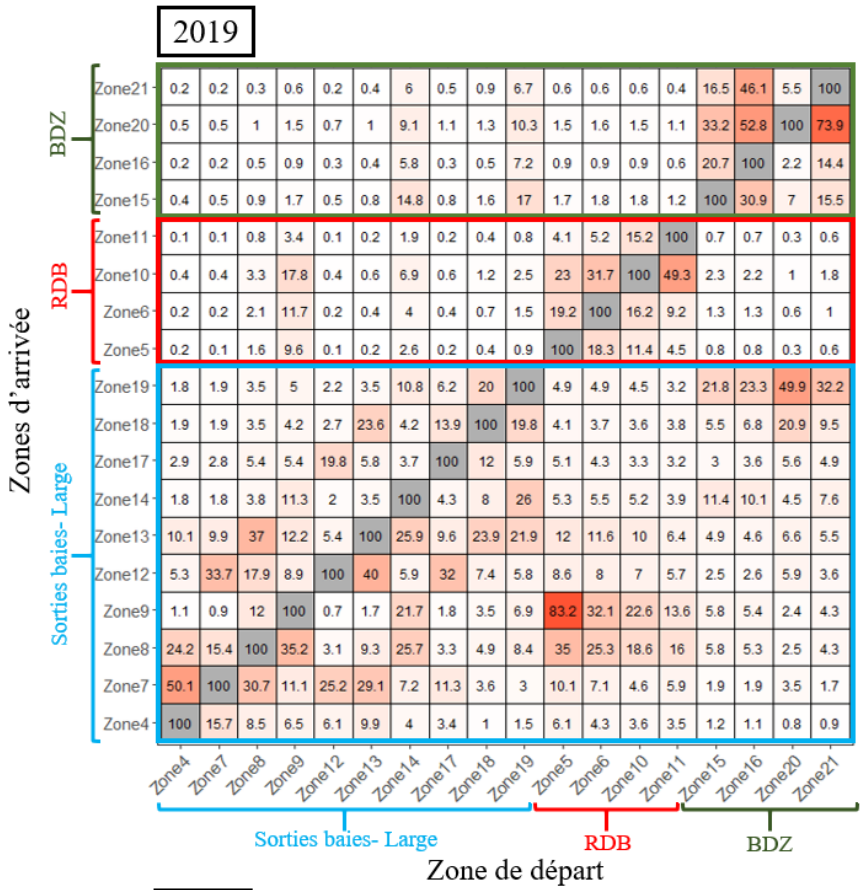
2019
Zones d'arrivée
BDZ
RDB
Sorties baies- Large
Zone21 0.2 0.2 0.3 0.6 0.2 0.4 6 0.5 0.9 6.7 0.6 0.6 0.6 0.4 16.5 46.1 5.5 100
Zone20 0.5 0.5 1 1.5 0.7 1 9.1 1.1 1.3 10.3 1.5 1.6 1.5 1.1 33.2 52.8 100 73.9
Zone16 0.2 0.2 0.5 0.9 0.3 0.4 5.8 0.3 0.5 7.2 0.9 0.9 0.9 0.6 20.7 100 2.2 14.4
Zone15 0.4 0.5 0.9 1.7 0.5 0.8 14.8 0.8 1.6 17 1.7 1.8 1.8 1.2 100 30.9 7 15.5
Zone11 0.1 0.1 0.8 3.4 0.1 0.2 1.9 0.2 0.4 0.8 4.1 5.2 15.2 100 0.7 0.7 0.3 0.6
Zone10 0.4 0.4 3.3 17.8 0.4 0.6 6.9 0.6 1.2 2.5 23 31.7 100 49.3 2.3 2.2 1 1.8
Zone6 0.2 0.2 2.1 11.7 0.2 0.4 4 0.4 0.7 1.5 19.2 100 16.2 9.2 1.3 1.3 0.6 1
Zone5 0.2 0.1 1.6 9.6 0.1 0.2 2.6 0.2 0.4 0.9 100 18.3 11.4 4.5 0.8 0.8 0.3 0.6
Zone19 1.8 1.9 3.5 5 2.2 3.5 10.8 6.2 20 100 4.9 4.9 4.5 3.2 21.8 23.3 49.9 32.2
Zone18 1.9 1.9 3.5 4.2 2.7 23.6 4.2 13.9 100 19.8 4.1 3.7 3.6 3.8 5.5 6.8 20.9 9.5
Zone17 2.9 2.8 5.4 5.4 19.8 5.8 3.7 100 12 5.9 5.1 4.3 3.3 3.2 3 3.6 5.6 4.9
Zone14 1.8 1.8 3.8 11.3 2 3.5 100 4.3 8 26 5.3 5.5 5.2 3.9 11.4 10.1 4.5 7.6
Zone13 10.1 9.9 37 12.2 5.4 100 25.9 9.6 23.9 21.9 12 11.6 10 6.4 4.9 4.6 6.6 5.5
Zone12 5.3 33.7 17.9 8.9 100 40 5.9 32 7.4 5.8 8.6 8 7 5.7 2.5 2.6 5.9 3.6
Zone9 1.1 0.9 12 100 0.7 1.7 21.7 1.8 3.5 6.9 83.2 32.1 22.6 13.6 5.8 5.4 2.4 4.3
Zone8 24.2 15.4 100 35.2 3.1 9.3 25.7 3.3 4.9 8.4 35 25.3 18.6 16 5.8 5.3 2.5 4.3
Zone7 50.1 100 30.7 11.1 25.2 29.1 7.2 11.3 3.6 3 10.1 7.1 4.6 5.9 1.9 1.9 3.5 1.7
Zone4 100 15.7 8.5 6.5 6.1 9.9 4 3.4 1 1.5 6.1 4.3 3.6 3.5 1.2 1.1 0.8 0.9
Zone4 Zone7 Zone8 Zone9 Zone12 Zone13 Zone14 Zone17 Zone18 Zone19 Zone5 Zone6 Zone10 Zone11 Zone15 Zone16 Zone20 Zone21
Sorties baies- Large
RDB
BDZ
Zone de départ

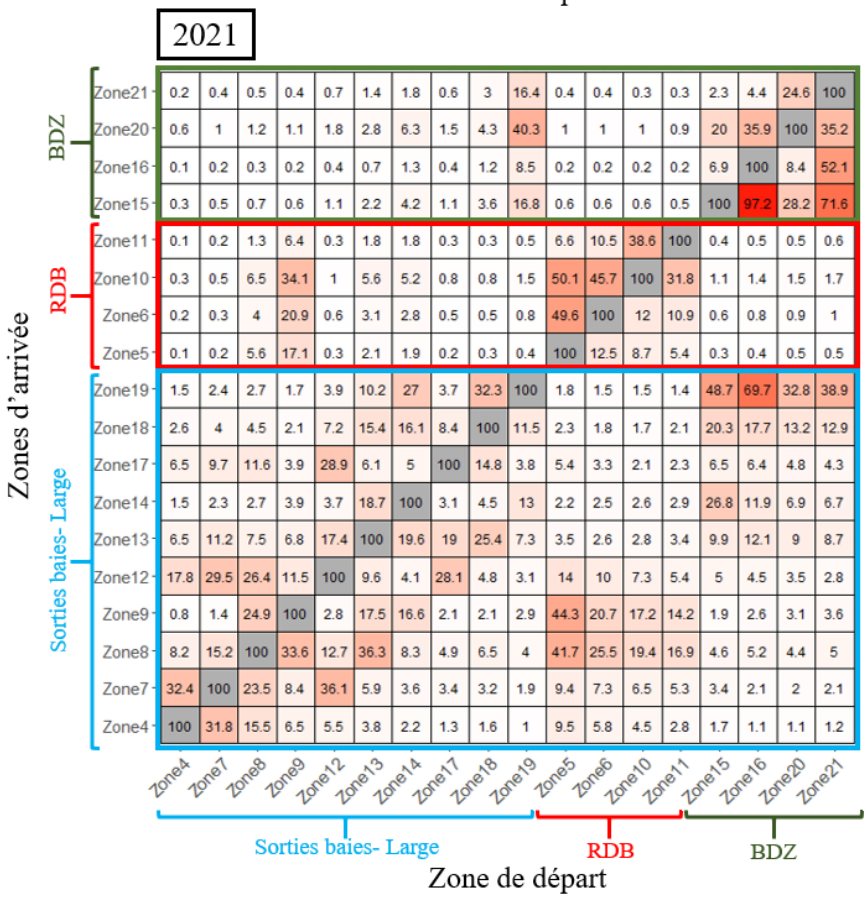
2021
Zones d'arrivée
BDZ
RDB
Sorties baies- Large
Zone21 0.2 0.4 0.5 0.4 0.7 1.4 1.8 0.6 3 16.4 0.4 0.4 0.3 0.3 2.3 4.4 24.6 100
Zone20 0.6 1 1.2 1.1 1.8 2.8 6.3 1.5 4.3 40.3 1 1 1 0.9 20 35.9 100 35.2
Zone16 0.1 0.2 0.3 0.2 0.4 0.7 1.3 0.4 1.2 8.5 0.2 0.2 0.2 0.2 6.9 100 8.4 52.1
Zone15 0.3 0.5 0.7 0.6 1.1 2.2 4.2 1.1 3.6 16.8 0.6 0.6 0.6 0.5 100 97.2 28.2 71.6
Zone11 0.1 0.2 1.3 6.4 0.3 1.8 1.8 0.3 0.3 0.5 6.6 10.5 38.6 100 0.4 0.5 0.5 0.6
Zone10 0.3 0.5 6.5 34.1 1 5.6 5.2 0.8 0.8 1.5 50.1 45.7 100 31.8 1.1 1.4 1.5 1.7
Zone6 0.2 0.3 4 20.9 0.6 3.1 2.8 0.5 0.5 0.8 49.6 100 12 10.9 0.6 0.8 0.9 1
Zone5 0.1 0.2 5.6 17.1 0.3 2.1 1.9 0.2 0.3 0.4 100 12.5 8.7 5.4 0.3 0.4 0.5 0.5
Zone19 1.5 2.4 2.7 1.7 3.9 10.2 27 3.7 32.3 100 1.8 1.5 1.5 1.4 48.7 69.7 32.8 38.9
Zone18 2.6 4 4.5 2.1 7.2 15.4 16.1 8.4 100 11.5 2.3 1.8 1.7 2.1 20.3 17.7 13.2 12.9
Zone17 6.5 9.7 11.6 3.9 28.9 6.1 5 100 14.8 3.8 5.4 3.3 2.1 2.3 6.5 6.4 4.8 4.3
Zone14 1.5 2.3 2.7 3.9 3.7 18.7 100 3.1 4.5 13 2.2 2.5 2.6 2.9 26.8 11.9 6.9 6.7
Zone13 6.5 11.2 7.5 6.8 17.4 100 19.6 19 25.4 7.3 3.5 2.6 2.8 3.4 9.9 12.1 9 8.7
Zone12 17.8 29.5 26.4 11.5 100 9.6 4.1 28.1 4.8 3.1 14 10 7.3 5.4 5 4.5 3.5 2.8
Zone9 0.8 1.4 24.9 100 2.8 17.5 16.6 2.1 2.1 2.9 44.3 20.7 17.2 14.2 1.9 2.6 3.1 3.6
Zone8 8.2 15.2 100 33.6 12.7 36.3 8.3 4.9 6.5 4 41.7 25.5 19.4 16.9 4.6 5.2 4.4 5
Zone7 32.4 100 23.5 8.4 36.1 5.9 3.6 3.4 3.2 1.9 9.4 7.3 6.5 5.3 3.4 2.1 2 2.1
Zone4 100 31.8 15.5 6.5 5.5 3.8 2.2 1.3 1.6 1 9.5 5.8 4.5 2.8 1.7 1.1 1.1 1.2
Zone4 Zone7 Zone8 Zone9 Zone12 Zone13 Zone14 Zone17 Zone18 Zone19 Zone5 Zone6 Zone10 Zone11 Zone15 Zone16 Zone20 Zone21
Sorties baies- Large
RDB
BDZ
Zone de départ

4.2. Tmax

Matrices de connectivité représentant les temps d'arrivée des pourcentages maximales de masses initiales des 19 traceurs dans les 19 zones pour les 4 années simulées. La matrice est à lire à l'horizontale en considérant dans les différentes zones, le temps d'arrivée des traceurs venant des 19 autres stations.

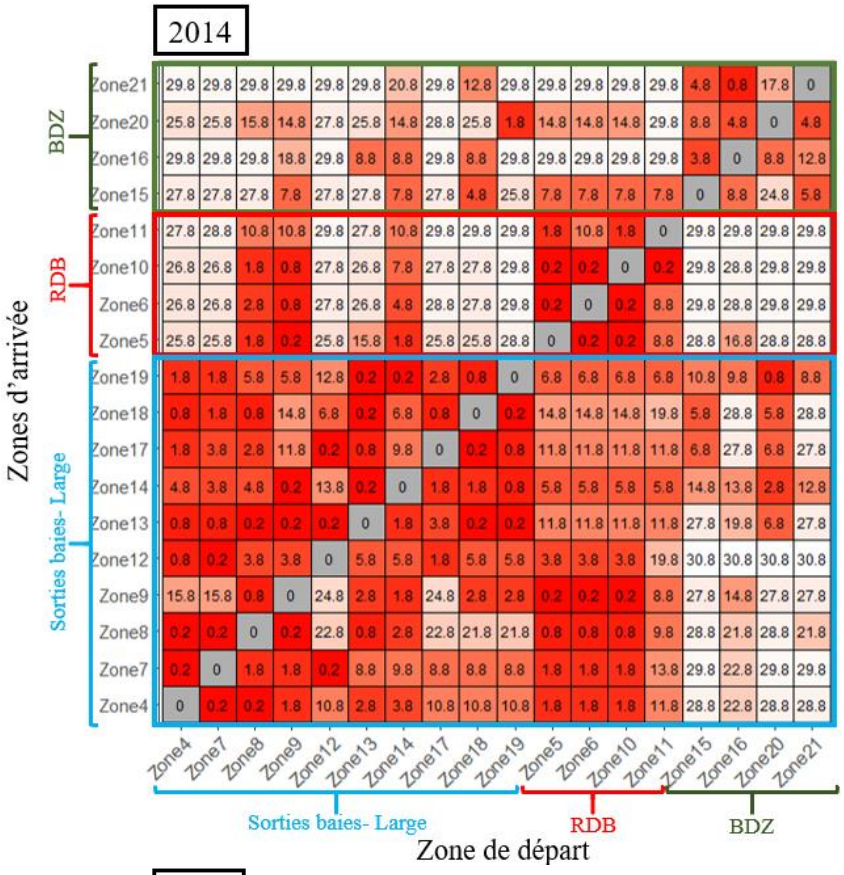

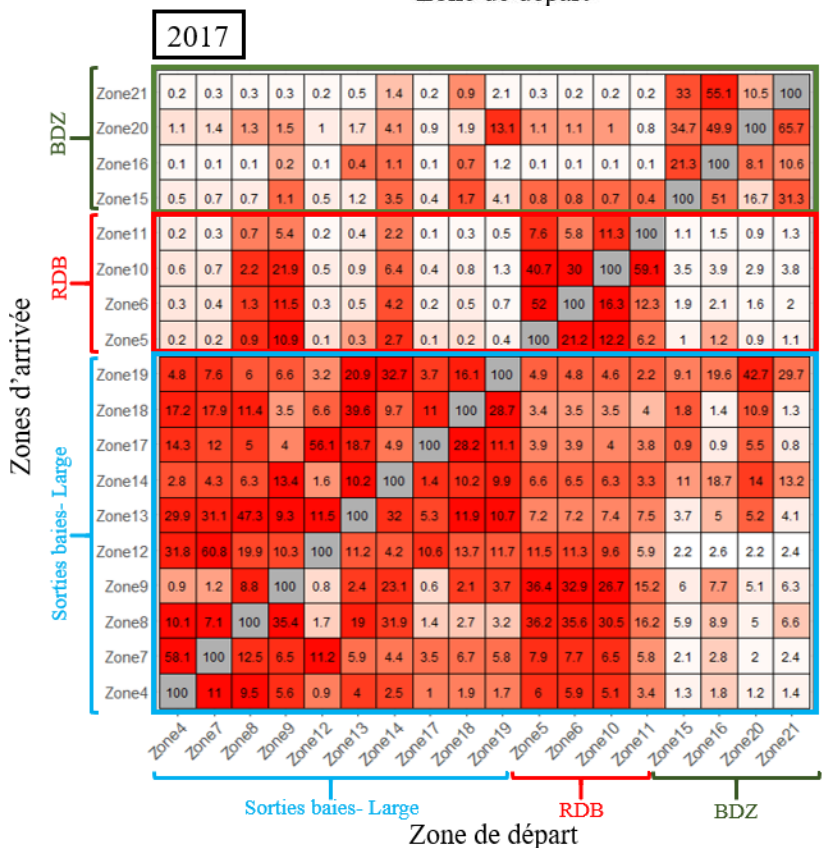

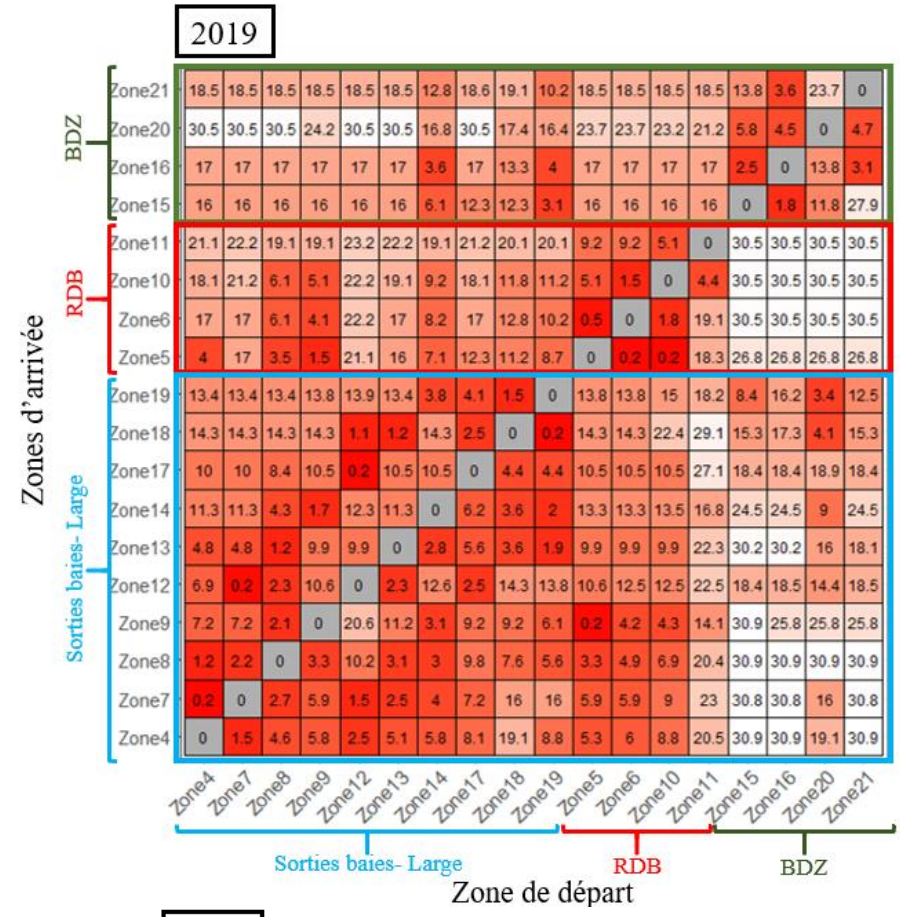
2019
Zones d'arrivée
BDZ
RDB
Sorties baies- Large
Zone21 18.5 18.5 18.5 18.5 18.5 18.5 12.8 18.6 19.1 10.2 18.5 18.5 18.5 18.5 13.8 3.6 23.7 0
Zone20 30.5 30.5 30.5 24.2 30.5 30.5 16.8 30.5 17.4 16.4 23.7 23.7 23.2 21.2 5.8 4.5 0 4.7
Zone16 17 17 17 17 17 17 3.6 17 13.3 4 17 17 17 17 2.5 0 13.8 3.1
Zone15 16 16 16 16 16 16 6.1 12.3 12.3 3.1 16 16 16 16 0 1.8 11.8 27.9
Zone11 21.1 22.2 19.1 19.1 23.2 22.2 19.1 21.2 20.1 20.1 9.2 9.2 5.1 0 30.5 30.5 30.5 30.5
Zone10 18.1 21.2 6.1 5.1 22.2 19.1 9.2 18.1 11.8 11.2 5.1 1.5 0 4.4 30.5 30.5 30.5 30.5
Zone6 17 17 6.1 4.1 22.2 17 8.2 17 12.8 10.2 0.5 0 1.8 19.1 30.5 30.5 30.5 30.5
Zone5 4 17 3.5 1.5 21.1 16 7.1 12.3 11.2 8.7 0 0.2 0.2 18.3 26.8 26.8 26.8 26.8
Zone19 13.4 13.4 13.4 13.8 13.9 13.4 3.8 4.1 1.5 0 13.8 13.8 15 18.2 8.4 16.2 3.4 12.5
Zone18 14.3 14.3 14.3 14.3 1.1 1.2 14.3 2.5 0 0.2 14.3 14.3 22.4 29.1 15.3 17.3 4.1 15.3
Zone17 10 10 8.4 10.5 0.2 10.5 10.5 0 4.4 4.4 10.5 10.5 10.5 27.1 18.4 18.4 18.9 18.4
Zone14 11.3 11.3 4.3 1.7 12.3 11.3 0 6.2 3.6 2 13.3 13.3 13.5 16.8 24.5 24.5 9 24.5
Zone13 4.8 4.8 1.2 9.9 9.9 0 2.8 5.6 3.6 1.9 9.9 9.9 9.9 22.3 30.2 30.2 16 18.1
Zone12 6.9 0.2 2.3 10.6 0 2.3 12.6 2.5 14.3 13.8 10.6 12.5 12.5 22.5 18.4 18.5 14.4 18.5
Zone9 7.2 7.2 2.1 0 20.6 11.2 3.1 9.2 9.2 6.1 0.2 4.2 4.3 14.1 30.9 25.8 25.8 25.8
Zone8 1.2 2.2 0 3.3 10.2 3.1 3 9.8 7.6 5.6 3.3 4.9 6.9 20.4 30.9 30.9 30.9 30.9
Zone7 0.2 0 2.7 5.9 1.5 2.5 4 7.2 16 16 5.9 5.9 9 23 30.8 30.8 16 30.8
Zone4 0 1.5 4.6 5.8 2.5 5.1 5.8 8.1 19.1 8.8 5.3 6 8.8 20.5 30.9 30.9 19.1 30.9
Zone4 Zone7 Zone8 Zone9 Zone12 Zone13 Zone14 Zone17 Zone18 Zone19 Zone5 Zone6 Zone10 Zone11 Zone15 Zone16 Zone20 Zone21
Sorties baies- Large
RDB
BDZ
Zone de départ

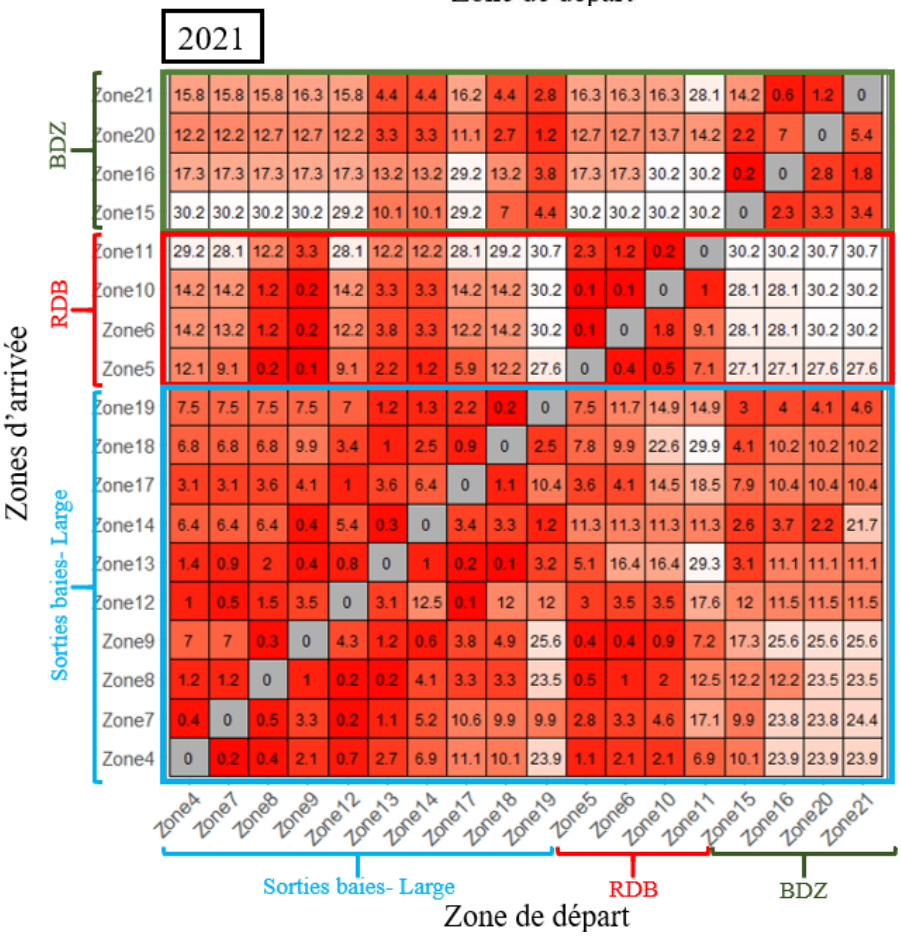
2021
Zones d'arrivée
BDZ
RDB
Sorties baies- Large
Zone21 15.8 15.8 15.8 16.3 15.8 4.4 4.4 16.2 4.4 2.8 16.3 16.3 16.3 28.1 14.2 0.6 1.2 0
Zone20 12.2 12.2 12.7 12.7 12.2 3.3 3.3 11.1 2.7 1.2 12.7 12.7 13.7 14.2 2.2 7 0 5.4
Zone16 17.3 17.3 17.3 17.3 17.3 13.2 13.2 29.2 13.2 3.8 17.3 17.3 30.2 30.2 0.2 0 2.8 1.8
Zone15 30.2 30.2 30.2 30.2 29.2 10.1 10.1 29.2 7 4.4 30.2 30.2 30.2 30.2 0 2.3 3.3 3.4
Zone11 29.2 28.1 12.2 3.3 28.1 12.2 12.2 28.1 29.2 30.7 2.3 1.2 0.2 0 30.2 30.2 30.7 30.7
Zone10 14.2 14.2 1.2 0.2 14.2 3.3 3.3 14.2 14.2 30.2 0.1 0.1 0 1 28.1 28.1 30.2 30.2
Zone6 14.2 13.2 1.2 0.2 12.2 3.8 3.3 12.2 14.2 30.2 0.1 0 1.8 9.1 28.1 28.1 30.2 30.2
Zone5 12.1 9.1 0.2 0.1 9.1 2.2 1.2 5.9 12.2 27.6 0 0.4 0.5 7.1 27.1 27.1 27.6 27.6
Zone19 7.5 7.5 7.5 7.5 7 1.2 1.3 2.2 0.2 0 7.5 11.7 14.9 14.9 3 4 4.1 4.6
Zone18 6.8 6.8 6.8 9.9 3.4 1 2.5 0.9 0 2.5 7.8 9.9 22.6 29.9 4.1 10.2 10.2 10.2
Zone17 3.1 3.1 3.6 4.1 1 3.6 6.4 0 1.1 10.4 3.6 4.1 14.5 18.5 7.9 10.4 10.4 10.4
Zone14 6.4 6.4 6.4 0.4 5.4 0.3 0 3.4 3.3 1.2 11.3 11.3 11.3 11.3 2.6 3.7 2.2 21.7
Zone13 1.4 0.9 2 0.4 0.8 0 1 0.2 0.1 3.2 5.1 16.4 16.4 29.3 3.1 11.1 11.1 11.1
Zone12 1 0.5 1.5 3.5 0 3.1 12.5 0.1 12 12 3 3.5 3.5 17.6 12 11.5 11.5 11.5
Zone9 7 7 0.3 0 4.3 1.2 0.6 3.8 4.9 25.6 0.4 0.4 0.9 7.2 17.3 25.6 25.6 25.6
Zone8 1.2 1.2 0 1 0.2 0.2 4.1 3.3 3.3 23.5 0.5 1 2 12.5 12.2 12.2 23.5 23.5
Zone7 0.4 0 0.5 3.3 0.2 1.1 5.2 10.6 9.9 9.9 2.8 3.3 4.6 17.1 9.9 23.8 23.8 24.4
Zone4 0 0.2 0.4 2.1 0.7 2.7 6.9 11.1 10.1 23.9 1.1 2.1 2.1 6.9 10.1 23.9 23.9 23.9
Zone4 Zone7 Zone8 Zone9 Zone12 Zone13 Zone14 Zone17 Zone18 Zone19 Zone5 Zone6 Zone10 Zone11 Zone15 Zone16 Zone20 Zone21
Sorties baies- Large
RDB
BDZ
Zone de départ

Chapter 4

Supplementary material

Spatio-temporal dynamics of *Pseudo-nitzschia australis* during a bloom: from gene expression to hydrodynamic

Léa Prigent[a], Julien Quéré[a], Marie Latimier[a], Florian Caradec[a], Fabienne Hervé[b], Lauriane Baudy[b], Zouher Amzil[b], Emilie Rabiller[a], Martin Plus[a], Mickaël Le Gac[a]

[a]Ifremer, DYNECO, F-29280 Plouzané, France.
[b]Ifremer, PHYTOX Unit, METALG Laboratory, F-44300 Nantes, France.

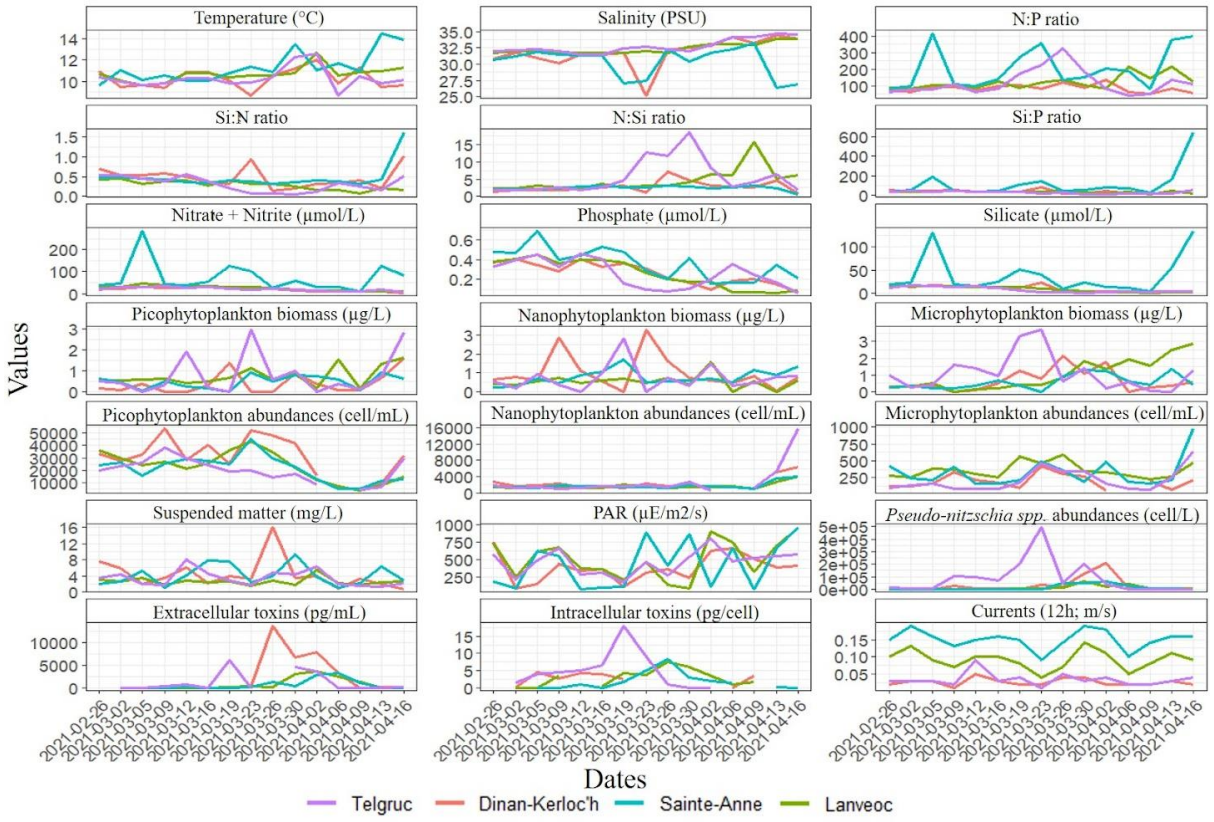

Fig.1: Temporal evolution of environmental parameters associated with spatio-temporal monitoring in 2021. The temporal evolution of the parameters of the Telgruc station are plotted in purple, the Dinan-Kerloc'h station in red, Lanvéoc in green and Sainte-Anne in blue.

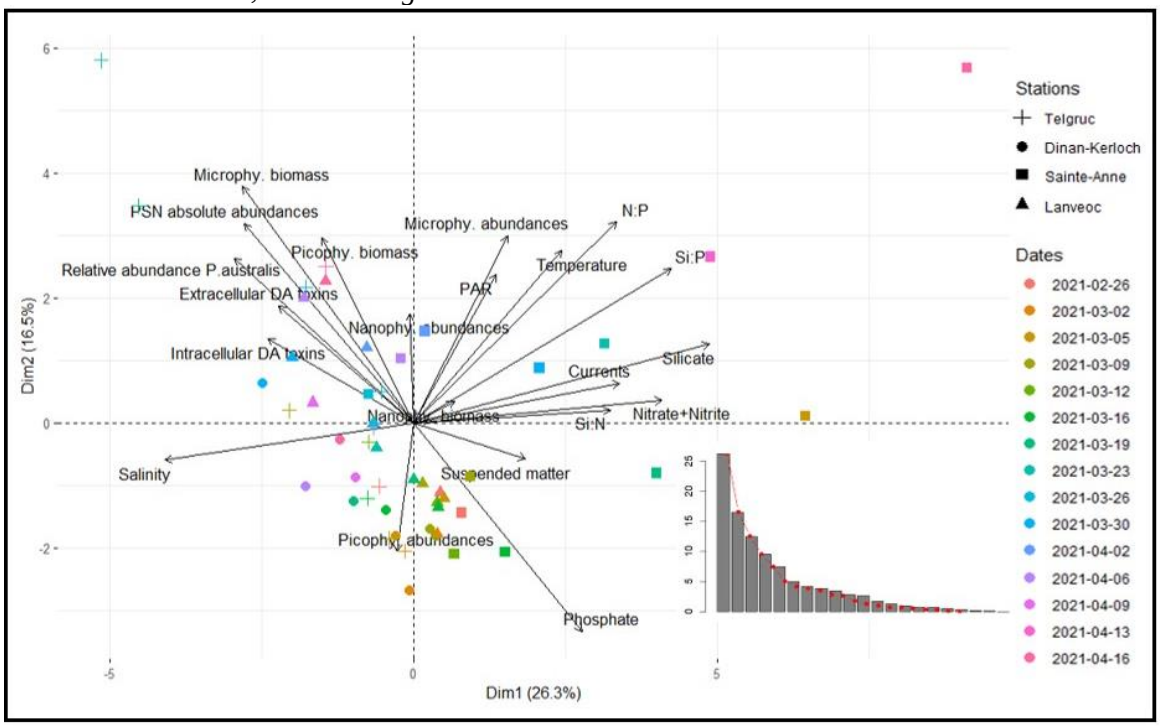

Fig. 2: First two components of a PCA showing relationships between biotic and abiotic environment (in black) and samples. The difference with the PCA in the article is the presence of nutrient ratios. Sampling dates (colors) and sampling stations (shapes) are indicated. The black arrows represent the biotic and abiotic variables, their position indicating the direction of their increase. The closer two arrows are, the more correlated they are.

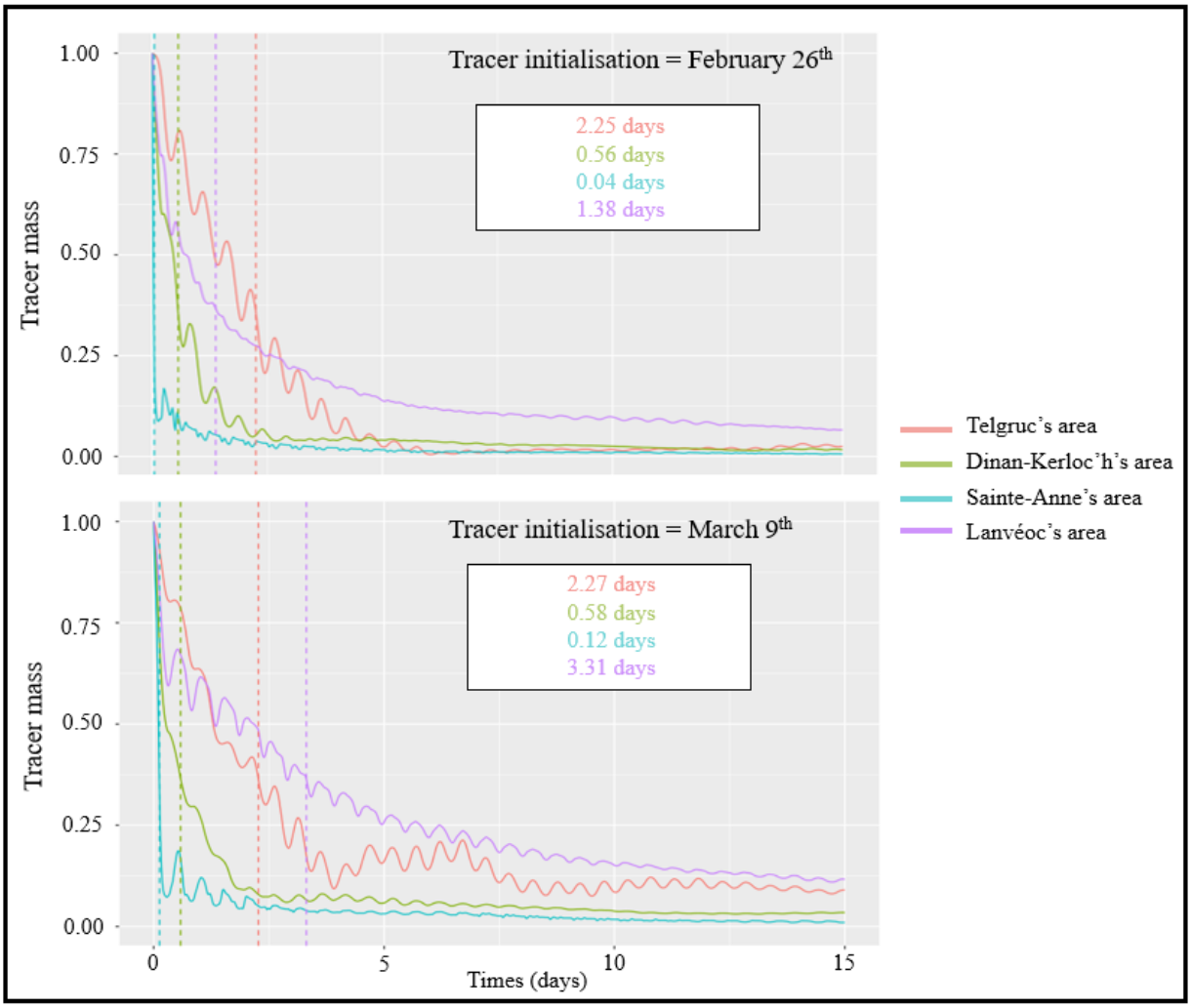

Fig. 3: Evolution of the mass of tracer leaving a zone. Each color represents a starting zone. Red for Telgruc, green for Dinan-Kerloc'h, blue for Sainte-Anne and purple for Lanvéoc. The calculated e-flushing times associated with each zone are indicated. This is the time needed for dilution to drop the tracer quantity to 37% of initial quantity in a particular area.

Chapitre 5

Supplementary material

Sexual reproduction, a major event determining the dynamics of gene expression during a *P. australis* bloom?

Léa Prigent[a], Julien Quéré[a], Martin Plus[a], Mickaël Le Gac[a]

[a]Ifremer, DYNECO, F-29280 Plouzané, France.

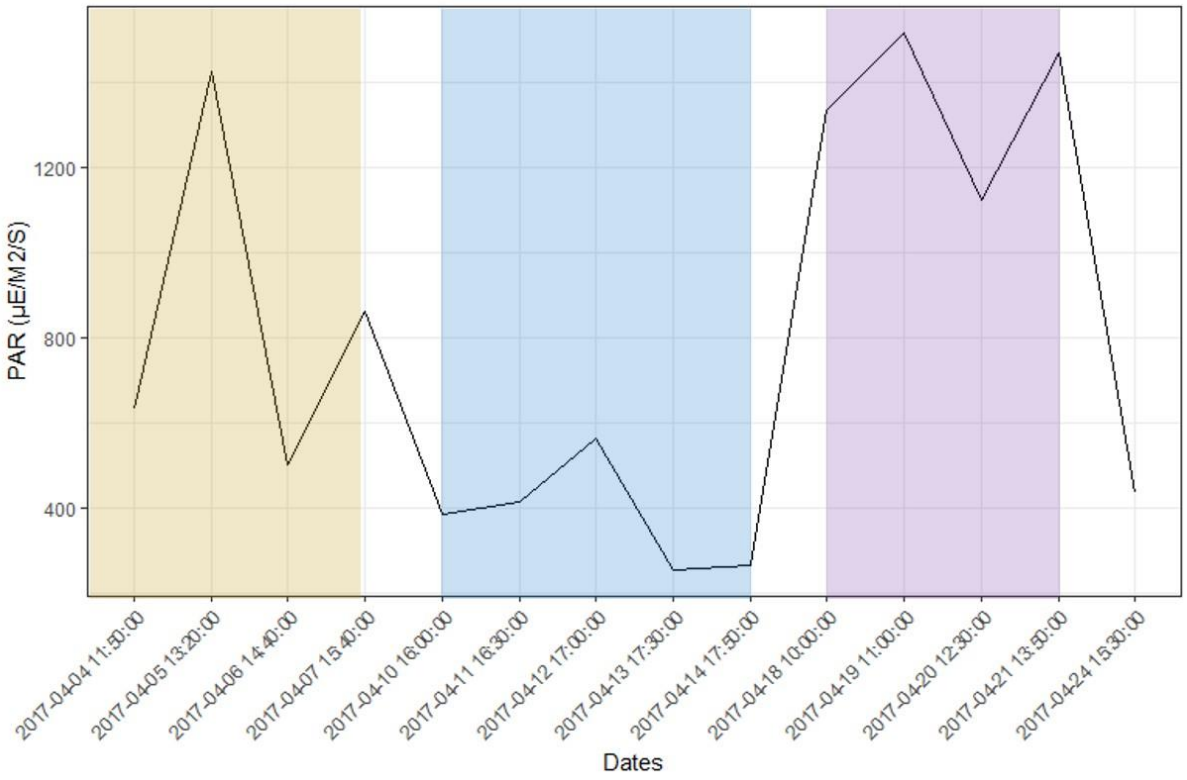

Fig. 1: PAR values at the time of sampling. The 3 colours represent the groups of samples on the basis of gene expression (yellow for the beginning of the bloom: 04/04; 04/05, 04/06 and 04/07; blue for the middle of the bloom: 04/10, 04/11, 04/12, 04/13 and 04/14; and purple for end of the bloom: 04/18, 04/19, 04/20 and 04/21).

1	5.82 m
2	4.88 m
3	3.88 m
4	3.19 m
5	3.01 m
6	3.34 m
7	4.04 m
8	4.74 m
9	5.26 m
10	5.63 m
11	5.67 m
12	5.65 m
13	5.47 m
14	5.13 m
15	4.63 m
16	4.01 m
17	3.34 m
18	2.70 m
19	2.20 m
20	2.05 m
21	2.44 m
22	3.21 m
23	4.19 m
24	5.17 m
25	6.02 m
26	6.61 m
27	6.90 m
28	6.92 m
29	6.55 m
30	5.85 m

Table 1: Average daily water level (in metres) between high and low tide.

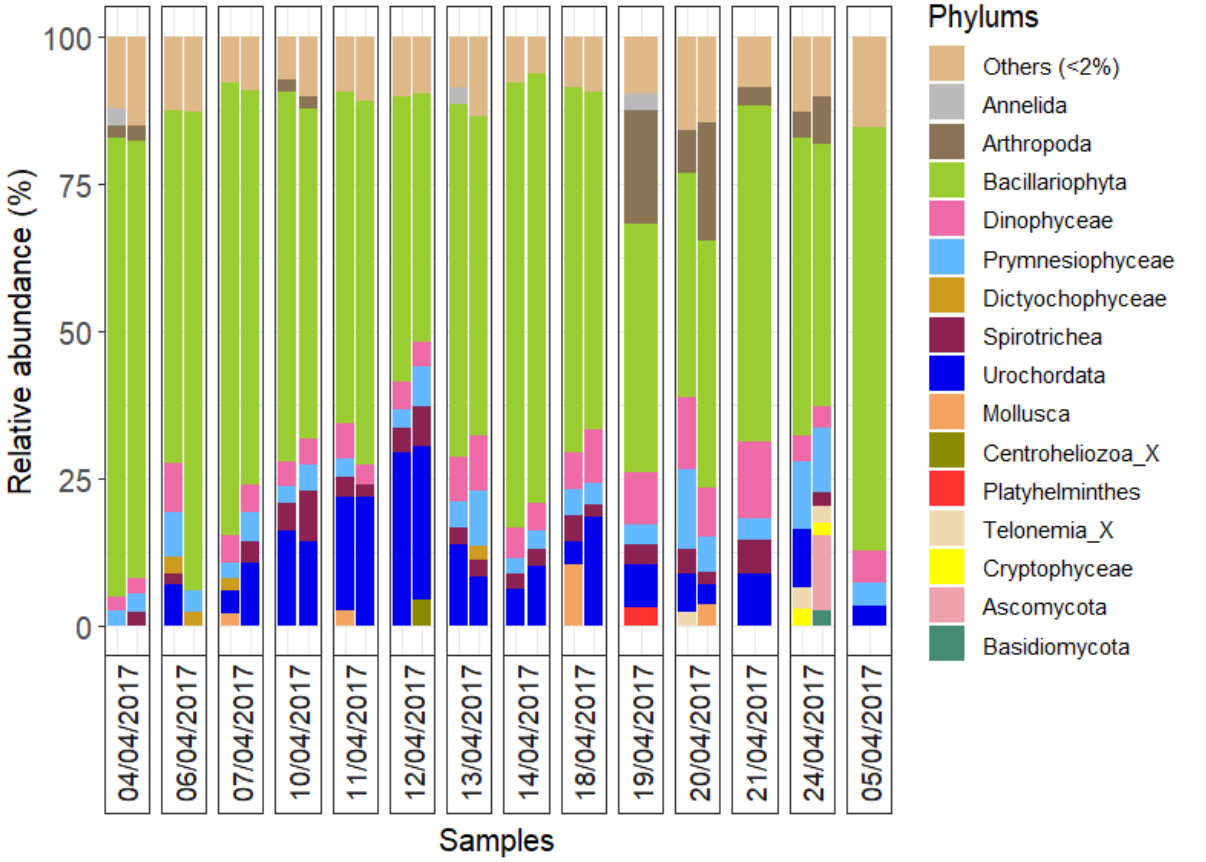

Fig. 2: Relative abundances of the phylum community composition during the 2017 monitoring (the category others regroup phylum lower 2% of total abundance).

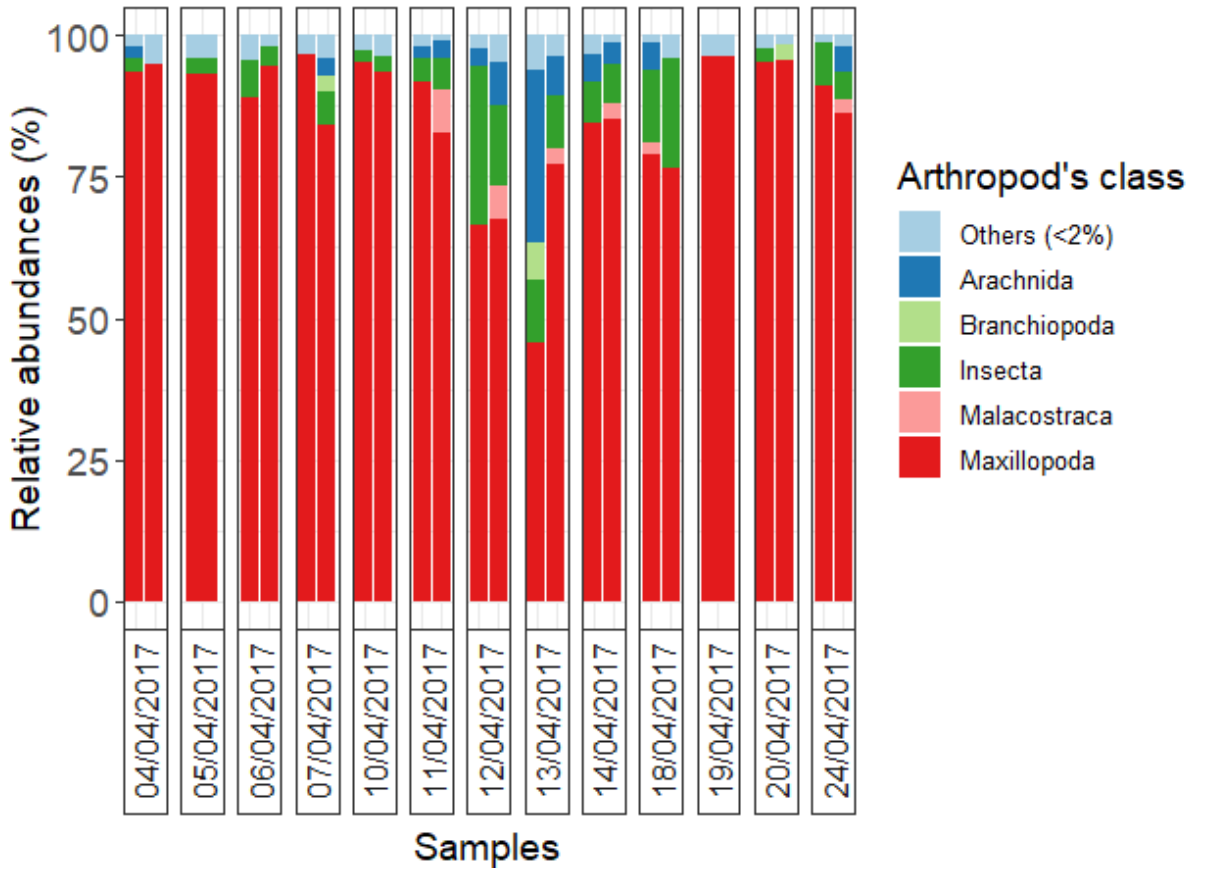

Fig. 3: Relative abundances of the Arthropod's class community composition during the 2017 monitoring (the category others regroup class lower than 2% of total abundance).

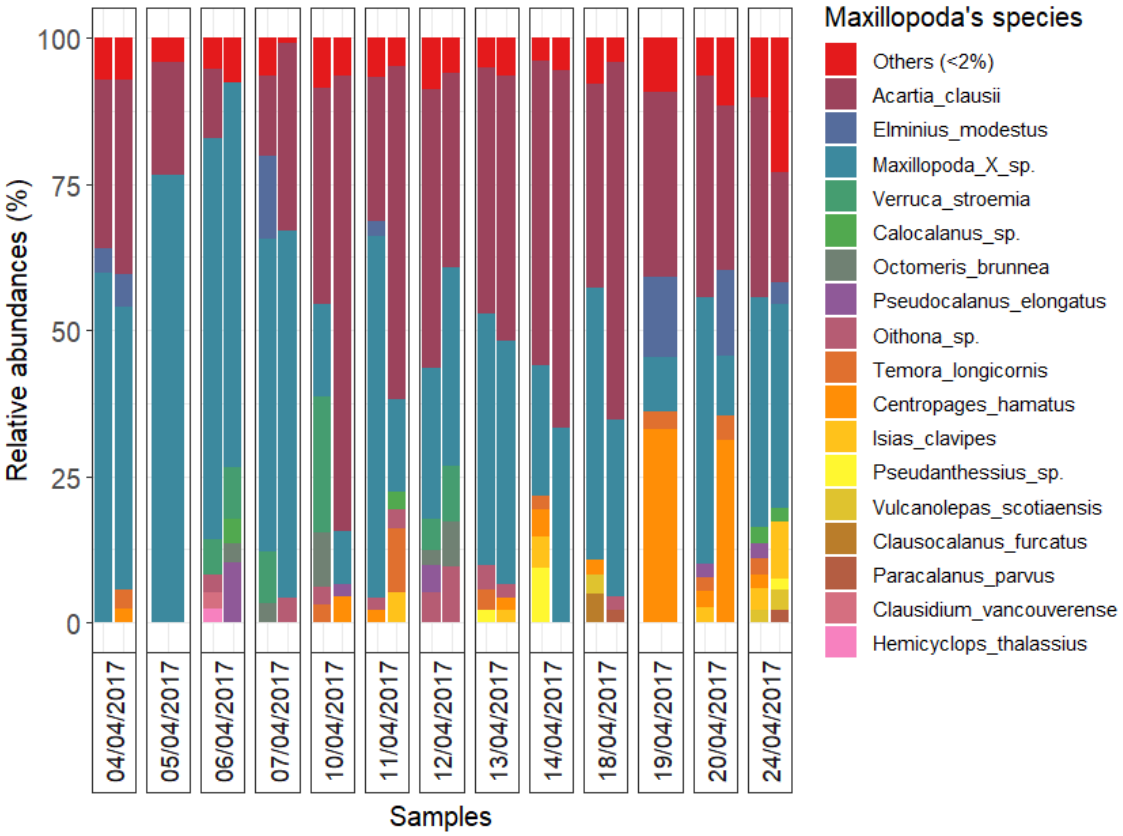

Fig. 4: Relative abundances of the Maxilopoda's class species community composition during the 2017 monitoring (the category others regroup species lower than 2% of total abundance).

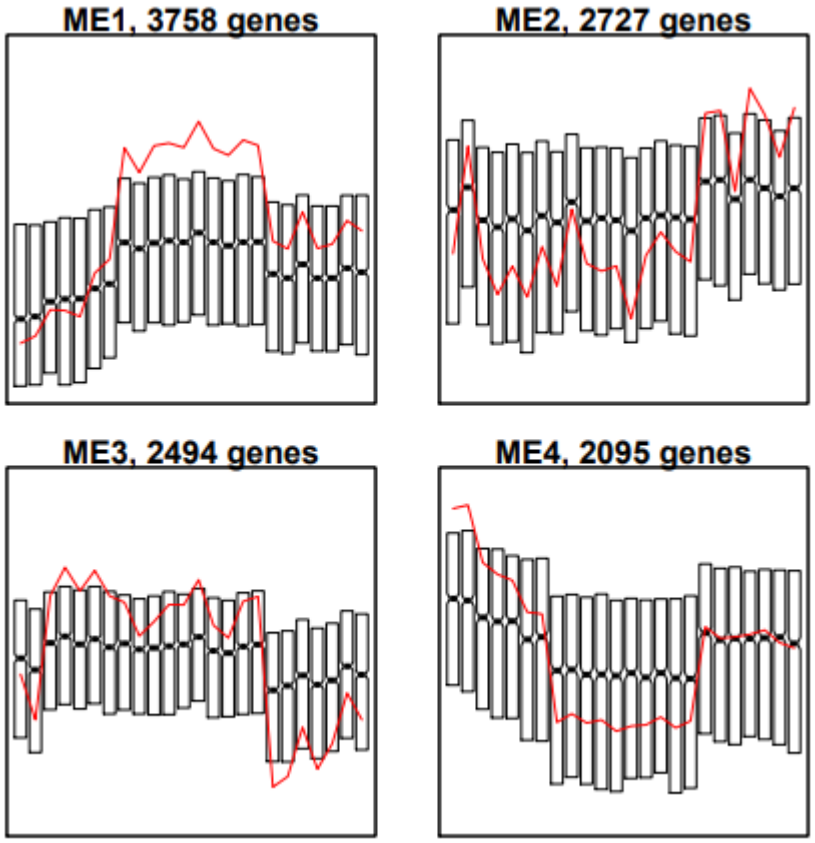

Fig. 5: Clusters of genes displaying similar gene expression dynamics (expressed as log2FC) across the 24 samples using WGCNA analysis.

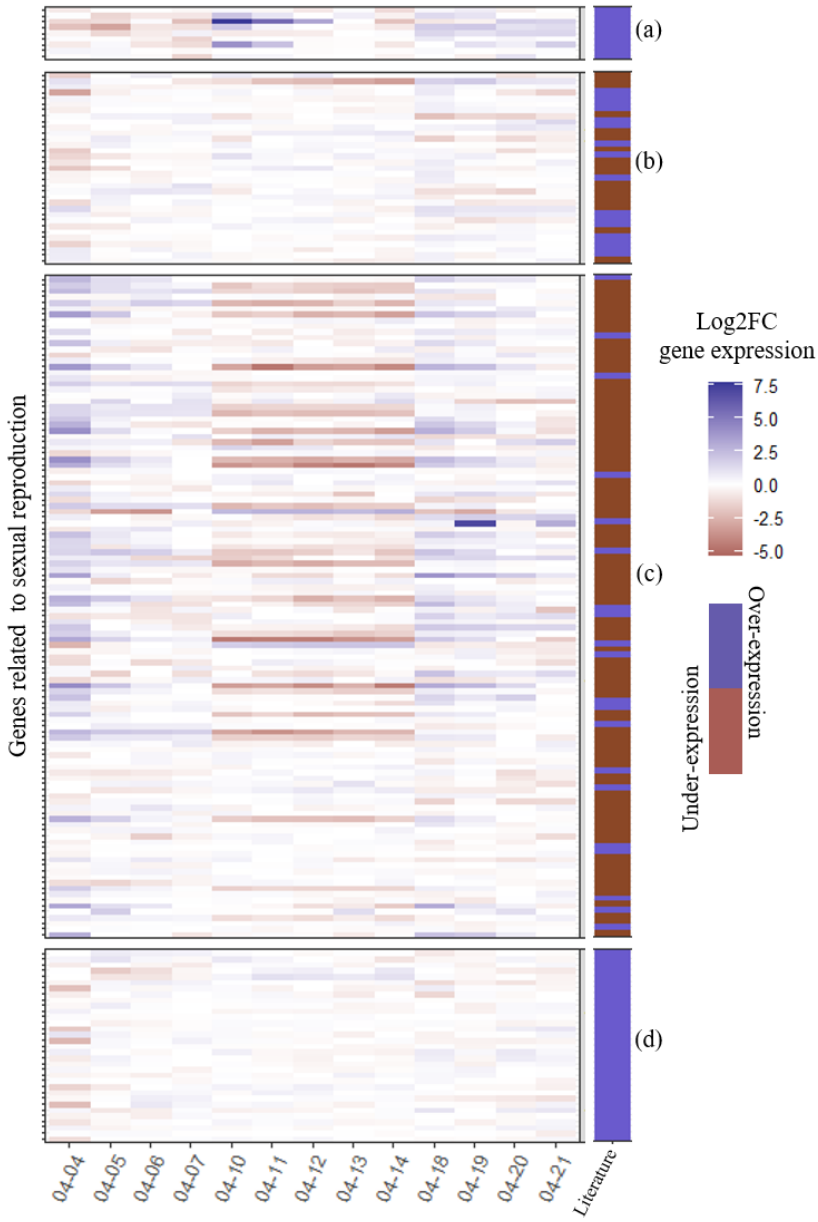

Fig. 6: Comparison of the expression level (under- in brown and over-expressed in blue) of genes identified as differentially expressed or involved in sexual reproduction in the literature with their homologs identified in the P. australis reference transcriptome. The different letters represent the gene expression analysis's timing after sexual reproduction in the literature: (a) Directly (Russo et al., 2018, and Bilcke. G personal communication); (b) 6h after opposite MT contact (Basu et al., 2017) (c) From 1 hour to 5 days (Annunziata et al., 2022) and (d) Sexual reproduction period (Patil et al., 2015). All homologous genes identified are found in the supplementary material, table 2 in comparison with the literature.

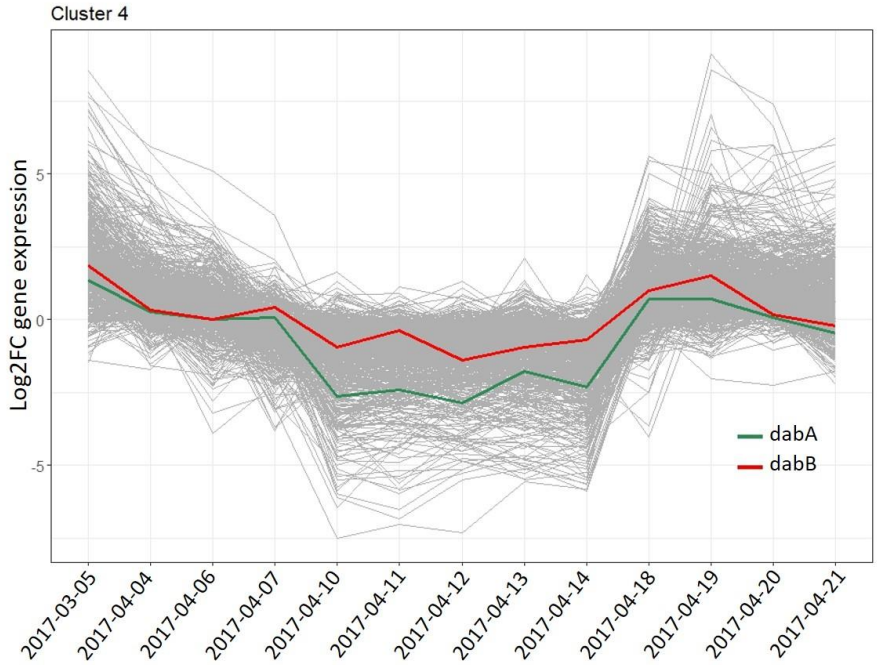

Fig. 7: DAB's gene expression dynamics in the cluster 4. Only dabA and dabB homologous genes were identified on it.

Table 2: Genes' markers of sexual reproduction identified in the literature associated with their homologue in the reference transcriptome of P. australis.

Functions	**Annotations**	**Papers**	**Gene expression**	**Analysis timing**
ATP-binding casette, subfamily B (MDR/TAP), member 1	ABC transporters	Basu et al., 2017	Over	6h after opposite MT contact
DNA repair protein RAD51 homologue 1, RAD51-A1	Cell cycle and meosis	Basu et al., 2017	Over	6h after opposite MT contact
DNA repair protein RAD51 homologue 3, RAD51-C	Cell cycle and meosis	Basu et al., 2017	Over	6h after opposite MT contact
Pds5	Cell cycle and meosis	Basu et al., 2017	Over	6h after opposite MT contact
Structural maintenance of chromosomes protein 5	Cell cycle and meosis	Basu et al., 2017	Over	6h after opposite MT contact
Structural maintenance of chromosomes protein 3	Cell cycle and meosis	Basu et al., 2017	Over	6h after opposite MT contact
Structural maintenance of chromosomes protein 1	Cell cycle and meosis	Basu et al., 2017	Over	6h after opposite MT contact
Cohesin complex subunit SCC1 (RAD21)	Cell cycle and meosis	Basu et al., 2017	Over	6h after opposite MT contact
Cohesin complex subunit SA-1/2 (SCC3)	Cell cycle and meosis	Basu et al., 2017	Over	6h after opposite MT contact
G2/mitotic specific cyclin S13-6 (dsCYC5)	Cell cycle and meosis	Basu et al., 2017	Down	6h after opposite MT contact
Cyclin-B2-2 (dsCYC4)	Cell cycle and meosis	Basu et al., 2017	Down	6h after opposite MT contact
Ferrodoxin-dependant glutamate synthase 2	Nitrate metabolism	Basu et al., 2017	Down	6h after opposite MT contact
Ammonium transper1, member 5	Nitrate metabolism	Basu et al., 2017	Down	6h after opposite MT contact
Nitrate/nitrite transporter NarU	Nitrate metabolism	Basu et al., 2017	Down	6h after opposite MT contact

Transcription factor SKN7	Transcription factors	Basu et al., 2017	Down	6h after opposite MT contact
Transcriptional activator Myb	Transcription factors	Basu et al., 2017	Down	6h after opposite MT contact
Major intracellular serine protease	Protein processing Receptor like	Basu et al., 2017	Down	6h after opposite MT contact
Probable leucine rich repeat receptor-like protein kinase At2g33170	Protein processing Receptor like	Basu et al., 2017	Over	6h after opposite MT contact
Probable leucine rich repeat receptor-like protein kinase At1g35710	Protein processing Receptor like	Basu et al., 2017	Down	6h after opposite MT contact
Receptor-like protein kinase 5	Protein processing Receptor like	Basu et al., 2017	Down	6h after opposite MT contact
Probable leucine-rich repeat receptor-like serine/threonine protein kinase At4g08850	Protein processing Receptor like	Basu et al., 2017	Down	6h after opposite MT contact
Receptor-like protein kinase HSL1	Protein processing Receptor like	Basu et al., 2017	Down	6h after opposite MT contact
Leucine-rich repeat receptor-like serine/threonine protein kinase GS02	Protein processing Receptor like	Basu et al., 2017	Down	6h after opposite MT contact
Somatic embryogenesis receptor kinase 1	Protein processing Receptor like	Basu et al., 2017	Down	6h after opposite MT contact
Probable leucine rich repeat receptor like serine/threonine protein kinase At4g26540	Protein processing Receptor like	Basu et al., 2017	Down	6h after opposite MT contact
Probable leucine-rich repeat receptor-like protein kinase	Protein processing Receptor like	Basu et al., 2017	Down	6h after opposite MT contact
Probable leucine-rich repeat receptor-like protein kinase	Protein processing Receptor like	Basu et al., 2017	Down	6h after opposite MT contact
Soluble guanylate cyclase 88E	Signalling Miscellaneous	Basu et al., 2017	Over	6h after opposite MT contact
Protein aardvark (adhesion protein)	Signalling Miscellaneous	Basu et al., 2017	Over	6h after opposite MT contact
Tetratricopeptide (TPR) repeat-containing protein (protein-protein interactions)	Signalling Miscellaneous	Basu et al., 2017	Over	6h after opposite MT contact

Salicylate carboxymethyltransferase	Signalling Miscellaneous	Basu et al., 2017	Over	6h after opposite MT contact
E3 ubiquitin-protein ligase Nedd-4	Signalling Miscellaneous	Basu et al., 2017	Over	6h after opposite MT contact
Heat shock protein 3	MT-specific Miscellaneous	Basu et al., 2017	Over	6h after opposite MT contact
Cathepsin D	MT-specific Miscellaneous	Basu et al., 2017	Over	6h after opposite MT contact
TPR repeat-containing protein (protein-protein interactions)	MT-specific Miscellaneous	Basu et al., 2017	Down	6h after opposite MT contact
MRP1	Mating type identification	Russo et al., 2018	Over	Directly
MRP2	Mating type identification	Russo et al., 2018	Over	Directly
MRP3	Mating type identification	Russo et al., 2018	Over	Directly
MRM1_1	Mating type identification	Russo et al., 2018	Over	Directly
MRM1_2	Mating type identification	Russo et al., 2018	Over	Directly
MRM2	Mating type identification	Russo et al., 2018	Over	Directly
Mcm2	DNA replication and chromosome maintenance	Patil et al., 2015	Over	Sexual reproduction period
Mcm3	DNA replication and chromosome maintenance	Patil et al., 2015	Over	Sexual reproduction period
Mcm4	DNA replication and chromosome maintenance	Patil et al., 2015	Over	Sexual reproduction period
Mcm5	DNA replication and chromosome maintenance	Patil et al., 2015	Over	Sexual reproduction period
Mcm6	DNA replication and chromosome maintenance	Patil et al., 2015	Over	Sexual reproduction period

Mcm7	DNA replication and chromosome maintenance	Patil et al., 2015	Over	Sexual reproduction period
Mcm8	DNA replication and chromosome maintenance	Patil et al., 2015	Over	Sexual reproduction period
Mcm9	DNA replication and chromosome maintenance	Patil et al., 2015	Over	Sexual reproduction period
Smc1	DNA replication and chromosome maintenance	Patil et al., 2015	Over	Sexual reproduction period
Smc2	DNA replication and chromosome maintenance	Patil et al., 2015	Over	Sexual reproduction period
Smc3	DNA replication and chromosome maintenance	Patil et al., 2015	Over	Sexual reproduction period
Smc4	DNA replication and chromosome maintenance	Patil et al., 2015	Over	Sexual reproduction period
Smc5	DNA replication and chromosome maintenance	Patil et al., 2015	Over	Sexual reproduction period
Smc6	DNA replication and chromosome maintenance	Patil et al., 2015	Over	Sexual reproduction period
Pds5	DNA replication and chromosome maintenance	Patil et al., 2015	Over	Sexual reproduction period
Scc3	DNA replication and chromosome maintenance	Patil et al., 2015	Over	Sexual reproduction period
Rad21	DNA replication and chromosome maintenance	Patil et al., 2015	Over	Sexual reproduction period
Spo11-2	Double strand break formation	Patil et al., 2015	Over	Sexual reproduction period
Spo11-3/Top VIA	Double strand break formation	Patil et al., 2015	Over	Sexual reproduction period
Rad50	DNA damage sensing and response	Patil et al., 2015	Over	Sexual reproduction period
Mre11	DNA damage sensing and response	Patil et al., 2015	Over	Sexual reproduction period

Mer3	Crossover regulation	Patil et al., 2015	Over	Sexual reproduction period
Mnd1	Crossover regulation	Patil et al., 2015	Over	Sexual reproduction period
Msh4	Crossover regulation	Patil et al., 2015	Over	Sexual reproduction period
Msh5	Crossover regulation	Patil et al., 2015	Over	Sexual reproduction period
Rad51-A(1)	Double strand break repair	Patil et al., 2015	Over	Sexual reproduction period
Rad51-A(2)	Double strand break repair	Patil et al., 2015	Over	Sexual reproduction period
Rad51-B	Double strand break repair	Patil et al., 2015	Over	Sexual reproduction period
Rad51-C	Double strand break repair	Patil et al., 2015	Over	Sexual reproduction period
Rec-A	Double strand break repair	Patil et al., 2015	Over	Sexual reproduction period
Rad52	Double strand break repair	Patil et al., 2015	Over	Sexual reproduction period
Rad1	Double strand break repair	Patil et al., 2015	Over	Sexual reproduction period
Msh2	Double strand break repair	Patil et al., 2015	Over	Sexual reproduction period
Msh6	Double strand break repair	Patil et al., 2015	Over	Sexual reproduction period
Mlh1	Double strand break repair	Patil et al., 2015	Over	Sexual reproduction period
Pms1	Double strand break repair	Patil et al., 2015	Over	Sexual reproduction period
Mus81	Double strand break repair	Patil et al., 2015	Over	Sexual reproduction period

Fancm	Double strand break repair	Patil et al., 2015	Over	Sexual reproduction period
Fen1	Accessory proteins required during meiosis	Patil et al., 2015	Over	Sexual reproduction period
Exo1	Accessory proteins required during meiosis	Patil et al., 2015	Over	Sexual reproduction period
Dna2	Accessory proteins required during meiosis	Patil et al., 2015	Over	Sexual reproduction period
Brca2	Accessory proteins required during meiosis	Patil et al., 2015	Over	Sexual reproduction period
Nark	Nitrogen	Annunziata et al., 2022	Down	from 1 hour to 5 days
Nark	Nitrogen	Annunziata et al., 2022	Down	from 1 hour to 5 days
Nark	Nitrogen	Annunziata et al., 2022	Down	from 1 hour to 5 days
Ntr	Nitrogen	Annunziata et al., 2022	Down	from 1 hour to 5 days
NarU	Nitrogen	Annunziata et al., 2022	Down	from 1 hour to 5 days
NirD	Nitrogen	Annunziata et al., 2022	Down	from 1 hour to 5 days
FNT	Nitrogen	Annunziata et al., 2022	Down	from 1 hour to 5 days
Fld	Nitrogen	Annunziata et al., 2022	Down	from 1 hour to 5 days
UT	Nitrogen	Annunziata et al., 2022	Down	from 1 hour to 5 days
HANT	Nitrogen	Annunziata et al., 2022	Down	from 1 hour to 5 days
HANT	Nitrogen	Annunziata et al., 2022	Down	from 1 hour to 5 days

HANT	Nitrogen	Annunziata et al., 2022	Down	from 1 hour to 5 days
Ntr	Nitrogen	Annunziata et al., 2022	Down	from 1 hour to 5 days
Amt	Nitrogen	Annunziata et al., 2022	Down	from 1 hour to 5 days
Amt	Nitrogen	Annunziata et al., 2022	Down	from 1 hour to 5 days
UT	Nitrogen	Annunziata et al., 2022	Down	from 1 hour to 5 days
NR	Nitrogen	Annunziata et al., 2022	Down	from 1 hour to 5 days
FdGOGAT	Nitrogen	Annunziata et al., 2022	Down	from 1 hour to 5 days
FdGOGAT	Nitrogen	Annunziata et al., 2022	Down	from 1 hour to 5 days
FdGOGAT	Nitrogen	Annunziata et al., 2022	Down	from 1 hour to 5 days
Amt	Nitrogen	Annunziata et al., 2022	Down	from 1 hour to 5 days
NiR	Nitrogen	Annunziata et al., 2022	Down	from 1 hour to 5 days
NR	Nitrogen	Annunziata et al., 2022	Down	from 1 hour to 5 days
NR	Nitrogen	Annunziata et al., 2022	Down	from 1 hour to 5 days
HANT	Nitrogen	Annunziata et al., 2022	Down	from 1 hour to 5 days
HANT	Nitrogen	Annunziata et al., 2022	Down	from 1 hour to 5 days
HANT	Nitrogen	Annunziata et al., 2022	Down	from 1 hour to 5 days

Amt	Nitrogen	Annunziata et al., 2022	Down	from 1 hour to 5 days
HANT	Nitrogen	Annunziata et al., 2022	Over	from 1 hour to 5 days
PPT2	Phosphorus	Annunziata et al., 2022	Down	from 1 hour to 5 days
PPT2	Phosphorus	Annunziata et al., 2022	Down	from 1 hour to 5 days
TPT	Phosphorus	Annunziata et al., 2022	Down	from 1 hour to 5 days
PPT3	Phosphorus	Annunziata et al., 2022	Down	from 1 hour to 5 days
PPT3	Phosphorus	Annunziata et al., 2022	Down	from 1 hour to 5 days
XPT	Phosphorus	Annunziata et al., 2022	Down	from 1 hour to 5 days
IMP3	Phosphorus	Annunziata et al., 2022	Down	from 1 hour to 5 days
SLC	Phosphorus	Annunziata et al., 2022	Down	from 1 hour to 5 days
SLC	Phosphorus	Annunziata et al., 2022	Down	from 1 hour to 5 days
PstS	Phosphorus	Annunziata et al., 2022	Down	from 1 hour to 5 days
IPT1	Phosphorus	Annunziata et al., 2022	Down	from 1 hour to 5 days
MPT	Phosphorus	Annunziata et al., 2022	Down	from 1 hour to 5 days
PIT	Phosphorus	Annunziata et al., 2022	Down	from 1 hour to 5 days
TPT	Phosphorus	Annunziata et al., 2022	Down	from 1 hour to 5 days

IMPA	Phosphorus	Annunziata et al., 2022	Down	from 1 hour to 5 days
MPT	Phosphorus	Annunziata et al., 2022	Over	from 1 hour to 5 days
MPT	Phosphorus	Annunziata et al., 2022	Over	from 1 hour to 5 days
MPT	Phosphorus	Annunziata et al., 2022	Over	from 1 hour to 5 days
SIT	Silicon	Annunziata et al., 2022	Down	from 1 hour to 5 days
SIT	Silicon	Annunziata et al., 2022	Down	from 1 hour to 5 days
SIT	Silicon	Annunziata et al., 2022	Down	from 1 hour to 5 days
SIT	Silicon	Annunziata et al., 2022	Down	from 1 hour to 5 days
SIT	Silicon	Annunziata et al., 2022	Down	from 1 hour to 5 days
SIT	Silicon	Annunziata et al., 2022	Down	from 1 hour to 5 days
SIT	Silicon	Annunziata et al., 2022	Down	from 1 hour to 5 days
SIT	Silicon	Annunziata et al., 2022	Down	from 1 hour to 5 days
SIT	Silicon	Annunziata et al., 2022	Over	from 1 hour to 5 days
G1S	Cyclins-Cdks	Annunziata et al., 2022	Down	from 1 hour to 5 days
Cyc	Cyclins-Cdks	Annunziata et al., 2022	Down	from 1 hour to 5 days
Cyc	Cyclins-Cdks	Annunziata et al., 2022	Down	from 1 hour to 5 days

J	Cyclins-Cdks	Annunziata et al., 2022	Down	from 1 hour to 5 days
Cdk5	Cyclins-Cdks	Annunziata et al., 2022	Down	from 1 hour to 5 days
CycU41	Cyclins-Cdks	Annunziata et al., 2022	Down	from 1 hour to 5 days
CycA2A	Cyclins-Cdks	Annunziata et al., 2022	Down	from 1 hour to 5 days
Cdk11	Cyclins-Cdks	Annunziata et al., 2022	Down	from 1 hour to 5 days
Cdk11	Cyclins-Cdks	Annunziata et al., 2022	Down	from 1 hour to 5 days
CycB21	Cyclins-Cdks	Annunziata et al., 2022	Down	from 1 hour to 5 days
CycB22	Cyclins-Cdks	Annunziata et al., 2022	Down	from 1 hour to 5 days
CycB22	Cyclins-Cdks	Annunziata et al., 2022	Down	from 1 hour to 5 days
CycY	Cyclins-Cdks	Annunziata et al., 2022	Down	from 1 hour to 5 days
CycH11	Cyclins-Cdks	Annunziata et al., 2022	Down	from 1 hour to 5 days
G2MCyc	Cyclins-Cdks	Annunziata et al., 2022	Down	from 1 hour to 5 days
G2MCyc	Cyclins-Cdks	Annunziata et al., 2022	Down	from 1 hour to 5 days
CdkD3	Cyclins-Cdks	Annunziata et al., 2022	Down	from 1 hour to 5 days
Cdk2	Cyclins-Cdks	Annunziata et al., 2022	Down	from 1 hour to 5 days
G1SCyc	Cyclins-Cdks	Annunziata et al., 2022	Down	from 1 hour to 5 days

Cdk1	Cyclins-Cdks	Annunziata et al., 2022	Down	from 1 hour to 5 days
Cdk20	Cyclins-Cdks	Annunziata et al., 2022	Down	from 1 hour to 5 days
CycB15	Cyclins-Cdks	Annunziata et al., 2022	Down	from 1 hour to 5 days
G2MCyc	Cyclins-Cdks	Annunziata et al., 2022	Down	from 1 hour to 5 days
Cyc0	Cyclins-Cdks	Annunziata et al., 2022	Down	from 1 hour to 5 days
CycT14	Cyclins-Cdks	Annunziata et al., 2022	Down	from 1 hour to 5 days
CdkC1	Cyclins-Cdks	Annunziata et al., 2022	Over	from 1 hour to 5 days
CycB214	Cyclins-Cdks	Annunziata et al., 2022	Over	from 1 hour to 5 days
CycB22	Cyclins-Cdks	Annunziata et al., 2022	Over	from 1 hour to 5 days
CdkC2	Cyclins-Cdks	Annunziata et al., 2022	Over	from 1 hour to 5 days
CycB13	Cyclins-Cdks	Annunziata et al., 2022	Over	from 1 hour to 5 days
G1SCyc	Cyclins-Cdks	Annunziata et al., 2022	Over	from 1 hour to 5 days
MCAT	FA synthesis	Annunziata et al., 2022	Down	from 1 hour to 5 days
3-OXO-ACPS	FA synthesis	Annunziata et al., 2022	Down	from 1 hour to 5 days
3-OXO-ACPS	FA synthesis	Annunziata et al., 2022	Down	from 1 hour to 5 days
FAD	FA synthesis	Annunziata et al., 2022	Down	from 1 hour to 5 days

FAD	FA synthesis	Annunziata et al., 2022	Down	from 1 hour to 5 days
HPO8	FA synthesis	Annunziata et al., 2022	Down	from 1 hour to 5 days
KCS-5	FA synthesis	Annunziata et al., 2022	Down	from 1 hour to 5 days
FAD	FA synthesis	Annunziata et al., 2022	Down	from 1 hour to 5 days
ACC	FA synthesis	Annunziata et al., 2022	Down	from 1 hour to 5 days
ACC	FA synthesis	Annunziata et al., 2022	Down	from 1 hour to 5 days
ACC	FA synthesis	Annunziata et al., 2022	Down	from 1 hour to 5 days
ACC	FA synthesis	Annunziata et al., 2022	Down	from 1 hour to 5 days
ELOVL	FA synthesis	Annunziata et al., 2022	Down	from 1 hour to 5 days
SCD5	FA synthesis	Annunziata et al., 2022	Down	from 1 hour to 5 days
FABI	FA synthesis	Annunziata et al., 2022	Over	from 1 hour to 5 days
FABI	FA synthesis	Annunziata et al., 2022	Over	from 1 hour to 5 days
FABI	FA synthesis	Annunziata et al., 2022	Over	from 1 hour to 5 days
FAD	FA synthesis	Annunziata et al., 2022	Over	from 1 hour to 5 days
ACC	FA synthesis	Annunziata et al., 2022	Over	from 1 hour to 5 days
FAD	FA synthesis	Annunziata et al., 2022	Over	from 1 hour to 5 days

FAD	FA synthesis	Annunziata et al., 2022	Over	from 1 hour to 5 days
ELOVL	FA synthesis	Annunziata et al., 2022	Over	from 1 hour to 5 days
ACAT	FA synthesis	Annunziata et al., 2022	Over	from 1 hour to 5 days
DEGS	FA synthesis	Annunziata et al., 2022	Over	from 1 hour to 5 days
ELOVL	FA synthesis	Annunziata et al., 2022	Over	from 1 hour to 5 days
FAD	FA synthesis	Annunziata et al., 2022	Over	from 1 hour to 5 days
FAD	FA synthesis	Annunziata et al., 2022	Over	from 1 hour to 5 days
ACS	FA synthesis	Annunziata et al., 2022	Over	from 1 hour to 5 days
ACC	FA synthesis	Annunziata et al., 2022	Over	from 1 hour to 5 days
ACS	FA synthesis	Annunziata et al., 2022	Over	from 1 hour to 5 days
ACS	FA synthesis	Annunziata et al., 2022	Over	from 1 hour to 5 days
3OXOACPS	FA synthesis	Annunziata et al., 2022	Over	from 1 hour to 5 days
3OXOACPS	FA synthesis	Annunziata et al., 2022	Over	from 1 hour to 5 days
FABI	FA synthesis	Annunziata et al., 2022	Over	from 1 hour to 5 days
FAD	FA synthesis	Annunziata et al., 2022	Over	from 1 hour to 5 days
FABI	FA synthesis	Annunziata et al., 2022	Over	from 1 hour to 5 days

ELOVL	FA synthesis	Annunziata et al., 2022	Over	from 1 hour to 5 days
DEGS	FA synthesis	Annunziata et al., 2022	Over	from 1 hour to 5 days
SCD5	FA synthesis	Annunziata et al., 2022	Over	from 1 hour to 5 days
HADH	FA synthesis	Annunziata et al., 2022	Over	from 1 hour to 5 days
ACS	FA synthesis	Annunziata et al., 2022	Over	from 1 hour to 5 days
ACS	FA synthesis	Annunziata et al., 2022	Over	from 1 hour to 5 days
DGAT	TAG synthesis	Annunziata et al., 2022	Down	from 1 hour to 5 days
DGAT	TAG synthesis	Annunziata et al., 2022	Down	from 1 hour to 5 days
LPAAT	TAG synthesis	Annunziata et al., 2022	Down	from 1 hour to 5 days
MOGAT	TAG synthesis	Annunziata et al., 2022	Down	from 1 hour to 5 days
DGAT	TAG synthesis	Annunziata et al., 2022	Down	from 1 hour to 5 days
DGAT	TAG synthesis	Annunziata et al., 2022	Down	from 1 hour to 5 days
DGAT	TAG synthesis	Annunziata et al., 2022	Down	from 1 hour to 5 days
PDAT	TAG synthesis	Annunziata et al., 2022	Down	from 1 hour to 5 days
PAP	TAG synthesis	Annunziata et al., 2022	Down	from 1 hour to 5 days
PAP	TAG synthesis	Annunziata et al., 2022	Down	from 1 hour to 5 days

GPAT	TAG synthesis	Annunziata et al., 2022	Down	from 1 hour to 5 days
PAP	TAG synthesis	Annunziata et al., 2022	Down	from 1 hour to 5 days
PDAT	TAG synthesis	Annunziata et al., 2022	Down	from 1 hour to 5 days
MOGAT	TAG synthesis	Annunziata et al., 2022	Down	from 1 hour to 5 days
PDAT	TAG synthesis	Annunziata et al., 2022	Over	from 1 hour to 5 days
LHCFs/LHCRs	Light Harvesting/photoprotection	Annunziata et al., 2022	Down	from 1 hour to 5 days
LHCFs/LHCRs	Light Harvesting/photoprotection	Annunziata et al., 2022	Down	from 1 hour to 5 days
LHCFs/LHCRs	Light Harvesting/photoprotection	Annunziata et al., 2022	Down	from 1 hour to 5 days
LHCFs/LHCRs	Light Harvesting/photoprotection	Annunziata et al., 2022	Down	from 1 hour to 5 days
LHFs/LHCRs	Light Harvesting/photoprotection	Annunziata et al., 2022	Down	from 1 hour to 5 days
LHFs/LHCRs	Light Harvesting/photoprotection	Annunziata et al., 2022	Down	from 1 hour to 5 days
LHFs/LHCRs	Light Harvesting/photoprotection	Annunziata et al., 2022	Down	from 1 hour to 5 days
LHFs/LHCRs	Light Harvesting/photoprotection	Annunziata et al., 2022	Down	from 1 hour to 5 days
LHFs/LHCRs	Light Harvesting/photoprotection	Annunziata et al., 2022	Down	from 1 hour to 5 days
LHFs/LHCRs	Light Harvesting/photoprotection	Annunziata et al., 2022	Down	from 1 hour to 5 days
LHFs/LHCRs	Light Harvesting/photoprotection	Annunziata et al., 2022	Down	from 1 hour to 5 days

LHFs/LHCRs	Light Harvesting/photoprotection	Annunziata et al., 2022	Down	from 1 hour to 5 days
LHFs/LHCRs	Light Harvesting/photoprotection	Annunziata et al., 2022	Down	from 1 hour to 5 days
LHFs/LHCRs	Light Harvesting/photoprotection	Annunziata et al., 2022	Down	from 1 hour to 5 days
LHFs/LHCRs	Light Harvesting/photoprotection	Annunziata et al., 2022	Down	from 1 hour to 5 days
LHFs/LHCRs	Light Harvesting/photoprotection	Annunziata et al., 2022	Down	from 1 hour to 5 days
LHFs/LHCRs	Light Harvesting/photoprotection	Annunziata et al., 2022	Down	from 1 hour to 5 days
LHFs/LHCRs	Light Harvesting/photoprotection	Annunziata et al., 2022	Down	from 1 hour to 5 days
LHFs/LHCRs	Light Harvesting/photoprotection	Annunziata et al., 2022	Down	from 1 hour to 5 days
LHFs/LHCRs	Light Harvesting/photoprotection	Annunziata et al., 2022	Down	from 1 hour to 5 days
LHFs/LHCRs	Light Harvesting/photoprotection	Annunziata et al., 2022	Down	from 1 hour to 5 days
LHFs/LHCRs	Light Harvesting/photoprotection	Annunziata et al., 2022	Down	from 1 hour to 5 days
LHFs/LHCRs	Light Harvesting/photoprotection	Annunziata et al., 2022	Down	from 1 hour to 5 days
LHFs/LHCRs	Light Harvesting/photoprotection	Annunziata et al., 2022	Down	from 1 hour to 5 days
LHFs/LHCRs	Light Harvesting/photoprotection	Annunziata et al., 2022	Down	from 1 hour to 5 days
LHFs/LHCRs	Light Harvesting/photoprotection	Annunziata et al., 2022	Down	from 1 hour to 5 days
LHFs/LHCRs	Light Harvesting/photoprotection	Annunziata et al., 2022	Down	from 1 hour to 5 days

LHFs/LHCRs	Light Harvesting/photoprotection	Annunziata et al., 2022	Down	from 1 hour to 5 days
LHFs/LHCRs	Light Harvesting/photoprotection	Annunziata et al., 2022	Down	from 1 hour to 5 days
LHFs/LHCRs	Light Harvesting/photoprotection	Annunziata et al., 2022	Down	from 1 hour to 5 days
LHFs/LHCRs	Light Harvesting/photoprotection	Annunziata et al., 2022	Down	from 1 hour to 5 days
LHFs/LHCRs	Light Harvesting/photoprotection	Annunziata et al., 2022	Down	from 1 hour to 5 days
LHFs/LHCRs	Light Harvesting/photoprotection	Annunziata et al., 2022	Down	from 1 hour to 5 days
LHFs/LHCRs	Light Harvesting/photoprotection	Annunziata et al., 2022	Down	from 1 hour to 5 days
LHFs/LHCRs	Light Harvesting/photoprotection	Annunziata et al., 2022	Down	from 1 hour to 5 days
LHFs/LHCRs	Light Harvesting/photoprotection	Annunziata et al., 2022	Down	from 1 hour to 5 days
LHFs/LHCRs	Light Harvesting/photoprotection	Annunziata et al., 2022	Down	from 1 hour to 5 days
LHCX	Light Harvesting/photoprotection	Annunziata et al., 2022	Over	from 1 hour to 5 days
LHCX	Light Harvesting/photoprotection	Annunziata et al., 2022	Over	from 1 hour to 5 days
LHCR	Light Harvesting/photoprotection	Annunziata et al., 2022	Down	from 1 hour to 5 days
LHCX	Light Harvesting/photoprotection	Annunziata et al., 2022	Over	from 1 hour to 5 days
LHCX	Light Harvesting/photoprotection	Annunziata et al., 2022	Over	from 1 hour to 5 days
PSIID1	Photosynthetic electron transport	Annunziata et al., 2022	Down	from 1 hour to 5 days

PSIID1	Photosynthetic electron transport	Annunziata et al., 2022	Down	from 1 hour to 5 days
CytC6	Photosynthetic electron transport	Annunziata et al., 2022	Down	from 1 hour to 5 days
CytB6sub	Photosynthetic electron transport	Annunziata et al., 2022	Down	from 1 hour to 5 days
st/as	Photosynthetic electron transport	Annunziata et al., 2022	Down	from 1 hour to 5 days
rcp	Photosynthetic electron transport	Annunziata et al., 2022	Down	from 1 hour to 5 days
Psb27	Photosynthetic electron transport	Annunziata et al., 2022	Down	from 1 hour to 5 days
PSIap	Photosynthetic electron transport	Annunziata et al., 2022	Down	from 1 hour to 5 days
PsbU	Photosynthetic electron transport	Annunziata et al., 2022	Down	from 1 hour to 5 days
Psb28	Photosynthetic electron transport	Annunziata et al., 2022	Down	from 1 hour to 5 days
CytB6sub	Photosynthetic electron transport	Annunziata et al., 2022	Down	from 1 hour to 5 days
ATPC	Photosynthetic electron transport	Annunziata et al., 2022	Down	from 1 hour to 5 days
PsbM	Photosynthetic electron transport	Annunziata et al., 2022	Down	from 1 hour to 5 days
CytB6sub	Photosynthetic electron transport	Annunziata et al., 2022	Down	from 1 hour to 5 days
ZEP2	Carotenoids synthesis	Annunziata et al., 2022	Down	from 1 hour to 5 days
PDS1	Carotenoids synthesis	Annunziata et al., 2022	Down	from 1 hour to 5 days
PDS1	Carotenoids synthesis	Annunziata et al., 2022	Down	from 1 hour to 5 days

PSY	Carotenoids synthesis	Annunziata et al., 2022	Down	from 1 hour to 5 days
CRT-OX	Carotenoids synthesis	Annunziata et al., 2022	Down	from 1 hour to 5 days
CRTISO	Carotenoids synthesis	Annunziata et al., 2022	Down	from 1 hour to 5 days
ZEP1	Carotenoids synthesis	Annunziata et al., 2022	Down	from 1 hour to 5 days
ZEP1	Carotenoids synthesis	Annunziata et al., 2022	Down	from 1 hour to 5 days
GGPS	Carotenoids synthesis	Annunziata et al., 2022	Down	from 1 hour to 5 days
VDL1	Carotenoids synthesis	Annunziata et al., 2022	Down	from 1 hour to 5 days
PSY	Carotenoids synthesis	Annunziata et al., 2022	Down	from 1 hour to 5 days
LCYB	Carotenoids synthesis	Annunziata et al., 2022	Down	from 1 hour to 5 days
VDL2	Carotenoids synthesis	Annunziata et al., 2022	Down	from 1 hour to 5 days
PDS	Carotenoids synthesis	Annunziata et al., 2022	Down	from 1 hour to 5 days
CRT-OX	Carotenoids synthesis	Annunziata et al., 2022	Down	from 1 hour to 5 days
VDR	Carotenoids synthesis	Annunziata et al., 2022	Down	from 1 hour to 5 days
CRTISO4	Carotenoids synthesis	Annunziata et al., 2022	Down	from 1 hour to 5 days
VDE	Carotenoids synthesis	Annunziata et al., 2022	Down	from 1 hour to 5 days
CRTIS03	Carotenoids synthesis	Annunziata et al., 2022	Down	from 1 hour to 5 days

CRTIS0	Carotenoids synthesis	Annunziata et al., 2022	Down	from 1 hour to 5 days
ZEP3	Carotenoids synthesis	Annunziata et al., 2022	Over	from 1 hour to 5 days
PRK	Carbon assimilation	Annunziata et al., 2022	Down	from 1 hour to 5 days
PGP	Carbon assimilation	Annunziata et al., 2022	Down	from 1 hour to 5 days
GAPDH	Carbon assimilation	Annunziata et al., 2022	Down	from 1 hour to 5 days
GAPDH	Carbon assimilation	Annunziata et al., 2022	Down	from 1 hour to 5 days
TKT	Carbon assimilation	Annunziata et al., 2022	Down	from 1 hour to 5 days
FBP	Carbon assimilation	Annunziata et al., 2022	Down	from 1 hour to 5 days
FBP	Carbon assimilation	Annunziata et al., 2022	Down	from 1 hour to 5 days
FBA	Carbon assimilation	Annunziata et al., 2022	Down	from 1 hour to 5 days
FBA	Carbon assimilation	Annunziata et al., 2022	Down	from 1 hour to 5 days
PGK	Carbon assimilation	Annunziata et al., 2022	Down	from 1 hour to 5 days
RPE	Carbon assimilation	Annunziata et al., 2022	Down	from 1 hour to 5 days
DXS	Carbon assimilation	Annunziata et al., 2022	Down	from 1 hour to 5 days
SBP	Carbon assimilation	Annunziata et al., 2022	Down	from 1 hour to 5 days
RPI	Carbon assimilation	Annunziata et al., 2022	Down	from 1 hour to 5 days

GAPDH	Carbon assimilation	Annunziata et al., 2022	Down	from 1 hour to 5 days
FBP	Carbon assimilation	Annunziata et al., 2022	Down	from 1 hour to 5 days
HAD-hydrolase	Carbon assimilation	Annunziata et al., 2022	Down	from 1 hour to 5 days
TPI	Carbon assimilation	Annunziata et al., 2022	Down	from 1 hour to 5 days
FBP	Carbon assimilation	Annunziata et al., 2022	Down	from 1 hour to 5 days
FBP	Carbon assimilation	Annunziata et al., 2022	Down	from 1 hour to 5 days
FBP	Carbon assimilation	Annunziata et al., 2022	Down	from 1 hour to 5 days
PGP	Carbon assimilation	Annunziata et al., 2022	Down	from 1 hour to 5 days
FBP	Carbon assimilation	Annunziata et al., 2022	Down	from 1 hour to 5 days
PGP	Carbon assimilation	Annunziata et al., 2022	Down	from 1 hour to 5 days
FBP	Carbon assimilation	Annunziata et al., 2022	Down	from 1 hour to 5 days
TPI	Carbon assimilation	Annunziata et al., 2022	Down	from 1 hour to 5 days
RPE	Carbon assimilation	Annunziata et al., 2022	Down	from 1 hour to 5 days
RPE	Carbon assimilation	Annunziata et al., 2022	Down	from 1 hour to 5 days
6PGL	Carbon assimilation	Annunziata et al., 2022	Down	from 1 hour to 5 days
6PGL	Carbon assimilation	Annunziata et al., 2022	Down	from 1 hour to 5 days

FBP	Carbon assimilation	Annunziata et al., 2022	Down	from 1 hour to 5 days
6PGD	Carbon assimilation	Annunziata et al., 2022	Down	from 1 hour to 5 days
6PGD	Carbon assimilation	Annunziata et al., 2022	Down	from 1 hour to 5 days
PGK	Carbon assimilation	Annunziata et al., 2022	Down	from 1 hour to 5 days
TKT	Carbon assimilation	Annunziata et al., 2022	Over	from 1 hour to 5 days
HAD-hydrolase	Carbon assimilation	Annunziata et al., 2022	Down	from 1 hour to 5 days
PDHB1	Carbon assimilation	Annunziata et al., 2022	Over	from 1 hour to 5 days
G6PD	Carbon assimilation	Annunziata et al., 2022	Over	from 1 hour to 5 days
RPE	Carbon assimilation	Annunziata et al., 2022	Over	from 1 hour to 5 days
Marker1	Putative sex marker genes	Bilcke. G	Over	Directly
Marker2	Putative sex marker genes	Bilcke. G	Over	Directly
Marker3	Putative sex marker genes	Bilcke. G	Over	Directly
Marker4	Putative sex marker genes	Bilcke. G	Over	Directly
Marker5	Putative sex marker genes	Bilcke. G	Over	Directly

Titre : Dynamique spatio-temporelle des efflorescences de *Pseudo-nitzschia australis* dans la mer d'Iroise : Une étude multidisciplinaire combinant l'expression de gènes, l'environnement et l'hydrodynamique.

Mots clés : *Pseudo-nitzschia australis*, efflorescence spatio-temporelle, mer d'Iroise, rade de Brest, metatranscriptomique, hydrodynamique

Résumé : Certaines espèces de diatomées du genre *Pseudo-nitzschia* produisent de l'acide domoïque, une neurotoxine responsable du syndrome d'intoxication amnésique chez l'Homme ou de mortalités chez des animaux marins. Les efflorescences de *Pseudo-nitzschia* et les toxicités qui en résultent constituent un problème mondial. En France, le Finistère est affecté de manière régulière au début du printemps par une des espèces les plus toxiques, *P. australis*. Cette thèse se concentre sur la dynamique spatio-temporelle des efflorescences de cette espèce dans la mer d'Iroise. En combinant simulations hydrodynamiques, metatranscriptomique, suivi des efflorescences et des conditions environnementales associées, cette thèse a mis en évidence un rôle important de l'hydrodynamique dans l'initiation et l'extension des efflorescences de *P. australis* (et d'autres espèces de diatomées). En effet, un transport hydrodynamique Sud-Nord des efflorescences a été identifié, avec un potentiel développement en baie de Douarnenez avant d'être transportées plus au nord, en rade de Brest. Ce développement local dans la baie de Douarnenez pourrait-être favorisé par une faible dilution, permettant l'accumulation des cellules. En revanche, aucune relation entre environnement local et décalage spatio-temporel des efflorescences n'a pu être mise en évidence. Par contre, il a été découvert que la reproduction sexuée joue un rôle essentiel dans la physiologie de *P. australis* lors d'une efflorescence *in situ*. Cette étude met en évidence le rôle combiné de l'environnement, de la connectivité hydrodynamique et du cycle de vie dans le développement, le transport, et la persistance d'une efflorescence en milieu naturel.

Title: Spatio-temporal dynamics of *Pseudo-nitzschia australis* blooms in the Iroise Sea: A multi-disciplinary study combining gene expression, environment, and hydrodynamics.

Keywords: *Pseudo-nitzschia australis*, spatio-temporal bloom, Iroise sea, Bay of Brest, metatranscriptomic, hydrodynamics

Abstract: Diatoms of the *Pseudo-nitzschia* genus produce domoic acid, a neurotoxin responsible for amnesic poisoning syndrome in humans, following consumption of filter-feeding mollusks, and mortality in mammals and seabirds. In France, West-Finistère is regularly affected in early spring by one of the most toxic species, *P. australis*. This thesis focuses on the spatio-temporal dynamics of blooms of this species in the Iroise Sea. By combining hydrodynamic simulations, metatranscriptomics, monitoring of blooms and associated environmental conditions, this thesis has highlighted the important role of hydrodynamics in the initiation and extension of *P. australis* blooms (and other diatom species). Hydrodynamic transport of the blooms from south to north has been identified, with potential development in the Bay of Douarnenez before being transported further north to the Bay of Brest. This local development in the Bay of Douarnenez could be favoured by low dilution, allowing cells to accumulate. However, no relationship between the local environment and the spatio-temporal shift in the blooms could be established. However, it was discovered that sexual reproduction plays an essential role in the physiology of *P. australis* during an *in situ* bloom. This study highlights the combined role of the environment, hydrodynamic connectivity and the life cycle in the development, transport and persistence of a bloom in a natural environment.